Impact of senescence and disease on the structural and functional performance of the visual pathway

Helena Louise Workman
Doctor of Philosophy

Aston University
December 2005

Aston University
Impact of senescence and disease on the structural and functional performance of the visual pathway
Helena Louise Workman
Doctor of Philosophy
2005

Thesis summary

The diagnosis and monitoring of ocular disease presents considerable clinical difficulties for two main reasons i) the substantial physiological variation of anatomical structure of the visual pathway and ii) constraints due to technical limitations of diagnostic hardware. These are further confounded by difficulties in detecting early loss or change in visual function due to the masking of disease effects, for example, due to a high degree of redundancy in terms of nerve fibre number along the visual pathway.

This thesis addresses these issues across three areas of study:

1. Factors influencing retinal thickness measures and their clinical interpretation

As the retina is the principal anatomical site for damage associated with visual loss, objective measures of retinal thickness and retinal nerve fibre layer thickness are key to the detection of pathology. In this thesis the ability of optical coherence tomography (OCT) to provide repeatable and reproducible measures of retinal structure at the macula and optic nerve head is investigated. In addition, the normal physiological variations in retinal thickness and retinal nerve fibre layer thickness are explored. Principal findings were:

- Macular retinal thickness and optic nerve head measurements are repeatable and reproducible for normal subjects and diseased eyes
- Macular and retinal nerve fibre layer thickness around the optic nerve correlate negatively with axial length, suggesting that larger eyes have thinner retinae, potentially making them more susceptible to damage or disease
- Foveola retinal thickness increases with age while retinal nerve fibre layer thickness around the optic nerve head decreases with age. Such findings should be considered during examination of the eye with suspect pathology or in long-term disease monitoring

2. Impact of glucose control on retinal anatomy and function in diabetes

Diabetes is a major health concern in the UK and worldwide and diabetic retinopathy is a major cause of blindness in the working population. Objective, quantitative measurements of retinal thickness, particularly at the macula provide essential information regarding disease progression and the efficacy of treatment. Functional vision loss in diabetic patients is commonly observed in clinical and experimental studies and is thought to be affected by blood glucose levels. In the first study of its kind, the short term impact of fluctuations in blood glucose levels on retinal structure and function over a 12 hour period in patients with diabetes are investigated. Principal findings were:

- Acute fluctuations in blood glucose levels are greater in diabetic patients than normal subjects
- The fluctuations in blood glucose levels impact contrast sensitivity scores, SWAP visual fields, intraocular pressure and diastolic pressure. This effect is similar for type 1 and type 2 diabetic patients despite the differences in their physiological status
- Long-term metabolic control in the diabetic patient is a useful predictor in the fluctuation of contrast sensitivity scores
- Large fluctuations in blood glucose levels and/or visual function and structure may be indicative of an increased risk of development or progression of retinopathy

3. Structural and functional damage of the visual pathway in glaucomatous optic neuropathy

The glaucomatous eye undergoes a number of well documented pathological changes including retinal nerve fibre loss and optic nerve head damage which is correlated with loss of functional

vision. In experimental glaucoma there is evidence that glaucomatous damage extends from retinal ganglion cells in the eye, along the visual pathway, to vision centres in the brain. This thesis explores the effects of glaucoma on retinal nerve fibre layer thickness, ocular anterior anatomy and cortical structure, and its correlates with visual function in humans. Principal findings were:

- In the retina, glaucomatous retinal nerve fibre layer loss is less marked with increasing distance from the optic nerve head, suggesting that RNFL examination at a greater distance than traditionally employed may provide invaluable early indicators of glaucomatous damage
- Neuroretinal rim area and retrobulbar optic nerve diameter are strong indicators of visual field loss
- Grey matter density decreases at a rate of 3.85% per decade. There was no clear evidence of a disease effect
- Cortical activation as measured by fMRI was a strong indicator of functional damage in patients with significant neuroretinal rim loss despite relatively modest visual field defects

These investigations have shown that the effects of senescence are evident in both the anterior and posterior visual pathway. A variety of anatomical and functional diagnostic protocols for the investigation of damage to the visual pathway in ocular disease are required to maximise understanding of the disease processes and thereby optimising patient care.

Keywords

Optical coherence tomography, retinal and retinal nerve fibre layer thickness, age and axial length effects, glaucoma, diabetes

Acknowledgements

My very grateful thanks to my supervisor Dr Sarah L Hosking without whose intellectual input and guidance this work would not have been possible. I would also like to thank Prof Krish Singh for both his supervisory contribution and involvement in the MRI part of this thesis. Thanks are also due to Dr Miriam Conway for unravelling the mystery of statistics, to Dr Rob Cubbidge for his clever visual field analysis, to Dr Nicola Logan for her wise words in all things and to Dr Emma Hilton who greatly helped me at the very beginning of this project.

And last but by no means least, my thanks to my family for their endless support, prayers, love and encouragement over the last few years, especially more recently to Nana for her excellent study facilities, Mum for her endless text messages and Nat for his patience, understanding and loving care.

List of figures

List of tables

List of equations

CHAPTER 1: Introduction

The following review describes the normal anatomy of the optic nerve head, retinal nerve fibre layer and retinal layer and explores the physiological variations and pathological changes which may occur. A description of glaucoma, namely primary open angle glaucoma (POAG) and its pathogenesis is reviewed. The epidemiology and risk factors of POAG are described, together with an introduction to the clinical assessment of the disease. Diabetes and risk factors for the development of diabetic retinopathy are explored. Current imaging modalities are reviewed, in particular the optical coherence tomographer (OCT) and its applications. The investigation of normal physiological variations in ocular structure and changes to retinal structure as measured by the OCT and retinal function in the diseased eye forms the basis of this thesis.

1.1 Anatomy of the eye

1.1.1 Retinal ganglion cells

Retinal ganglion cells, of which there are 1.25 million in each human eye, can be broadly divided into three types, parvocellular (70%), magnocellular (8-10%) and koniocellular groups (1-10%). Parvocellular (P, midget) cells are specialised in the detection of fine spatial detail, colour and spatial contrast sensitivity, due to their small dendritic fields and small receptive field size, small axonal diameters and their ability to conduct information at moderate speeds. This cell type is predominately found in the foveal area and these fibres project to the parvocellular layers of the lateral geniculate nucleus. Magnocellular (M, parasol) cells have large dendritic fields and subsequently large receptive field sizes and large axonal diameters. They respond transiently to the onset and offset of lights, have rapid conduction and as such are specialised in detection of high temporal frequency stimuli but poor at fine spatial detail. These cells are situated in the retinal periphery and project to the magnocellular layers of the lateral geniculate nucleus (Perry, Oehler, Cowey, 1984). Koniocellular cells have blue- yellow

opponency and receive input from blue-yellow cone bipolar cells. They project their axons to the interlaminar konicellular layers of the lateral geniculate nucleus (Martin, White, Goodchild *et al.*, 1997).

1.1.2 Anatomy of the retinal nerve fibre layer (RNFL)

The RNFL is composed mainly of ganglion cell axons together with neuroglial cells and astrocytes. Retinal ganglion cell axons curve sharply at the optic nerve margin and form the optic nerve, passing through the lamina cribrosa, and converge upon the optic chiasm to form the optic tract before reaching the lateral geniculate nucleus. From the LGN, relay neurons projecting to the primary visual cortex make up the final part of the visual pathway.

Retinal nerve fibres can be classified according to their position and subsequent pathway to the optic nerve as follows:

Superior arcuate fibres - start from the horizontal raphe, follow an arcuate path around the papillomacular bundle to form the superotemporal portion of the optic disc

Inferior arcuate fibres - start from the horizontal raphe, follow an arcuate path around the papillomacular bundle to form the inferotemporal portion of the optic disc

Superior radiating fibres – start from the superonasal retina and project in direct radial lines towards the superonasal portion of the optic disc

Inferior radiating fibres – start from the inferonasal retina and project in direct radial lines towards the inferonasal portion of the optic disc

Papillomacular bundle – large number of ganglion cell axons starting at the fovea that project directly to the optic nerve. Fibres on the temporal side of the fovea follow an arcuate pattern around the fibres from the nasal fovea divided superiorly and inferiorly by the horizontal raphe. The papillomacular bundle forms a large proportion of the temporal optic disc

1.1.3 Anatomy of the optic nerve

The optic nerve measures approximately 50mm in length and is made up of between 1.1-1.3 million retinal ganglion cell axons which arise from the retinal ganglion cells and pass to the lateral geniculate body before being relayed to the visual cortex.

It can be divided into four regions:

1. Intraocular
2. Intraorbital
3. Intracanalicular
4. Intracranial

The intraocular portion of the optic nerve is the optic nerve head and may be further described in terms of its position relative to the lamina cribrosa: prelaminar, laminar and postlaminar. The retrobulbar optic nerve consists of the intraorbital, intracanalicular and intracranial portion.

Prelaminar optic nerve head

At the optic disc margin, the retinal ganglion cell axons curve sharply and form the optic nerve. In this region the axons are unmyelinated and separated into bundles by astrocytes. The optic nerve fibre bundles exit the eyeball via the lamina cribrosa (Birch, Brotchie, Roberts *et al.*, 1997).

Laminar optic nerve head

The bundles pass through the collagen sheets of the lamina cribrosa and become gradually myelinated toward the posterior part of the lamina. The astrocytes surrounding the nerve fibres reduce to a thin covering and separate the fibres from the collagenous lamina cribrosa extracellular matrix.

Lamina cribrosa

The lamina cribrosa is made up of about ten perforated sheets mainly consisting of elastin fibres, collagen fibrils and fibroblasts (Hernandez, Luo, Igoe *et al.*, 1987). The perforations or pores vary from 200-400 in number, are positioned irregularly and vary in size from 10 to 100μm. Pores in the centre appear to be smaller than those located in

the periphery while the superior and inferior portions of the lamina cribrosa are larger in size compared to those in the temporal and nasal regions (Mikelberg *et al.*, 1989). The pores allow the passage of nerve fibre bundles and facilitate axonal transport. This is defined as the movement of material along an axon either from the terminal to the cell body (retrograde) or from the cell body to the terminal (anterograde) (Birch *et al.*, 1997; Anderson, 1977).

Post laminar optic nerve

The post laminar optic nerve is surrounded by the pia, arachnoid and dura maters. Nerve fibre bundles are separated by the pial septa which comprise collagen and elastic fibres together with fibroblasts, nerves and vessels. The pial septa provide both nutritional and mechanical support.

1.1.4 Normal vasculature of the optic nerve

The superficial nerve fibre layer is supplied from the branches of the central retinal arteries. The blood supply to the prelaminar and laminar regions is provided by branches either from the circle of Zinn-Haller or from the short posterior ciliary arteries. The retrolaminar region is supplied by branches of the short posterior ciliary arteries and pial arteries in addition to occasional branches of the central retinal artery (Onda, Cioffi, Bacon *et al.*, 1995; Zhao and Cioffi, 2000).

1.1.5 Aqueous humour

Aqueous humour is a transparent colourless liquid essential for the nutrition of the iris, lens and cornea and the removal of metabolic waste. It is formed in the ciliary body at a rate of approximately 2ml/min, from where it passes round the equator of the lens through the pupil into the anterior chamber. Aqueous drains into the venous circulation via the trabecular meshwork and independently through the uveoscleral outflow pathway. Intraocular pressure is regulated by a balance between the secretion and drainage of the aqueous humour (Lawrenson, 1998; Weinreb and Khaw, 2004).

1.1.6 Optic nerve head in normal eyes

The optic nerve head or optic disc are the terms used to describe the tissues comprising the region of the intraocular optic nerve extending from the lamina cribrosa to the disc surface. Elevations on the disc surface as a result of the convergence of many retinal ganglion cell axons are described as papilla. The optic disc comprises the neuroretinal rim and the optic cup. The neuroretinal rim comprises the nerve fibres while the optic cup is the central pale depression of the disc devoid of nerve fibres. The scleral ring of Elsching is a thin, cream coloured border which usually encircles the optic nerve head, marking the termination of the retinal pigment epithelium (RPE). Choroidal crescents represent the RPE terminating short of the disc and exposing the underlying choroid, while scleral crescents represent both the RPE and choroid failing to reach the disc and exposing the underlying scleral tissue.

1.1.7 Neuroretinal rim shape in normal eyes

The normal optic nerve head/optic disc comprises the optic cup, a pale depression, within the darker coloured neuroretinal rim. The neuroretinal rim exhibits a characteristic configuration in normal eyes. It is normally broadest in the inferior disc region, followed by the superior disc region, the nasal disc and finally the temporal disc area, otherwise known as the ISNT rule (Jonas, Gusek, Naumann, 1988). The size of the optic disc varies greatly within individuals and is on average 1.75mm by 1.65mm. Optic cup size is dependent on the size of the disc. Large discs tend to have large cups while small discs may have little or no cup. The cup: disc ratio is the diameter of the cup divided by the diameter of the disc and is routinely measured during ophthalmoscopic examination. It can be estimated in both vertical and horizontal meridians and on average measures 0.3 vertically (range 0.0-0.9) in a normal population (Jonas *et al.*, 1988). Cup: disc ratios of greater than 0.5 are considered suspicious as they may indicate enlargement of the cup size as neuroretinal rim tissue is lost. Features of the optic disc to be assessed in clinical examination include its colour, shape, margins, optic cup and neuroretinal rim appearance and vasculature.

1.2 Anatomy of the lateral geniculate nucleus (LGN)

The LGN is the major target of retinal ganglion cell axons before visual information is relayed to the visual cortex. It consists of six layers that are superimposed upon each other and separated by cell-sparse interlaminar zones. The two most ventral layers (1 and 2) are the magnocellular layers and consist of neurons with large cell bodies. These layers receive input from the M cells. The dorsal-most four layers (3, 4, 5 and 6) are referred to as the parvocellular layers, consist of smaller cell bodies and receive their input from P cells. Each nucleus receives axons from the contralateral nasal hemiretina and the ipsilateral temporal retina due to the partial decussation of axons at the optic chiasm. In both the magno and parvo layers, M and P cell inputs from each eye will remain separate and reach different layers. Within each LGN layer a neural retinotopic map exists in which neighbouring regions of the retina are represented. The cells of both the magno and parvocellular layers send axons to the primary visual cortex via the posterior limb of the internal capsule and the optic radiations (Hubel, 1988).

1.3 Primary visual cortex

The primary visual cortex is located at the posterior pole of the occipital lobe and is referred to as area 17 or V1. It comprises six distinct cellular layers with an underlying white matter comprising the axons which provide input and output to the region.

Layer 1: the molecular layer. This is the most superficial layer and contains a few scattered neurons.
Layer 2: the external granular layer. This contains small neurons that extend their axons only to deeper cortical layers.
Layer 3: the external pyramidal layer. This contains larger neurons that send axons mainly to other cortical regions.
Layer 4: the internal granular layer. This consists mainly of granular cells and is subdivided into layers 4A, 4B and 4C. Layer 4C receives the predominant input from the LGN and retains the segregation of inputs in the LGN. Layer 4Cα receives its input from axons from the magnocellular LGN layers and 4Cβ from the parvocellular layers. Layer 4B cells send axons to more superficial layers and to other visual cortical areas.

Layer 5: the internal pyramidal layer. This consists of larger neurons which send axons to the superior colliculus and other structures within the brainstem.
Layer 6: the multiform layer. This comprises a variety of cell types and most of the axons project back to the LGN (Hubel, 1988).

1.4 Normal retinal thickness

A number of studies have used the Optical Coherence Tomographer (OCT) and the Retinal Thickness Analyzer (RTA) to measure foveal retinal thickness in normal subjects as summarised in table 1.1.

Author	Year	Foveal retinal thickness
Optical Coherence Tomography		
Hee, Puliafito, Wong *et al.*	1995b	147 ± 17μm
Hee, Puliafito,Duker *et al.*	1998	152 ± 21μm
Baumann, Gentile, Liebmann, Ritch	1998	154 ± 13μm
Otani, Kishi and Maruyama	1999	133 ± 9μm
Goebel, Hartmann and Haigis	2001	142 ± 18μm
Konno, Akiba and Yoshida	2001	155.1 ± 14.9μm
Sanchez- Tocino, Alvarez- Vidal *et al*	2002	145 ± 16μm
Goebel and Kretzchmar-Gross	2002	153 ± 15μm
Retinal Thickness Analyzer		
Weinberger, Axer-Siegel and Landau	1998	178 ± 44μm
Konno, Akiba and Yoshida	2001	107.8 ± 18.6μm

Table 1.1 Summary of reported retinal thickness values for normal subjects

1.5 Physiological variation in retinal thickness

1.5.1 Age effects

There is considerable physiological variation in retinal thickness (RT) and retinal nerve fibre layer thickness (RNFL) in normal healthy subjects. There is also evidence that retinal thickness and retinal nerve fibre layer thickness may be affected by age. Studies to determine whether age has an effect on retinal and RNFL thickness are numerous and provide contradictory results. Conclusive findings are complicated by the variety of imaging techniques and particular type of scan employed in each study. While some authors report no correlation between age and RNFL, others have found that the RNFL decreases with age, a result confirmed by post-mortem studies (Dolman, McCormick and Drance 1980; Balazsi, Rootman, Drance *et al.*, 1984; Johnson, Miao and Sudan, 1987; Mikelberg, Drance, Schulzer *et al.*, 1989; Repka and Quigley, 1988; Jonas, Muller-Bergh *et al.*, 1990; Poinoosawmy, Fontata, Wu *et al.*, 1997; Funaki, Shirakashi, Funaki *et al.*, 1999). More recently, studies using optical coherence tomography have demonstrated that RNFL significantly decreased with age (Alamouti and Funk, 2003; Kanamori, Escano, Eno *et al.*, 2003).

Oshima, Emi, Yamanishi *et al.* (1999) reported that macular retinal thickness in normal subjects was independent of age using the Retinal Thickness Analyzer (RTA). This was confirmed by Asrani, Zou *et al.* (1999) who, using similar imaging techniques, concluded that age has little effect on the retinal thickness at the posterior pole. Varma, Bazzaz *et al.* (2003) used OCT model 2000 to measure retinal thickness across the macular region using 6 linear scans each 30 degrees apart centred on the fovea. They too observed no significant difference between the macular thickness in older and younger individuals ($p=0.72$). Similarly, Massin, Erginay, Haouchine *et al.* (2002) using the OCT macular scan found no significant difference in retinal thickness according to age.

This finding is in contrast to Landau, Schneidman, Jacobovitz *et al.* (1997) who found that foveola thickness increased with age.

Other workers have reported that retinal thickness decreases with age as a result of the degeneration of the nerve fibre layer (Mikelberg *et al.*, 1989). This is confirmed in a later study using the OCT by Alamouti and Funk (2003) who report a significant decrease of 0.53μm per year in retinal thickness with age.

1.5.2 Axial length effects

The myopic eye has a greater axial length than the normal eye which produces scleral thinning which is more marked at the posterior pole. It is logical to suggest that highly myopic eyes also have thinner retinal tissue compared with emmetropic eyes. Studies investigating the effect of myopia on retinal and retinal nerve fibre layer tissue have drawn inconsistent conclusions. Retinal thickness in the macular area is not influenced by the axial length of the eye according to Garcia-Valenzuela, Mori, Edward *et al.* (2000) and Wakitani, Sasoh, Sugimoto *et al.* (2003). Goebel, Hartmann and Haigis (2001) using OCT line scans placed through the fovea, also reported no influence of axial length on macular thickness. However, a relationship between macular retinal thickness and degrees of myopia has been reported by Mrugacz and Bakunowicz-Lazarczyk (2005). Kremser, Troger, Baltaci, *et al.* (1999) using the Retinal Thickness Analyzer (RTA) report retinal thinning at the posterior pole of myopic eyes.

1.6 Normal retinal nerve fibre layer

The peripapillary retinal contour follows a double hump pattern whereby the retinal nerve fibre layer thickness is greatest at the inferior and superior poles of the optic disc and thinnest at the temporal and nasal disc margins (Dichtl, Jonas, Naumann, 1999). The RNFL is not easy to visualise but is best examined using red-free ophthalmoscopy or photography, preferably with a stereoscopic view. The normal retinal nerve fibre layer looks slightly opaque, with fine pale striations. The nerve fibre bundles are most visible in the inferotemporal sector, followed by the superotemporal area (where there are a greater number of fibres), the nasal superonasal region and finally the inferonasal sector (Jonas and Dichtl, 1996). It is least visible in the superior, inferior, temporal horizontal and nasal horizontal regions. More recently, scanning laser tomography,

scanning laser polarimetry and optical coherence tomography techniques have been employed to assess the RNFL.

1.6.1 Histological studies

Histological studies of human eyes are understandably limited. Varma, Skaf and Barron, (1996) provided the first histologically measured estimates of RNFL thickness at the optic disc margin, fovea and periphery of human eyes. They found mean superior, inferior, nasal and temporal RNFL thickness at the disc margin to be 405,376,372 and 316μm respectively. This double hump configuration was confirmed in a study by Dichtl, Jonas and Naumann (1999) who reported highest mean thickness in the inferior quadrant (266±64μm), followed by the superior quadrant (240±57μm), the nasal quadrant (220±70μm) and finally the temporal quadrant (170±58μm). Differences between findings of the two studies may be explained by a longer postmortem time for the eyes in the earlier study and differing methodologies.

According to Varma and co-workers, retinal nerve fibre layer thickness decreases with increasing distance from the disc margin in all quadrants (Varma *et al.*, 1996).

1.6.2 In vivo morphological studies

There appears to be a good correlation between measurements of retinal nerve fibre layer thickness using the optical coherence tomographer (OCT) compared with histological data. The OCT has been used in several studies to measure the retinal nerve fibre layer of both normal and diseased eyes and has been found to be both reliable, repeatable and reproducible (Hee, Puliafito, Wong, *et al.* 1995b; Hee, Izatt, Swanson *et al.*, 1995a; Schuman, Hee, Puliafito *et al.*, 1995; Massin *et al.*, 2001). Kanamori *et al.* (2003) found the RNFL in normal eyes to exhibit the double hump pattern. RNFL was greatest in the superior and inferior quadrants and significantly thinner in the nasal and temporal quadrants in comparison to the vertical pole. This was confirmed by Varma *et al.* (2003) who investigated the RNFL thickness in 312 normal eyes using the OCT.

They noted the RNFL to be thicker in the inferior and superior quadrants and thinner in the nasal and temporal quadrants.

The normal RNFL is asymmetric with respect to the horizontal midline for individual eyes and also to the vertical meridian for the two eyes (Kurimoto, Matsuno, Kaneko *et al.*, 2000). The authors recommend that such findings should be considered during RNFL examination of diseased eyes.

1.7 Physiological variation in retinal nerve fibre layer thickness

1.7.1 Age effects

There is considerable evidence of an inverse relationship between retinal nerve fibre layer thickness and age (Schuman *et al.*, 1995; Mok, Lee and So, 2002; Alamouti and Funk, 2003). Varma *et al.* (2003) observed a statistical difference in the peripapillary RNFL thickness between older and younger normal subjects. The effect of age appears to vary according to the region of retina being tested. RNFL thickness, particular in the temporal quadrant, significantly decreases with age according to Kanamori *et al.* (2003).

Soliman, van den Berg, Ismaeil *et al.* (2002) found that RNFL thickness decreased with increasing age when assessed by both the OCT and red-free photography. Jonas, Nguyen, Naumann (1989) using red-free photography also reported that RNFL decreased with age.

Histological studies have shown that the superonasal and inferotemporal RNFL thickness at the disc margin was inversely related to age (Varma *et al.*, 1996). The authors were unable to detect a consistent negative association between all RNFL thickness measurements and age but their small sample size (n=10) may explain this.

Analyses of RNFL variations with age using scanning laser polarimetry have proved inconsistent. Poinoosawmy *et al.* (1997) report a progressive reduction in thickness as age increases, with a decay of 0.38μm per year. Similar findings were reported by Chi, Tomita, Inazumi, *et al.* (1995) who calculated a decrease in RNFL thickness of 0.2μm

per year. Lee and Mok (2000) found a significant negative correlation in average RNFL values with increasing age (approximately 1.9μm per decade).

However, Funaki *et al.* (1999) found no significant relationship between RNFL thickness and age. Laser scanning polarimetry technique is based on changes in polarisation of light and retardation which is related to retinal nerve fibre layer thickness. Change in polarisation is converted into a topographical map of RNFL thickness measurements from which software analysis can be performed. However, a limitation of the scanning laser polarimeter is that the RNFL is not the only birefringent structure of the eye - both the cornea and lens have birefringence properties. The possibility that they may influence findings should be considered.

1.7.2 Gender effects

Several reports have investigated the effect of gender on the nerve fibre layer thickness of normal subjects. Schuman *et al.* (1995) reported that nerve fibre layers of women tended to be thinner than in men but not to a significant degree. Varma *et al.* (2003) observed no statistically significant differences in RNFL thickness between men and women at the macula, peripapillary circumference and superior, temporal and nasal quadrants.

1.8 Physiological variations of the optic nerve

1.8.1 Normal optic nerve axon count

Mikelberg *et al.* (1989) investigated the axonal count and axon diameter distribution in normal eyes using computerized image analysis. Mean axon count was 969,279 ± 239,740 axons per nerve. Other workers found lower mean counts although the mean age of their samples was higher for example, Quigley, Dunkelberger and Green (1988) calculated the mean count at 689,500±136,300 while Repka and Quigley (1989) observed a mean count of 693,316. Balazsi *et al.* (1984) calculated the mean axon count to be 1,244,005 using a manual technique. Jonas, Muller-Bergh, Schlotzer-Schrehardt, *et al.* (1990) report a mean fibre count of 1,159,000 ± 196,000. Yucel, Gupta,

Kalichman *et al.* (1998) reported mean nerve fibre number in monkey eyes to be 1,073,205 ± 134,119. Discrepancies between studies may be explained by the different techniques employed since automated analysis counts axons that are well preserved while the manual technique is able to count more damaged axons.

1.8.2 Axon diameter

Mean axon diameter varies according to each study and has been recorded as being 0.72μm (Mikelberg *et al.*, 1989), 0.96±0.09μm (Repka and Quigley, 1989) and 1.00 ±0.06μm (Jonas *et al.*, 1990). Johnson *et al.* (1987) measured mean axon diameter size range of 0.65 to 1.10μm. In a study of 13 normal optic nerves Quigley *et al.* (1988) report a mean fibre diameter of 0.95±0.07μm. Such variability can be explained by the large patient variability, small sample size and methodology employed.

There is considerable evidence to show higher axonal density is found in the inferotemporal segment of the nerve. This is consistent with the observation that the major portion of the papillomacular bundle enters at this point. The superonasal segment of the optic nerve contains axons with higher mean diameters which is in agreement with the observation that a greater number of larger diameter axons enter this quadrant of the nerve (Quigley *et al.*, 1988; Mikelberg *et al.*, 1989; Jonas *et al.*, 1990). Previous studies have shown that in glaucomatous eyes neural loss takes place predominantly at the vertical poles of the optic nerve head (Quigley, Addicks and Green, 1982) while large diameter fibres appear particularly prone to damage and eventual loss (Quigley, Sanchez, *et al.*, 1987; Quigley *et al.*, 1988).

Jonas *et al.* (1990) found that the optic nerve cross-section area was correlated with the nerve fibre count and can therefore be taken as an indicator of the nerve fibre number. Studies have shown that eyes with large optic discs have a greater number of optic nerve fibres and larger nerve fibre layer volume compared with eyes with small optic nerve heads (Quigley, Coleman and Dorman-Pease, 1991: Jonas, Schmidt, Muller-Bergh *et al.*, 1992). A correlation has also been found between optic disc size and retinal photoreceptor count. Large optic nerve heads are reported to have a higher count of rods and cones (Panda-Jonas, Jonas, Jakobczyk *et al.*, 1994). Previous studies have

shown a loss of photoreceptors in glaucomatous eyes (Panda and Jonas, 1992). Panda-Jonas *et al.* (1994) therefore suggest a higher anatomic reserve capacity in glaucomatous eyes with large optic discs as compared to glaucomatous eyes with small optic discs. Furthermore, they postulate that the area of the optic nerve head may be a useful predictor of the anatomic resources of the retina and that this hypothesis may be extended to retinal ganglion cells. Such a view is disputed by Jonas, Fernandez and Naumann (1991) who report that optic nerve damage in white patients with POAG is independent of the size of the optic disc.

The majority of studies report that optic nerve axon number decreases with age (Balazsi *et al.,* 1984; Johnson *et al.*, 1987; Dolman *et al.*, 1980). Conversely, Quigley and associates found no fibre loss with age in five normal nerves (Quigley *et al.*, 1982) but this may be explained by the small number of nerves tested. A later study by Repka and Quigley (1989) on cadaver eyes revealed no significant decline in fibre number or neural area with increasing age. However, the patients in this study showed a large variation in axonal count which could mask small age effects. Studies of this kind are inherently difficult due to the difficulty in methodology and due to the substantial variability of the total number of axons between individuals and even between fellow eyes. The above studies employ a variety of methods to count nerve fibres and measure nerve diameter which itself is a source of variability when comparing results. Automated image analysis technique counts axons that are well preserved, while manual techniques tend to include more damaged axons.

The relationship between axon diameter and age has been investigated with varying results. Axon diameter has been shown to be independent of age (Johnson *et al.*, 1987; Mikelberg *et al.*, 1989) while others report a slight decrease in mean axon diameter although not statistically significant (Repka and Quigley, 1989). The authors suggest that this could be explained by a selective loss of large nerve fibres.

1.9 Glaucoma: Facts & Figures

Glaucoma is a term used to describe a variety of eye conditions, all of which are associated with characteristic optic nerve damage. Glaucoma may be classified as a primary disease, which has no particular association with any other systemic or ocular disease or secondary, which occurs as a consequence of another disease, abnormality or injury or congenital factors. It may be described as open angle or closed angle depending on the nature of the anterior chamber angle. Closure of this structure leads to a reduction or cessation of normal aqueous drainage and can cause a rise in IOP.

Primary open angle glaucoma (POAG) is of particular interest in this study and is described as a syndrome of progressive optic neuropathy with characteristic optic nerve damage and defects in retinal sensitivity leading to loss of visual function (Fechtner and Weinreb, 1994).

1.9.1 Epidemiology of glaucoma

It was estimated in 1996 that glaucoma would affect more than 66 million individuals worldwide with at least 6.7million bilaterally blind by the year 2000 (Quigley, 1996). According to the World Health Organisation statistics, glaucoma is the second leading cause of blindness globally, at 12.3% of total blindness (Resnikoff, Pascolini, Etya'ale *et al.*, 2002).

Several epidemiological studies have attempted to determine the prevalence and incidence of glaucoma. Estimates vary as a result of the different populations studied, the differing methodologies employed with regard to sampling the populations and variations in the way in which glaucoma is defined. Table 1.2 outlines the prevalence of POAG according to several studies.

Study	Author	Age range	Total Prevalence (%)
Ferndale	Hollows *et al.* 1966	40-75	0.4
Framingham	Kahn *et al.* 1980	52-85	2.2 (3.3*)
Dalby, Sweden	Bengtsson 1981	55-69	0.93
St. Lucia	Mason *et al.* 1989	30+	8.8
Baltimore (whites)	Tielsch *et al.* 1991	40-85+	1.3
Baltimore (blacks)	Tielsch *et al.*1991	40-85	4.7
Beaver Dam	Klein *et al.* 1992	43-84	2.1
Roscommon Ireland	Coffey *et al.* 1993	50-80+	1.9
South Africa	Salmon *et al.* 1993	40+	1.5
Rotterdam	Dielemans *et al.* 1994	55-85+	1.1
Barbados	Leske *et al.*1994	40-84	6.7
Casteldaccia	Giuffre *et al.* 1995	40+	1.2
Tierp	Ekstrom 1996	65-74	5.7
Blue Mountains	Mitchell *et al.* 1996	49-97	2.4 (3.0*)
Melbourne	Wensor *et al.* 1998	40-98	1.7 (2.2*)
Egna-Neumarkt	Bonomi *et al.* 1998	40+	1.4

Table 1.2 Prevalence of POAG previously reported in other studies

(*) Definite and probable glaucoma cases combined

Until 1991, prevalence studies had predominantly studied racially separate populations. This lack of comparable data meant there was little information regarding the effect of race on the likelihood of developing POAG. The Baltimore Eye Survey (Tielsch, Sommer, Katz *et al.*, 1991) was specifically designed to compare the racial variations in the prevalence rates between black and white Americans by applying the same rigorous examination criteria on a representative sample of both black and white subjects from similar socio-economic backgrounds. Results from this study, together with the Baltimore and St Lucia study, suggested a racial disparity in the prevalence of POAG (see table 1.2).

1.9.2 Risk factors in glaucoma

Risk factors associated with POAG can be broadly divided into demographic, ocular, systemic, genetic and miscellaneous factors. Some of these will be explored in detail in the following sections.

Type	Description
Demographic	Age Gender Race
Ocular	Intraocular pressure (IOP) Optic nerve head (ONH) Myopia Hypermetropia
Systemic	Diabetes Systemic hypertension Systemic hypotension Peripheral vascular disease Vasospasm Migraine Hormonal influences
Genetic	Family history of glaucoma
Other	Cigarette smoking Caffeine intake Alcohol intake Socio-economic factors

Table 1.3 Risk factors in glaucoma

Age

Increasing age is one of the most significant risk factors for POAG. Age specific prevalence figures increase from 0.2% in age group 55-59 years to 3.3% in the age group 85-89 years in the Rotterdam study (Dielemans, Vingerling, Wolfs *et al.*, 1994). Wensor, McCarty, Stanislavsky *et al.*, (1998) report a steady increase in POAG with age, from 0.1% at ages 40-49 to 9.7% in patients aged 80-89years. The Beaver Dam study reports a prevalence of 0.9% in people 43-54 years to 4.7% in 75+years. The Barbados Eye Study investigated the prevalence rates of POAG in a predominantly black study population. The authors found that prevalence was high, especially at older ages and in men. Among subjects 50 years and older, 1 in 11 had POAG and prevalence increased to 1 in 6 at age 70 years and above (Leske, Connell, Schachat *et al.*, 1994). A significant increase in glaucoma prevalence with age also occurred according to Weih,

Nanjam, McCarty *et al.* (2001) while Mitchell, Smith, Attebo *et al.* (1996) record an exponential rise in prevalence with increasing age.

Gender

Studies regarding the association of gender with glaucoma have produced widely differing results. Early studies report increased IOP levels in females which have been attributed to hormonal and menopausal influences (Hollows and Graham, 1966, Armaly, 1965). Subsequent work has demonstrated higher prevalence rates in men than women. The Barbados Eye Study found higher prevalence in men than women at 8.3% and 5.7% respectively (Leske *et al.*, 1994). According to the Rotterdam study men have more than three times the risk of having POAG than women (Dielemans *et al.*, 1994).

Mitchell *et al.* (1996) contradict these findings in their study which finds a higher prevalence of POAG in women compared to men after adjusting for age. However, the Baltimore Eye Survey revealed no difference in rates of POAG between men and women for all patients examined (Tielsch *et al.*, 1991). Klein and colleagues also failed to find a significant effect of gender on prevalence rates on glaucoma after adjusting for age (Klein, Klein and Sponsel *et al.*, 1992). This finding is confirmed by Wensor *et al.* (1998) who found no relationship between prevalence rates and gender.

Race

While average IOP among white and black subjects in a general population is similar (Hollows and Graham, 1966; Mason, Kosoko, Wilson *et al.*, 1989; Sommer Tielsch, Katz *et al.*, 1991) studies have shown that black people are 4-6.8 times more likely to develop glaucoma than Caucasian subjects (Tielsch *et al.*, 1991; Wilson, Hertzmark, Walker *et al.*, 1987).

The Barbados Eye Study evaluated the risk factors for POAG among black participants. It concluded that the subjects most likely to have POAG were older men, with elevated IOP, lean body mass, cataract history and a positive family history of POAG (Leske, Connell, Wu, 1995).

IOP

Elevated IOP is known to be a prominent risk factor for the development of optic nerve damage (Anderson, 1989). According to the Baltimore Eye Survey, glaucomatous eyes in both white and black subject groups exhibited higher screening IOP than the general population. The risk of glaucomatous optic neuropathy in all subjects increased with the height of the screening IOP, particularly at levels of 22-29 and 30mmHg and above (Sommer *et al.*, 1991). Longitudinal studies have reported the risk of developing a field defect is directly related to the height of their pre-existing IOP (Armaly, Krueger and Maunder, 1980).

Studies have also shown an association between IOP and pathological changes to the optic disc structure and progression of visual field loss (Rath, Shin, Kim *et al.*, 1996; Vogel, Crick, Newson *et al.*, 1990). Several studies have demonstrated a relative improvement to optic nerve head topography and visual field sensitivity of glaucoma patients following a reduction in their IOP (Mikelberg, 1993; Shiose, 1989; Spaeth, 1994).

While elevated IOP is unquestionably a strong risk factor in the development of POAG, there are several other factors which must be considered. (See section 1.9.3 mechanical (pressure related) theory of glaucoma).

Optic disc size

The size of the optic disc has been considered to be important in the development of glaucoma. It has been postulated that the higher susceptibility of black subjects compared to Caucasians in developing glaucoma may be due to their larger optic disc areas (Martin, Sommer and Gold, 1985). However, work by Dandona, Quigley, Brown *et al.* (1990) reported no morphometric differences of the lamina cribrosa between black and white subjects, despite the larger area of lamina in black subjects. Furthermore, a study by Jonas *et al.* (1991) reported that in a group of white subjects, susceptibility to glaucomatous optic nerve fibre loss is independent of optic disc size.

Myopia

A strong association between myopia and POAG has been confirmed by a number of studies (Wilson, Hertzmark, Walker *et al.*, 1987; Chihara, Liu, Dong *et al.*, 1997). Mitchell and colleagues found a two-three fold increased risk of glaucoma in myopic patients compared to non-myopic patients, independent of other risk factors and IOP (Mitchell, Hourihan, Sandbach *et al.*, 1999). Such a finding may be explained by the fact that a more myopic eye is more structurally prone to glaucomatous damage from elevated or normal IOP (Chihara *et al.*, 1997; Jonas Gusek and Naumann, 1988b) compared to a normal eye. It has also been suggested that glaucoma and myopia may share a common genetic link, based on the fact that both conditions have strong familial tendencies (Stone, Fingert, Alward *et al.*, 1997; Mitchell *et al.*, 1999).

Diabetes

The relationship between diabetes and POAG is controversial. Several studies found a positive correlation between the two diseases (Mitchell, Smith, Chey *et al.*, 1997; Klein, Klein and Jensen, 1994) while others have failed to do so (Tielsch, Katz, Quigley *et al.*, 1995). Such studies are often confused by the use of varying definitions of both the disease and the experimental conditions employed.

Early clinical findings support a relationship between increased IOP and diabetic patients compared with normals (Armstrong, Daily, Dobson *et al.*, 1960). The Baltimore Eye Survey found no definite evidence to support an association between diabetes and POAG after adjustment for age and race. Tielsch *et al.* (1995) suggest that selection bias could explain the positive correlation between diabetes and POAG in the clinical setting. They argue that patients with diabetes are more likely to be diagnosed with glaucoma as a result of more frequent eye examinations.

Nevertheless, substantial evidence exists to support an association between these two diseases. Mitchell *et al.*, (1997) report a significant and consistent association between diabetes and glaucoma, which appeared independent of the effect of diabetes on IOP. The prevalence of glaucoma was increased in diabetic patients (5.5%) compared to non-diabetics (3.5%). Diabetes was present in 13.0% of glaucoma patients, compared with

6.9% of non-glaucoma subjects. Klein *et al.* (1994) conclude in their population based study of age related disease that the presence of POAG is increased with older-onset diabetes. The mechanism for this association is unclear but it has been suggested that the increased prevalence may reflect optic nerve damage caused as a result of vascular or other effects of diabetes (Becker, 1971). A genetic link between the two diseases has been suggested by Mapstone and Clark (1985) who report an increased family history of type 2 diabetes in ocular hypertensive patients. However this fails to receive support by a more recent study by Mitchell *et al.* (1997) who, while observing an involvement of genetic factors for both diseases, conclude that any genetic influence may be independent of the relation between diabetes and glaucoma.

Vascular factors

The vascular theory of glaucomatous optic neuropathy purports that damage occurs as a result of inadequate perfusion of the proximal portion of the optic nerve and may occur in systemic hypertension and/or hypotension. (Perfusion pressure expresses the difference between arterial and venous pressure). In the former case, this may be explained by increased peripheral resistance in the small vessels. Conversely, a reduction in systemic blood pressure (hypotension) may create insufficient perfusion pressure in the optic disc and lead to pathological conditions (Drance, Sweeney, Morgan *et al.*, 1973, Van Buskirk and Cioffi, 1992).

Systemic hypertension

Several studies have reported a relationship between increased systolic and diastolic blood pressure and elevated IOP (Kahn, Leibowitz, Ganley *et al.*, 1977; Leske and Podgor, 1983). Since elevated IOP is major risk factor for POAG it is to be expected that systemic blood pressure itself would be a risk factor for POAG. Wilson and colleagues (1987) found a strong association between systolic blood pressure and incident glaucoma. Dielemans, Vingerling, Algra *et al.* (1995) reported an association between high tension glaucoma and systolic blood pressure and hypertension. In addition, no association was found between blood pressure or hypertension and normal tension glaucoma.

The Barbados Eye Study suggests that high blood pressure alone is not a risk factor for POAG in their black subjects. Leske and colleagues (1995) concluded that hypertension was not a major direct contributor to the high prevalence of POAG.

Systemic hypotension

There is considerable evidence to suggest that glaucoma is associated with low levels of systemic blood pressure (Leske *et al.*, 1995; Tielsch, Katz, Sommer *et al.*, 1995).

A reduction in perfusion pressure (blood pressure – intraocular pressure) has been found to be strongly associated with an increased prevalence of POAG. Subjects with diastolic perfusion pressure below 30mmHg had six times the risk of POAG than those with perfusion pressures of 50mmHg. Prevalence rates remained constant at pressures above 50mmHg, below which rates increased dramatically with further decreases in perfusion pressure. Such findings are confirmed by a study by Bonomi, Marchini, Marraffa *et al.* (2000) who report an association between lower diastolic perfusion pressure and marked, progressive increase in the frequency of POAG.

Family history

A positive family history of glaucoma has been identified as an important risk factor in developing the disease. Wolfs, Klaver, Ramrattan *et al.* (1998) studied the familial aggregation of POAG and the risk of first degree relatives developing the condition. They reported the prevalence of glaucoma as 10.4% in siblings of patients, 1.1% in children of patients compared to 0.7% in siblings of controls and 0% in children of controls. Life time risk of enlarged cup-disc ratios was 62.2% in relatives of patients compared to 16.6% in controls' relatives. Life time risk of elevated IOPs was also more prevalent in relatives of glaucoma patients at 42.5% compared with relatives of normals at 6.7%. Enlarged cup: disc (C:D) ratio was the earliest and most prominent feature of familial aggregation. Their studies failed to establish whether the cause of familial aggregation was of a genetic or environmental origin.

A later study in Tasmania suggests that a higher percentage of adult POAG may be inherited than previous work demonstrates. McNaught, Allen, Healey *et al.* (2000)

found that even in large pedigrees, 27% of previously diagnosed glaucoma patients were not aware of their positive family history. Such findings demonstrate the potential lack of reliability and accuracy of reported family history data.

Genetic

POAG is likely to be a genetically heterogeneous disorder that results from the interaction of multiple genes and environmental factors. Several genes have been identified as being possible causative factors in the development of the disease. Identification of mutated genes will aid the early diagnosis and better long term prognosis of patients with POAG (Stone *et al.*, 1997).

Lifestyle factors

The Framingham Eye Study suggests a relationship of history of alcohol use and POAG (Kahn and Milton, 1980) while Wilson *et al.* (1987) suggests an association between cigarette smoking and glaucoma. However, Klein, Klein and Ritter (1993) demonstrate that neither heavy drinking nor cigarette smoking is related to the prevalence of POAG.

1.9.3 Pathogenesis of POAG: Mechanical (pressure related) theory of glaucoma

The pathogenesis of POAG remains unclear and may be multifactorial in origin. Two theories are considered to exist, the mechanical and vascular theory.

The mechanical theory for the pathogenesis of glaucoma suggests that optic nerve damage can be induced by elevated intraocular pressure through structural or biochemical factors. It supposes that glaucomatous optic neuropathy is a direct consequence of IOP, damaging the lamina cribrosa and neural axons (Yan, Coloma, Metheetrairut *et al.*, 1994). It is well established that a prominent risk factor in the development of glaucomatous optic neuropathy is the elevation of IOP (Anderson, 1989). That high IOP can contribute to optic nerve damage is reinforced by the direct relationship observed between IOP and glaucomatous damage (Armaly *et al.*, 1980; David, Livingston and Luntz, 1980; Sommer, 1989). In primate experimental glaucoma

studies with sustained elevated IOP, optic neuropathy develops which is similar to human POAG in both clinical and histological terms (Quigley, Hohman and Addicks, 1980). In patients with normal tension glaucoma and asymmetrical IOPs the eye with higher IOP tends to have more marked visual field loss (Cartwright and Anderson, 1988) although there are exceptions to these findings (Haefliger and Hitchings, 1990). Several ocular conditions such as congenital glaucoma, angle-closure glaucoma or secondary glaucomas demonstrate that elevated IOP is sufficient to lead to glaucomatous optic neuropathy (Flammer, Orgul, Costa *et al.*, 2002).

Optic nerve fibre damage is predominantly located at the lamina cribrosa according to evidence from both from histological and experimental studies. The lamina provides structural support and nourishment to the nerve fibres which pass within its lamellar sheets through channels created by the alignment of pores. Histological studies document an average of 400 channels occurring at choroidal level with an increase to 550 more posteriorly at lamina level. This increase can be explained by the branching and division of nerve fibre bundles in this area.

Regional differences in lamina structure make specific portions of the optic nerve more susceptible to pressure distortion. The superior and inferior parts of the lamina at scleral level contain larger pores and thinner connective tissue support for the passage of nerve fibre bundles compared to the nasal and temporal parts (Quigley and Addicks, 1981; Radius and Gonzales, 1981). This correlates well with the pattern of glaucomatous field loss observed in the arcuate regions while the central and temporal potions of the visual field are relatively spared (Quigley and Addicks, 1981; Quigley, Addicks, Green *et al.*, 1981; Radius, 1981). Fechtner and Weinreb (1994) suggest that IOP induced changes within the lamina may result in a change of orientation or collapse of the laminar plates. The mechanical theory proposes that subsequent misalignment of the laminar cribiform plates and pores would cause direct mechanical axonal damage. Furthermore, this process may lead to a compromised blood supply and reduced nutritional input to the ganglion cell axons.

The lamina in patients with glaucoma undergoes a number of changes. Patients with moderate visual glaucomatous field loss have compression of the lamina cribrosa plates. Miller and Quigley (1988) observed elongated lamina pores in some eyes with moderate

to severe visual field damage compared to eyes with normal visual fields. Hernandez (1992) observed several pathological changes to the extracellular matrix in patients with mild glaucoma. These include a reduction in collagen fibre number, increase in glial cell number, thickening of the basement membrane and alterations to the elastic fibres, specifically loss of their tubular structure. Quigley, Pease and Thibault (1994) reported a change in the structure or appearance of elastin in the lamina of glaucomatous eyes compared to normal eyes. It is unclear whether changes of the extracellular matrix contribute to glaucomatous optic neuropathy or are a consequence of the disease process.

Neuronal function and survival is dependent on axonal transport. This is the process by which neuronal components are moved from their site of synthesis in the cell body along the cell axon while cellular components to be recycled are transported back to the cell body. Experimental glaucoma studies clearly show that both orthograde (away from the cell body) and retrograde (toward the cell body) axonal transport is disrupted by elevated IOP (Minckler, Bunt and Johanson, 1977; Minckler, Bunt and Klock, 1978).

That the elevation of IOP has a role in the development of optic nerve damage is not in question. The prevalence of glaucoma in a population increases as the level of IOP increases. In experimental acute glaucoma and human secondary glaucoma studies, changes to the retinal nerve fibre layer and optic nerve head as a result of increasing the IOP mimic those seen in primary glaucoma (Quigley and Pease, 1996). Tielsch *et al.* (1995) reported higher mean IOP levels in groups of glaucoma subjects compared to age matched normals.

However, several studies provide evidence which would question the theory that elevated IOP is the sole mechanism for glaucomatous optic nerve damage. The incidence of normal tension glaucoma in females is approximately twice that of males although men and women have approximately the same IOP (Orgul, Flammer and Gasser, 1995). While the incidence of glaucoma in Japan increases with age in accordance with Europe and America populations, actual IOP in Japan is inversely related to age (Shiose, Kitazawa, Tsukuhara *et al.*, 1991). A study by Leske *et al.* (1994) suggests that the prevalence of POAG may be nearly five times greater in black compared to white Americans. Such findings are confirmed by the Baltimore Eye

Survey where researchers investigated the relationship between IOP and POAG among white and black Americans. The prevalence of glaucoma was four times greater in black compared to white Americans although the level of IOP was similar for the two groups. Weber, Koll and Krieglstein (1993) suggest that the relationship between IOP and the presence and progressions of glaucomatous damage is tenuous.

1.9.4 Indirect theory: The vasogenic mechanism of damage

The role of elevated IOP alone is insufficient to explain the results of every experimental and clinical investigation of glaucoma. The existence of both normal tension glaucoma patients and ocular hypertensive patients, together with the fact that optic nerve damage may progress in some patients even when their IOP is reduced would suggest that there are other contributory factors involved. The vascular theory for the pathogenesis of POAG proposes that reduced perfusion of the optic nerve head results in retinal ganglion cell axon death (Drance *et al.*, 1973; Van Buskirk and Cioffi, 1992).

There is considerable evidence suggesting that compromise of the microvasculature of the optic nerve may have a role in the development of glaucomatous optic neuropathy. The observation of vascular abnormalities in glaucomatous eyes such as flame-shaped splinter optic disc haemorrhages may add to the evidence that the pathogenesis of glaucoma has a vascular element. These may be an indication of local capillary ischaemia or may be the result of mechanical trauma following damage to the lamina itself. In early glaucoma they are usually located in the infero and supero-temporal disc regions. They are associated with neuroretinal rim notches and localised RNFL defects (Airaksinen, Mustonen, Alanko, 1981).

Fechtner and Weinreb (1994) suggest a number of ways in which the microvasculature of the optic nerve may fail to nourish the ganglion cell axons. These include changes in capillaries, including loss of capillaries or alteration of blood flow within existing capillaries, other changes which interfere with the delivery of nutrients or removal of metabolic products from the axons, alterations in choroidal blood flow, failure of

regulation of blood flow, delivery of injurious vasoactive substances to the blood vessels of the optic nerve or a combination of these factors.

1.9.5 Autoregulation of blood flow

Autoregulation is automatic adjustment of blood flow to a tissue in proportion to its requirements. In the eye, as levels of IOP change the rate of blood flow in the ocular vessels alters accordingly. While the optic nerve appears capable of autoregulation this is not the case for choroidal blood flow. It has been proposed that faulty autoregulation of ocular microcirculation may play a role in the pathogenesis of POAG (Fechtner and Weinreb, 1994).

1.9.6 Chemical mediators as a mechanism for glaucoma

Aptosis, or programmed cell death is a genetically-coded response to damage or disuse of cells. This process has been implicated as a causative factor in studies of ganglion cell death in glaucoma (Kerrigan, Zack, Quigley *et al.*, 1997). Retrograde transsynaptic degeneration describes the degeneration of a neuron following the death of its target cell. Such a mechanism could explain the loss of cells in glaucomatous optic neuropathy. The target cell is a source of essential neurotrophic factors without which the neuron cannot survive. Disruption to axoplasmic flow as a result of IOP induced lamina cribrosa damage could lead to retinal ganglion cell damage.

An excitotoxic mechanism may also be responsible for ganglion cell damage in glaucoma. Glutamate, an excitatory amino acid may produce neurotoxic effects in the eye. Levels of glutamate in the vitreous of a group of glaucoma patients was found to be double that in a control population of patients with cataracts only. Such levels are potentially toxic to retinal ganglion cells. According to a study by Dreyer, Zurakowski, Schumer *et al.* (1996), glutamate is more toxic to larger ganglion cells.

1.9.7 Selective loss theory

Selective cell loss theory in human and experimental glaucoma has received considerable support. Histologic analysis of the distribution of retinal ganglion cell body sizes reveals a selective loss of larger retinal ganglion cells in both mid- peripheral and central retina (Glovinsky, Quigley and Dunkelberger, 1991; Glovinsky, Quigley and Pease, 1993). Further histological work suggests that glaucomatous damage primarily affects ganglion cells with larger diameter axons (Quigley, Sanchez, Dunkelberger *et al.*, 1987; Quigley, Dunkelberger and Green, 1988. In both experimental glaucoma and in human studies optic nerve fibres larger than the mean diameter were killed more rapidly than smaller fibres. Quigley *et al.*, (1988) suggest that this can be partly explained by the fact that the larger fibres are normally found in greater numbers in the vertical poles. However, larger fibres lying in comparatively spared zones are still destroyed, indicating an inherently greater susceptibility.

Anderson and O'Brien (1997) provide psychophysical evidence for a selective loss of M ganglion cells in glaucoma in a study of normal, ocular hypertensive and glaucoma subjects. Stationary gratings and phase reversed gratings (30Hz) were employed to selectively stimulate parvocellular ganglion cells and magnocellular cells respectively. P-cell related peripheral resolution was significantly reduced in glaucoma patients and less so in ocular hypertensives. Loss of peripheral resolution acuity was greater with the phase reversal grating. The authors suggest their findings are explained by a selective loss of M ganglion cell density over P ganglion cell density in glaucoma.

However, the theory that selective cell death first affects large fibre ganglion cells has been questioned (Morgan, 1994).

While many have interpreted the loss of larger axons to describe the loss of the M ganglion cells, this may not be the case. Findings are based on evidence that M retinal ganglion cell bodies and their axons are relatively larger compared with cell bodies and axons of retinal ganglion cells projecting to the parvocellular layers. However, identification of cell type based on size alone may not be a reliable method of classification since there is an overlap in cell body size between M and P cells in normal human and monkey retina (Yucel, Zhang, Gupta *et al.*, 2000). Blue-yellow ganglion

cells are also larger than parvocellular cells. In addition, since the size of fibres is dependent on eccentricity, it is possible that some eccentric parvocellular cells may be larger than central magnocellular cell axons (Sample, 2000). Furthermore, atrophic changes in glaucoma include a reduction in cell body size and axon diameter of retinal ganglion cells (Weber, Kaufmann and Hubbard, 1998).

Similar findings were reported by in later studies by Smith, Chino, Harweth *et al.* (1993) who employed microelectrode recording techniques to analyse the response properties of individual LGN neurons. They concluded that ganglion cells projecting to the magnocellular LGN are not selectively damaged. They hypothesise that the larger members of all functional retinal ganglion cell types are more prone to glaucomatous damage than their respective smaller members. Vickers, Schumer, Podos *et al.* (1995) also demonstrate that all retinal ganglion cells are affected to some degree.

Several studies do not support the hypothesis of selective loss of M cells. Morgan Uchida and Caprioli (2000) used horseradish peroxidase (HRP) to retrogradely label retinal ganglion cells of ocular hypertensive primates. Basing their study on the proportion of identifiable magno to parvocellular retinal ganglion cells, they found no evidence for selective loss.

Psychophysical testing has also revealed non selection of ganglion cell loss. Short wavelength automated perimetry (SWAP) and motion automated perimetry (MAP) was employed by Sample, Bosworth and Weinreb (1997) to investigate functional loss in glaucoma. Notable overlap in visual field defects measured with each technique would suggest that glaucomatous damage is non selective for either ganglion cell type. The authors suggest that the type of ganglion cell damaged in early glaucoma may vary between subjects.

1.9.8 Reduced redundancy theory

The reduced redundancy theory supports the view that all pathways are equally damaged in the disease process. Since blue cones only constitute 5-10% of the total

number of retinal cones, the blue response pathway would be affected earlier in the disease process than the other spectral pathways (Curcio, Allen, Sloan *et al.*, 1991).

1.9.9 Retinal ganglion cell shrinkage in glaucoma

The notion of cell shrinkage has been proposed to explain the apparent selective loss of large retinal ganglion cells. If the entire cell population was subjected to identical percentage shrinkage, there would be a marked effect on larger cells. Evidence for such a theory is provided by Weber *et al.* (1998) and Morgan *et al.* (2000) who report a reduction in the mean soma size of both M and P cells in ocular hypertensive primates. Morgan (1994) attributed findings of a more marked decrease in anterograde labelling of LGN M cells by Dandona, Hendrickson and Quigley (1991) to greater shrinkage and retraction of the terminal area of the M cell.

1.10 Clinical examination of the glaucomatous eye

Conventionally, the assessment of glaucoma has been based on the measuring of intraocular pressures (IOP), visual fields and examination of the optic nerve head.

1.10.1 Tonometry

Elevated IOP is an important risk factor for the development of POAG and therefore regular monitoring of IOP in the clinical setting and prescribing drops to lower IOP has a major role in the treatment of glaucoma. Goldmann tonometry is considered to be the gold standard testing method and is widely used in the hospital setting while the quicker, less invasive non contact method is routinely used for screening in most optometric practices.

Studies have shown that tonometry alone is neither an effective nor an efficient screening tool for POAG (Sommer *et al.*, 1991). Traditionally, IOPs above 22mmHg are regarded as suspicious. However, patients with glaucomatous visual field loss may have normal pressures (i.e. below 22mmHg) while some patients exhibiting IOPs

greater than 22mmHg show no glaucomatous changes either in their visual fields of optic nerve head appearance. IOP measurement is therefore no longer the most important factor in the confirmation of a diagnosis of glaucoma.

1.10.2 Visual field

The visual field can be defined as all the space that one eye can see at any given instant (Tate and Lynn, 1977). The normal monocular visual field is measured from the line of sight and extends 60 degrees superiorly, 75 degrees inferiorly, 100 degrees temporally and 60 degrees nasally. It is described as an island of vision surrounded by a sea of darkness. Visual sensitivity is highest at the peak, the fovea and declines towards the periphery.

Visual field assessment can be performed using kinetic perimetry, in which a stimulus of constant intensity and size is moved across the field (Goldmann perimeter) or by static perimetry in which the stimulus remains stationary (Humphrey Field Analyser). Computerised automated static examination field testing is generally quicker, more consistent and provides quantitative numerical analysis.

1.10.3 Humphrey Visual Field Analyser

1.10.3.1 White on white perimetry

Visual threshold is regarded as the minimum brightness which the patient can see at a given location in the visual field. This is determined by the Humphrey Visual Field Analyser using a 4-2dB double staircase strategy. An initial stimulus is presented at intensity brighter than the patient's expected threshold. If seen, the intensity of the stimulus is decreased in 4dB increments until no longer seen. Intensity is increased in steps of 2dB until patient first sees the stimulus and this is subsequently set as the threshold (Haley, 1987). The Full Threshold test employs this bracketing technique at 4 primary points across the visual field which in turn determines the starting levels for neighbouring points in the pattern.

The 30-2 and 24-2 (shorter testing time with minimal loss of data) program is recommended for testing glaucoma and glaucoma suspects.

Global indices are provided to aid the practitioner to assess the patient's overall visual field pattern. They are based on calculations from deviations in age-corrected normals data and are as follows:

Mean Deviation (MD) - the average depression or elevation of the patient's overall field compared to the normal reference field

Pattern Standard Deviation (PSD) – a measure of the degree to which the shape of the patient's visual field differs from the normal reference field

Short term Fluctuation (SF) – a measure of the consistency of the patient's responses throughout the visual field test

Corrected Pattern Standard Deviation (CPSD) – a measure of the degree to which the total shape of the patient's visual field differs from the shape of the normal age matched hill of vision, corrected for intra test variability (SF)

All are printed as sensitivity measures in decibels (dB) together with the probability value (p-value) that these are normal.

1.10.3.2 HFA Visual field analysis

The Humphrey Visual Field Analyser uses STATPAC, a statistical program to analyse threshold visual field results. Firstly, a grayscale representation of the patient's visual field indicates the presence and severity of any defect, with each step in the pattern representing a 5dB change in sensitivity. These defects are represented numerically in the defect depth grid. A further numeric grid gives the threshold in decibels for all locations tested.

Total deviation plots show the difference in decibels between the patient's test results and the age corrected normal values for each point tested. Analysis is displayed both in

a numerical and grey scale format. Pattern deviation plots are similar to the total deviation plots with the exception that any change in overall sensitivity has been taken into account. This may take the form of a reduction in the case of cataracts and small pupils or an increase in the case of exceptional sensitivity. The numeric pattern deviation plot indicates the deviation in decibels from the age corrected normal values, while the probability pattern plot displays the statistical significance of the result at each point.

1.10.3.3 Blue-on-yellow perimetry

Achromatic automated perimetry (SAP) is the standard technique used to assess the visual field. However, short wavelength automated perimetry (SWAP) has been reported to detect functional visual loss before standard SAP in patients with glaucoma and ocular hypertension and is superior to standard field testing for following glaucoma progression (Polo, Larrosa, Pinilla *et al.*, 2002; Heron, Adams and Husted, 1988; Johnson, Adams, Casson *et al.*, 1993; Sample, Taylor, Martinez *et al.*, 1993).

SWAP is conducted by projecting a large blue stimulus onto a bright yellow background. This type of stimulus is specifically detected by the short wavelength cones and processed through the blue-yellow ganglion cells. The yellow background adapts the rods and both the middle and long wavelength cones in order to isolate and test the short wavelength pathways.

1.10.3.4 Frequency doubling contrast test (FDT)

Frequency doubling contrast test (FDT) is designed to exploit the properties of the magnocellular cells. M cells comprise 25% of the ganglion cell population. They are particularly susceptibile to damage and appear to be preferentially lost in early glaucoma. A loss of just a small number of cells will have a considerable effect on visual function. A frequency doubling illusion is produced when a low spatial frequency sinusoidal grating (<1 cycle per degree) undergoes high temporal frequency counterphase flicker at 15Hz. The rapid contrast reversal in which the dark bars become light and vice versa creates the illusion if the grating being twice its actual frequency (Johnson and Samuels, 1997).

FDT perimetry is highly sensitive and specific in the detection of glaucomatous visual field loss. A recent study by Iester, Mermoud and Schnyder (2000) suggests that FDT could be used to screen and monitor visual field loss in its early and moderate stages.

1.10.3.5 Physiological changes to visual field

Studies have shown that a decline in luminance sensitivity occurs with increasing age. This is due to a number of factors including, ocular media changes, reduction in pupil size, reduction in absorbance efficiency of photopigments and neural losses in the retina and retinal nerve pathway (Barton and Benatar, 2002).

1.10.4 Optic nerve head examination

The most widely employed method of examining the optic nerve head in optometric practice is the direct ophthalmoscope. However, drawbacks of magnification effects (15x for the emmetropic eye) and two dimensional view limits its use in detecting subtle retinal tissue changes that may occur for example in diabetic retinopathy and optic nerve head changes in glaucoma. Binocular indirect methods permit both a stereoscopic and improved field of view. Head mounted systems offer an excellent field of view with magnification for the emmetropic eye of only 2x. Subtle structural changes in the eye may therefore be difficult to observe. Slit lamp binocular indirect ophthalmoscopy provides a good field of view and optimum magnification for the task can be provided by adjusting both the auxiliary lens and magnification level on the slit lamp itself.

It is difficult to detect early glaucomatous damage by observation of the ONH due to the variability in appearance of normal eyes and also the disagreement between observers of the findings (Tielsch, Katz, Quigley *et al.*, 1988; Varma, Steinmann and Scott, 1992).

Ophthalmic examination of the RNFL may reveal generalised deterioration, slit defects or wedge shaped defects. Diffuse atrophy is more difficult to evaluate than localised atrophy. Studies have shown that field defects are preceded by changes of the optic nerve head or loss of the RNFL (Sommer, Katz, Quigley *et al.*, 1991; Tuulonen, Lehtola and Airaksinen, 1992). Visual field defects only occur after irreversible damage to the nerve fibre layer. Studies have also shown that a reduction in RNFL thickness may precede pathological changes to the structure of the optic nerve head (Sommer, Miller,

Pollack *et al.*, 1977). The advent of imaging devices such as the Nerve Fibre Analyser (NFA) and Optical Coherence Tomography (OCT) has allowed earlier diagnosis and more reliable monitoring of pathological changes to the RNFL and optic nerve head structure.

1.10.5 Heidelberg Retinal Tomographer (HRT)

The Heidelberg Retina Tomographer quantitatively measures optic disc parameters such as cup area and volume and rim area and volume and is widely accepted as a useful tool in the diagnosis and follow-up of glaucoma patients. Image analysis on the HRT facilitates measurement of the cup:disc area ratio and allows the clinician to accurately monitor optic nerve head changes over time. The literature suggests that the HRT technique is repeatable, reproducible and accurate (Mikelberg, Wijsman, Schulzer, 1993; Azuara-Blanco, Harris and Cantor, 1998).

Beatty, Good, McLaughlin *et al.* (1998a) evaluated optic disc cupping using the new Biovision B-Scan Probe, a high resolution 2D ultrasound scanner. They found a strong correlation between optic disc measurements made with the HRT and ultrasound and suggested such a technique would be useful in a clinical setting without the use of expensive specialist machines such as the HRT and OCT especially for patients with dense media opacities which would not affect acquisition results. They concluded that while pathological cupping cannot be distinguished from a normal cup based on size alone a small cup is less likely to be diseased. A large observed change in 2D optic cup parameters over time could be regarded as evidence of progression in cupping.

The laser tomographer scanner /scanning laser ophthalmoscope uses a confocal optical system to accurately and reliably produce 3D topographic images and calculate topometric variables of the optic nerve and retinal structure (Kruse, Burk, Volcker, *et al.*, 1989; Dreher, Tso and Weinreb, 1991; Cioffi, Robin, Eastman *et al.*, 1993; Rohrschneider, Burk and Volcker, 1993) even in patients with undilated pupils (Lusky, Bosem and Weinreb, 1993). The Heidelberg Retina Tomographer is based on this technique and has several improvements including faster image acquisition, image quality and easier handling. The HRT uses a 670nm diode laser which scans the optic disc over 1.6.seconds and produces 32 consecutive optical section images at depths of

1.5 to 4mm. A topographic map is then produced showing the height of the retinal surface from the focal plane of the eye.

Studies have shown that the ability of the HRT to differentiate between normal and glaucomatous eyes is adversely affected by the variation of size and shape of the normal optic disc and the close correlation between disc and rim and cup sizes i.e. larger optic discs contain a larger number of nerve fibres with a larger rim area and cup area. The HRT uses a reference plane which may not equate to the individual's eye anatomy it is measuring and hence lead to inaccuracies. Miglior, Casula, Guareschi *et al.* (2001) found that while the HRT exhibits only fair to poor agreement with the standard visual field examination, the analysis provided with the updated software version 2.01 to distinguish normal from glaucomatous eyes may be acceptable diagnostically.

In the same way, Tannenbaum, Zangwill, Bowd *et al.* (2001) found considerable overlap in HRT RNFL measurements in eyes with large cup to disc ratios and abnormal visual fields as compared with eyes with large cup to disc ratios and normal visual fields. They suggest that this may limit the clinical ability of the HRT to detect early glaucoma in patients with large cup to disc ratios.

1.10.6 Optical coherence tomography

Optical coherence tomography (OCT) is a non contact and non invasive method of assessing and quantitatively measuring the retinal nerve layer thickness and retinal thickness. OCT has been demonstrated to detect tissue thickness changes with micrometer-scale sensitivity (Huang, Swanson, Lin *et al.*, 1991). Good correlations between OCT estimates and histological measures of retinal nerve fibre layer thickness have been reported (Chauhan and Marshall, 1999; Huang, Schuman, Pedut-Kloizman *et al.*, 1997; Toth, Narayan, Boppart *et al.*, 1997). Studies have shown that this technique is both an accurate and repeatable method of identifying early changes in diseased eyes (Hee, Izatt, Swanson *et al.*, 1995a; Schuman, Pedut-Kloizman, Hertzmark *et al.*, 1996; Baumann, Gentile, Liebman *et al.*, 1998; Koozekanani, Roberts, Katz *et al.*, 2000; Massin, Vicaut, Haouchine *et al.*, 2001; Muscat, Parks, Kemp *et al.*, 2002) and

reproducible between-visit (Schuman *et al.*, 1996; Jones, Sheen, North *et al.*, 2001; Massin *et al.*, 2001; Muscat *et al.*, 2002).

1.11 Structural changes in glaucoma

1.11.1 Neuroretinal rim in glaucomatous eyes

Glaucomatous optic neuropathy may take the form of excavation, pallor and haemorrhage. It is characterised by ganglion cell axon loss which is exhibited as a decrease in neuroretinal rim area with a reciprocal increase in cup area. The larger the optic disc, the larger the optic cup and neuroretinal rim. Consequently, a large cup in a large optic disc can be normal, while glaucomatous optic nerve damage may be exhibited in an individual with a small optic cup in a very small disc (Jonas, Fernandez, Naumann, 1990). Cupping may be uniform or may take the form of localised notching. As neuropathy develops the lamina cribrosa may become more visible. POAG is usually asymmetric in nature which is reflected in the difference in appearance of the optic nerve head in its early stages. Asymmetry of 0.2 or greater should be regarded as suspicious (Hodapp, Parrish and Anderson, 1993). Changes in cup: disc ratios over time may also indicate potential pathological changes.

Glaucomatous rim loss is mostly diffuse in nature but tends to follow a characteristic pattern depending on disease progression. Early glaucomatous damage shows rim loss predominantly in the infero and supero-temporal regions, followed by loss in the temporal horizontal disc region. In advanced glaucoma, the neuroretinal rim is finally lost from the nasal inferior margin followed by the nasal superior region. This sequence of loss correlates well with patterns of glaucomatous visual field loss (Tuulonen and Airaksinen, 1991; Jonas *et al.*, 1989, Jonas, Fernandez and Sturmer, 1993).

1.11.2 Neuroretinal rim pallor

Increasing pallor of the optic disc and specifically of the neuroretinal rim is typically observed in the glaucomatous eye (Jonas *et al.*, 1988b).

1.11.3 Disc haemorrhages in glaucomatous eyes

Splinter-shaped or flame-shaped haemorrhages at the optic disc margin are characteristic of glaucomatous optic neuropathy and are detected in approximately 4-7% of eyes with glaucoma. They are associated with localised RNFL defects and neuroretinal rim notches and in early glaucoma are usually located in the infero and supero-temporal disc regions (Airaksinen, Mustonen and Alanko, 1981). Jonas and Xu (1994) report that their frequency increases as the disease progresses from an early stage of glaucoma to a moderate stage, while in more advanced glaucoma tend to be less frequent. Other changes occurring in the optic nerve head vasculature include baring of the circumlinear blood vessels, fly-over vessels (where a blood vessel has been isolated from the floor of the optic cup) and bayonetting (where a blood vessel disappears over an undercut rim edge, only to re-appear on the floor of the optic cup).

1.11.4 Retinal nerve fibre layer in glaucomatous eyes

In 1973 Hoyt, Frisen and Newman first reported that photographs of the retinal nerve fibre layer could show glaucomatous fibre loss even in the absence of visual field defects and optic disc changes. Several early studies by Sommer and colleagues demonstrated that visible atrophy of the nerve fibre layer preceded visual field loss by as much as five years and was at least as accurate in predicting further damage as optic disc examination (Sommer, Miller Pollack *et al.*, 1977; Sommer, Pollack and Maumenee, 1979). Such findings have since been confirmed by numerous studies.

Quigley, Miller, George (1980) reported that observed RNFL abnormalities accurately corresponded with areas of visual field loss. They observed that RNFL defects in suspect glaucoma patients were more localized in comparison with diffuse atrophy found in eyes with established visual field loss. Airaksinen, Drance and Douglas (1984) observed a combination of general decline in fibres and more specific fibre loss often situated in the arcuate fibre bundle areas, in the glaucomatous eye.

In a study of nerve fibre loss, Sommer *et al.* (1991) report that mild defects were more readily recognized than more severe diffuse atrophy and that fibre defects expanded

with time, often by the development and coalescence of adjacent areas of damage. Generalised thinning of the RNFL produces a reduction in mean sensitivity in visual field tests while focal defects produce small deep field defect (Pieroth, Schuman, Hertzmark *et al.,* 1999).

Defects of the RNFL may be diffuse or localised in nature. Localised defects appear as dark, wedge shaped areas within the supero-temporal and infero-temporal retinal arcades (Airaksinen *et al.,* 1981). They can be found in 20% or more of all eyes and in the same way as disc haemorrhages, vary in their frequency according to the stage in the disease process (Jonas and Dichtl, 1996). According to a study by Jonas and Schiro (1994), they occur most often in normal tension glaucoma, followed by POAG and lastly by secondary open angle glaucoma. They are positively associated with disc margin haemorrhages and showed a high specificity to indicate optic nerve damage (Jonas and Schiro, 1994). Diffuse nerve fibre loss can also be found in eyes with optic nerve damage and is exhibited as a decreased visibility of the RNFL. Nerve fibre layer defects are highly correlated with positions of subsequent visual field loss (Quigley, Katz, Derick *et al.*, 1992).

1.11.5 Retinal nerve fibre layer in ocular hypertension

While reports regarding retinal nerve fibre layer changes in glaucoma are generally consistent, retinal nerve fibre layer changes in ocular hypertension are less established. While several studies report significant differences between OHT and normal eyes, others have failed to do so.

Tjon-Fo-Sang and associates (1996) using scanning laser polarimetry, report RNFL thickness to be significantly reduced in ocular hypertensives compared with normals. Bowd, Weinreb, Williams *et al.* (2000) reported the RNFL to be significantly thinner in OHT eyes than in normals in the inferior and nasal quadrants and through 360 degrees around the circular scan but similar in the superior and temporal quadrants. The RNFL was thinner in ocular hypertensive eyes compared with normal eyes and more markedly different in the nasal quadrant and especially the inferior quadrant.

with time, often by the development and coalescence of adjacent areas of damage. Generalised thinning of the RNFL produces a reduction in mean sensitivity in visual field tests while focal defects produce small deep field defect (Pieroth, Schuman, Hertzmark *et al.*, 1999).

Defects of the RNFL may be diffuse or localised in nature. Localised defects appear as dark, wedge shaped areas within the supero-temporal and infero-temporal retinal arcades (Airaksinen *et al.*, 1981). They can be found in 20% or more of all eyes and in the same way as disc haemorrhages, vary in their frequency according to the stage in the disease process (Jonas and Dichtl, 1996). According to a study by Jonas and Schiro (1994), they occur most often in normal tension glaucoma, followed by POAG and lastly by secondary open angle glaucoma. They are positively associated with disc margin haemorrhages and showed a high specificity to indicate optic nerve damage (Jonas and Schiro, 1994). Diffuse nerve fibre loss can also be found in eyes with optic nerve damage and is exhibited as a decreased visibility of the RNFL. Nerve fibre layer defects are highly correlated with positions of subsequent visual field loss (Quigley, Katz, Derick *et al.*, 1992).

1.11.5 Retinal nerve fibre layer in ocular hypertension

While reports regarding retinal nerve fibre layer changes in glaucoma are generally consistent, retinal nerve fibre layer changes in ocular hypertension are less established. While several studies report significant differences between OHT and normal eyes, others have failed to do so.

Tjon-Fo-Sang and associates (1996) using scanning laser polarimetry, report RNFL thickness to be significantly reduced in ocular hypertensives compared with normals. Bowd, Weinreb, Williams *et al.* (2000) reported the RNFL to be significantly thinner in OHT eyes than in normals in the inferior and nasal quadrants and through 360 degrees around the circular scan but similar in the superior and temporal quadrants. The RNFL was thinner in ocular hypertensive eyes compared with normal eyes and more markedly different in the nasal quadrant and especially the inferior quadrant.

Conversely, others have found no difference between the RNFL in normals and ocular hypertensives but this may be the result of different imaging techniques, sample size and study group demographics (Zangwill, Van Horn, de Souza Lima *et al.*, 1996; Iester, Broadway, Mikelberg *et al.*, 1997).

Hoh, Greenfield, Mistlberger *et al.* (2000) were unable to identify differences between normal and ocular hypertensive eyes. They reported considerable measurement overlap among normal, ocular hypertensive and glaucomatous eyes when examined with both OCT and SLP. These techniques were capable of differentiating between glaucomatous eyes and non glaucomatous eyes but were unable to distinguish normal from ocular hypertensives.

1.11.6 Macular volume in glaucoma

Glaucoma leads to a loss of retinal ganglion cells and since these cell types make up 30-35% of the retinal thickness in the macular region it is likely that glaucomatous changes are apparent both here and at the optic nerve head (Zeimer, Asrani, Zou *et al.*, 1998). Studies by Glovinsky and colleagues have shown that the size and anatomical distribution of retinal ganglion cells varies throughout the posterior pole (Glovinsky *et al.*, 1991; Glovinsky *et al.*, 1993). Their animal studies showed that a substantial loss of retinal ganglion cells of the primate macula occurs in experimental glaucoma. Garway-Heath, Caprioli, Fitzke *et al.* (2000) demonstrated that due to the redundancy of ganglion cells in the macular area greater loss of ganglion cells is required in the central compared to the peripheral visual field for equal effects on visual sensitivity. It has been suggested that macula imaging may aid in the early detection of glaucomatous damage due to the 10-20 fold increase in ganglion cell bodies compared to the diameter of their axons (Zeimer *et al.*, 1998; Greenfield, Bagga and Knighton, 2003).

Several studies explored the relationship between macular thickness and volume with RNFL in both normal and glaucomatous eyes. Giovannini and colleagues (2002) report that OCT macular volume was greater in normals compared to glaucomatous eyes. They conclude that volumetric analysis of macular thickness using OCT is a useful method of monitoring glaucomatous optic neuropathy. In a similar study, Greenfield *et al.* (2003)

found that macular thickness changes are well correlated with changes in visual function and RNFL structure in glaucoma and postulate macular thickness measurements may be a surrogate indicator of retinal ganglion cell loss. Guedes, Schuman, Hertzmark *et al.* (2003) demonstrated a statistically significant correlation between macular thickness and glaucoma (although RNFL was more strongly associated). Wollstein, Schuman Price *et al.* (2004) showed that macular retinal thickness was capable of detecting glaucomatous damage and corresponded with peripapillary RNFL thickness. However, they observed that specificity and sensitivity for the detection of visual field changes was higher with peripapillary RNFL thickness measures.

Lederer and colleagues (2003) demonstrated decreasing macular volume with more advanced glaucomatous disease. They found a significant difference in macular volume between normal, glaucoma suspect and early glaucomatous eyes, compared with advanced glaucomatous eyes and a significant difference between normal eyes and early glaucomatous eyes. They suggest that macular volume can be a valuable indicator of glaucoma status and may provide a useful, objective and quantitative parameter for glaucoma evaluation and monitoring.

1.11.7 Optic nerve in glaucoma

The pattern of glaucomatous nerve damage follows an hour-glass shape, with selectively greater damage in the vertical polar regions. This correlates well with the pattern of field loss observed in the arcuate regions. Quigley and Addicks (1981) demonstrated how regional differences in the structure of the lamina cribrosa could explain the greater susceptibility of superior and inferior nerve fibres to be lost in glaucoma. They found that the superior and inferior parts of the lamina at scleral level contained larger pores and thinner connective tissue support for the passage of nerve fibre bundles compared to the nasal and temporal parts.

1.11.8 Retrobulbar optic nerve

Variation in both the number of nerve fibres and the overall diameter of the retrobulbar nerve in the normal eye leads to difficulty in assessing the retrobulbar optic nerve for

glaucomatous damage. Ganglion cell death results in a decrease in the diameter of the retrobulbar optic nerve. As optic nerve thickness decreases, neuroretinal rim area decreases (Dichtl and Jonas, 1996). These findings are confirmed by Beatty *et al.* (1998a) who studied the relationship between orbital optic nerve dimensions and optic nerve head morphology. They demonstrated that the orbital optic nerve diameter and cross sectional area correlates positively and significantly with neuroretinal rim area.

Jonas *et al.* (1995) studied the relationship between the calibre of the optic nerve and the numbers of optic nerve fibres present. They established that for every millimetre increase in optic nerve diameter (starting at baseline 1.89mm) the optic nerve fibre count increases significantly by 777,000 fibres. They concluded that optic nerve fibre count can be estimated in routine histology by measuring optic nerve diameter. Jonas *et al.* (1995) suggests that greater retrobulbar optic nerve calibre may indicate structural reserve capacity.

Beatty, McLaughlin and O'Neill (1998b;1998c) used the B scan ultrasonographer to measure retrobulbar optic nerve dimensions in glaucomatous eyes, ocular hypertensive and normal eyes. They found that normal eyes had the greatest optic nerve diameter and cross sectional area and glaucomatous eyes had significantly smaller readings in comparison. Eyes with ocular hypertension had readings that were statistically comparable to normal subjects, but significantly greater than those with glaucoma. Their findings regarding normal optic nerve diameter were consistent with those of previous studies (Dichtl and Jonas, 1996). This study suggests that ocular hypertensives have normal optic nerve diameters and cross sectional areas or that optic nerve changes in ocular hypertension are too subtle for detection by this technique, reflected in the fact that there is little statistical difference between age matched normal and eyes with ocular hypertension. In addition to a decrease in ON diameter, Beatty *et al.* (1998c) found greater interocular asymmetry in glaucomatous eyes which is in keeping with optic disc changes in diseased eyes. They conclude that ultrasonographic measurements are a useful measure of change.

In a similar study, Beatty *et al.* (1998a) investigated the relationship between ONH topographical dimensions and orbital optic nerve dimensions. The optic nerve was measured with high resolution ultrasound B scanner 2-4mm posterior to the globe while

the HRT was used to image the ONH. It was found that the retrobulbar optic nerve dimensions correlate significantly and positively with neuroretinal rim area.

Jonas *et al.* (1992) reports that nerve fibre count was positively correlated with the retrobulbar optic nerve cross sectional area which would suggest that a thin retrobulbar optic nerve can be taken as an indicator of optic nerve atrophy. In addition, optic nerve cross section area was related to optic disc size. These correlations have an important role in the examination of a glaucoma patient. In glaucomatous human optic nerves Quigley *et al.* (1988) reported a slight decrease in fibre diameter at 0.94±0.11 compared to normal eyes (0.95±0.07) but this failed to reach significance. Mean nerve fibre number was significantly different in experimental glaucomatous animal eyes (519,610±470,273) compared to control eyes (1,073,205±198,254) according to a study by Yucel *et al.* (1998). In addition they found a correlation between optic disc topography and optic nerve fibre number.

1.11.9 LGN in glaucoma

Glaucomatous neuropathy extends beyond the RNFL and optic nerve according to several studies investigating the effect of experimental glaucoma on the LGN. Dandona *et al.* (1991) demonstrated that rapid phase axonal transport from M ganglion cells to the magnocellular layers of the LGN was decreased selectively in chronic experimental glaucoma. In a similar investigation, postmortem examination of the LGN of human glaucoma patients has shown a preferential reduction of neuron density in the human LGN magnocellular layer (Chaturvedi, Hedley-White and Dreyer, 1993). These studies support the theory of selective cell loss (see section 1.9.7).

Within the LGN there are two types of neuron, relay neurons whose projections terminate in the visual cortex and interneurons whose projections are confined to the LGN. Using parvalbumin, a calcium-binding protein, to selectively identify relay neurons Yucel and colleagues (2000) explored changes of LGN in experimental glaucoma. They measured a significant relay neuronal loss in the magnocellular and parvocellular layers of the lateral geniculate nucleus and found a positive correlation between neuronal loss and optic nerve fibre loss. The results of their study suggest that glaucomatous damage extends to the primary visual cortex. They found no significant

decrease in the neuronal density in these layers. In a later study Yucel, Zhang, Weinreb *et al.*, (2001) demonstrated that relay LGN neurons in the parvocellular layers undergo significantly more shrinkage than neurons in magnocellular layers.

Experimental glaucoma studies demonstrate the effects of chronic IOP elevation on the cytoartichecture of the primate LGN. Weber and colleagues (2000) report larger reductions in soma size of both M and P cells with longer durations of elevated IOP. They found percentage decreases in mean cell area of both the M and P layers were comparable and that the largest neurons in both areas are likely to be most severely affected. The results would suggest that both cell loss and cell shrinkage contribute to the reduction of soma size within the M and P layers. Further, that general size shrinkage may contribute to a greater extent in the determining final P layer cell size, while actual cell loss occurs in the M layers.

1.11.10 Anterior visual pathway in glaucoma

Glaucoma affects the anterior visual pathway anterogradely at least up to the optic chiasm according to magnetic resonance imaging (MRI). Kashwagi, Okubo, Tsukahara (2004) report that optic nerve diameter and height of the optic chiasm in glaucoma patients is significantly different from that in normal subjects. Optic nerve diameter measured 2.25±0.33mm in glaucoma patients compared with 2.47±0.24mm in controls. Optic chiasm height was significantly shorter in glaucoma (2.12±0.37mm) than in normals (2.77±0.36mm). The authors found a good correlation between recorded morphologic changes and glaucomatous optic nerve damage.

1.12 Functional changes in glaucoma

1.12.1 Contrast sensitivity in glaucoma

Investigative studies of visual function in terms of contrast sensitivity in glaucoma have reported conflicting results. Arden and Jacobson (1978) and Ross, Bron and Clarke (1984) found a decrease in the contrast sensitivity function while Lundh (1983) reports

no change in sensitivity in glaucoma subjects. Such differences may be attributed to differing methodologies and/or subject groups.

1.12.2 Visual field loss in glaucoma

Glaucomatous field defects are typically due to damage of the retinal nerve fibre bundles at the optic nerve head. Their characteristic location and shape corresponds to the anatomy of the retinal nerve fibre layer itself. Most visual field defects occur within the central 30 degrees and can be classified as:

Paracentral
Arcuate
Nasal step
Overall depression
Baring of the blind spot
Enlargement of the blind spot

Early defects are usually paracentral, arcuate scotomas or nasal steps and are often found together. 70% of all early defects have a paracentral defect and occur more frequently in the superior field and between 10-20 degrees of eccentricity.

Arcuate defects occur in more advanced glaucoma and are located in the Bjerrum regions above and /or below the macular, more frequently in the superior field.

Nasal step is associated with a difference in sensitivity across the horizontal midline in the nasal field and is more prevalent in the superior field.

Overall depression is believed to occur as a result of diffuse loss of nerve fibres and has been reported to exist in up to 39% of patients with glaucomatous loss. More specifically, depression of the nasal field with contraction of the nasal isopters is characteristic of glaucomatous loss. Both baring and enlargement of the blind spot is associated with glaucoma but is not considered specific to it (Henson, 1993).

1.13 Optical principles of the OCT

OCT imaging of the posterior segment is able to identify the cross sectional morphology of the fovea, optic disc and retinal structure together with the normal variations in retina and nerve fibre layer thickness. This technique is based on the principle of Michelson Interferometry. Low coherence light is split by a beam splitter into a reference optical delay path and a probe beam incident on the retina. Light passing through the eye is reflected by structures in different retinal tissue layers. A detector recombines the beams and only when the propagation distances of both match within the source coherence length does an interference signal occur. An A-scan profile of reflectivity versus depth into the retina is produced by measuring the interference signal while varying the length of the reference optical delay path by varying the distance between the beam splitter and the reference mirror. While the probe beam is automatically scanned across the retina a series of one dimensional A-scan reflectivity profiles are obtained to produce the cross sectional B-scan image. OCT software generates a colour coded image for the display of these interferometric signals from which retinal thickness measurements are made using computer algorithms (Hrynchak and Simpson, 2000).

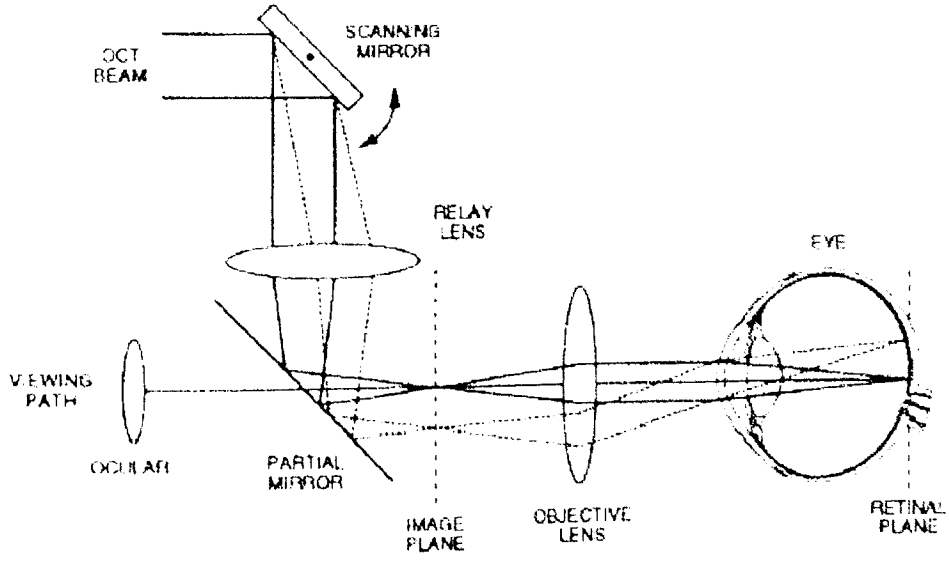

Figure 1.1 Schematic diagram of the optical system for OCT imaging of the retina (from Schuman, Puliafito and Fujimoto, 2004)

Images are shown in false-colour where dim colours (blue to black) represent areas of minimal or no reflectivity and bright colours correspond to regions of high relative optical reflectivity. The inner retinal margin is well defined due to the contrast between the backscattering retina and the non reflective vitreous. The foveal depression and lateral displacement of the retina anterior to Henle's fibre layer is obvious while a low reflectance membrane anterior to the foveal pit represents the posterior hyaloid. The choriocapillaris and retinal pigment epithelium are identified by a highly reflective band while the photoreceptors lying anterior to the choriocapillaris provide weak backscattering. The nerve fibre layer is seen as a red layer (highly scattering) at the inner margin of the retina (Puliafito *et al.*, 1995; Hee *et al.*, 1995a).

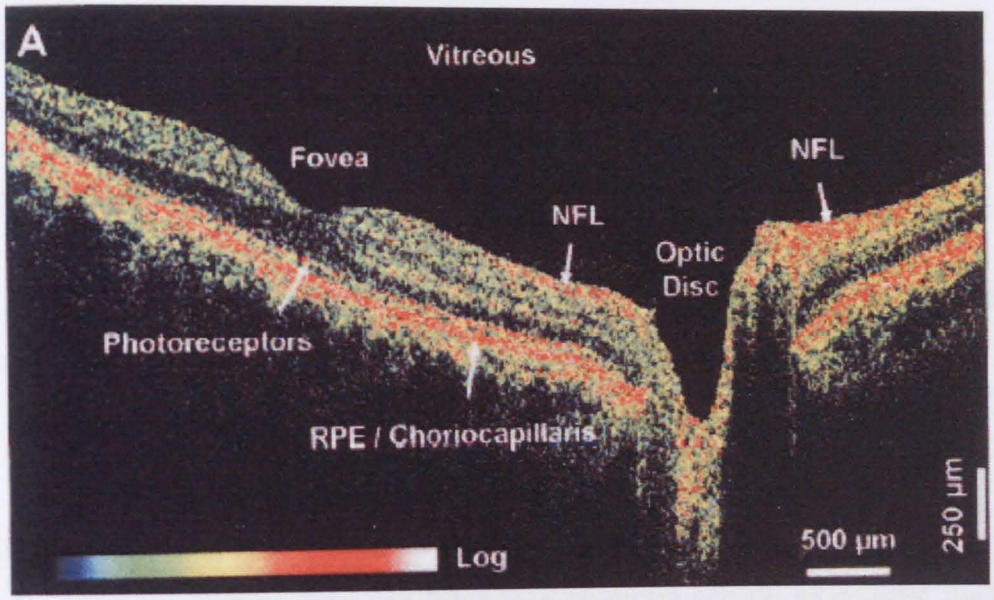

Figure 1.2 OCT tomogram of a normal fovea and optic disc taken along the papillomacular axis (Schuman *et al.*, 2004)

OCT was first introduced in 1991 and since then has undergone several updates and modifications. Several studies examined the properties of the prototype and commercially available OCT models OCT 1/ OCT2 and the latest model OCT3/Stratus. While the instruments vary in a number of ways including their optics, internal amplification, output interface and super luminescent (SLD) power range, studies have

reported that repeatability obtained with commercial instruments is comparable to the prototype (Schuman *et al.*, 1996; Koozekanani *et al.*, 2000; Jones *et al.*, 2001).

The latest OCT model- the Stratus OCT (OCT 3 model 3000) projects a bandwidth near-infrared light beam of 820nm from a superluminsecent diode to produce cross sectional retinal images with axial resolution of ≤10microns and transverse resolution of 20 microns. The OCT interferometer electronically detects, collects, processes and stores the echo delay patterns from the retina. Every scan pass captures 128-768 axial A-scans. Each A-scan consists of 1024 data points over 2mm depth. A tomogram therefore comprises 131,072 to 768,432 data points.

The Stratus OCT offers 18 scan types, along with 18 analysis protocols. The most widely used scan types employed by current studies are the macular thickness scan, optic nerve head scan and circular RNFL scan.

1.13.1 Scan type

Macular thickness map: this scan is a version of the radial lines pattern consisting of 6-24 equally spaced line scans through a common axis, each measuring 6mm. Line number is adjustable depending on the examiner's requirements.

Optical disc map: this scan consists of a radial line pattern with 6-24 equally spaced lines each measuring 4mm, arranged through a common central axis. Line number is adjustable depending on the examiner's requirements.

RNFL (3.4): this allows the examiner to acquire three circle scans of 3.4mm centred on the optic disc. Parameters are fixed. This represents a standard size scan to measure the RNFL and is employed by many studies.

Circle scan: multiple circle scans can be acquired without retuning to the main window. These are generally applied around the optic nerve head and circle radius can be tailored to each patient depending on examiner's requirements. Circle size can be

altered during period of scanning and same size scans can be averaged later in analysis. Default circle radius is 1.73mm. This is analysed using the RNFL analysis protocol.

Fast scans

These are designed to reduce acquisition time and simplify the scanning process. The advantage of using this technique is improved accuracy. Scan alignment and set up is required only once which improves accuracy because scans are acquired almost simultaneously and reduces possible patient eye movement and fixation loss. Multiple scans can be acquired without having to return to the main window, leading to greater scan production in a shorter time period.

Fast scans acquire 768 A-scans (128 A-scans multiplied by 6) or three times 256 A-scans for the circular scan. It should be noted that this is less than if acquiring scans individually at 512 A-scans. However, the time taken to acquire this higher resolution is likely to produce errors due to fixation loss.

Fast macular thickness map protocol compresses the six radial line scans into one scan in 1.92 seconds. This scan is designed for use with the retinal thickness analyses.

Fast Optical Disc protocol compresses the six optical disc scans into one scan and acquires all six 4mm radial line scans in 1.92 seconds of scanning. This scan is designed to examine the optic disc for indications of glaucoma and scans are analysed with the optic nerve head analysis protocol.

Fast RNFL thickness (3.4) protocol compresses the three circle scans into one scan in 1.92 seconds of scanning. This glaucoma protocol is analysed with the RNFL analyses.

1.13.2 Analysis protocol

The Stratus OCT calculates retinal and RNFL thickness as the distance between the vitreoretinal interface and the anterior surface of the retinal pigment epithelium (RPE)/choriocapillaris. The vitreoretinal surface is detected by the algorithm by

searching each A- scan axially from anterior to posterior for a reflecivity shift above a threshold rate. It searches for the RPE surface from below the retinal surface. The retinal thickness algorithm locates the highest changes in reflectivity. The RNFL thickness algorithm searches for the RPE in two stages. Firstly it detects the highest rates of reflectivity change and secondly identifies reflectivity above a threshold value.

Retinal thickness/volume analysis produces a circular map of average retinal thickness or volume in each of the nine scan sectors. Map circle default diameters are 1, 3 and 6mm. Circle diameters can be changed to 1, 2.22 and 3.45mm for further analysis. The display also includes a foveal thickness measurement which represents the calculation of average thickness in microns +/- the standard deviation for the centre point (area 1) where all the scans intersect and total macular volume of the retinal map area in mm^3.

RNFL thickness analysis produces a number of data displays. A graph shows how RNFL thickness varies around the circular scan (with x and y axis representing A-scan location and RNFL thickness respectively). At any point on the A-scan, RNFL thickness can be measured by applying the pointer. Calipers can be employed to quantify specific parameter measures. In addition, circular diagrams represent average RNFL thickness in the four quadrants (inferior, superior, nasal, and temporal) and around 12 clock hour positions. Overall RNFL average thickness is also displayed.

Optic nerve head analysis detects the anterior surface of the RNFL and the RPE and is then able to identify features of the optic disc based on anatomical markers (disc reference points) on each side of the disc where the RPE ends. The RNFL surface is located by the algorithm searching each A-scan from anterior to posterior until it finds reflectivity above a threshold value. The RPE surface is located by searching each A-scan posteriorly (from below the RNFL) for the highest rate of reflectivity change. The algorithm is able to detect and quantify optic nerve head topography using reference points located at the disc edge where the RPE ends. Disc diameter is measured by a straight line traced between the two disc reference points. Cup diameter is measured on a line parallel to the disc line offset by 150 microns and rim area is calculated using the cup line as a posterior boundary.

For each individual scan, the computer algorithm identifies and measures disc diameter, cup diameter, rim area (vertical cross section), horizontal rim length and average nerve width at the disc. Optic nerve head analysis results combines the analysis and measurement of each individual scan to give vertical integrated rim area (volume), horizontal integrated rim width (area), disc area, cup area, rim area, cup:disc area ratio, cup:disc horizontal ratio and cup:disc vertical ratio. It is possible to adjust the placement of the disc reference points and therefore the resulting measurements.

1.13.3 Comparison of OCT with traditional techniques

Traditional methods of evaluating retinal and, more specifically, macular thickness such as slit lamp biomicroscopy, stereoscopic photography and fluorescein angiography are only qualitative and relatively insensitive to small changes (Shahidi, Ogura, Blair *et al.*, 1991). Ultrasound techniques are limited by the acoustic wave length in ocular tissue to approximately 150μm (Olsen, 1989; Pavlin, Sherar and Foster, 1990). High frequency ultrasound increases the resolution to about 20μm but limited penetration does not permit imaging of the posterior fundus (Pavlin, Harsiewicz, Sherar *et al.*, 1991). Computed tomography and magnetic resonance imaging is also limited. Ocular aberrations and the numerical aperture available through the pupil, limit cross sectional imaging by scanning laser ophthalmoscopy and scanning laser tomography to 300μm of axial resolution. The Glaucoma Scope can only image the optic nerve head itself while the confocal scanning laser ophthalmoscope is limited to coronal sections of the ONH and retina and the optic Nerve Fibre Analyser (NFA) is subject to birefringence effects from the cornea and lens as it measures the change in polarisation of light reflected from the eye (Schuman *et al.*, 1996).

The OCT has been compared with already known imaging techniques to determine its accuracy. Jones *et al.* (2001) suggest that while measurements are consistent with the properties of the retinal nerve fibre layer (RNFL) the OCT underestimates its thickness. However, entire retinal thickness measurements show greater reproducibility and are more in agreement with histological data (Koozekanani *et al.*, 2000). A more recent conflicting report demonstrates that the OCT tends to overestimate the RNFL thickness and suggests this may limit its ability to detect subtle changes (Soliman *et al.*, 2002).

Several studies suggest that the OCT may be superior to other imaging devices such as scanning laser polarimetry and HRT for detecting a specific pattern of reduction in the average or focal RNFL thickness (Zangwill, Bowd, Berry *et al.*, 2001; Hoh *et al.*, 2000).

1.13.4 Advantages of the OCT

OCT differs from the HRT and Nerve Fibre Analyser (NFA) because cross sectional images of the retina are made from which direct measurements of the NFL thickness are made. OCT has greater resolution than the scanning laser ophthalmoscope at approx 14μm in air, 10μm in clear biological tissues compared with resolution of approx 30μm respectively (Huang *et al.*, 1991).

OCT is not affected by the refractive status or axial length of the eye. Unlike other imaging techniques OCT differentiates between light back scattered from different depths in the retina which allows characterisation of internal structures (Schuman *et al.*, 1996). OCT allows a number of different scans to be made, each most appropriate to the structure being analysed. Unlike slit lamp observation or fluorescein angiography OCT measurements enable the objective monitoring of disease progression or resolution with a single recorded number. Nuclear sclerotic changes appear to have no effect on OCT imaging. Unlike other imaging modalities structural information is not dependent on an arbitrarily defined reference plane.

OCT can be used with undilated pupils (Baumann *et al.*, 1998; Koozekanani *et al.*, 2000). Acquiring data is therefore possible with elderly patients and those who are using topical pilocarpine and have been diagnosed with exfoliation syndrome, pseudo exfoliation syndrome, chronic diabetes (Koozekanani *et al.*, 2000). The advantage of not having to dilate the pupils, together with the fact that infra red illumination is used, is increased comfort and tolerance for the patient compared with other more invasive techniques such as fluorescein angiography or fundus photography.

1.13.5 Factors affecting the accuracy of the OCT

Accuracy of the OCT is affected by the reproducibility with which the examiner can locate the same retinal position on subsequent patient visits (although overcome to a certain degree by the fixation light and the repeat function on the Stratus OCT). Reduction of the accuracy of the OCT will also be a consequence of the inability of different observers to obtain the same image quality (Massin *et al.*, 2001).

The OCT is based on infrared interferometry and is therefore not affected by changes in nuclear sclerotic cataract density. However, dense subcapsular and cortical opacities may impair the ability to perform OCT (Schuman *et al.*, 1996). Hee *et al.* (1998) advocate the usefulness of the OCT in quantifying macular thickness in patients with diabetic macular oedema but they acknowledge that accuracy of the OCT could be reduced in patients with eccentric or varying fixation, by refractive error and saccadic eye motion. While the OCT allows accurate measurement of the retinal nerve fibre layer and retinal thickness, precise measurement of specific retinal layers is, as yet, not possible (Chauhan and Marshall, 1999).

1.13.6 Repeatability and Reproducibility of the OCT

In order for any technology to be reliable in the monitoring of disease, measurements must be reproducible. Repeatability and reproducibility studies of measures of the normal and diseased eye are extensive. The OCT provides quantitative measurements of retinal thickness, RNFL thickness and optic nerve head parameters which are accurate, repeatable within-visit (Schuman *et al.*, 1996; Baumann *et al.*, 1998; Koozekanani *et al.*, 2000; Massin *et al.*, 2001; Muscat *et al.*, 2002) and reproducible between-visit (Schuman *et al.*, 1996; Jones *et al.*, 2001; Massin *et al.*, 2001; Muscat *et al.*, 2002). Although OCT technology has developed in terms of both hardware and software since its introduction in the early 1990s, measurements made with prototype and commercial instruments have been shown to be highly correlated and similar despite different system components (Guedes *et al.*, 2003).

Early studies using the prototype OCT have shown standard deviations (SDs) of measurement of RNFL and retinal thicknesses of approximately 10-20μm (10-20%) in normal and glaucomatous eyes (Schuman *et al.*, 1995; Schuman *et al.*, 1996; Baumann *et al.*, 1998).

More recently, Gurses-Ozden, Teng, Vessani *et al.* (2004) report that the newest version of the technology, the Stratus OCT displays both intra and inter operator reproducibility for normal eyes. The Stratus OCT is the most recently introduced model and has undergone a number of improvements. The acquisition of more A-scans has improved image resolution but resulted in greater acquisition time. The Stratus OCT demonstrates reproducible measurements of RNFL macular and optic nerve head parameters for normal eyes (Paunescu, Schuman, Price *et al.*, 2004). According to Paunescu and colleagues (2004) the Stratus OCT showed a SD of 3μm for mean macular thickness measurements. For the circular RNFL scan, within-visit and between-visit SDs were approximately 1-15μm for clock hour positions (segments 1-12), 7μm for four quadrants and 4μm for mean RNFL thickness. Such findings compare well with previous studies by Schuman *et al.* (1996) using the prototype OCT and Jones *et al.* (2001) who investigated the reproducibility of the OCT 2000 in normal eyes. Schuman and colleagues (1996) reported SDs of 11-30μm for RNFL clock hour analysis, 11-26μm for quadrant analysis and 10-20μm for mean RNFL thickness. Jones and colleagues (2001) showed that OCT model 2000 could provide reproducible measurements of retinal structures that are consistent with the properties of the RNFL. They demonstrated SDs of 11 μm, 10μm and 6μm for clock hour, quadrant and mean RNFL analyses respectively.

RNFL thickness measurements of normal and glaucomatous eyes using the prototype OCT provide adequate reproducibility (Schuman *et al.*, 1996). Confirmation of such findings were documented in a later study by Blumenthal and colleagues (2000), who used the 3.4mm diameter circular scan of the first commercially available OCT to acquire reproducible RNFL measurements for both normal and glaucomatous eyes. Carpineto, Ciancaglini, Zuppardi *et al.* (2003) evaluated the reliability of RNFL thickness measurements by OCT in age matched normal and glaucomatous eyes. Each subject underwent five repetitions of a series of scans on five separate occasions within

a two week period and intersubject, within-visit and between-visit components were evaluated.

1.13.7 Comparison of OCT with histological studies

According to Jones *et al.* (2000) the Humphrey OCT (model 2000) tends to underestimate RNFL thickness when compared to histological data by an average of 37%. However, entire retinal thickness measurements show better agreement with human histology.

1.13.8 Comparison of imaging methods

Authors have aimed to establish the validity of the OCT by comparing with existing assessment methods. Zangwill and associates (2001) compare the ability of the HRT, GDx and OCT to discriminate the normal eye from those with early to moderate glaucomatous visual field loss. They found that while the area under the ROC curves was similar among the best parameters for each instrument, qualitative assessment of stereophotographs and measurements from the HRT and OCT generally had greater sensitivities than GDx measurements.

Soliman *et al.* (2002) demonstrates high correlation with OCT and red free photographic scores and visual field defects therefore illustrating high validity for the measurement of RNFL thickness.

Both OCT and scanning laser polarimetry techniques have been shown to be capable of differentiating glaucomatous eyes from non glaucomatous eyes but are unable to differentiate between normal and ocular hypertensive eyes (Hoh *et al.*, 2000).

Varma *et al.* (1996) question the reliability of RNFL thickness measurements made by various imaging instruments on the basis that the majority of instruments either determine the thickness relative to the surrounding elevation values (Topcon Imagenet, ONHA HRT), while some measure the degree of polarisation based on the assumption that tubules in the RNFL contribute primarily to a change on the polarisation of incident

light (NFL analyser). In the case of the OCT, the depth of various retinal layers is based on the time delay of backscattered light using interferometry. They acknowledge the benefit of alternative techniques in that they measure some aspect of retinal thickness but suggest that without a standard in humans for histological RNFL thickness measurements it is difficult to assess the accuracy. In the absence of such absolute data, instruments such as the OCT and HRT still provide invaluable information about any changes and progression in retinal tissue during the disease process.

Greaney, Hoffman, Garway-Heath *et al.* (2002) compared the ability of qualitative assessment of optic nerve head stereophotographs (ONHPs), confocal scanning laser ophthalmoscopy (CSLO) scanning laser polarimetry (SLP) and optical coherence tomography (OCT) to distinguish normal eyes from those with early to moderate glaucoma as determined by loss of visual field. They concluded that the quantitative methods CSLO, SLP, OCT had no advantage over qualitative assessment of disc photographs by experienced observers in distinguishing between the normal and early to moderate glaucomatous eyes. They supported the view that combining such imaging methods would significantly improve accurate diagnosis. Mistlberger, Liebmann, Greenfield *et al.* (1999) reported that OCT, SLO and scanning laser polarimetry failed to distinguish between normal eyes and ocular hypertensive eyes that displayed normal achromatic and SWAP fields.

1.14 Clinical investigation of glaucomatous optic neuropathy using the OCT

1.14.1 OCT assessment of the RNFL

Histological studies have shown that 50% of the retinal nerve fibre layer may atrophy before detection by the above methods (Quigley and Addicks, 1982). Changes in RNFL thickness may therefore be a sensitive indicator of the presence of glaucoma and precede other indicators such as cupping.

OCT allows direct measurement of nerve fibre layer thickness by *in-vivo* visualisation of cross sectional images of the retinal and nerve fibre layer at histologic levels of resolution. There is considerable evidence that the OCT is a reliable and reproducible

method of identifying and quantifying RNFL and topographic optic nerve head changes in glaucoma. OCT can be used to image the optic nerve head and peripapillary region and is useful in the early diagnosis and therefore early treatment and monitoring of glaucoma (Schuman *et al.*, 1996; Blumenthal *et al.*, 2000; Carpineto *et al.*, 2003; Gurses-Ozden *et al.*, 2004; Zafar, Gurses-Ozden, Vessani *et al.*, 2004; Budenz, Chang, Huang *et al.*, 2005).

The ability of the OCT to differentiate normal from glaucomatous eyes, based on measurements of the RNFL has been widely reported. These studies have measured a decrease in RNFL thickness in glaucomatous eyes compared with normal eyes (Schuman *et al.*, 1995; Pieroth *et al.*, 1999; Zangwill *et al.*, 2000; Hoh *et al.*, 2000; Bowd *et al.*, 2000; Soliman *et al.*, 2002).

The OCT is able to accurately assess RNFL thinning in the areas corresponding to notching of the optic disc. Abnormal changes in RNFL thickness correlate well with loss of functional vision such as visual field examination results. Early abnormal changes in the RNFL in glaucomatous eyes can be diffuse or more localised and both precede visual field defects. It is more difficult to detect diffuse defects than focal defects using traditional perimetry tests. Generalised thinning of the RNFL produces a reduction in mean sensitivity in visual field tests while focal defects produce small deep field defect (Pieroth *et al.*, 1999).

Schuman *et al.* (1995) found that RNFL thickness was a more reliable predictor of functional visual loss than both optic nerve cupping and neuroretinal rim area. As expected, thinning of the inferior RNFL was associated with superior field defects while loss of tissue superiorly was associated with inferior defects. Using the OCT, Bowd *et al.* (2000) showed that RNFL thickness around the optic disc has a characteristic double hump pattern with RNFL thickness peaks in the superior and inferior quadrants and troughs in the temporal and nasal quadrants. Patients with glaucoma exhibited a similar but depressed pattern. In all quadrants, the RNFL thickness in glaucomatous eyes was less compared to that of normal and ocular hypertensive eyes.

OCT measurements of RNFL thickness compare well with established techniques of RNFL photography and visual field testing in the investigation of glaucomatous optic

neuropathy (Zangwill, Williams, Berry *et al.*, 2000). OCT measurement of RNFL thickness is topographically related with glaucomatous visual field defects assessed with SWAP. Kanamori, Nakamura, Escano *et al.* (2003) found RNFL thickness was significantly reduced at the superior and inferior quadrants in the glaucomatous eye compared with normal eyes. They suggest that OCT measurements of RNFL thickness may be useful in detecting early RNFL damage.

1.14.2 Correlation between OCT measures of RNFL thickness and visual fields

The OCT is able to discriminate the glaucomatous eye from the normal eye when glaucoma is defined on the basis of achromatic visual fields as tested by the Humphrey Field Analyser (Bowd *et al.*, 2001; Greaney *et al.*, 2002; Kanamori *et al.*, 2003; Mistlberger *et al.*, 1999; Hoh *et al.*, 2000; Bowd *et al.*, 2000).

Mok, Lee and So (2003) report a significant reduction of RNFL thickness in glaucoma suspects with abnormal SWAP in the inferotemporal and superotemporal sectors of the peripaillary area. Findings would suggest a good correlation between OCT RNFL measurements and SWAP abnormalities in glaucoma. Mok and associates suggest that the OCT may detect glaucomatous damage earlier than standard achromatic perimetry and consequently has the ability to identify the earliest evidence of structure alterations in POAG.

More recently, Nouri-Mahdavi, Hoffman, Tannenbaum *et al.* (2004) investigated the ability of the OCT to discriminate between normal eyes and those with early glaucoma and glaucoma suspects. Glaucoma suspects were defined as those with normal achromatic visual fields but abnormal disc appearance consistent with glaucoma. Early glaucoma was described as the presence of a glaucomatous defect regardless of optic disc appearance. They found that the OCT discriminates well between eyes with early perimetric glaucoma and normal eyes but its ability to identify glaucoma suspects is less adequate.

RNFL structural measurements are well correlated with visual function (Hoh *et al.*, 2000).

There is mounting evidence that a relationship exists between visual field and RNFL thickness as measured by OCT. Soliman and colleagues (2002) note the relationship between RNFL loss and visual field damage can be approximated by an exponential model rather than a linear plot. An initial steep gradient followed by a relative plateau representing a considerable loss of RNFL before the observation of visual field damage concurs with previous reports that RNFL loss precedes field defects. They suggest that nerve fibre loss in the absence of visual field damage in early glaucoma is most easily detected with OCT, while advanced glaucomatous changes are better detected with field testing.

Kanamori *et al.* (2003) found a significant relationship between the mean deviation (MD) measured with the Humphrey Field Analyser using the central full threshold program 30-2 and average RNFL thickness measured around the optic disc by a circular scan of 3.4mm diameter. El Beltagi, Bowd, Boden *et al.* (2003) showed that regional OCT measured RNFL thinning in glaucomatous eyes is related to decreases in visual field sensitivity in terms of both location and severity. RNFL was reduced more inferiorly than in other locations, corresponding to superior field loss and supporting the findings of Quigley *et al.* (1981) of preferential loss of inferior arcuate fibres in early glaucoma.

1.15 Diabetes: Facts and Figures

Diabetes mellitus is a heterogenous metabolic disease in which hyperglycaemia is a central feature. The associated abnormalities in protein, carbohydrate and fat metabolism are the result of insufficient insulin action on peripheral target tissues due to insufficient insulin secretion in the case of Type 1 diabetes (IDDM), or diminished tissue response to insulin in Type 2 diabetes (NIDDM) or a combination of both. Pathophysiology of NIDDM involves both impaired insulin secretion from the beta cells of the pancreas and cellular resistance to the action of insulin.

Type 1 diabetes usually manifests itself between the ages of 10-20 years although older patients may acquire the disease (Alberti and Zimmer, 1998). Patients depend on exogenously supplied insulin for survival.

Type 2 is an acquired form of the disease which usually develops between the ages of 50-70 years (Alberti and Zimmer, 1998). Most patients can control this condition with a good diet. The majority will also require oral hypoglycaemic agents to control blood glucose levels and a significant number will also require insulin. The major cause of death in NIDDM, accounting for two thirds in total is macrovasular disease- coronary artery, peripheral vascular and cerebrovascular disease (Zimmet, McCarty and De Courten, 1997).

1.15.1 Epidemiology of diabetes

Diabetes is among the five leading causes of death by disease in most countries (WHO, 1994) and forecasts have predicted that by 2010 215 million people will suffer the disease (McCarty and Zimmet, 1994). King, Aubert and Herman (1998) have proposed that the number of adults with diabetes will have risen from 135 million in 1995 to 300 million by 2025. Non-insulin diabetes (NIDDM) constitutes approximately 85% of all cases of diabetes in developed countries, with epidemic proportions in many developing nations (Zimmet *et al.*, 1997).

1.15.2 Risk factors in diabetes

Age

This is the single most important factor influencing the prevalence of diabetes. Epidemiological studies show an increased rate with advancing age with a possible decline in very old age groups (Gadsby, 2002).

Gender

There is no clear trend regarding the prevalence rates of diabetes among the sexes (Gadsby, 2002).

Country

Rates of diabetes vary between 3-10% in Europe, with increased rates of 14-20% for Arab, Asian Indian and Hispanic American populations. Prevalence rates of 50% have been reported in natives of Nauru (Pacific Island) and the Pima Indians (USA) (King and Rewers, 1993).

Socio-economic factors

Poor diet and poor lifestyle resulting from socio-economic deprivation are linked to high incidence of diabetes (Gadsby, 2002).

Obesity

Strong evidence exists for obesity being an independent risk factor for the development of diabetes (Harris, Flegal, Cowie *et al.*, 1998).

1.16 Diabetic retinopathy

Diabetic retinopathy is principally a micro-angiopathy, a disorder of the small blood vessels: capillaries, venules and arterioles. The main pathological processes responsible for retinopathic changes are microvascular occlusion and microvascular leakage. Microvessels undergo structural changes, namely thickening of the basement membrane, selective loss of pericytes and endothelial cell changes. One of the earliest clinically detectable signs of diabetic retinopathy is increased vascular permeability due to a breakdown in the blood retinal barrier causing macular oedema (Cunha-Vaz, Faria de Abreu, Campos *et al.*, 1975). As the disease progresses, retinal changes include development of vascular microaneurysms, drusen and vascular proliferation.

Diabetic retinopathy can be classified into the following groups, according to the severity of retinal changes (Ferris, 1993):

1. Background retinopathy
2. Maculopathy
3. Pre-proliferative retinopathy
4. Proliferative retinopathy

1.16.1 Background Retinopathy

Clinical features of background retinopathy include:
Microaneurysms – the first clinically detectable lesions of diabetic retinopathy. They appear as bright red dots and range in size 10- 100μm. Microaneurysms occur mainly in the inner nuclear layer and are found most frequently at the posterior pole.
Exudates – have a yellow, waxy appearance and occur in individual streaks and clusters or in larger circinate patterns surrounding clusters of microaneurysms. They consist of condensed fluid plasma leaked from damaged capillaries and are located in the outer plexiform retinal layer.
Haemorrhages – vary in appearance according to their location. Dot haemorrhages are located within the outer plexiform and inner nuclear retinal layers and have distinct borders. Blot haemorrhages are similar in appearance with indistinct edges. Flame shaped haemorrhages occur in the superficial nerve fibre layer.
Cotton wool spots – have a poorly defined, white roundish appearance. They represent an ischaemic response and are small infarcts occurring within the nerve fibre layer caused by a closure or reduction within a capillary. Transported material in the ganglion cell axons builds up leading to swelling of the neural tissue.

1.16.2 Maculopathy

Background diabetic retinopathy involving the macular area is referred to as maculopathy and can result in loss of vision. Diabetic maculopathy can co-exist with proliferative retinopathy.

Focal maculopathy – focal leakage from microaneurysms and capillaries occurs and leads to the formation of focal oedema and circinate hard exudate surrounding the leakage point.

Diffuse maculopathy – diffuse macular oedema as a consequence of extensive fluid accumulation in retinal tissue (Ferris and Patz, 1984).

Ischaemic maculopathy – this is due to capillary closure and subsequent retinal non-perfusion and ischaemia. Clinical signs include vascular changes, intra-retinal microvascular abnormalities, large blot haemorrhages and multiple cotton wool spots.

1.16.3 Pre-proliferative retinopathy

Multiple cotton wool spots – greater than 5.

Larger blot haemorrhages – these originate from the deep capillary plexus and are located in the inner plexiform and outer plexiform retinal layers. They have a dark red appearance.

Intraretinal microvascular abnormalities (IRMA) – appear as small areas of very fine abnormal branching small blood vessels lying flat within the retina. They occur as a result of newly developed capillary networks to compensate for areas of capillary closure.

Venous abnormalities – tortuosity and dilatation which may progress to venous beading (an irregular increase in vessel calibre) and looping.

1.16.4 Proliferative retinopathy

Severe retinal ischaemia and subsequent release of angiographic growth factors produce retinal changes as follows:

Neovascularisation – the formation of new networks of fine vessels from the optic disc (neovascularisation of the disc: NVD) or from the surface of the retina (neovascularisation elsewhere: NVE) most frequently in the posterior pole within 45 degrees of the optic disc. The vessels originate from within the retina and in time pass through the internal limiting membrane onto the surface of the retina. These new vessels are associated with pre-retinal and vitreous haemorrhage.

Retinal detachment – new vessels tend to be fibrous and subsequent contraction can lead to retinal detachment.

End stage diabetic retinopathy – iris neovascularisation may lead to glaucoma.

1.16.5 Risk factors in diabetic retinopathy

Diabetic retinopathy is one of the most frequent and serious complications of diabetes and has several associated risk factors which will be described in the following section. The Pittsburgh Epidemiology of Diabetes Complications (EDC) study suggests that risk factors for the development of retinopathy vary with time, according to the stage of the disease. Baseline diastolic blood pressure was significantly associated with the incidence of new retinopathy, while both retinopathy progression and proliferative retinopathy were significantly associated with baseline glycosylated haemoglobin and baseline severity of retinopathy (Lloyd, Klein, Maser *et al.*, 1995).

Race

Several studies have investigated the effect of race on the development of diabetic retinopathy. Prevalence and severity of diabetic retinopathy has been shown to be greater in non-Hispanic blacks and Mexican Americans with type 2 diabetes in the U.S population than in non-Hispanic whites (Harris, Klein Cowie *et al.*, 1998). In a later study, Harris, Sherman and Georgopoulos (1999) demonstrate that black individuals with Type 2 diabetes are more likely to develop retinopathy than white individuals, even after accounting for potential risk factors. The authors suggest that differences in prevalence may be explained by differential (genetic) susceptibility to the adverse effects on increased levels of blood glucose and/or blood pressure.

Evidence suggests that NIDDM is pathogenetically heterogenous in different ethnic groups. Genetic factors appear to affect the mechanisms by which diabetes is developed in these subjects. It has been suggested that insulin resistance is reduced in individuals of African heritage compared with those of European, Asian and Latin backgrounds (Abate, Garg, Peshock *et al.*, 1996).

Duration of diabetes

The risk of developing diabetic retinopathy increases with duration of the disease. 98% of diabetic patients who have had the disease for 15 years have non-proliferative retinopathy to a certain extent. After 35 years proliferative retinopathy is found in 67% of patients (Harper, O'Day and Taylor, 1995). The risk of developing DR is higher in patients with IDDM (Cerrutti, Sacchetti, Vigo *et al.*, 1989).

Genetic

A number of gene polymorphisms involving pathways of insulin secretion and insulin action have been identified within specific ethnic groups (Abate and Chandalia, 2003). These can either offer protection against DR or predispose individuals to the development of DR. There are currently 10 candidate genes thought to be associated with diabetic retinopathy (Jain, Sarraf and Fong, 2003).

Hypertension

Hypertension is an important risk factor in the development and progression on diabetic retinopathy. The United Kingdom Prospective Diabetes Study (UKPDS) reported a 34% reduction in the risk of DR progression in subjects whose blood pressure was tightly controlled (BP≤144/82) (UKPDS, 1998).

Cigarette smoking

Evidence regarding the association between smoking and diabetic retinopathy is controversial. Moss, Klein and Klein (1996) did not find smoking to be a risk factor for the long term incidence of retinopathy while other studies do report an association between the two (Mulhauser, Bender, Bott *et al.*, 1996). Smoking causes a significant deterioration in contrast sensitivity of patients with IDDM according to Moloney and Drury (1982).

Pregnancy

This is a major risk factor for the progression of DR in the short term but not in the long term (Chen, Newsom, Patel *et al.*, 1994; Schocket, Grunwald, Tsang *et al.*, 1999).

1.17 Blood retinal barrier

Diabetic retinopathy can be described as a micro-angiopathy, a disorder of small blood vessels – arterioles, venules and capillaries. Arterioles and venules are sited within the ganglion cell and nerve fibre layers, while capillaries are located within the inner nuclear and inner plexiform layers. Retinal vessel walls comprise endothelial cells and pericytes enclosed by a basement membrane (comprised of collagen and glycoproteins). Endothelial cells regulate haemostatic functions and pericytes regulate retinal vascular flow by dilating and contracting. Complex tight junctions join adjacent endothelial cells together while the outer pericyte cell layer provides mechanical support and stability to form a selective permeability barrier. The purpose of such a barrier is to prevent movement of ions and hydrophilic molecules from the bloodstream into retinal tissue. (Regulation of solutes from the choroidal layer into the retina is performed by a second barrier made up by the tight junctions between retinal pigment epithelium cells).

Macroglial cells serve to regulate retinal metabolism and modulate the function of blood vessels and can be divided into two groups. The Muller cells span the entire thickness of the retina from the outer limiting membrane to the retinal ganglion cell layer. Their role is to regulate glutamate metabolism, extracellular ionic balance and neuronal function. Astrocytes are fewer in number and situated in the retinal nerve fibre layer alone.

There are several types of retinal neurons including photoreceptors, bipolar cells, amacrine cells and ganglion cells which together are responsible for the convection of nerve impulses from retina to brain. These cells are very sensitive to changes in extracellular ion concentration and the potentially cytotoxic components of the blood. The blood retinal barrier serves to separate the retinal neural layer from the blood circulation.

Disruption to the blood retinal barrier is identified using fluorecscein angiography. This involves the intravenous injection of sodium fluorescein. In the healthy eye this is unable to pass the blood vessel wall. However, in the diseased eye where the blood retinal barrier has been compromised, areas of fluorescein leakage from the retinal vasculature are observed. Vitreous fluorophotometry is the process used to quantify the

amount of leakage by measuring the concentration of fluorescein in the vitreous gel (Gardner, Antonetti, Barber *et al.*, 2002).

The causal relationship between vascular and neuronal changes in diabetes is not clear. Gardner *et al.* (2002) propose two alternative theories. An initial impairment of the blood retinal barrier affects neuronal, microglial and macroglial function and the way in which they interact. Conversely, particular cell types have a propensity to being altered by certain metabolic changes occurring in diabetes. The authors suggest that metabolic insult or stress to neuronal or glial cells may instigate changes in retinal blood flow and vascular permeability leading to haemorrhages and microaneurysms.

1.17.1 Retinal microvascular changes in diabetes

The capillary basement membrane in diabetic retinopathy increases in thickness (Ashton, 1974). The diabetic eye shows a selective loss of pericytes and alterations to the endothelial cell tight junctions and endothelial cell death leading to increased vascular permeability. Ophthalmoscopically this is manifest as hard exudates, oedema and intra-retinal haemorrhages.

1.17.2 Neurodegeneration in diabetes

There is increasing evidence to suggest that in addition to the vascular changes occurring in diabetic retinopathy, chronic neurodegeneration of the retina plays a critical role in the development of diabetic eye disease. This includes neural apoptosis, loss of ganglion cell bodies, decrease in thickness of the inner retina, glial reactivity, neurofilament abnormality, reduction of retrograde transport in the optic nerve, changes in electrophysiology activity (Barber, 2003).

Several reports concerned with electrophysiological and psychophysical measurements of retinal function appear to suggest that retinal neuron function is affected before the breakdown of the blood retinal barrier and subsequent observable vascular lesions. Electroretinogram (ERG) testing revealed a reduction in the amplitude of oscillatory

amount of leakage by measuring the concentration of fluorescein in the vitreous gel (Gardner, Antonetti, Barber *et al.*, 2002).

The causal relationship between vascular and neuronal changes in diabetes is not clear. Gardner *et al.* (2002) propose two alternative theories. An initial impairment of the blood retinal barrier affects neuronal, microglial and macroglial function and the way in which they interact. Conversely, particular cell types have a propensity to being altered by certain metabolic changes occurring in diabetes. The authors suggest that metabolic insult or stress to neuronal or glial cells may instigate changes in retinal blood flow and vascular permeability leading to haemorrhages and microaneurysms.

1.17.1 Retinal microvascular changes in diabetes

The capillary basement membrane in diabetic retinopathy increases in thickness (Ashton, 1974). The diabetic eye shows a selective loss of pericytes and alterations to the endothelial cell tight junctions and endothelial cell death leading to increased vascular permeability. Ophthalmoscopically this is manifest as hard exudates, oedema and intra-retinal haemorrhages.

1.17.2 Neurodegeneration in diabetes

There is increasing evidence to suggest that in addition to the vascular changes occurring in diabetic retinopathy, chronic neurodegeneration of the retina plays a critical role in the development of diabetic eye disease. This includes neural apoptosis, loss of ganglion cell bodies, decrease in thickness of the inner retina, glial reactivity, neurofilament abnormality, reduction of retrograde transport in the optic nerve, changes in electrophysiology activity (Barber, 2003).

Several reports concerned with electrophysiological and psychophysical measurements of retinal function appear to suggest that retinal neuron function is affected before the breakdown of the blood retinal barrier and subsequent observable vascular lesions. Electroretinogram (ERG) testing revealed a reduction in the amplitude of oscillatory

potentials in insulin dependent diabetic patients in the absence of vascular retinopathic changes (Simonsen, 1980; Frost-Larsen, Larsen and Simonsen, 1980; Juen and Kieselbach, 1990). Sokol, Moskowitz, Skarf *et al.* (1985) report reduced contrast sensitivity scores for non-insulin diabetic patients which preceded vascular retinopathy while Della-Sala, Bertoni, Somazzi *et al.* (1985) found reductions in contrast sensitivity to be unrelated to observed diabetic changes in the retina.

Diabetes affects the function of the macroglial cells to maintain the blood retinal barrier and causes an impairment of glutamate metabolism and the release of inflammatory mediators. Microglia (normally dormant in the healthy eye) become activated in diabetes and through a series of processes exacerbates retinal vascular permeability (Gardner *et al.* 2002).

Barber, Lieth, Khin *et al.* (1998) describe the process of apoptosis of retinal ganglion cells and inner nuclear cells in the early stages of diabetes leading to increased atrophy of the inner retina, and a subsequent reduction in retinal nerve fibre layer thickness and number of axons in the optic nerve (Lopes de Faria, Russ and Costa, 2002; Scott, Foote, Peat *et al.*, 1986). It may be expected that loss of axonal fibres would cause functional loss. This is confirmed by Zhang, Inoue, Dong *et al.* (1998, 2000) who noted deficits in retrograde axonal transport. Furthermore, animal studies using diabetic rats demonstrated a reduction in the ability to perform a task relying on hippocampal function and spatial memory with reductions in neurons in the hippocampus.

1.17.3 Theories regarding cell apoptosis

Several theories have been proposed to explain the increase of cell apoptosis in diabetes. King and Brownlee (1996) suggest hyperglycaemia, oxidative stress and advanced glycation end products may be responsible. Others propose that the role of insulin is to regulate glutamate processing in glial cells. A loss in the diabetic eye alters glutamate metabolism and transport, leading to an increase in extracellular glutamate (Zhu, Kum, Ho *et al.*, 1990; Aizenman and de Vellis, 1987). Insulin may also be regarded as having a role in the protection of retinal neurons, which when reduced in diabetes directly leads

to cell death (Barber, Antonetti and Gardner, 2000, Nakamura, Barber, Antonetti *et al.*, 2001).

1.17.4 Vascular endothelial growth factors (VEGF)

VEGF is elevated in diabetic retinopathy and leads to proliferation and increased vascular permeability by altering vascular endothelial tight junctions (Antonetti, Barber, Khin *et al.*, 1998, Antonetti, Barber, Hollinger *et al.*, 1999). There is evidence to show that glial and neuronal retinal cells produce this cytokine which may have a secondary effect on the blood retinal barrier. VEGF also facilitates survival of endothelial cells and neurons by way of a neuroprotective effect and encourages neovascularisation in hypoxic regions of tissues.

1.18 Structural changes in diabetes

1.18.1 Diabetes and retinal thickness

Diabetic retinopathy is characterised by ischaemia of the retinal tissue followed by new vessel formation and breakdown of the blood retinal barrier. Lobo and colleagues in a series of three studies have investigated alterations in retinal thickness and the blood retinal barrier. In their first study Lobo, Bernandes and Cunha-Vaz (2000) postulate that in preclinical diabetic retinopathy two types of increased retinal thickness may occur; one directly associated with a change of the blood retinal barrier (vasogenic) and a second type occurring in the absence of apparent breakdown (cytotoxic). In their investigation of type 2 diabetics (n=10) maps of retinal leakage and retinal thickness were aligned and integrated in the same image to correlate leakage with thickness. The majority of patients (n=6) demonstrated good coincidence between location of areas of increased retinal thickness and those of increased leakage. In the 4 remaining eyes however, no relationship was found between sites exhibiting retinal thickness and those with abnormal fluorescein leakage. Furthermore, areas of retinal thickness increase were observed without abnormal leakage being present. Zeimer, Blair and Cunha-Vaz (1983) suggest that this may be associated with an excitatory release of glutamate or lactic acidosis. Alternative theories proposed to explain the presence of oedema without

blood retinal barrier alteration include residual extracellular oedema from earlier areas of leakage, blood retinal barrier breakdown located away from the location of oedema, varying rates of fluid reabsorption at particular sites or tendencies of particular retinal areas to collect fluid (Lobo *et al.*, 2000).

In a subsequent study, Lobo, Bernandes, De Abreu *et al.* (2001) examined alterations of the blood retinal barrier and changes in macular retinal thickness in type 2 diabetics with mild non proliferative retinopathy over a twelve month period. Increases in retinal thickness varied in magnitude and position at each visit (baseline, 6 months and 12 months). A correlation was found between the locations of retinal thickness increases and that of fluorescein leaking sites as measured by the Retinal Leakage Analyser (RLA). The authors concluded that retinal oedema appears to be a consequence of retinal vascular leakage and is of an extracellular form which is associated with an alteration of the blood retinal barrier. Retinal vascular damage appears to be reversible and directly associated with variations in glycaemic metabolic control. No correlation was found between retinal thickness changes and variations in HbA1c levels or blood pressure variations.

Such findings were confirmed in a prospective 3 year follow-up study using multimodal imaging of the macular area in 14 eyes of 14 patients with type 2 diabetes and mild non proliferative diabetic retinopathy (Lobo, Bernandes, Figueira *et al.*, 2004).

Several studies report a strong correlation between retinopathy progression and high blood retinal barrier permeability as measured by vitreous fluorometry in type 2 diabetics (Cunha-Vaz, Gray, Zeimer *et al.*, 1985; Engler, Krogsaa and Lund-Andersen, 1991).

1.18.2 Diabetes and retinal nerve fibre layer thickness

Focal retinal nerve fibre layer defects in type 2 diabetic patients with no diabetic fundus changes have been reported (Chiara, Matsuoka, Ogura *et al.*, 1993; Bartz-Schmidt and Schmitz-Valckenberg, 1994). Retinal nerve fibre loss has also been reported in type 1 diabetic patients without retinopathy by Lopes de Faria *et al.* (2002) who, using

scanning laser polarimetry observed a significant reduction in the RNFL thickness of the superior polar quadrant of the retina in their type 1 diabetic patients compared to the aged-matched control group. The authors hypothesise that their findings may suggest that neurodegeneration may be an event in the pathogenesis of diabetic retinopathy. The apparent asymmetry of nerve fibre loss mirrors evidence that retinal changes such as microaneurysms are twice as common in the superior than in the inferior retina (Kern and Engerman, 1995).

1.18.3 Diabetic macular oedema

Diabetic macular oedema is one of the main causes of visual loss in diabetic patients (Klein, Klein, Moss *et al.*, 1984; Ferris and Patz, 1984). It is the result of the breakdown of the blood-retinal barrier leading to the accumulation of abnormal fluid in the retinal tissue and is defined as an increase in retinal volume and is manifest as an increase in retinal thickness. Traditional methods of examination, for example slit lamp biomicroscopy, fundus photography and fluorescein angiography, have a number of limitations in terms of resolution and lack of objectivity and reproducibility.

The incidence of diabetic macular oedema after 10 years of follow-up has been reported to be 20.1 % in type 1 diabetics, 13.9% in type 2 non-insulin diabetics and 25.4 % in type 2 insulin- dependent diabetics (Klein *et al.*, 1984).

The Early Treatment Diabetic Retinopathy Study Research (EDTRS) (1985) defined macular oedema as thickening of the retina and/or hard exudates within 1 disc diameter of the centre of the macula.

Clinically significant macular oedema is defined as one or more of the following:

1. Thickening of the retina at or within 500μm of the centre of the macula
2. Hard exudates at or within 500μm of the centre of the macula, associated with thickening of the adjacent retina
3. A zone or zones of retinal thickening one disc area or larger, any part of which is within one disc diameter of the centre of the macula

The retinal layer undergoes a number of changes in diabetic macular oedema including retinal swelling, serous retinal detachment and cystoid macular oedema (Otani, Kishi, Maruyama, 1999). The correlation between visual acuity and retinal thickness was independent of the different tomographic features. This correlates well with the findings of Kang, Park and Ham (2004).

Since laser photocoagulation is indicated in patients with clinically significant diabetic macular oedema, objective quantitative measurement of retinal thickness is essential in the clinical assessment of the diabetic patient (ETDRS, 1985, 1987, 1995). Technologies such as the retinal thickness analyzer and optical coherence tomography can play an important role in such assessments.

1.18.4 Clinical examination of macular oedema

Slit lamp biomicroscopy and fundus photography are both subjective techniques and are unable to identify the subtle changes of macular thickening or diffuse oedema. Shahidi *et al.* (1991) reported that retinal thickening using slit lamp biomicroscopy is detected only when it is more than 60% of normal retinal thickness and as such unlikely to detect mild or localised macular thickening. Hee *et al.* (1995b) suggest that slit lamp examination is unreliable in detecting an increase in central macular thickness less than 250μm.

Oedema formation is a variable process which is dependent on the balance between rate of leakage and the reabsorption of fluid by the retinal pigment epithelium. Leakage is not always accompanied by an appreciable fluid accumulation in the retina at the subclinical stage. Fluorescein angiography can identify localised blood-retinal barrier breakdown and subsequent leakage and therefore the site of possible oedema but is unable to measure the extent of fluid accumulation and subsequent retinal thickening. Nussenblatt, Kaufman, Palestine *et al.* (1987) describes the poor correlation between macular oedema and leakage detected by fluorescein angiography.

Optical Coherence Tomography (OCT) and the Retinal Thickness Analyzer (RTA) are quick, non invasive methods to obtain objective, quantitative measurements of retinal

thickness. A number of studies have been performed to determine whether clinical measurement of retinal thickness may be useful in the screening, and monitoring of diabetic patients. Hee *et al.* (1995b) using the OCT suggest that a foveal thickness of more than 185μm be regarded as abnormal. This finding is confirmed by Sanchez – Tocina *et al.* (2002) who suggest that a foveal thickness measure of more than 180μm should be regarded as abnormal macular thickening and recommend that careful follow up of such patients is performed. Goebel and Kretzchmar-Gross (2002) found a high correlation between foveal thickness and average thickness across the OCT scan and suggested that measurements of foveal thickness alone may be sufficient for clinically significant macular oedema screening.

A number of studies show that the criterion of CSMO is insufficient in identifying macular oedema (Yang, Cheng, Lee *et al.*, 2001). In the absence of detectable fluorescein leakage or CSMO the OCT is able to detect retinal changes (Hee *et al.*, 1998). Schaudig, Glaefke, Scholz *et al.* (2000) demonstrated the presence of significant diabetic macular thickening in the absence of CSMO using the OCT. A later study by Goebel and Kretzchmar-Gross (2002) using the OCT found the increase in retinal thickness in diabetic patients compared to normals was more marked than previous work. They found increased retinal thickness was more closely related to CSMO than with angiographically detectable leakage.

Such findings have two clear implications for the treatment of diabetic patients. Firstly, the routine use of OCT in the eye examination and earlier detection of macular thickening is likely to indicate earlier intervention of laser photocoagulation. Secondly, the fact that laser photocoagulation is not without side effects, namely the production of paracentral scotomas, should not be overlooked. Without the OCT to confirm clinical findings of suspected oedema, treatment may be unnecessary (Browning, McOwen, Bowen *et al.*, 2004).

The Early Treatment of Diabetic Retinopathy Study group demonstrated that focal or grid laser photocoagulation for CSMO reduced moderate visual loss by 50% (ETDRS, 1985) However, even with treatment, visual outcomes for retinal thickening as a result of cystoid macular oedema or diffuse macular oedema are poor. Early detection of macular thickening will contribute to a better outcome for the diabetic patient.

Hee *et al.* (1995b) report a close relationship between known histopathological characteristics of cystoid oedema and cross sectional tissue scans using the OCT. A study by Kang *et al.* (2004) reports a significant correlation between the features of OCT and fluorescein angiography in CSMO. Focal leakage observed using fluorescein angiography correlated closely with homogenous foveal thickening on OCT and diffuse or diffuse cystoid leakage correlated well with fluid collection, mainly in the outer retinal or subretinal space. The authors suggest that a greater understanding of anatomical and physiological characteristics of CSMO may be provided by the combination of fluorescein angiography and OCT data.

Recent studies report on the effectiveness of alternative treatment modalities such as vitrectomy. The OCT has also been used to evaluate the structure of the macula as a way of assessing the outcome of vitrectomy surgery to treat macular oedema (Otani and Kishi, 2000; Terasaki, Kojima, Niwa *et al.*, 2003). OCT investigations show good resolution of oedema following vitrectomy. Massin, Duguid, Erginay *et al.*, (2003) used the OCT to diagnose subtle vitreomacular traction, undetected by biomicroscopy. They found the OCT to be useful in providing accurate evaluations of macular thickness pre- and post-vitrectomy treatment for diffuse oedema.

A study by Weinberger *et al.* (1998) suggest that the RTA is a useful and sensitive tool for the diagnosis and follow up of diabetic macular oedema and in the assessment of laser treatment. Retinal thickness in diabetic patients without diabetic retinopathy was reported to be greater than normal subjects according to a study by Fritsche, van der Heijde, Suttorp-Schulten *et al.* (2002). They also found that mean foveal thickness was significantly greater than that of the normal group. Similarly, central macular thickness was reported as being significantly greater in eyes with diabetic retinopathy than in normal subjects, even in patients clinically diagnosed without CSMO according to ETDRS standards in a study by Oshima *et al.* (1999) using the RTA.

Several reports have indicated that macular thickness measures by the RTA and OCT are highly correlated (Neubauer, Priglinger, Ullrich *et al.*, 2001; Konno *et al.*, 2001; Polito, Shah, Haller *et al.*, 2002). Polito *et al.* (2002) suggest that the OCT, compared to the RTA, provides greater resolution, faster acquisition time and is unaffected by media opacities, while the advantage of the RTA is rapid scanning and the ability to provide an

overall contour map of the macula. Pires, Bernandes, Lobo *et al.* (2002) compared retinal thickness of eyes with mild nonproliferative retinopathy using the RTA and OCT. They concluded that the OCT is less sensitive that the RTA in detecting localised increases in the initial stages of diabetic retinal disease.

B-scan ultrasonography can be used as an alternative to optical coherence tomography and fluorescein angiography (FA) to assess macular thickening in patients who are unable to tolerate these techniques or who have media opacities, according to work by Lai, Stinnet and Jaffe (2003). The authors found good correlation between ultrasonographic detection of macular thickening and that of slit-lamp biomicroscopy, OCT and FA.

The correlation between visual acuity and macular oedema has been widely investigated. Nussenblat *et al.* (1987) reports a good correlation between macular oedema and visual acuity. Sanchez-Tocino *et al.* (2002) also found a correlation between best corrected visual acuity in normal and diabetic eyes. Similarly, Otani *et al.* (1999) report a correlation between retinal thickness and visual acuity in eyes with diabetic macula oedema with or without cystoid macular oedema. Oshima *et al.* (1999) report that central macular thickness is highly correlated with logarithmic converted visual acuity in diabetic macular oedema.

Frank, Schulz, Abe *et al.* (2004) demonstrated using optical coherence tomography, that macula oedema reduces in diabetic subjects over the course of the day. The authors attribute this to the change from the recumbent position to upright body position and suggest that their findings have a clear implication for the time of follow-up examinations of diabetic patients.

1.19 Functional changes in diabetes

Development of diabetic retinopathy and reduced visual acuity is often preceded by central vision abnormalities in diabetic eyes which may by exhibited as contrast sensitivity defects (Moloney and Drury, 1982; Della Salla *et al.*, 1985; Sokol *et al.*, 1985; Gharfour, Foulds, Allan *et al.*, 1982) or acquired hue colour vision defects

(Bresnick, Condit, Palta *et al.*, 1985; Roy, Gunkel and Podgor, 1986; Moloney and Drury, 1982).

Clinical studies have shown that there is often dissociation between contrast sensitivity scores and levels of visual acuity in patients with diseased eyes (Wolkstein, Atkin and Bodis-Wollner, 1980; Hyvarinen, Laurinen and Rovamo, 1983). In a study of the visual function of young Type 1 diabetics, Banford, North and Dolben *et al.* (1994) found no significant differences in visual acuity between subjects and the control group. No significant variation of visual acuity in individual diabetics was observed. However, significant differences between normals and diabetics were reported for colour vision and contrast sensitivity.

1.19.1 Contrast sensitivity

It is well established that eyes with diabetes mellitus have reduced contrast sensitivity (Arend, Remky, Evans *et al.*, 1997; Dosso, Bonvin, Morel *et al.*, 1996; Ismail and Whitaker, 1998; Sokol *et al.*, 1985; Verrotti, Lobefalo, Petitti *et al.*, 1998). Significant differences between contrast sensitivity thresholds as measured by the Pelli-Robson Test Chart for non diabetic retinopathy and background retinopathy subject groups have been demonstrated (Mackie and Walsh, 1998). However, the Pelli-Robson was unable to distinguish between normal subjects and those with no diabetic retinopathy, or between background and pre-proliferative retinopathy, pre-proliferative and treated proliferative retinopathy, or treated proliferative retinopathy and treated maculopathy. It is, therefore, not effective as a screening test for diabetic retinopathy. This is confirmed by Ismail and Whitaker (1998) who demonstrated that Pelli-Robson was able to distinguish between non diabetics and early diabetic subjects but lacked sensitivity in grading the degree of diabetic retinopathy.

Several explanations for contrast sensitivity reduction have been proposed including fluctuations in glucose levels (Verrotti *et al.*, 1998) perifoveal capillary dropout (Arend *et al.*, 1997), functional loss of retinal ganglion cell dendrites, secondary to retinal ischaemia (Regan and Neima, 1984) and progressive neuronal damage to the visual pathways from repeated hypoglycaemic episodes (Di Leo, Caputo, Falsini *et al.*, 1992).

Early studies demonstrated increased retinal blood flow rates in diabetics with diabetic retinopathy (Kohner, 1976) which was attributed to impaired autoregulation of blood flow (Sinclair, Graunwald, Riva *et al.*, 1982).

1.19.2 Colour vision

Many studies have reported colour vision defects in diabetes (Green, Ghafour, Allan *et al.*, 1985; Bresnick *et al.*, 1985; Trick, Burde, Gordon *et al.*, 1988; Roy, McCulloch, Hanna *et al.*, 1984). The Farnsworth-Munsell 100 Hue Test (Farnsworth, 1943) has been widely used to investigate the effect of diabetes on colour vision. Roth (1969) observed significantly increased error scores in diabetics compared with normal subjects with no correlation between age, sex, age of onset, duration of disease or metabolic control. Similarly, Moloney and Drury (1982) observed that 66% of diabetics in their study group (n=132) had significantly raised error scores. They found no correlation between score and age, duration of diabetes or degree of retinopathy. Early studies debated the question of which area of the spectrum was most affected in diabetes. While some authors suggested an indiscriminate loss of function (Trick *et al.*, 1988, Hardy, Lipton, Scase *et al.*, 1992; Kurtenbach, Wagner, Neu *et al.*, 1994) others observed a selective increase in error score along the blue-yellow colour axis (Lakowski, Aspinall and Kinneer, 1972; Moloney and Drury, 1982; Greenstein, Sarter, Hood *et al.*, 1990). Ismail and Whitaker (1998) suggest that differences in findings may be explained by the level of retinopathy exhibited by each subject in the different study sample groups. In their study they observed that selective blue-yellow defects became more apparent with increasing retinopathy.

1.19.3 Visual fields in diabetes

Short wavelength sensitive cone mediated mechanisms are specifically affected in retinal diseases that involve the inner retina (Greenstein, Hood, Ritch *et al.*, 1989; Nork, Wang and Poulson, 1994). Such findings form the basis of several reported functional studies of diabetic eyes (Nomura, Terasaki, Hirose *et al.*, 2000; Remky, Arend and Hendricks, 2000; Greenstein *et al.*, 1990; Greenstein, Shapiro, Zaidi *et al.*, 1992). Diabetic patients with and without diabetic retinopathy exhibit reduced sensitivity to

short wavelength stimuli and reduced hue discrimination (Greenstein *et al.*, 1990; Trick *et al.*, 1988; Utku and Atmaca, 1992; Kurtenbach *et al*, 1994).

Blue-on-yellow automated perimetry has been shown to be more sensitive in detecting early glaucomatous field loss than standard achromatic perimetry (Sample and Weinreb, 1990; Johnson *et al.*, 1993). In addition, short-wavelength sensitive (SWS) cone mediated mechanisms are reported to be susceptible to damage in diabetic retinopathy (Greenstein *et al.*, 1989; Greenstein *et al.*, 1990; Nomura *et al.*, 2000). SWAP perimetry, compared with conventional automated static threshold perimetry, has been shown to provide improved sensitivity for the psychophysical detection of clinically significant diabetic macular oedema (Hudson, Flanagan, Turner *et al.*, 1998). Furthermore, Remky *et al.* (2000) suggest that this technique may assist early detection of visual functional loss in early diabetic maculopathy and the prediction of early ischaemic macular damage.

A recent study involving Type 1 diabetics has shown that short wavelength sensitive cones are vulnerable to damage from hyperglycaemia (Afrashi, Erakgun, Kose *et al.*, 2003). The authors compared white-on-white perimetric parameters with blue-on-yellow perimetric parameters in a group of type 1 diabetic patients without diabetic retinopathy and visual acuity of 6/6 normal subjects. They found that achromatic visual indices (MD, SF, PSD and CPSD) were similar between the diabetic subjects and their control subjects. Blue-on-yellow SF, PSD and CPSD values were also similar between groups. However, the blue-on-yellow perimetry MD score was significantly different between groups ($p=0.001$). Afrashi *et al.* (2003) propose that blue-on-yellow perimetry is a useful method of detecting and monitoring early visual functional deficits in diabetic patients without retinopathy.

Realini, Lai and Barber (2004) investigated the impact of diabetes in glaucoma screening using frequency-doubling techniques. It reported abnormal field plots in diabetic patients, including some who exhibited no evidence of diabetic retinopathy and advised caution when interpreting field results in glaucoma screening as diabetes may be a source of "false-positive" test results.

1.20 Clinical investigation of diabetic macular oedema using the OCT

The OCT has been widely used to evaluate the pattern and severity of macular oedema in diabetic eyes and its correlates with visual function. In one of the earliest studies of the capability and clinical use of the OCT Hee *et al.* (1998) compared the macular retinal thickness of healthy volunteers, diabetic patients exhibiting diabetic retinopathy and diabetic patients with no ophthalmoscopic evidence of retinopathy. They observed that OCT was able to quantify the development and resolution of both foveal and extrafoveal macular thickening. Studies have shown that the OCT provides valuable information on the retinal morphological changes associated with macular oedema in the diabetic eye and in eyes with other pathologies for example, uveitis, and central retinal vein occlusion. A number of authors have devised classification systems for oedema based on OCT images to aid the clinical diagnosis and monitoring of treatment outcomes (Otani *et al.*, 1999; Panozzo, Parolini, Gusson *et al.*, 2004).

1.21 Functional magnetic resonance imaging (fMRI)

Functional MRI (fMRI) is a non invasive method for measuring haemodynamic responses to changes in neural activity in the brain. Broadly speaking, an increase in neural activity, leads to an increase in regional cerebral blood flow and a subsequent decrease in the local concentration of deoxygenated haemoglobin. This decrease results in a localised increase in the fMRI signal in the brain. fMRI signal intensity is correlated with localised changes in neural activity (Courtney and Ungerleider, 1997). fMRI is used to demonstrate activity in particular regions of the brain and neural systems in response to a subject performing simple motor and sensory tasks and complex tasks such as reading, memory or spatial visualisation. It is an invaluable tool both in the neuroclinical and surgical environment and more specifically in relation to this work as a method of investigating the topography and functional organization of the visual cortex.

During MRI investigation the subject is placed into a scanner which creates a strong homogenous magnetic field with which all atomic nuclei (neutrons and protons) in the body are aligned. A second magnetic field is briefly applied along an orthogonal path

to the original field causing some of the protons to align perpendicular to the original field, giving rise to a voltage in the receiver coil, the magnitude of which is the MRI signal. When the second magnetic field is switched off the protons return to their original position. The rate at which this occurs is described by the longitudinal and transverse relaxation, the latter of which is utilised in fMRI. Different tissues within the brain exhibit different transverse relaxation rates and therefore produce different MRI signal intensity. This phenomenon forms the basis of MRI contrast (Cohen and Bookheimer, 1994; Yarmish and Lipton, 2003).

Neuronal activity in the brain is observed indirectly through the changes in blood flow, blood volume and oxygenation which it creates. The most common fMRI technique detects variations in the concentration of deoxy-haemoglobin (Ogawa, Tank, Menon *et al.*, 1992) and is referred to as blood oxygen level dependent (BOLD) contrast. Haemoglobin exhibits different magnetic states according to its oxygenation. The BOLD effect represents alteration in the ratio of deoxygenated to oxygenated haemoglobin within the tissue of the brain which gives rise to changes in MRI signal intensity.

CHAPTER 2: Research rationale

There is evidence that reductions in retinal nerve fibre layer thickness may precede pathological changes to the structure of the optic nerve head (Sommer *et al.*, 1977) while visual field defects are preceded by changes of the optic nerve head or loss of the RNFL (Sommer *et al.* 1991; Tuulonen *et al.*, 1992). The ability to quantify such anatomical changes is essential. In order to diagnose and monitor disease it is important to have diagnostic tools that are reliable in terms of their repeatability and reproducibility and for which confounding variables are understood. A clear understanding of the normal physiological changes in morphology, especially those known to be associated with age and acute changes such as diurnal variation is also essential. Finally, it is important to be able to relate known functional losses of vision with morphological changes in the visual pathway. This thesis addresses some of these issues.

2.1 Research aims

There were three principal aims to this thesis:

1. To identify the repeatability and reproducibility of the new Stratus OCT (OCT3 Model 3000).
2. To investigate the effects of axial length and age in normal healthy eyes
3. To investigate the effects of disease, particularly glaucoma and diabetes on the structural and functional performance of the visual pathway.

2.2 Repeatability and reproducibility of the Stratus OCT

For any imaging technique to be effective in identifying and monitoring pathological change over time, it is important that acquired measures are repeatable and reproducible. Studies have reported that the OCT version 1 and 2 provides repeatable

measurements within and between visit for normal and diseased eyes (Baumann *et al.*, 1998; Koozekanani *et al.*, 2000; Massin *et al.*, 2001; Muscat *et al.*, 2002).

The Stratus OCT (OCT 3) has been subject to a series of upgrades to provide a wider choice of scan types, shorter acquisition time and higher image resolution. The within-visit repeatability and between-visit reproducibility of this instrument in normal subjects has been investigated (Gurses-Ozden *et al.*, 2004; Paunescu *et al.*, 2004) but to our knowledge no studies have investigated the repeatability of measures of diseased eyes. The aim of this study was to investigate the repeatability and reproducibility of macular retinal thickness measures and optic nerve head measurements using the Stratus OCT. The subject sample comprised 20 normal healthy eyes, 20 eyes with diabetic maculopathy and 20 glaucomatous eyes.

2.3 Relationship between axial length and retinal thickness and retinal nerve fibre layer thickness

Identifying pathological change in the eye is inherently difficult due to physiological variations in normal eyes. In order to identify changes associated with disease it is imperative that the diverse physiological traits of the normal healthy eye are understood.

Increased axial length in myopic eyes may be associated with scleral thinning and possibly a related stretching and subsequent reduction in retinal and retinal nerve fibre layer thickness. To date, studies investigating the effect of myopia on retinal and retinal nerve fibre layer tissue have produced inconsistent results. While some authors report no relationship between axial length and retinal thickness (Garcia-Valenzuela *et al.*, 2000; Gobel and Hartmann, 2001; Wakatani *et al.*, 2003), a relationship between macular retinal thickness and degrees of myopia has been reported by Mrugacz and Bakunocicz-Lazarczyk (2005).

The aim of this study was to investigate the relationship between axial length and retinal thickness and retinal nerve fibre layer thickness and more specifically to assess the possibility of retinal thickness and retinal nerve fibre layer thickness being reduced in normal healthy eyes with greater axial length. Macular retinal thickness measurements

through the fovea were acquired for 66 eyes of 66 normal subjects. Retinal nerve fibre layer thickness measurements around the optic nerve head were acquired for 64 eyes of 64 normal subjects.

2.4 The effect of age on retinal thickness and retinal nerve fibre layer thickness

It is necessary to establish whether observed alterations in tissue thickness are due to either disease alone or the result of physiological change before accurate and reliable long term monitoring of pathological retinal changes due to glaucoma for example, can take place. There is some evidence to suggest that retinal and nerve fibre tissue may be affected by age, however results are largely inconsistent. Reduced retinal thickness with increasing age has been reported by several authors (Baquero Aranda, Morillo Sanchez and Garcia Campos, 2005; Kanai, Abe, Murayama *et al.*, 2002; Alamouti and Funk, 2003; Tewari, Wagh, Sony *et al.*, 2004) while others found no such effect (Oshima *et al.*, 1999). Several studies describe a reduction in retinal nerve fibre layer thickness with increasing age (Poinoosawmy *et al.*, 1997; Funaki *et al.*, 1999; Mok *et al.*, 2002; Kanamori *et al.*, 2003; Sony, Sihota, Tewari *et al.*, 2004).

The aim of this study was to determine the ability of the Stratus OCT3 to measure the effects of age on retinal tissue. The study consisted of 2 parts: firstly to determine the effects of age on retinal thickness and secondly on retinal nerve fibre layer thickness. For the retinal macular thickness study, the subject sample consisted of 120 normal healthy volunteers, subdivided according to age (under 40 years of age and over 40 years of age). The second part of the study investigated the effects of age on retinal nerve fibre layer thickness around the optic nerve head at different eccentricities for a subject sample of 115 normal healthy volunteers, subdivided according to age (under 40 years of age and over 40 years of age).

2.5 Nerve fibre loss in glaucomatous optic neuropathy

Glaucoma is a disease that is characterised by a loss of retinal ganglion cells and their axons and subsequent decrease in the retinal nerve fibre layer. Studies have shown a

reduction in nerve fibre layer thickness can precede visual field defects (Quigley, Addicks *et al.*, 1982; Quigley *et al.*, 1989; Sommer *et al.*, 1991). Optical coherence tomography (OCT) has been shown to be an objective and reliable method of providing quantitative measurements of retinal nerve fibre layer thickness (Huang *et al.*, 1991; Schuman *et al.*, 1995; Schuman *et al.*, 1996; Blumenthal *et al.*, 2000; Carpineto *et al.*, 2003) and as such has the potential to identify early and long term changes in glaucoma. The OCT has previously been widely used to investigate the effects of glaucoma on the retinal nerve fibre layer (Schuman *et al.*, 1995; Bowd et *al.*, 2000; Kanamori *et al.*, 2003; Nouri-Mahdavi *et al.*, 2004; Leung, Chan, Yung *et al.*, 2005). The majority of studies have identified changes of the nerve fibre layer around the optic nerve head at one particular location, (usually at the default setting of the instrument). However, little has been reported on the effects of glaucomatous eye disease with increasing distance from the optic disc margin.

The aim of this study was to determine the rate of reduction in retinal nerve fibre layer thickness with eccentricity from the optic nerve head in normal subjects and glaucoma patients in order to identify the most appropriate imaging protocol for the detection of glaucomatous nerve fibre loss. The subject sample consists of one eye each of 40 normal subjects and 40 glaucoma patients.

2.6 Short term relationship between blood glucose levels, retinal thickness, retinal nerve fibre layer thickness and visual function

Changes in the visual function of diabetic patients have been well documented in the literature and according to patients' subjective experience. Deficits in contrast sensitivity (Arend *et al.*, 1997; Dosso *et al.*, 1996; Ismail and Whitaker, 1998; Sokol *et al.*, 1985; Verrotti *et al.*, 1998), colour vision (Green *et al.*, 1985; Bresnick *et al.*, 1985; Trick *et al.*, 1988; Roy *et al.*, 1984 and SWAP fields (Greenstein *et al.*, 1989; Greenstein *et al.*, 1990; Nomura *et al.*, 2000) are widely reported in diabetic patients compared to normal subjects. Structural changes in retinal anatomy due to diabetic eye disease, for example macular oedema, are consistently observed both in the clinical setting and in experimental studies. Optical coherence tomography has been used in several studies to quantify changes in retinal thickness and retinal nerve fibre layer

thickness of diabetic patients (Lobo *et al.*, 2000, 2001, 2004; Lopes de Faria *et al.*, 2002).

To date, the majority of experimental studies investigating the effect of blood glucose on the diabetic eye have investigated visual performance by chemically inducing changes to blood glucose levels of diabetic patients, and either fixing glucose levels at different levels (Hardy, Scase, Foster *et al.*, 1995) or comparing visual function at the highest and lowest glucose levels (Volbrecht, Schneck, Adams *et al.*, 1994). To our knowledge, no study has investigated the impact of acute changes in glucose control on ocular anatomy or visual function. Such a study has the potential to offer explanations for the variation in vision reported throughout the day of the typical diabetic patient.

The aim of this study was to determine the short term impact of fluctuations in blood glucose levels on retinal structure and function over a 12 hour acute period in patients with diabetes. The subject sample consisted of 20 type 1 diabetic patients and 21 Type 2 diabetic patients. A battery of visual function and ocular imaging tests were carried out at 2 hourly intervals for each of the diabetic patients whilst normal routines of medication, food and drink intake and exercise were maintained.

2.7 Anatomical and functional changes in the visual cortex of patients with glaucoma

There is evidence of a wide variation in the size of the components of the visual pathway of normal subjects and furthermore, that a dimensional relationship exists between the components of the visual pathway i.e. a large visual cortex is associated with a large LGN and optic tract and vice versa (Andrews, Halpern and Purves, 1997). These variations must be considered before making decisions about the effects of disease. Studies suggest that glaucomatous damage affects each component of the visual pathway from the retinal ganglion cells in the eye, retinal nerve fibre layer, along the visual pathway including the lateral geniculate nucleus to the primary visual cortex.

This study will investigate the relationship between visual function, cortical responses, and anatomy of the visual pathway in normal and diseased eyes. The subject sample

consisted of 6 normal healthy subjects and 4 patients previously diagnosed with primary open angle glaucoma (POAG).

CHAPTER 3: Repeatability and Reproducibility of macular thickness measurements using Optical Coherence Tomography (Stratus OCT 3) in normals and diabetics

3.1 Abstract

Purpose: Optical coherence tomography is a technique recommended for use in the diagnosis and monitoring of ocular disease. While previous models (OCT1 and 2000) have demonstrated both good repeatability and reproducibility, little has been reported for the Stratus OCT. The purpose of this study was therefore to determine the within-visit repeatability and between-visit reproducibility of macular thickness measurements using the Stratus OCT (OCT3 Model 3000, Carl-Zeiss Meditec, Dublin, CA) in normal subjects and diabetic patients.

Methods: Macular thickness measurements were obtained at each of two visits using multiple radial line scans, 6mm in length, centred through the fixation point of 20 normal control subjects (58.9±13.1 years; range 41-74 years) and 20 diabetic patients diagnosed with early diabetic maculopathy (60.1±9.4 years; range 40-73years). Retinal thickness analysis software (version 3.0) was used to produce a circular map comprising 9 sectors depicting average retinal thickness. Coefficient of repeatability (CoR 1) and coefficient of variation (CoV) were used to determine the repeatability of measures within visit, while coefficient of reproducibility (CoR 2) and intraclass correlation coefficients (ICC) were used to determine the reproducibility of measures between visits.

Results: The within-visit CoV was 1.64% for normal subjects and 1.58% for diabetic patients. The CoR (1) was 1.64±0.39% for normal subjects and 1.58±0.29% for diabetic patients. The between-visit CoR (2) was 2.87±1.12% for normal subjects and 2.6±1.33% for diabetic patients. For normal subjects ICC's for between-visit reproducibility ranged from 77% to 97% (mean 91%). For diabetic patients, ICC's ranged from 67% to 98% (mean 91%)

Conclusion: Measurements of macular thickness made with the Stratus OCT are highly repeatable and reproducible for both normal subjects and diabetic patients suggesting that the technology is of value in the diagnosis and monitoring of macula disease.

3.2 Introduction

The OCT offers a non invasive imaging technique to assess retinal and nerve fibre layer thickness, providing potential clinical applications in the diagnosis and monitoring of diseases of the retina. For an imaging method to be effective, measures must be repeatable and reproducible, in order that any deviation from normality or change over time can be detected over and above the normal measurement variability.

Several studies have investigated the repeatability and reproducibility of measurements of the macula and optic nerve head taken with early models of the OCT using a variety of experimental designs and statistical methods. Although this imaging modality has undergone a series of hardware and software improvements since its introduction in the early 1990s, the OCT has exhibited good repeatability and reproducibility at all stages of development. For example, one of the earliest prototype systems showed repeatable measures of retinal macular thickness measures during a single visit (Baumann *et al.*, 1998) while several studies have confirmed that the within-visit repeatability and between-visit reproducibility of macular thickness measurement of normal subjects using the OCT 1 and OCT 2000 is high (Koozekanani *et al.*, 2000; Massin *et al.*, 2001; Muscat *et al.*, 2002). Of more clinical relevance is the ability of the OCT to reliably measure retinal thickness in diseased eyes. Repeatable measures of retinal thickness in eyes with clinically significant oedema due to diabetic eye disease have also been observed (Massin *et al.*, 2001) while OCT measures have been found to be accurate and reliable even with degraded signal strength (Muscat *et al.*, 2002).

The most recent version of the OCT is the Stratus OCT 3 (model 3000) which offers a greater choice of scanning protocols and provides increased image resolution. There are few studies that have investigated the repeatability and reproducibility of this third generation instrument in normal subjects (Gurses-Ozden *et al.*, 2004; Paunescu *et al.*, 2004) and to our knowledge none have investigated the repeatability of macular retinal thickness measures in diseased eyes. This study investigates the properties of the Stratus OCT in both healthy and diseased eyes.

3.3 Aim and objectives

To determine the number of images required to achieve repeatable and reproducible data and to assess the within-visit repeatability and between-visit reproducibility of macular thickness measurements using the new Stratus OCT (OCT3 model 3000) instrument in normal subjects and diabetic patients.

3.3.1 Hypothesis

Stratus OCT provides repeatable and reproducible measurements of retinal thickness at the macula of normal and diabetic eyes.

3.4 Study sample and investigations

3.4.1 Inclusion Criteria

All subjects and patients were subjected to a clinical eye examination to assess their fitness to participate in the study based on the following criteria.

3.4.2 Normal group

Normal healthy subjects were recruited from attendees at the optometry clinic at Aston University and from staff at Birmingham Heartlands Hospital Ophthalmology Department. A full eye examination was performed by an optometrist (HLW) to establish whether the study inclusion criteria were met. Subjects were included if they exhibited:

- No abnormalities on ophthalmoscopic examination
- Minimal or no lens opacities allowing a clear fundus view
- No history or evidence of intraocular surgery or laser therapy
- No history or evidence of retinal pathology or glaucoma
- Snellen visual acuity (VA) 6/6 or better
- Less than 6 dioptres of spherical ametropia and 2 dioptres of astigmatism

- Absence of visual field defects (Humphrey Visual Field Analyser program 24-2)
- Intraocular pressure (IOP) less than 21mmHg (non contact tonometry- Pulsair 3000)

3.4.3 Diabetic group

Diabetic patients were recruited from the Ophthalmology Department of Birmingham Heartlands Hospital Diabetic Clinic and were included if they had type 1 or type 2 diabetes and evidence of diabetic macular changes. A full ocular examination was carried out by a collaborating ophthalmologist (JMG) using slit lamp indirect ophthalmoscopy (Volk lens) to establish the presence of diabetic maculopathy. Diabetic maculopathy was classified as those diabetic retinopathic changes occuring in the macular area and included macular oedema, dot and blot haemorrhages, exudates and cotton wool spots.

Following confirmation of diabetic maculopathy, patients were only included if they exhibited:

- Snellen visual acuity (VA) 6/12 or better
- Minimal or no lens opacities allowing a clear fundus view
- No history or evidence of intraocular surgery or laser therapy
- No history or evidence of retinal pathology other than diabetic maculopathy
- Less than 6 dioptres of spherical ametropia and 2 dioptres of astigmatism
- Absence of visual field defects (Humphrey Visual Field Analyser program 24-2)
- Intraocular pressure (IOP) less than 21mmHg (non contact tonometry- Pulsair 3000)

3.4.4 Subject sample statistics

The subject sample consisted of 20 normal healthy volunteers and 20 diabetic patients previously diagnosed with mild diabetic maculopathy by collaborating ophthalmologists. Details of the subject sample are given in table 3.1.

	Gender		Test eye		Mean Age ± SD (range)
Subject Group	Male	Female	Right	Left	
Normal (n=20)	10	10	10	10	58.9±13.1 years (41-74)
Diabetic (n=20)	10	10	10	10	60.1± 9.4 years (40-73)

Table 3.1 Summary of the subject sample

3.4.5 Ethical approval and informed consent

Ethical approval was obtained from the ethical committee boards of Birmingham Heartlands and Solihull NHS Trust and Aston University. Approval conformed to the tenets of the Declaration of Helsinki. Written informed consent was obtained from all subjects and patients.

3.5 Methods

Subjects were required to attend the Heartlands Hospital Ophthalmology Clinic on two occasions. At visit 1 screening of all patients was conducted as per the requirements set and listed above. Pupil dilation was performed to allow a clear view of the fundus for assessing diabetic maculopathy and for ease of OCT scanning. One drop of 0.5% tropicamide was instilled into the test eye. After 20 minutes full mydriasis was confirmed by the pupillary light reflex. The first set of OCT scans was performed for within-visit analysis.

OCT scans were repeated at visit 2, within a fortnight of the patient's first visit. In order to mimic a realistic follow up clinic visit it was not necessary to rebook the patient at the same time as their first.

3.5.1 Macular thickness measurements: Optical coherence tomography

The Stratus OCT (OCT 3) projects a broad bandwidth near-infrared light beam of 820nm wavelength from a super luminescent diode onto the retina. Echo time delays of

light reflected from a reference mirror at known distance are compared with that reflected from the retinal tissue. Interference occurs when these light rays are combined by the OCT 3 interferometer and the photodetector measures this interference. (For a detailed description of the OCT see section 1.13).

Prior to image acquisition, subject details were entered into the database of the OCT. The subjects were instructed to place their chin on the chin rest and forehead against the top bar and instructed to fixate on a green target within the centre of the camera. To optimise the scan image and yield the strongest scan signal, both the Z-offset (axial range) and polarisation was adjusted. Fixating on the central green target during the scanning process in both visits 1 and 2 ensured that the radial line scan passed directly through the fovea. No adjustment to the scan position was required on either occasion.

The fast macular thickness protocol was carried out to obtain macular thickness measurements for all subjects. The macular scans consist of six radial line scans (6mm in length) arranged in a spoke-like pattern centred on the fovea with each radial scan spaced 30 degrees from each other as shown in figure 3.1. Each radial line scan contains 128 A-scans taken in a single session of 1.92 seconds. OCT software calculates retinal thickness as the distance between the vitreoretinal surface and the junction between the inner and outer segment of photoreceptors located just above the retinal pigment epithelium. This fast protocol scan compresses the six radial line scans into one scan and uses interpolation to fill the gaps between scans. Retinal thickness analysis produces a circular map of average retinal thickness which is divided using concentric circles into three zones fovea, inner macula and outer macula and further divided into quadrants to produce nine locations across the scan 1 being the fovea, 2-5 inner macula and 6-9 outer macula (representing the 9 Early Treatment Diabetic Retinopathy (EDTRS) areas. In this study the map circle default diameters of 1, 3 and 6mm were used to divide the macular thickness map as shown in figure 3.2. The map is displayed as a false colour image in which retinal thickness at each point is represented by a different colour. Thicker macular sections are shown by red and white shading while thin areas are seen as blue and black. Intermediate thickness locations are indicated by green and yellow shading.

a)

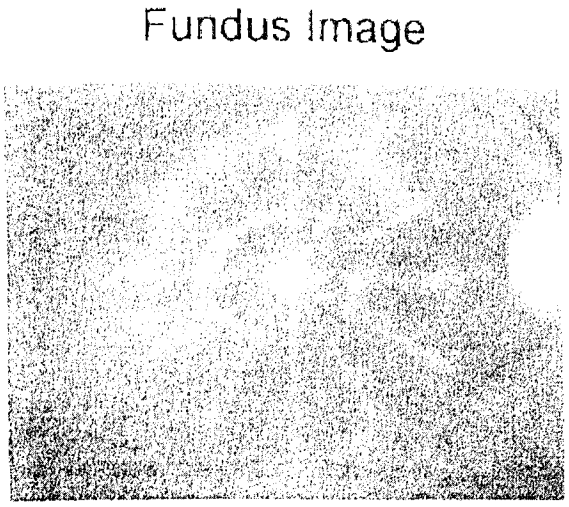

b)

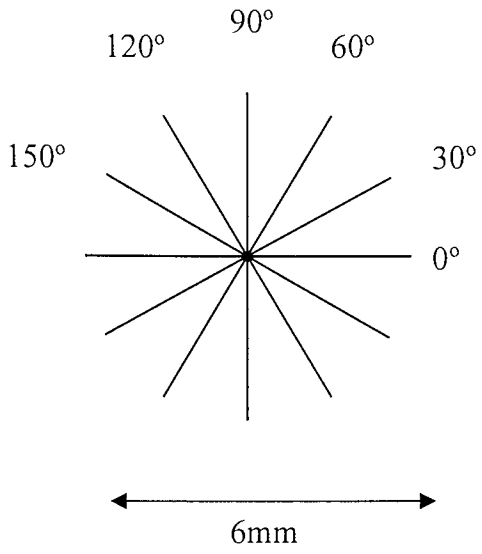

Figure 3.1 a) Example of a fundus image produced during OCT scan macular scan acquisition b) Schematic diagram of fast macular thickness scan, centred through the fovea.

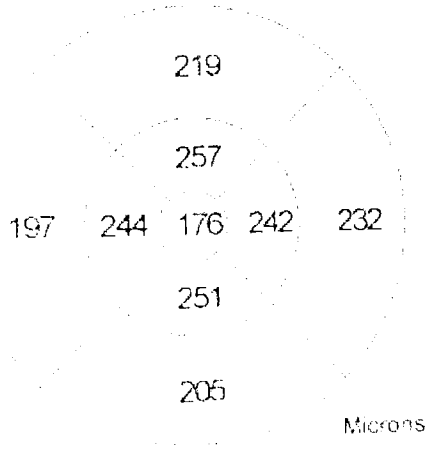

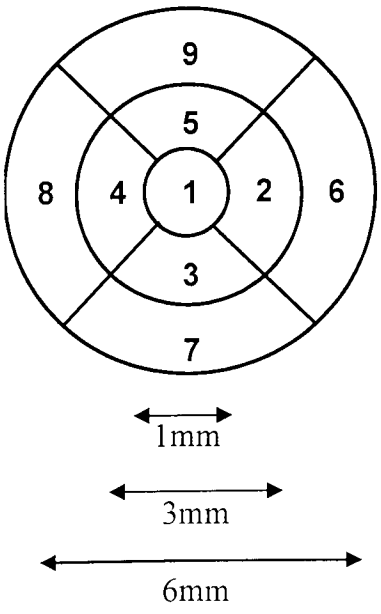

Figure 3.2 a) Example of retinal thickness map produced by OCT software b) Schematic illustration of retinal thickness map showing retinal positions

In total, 12 macular thickness scans were acquired for each patient. Following inspection of retinal map output by the OCT software, scans were rejected if it was obvious that the patient had lost fixation and/or if signal strength (polarisation) was poor. On occasions, the scan could not be analysed due to poor scan data. Erroneous results were produced if the inner or outer retina was not identified correctly by the OCT software and these scans were rejected. Although all steps were made to ensure this was avoided, if the Z offset (axial range) was incorrect the lower or upper part of the scan was missing and the scan was rejected.

Each of the macular thickness measurements in retinal positions 1-9 across the scan were evaluated in this study.

3.5.2 OCT software

All data acquisition and image processing was with OCT software version 3.0.

3.6 Statistical analysis

All statistical analyses were performed using SPSS version 11.5 for Windows. To allow comparison with other studies a variety of statistical tests were performed to assess repeatability and reproducibility.

3.6.1 Differences between groups

An independent samples *t*-test was performed to assess whether the groups differed significantly in terms of their age.

3.6.2 Number of images

12 macular thickness scans were taken in total. Of these, 10 scans were chosen on the basis of a good image quality indicated by the percentage of A-scans, lack of artefacts and good patient fixation as indicated by the foveal pit being centred within the central

1mm retinal map of the output analysis. Before analysis took place the minimum number of scans required per visit for the normal and the diabetic patients was calculated. For each of the nine locations the standard deviation of 2,3,4,5,6,7,8,9 and 10 images was plotted against the number of images and the point at which the graph plateaus was identified. It is assumed that from this point on, any extra images provide no additional information. Statistical analysis was performed on the basis of this finding.

3.6.3 Repeatability within-visit

According to definitions adopted by the British Standards Institution (BSI, 1994) repeatability conditions are those where independent test results are obtained by the same operator and on the same set of equipment, with the shortest time lapse possible between successive sets of readings.

For each retinal macular location (1-9) the coefficient of repeatability (CoR 1) and coefficient of variation (CoV) were used to determine the repeatability of macular thickness measures within-visit where:

- Coefficient of Variation (CoV) is defined as the standard deviation divided by the mean (usually expressed as a %)
- Standard Deviation (SD) is the average deviation from the mean for a number of observations.
- Coefficient of Repeatability (CoR 1) as recommended by Bland and Altman (1986) (who based their definitions on the recommendations of the British Standards Institution) is defined as the SD of the difference of each measurement from the mean of repeated measurements, divided by the average response (usually expressed as a % (Muscat *et al.*, 2002)).

3.6.4 Reproducibility between-visit

Reproducibility conditions are those where sets of readings are obtained using the same method but on different occasions (BSI, 1994).

For each retinal macular location (1-9) the coefficient of reproducibility (CoR 2) and intraclass correlation coefficient (ICC) were used to determine the reproducibility of macular thickness measures between visits where:

- Coefficient of Reproducibility (CoR 2) is defined as the SD of the differences between pairs of measurements obtained during different sessions, divided by the average of the means of each pair of readings (usually expressed as a % (Muscat *et al.*, 2002)).
- The intraclass correlation (ICC) was determined using the following formula taken from ANOVA:

  ICC = (Within variance – between variance)
  (Within variance + between variance)

  or:

  $$r_I = \frac{mSS_B - SS_T}{(m-1)SS_T}$$

  where:
  rl = ICC (finally expressed as a percentage)
  m = the number of observations per subject
  SS_T = Total sums of squares
  SS_B = Sums of squares between subjects

Equation 1.1

(Bland and Altman, 1996)

The ICC was determined by entering subject data into a statistical software package (Statistica). The total sums of squares and the sums of squares between subjects calculated during ANOVA were used to determine the ICC.

A paired samples *t*-test was conducted to evaluate the reproducibility of retinal thickness measurements between visit 1 and visit 2 for normal subjects and diabetic patients.

3.7 Results

3.7.1 Actual macular retinal thickness values for normal subjects and diabetic patients

Table 3.2 shows the actual mean ±SD retinal thickness values for each location across the macular scan for both groups and both visits.

	Normal group Retinal thickness values (microns)		Diabetic group Retinal thickness values (microns)	
Retinal location	Visit 1	Visit 2	Visit 1	Visit 2
Position 1	219.51 ± 21.43	216.04 ± 21.04	224.34 ± 27.30	226.42 ± 27.79
Position 2	281.46 ± 21.00	279.46 ± 22.34	276.18 ± 19.26	277.44 ± 18.30
Position 3	282.66 ± 15.03	281.29 ± 14.89	271.99 ± 19.04	274.08 ± 19.18
Position 4	270.89 ± 17.93	270.02 ± 16.95	265.56 ± 19.04	267.93 ± 17.69
Position 5	282.05 ± 23.12	280.46 ± 21.05	276.82 ± 17.60	277.99 ± 17.54
Position 6	269.39 ± 21.01	268.36 ± 19.88	263.42 ± 15.77	262.19 ± 14.19
Position 7	245.92 ± 17.92	243.50 ± 15.93	238.23 ± 15.63	239.50 ± 15.56
Position 8	234.15 ± 17.10	234.36 ± 15.18	230.08 ± 23.07	231.84 ± 20.94
Position 9	248.93 ± 21.07	246.56 ± 17.56	243.24 ± 14.50	244.83 ± 14.55
MeanRT	259.44 ± 17.93	257.78 ± 16.32	254.43 ± 14.45	255.80 ± 14.01

Table 3.2 Table showing the actual mean (± SD) retinal thickness values for each group at each visit.

An independent samples *t*-test was conducted to compare retinal thickness values for the normal and diabetic group at each visit for each retinal location. In terms of their actual retinal thickness values the groups did not differ significantly for either visit nor in any location ($p>0.05$).

3.7.2 Differences between groups

The groups did not differ significantly in terms of age according to an independent samples *t*-test ($p>0.05$).

3.7.3 Number of images

For each retinal location the mean standard deviation of 2,3,4,5,6,7,8,9,10 scans was calculated and plotted as a function of the number of scans as shown in figure 3.3. The asymptote of each curve was identified to provide guidelines as to the minimum number of scans required for the practical acquisition of reliable measurements.

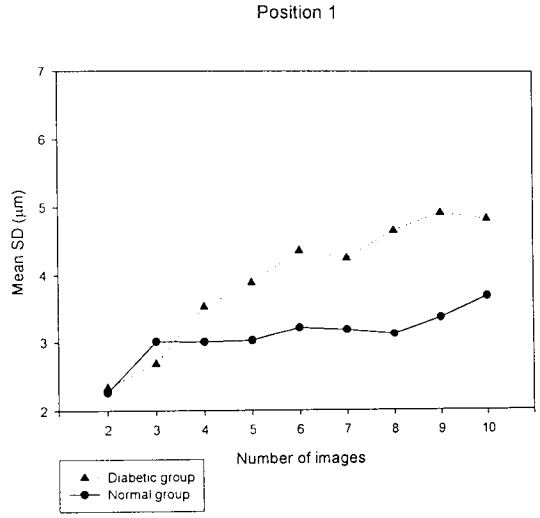

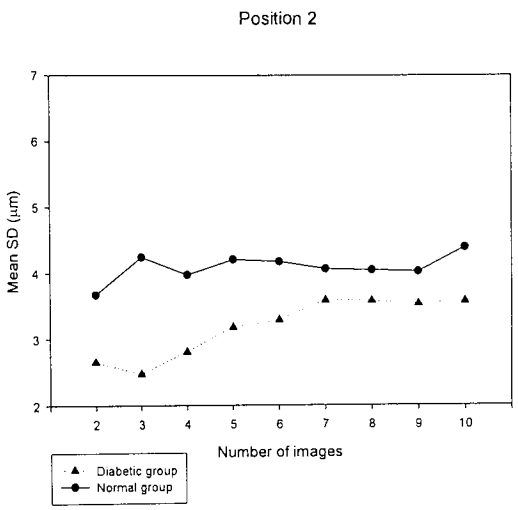

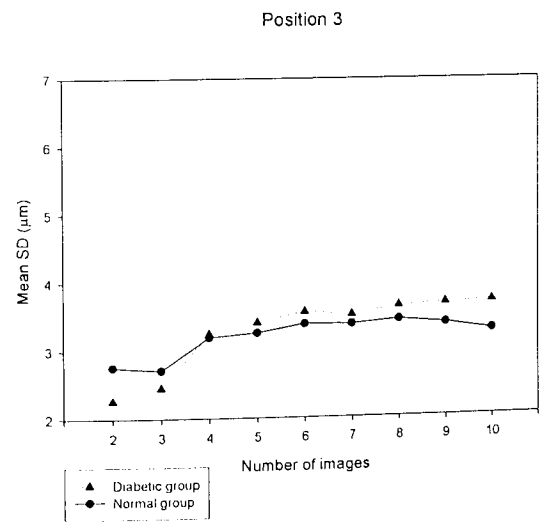

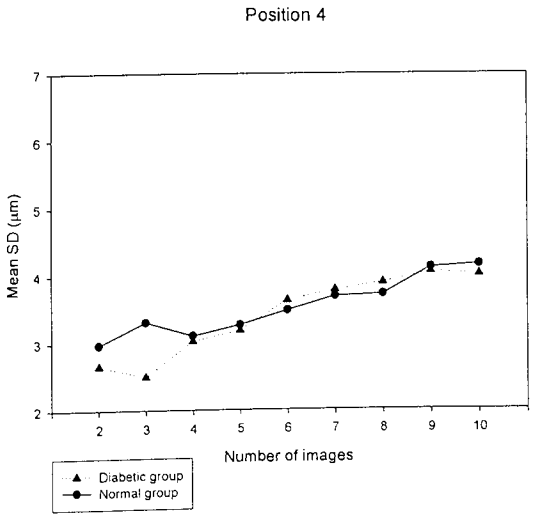

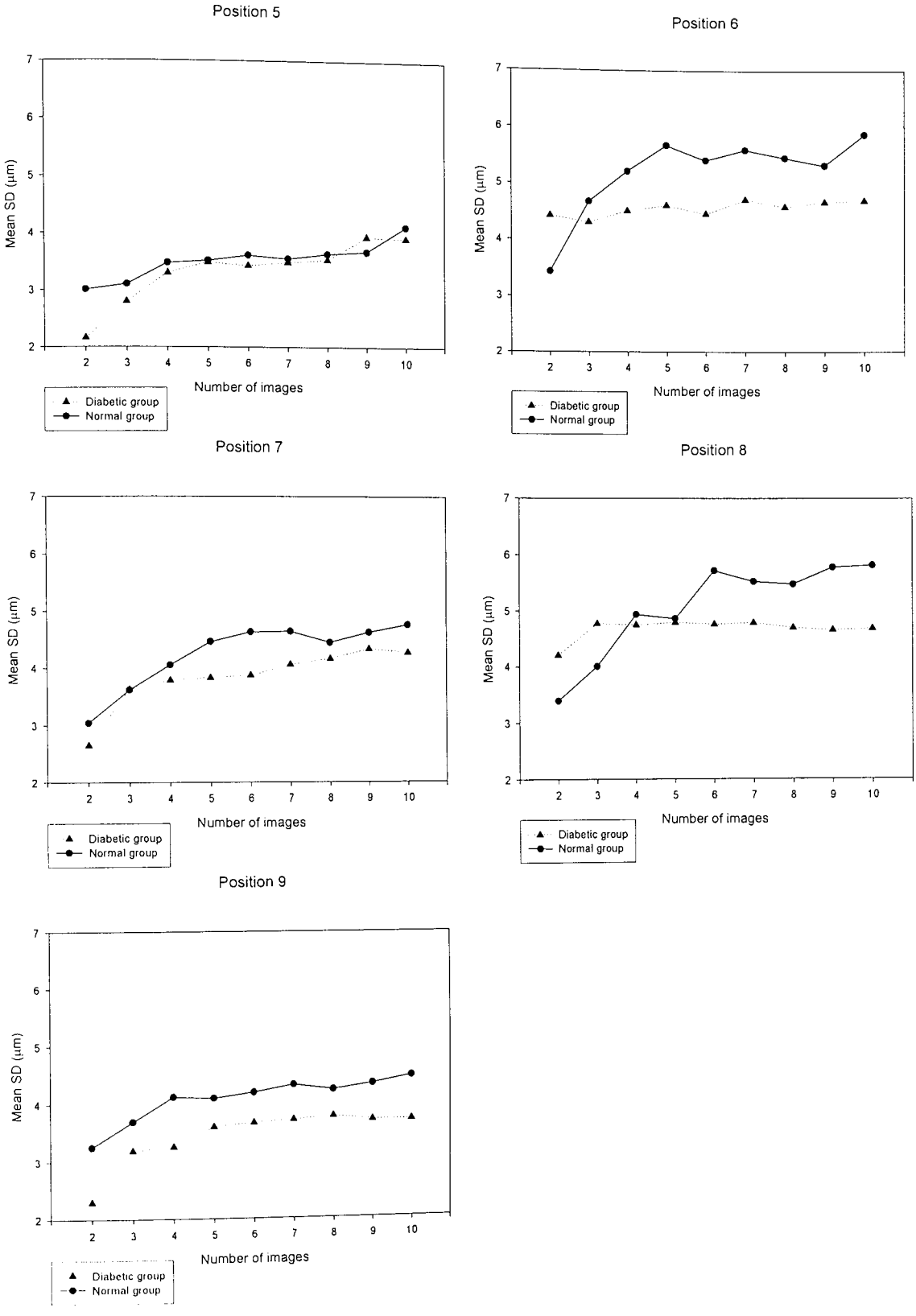

Figure 3.3 Graph showing group mean change in Mean SD for each retinal location 1-9 as a function of the number of scans for normal and diabetic subjects.

3.7.4 Repeatability (within-visit) of macular thickness measurements

As table 3.3 shows, the mean within-visit CoV was 1.64% for normal subjects and 1.58% for diabetic patients. The CoR (1) was 1.64±0.39% for normal subjects and 1.58±0.29% for diabetic patients.

	Normals		Diabetics	
Retinal location	CoV (%)	CoR 1 (%)	CoV (%)	CoR 1 (%)
1	1.45	1.45	1.89	1.89
2	1.44	1.44	1.30	1.30
3	1.19	1.19	1.29	1.29
4	1.36	1.36	1.42	1.42
5	1.26	1.26	1.26	1.26
6	2.08	2.08	1.79	1.79
7	1.89	1.89	1.70	1.70
8	2.36	2.36	2.08	2.08
9	1.73	1.73	1.53	1.53
Mean	1.64±0.39	1.64±0.39	1.58±0.29	1.58±0.29

Table 3.3 Summary of repeatability (within-visit) results for normal and diabetic group

Normal group

The CoV ranges from 1.19% to 2.36% (mean 1.64±0.39%) and CoR ranges from 1.19% to 2.36% (mean 1.64±0.39%) indicating highly repeatable macular thickness measures in all retinal locations. CoV and CoR varies little over each location.

Diabetic group

The CoV ranges from 1.26% to 2.08% (mean 1.58±0.29%) and CoR ranges from 1.26% to 2.08% (mean 1.58±0.29%) indicating highly repeatable macular thickness measures in all retinal locations. CoV and CoR varies little over each location.

3.7.5 Reproducibility (between-visit) of macular thickness measurements

Reproducibility results for each location of the macular scan are summarised in table 3.4. The mean between-visit CoR (2) was 2.87±1.12% for normal subjects and 2.60 ±1.33% for diabetic patients. Mean ICC was 91% for normal subjects and 91% for diabetic patients.

	Normals		Diabetics	
Retinal location	ICC (%)	CoR 2(%)	ICC (%)	CoR 2 (%)
1	91	3.86	97	2.61
2	97	1.72	98	1.33
3	95	1.54	97	1.46
4	95	2.05	94	2.25
5	97	1.96	96	1.69
6	91	3.12	86	2.99
7	83	3.92	96	1.65
8	77	4.67	88	4.64
9	92	3.04	67	4.83
Mean	91	2.87±1.12	91	2.60±1.33

Table 3.4 Summary of reproducibility (between-visit) results for normal and diabetic group

Normal group

The CoR (2) ranges from 1.54% (location 3: inner inferior macular position) to 4.67% (location 8: outer temporal macular position) and has a mean of 2.87±1.12%. ICC's are very high ranging from 77% (location 8) temporal to 97% (location 2) with a mean ICC of 91%. Bland and Altman plots for all retinal locations are shown in figure 3.4 in which the solid horizontal line represents the group mean difference between visits for each parameter and the two dotted lines are the 95% limits of agreement between visits. The coefficient of reproducibility (the difference divided by the mean) is illustrated as a scatter plot within each graph (Bland and Altman, 1986).

Position 1

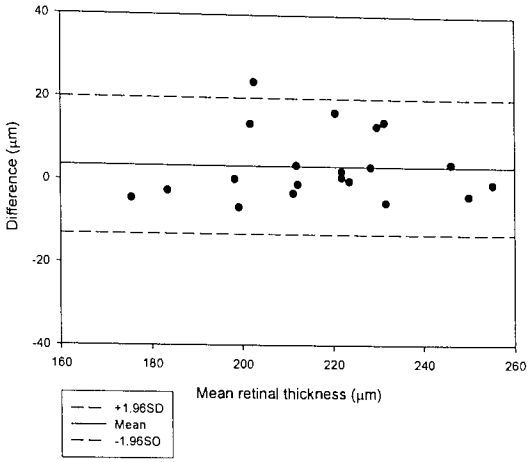

Position 2

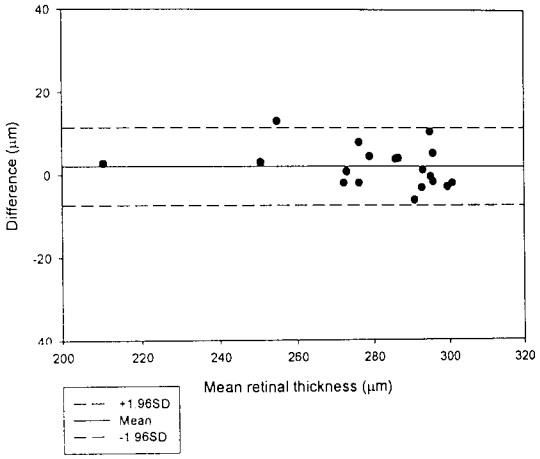

Position 3

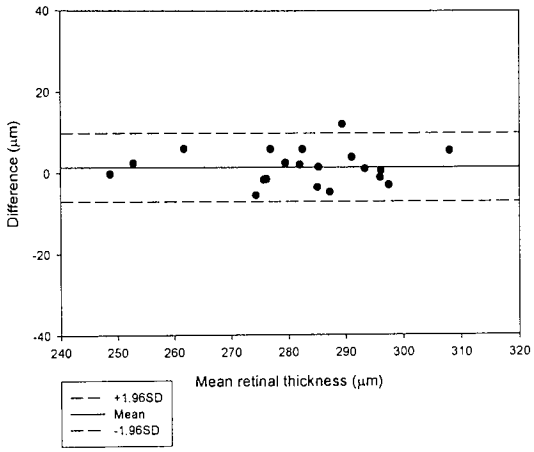

Position 4

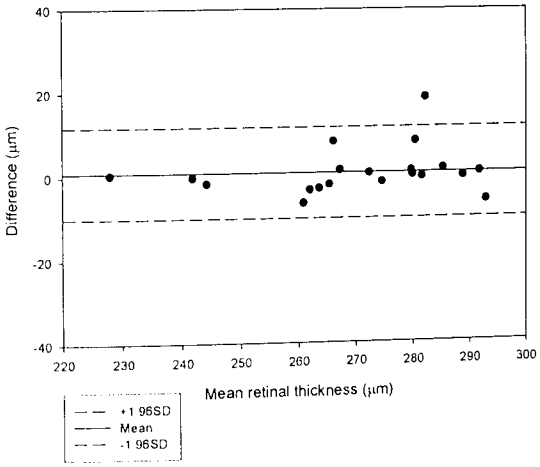

Position 5

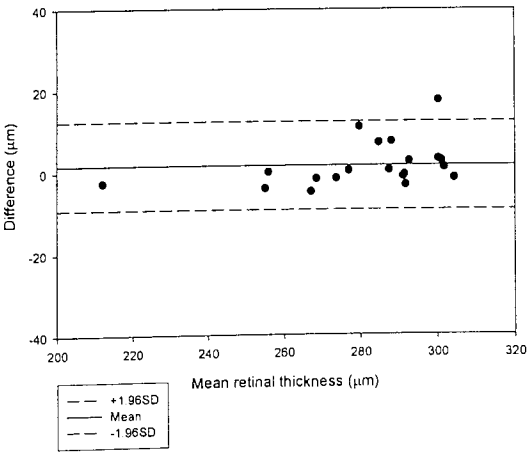

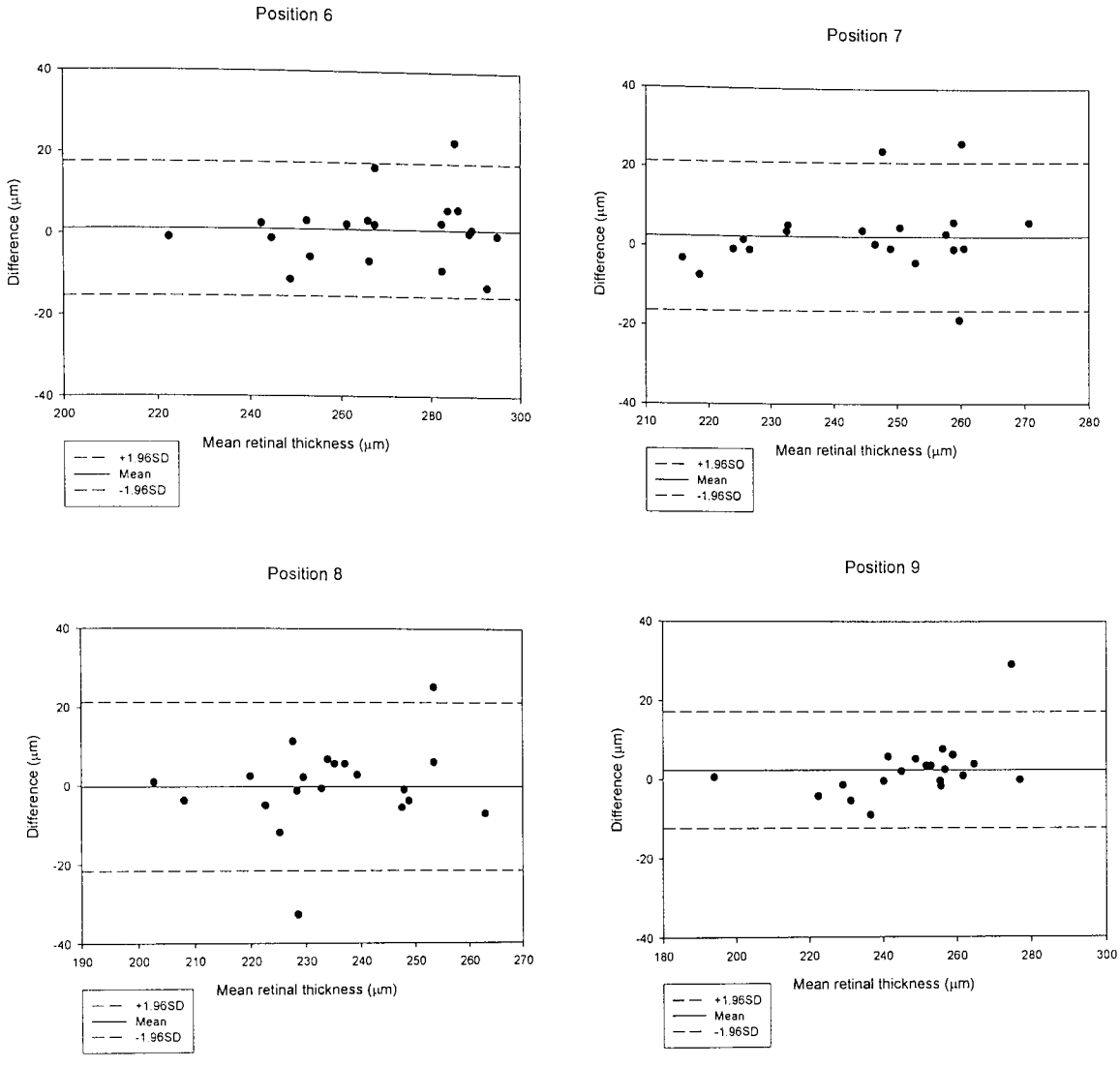

Figure 3.4 Graph showing the reproducibility of OCT macular retinal thickness measurements at each location 1-9 for normal subjects.

A paired *t*-test showed no difference in retinal thickness measurements between visit 1 and visit 2 for any position ($p<0.005$ after Bonferroni correction for multiple comparisons).

Diabetic group

The CoR (2) ranges from 1.33% (location 2: inner nasal) to 4.83% (location 9: outer superior) and has a mean of 2.60±1.33%. ICCs are high, ranging from 67% at location 9 to 98% at location 2. Bland and Altman plots for all retinal locations are shown in figure 3.5 in which the solid horizontal line represents the group mean difference between visits for each parameter and the two dotted lines are the 95% limits of agreement

between visits. The coefficient of reproducibility (the difference divided by the mean) is illustrated as a scatter plot within each graph (Bland and Altman, 1986).

Position 1

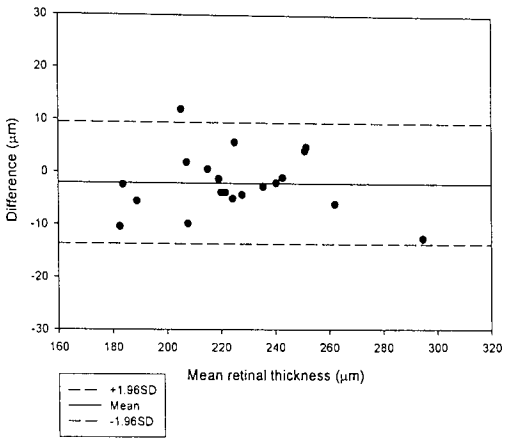

Position 2

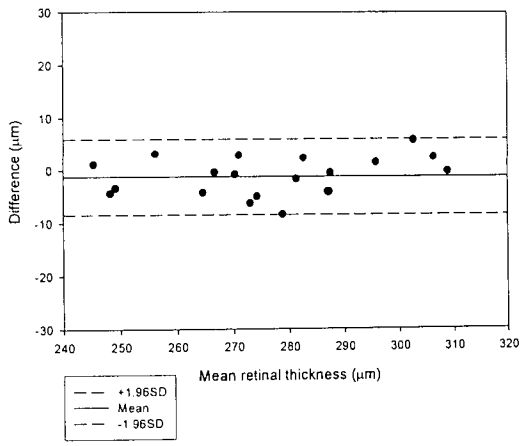

Position 3

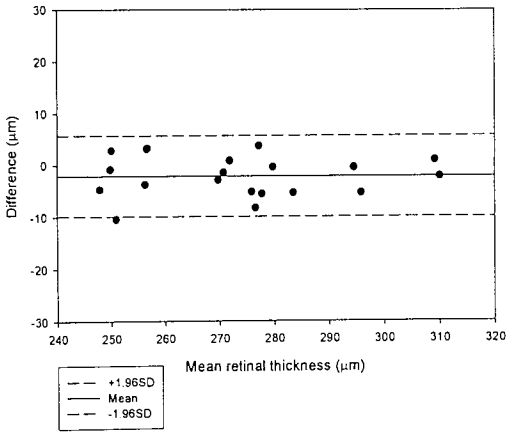

Position 4

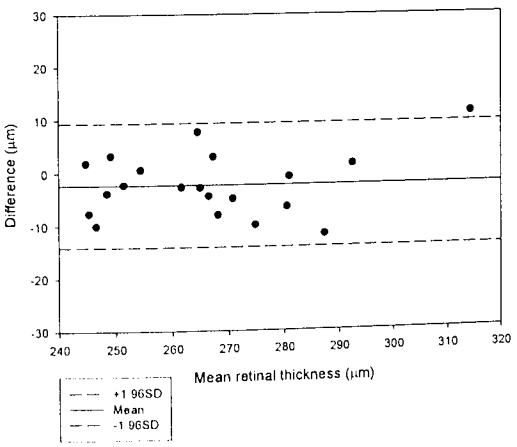

Position 5

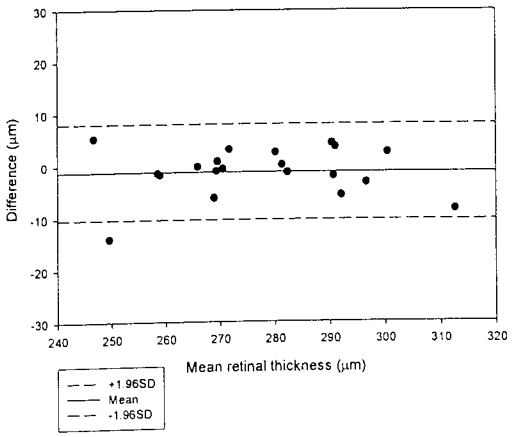

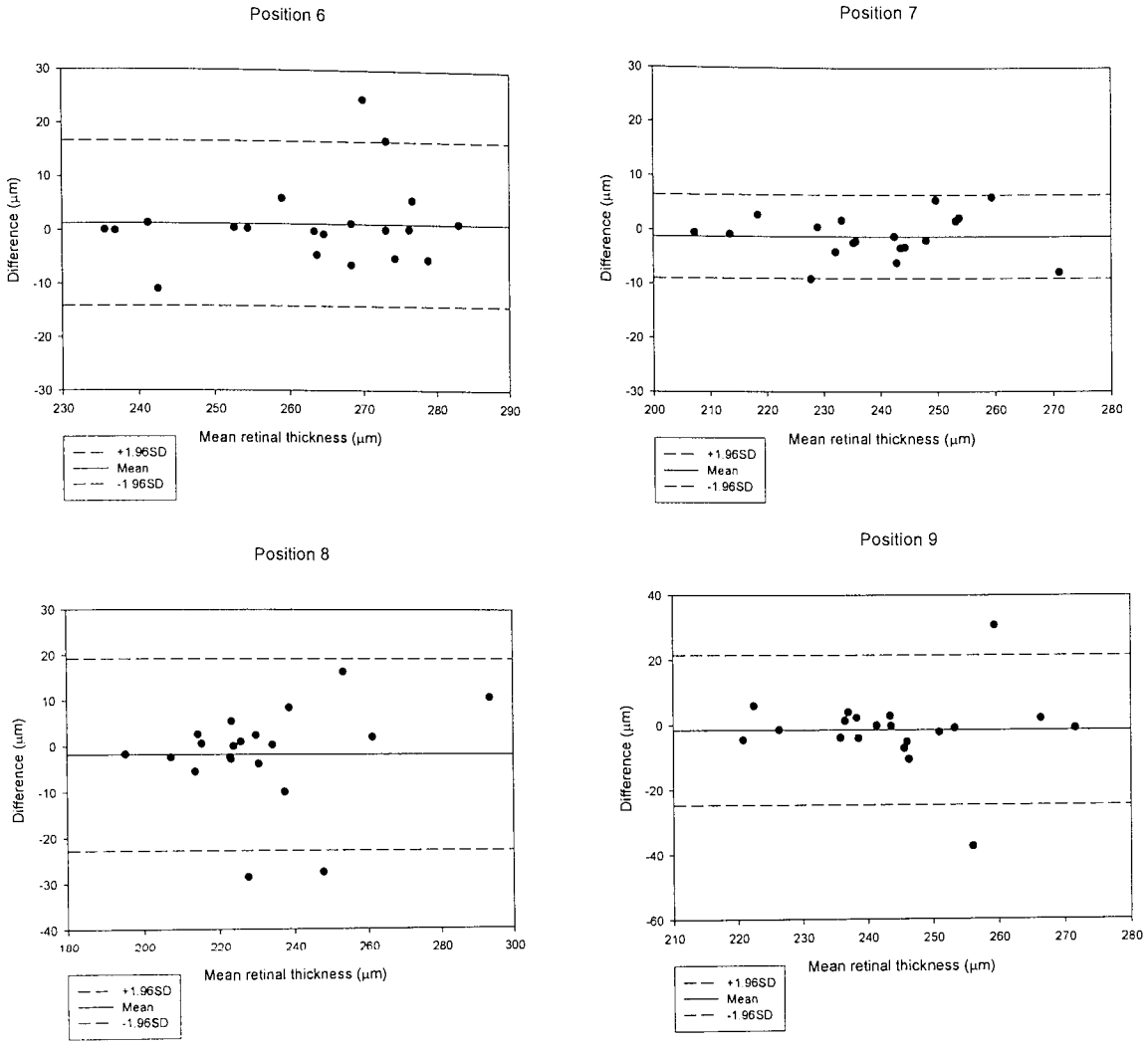

Figure 3.5 Graph showing the reproducibility of OCT macular retinal thickness measurements in each retinal location 1-9 for diabetic patients.

A paired samples *t*-test showed no difference in retinal thickness measurements between visit 1 and visit 2 for any position ($p<0.005$ after Bonferroni correction for multiple comparisons).

3.7.6 Difference between groups

Independent samples *t*-tests were performed to establish whether significant differences existed between groups in terms of the repeatability or reproducibility results. There were no significant differences for CoV, CoR1, and CoR2 and ICC values ($p>0.05$).

3.8 Discussion

This study explored the repeatability and reproducibility of retinal thickness measured in normal subjects and diabetic patients. In all retinal locations the data were found to exhibit high degrees of repeatability both within-visit and between-visit for normals and diabetics.

Graphical representation of the coefficient of reproducibility in the Bland and Altman plots shows, not surprisingly for reproducible measures, that the mean of the difference is approximately 0 for retinal locations in both the normal subjects and diabetic patients. The reproducibility of acquired measures is indicated by the width of the upper and lower limits of agreement with very reproducible measures indicated by a very narrow range. Overall, the limits of agreement are excellent in all locations for all subjects indicating excellent reproducibility. Furthermore, the limits of agreement appear to differ between retinal locations for all subjects, at different distances from the fovea. For normal subjects the limit of agreement at the fovea (position 1) is approximately 35μm, while for the inner ring on the retinal map analysis output (positions 2-5) the limits of agreement measure approximately 20μm indicating greater reproducibility. In positions 6-9 of the outer ring on the retinal map the limits of agreement are greater at around 40μm. In diabetic subjects the limits of agreement do not appear to follow this trend as closely. Positions 1 and 4 exhibit confidence limits of approximately 18μm, while positions 2, 3, 5 and 7 show limits of agreement of 15μm. Limits of agreement for position 6 are 30μm and finally, worse reproducibility is exhibited by position 8 and 9 at 40μm.

There were no significant differences between normal subjects and diabetic patients in terms of their repeatability and reproducibility, indicating that measurements are robust even in eyes with some degree of pathology. Our findings suggest that in a clinical situation, any significant changes in macular retinal thickness measurements observed over different scanning sessions are likely to be a result of variations in the retinal thickness of the patient and not due to poor reliability and inaccuracies of the OCT.

3.8.1 Actual retinal thickness values

In our study, retinal macular retinal thickness (average positions 1-9) measured 258.61±1.17μm for normal subjects (average of visit 1 and 2). This compares well with a similar study using Stratus OCT fast macular scanning of 10 normal subjects (mean age 30.5±7.4years) by Paunsecu *et al.* (2004) who reported an average retinal thickness (positions 1-9) of 241.97±25.81μm. Similarly, Polito, Del Borello, Isola *et al.* (2005) using the Stratus OCT report an average retinal thickness of 264.67±28.40μm and 265.89±27.23μm for a group of 10 normal subjects undilated and dilated respectively. Pierre-Khan, Tadayoni, Haouchine *et al.* (2005) reported mean retinal thickness at position 1 (fovea) of 191.4±17.6μm using the Stratus OCT in a group of 17 normal subjects (37.5±8.6years). Our study found slightly higher foveal thickness at 219.51±21.43μm at visit 1 and 216.04±21.04μm at visit 2.

In our study average retinal thickness over both visits for diabetic patients measured 255.12±0.97μm. (Comparison with previous work is impossible because to our knowledge there are no reports of retinal thickness values for diabetic patients with early maculopathy). There is very little difference between retinal thickness measurements at each location between normals and diabetics which suggests that early maculopathy is not associated with oedema. More specifically, at the fovea the retinal thickness is more for the diabetic group than the normal subjects. In all other locations 2-9 the retinal thickness is less in diabetics than normals. However, differences between groups in terms of their retinal thickness did not reach statistical significance in any location according to an independent samples *t*-test.

3.8.2 Number of images

For each location the mean standard deviation (MSD) was calculated for 2 scans, 3 scans, 4 scans etc and plotted against the number of scans taken. It can be seen that for all locations in both the normal and diabetic group, the mean standard deviation is very low (<7μm). For each graph the point at which the curve reached a plateau was identified. There was no definitive point at which the variance was stable for all retinal locations, with some curves reaching a plateau at 2 scans while others levelled at 6 or 7

scans. However, for the majority of locations, beyond the third or fourth scan there is little further improvement in the data overall. There is an argument for using one image in a clinical setting but for statistical analysis and for research purposes, the use of 3 scans would be robust. These data suggest that 3 images are the minimum acceptable for repeatable measures while remaining clinically acceptable. Repeatability and reproducibility analyses were based on these findings. The use of 3 scans was employed throughout all subsequent studies in this work.

3.8.3 Repeatability and reproducibility

Our findings are similar to those reported in the literature for earlier models and most recently for the Stratus OCT in normal subjects. OCT technology has developed in terms of both hardware and software since its introduction in the early 1990s. OCT 1 and OCT 2000 had an axial resolution of approximately 15μm (500 pixels for each A-scan) while the Stratus OCT offers resolution of 8-10μm (1000 pixels per scan). Stratus OCT, unlike its predecessors, also offers a fast scanning option in which the six component radial line scans are compressed to form one scan reducing scan acquisition time to 1.92 seconds in total, compared with 1 second per single linear scan (6 seconds in total) using the OCT 2000. This allows the acquisition of more reliable scans due to improved patient tolerability and fixation. The number of A-scans per optical cross section has increased from 100 using the OCT 2000 to 128 using the Stratus OCT. Tranverse resolution along each scan line with the OCT 2000 was 60μm compared to 49μm with the Stratus OCT. In every retinal position 1-9 of the macular thickness map, the density of measurements has increased from 100 with the OCT 2000 to 128 using the Stratus OCT for position 1, 50 to 64 for position 2-5 and from 75 to 96 for positions 6-9 . While it is not appropriate to compare results of previous studies directly, due to the inconsistencies of scan types and position, the variability of the instruments used and the way in which the data are analysed according to the literature, repeatability and reproducibility of measurements acquired by all models is high.

One of the first OCT repeatability within-visit studies was performed by Baumann *et al.* (1998) who used an OCT scanner prototype to image the macular region of normal subjects. Multiple vertical scans of length 2.88mm (divided into 7 sections) were

centred through the fovea of 18 eyes and analyses performed using a manual method (where the observer visualised the A-scan and manually placed measurement cursors at the steepest portion of each rising slope produced at the internal limiting membrane (ILM) and retinal pigment epithelium (RPE)) and an automated method using system software. Coefficient of variation (CoV) of 5 repeated measurements of a single scan (at each of the 7 locations) indicated high intraobserver reproducibility. Mean CoV was less than 10% for all locations (range 3.2- 8.1%) with the manual method. Higher CoVs were observed for the regions within 500μm of fixation. At all locations the CoV was higher using the automated method due to its failure to detect the ILM. This effect was more marked near fixation and gave rise to CoV of approximately 30%. The authors concluded that the OCT is capable of reproducible measurement of retinal thickness in normal eyes but suggests refinement of automated measurements of retinal thickness near fixation. Such recommendations were implemented in the commercial OCT models.

Individual OCT line scan measures, although repeatable, gave an incomplete assessment of macular thickness since the retinal thickness could only be measured along the scan line and therefore the topographic mapping protocol was developed by Hee *et al.* (1998). This comprised 6 radial tomograms obtained in a spoke like pattern through a common centre, from which one scan and a retinal thickness map was produced by the OCT software using mathematical interpolation to fill the gaps between the line scans. This map displayed retinal thickness values for 9 locations across the macula and formed the basis of the fast macular thickness scan analysis used in our study.

Following the commercialisation of the OCT equipment several software programs became available. Massin *et al.* (2001) assessed the reproducibility of retinal thickness measurement using A5 mapping software of OCT 1 (which included the 6 radial line scanning protocol and false-colour plot for 9 locations across the scan) for normal (n=10, mean age 35 years) and diabetic patients (n=10, mean age 61 years) with clinically significant oedema. Measurement reproducibility was assessed by means of 3 series of 6 scans performed by 2 different observers on 2 different days, separated by a 1 week interval. In healthy subjects, intraobserver, interobserver and between-visit reproducibility was excellent with ICCs of greater than 89%. In diabetic patients, within-visit repeatability ICC of each location was greater than 98%. Our results

compare favourably with between-visit reproducibility exhibiting ICCs of 91% for both subject groups.

The Humphrey 2000 OCT system has been subject to examination in terms of intrasession and intersession repeatability by a number of research groups. Koozekanani *et al.* (2000) reported repeatable macular thickness measurements for 26 normal volunteers (mean age 31±9 years) using horizontal scans, 3mm in length through the patient's fovea. Five scans were acquired from each subject in each session. Each subject was imaged during three independent sessions. Repeated-measures analysis found no significant differences between scans within or between sessions.

Such findings were also confirmed by Muscat *et al.* (2002), who assessed the repeatability and reproducibility of macular thickness measurements in 20 normal subjects (mean age 31.9 years) with dilated pupils using the Humphrey OCT system. Initially a series of horizontal single-line scans were taken across the fovea in each subject. Despite the use of the repeat scan option that provides a landmark cursor to facilitate the repeat positioning of subsequent scans the authors detected inaccuracies in the positioning of the cursor with displacements up to 0.2-0.3mm. Such inaccuracies would lead to a misrepresentative reduction in the coefficients of repeatability and reproducibility. Macular thickness was subsequently measured using the OCT raster-line scan which comprised six closely spaced scan lines (of width 4mm and separation 0.1mm) located in an aiming rectangle, at least 4 of which traversed and were centred on the foveal pit. For the purposes of analysis, these scan lines were divided into 10 sections, for which the coefficients of repeatability and reproducibility were calculated. In total 10 sets of scans were taken for within-visit analysis. Between-visit reproducibility was investigated by taking readings in the morning and afternoon on five consecutive days, the separation of which was just 5 hours and the OCT remained switched on during this time. Muscat *et al.* (2002) found that the coefficients of repeatability were between 0.75% and 4.78% and coefficients of reproducibility were between 1.24% and 4.20% for their study sample of normal subjects (average age 31.9 years). Our study indicates similar within-visit repeatability values for both normal (1.19 - 2.36%) and diabetic eyes (1.26 - 2.08%). Between-visit reproducibility is similar to results obtained by Muscat *et al.* (2002) for both normal subjects (1.54 - 4.67%) and diabetics (1.33 - 4.83). Such findings are encouraging when considering the older age

group of our normal subjects and the inclusion of a diseased eye group. When compared to earlier studies, in terms of between-visit reproducibility, our study more accurately reflects the time period between patient visits in a clinical setting i.e. two weeks as opposed to the minimum 5 minutes for the study by Koozekanani *et al.* (2000) and the 5 hour session separation in the study by Muscat *et al.* (2002).

One of the advantages of the new Stratus OCT system is the use of the fast scan protocols for the macular, RNFL circle scan and the optic nerve head cross sectional scan. Unlike its predecessors, the Stratus OCT offers the fast macular thickness scan option in which the six component radial line scans are compressed to form one scan and subsequently analysed to form a retinal thickness map. No adjustments of scan position by the operator are required during the entire scanning session since the default location of the six radial lines is directly through the fovea of the patient, when the patient accurately fixates the internal fixation light. At subsequent scanning sessions the use of the repeat scan is unnecessary due to the fact that the patient once again fixates looks at the fixation light and the radial line scan is automatically placed through the fovea. Scanning time is reduced, which reduces the potential for fixation loss and potentially increases the repeatability of thickness measures. Baumann *et al.* (1998) and Muscat *et al.* (2002) found that retinal thickness measurements closest to the fixation point were less reproducible than those sections further away. This is probably explained by the difficulties they experienced in re-positioning their scan lines. For all scan types, inaccuracies in fixation are going to impact the fovea to a greater extent than the peripheral areas of the posterior pole due to the large changes in retinal thickness across the foveal slope and the shape of the foveal depression. Repeatability and reproducibility values in our study varied little for each location across the retinal map, with position 1 (fovea) comparing favourably with the more eccentric macular locations. This is consistent with the repeatability findings for Massin *et al.* (2001) who observed highly reproducible measurements in the central macular area. This is likely to be the result of the large number of points being measured in this area with the mapping protocol (position 1) compensating for the theoretically greater variability due to the changes in retinal thickness occurring in this area.

Muscat *et al.* (2002) using a test object with an air gap of known thickness which was filled with water and glycerin to mimic the reduction of signal with retinal disease,

determined that OCT scans were accurate, precise, repeatable and reproducible even when there is significant degradation of the OCT signal. They found coefficients of repeatability for 10 consecutive scans of 0.29% for the air filled gap, 0.34% for the water filled gap and 0.43% for the glycerin filled gap. Coefficients of reproducibility for 10 scans during two different sessions for air, water and glycerin were 0.67%, 1.05% and 0.45% respectively. Paired *t*-tests revealed no statistically significant differences between measurements obtained in the morning and afternoon scanning sessions.

Our study suggests that retinal thickness measures are repeatable with eyes exhibiting diabetic macular changes. All diabetic subjects had a fairly good level of vision despite the pathological changes and would have been able to accurately fixate the target light within the OCT camera. A further extension of this work would be to assess the repeatability and reproducibility of OCT scans for patients whose visual acuity was reduced to a greater extent. The use of the external fixation light in these cases would ensure the most reliable measures were acquired. Massin *et al.* (2001) observed high within-visit repeatability even for diabetic patients with macular oedema whose visual acuity is likely to be impaired. They suggested that this may partly be due to the thickening and flattening of the macula with a resultant loss of foveal depression as a consequence of macular oedema.

A study by Pierre-Khan *et al.* (2005) compared macular retinal thickness measurements of normal and diabetic patients made by the OCT 1 (version A6.2) and Stratus OCT (version 2.0). They observed that measures of the same eye with the Stratus OCT were significantly higher than those measured by its predecessor. The Stratus OCT produced fewer artefacts than the OCT 1 in pathological cases. The authors recommend that extrapolation of retinal thickness measurements from OCT 1 and Stratus OCT should take into account a correcting value.

In a study by Gurses-Ozden *et al.* (2004) the repeatability of macular thickness measurements in 10 normal subjects were made with the Stratus OCT (OCT 3) using both the fast macular thickness protocol. Analysis of variance (ANOVA) revealed no significant differences for macular thickness over the course of three visits- 3 days within a 1 month period with $p>0.05$ nor between examiners (paired *t*-test $p> 0.05$). Our

study would support these findings with no significant differences between macular thickness observed on each visit for both the normal and diabetic groups.

Similarly, Paunescu *et al.* (2004) reported that the Stratus OCT demonstrates reproducible measurements of macular thickness for normal subjects. Ten normal subjects were imaged 6 times (3 before dilation and 3 after dilation) per day and the series was repeated on three different days within a 5 month period. Standard density (fast macular) scans and high density (slow acquisition) scan protocols were performed on each subject and results compared. Fast macular scan ICCs ranged from 52-92% for the undilated eye and 55-97% for the dilated eye. These values compare well with our findings of between-visit reproducibility ICC values of 91% for normal subjects. High density scans showed ICCs of between 35 and 96% for undilated eyes and 65-95% for dilated eyes. The effects of dilation did not reach significance for any of the macular parameters (positions 1-9). In general terms, the study revealed that high density /slow acquisition scanning (where each radial line scan is acquired consecutively after manual repositioning) is more susceptible to fixation problems, eye movements and inaccuracies in scan placement by the operator and subsequently displays greater measurement variability. The fast macular thickness scanning protocol therefore appears to be a valid and reliable imaging technique.

Our study was the first of its kind to investigate the repeatability and reproducibility of the Stratus OCT for both normal and diabetic eyes. An interesting extension of this work would be to conduct a similar study in a group of diabetic subjects with greater degrees of maculopathy and macular oedema and associated visual acuity reduction. Since completion of our work a similar study has been carried out by Polito *et al.* (2005) who investigated the repeatability and reproducibility of retinal thickness measurements using the fast macular thickness mapping protocol of the Stratus OCT in one eye each of 10 healthy subjects (mean age 40 years) and 15 diabetic patients (mean age 64 years) with clinically significant oedema. They reported coefficients of repeatability of between 1.57 and 7.43% in healthy subjects and between 3.41 and 6.19% in diabetic patients. These values indicate worse repeatability than in our study where we found CoR 1 ranged from 1.19-2.36% for normal subjects and 1.26-2.08% for diabetic patients. The discrepancy between the diabetic groups is likely to be explained by the presence of macular oedema and poorer visual acuity (6/6 to 6/30) in their study sample

compared to ours. Likewise, between-visit reproducibility was lower than in our study, with coefficients of reproducibility between-visit for normal subjects, reported by Polito *et al.* (2005) ranging from 2.43 to 8.83% compared to our study results of 1.54 to 4.67% for normal subjects. Between-visit ICCs reported by Polito *et al.* (2005) ranged from 81% to 95% in healthy eyes while healthy subjects in our study exhibited ICCs of between 77% and 97%. Polito *et al.* (2005) did not measure between-visit reproducibility in their diabetic patients since observed differences may have been dependent on variations in macular oedema.

Our findings of good repeatability and reproducibility are confirmed by Polito and colleagues (2005) who conducted a Wilcoxon paired-measurements test ($p=0.05$) to show that there were no statistically significant differences between measurements obtained during different visits in healthy and diabetic patients with macular oedema.

3.9 Conclusion

Measurements of macular thickness made with the Stratus OCT are repeatable and reproducible for both normal and diabetic patients. Three scans for each visit will provide repeatable and reproducible measurements. Stratus OCT therefore provides quantitative measurements of retinal structure and can be used to monitor the progression of disease over a period of time allowing more effective management and treatment of disease.

CHAPTER 4: Repeatability and reproducibility of optic disc parameters measured by the Optical Coherence Tomographer (Stratus OCT 3) in normal subjects and glaucoma patients

4.1 Abstract

Purpose: Optical coherence tomography is a technique recommended for use in the diagnosis and monitoring of ocular disease such as glaucoma. The OCT has demonstrated both good repeatability and reproducibility in terms of measuring retinal thickness across the macula and retinal nerve fibre layer thickness around the optic nerve head. However, very little investigation has been made of the ability of the OCT to measure optic disc parameters. The purpose of this study was therefore to determine the within-visit repeatability and between-visit reproducibility of optic disc parameters using the Stratus OCT (Model 3000 OCT, Carl-Zeiss Meditec, Dublin, CA) in normal subjects and glaucoma patients.

Methods: Optic nerve head measurements were obtained at each of two visits using multiple radial line scans, 4mm in length, centred through the optic disc of 20 normal control subjects (63.15±11.76 years; range 46-80years) and 20 patients (67.75±10.31; range 48-83 years) diagnosed with primary open angle glaucoma (POAG). Optic nerve head analysis combines the analysis and measurement of each individual scan to calculate mean vertical integrated rim area (volume), horizontal integrated rim width (area), disc area, cup area, rim area, cup:disc area ratio, cup:disc horizontal ratio and cup:disc vertical ratio. Coefficient of repeatability (CoR 1) and coefficient of variation (CoV) were used to determine the repeatability of measures for each parameter within a visit, while coefficient of reproducibility (CoR 2) and intraclass correlation coefficients (ICC) were used to determine the reproducibility of measures between visits.

Results: For normal subjects, the within-visit CoV for each of the disc parameters ranged from 4.36% for horizontal integrated rim width (area) to 11.08% for vertical integrated rim area (vol). For glaucoma patients the within-visit CoV ranged from 4.18% for cup:disc horizontal ratio to 17.63% for vertical integrated rim area (vol). The CoR (1) ranged from 4.36% to 11.08% for normal subjects and from 4.18% to 17.63% for glaucoma patients. The between-visit CoR (2) ranged from 4.87% (horizontal integrated rim width (area) to 12.96% (cup:disc area ratio) for normal subjects and from 3.66% (cup:disc horizontal ratio) to 27.16% (vertical integrated rim area) for glaucoma patients. ICC's for between-visit reproducibility ranged from 91.6% (disc area) to 98.3% (cup area) in normal subjects; ICC's ranged from 90.6% (disc area) to 95.5% (cup:disc horizontal ratio) for glaucoma patients.

Conclusion: Measurements of optic disc parameters made with the Stratus OCT are repeatable and reproducible for both normal and glaucoma patients. In general the Stratus OCT provides quantitative measurements of retinal structure and can be used to monitor the progression of disease over a period of time allowing more effective management and treatment of disease.

4.2 Introduction

Optical coherence tomography provides quantitative measurements of macular retinal thickness, nerve fibre layer thickness and topographical measurements of the optic nerve head. Since its introduction in the early 1990's, several studies have used the OCT to evaluate retinal nerve fibre layer thickness changes around the optic nerve head in glaucomatous damage and its ability to discriminate between the normal and glaucomatous eye using the prototype instrument (Schuman *et al.,* 1995), the OCT 2000 (Bowd et *al.*, 2000; Kanamori *et al.*, 2003; Nouri-Mahdavi *et al.*, 2004) and the Stratus OCT (Leung *et al.*, 2005). OCT measurements of the retinal nerve fibre layer around the optic nerve head using circular scans centred on the optic disc have been found to be both repeatable and reproducible (Schuman *et al.*, 1996; Bumenthal *et al.*, 2000; Carpineto *et al.*, 2003; Gurses-Ozden *et al.*, 2004; Zafar *et al.*, 2004; Budenz *et al.*, 2005). Despite the fact that examination of the optic nerve head performs a key role in the detection of glaucomatous damage, few studies have employed the OCT to measure optic nerve head structure. The ability of the Stratus OCT to provide repeatable and reproducible measures of optic nerve head morphometry using the cross sectional scan protocol in normal subjects has been documented in just two studies (Paunescu *et al.*, 2004; Olmedo, Cadarso-Suarez, Gomez-Ulla *et al.*, 2005). Furthermore, to our knowledge, of these, only one has investigated the ability of the OCT to provide repeatable measures of optic disc parameters in diseased eyes (Olmedo *et al.*, 2005). The Stratus OCT (OCT 3 Model 3000) has an advanced fast optical scan protocol option which uses 6 radial line scans (each measuring 4mm in length) centred on the optic disc, to produce a detailed output of disc parameters including vertical integrated rim area (volume), horizontal integrated rim width (area), disc, cup and rim area, and both horizontal and vertical cup:disc ratio. The ability of the OCT 3 to provide repeatable and reproducible measurements of these parameters in normal eyes and diseased eyes is investigated in this study.

4.3 Aims and objectives

The purpose of this study was to determine the within-visit repeatability and between-visit reproducibility of optic nerve head parameters measured using the new Stratus OCT instrument for normal subjects and glaucoma patients.

4.3.1 Hypothesis

Stratus OCT provides repeatable and reproducible measurements of the optic nerve head of normal and glaucomatous eyes.

4.4 Study sample and investigations

4.4.1 Inclusion Criteria

All subjects and patients were subjected to a clinical eye examination to assess their fitness to participate in the study based on the following criteria.

4.4.2 Normal group

The inclusion criteria and recruitment procedures were as for Chapter 3.

4.4.3 Glaucoma patients

Glaucoma patients were recruited from the Ophthalmology Department of Birmingham Heartlands Hospital Glaucoma Clinic and had been previously diagnosed with primary open angle glaucoma (POAG) by a collaborating ophthalmologist in the glaucoma clinic. Subjects were included in the study if they showed:

- Optic nerve head cupping consistent with glaucomatous changes including:
  Notching (focal extension of the cup)
  Focal or geneneralised narrowing or disappearance of the neuroretinal rim
  Pallor of the neuro-retinal rim
  Cup:disc (C:D) asymmetry

- Repeatable mild to moderate repeatable visual field defect consistent with a diagnosis of glaucoma on at least two consecutive assessments as assessed by the Humphrey Visual Field Analyser (program 24-2)
- Minimal or no lens opacities allowing a clear fundus view
- No history or evidence of intraocular surgery or laser therapy
- No history or evidence of retinal pathology other than glaucoma
- Snellen visual acuity (VA) 6/9 or better
- Less than 6 dioptres of spherical ametropia and 2 dioptres of astigmatism

4.4.4 Subject sample statistics

The subject sample consisted of 20 normal healthy volunteers and 20 glaucoma patients previously diagnosed as having POAG by collaborating ophthalmologists. Details of the subject sample are given in table 4.1.

	Gender		Test eye		Mean Age ± SD(range)
Subject Group	Male	Female	Right	Left	
Normal (n=20)	10	10	10	10	63.15 ± 11.76 years (46-80)
Glaucoma (n=20)	10	10	11	9	67.75 ± 10.31 years (48-83)

Table 4.1 Summary of the subject sample

4.4.5 Ethical approval and informed consent

Ethical approval was obtained from the ethical committee boards of Birmingham Heartlands and Solihull NHS Trust and Aston University. Approval conformed to the tenets of the Declaration of Helsinki. Written informed consent was obtained from all subjects and patients.

4.5 Methods

Subjects were required to attend the Heartlands Hospital Ophthalmology Clinic on two occasions. At visit 1 screening of all patients was conducted as per the requirements set

and listed above. The first set of OCT scans was performed for within-visit analysis. OCT scans were repeated at visit 2, within a fortnight of the patient's first visit. In order to mimic a realistic follow up clinic visit it was not necessary to rebook the patient at the same time as their first.

4.5.1 Optic disc parameters: Optical Coherence Tomography

Prior to image acquisition, subject details were entered into the database of the OCT. The subjects were instructed to place their chin on the chin rest and forehead against the top bar and instructed to fixate on a green target placed to the periphery of the camera depending on whether the R or L eye was being scanned. The scan was positioned directly over the optic nerve head using the cursor and both Z-offset and polarisation adjusted to optimise the scan. The fast optical disc scanning protocol was carried out to obtain optic nerve head measurements for all subjects. This scan consists of six radial lines (4mm in length) arranged in a spoke-like pattern centred on the optic nerve head. The OCT interpolates between the scans to provide measurements throughout the optic nerve head. The fast protocol scan compresses these six optical disc scans into one scan and acquires all six 4mm radial line scans in 1.92 seconds of scanning. This scan is designed to examine the optic disc for indications of glaucoma and scans are analysed with the optic nerve head analysis protocol.

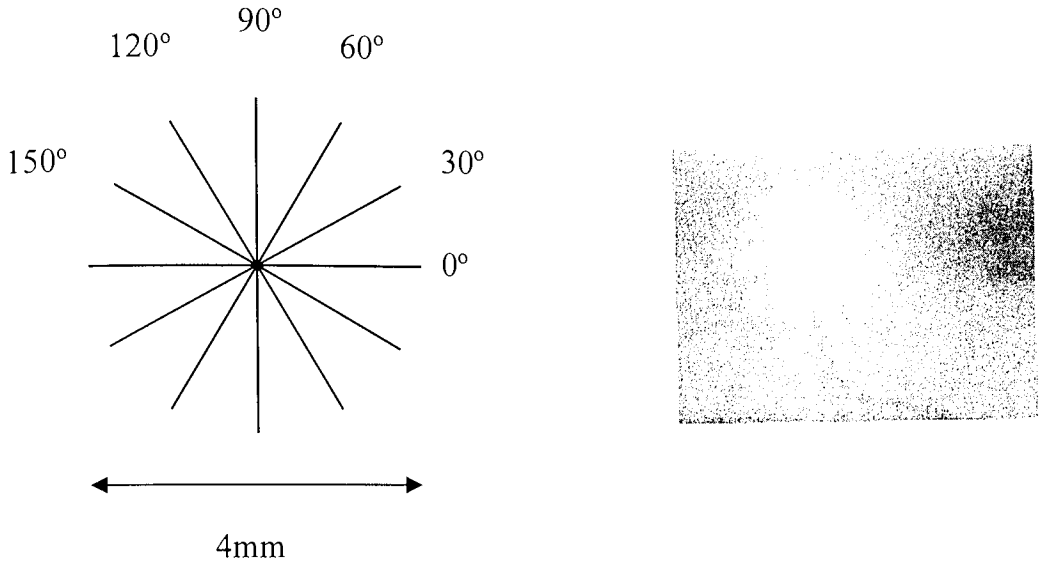

Figure 4.1 a) Schematic diagram of fast optical disc scan centred through the optic nerve head b) Example of a fundus image produced during OCT fast optical disc scan acquisition

During OCT analysis the optic disc margin is defined as the end of the retinal pigment epithelium/choriocapillaris layer. Optic nerve head analysis software detects the anterior surface of the RNFL and the RPE and is then able to identify features of the optic disc based on anatomical markers (disc reference points) on each side of the disc where the RPE ends. For each individual scan, the computer algorithm identifies and measures disc diameter, cup diameter, rim area (vertical cross section), horizontal rim length and average nerve width at the disc. Optic nerve head analysis results combines the analysis and measurement of each individual scan to give vertical integrated rim area (volume), horizontal integrated rim width (area), disc area, cup area, rim area, cup:disc area ratio, cup:disc horizontal ratio and cup:disc vertical ratio. It is possible to adjust the placement of the disc reference points and therefore the resulting measurements if required. However, during this study the default positions for both visits were used to reduce subjective elements.

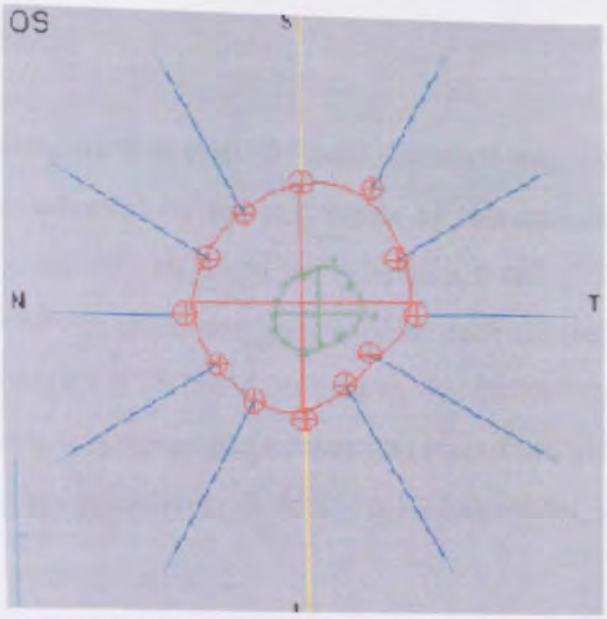

Figure 4.2 Example of the OCT fast optical disc scan analysis output

Scanning for visit 1 involves eccentric viewing and placement of the radial lines across the optic nerve head. Every subsequent scan during the session remained at this position. To ensure the scan was taken across the identical position at visit 2, the patient was set up in a comfortable position and fixated as per visit 1. Choosing the repeat option on the scanning menu allowed the scan to be taken in the same position as that during visit 1. This could be confirmed by displaying the x and y co-ordinates of the original scan.

In total, 12 fast optical disc scans were acquired for each patient. Following inspection of retinal map output by the OCT software, scans were rejected if it was obvious that the patient had lost fixation and/or if signal strength was poor. On occasions, the scan could not be analysed due to poor scan data.

4.5.2 OCT software

All data acquisition and image processing was with OCT software version 3.0.

4.6 Statistical analysis

All statistical analysis was performed using SPSS version 11.5 for Windows.

4.6.1 Number of images

12 optical disc scans were taken in total. Of these, 10 scans were chosen on the basis of a good image quality indicated by the percentage of A-scans and lack of artefacts. Before analysis took place we calculated the minimum number of scans required per visit for the normal and the glaucoma patients. For each of the test parameters the standard deviation of 2,3,4,5,6,7,8,9 and 10 images was plotted against the number of images and the point at which the graph plateaus was identified. It is assumed that from this point on, any extra images provide no additional information.

4.6.2 Repeatability within-visit

For each parameter tested, the coefficient of repeatability (CoR 1) and coefficient of variation (CoV) were used to determine the repeatability of measures within a visit (section 3.6.3)

4.6.3 Reproducibility between -visit

For each parameter tested, the coefficient of reproducibility (CoR 2) and intraclass correlation coefficient (ICC) were used to determine the reproducibility of measures between visits (section 3.6.4)

A paired samples *t*-test was conducted to evaluate the reproducibility of optic disc measurements between visit 1 and visit 2.

4.7 Results

4.7.1 Optic disc characteristics of normal subjects and glaucoma patients

The actual optic disc characteristics for both subject groups at each visit are summarised in table 4.2

	Normal subjects		Glaucoma patients	
Disc parameter	Visit 1	Visit 2	Visit 1	Visit 2
Vert. int. rim area (Vol) (mm^3)	0.45 ± 0.25	0.46 ± 0.25	0.13 ± 0.09	0.14 ± 0.09
Horiz. int. rim width (Area) (mm^2)	1.75 ± 0.26	1.76 ± 0.27	1.22 ± 0.24	1.22 ± 0.24
Disc area (mm^2)	2.48 ± 0.44	2.51 ± 0.40	2.49 ± 0.50	2.44 ± 0.37
Cup area (mm^2)	0.67 ± 0.39	0.68 ± 0.42	1.54 ± 0.66	1.49 ± 0.49
Rim area (mm^2)	1.81 ± 0.48	1.84 ± 0.46	0.96 ± 0.36	0.95 ± 0.34
Cup/Disc Area ratio	0.27 ± 0.14	0.27 ± 0.15	0.61 ± 0.13	0.61 ± 0.13
Cup/Disc Horiz ratio	0.52 ± 0.16	0.51 ± 0.16	0.80 ± 0.09	0.80 ± 0.10
Cup/Disc Vert ratio	0.48 ± 0.14	0.48 ± 0.15	0.75 ± 0.09	0.75 ± 0.09

Table 4.2 Optic disc characteristics for normal subjects and glaucoma patients

Independent samples *t*-tests were conducted to establish whether disc parameter measurements at both visit 1 and 2 were different for normal subjects and glaucoma patients. For every disc parameter with the exception of the disc area, a significant difference between groups was found. p values of <0.05 were considered statistically significant and indicated by * as shown in table 4.3.

Disc parameter	Significance levels Visit 1	Significance levels Visit 2
Vert. int. rim area (Vol) (mm^3)	0.000*	0.000*
Horiz. int. rim width (Area) (mm^2)	0.000*	0.000*
Disc area (mm^2)	0.919	0.561
Cup area (mm^2)	0.000*	0.000*
Rim area (mm^2)	0.000*	0.000*
Cup/Disc Area ratio	0.000*	0.000*
Cup/Disc Horiz ratio	0.000*	0.000*
Cup/Disc Vert ratio	0.000*	0.000*

Table 4.3 Statistical differences in optic disc parameter values between the normal and glaucoma group * denotes statistical significance

4.7.2 Number of images

For each optic disc test parameter, the mean standard deviation of 2,3,4,5,6,7,8,9,10 scans was calculated and plotted as a function of the number of scans as shown in figure 4.3. The asymptote of each curve was identified to provide guidelines as to the minimum number of scans required for the practical acquisition of reliable measurements.

Vert Integrated rim area

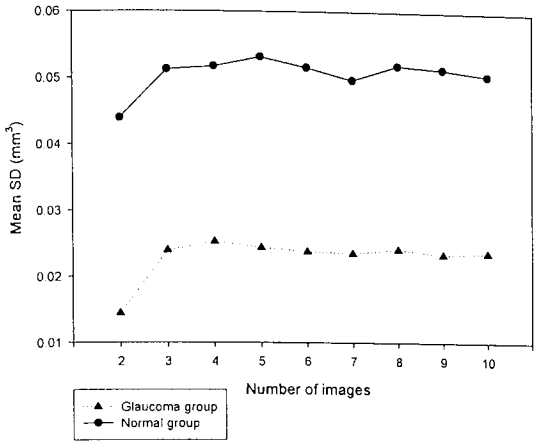

Horiz integrated rim width

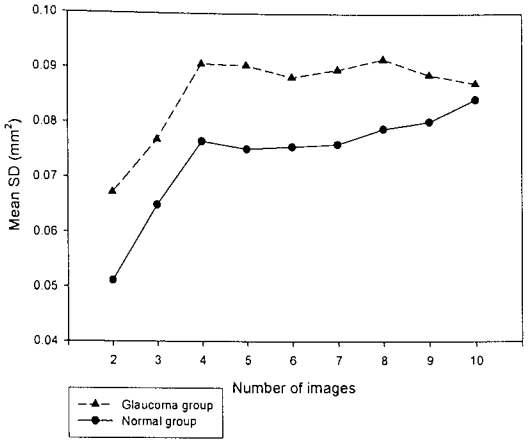

Disc area

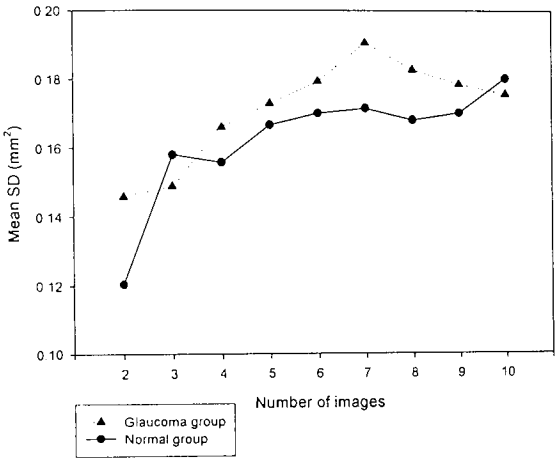

Cup area

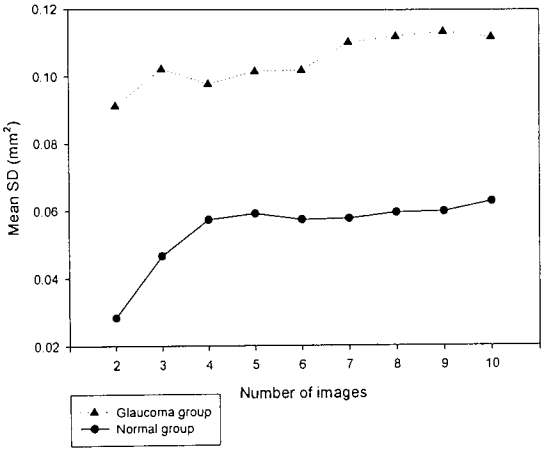

Rim area

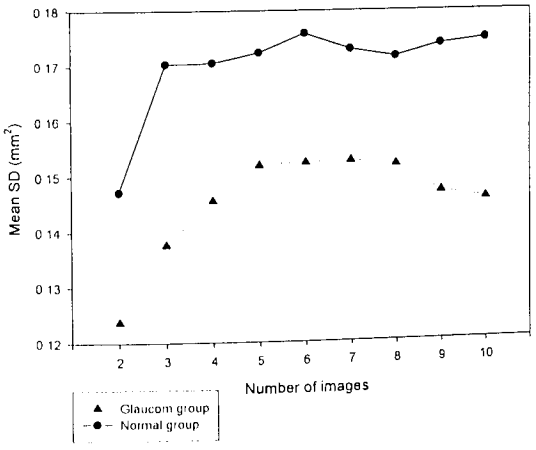

Cup:disc area ratio

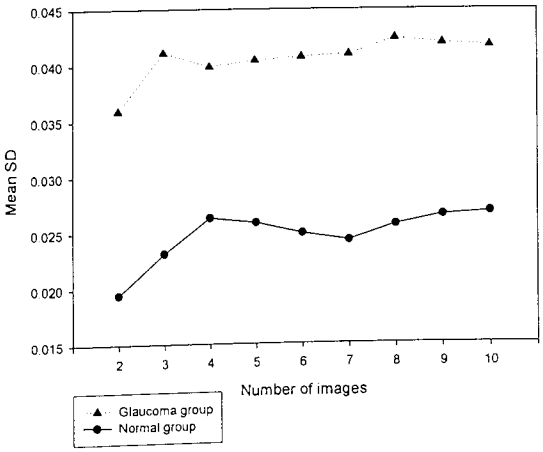

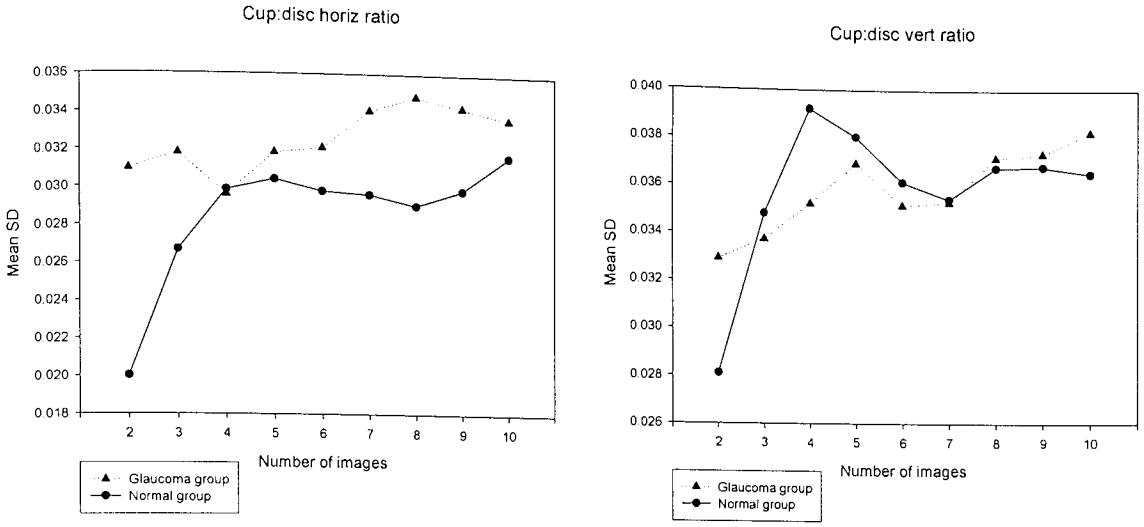

Figure 4.3 Graph showing group mean change in Mean SD for each optic disc parameter as a function of the number of scans for normal and glaucoma subjects.

4.7.3 Repeatability within-visit of optic disc measurements

The repeatability data (CoV and CoR1) for normals and glaucoma patients are summarised in table 4.4.

Parameter	Normals		Glaucoma	
	CoV (%)	CoR 1(%)	CoV(%)	CoR 1(%)
Vert. integrated rim area (Vol)	11.08	11.08	17.63	17.63
Horiz. integrated rim width (Area)	4.36	4.36	7.32	7.32
Disc area	6.91	6.91	7.68	7.68
Cup area	8.58	8.58	7.18	7.18
Rim area	9.57	9.57	15.79	15.79
Cup:Disc Area ratio	8.97	8.97	6.75	6.75
Cup:Disc Horiz ratio	5.75	5.75	4.18	4.18
Cup:Disc Vert ratio	7.31	7.31	4.71	4.71
Mean	7.82±2.17	7.82±2.17	8.91±5.00	8.91±5.00

Table 4.4 Repeatability (within-visit) results for the normal subjects and glaucoma patients

Normal group

The CoV/CoR1 ranges from 4.36% for the horizontal integrated rim width (area) to 11.08% for the vertical integrated rim area (vol). Repeatability is generally high for all parameters measured by the Stratus OCT for normal subjects.

Glaucoma group

The CoV/CoR1 ranges from 4.18% for the horizontal cup:disc area ratio to 17.63% for the vertical integrated rim area (vol). Repeatability is generally high for all parameters measured by the Stratus OCT for glaucoma patients.

4.7.4 Reproducibility between-visit

The between-visit reproducibility data for normal subjects and glaucoma patients are summarised in table 4.5.

Parameter	Normals		Glaucoma	
	ICC (%)	CoR 2 (%)	ICC (%)	CoR 2 (%)
Vert. integrated rim area (Vol)	98.1	10.47	91.8	27.16
Horiz. integrated rim width (Area)	94.6	4.87	91.1	8.38
Disc area	91.6	6.76	90.6	7.48
Cup area	98.3	10.99	92.1	14.73
Rim area	92.9	9.53	92.2	14.52
Cup:Disc Area ratio	97.2	12.96	94.4	7.15
Cup:Disc Horiz ratio	97.8	6.55	95.5	3.66
Cup:Disc Vert ratio	97.0	7.18	93.7	4.33
Mean	95.94±2.57	8.66±2.74	92.68±1.70	95.94±2.57

Table 4.5 Reproducibility (between-visit) results for normal subjects and glaucoma patients

Normal group

ICCs are high for each of the disc parameters measured by the Stratus OCT (see table 4.5). The disc area appears to have the lowest reproducibility at 91.6% (although this can still be considered to be very repeatable overall) while greatest between-visit reproducibility is displayed by the cup area at 98.3%. CoR 2 ranges from 4.87% to

12.96% indicating good reproducibility. Bland and Altman plots for all test parameters are displayed in figure 4.4 in which the solid horizontal line represents the group mean difference between visits for each parameter and the two dotted lines are the 95% limits of agreement between visits. The coefficient of reproducibility (the difference divided by the mean) is illustrated as a scatter plot within each graph (Bland and Altman, 1986).

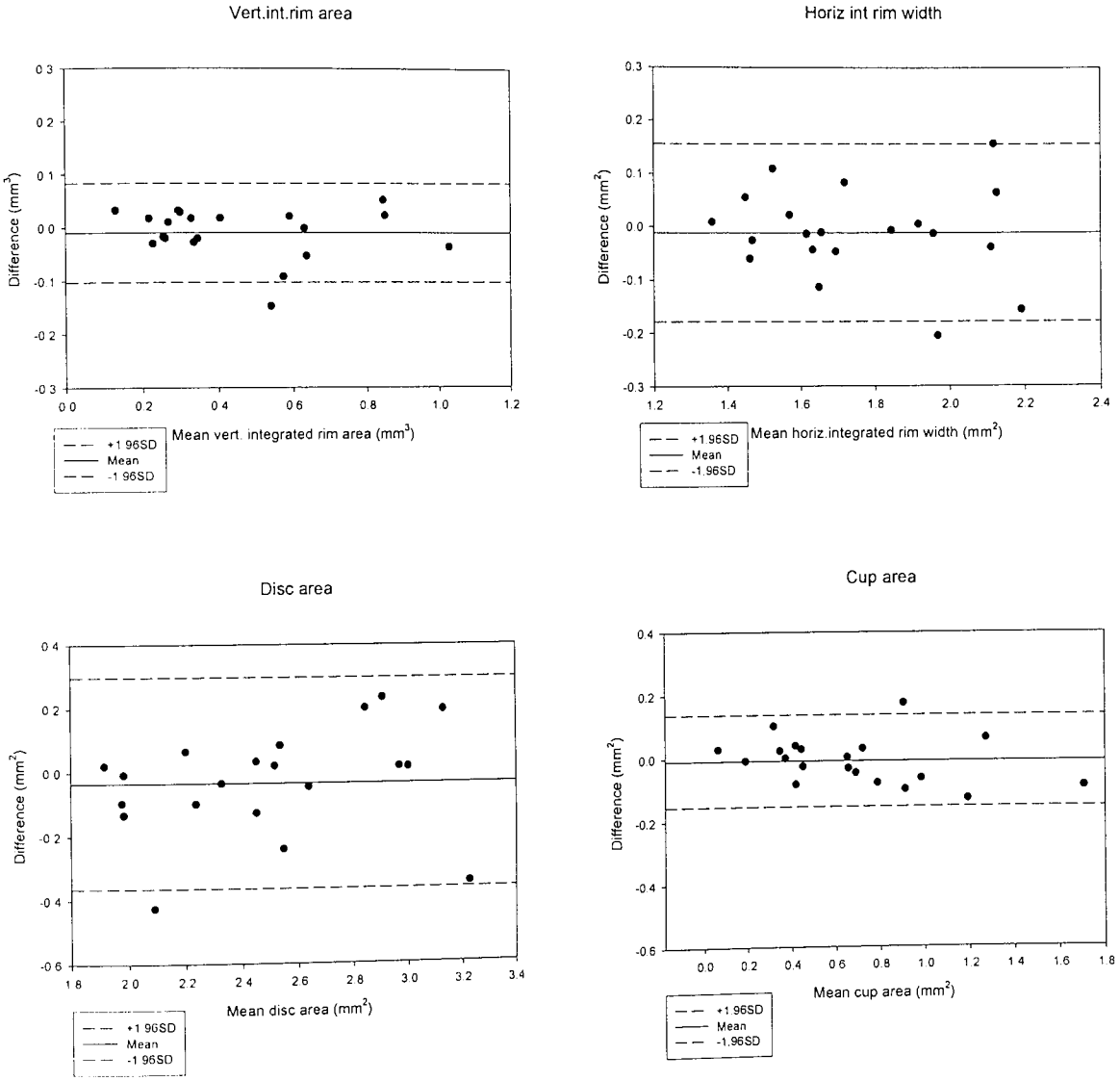

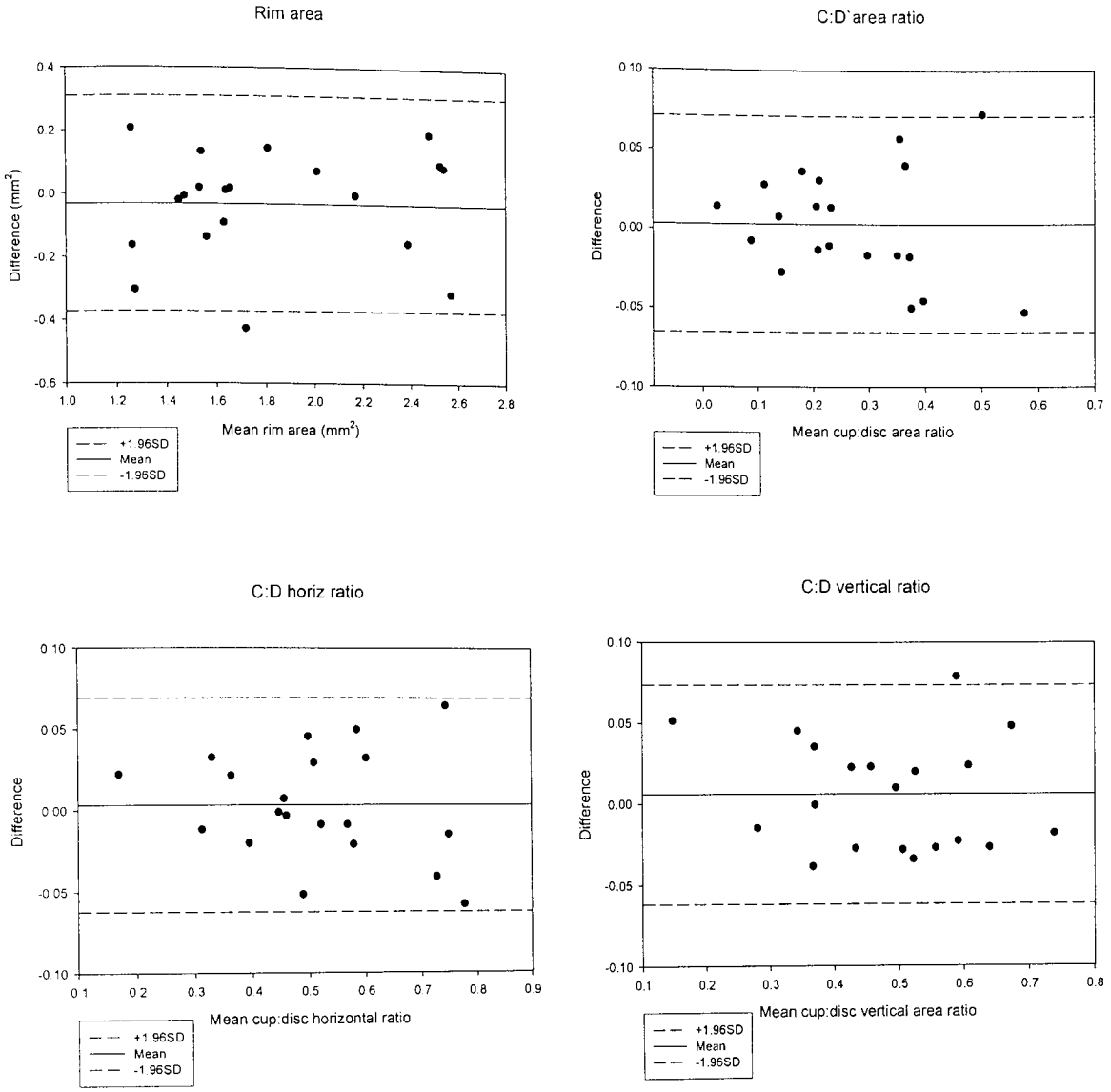

Figure 4.4 Graph showing the reproducibility of optic disc parameter measurements using the OCT in normal subjects.

A paired t-test showed no difference between visit 1 and visit 2 for any disc parameter ($p<0.0062$ after Bonferroni correction)

Glaucoma group

ICCs are high for each of the optic disc parameters measured by the OCT and range from 90.6% for the disc area to 95.5 % for the cup:disc horizontal ratio. CoR 2 ranges from 3.66% to 27.16%. Bland and Altman plots for all test parameters are displayed graphically in figure 4.5 in which the solid horizontal line represents the group mean difference between visits for each parameter and the two dotted lines are the 95% limits

of agreement between visits. The coefficient of reproducibility (the difference divided by the mean) is illustrated as a scatter plot within each graph (Bland and Altman, 1986).

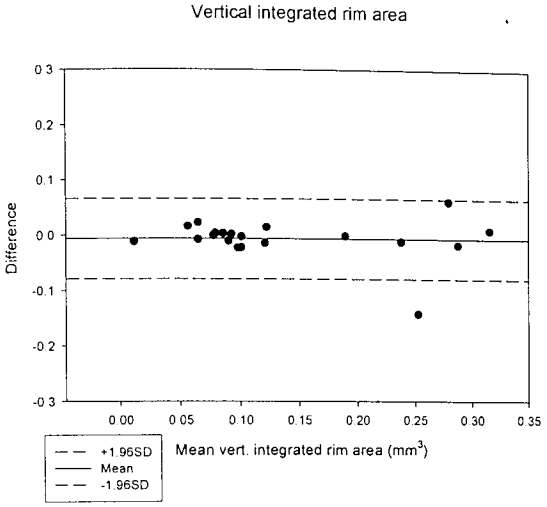

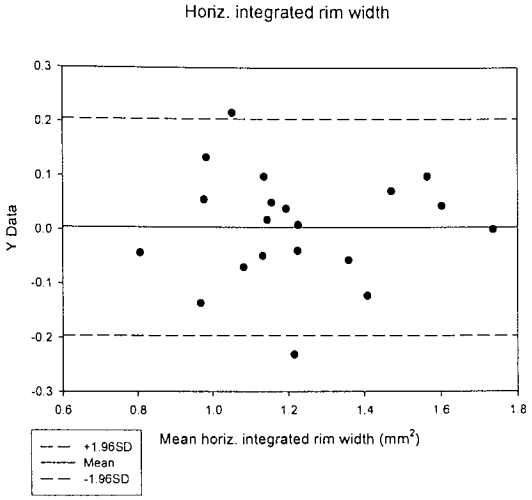

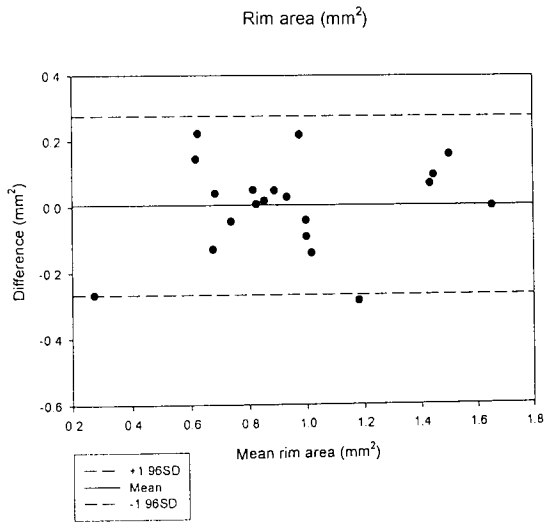

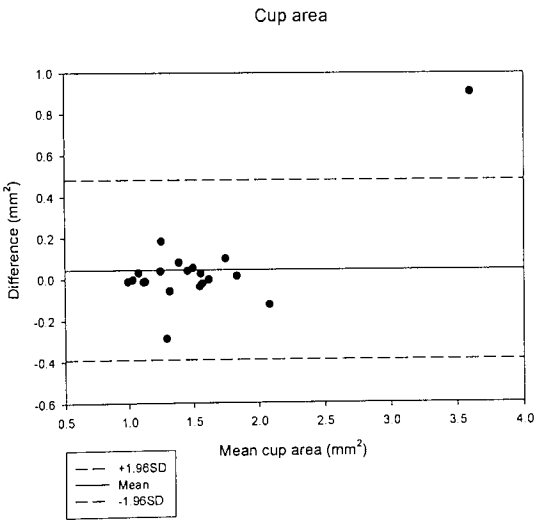

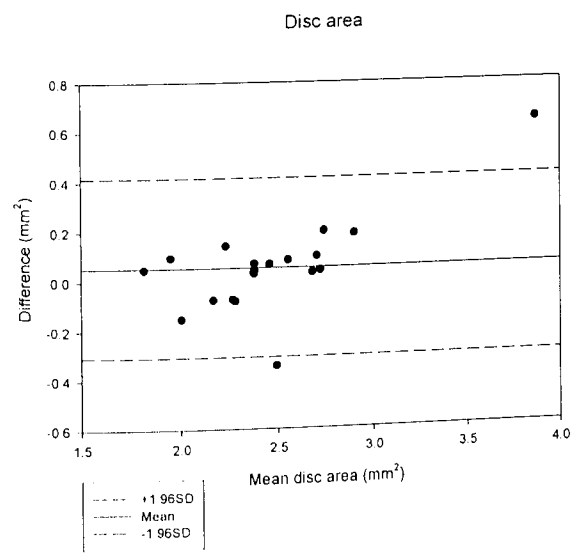

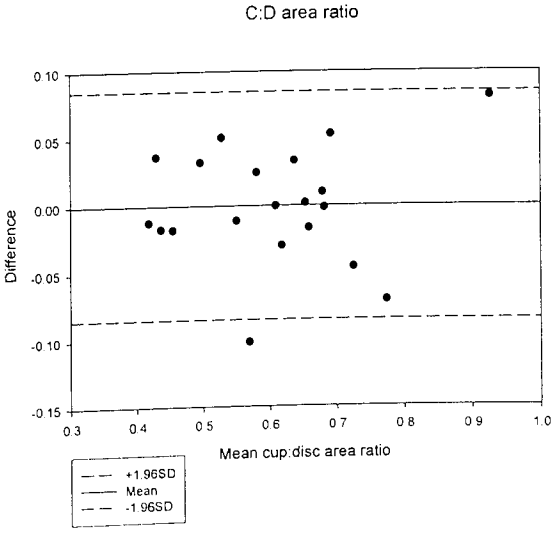

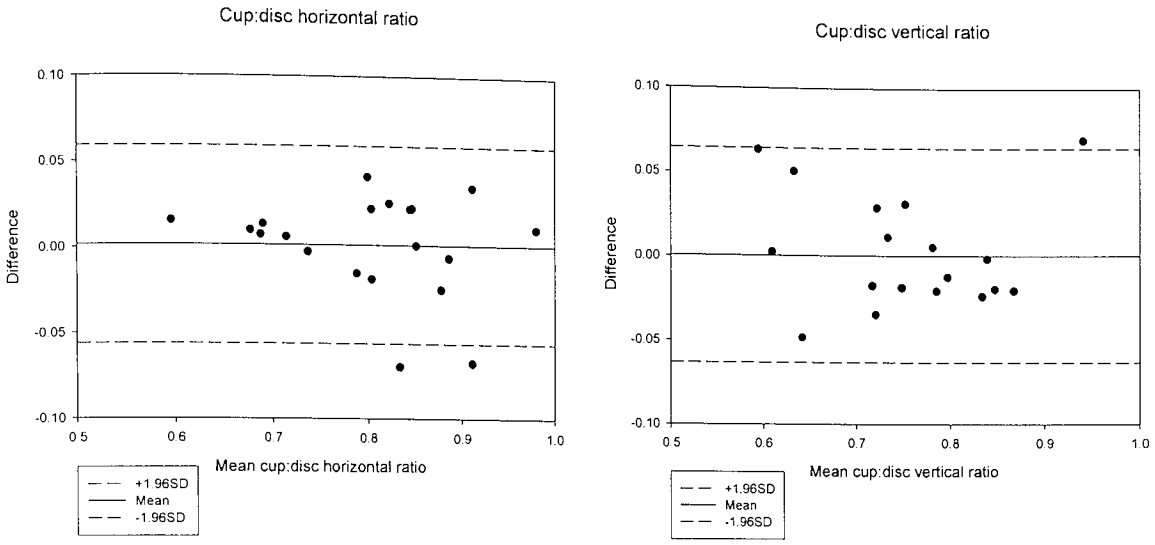

Figure 4.5 Graph showing the reproducibility of optic disc parameter measurements using the OCT in glaucoma patients.

A paired *t*-test showed no difference between visit 1 and visit 2 for any disc parameter ($p<0.0062$ after Bonferroni correction).

4.7.5 Difference between groups

Independent sample *t*-tests were performed to establish whether significant differences existed between groups in terms of the repeatability or reproducibility results. There were no significant differences for CoV, CoR1 ($p=0.581$), and CoR2 ($p=0.457$). However, ICC values differed significantly between groups ($p=0.010$).

4.8 Discussion

This study shows that measurements of optic disc parameters made with the Stratus OCT are both repeatable and reproducible for normal subjects and glaucoma patients. Within-visit repeatability is generally high for both groups although there is a wide range of repeatability values for each parameter. Repeatability is greater in normal subjects compared to glaucoma patients for the vertical integrated rim area (vol), horizontal integrated rim width (area), disc area and rim area while for the cup area,

cup: disc area ratio, cup: disc horizontal and vertical ratio glaucoma patients display the greatest repeatability.

For every parameter the ICC values are higher in normal subjects than glaucoma patients. With regard to the CoR 2, greater reproducibility is displayed for every parameter in the normal subjects compared with the glaucoma patients with the exception of the cup:disc area ratio, cup:disc horizontal area ratio and cup:disc vertical area ratio. While the between-visit reproducibility varies for each of the optic disc parameters it is generally very high.

Graphical representation of the coefficient of reproducibility in the Bland and Altman plots shows, not surprisingly for reproducible measures, that the mean of the difference is approximately 0 for all disc parameters in both the normal subjects and glaucoma patients. The reproducibility of acquired measures is indicated by the width of the upper and lower limits of agreement with very reproducible measures indicated by a very narrow range. Whilst it is not appropriate to draw comparisons between test parameters due to their being on different scales, every disc parameter exhibits an excellent degree of reproducibility.

4.8.1 Optic disc characteristics

Every disc parameter with the exception of disc size was significantly different between the normal subjects and the glaucoma group. Vertical integrated rim area, horizontal integrated rim width and rim area was greater in the normal subjects compared with the glaucoma patients. Cup area, and cup: disc ratios in terms of area, horizontal and vertical dimensions was smaller in the normal subjects than the glaucoma subjects. Our optic nerve head parameters are very similar to that reported by Paunescu *et al.* (2004) using the Stratus OCT to measure 10 normal subjects (mean age 30.5±7.4years) as shown in table 4.6.

Disc parameter	Study results	Paunescu *et al.* (2005)
Vert. integrated rim area (Vol) (mm^3)	0.45 ± 0.25	0.55 ± 0.39
Horiz. integrated rim width (Area) (mm^2)	1.75 ± 0.26	1.77 ± 0.28
Disc area (mm^2)	2.48 ± 0.44	2.19 ± 0.35
Cup area (mm^2)	0.67 ± 0.39	0.70 ± 0.57
Rim area (mm^2)	1.81 ± 0.48	1.49 ± 0.65
Cup:Disc Area ratio	0.27 ± 0.14	0.33 ± 0.26
Cup:Disc Horiz ratio	0.52 ± 0.16	0.55 ± 0.20
Cup:Disc Vert ratio	0.48 ± 0.14	0.51 ± 0.21

Table 4.6 Optic disc characteristics reported by comparative studies

The results of our study support the well documented pathological changes that occur in the glaucoma with loss of neural retinal rim tissue and increase in cup size (Jonas *et al.*, 1988b; Jonas, Fernandez and Sturmer, 1993).

4.8.2 Number of images

For each optic disc parameter of the normal subjects and glaucoma patients the mean standard deviation (MSD) was calculated for 2 scans, 3 scans, 4 scans etc and plotted against the number of scans taken. For each graph the point at which the curve reached a plateau was identified. While there was no specific point at which the variance was stable, the majority of locations reached a plateau around three or four scans, beyond which point there was little further improvement in the data overall. Our data suggest that 3 images are the minimum acceptable for repeatable measures while remaining clinically acceptable. Repeatability and reproducibility analyses were based on these findings. The use of 3 scans was employed throughout all subsequent studies in this work.

4.8.3 Repeatability and reproducibility

To date, studies to assess the repeatability and reproducibility of the OCT to measure optic disc parameters have been scarce. At the time of our study, to our knowledge no

literature regarding the repeatability and reproducibility optic nerve head measures had been published. Since completion of our work there have been two studies investigating the ability of the Stratus OCT to measure optic nerve head morphometry. In a study by Paunescu *et al.* (2004) using the Stratus OCT, ten normal subjects were imaged six times (three before dilation and three after dilation) per day and the series was repeated on three different days within a 5 month period. The standard density (fast acquisition) and high density (slow acquisition) six radial line scans were centred on the optic disc. ICCs ranged from 60-94% for the standard density scan with an undilated pupil and 45-97% with dilated pupils. ICCs ranged from 21- 92% for the undilated high density scan and 3-81% for the dilated high density scan. Highest reproducibility was markedly higher for dilated standard scanning (fast optical disc scan) for most of the parameters. This is explained by the fact that the fast optical scan acquisition time is quicker than the high density (slow) scan and therefore less affected by eye movements and scan placement. Reliability of measurements for optic nerve head scanning is more challenging for the patient because they are required to view an eccentric fixation light while the scan is taken of the optic disc. A further source of variability is the requirement of the operator to manually place the scan directly over the optic disc. This effect was limited in our study by the use of the fast optical disc scan only, which required the manual placement of the scan on one occasion only at the start of the scanning procedure. Our study found higher reproducibility values with ICCs ranging from 91.6% to 98.3% compared with that of Paunsecu *et al.* (2004) who reported ICCs of 45-97%. In both cases, the fast optical scan was performed for dilated pupils.

Since the completion of our study, Olmedo *et al.* (2005) has investigated the ability of the OCT to measure optic disc parameters in diseased eyes. Olmedo *et al.* (2005) evaluated the reproducibility of optic nerve head morphometry measurements obtained by OCT (model 3000) for 20 eyes (10 eyes of normal subjects and 10 eyes of glaucoma patients). For the normal group, the majority of optic nerve dimensions displayed ICCs above 81% with the exception of the horizontal integrated rim width (23.1%) rim area (33.3%) and disc area (64.7%). Our findings indicate much higher reproducibility in these areas with ICC values of 94.6% for the horizontal integrated rim area, 92.9% for the rim area and 91.6% for the disc area. All other parameters in our study exhibited ICCs of greater than 91.6% compared to the 81% by Olmedo *et al.* (2005). According to Olmedo and colleagues (2005) their glaucomatous eyes exhibited higher

reproducibility than in the normal group with all parameters having ICCs above 85% except the disc area with an ICC of 68.1%. This is not the case in our study where normal eyes exhibit greater reproducibility between 91.6% and 98.1% compared to the glaucoma group where ICCs range from 90.6% to 95.5%.

Both our repeatability and reproducibility results appear worse for the optic disc parameters than for macular thickness measurements (see Chapter 3). This is likely to be due to the fact that the optic nerve head is a much larger and more varied structure and is therefore more affected by the position and centration of images. Macular scanning involves the patients fixating centrally and no intervention is required on the part of the operator to align scan images – the default scanning position is directly through the fovea providing fixation is accurate. Throughout the scanning process it is relatively easy to check the accuracy of a patient's fixation by viewing the scanning line. The foveal pit should always be seen central in the viewing window – if this is not the case the patient should be reminded to fixate the green fixation light. For optic nerve head scanning the patient is required to view an eccentric fixation target which is inherently more difficult to view accurately, while the scan is located centrally in the camera. Fixation losses are more likely because the scanning lines and fixation point are no longer coincident. Checking fixation for optic nerve head scans is more problematic compared with for the macular scan. Another potential source of inaccuracy is the requirement for the operator to manually place the scanning lines centrally through the optic disc at the beginning of the scanning session. It is imperative at this stage that fixation is accurate because this scan position remains the same for the rest of the scanning procedure.

Reproducible between-visit measurements are aided by the OCT facility to perform the repeat scan protocol. The scan is placed in the exact same position as visit 1 – this can be checked by taking note of the x and y co-ordinates of the scan and fixation position. Provided the patient's position is set up in the same way as visit 1 and they remain fixated on the target light, acquired data should be reproducible. This has clear implications for the long-term monitoring of diseased eyes.

During all OCT scanning, especially for the optic nerve head scans, it is important that the patient is in a comfortable and maintainable position with their forehead placed on

the forehead rest. Any fluctuation in head and body position is likely to reduce accuracy and repeatability of the scans. Practiced operators are more likely to achieve repeatable and reproducible results due to the fact that their scanning time is quicker and this in turn offers the patient less time to move position or experience fatigue during scanning.

4.9 Conclusion

The OCT provides repeatable and reproducible measurements of optic disc parameters for both normal and glaucomatous eyes. Three scans for each visit will provide repeatable and reproducible measurements. Optical coherence tomography can be regarded as a useful tool in the monitoring of progression and effectiveness of the treatment of glaucoma.

CHAPTER 5: Relationship between axial length and retinal thickness and retinal nerve fibre layer thickness

5.1 Relationship between axial length and retinal thickness at the macula and optic nerve head

5.1.1 Abstract

Purpose: To determine the relationship between axial length (AL), macular retinal thickness (MRt) and retinal nerve fibre layer thickness (RNFLt) using the IOLMaster (Carl Zeiss Meditec, Germany. Software version 3.xx) and the Stratus Optical Coherence Tomographer (OCT3 Model 3000, Carl-Zeiss Meditec, Dublin, CA).

Methods: Axial length and MRt measurements were obtained for one eye each of 66 normal healthy volunteers; 29 male, 37 female subjects (mean age 22.45±4.3 years; range 19-39 years). MRt measurements were obtained using OCT multiple radial line scans, 6mm in length, centred through the fixation point of each patient. Retinal thickness analysis software (version 3.0) produced a circular map comprising 9 sectors depicting average retinal thickness. Axial length and RNFLt measurements were obtained for one eye each of 64 normal healthy volunteers; 29 male, 35 female subjects (mean age mean age 22.42±4.36 years; range 19-39 years) using a series of OCT circular scans centered on the optic disc, scanning around the optic disc margin. Measurements of RNFLt were taken close to the optic disc margin and at two further locations at increasing distances from the optic disc margin. Average RNFL thickness measurements were obtained for the overall 360 degree scan and for each of the superior, nasal, inferior and temporal quadrants for each of the three scan sizes. The relationship between axial length and tissue thickness was investigated using Pearson product-moment correlation with Bonferroni correction for multiple comparisons.

Results: The group mean axial length was 24.27±1.3 mm (range 22.08- 27.71mm). There was a moderate negative relationship between axial length and retinal thickness in positions 6 (outer nasal retina) p=0.014, positions 7 (outer inferior retina) p=0.002, 8 (outer temporal retina) p=0.003, and 9 (outer superior retina) p=0.002. For the 2nd and 3rd radius scans RNFLt was negatively correlated with axial length for the mean 360° thickness (p=0.000, p=0.000 respectively) and for the inferior (p=0.000, p=0.000 respectively), superior (p=0.000, p=0.000 respectively), and nasal quadrants (p=0.000, p=0.002 respectively) but not for the temporal quadrant (p=0.277, p=0.993 respectively).

Conclusion: MRt and RNFLt at the optic nerve head correlate negatively with axial length. These data suggest that eye size may be a factor in susceptibility to diseases of the macula and optic nerve head, and should be factored in to the clinical interpretation of clinical data and associated risks.

5.2 Introduction

Optical coherence tomography may be of value in the diagnosis and monitoring of diseases of the eye that affect the retina and nerve fibre layer for example in patients with diabetes or eyes with glaucoma (Puliafito *et al.*, 1995; Schuman *et al.*, 1995; Hrynchak and Simpson, 2000; Guedes *et al.*, 2003; Jaffe and Caprioli, 2004; Hussain, Hussain and Netheti, 2005). Macular oedema due to diabetic retinopathy, uveitis and retinal vein occlusion will all lead to an increase in retinal thickness. Conversely, loss of retinal ganglion cell axons with age or in glaucoma, or atrophy in the retinal pigment epithelium layer in age related macular degeneration (ARMD), will lead to a decrease in retinal nerve fibre layer thickness. In order that clinical data can be interpreted accurately, all possible reasons for tissue thickness changes should be understood before explanations for an increase or decrease are given. The axial length of the globe in myopic eyes is associated with a subsequent thinning of the scleral tissue and since this may also result in stretching of the retinal tissue, it has been suggested that there may be consequential thinning of the retina in eyes with a greater volume (Asrani *et al.*, 1999; Yanoff and Fine, 1989). Such an association between retinal volume (and its correlates) and retinal thickness, should be known prior to interpretation of OCT scans of diseased eyes. To date, studies investigating the effect of myopia on retinal and retinal nerve fibre layer tissue have produced conflicting reports. Garcia-Valenzuela *et al.* (2000) observed no relationship between axial length and retinal thickness as measured by the Retinal Thickness Analyzer (RTA). Such findings are confirmed by both Wakatani *et al.* (2003) and Goebel *et al.* (2001) who, using OCT line scans placed through the fovea, reported no influence of axial length on macular thickness. However, a relationship between macular retinal thickness and degrees of myopia has been reported by Mrugacz and Bakunowicz-Lazarczyk (2005) using the OCT to image young myopes. In addition, Kremser *et al.* (1999) using a prototype RTA report retinal thinning at the posterior pole of myopic eyes.

In this study we examine the possibility of retinal thickness and retinal nerve fibre layer thickness being reduced in normal healthy eyes with greater axial length i.e. in subjects with axial myopia. Since the basis of our study is that longer eyes have thinner retinae,

the prescription of our subject sample *per se* will not be regarded as a factor in this work.

5.3 Aims and objectives

This study consisted of 2 parts:

1) To determine the relationship between axial length and retinal thickness measured at the macula in normal human eyes.
2) To determine the relationship between axial length and retinal nerve fibre layer thickness measured around the optic nerve head in normal human eyes

5.3.1 Hypothesis

Retinal thickness and retinal nerve fibre layer thickness decrease with increasing axial length.

5.4 Study sample and investigation

5.4.1 Inclusion Criteria

Normal healthy subjects were recruited from attendees at the Optometry Clinic at Aston University and from the University's student population. A full eye examination was performed by an optometrist (HLW) to establish whether the study inclusion criteria were met. Subjects were included if they exhibited:

- No abnormalities on ophthalmoscopic examination
- Minimal or no lens opacities allowing a clear fundus view
- No history or evidence of intraocular surgery or laser therapy
- No history or evidence of retinal pathology or glaucoma
- Snellen visual acuity (VA) 6/9 or better
- Absence of visual field defects (Humphrey Field Analyser program 24-2)
- Intraocular pressure (IOP) less than 21mmHg (non-contact tonometry Pulsair 3000)

5.4.2 Subject sample: Macular thickness measurements

The subject sample consisted of one eye each of 66 normal healthy volunteers. Details of the subject sample are given in table 5.1.

	Gender		Test eye		Age years mean ± SD (range)	Axial length mm Mean ± SD (range)	Refractive error Sph. equiv (DS) Mean ± SD (range)
	Male	Female	Right	Left			
MRt (n=66)	29	37	31	35	22.45±4.3 (19-39)	24.27±1.3 (22.08-27.71)	-2.43±2.75 (0-10)

Table 5.1 Details of the subject sample (MRt measurements)

5.4.3 Ethical approval and informed consent

Ethical approval was obtained from the ethical committee boards of Aston University. Approval conformed to the tenets of the Declaration of Helsinki. Written informed consent was obtained from all subjects.

5.5 Methods

Following recruitment as per the requirements set and listed above, subjects attended for one visit only.

5.5.1 Axial length

Axial length measurements were obtained using the IOL Master (Carl Zeiss Meditec, Germany. Software version 3.xx). The IOLMaster is a non contact ocular biometer used to measure parameters of the human eye including axial length, corneal curvature, anterior chamber depth. It uses a semiconductor diode laser of wavelength 780nm. Axial length calculation is based on the process of partial coherence interferometry, whereby an interference signal is produced if the measuring light is reflected by the tear film and the retinal pigment epithelium. The IOLMaster employs an internal statistically

verified calculation algorithm which serves to adjust for the distance between the pigment epithelium and the inner limiting membrane. This ensures that IOLMaster data is comparable to axial length measurements made by ultrasonic immersion instruments which measure the axial length as the distance between the cornea and the inner limiting membrane- the point at which the sound waves are reflected. Studies have shown that the IOLMaster shows good repeatability and accuracy of axial length measurement both with trained examiners (Lam, Chan and Pang, 2001) and inexperienced operators (Kielhorn, Rajan, Tesha *et al.*, 2003).

Prior to axial length calculation, subject details were entered into the database of the IOLMaster. The subjects were instructed to place their chin on the chin rest and forehead against the top bar and instructed to look at the red fixation light. Five readings were taken and reviewed. Measures with signal-to-noise ratios (SNR) less than 2 were rejected (according to manufacturer's guidelines). Of those reliable readings accepted the measure with the greatest SNR was used for analysis.

5.5.2 Macular retinal thickness (MRt) measurements

Retinal thickness scans of the macular were taken using the optical coherence tomographer. Prior to OCT image acquisition, subject details were entered into the database of the OCT. The subjects were instructed to place their chin on the chin rest and forehead against the top bar and instructed to fixate on a green target within the centre of the camera. To optimise the scan image and yield the strongest scan signal both the Z-offset (axial range) and polarisation was adjusted.

Five consecutive fast macular thickness scans (of which the 3 best images were selected for analysis), centred through the fixation point were taken for each subject. Each scan comprised a radial line pattern consisting of 6 equally spaced lines, each measuring 6mm. The fast macular thickness map protocol compresses the six radial line scans into one scan in 1.92 seconds. Retinal thickness analysis software produced a circular map comprising 9 sectors depicting average retinal thickness. Map circle default diameters are 1, 3 and 6mm (See chapter 1)

5.6 Statistical analysis

Pearson product-moment correlation (r) was performed to assess the relationship between axial length (AL) and macular retinal thickness (MRt) in all retinal locations (1-9). This provides a numerical summary of the direction and strength of the linear relationship between AL and MRt where a correlation of 1 indicates a perfect correlation and a correlation of 0 indicates no relationship at all. In total, comparisons for 10 locations (1-9 and mean MRt) were made and it was therefore necessary to set a more stringent alpha level for comparison. This was achieved using Bonferroni adjustment whereby the new alpha level was calculated from 0.05 (usual significance level) divided by 10 (the number of comparisons) to give p=0.005. Preliminary analyses were performed to ensure no violation of the assumptions of normality, linearity and homoscedasticity.

5.7 Results

5.7.1 Macular retinal thickness values

Average macular retinal thickness values are displayed in table 5.2.

Location	Macular thickness
Position 1 (fovea)	195.84± 18.32 mm
Position 2 (inner nasal)	275.52± 15.20 mm
Position 3 (inner inferior)	269.74± 13.15 mm
Position 4 (inner temporal)	259.04± 12.75 mm
Position 5 (inner superior)	273.56± 14.03 mm
Position 6 (outer nasal)	254.22± 14.14 mm
Position 7 (outer inferior)	226.51± 12.69 mm
Position 8 (outer temporal)	216.74± 13.11 mm
Position 9 (outer superior)	236.08± 13.52 mm
Mean retinal thickness	244.92± 11.74 mm

Table 5.2 Mean ± SD retinal thickness values for each macular retinal location

5.7.2 Correlation analysis: AL versus MRt

The relationship between axial length as measured by the IOL master and macular retinal thickness in all 9 positions and mean retinal thickness of the scan as measured by OCT was investigated using Pearson product-moment correlation. Correlation analysis results are summarised in table 5.3. Statistical significance is indicated by *.

Scan position	Pearson Correlation (r)	Significance (2 tailed)
1	0.194	0.119
2	-0.053	0.675
3	-0.108	0.388
4	-0.056	0.657
5	-0.116	0.352
6	-0.296	0.016
7	-0.378	0.002*
8	-0.375	0.003*
9	-0.368	0.002*
Mean	-0.186	0.135

Table 5.3 Pearson product moment correlation between axial length and retinal thickness

*denotes statistical significance

The results indicate a moderate negative relationship between axial length and retinal thickness in positions 7 (outer inferior retina; p=0.002), 8 (outer temporal retina; p=0.003), and 9 (outer superior retina; p=0.002). There was also a similar trend in position 6. However, this was not statistically significant after Bonferroni correction. The relationship between axial length and MRt for these positions are illustrated in the scatter plots in figure 5.1.

a)

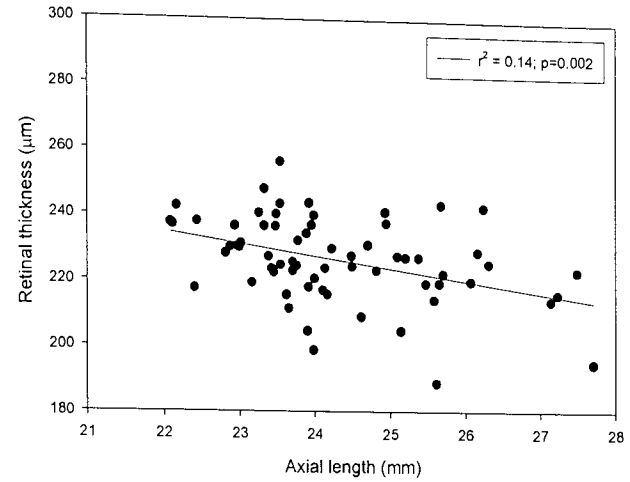

b)

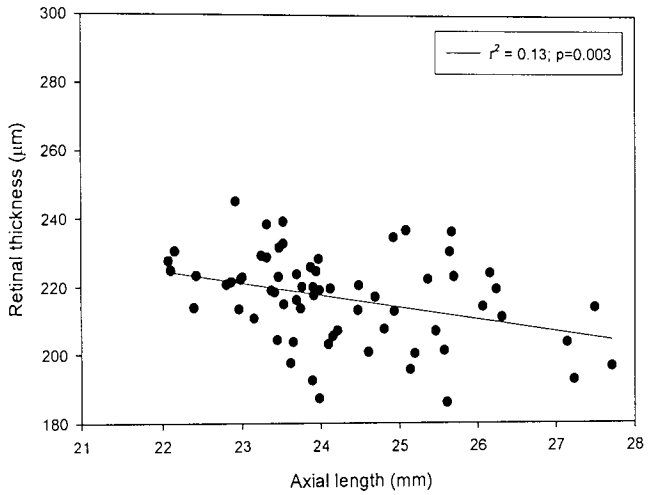

c)

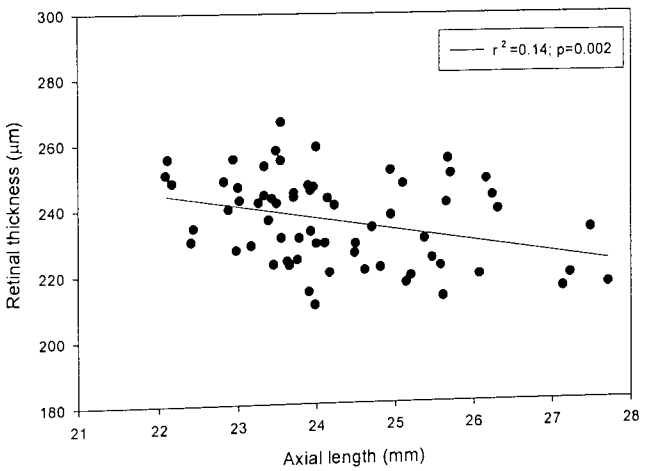

Figure 5.1 Scatterplots showing negative linear trends between axial length and a) position 7 (outer inferior retina) b) position 8 (outer temporal retina) c) position 9 (outer superior retina)

5.8 Subject sample: RNFLt at the optic nerve head

The subject sample consisted of one eye each of 64 normal healthy volunteers; 29 male, 35 female subjects. Their mean age was 22.42±4.36 years (range 19-39 years). The group had mean axial length 24.24±1.32 mm. Details of the subject sample are summarised in table 5.4.

	Gender		Test eye		Age years mean ± SD (range)	Axial length mm Mean ± SD (range)	Refractive error Sph. equiv (DS) Mean ± SD (range)
	Male	Female	Right	Left			
RNFLt (n=64)	29	35	31	33	22.42± 4.36 (19-39)	24.24± 1.32 (22.08-27.71)	-2.41±2.74 (0-10)

Table 5.4 Details of the subject sample (RNFLt)

5.9 Methods

Following recruitment as per the requirements set and listed above, subjects attended for one visit only. Following informed consent, axial length measurements were obtained using the IOL master (see section 5.5.1).

Retinal nerve fibre layer thickness scans around the optic nerve head were taken using the optical coherence tomographer. Prior to OCT image acquisition, subject details were entered into the database of the OCT. The subjects were instructed to place their chin on the chin rest and forehead against the top bar and instructed to fixate on a green target within the centre of the camera. To optimise the scan image and yield the strongest scan signal both the Z-offset (axial range) and polarisation was adjusted.

Retinal nerve fibre layer thickness (RNFLt) was assessed using a series of OCT circular scans centered around the optic disc margin. Measurements of RNFLt were taken at the optic disc margin and at two further locations at increasing distance from the optic disc margin using circle scan radii specific to each subject. The initial scan was placed at the

subjects' disc margin and designed to fit closely around the optic disc margin whilst ensuring that the entire optic disc fell within the scanning circle. The radius of the circle scan was then increased to 2x and then 3x the initial radius to allow investigation of the RNFL at several eccentricities (i.e. using ratio of 1:2:3). RNFL analysis software produced a circular map depicting RNFL thickness measurements for each of the four 90 degree quadrants (superior, nasal, inferior and temporal) and for the entire scan through 360 degrees as shown in figure 5.2 and figure 5.3.

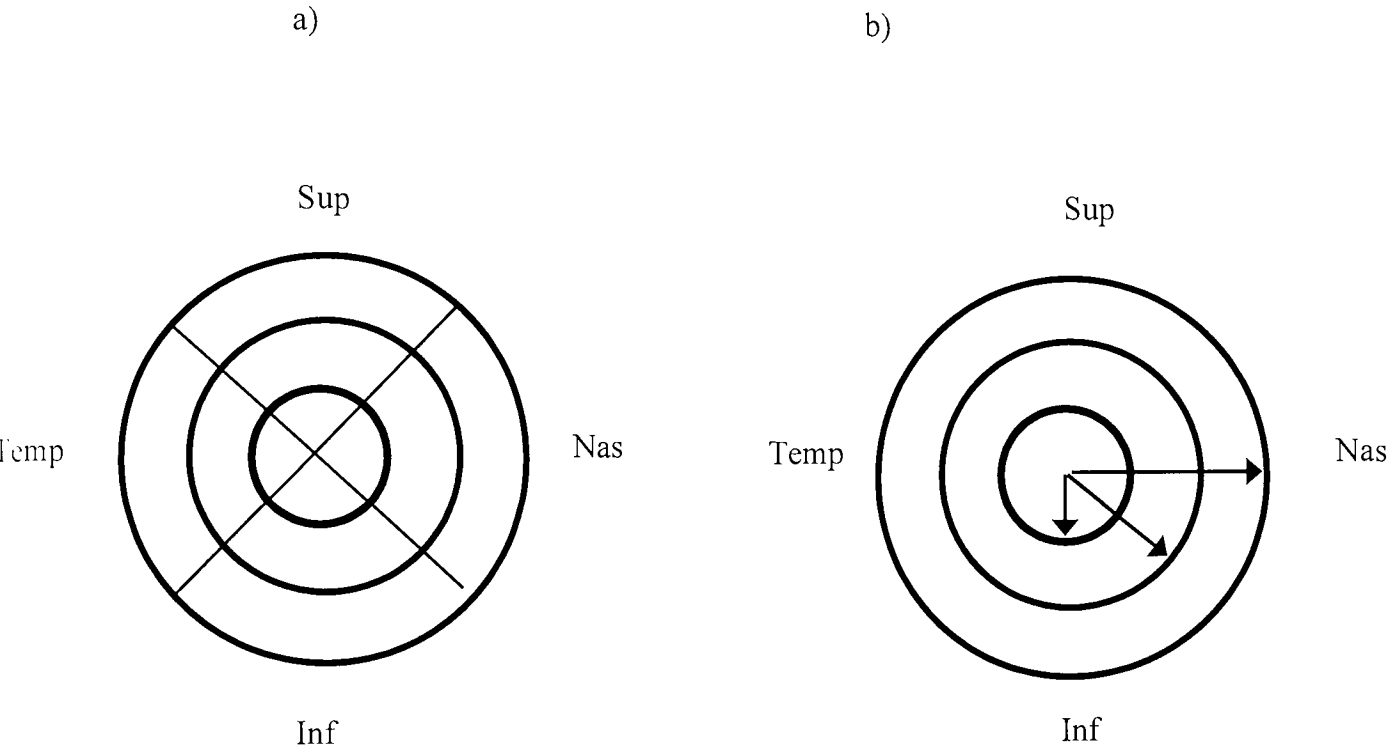

Figure 5.2 Schematic representing a) the OCT software output depicting RNFLt in each quadrant and b) the concentric circle scans of three different radii centred on the optic disc

a) b)

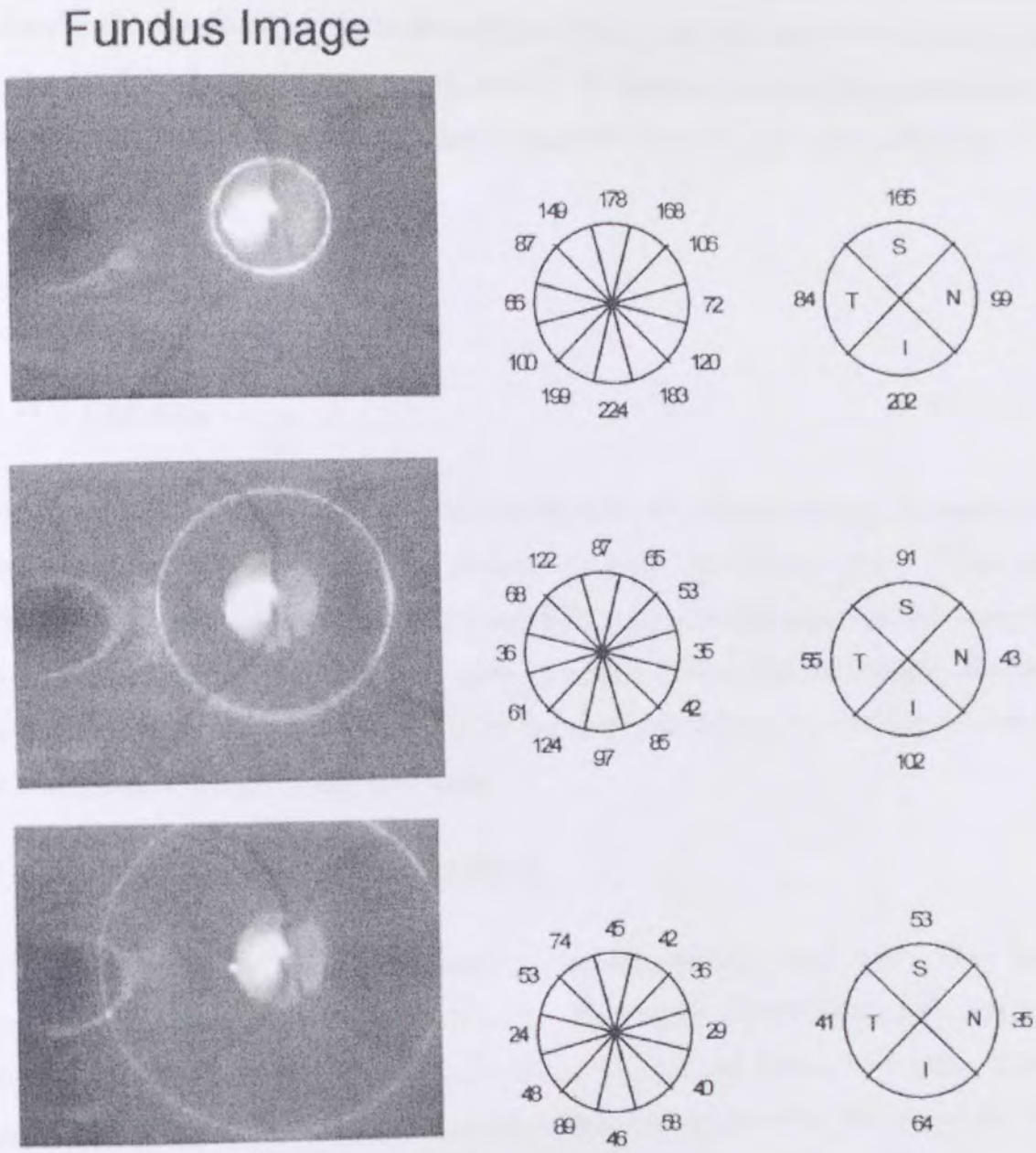

Figure 5.3 a) Example of a fundus image during OCT RNFLt scan acquisition and b) OCT RNFLt analysis per clock hour position and per quadrant

5.10 Statistical analysis

Pearson product-moment correlation was performed to assess the relationship between axial length and retinal nerve fibre layer thickness for the mean 360° scan and in each quadrant (superior, nasal, inferior and temporal) for each of the three scans (disc margin scan, 2nd and 3rd radius scan). In total, for each scan, comparisons for 5 locations (each quadrant and mean RNFLt) were made and it was therefore necessary to set a more

stringent alpha level for comparison. This was achieved using Bonferroni adjustment whereby the new alpha level was calculated as 0.05 (usual significance level) divided by 5 (the number of comparisons) to give p=0.01. Preliminary analyses were performed to ensure no violation of the assumptions of normality, linearity and homoscedasticity.

5.11 Results

5.11.1 Disc area

The relationship between disc area and retinal nerve fibre layer thickness for each scan was investigated using Pearson product moment correlation. After Bonferroni correction for multiple comparisons (5: superior, nasal, inferior, temporal and mean) the p level was adjusted to 0.01. There were no significant correlations between disc area and retinal nerve fibre layer thickness for the mean nerve fibre layer or for each of the four quadrants in each of the three scans.

5.11.2 Retinal nerve fibre layer thickness

The following table (table 5.5) details the actual average retinal nerve fibre layer thickness for each quadrant of each scan. The results are displayed graphically in figures 5.4. The majority of scans had radii of 1.0, 2.0 and 3.0mm or 1.1mm, 2.2mm and 3.3mm. The size of the scans for each subject was governed by the size of the first scan which was placed at the subjects' disc margin and designed to fit closely around the optic disc margin whilst ensuring that the entire optic disc fell within the scanning circle. The radius of the circle scan was then increased to 2x and then 3x the initial radius to allow investigation of the RNFL at several eccentricities (i.e. using ratio of 1:2:3).

Quadrant	Disc margin (microns)	2nd radius (microns)	3rd radius (microns)
Superior	165.77± 19.73	101.89± 14.53	66.44 ± 10.33
Nasal	128.31 ± 29.03	60.80 ± 17.37	40.89 ± 7.10
Inferior	178.13± 27.98	101.04± 12.93	64.17 ± 9.62
Temporal	93.98± 22.64	60.12 ± 9.53	45.23 ± 7.23
Mean	141.55± 17.36	80.96± 9.20	54.18± 6.37

Table 5.5 Retinal nerve fibre layer thickness values in each quadrant for each scan radii

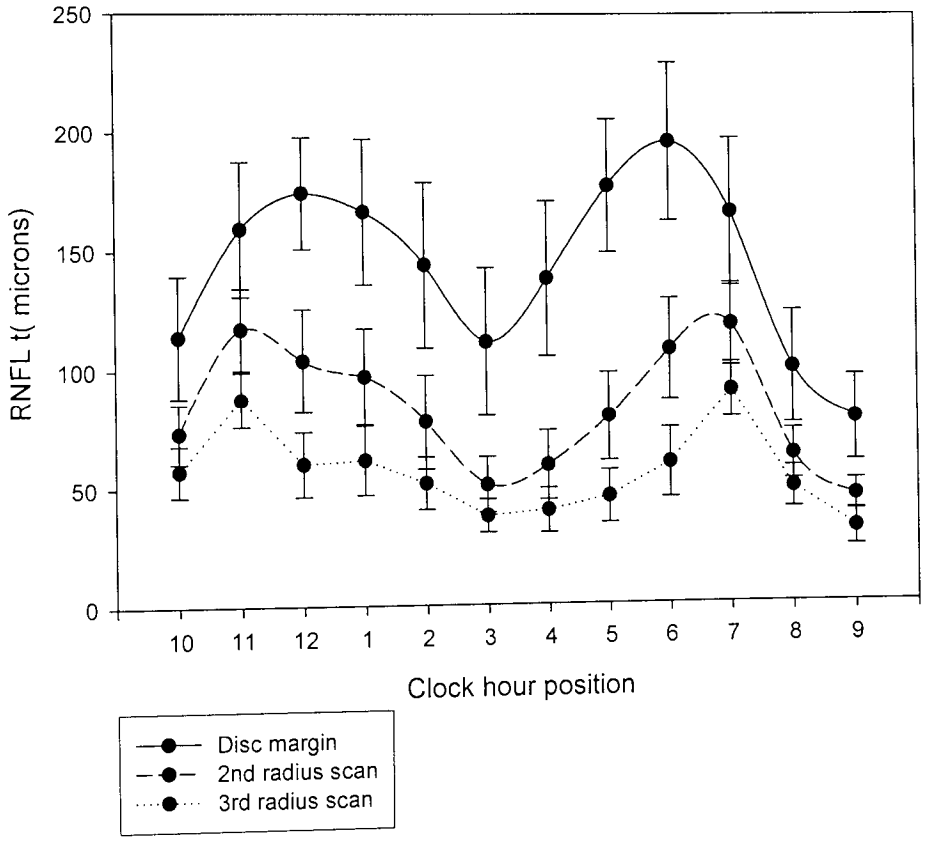

Figure 5.4 Graph to show the RNFLt variation around the optic nerve head for each scan size

5.11.3 Correlation analysis

Pearson product-moment correlation was conducted to investigate the relationship between axial length and retinal nerve fibre layer thickness in each quadrant and for each scan. The results are displayed in table 5.6 where statistically significant values are indicated by *

5.11.3.1 Disc margin

Disc margin RNFL position	Pearson Correlation (r)	Significance
Superior quadrant	-0.080	0.527
Nasal quadrant	-0.307	0.014
Inferior quadrant	-0.092	0.469
Temporal	0.038	0.768
Mean RNFL	-0.176	0.164

Table 5.6 Relationship between axial length and retinal nerve fibre layer thickness at the disc margin

A summary of the findings is given in table 5.6. Pearson product-moment correlation coefficient showed a negative trend between axial length and retinal nerve fibre layer thickness in the nasal quadrant (r=-0.307, p=0.014) with greater axial length associated with thinner nerve fibre layer. However, this failed to reach statistical significance after Bonferroni correction.

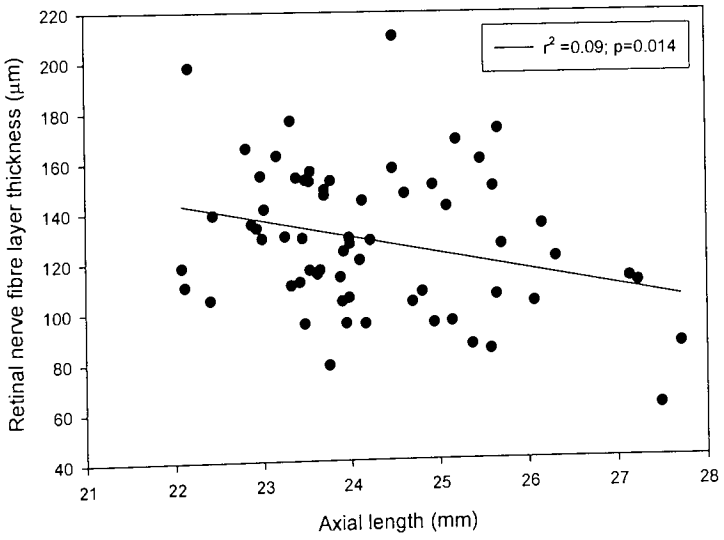

Figure 5.5 Scatterplot to show the negative trend between axial length and nasal RNFL at the disc margin

5.11.3.2 2nd radius scan

The findings are summarised in table 5.7. Significance is shown by *

2nd radius RNFL position	Pearson Correlation (r)	Significance
Superior quadrant	-0.437	0.000*
Nasal quadrant	-0.549	0.000*
Inferior quadrant	-0.477	0.000*
Temporal	0.138	0.277
Mean RNFL	-0.530	0.000*

Table 5.7 Relationship between axial length and retinal nerve fibre layer thickness for the 2nd radius scan * denotes statistical significance (p=0.01 after Bonferroni correction)

Pearson product- moment correlation coefficient showed a strong negative correlation between axial length and retinal nerve fibre layer for the superior, nasal and inferior quadrants and for the mean fibre layer for the 2nd radii. In these quadrants greater axial length is associated with a thinner retinal nerve fibre layer.

The following figure (5.6) shows the above results in graph format.

a)

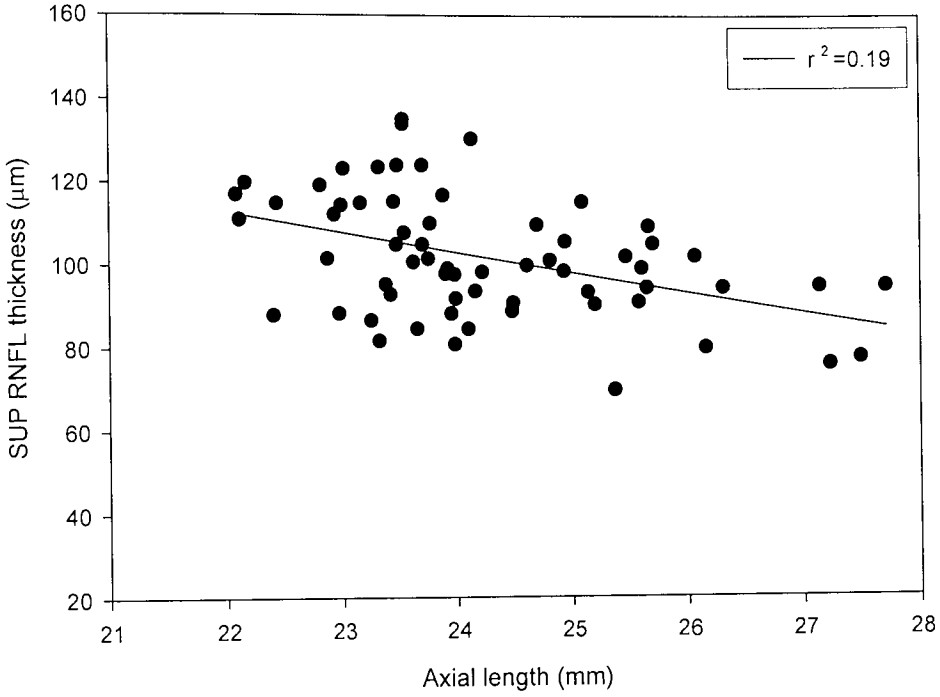

b)

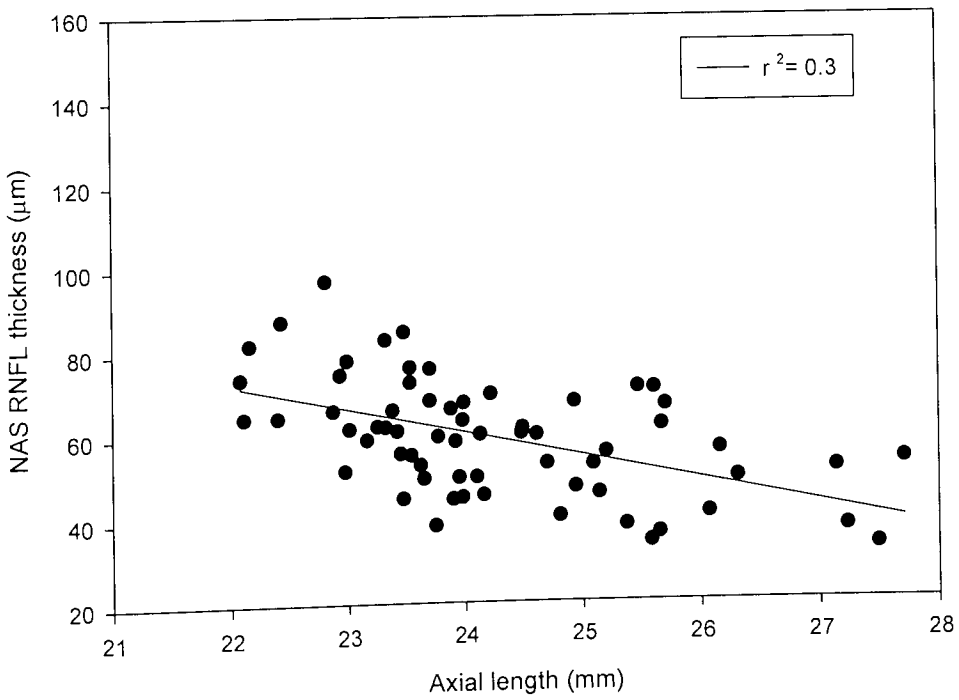

c)

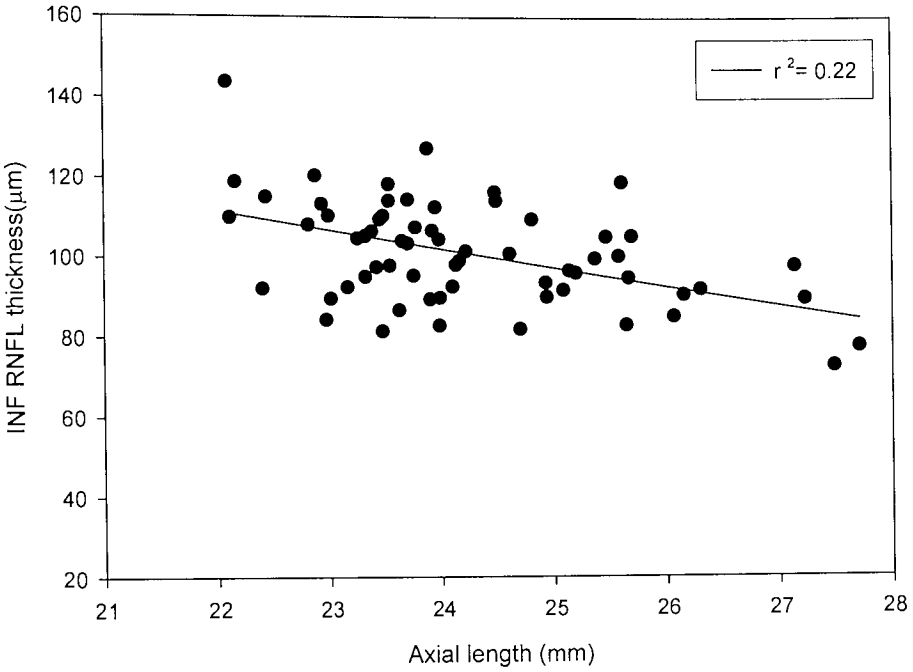

d)

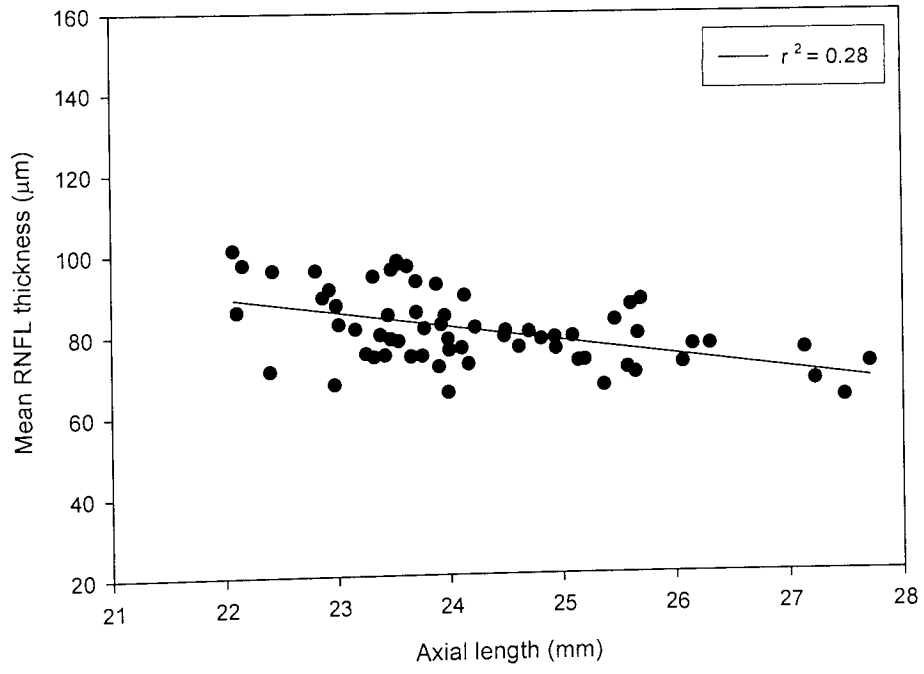

Figure 5.6 Scatterplot to show the negative correlation between axial length and a) superior RNFL and b) nasal RNFL c) inferior RNFL and d) mean RNFL for the 2nd radius scan.

5.11.3.3 3rd radius scan

The findings are summarised in table 5.8. Significance is shown by *

3rd radius RNFL position	Pearson Correlation (r)	Significance
Superior quadrant	-0.423	0.000*
Nasal quadrant	-0.374	0.002*
Inferior quadrant	-0.442	0.000*
Temporal	-0.011	0.993
Mean RNFL	-0.445	0.000*

Table 5.8 Relationship between axial length and retinal nerve fibre layer thickness for the 3rd radius scan

Pearson product- moment correlation coefficient showed a strong negative correlation between axial length and retinal nerve fibre layer for the superior, nasal, inferior quadrant and for the mean fibre layer for the 3nd radii. In these quadrants greater axial length is associated with a thinner retinal nerve fibre layer.

The following figure (5.7) shows the above results in graph format.

a)

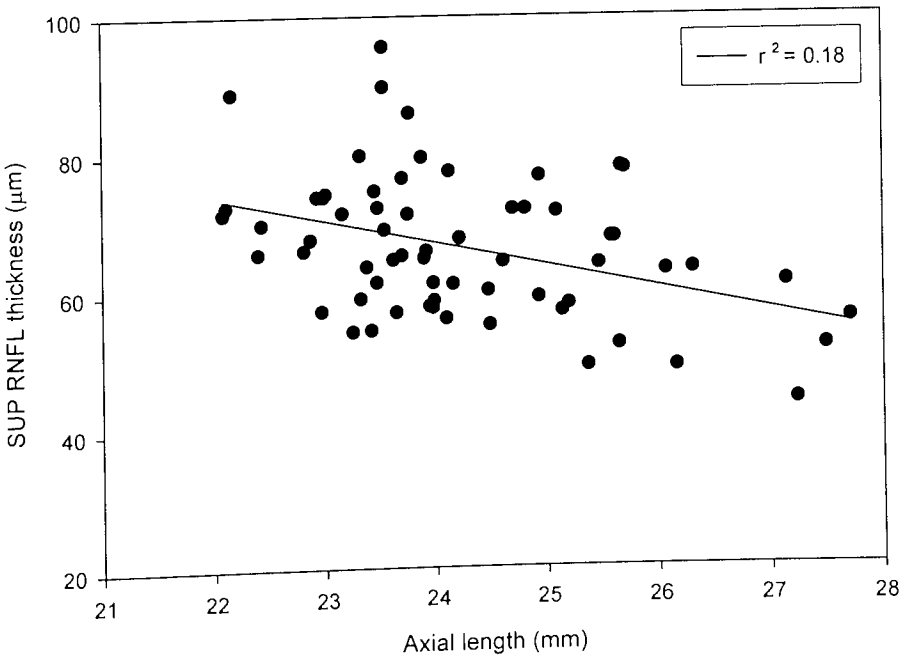

b)

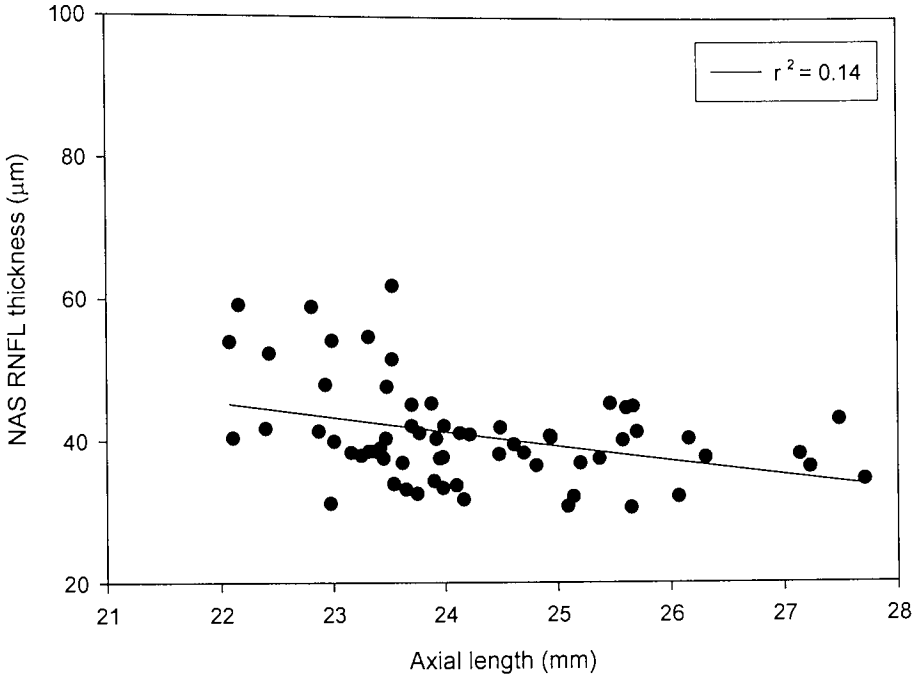
r 2 = 0.14
NAS RNFL thickness (µm)
100
80
60
40
20
21
22
23
24
25
26
27
28
Axial length (mm)

c)

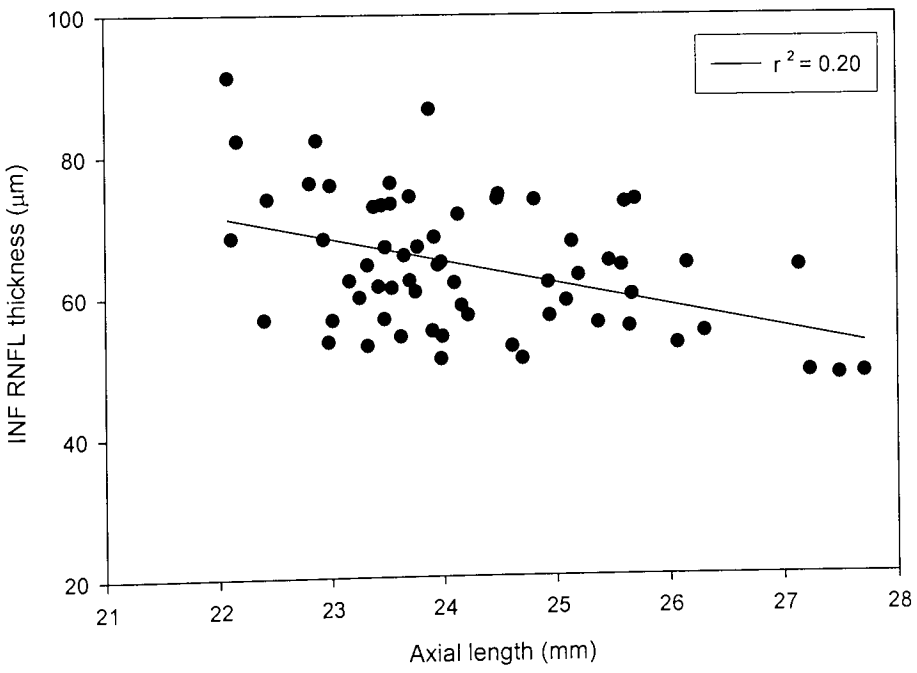
r 2 = 0.20
INF RNFL thickness (µm)
100
80
60
40
20
21
22
23
24
25
26
27
28
Axial length (mm)

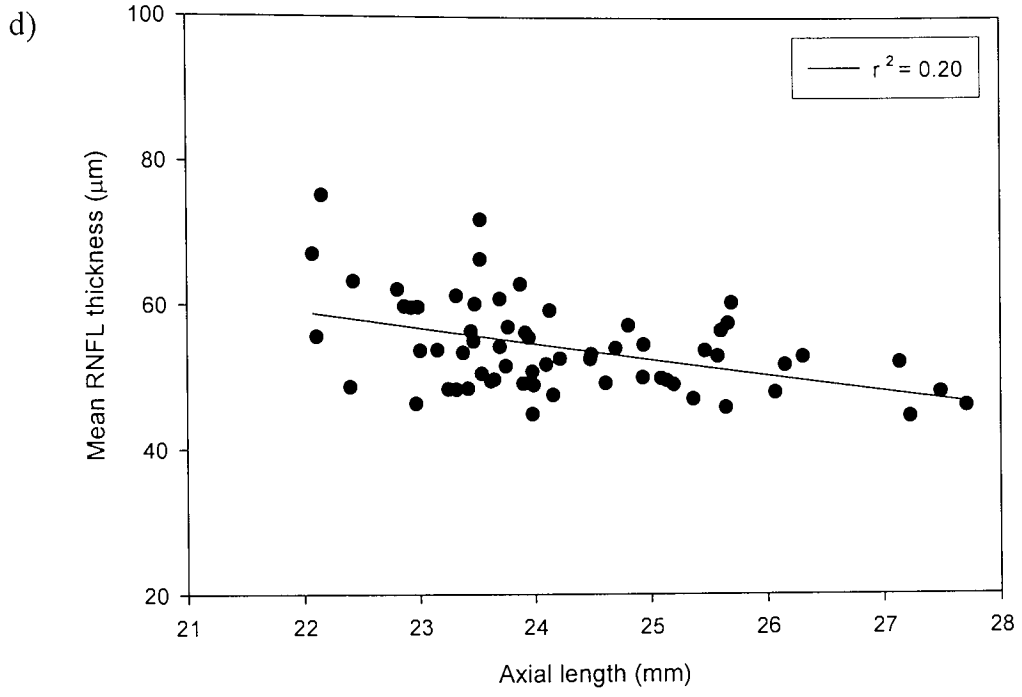

Figure 5.7 Scatterplot to show the negative correlation between axial length and a) superior RNFL and b) nasal RNFL c) inferior RNFL and d) mean RNFL for the 3rd radius scan.

5.12 Discussion

This study shows that the relationship between axial length and retinal thickness is not consistent across the entire macular scan. Our results suggest that axial length exerts greater influence over the retinal thickness in the macular region at increased distances from the fovea. In position 1 (fovea) there does not appear to be a correlation between axial length and retinal thickness. This is also the case for those retinal locations 2-5 which make up the inner 3mm diameter of the radial line scan. However, the retinal thickness in locations 6-9 of the outer ring shows a negative correlation with axial length. As axial length increases, the retinal thickness decreases in these positions.

Secondly, this study demonstrates that retinal nerve fibre layer thickness alters according to the axial length of the subject. The magnitude of its influence however, is not consistent at all retinal locations around a scan, i.e. at all retinal locations equidistant from the optic disc margin. The degree to which the retinal nerve fibre layer is correlated with axial length also is dependent on the distance from the disc margin.

Data analysis for the disc margin scan fails to show any significant relationships between axial length and retinal nerve fibre layer thickness although there is an observable trend between the RNFL in the nasal quadrant and axial length. For the second radius scan, mean RNFL thickness is highly correlated with axial length in addition to each quadrant, with the exception of the temporal quadrant. This is also true for the third radius scan where a strong correlation was found between mean RNFL and the superior, nasal, and inferior quadrant. However, there was no evidence of a relationship between axial length and retinal nerve fibre layer thickness in the temporal quadrant.

5.12.1 Macular retinal thickness

The overall average macular retinal thickness (positions 1-9) in this study was 244.92 ± 11.74μm which despite differences in subject sample age groups and axial length compares favourably with the retinal thickness found in other Stratus OCT studies using the fast macular scan and retinal mapping protocol. Paunsecu *et al.* (2004) reported an average retinal thickness (positions 1-9) of 241.97±25.81μm in 10 normal subjects (mean age 30.5±7.4years). Similarly, Polito *et al.* (2005) using the Stratus OCT reported an average retinal thickness of 264.67±28.40μm and 265.89±27.23μm for a group of 10 normal subjects undilated and dilated respectively (mean age 40 years). Pierre- Khan *et al.* (2005) reported mean retinal thickness at position 1 (foveola) of 191.4±17.6μm using the Stratus OCT in a group of 17 normal subjects (37.5±8.6years). Our study found very similar foveal thickness of 195.84±18.32μm.

5.12.2 Relationship between axial length and macular retinal thickness

To date, studies investigating the effect of axial length on retinal thickness have reported varying and inconsistent results. Difficulties in producing clear hypotheses arise from the fact that each study employs different methodologies, scan types and subject samples.

Kremser *et al.* (1999) used a commercially available prototype Retinal Thickness Analyzer (RTA) to test a subject sample of 129 eyes of 79 healthy volunteers. Subjects

were aged between 16 and 80 years (mean 41 years, 45.5% aged between 20 and 30 years) with refractive errors (spherical equivalent) between +2DS and -14DS. They reported a significant decrease in retinal thickness as axial myopia levels increased. A decrease of 4.8μm/ spherical equivalent in the foveolar region and 6.6μm/ spherical equivalent in the other areas of the posterior pole was noted.

Conversely, Garcia-Valenzuela *et al.* (2000) using similar technology, reported that average retinal thickness in the temporal peripapillary retinal area was not influenced by the axial length of the eye in 43 normal subjects aged 15 to 64 years (mean age 38±15 years) with an axial length range of 19.30mm to 27.35mm and refractive error (spherical equivalent) from +8.25 to -12.75DS. Retinal thickness mapping was used to generate a series of 20 optical sectional images across a 2 x 2mm area of the temporal retina, within one disc diameter of the optic disc margin. According to linear regression analysis, the separation of the retinal interfaces decreased significantly with increasing axial length. However, after adjusting for the magnification of the imaging system and the optical dimensions of the eye (Rudnicka, Burk, Edgar *et al.*, 1998) the authors reported a lack of significant variation in the thickness of the temporal peripapillary retina with a change of axial length. No statistically significant differences were found in the retinal thickness either between myopes and emmetropes or between hyperopes and emmetropes.

Despite the use of the same device in the above two studies, analysed results may also be biased. The study by Garcia-Valenzuela *et al.* (2000) differs from the work by Kremser *et al.* (1999) in that the magnification characteristics of the imaging system were taken into account during retinal thickness calculations. Kremser (1999) appeared to fail to consider the magnification difference in the transverse direction and as a result the size of the area in each eye may not have been constant, leading to inaccurate results.

The employment of different imaging devices and their model number makes comparisons between studies difficult. The RTA used by Garcia-Valenzuela *et al.* (2000) and Kremser *et al.* (1999) in their studies is based on the principle of slit-lamp biomicroscopy and as such its measurements are affected by the axial length and refractive power of the eye. Kremser *et al.* (1999) report that the instrument they used

can be adversely affected by media opacities and furthermore that although the RTA was able to distinguish between different histologic layers, the exact correlation between retinal layers and reflection layers in the slit image was unclear at that stage in its development. These factors are likely to lead to inconsistencies in the data collected. The advantage of the optical coherence tomographer is that measurements are unaffected by axial length variations and correction for optical magnification is unnecessary with this technology. Theoretically, this in turn may produce more reliable results.

In a study by Wakatani *et al.* (2003), macular retinal thickness scans were acquired using the OCT 2000 for 203 healthy subjects of mean age 46.2±15.9 years (range 12-74 years). Four single line OCT scans, arranged in a radial spoke pattern, each 3mm in length were centred through the foveal pit at orientations of 0, 45, 90 and 135 degrees. Retinal thickness was assessed in three circular areas centred on the central fovea, firstly a region measuring 350μm in diameter (representing the foveola), secondly within an area 1850μm in diameter (fovea) and thirdly an area of diameter 2850μm (parafoveal region). Optical ray tracing and scan length magnification equations were used to quantify the retinal thickness in these areas for each group in the subject sample which had been subdivided into groups by axial length (emmetropia and low myopia: < 25.00mm, n=55), moderate myopia (≥25.00 and <27.00mm, n=95) and high myopia (≥ 27.00mm, n=53). The authors reported no statistically significant change in the retinal thickness with increasing axial length as calculated by linear regression. The axial length of the eyes ranged from 22.68 to 30.22mm. In terms of scan selection, both our study and that of Wakatani (2003) uses a radial line pattern through the fovea. However, the scan line is half the length in Wakatani's study and the retinal thickness analysis reflects this. The retinal map in our study provides measures for a 1mm, 3mm and 6mm diameter circle and direct comparisons are impossible. Generally speaking, the largest area analysed, with diameter 2850 μm or 2.850mm approximates in terms of dimensions to the central fovea (position 1) plus the inner ring of our retinal thickness map. In both studies there was no evidence of a relationship between axial length and retinal thickness. Such an effect was only noted more peripherally in our study (outer ring).

Consideration must also be given to the way in which the scan is set up. Although a similar radial line scan was used in the study by Wakatani *et al.* (2003) and ourselves, the scan set-up was not automated (unlike in our study) and results may therefore be subject to the discrepancies caused by the intervention of the operator. Initial scan set-up involved the cross sectional scan being roughly centred on the fovea, which was then manually adjusted in order that the image of the foveal pit appeared as deep as possible in the centre of the scan, assuming that the deepest part of the foveal pit was at the centre. It is unclear whether the 4 line scans were taken simultaneously but this is unlikely when considering the model and software employed. The time taken to align the scans and the apparent subjectivity of the process may have lead to fixation loss by the patient and possible discrepancies in the data collected. In our study, using the fast macular scan, the six radial lines are compressed to form one scan in just 1.92 seconds during which time there is no need to adjust the position of the scan line. Reduced acquisition time leads to greater patient tolerance, improved fixation and better quality scans. Furthermore, during fast macular scanning, fixation losses can be observed in real time as the trace moves across the viewing window; the foveal pit should be located at the centre of the 6mm line scan. The patient should be reminded to fixate and only when the examiner is satisfied is the image captured and saved.

Similarly, Lim, Hoh, Foster *et al.* (2005) found that average retinal thickness did not vary with increasing myopia or axial length, using the first generation OCT 1. However, this was not true for each location tested, and the authors reported a range of axial length effects for different retinal locations in a sample of 139 males aged 19-24 years with myopia of -0.25 to -14.25DS (spherical equivalent). Three good quality horizontal and vertical scans each 6mm long centred through the fixation point of each eye were taken by the same operator. Each scan comprised 100 A-scans, effectively providing 100 data points of retinal thickness. Retinal thickness measurements were recorded manually by the operator at every 10 equally spaced points (0-100 along the length of the scan line). Maximum retinal thickness was taken to be either side of the fovea (approximately points 25 and 75 according to subjective examination) and recorded for the superior and inferior (vertical scan) and nasal and temporal (horizontal scan) positions. Minimum retinal thickness was assumed to be the fovea (approximately point 50). Mean maximum retinal thickness (assumed to be the parafovea) significantly decreased with increasing axial length ($p=0.03$) while mean minimum retinal thickness

at the fovea was positively correlated with axial length (p=0.015). Both our study and that of Lim *et al.* (2005) employ optical coherence tomography and scan lines of length 6mm, although scan set up and analysis differ; Lim *et al.* (2005) use a horizontal and vertical line scan through the fovea with 100 data points in total, along which retinal thickness measurements are taken at regular locations while we use the fast macular scan comprising 6 radial line scans, each of which has 128 data points, compressed to form one image. Retinal thickness map output with the Stratus OCT allows measurement of retinal thickness across a wider circular area (6mm in diameter) across the fovea, where computer algorithms interpolate the data along these 6 radial lines for 9 retinal positions. The maximum retinal thickness measures may be compared with the inner ring (positions 2-5) of our retinal map analysis. However, while a correlation was found for their maximum retinal thickness measures and axial length, no such effect was found in this study. This was also true for the fovea results whereby our study revealed no relationship between axial length and retinal thickness while Lim *et al.* (2005) reported a positive correlation. It is unlikely that discrepancies can be explained by fixation losses in either study due to the scanning of young subjects with accurate visual acuity.

5.12.3 Sample group characteristics

The axial length of our subjects, varied from 22.08mm to 27.71mm which appears to be slightly narrower in range than that reported in other work. Axial length for subjects in the study by Garcia-Valenzuela *et al.* (2000) using the RTA, ranged from 19.30 to 27.35mm, while those in the OCT study by Wakatani *et al.* (2003) ranged from 22.68 and 30.22 and between 23.33 to 29.23mm for Lim *et al.* (2005), also employing the OCT.

Other studies appear to be based on refractive myopia rather than axial myopia. Kremser *et al.* (1999) who reported a significant decrease in retinal thickness as myopia increased did not publish axial length data for their subjects, making comparisons impossible. Instead, they used refraction to classify their subjects where refraction levels were subdivided into 7 groups with unequal numbers of subjects in each group. The majority of their test subjects fell between +2DS and -8DS (n= 124) while four

subjects fell in the -8DS to -10DS group and only 1 subject had a refraction between -10DS and -14DS. Certainly for the latter group results gained may be atypical and consequently unreliable. Their results may also be influenced by the fact that they used both eyes of most of their subjects (129 eyes of 79 volunteers).

Any possible limitation of our axial length range is compensated by the well defined subject sample age range. All our subjects were under the age of 40 years, with the majority aged 19-24 years (n=55) and 11 subjects between the ages of 25 and 39 years. With the exception of Lim *et al.* (2005) who tested male subjects between the age of 19 and 24 years, all studies have employed subjects with a broad spectrum of ages. Kremser *et al.* (1999) used subjects aged between 16 and 80 years old, Garcia-Valenzuela *et al.* (2000) employed subjects aged 15 to 64 years old while subjects aged between 12 and 74 years of age participated in the study by Wakatani *et al.* (2003). To our knowledge data analysis was undertaken without considering age as a factor. Age could be a confounding factor because it most likely causes a decrease in retinal thickness. This may account for discrepancies in findings and study results may not give a true account of the relationship between axial length and retinal thickness.

Consideration into subject samples employed should be taken when drawing conclusions. Studies employing young subjects with good visual acuity and no evidence of pathology may bias results. That older myopic subjects may experience greater ocular pathology cannot be precluded.

Eyes with pathological myopia were excluded from studies by both Wakatani (2003) and Garcia-Valenzuela (2000) which may explain the observed lack of significant thickness differences between myopes and emmetropes. Furthermore, the subjects in each of the three samples (emmetropes, myopes and hypermetropes) for Wakatani's study (2003) were not age matched and this in itself may be a potential source of inaccuracy. The portion of the retina scanned for each subject in the study by Garcia-Valenzuela (2000) did not remain constant due to the fact that retinal thickness measurement at a specific distance from the optic disc margin corresponds to an area further away from the disc centre in a myopic eye compared with a hyperopic and emmetropic eye.

5.12.4 Retinal locations

The location of the retinal position at which thickness measurements are made affects the findings in all studies of this type. Our study suggests that the fovea (position 1) and Henle's layer (2-5) are unaffected by axial length but that the retinal layers area immediately adjacent (6-9) are. Kremser *et al.* (1999) suggests that differences between axial length effects at each location may be explained by the differences between the actual retinal thicknesses in each of the locations. The fovea (corresponding in our study to position 1) is thinner *per se* and therefore thinning in this area cannot occur to the extent observed in the other areas. At the centre of the fovea, the outer nuclear layers of the retina are displaced concentrically to form the foveal pit composed predominantly by cones. In this rod-free region, measuring approximately 500 microns in diameter the cones are elongated and densely packed (175 000 cones per mm^2), represented in this study by retinal thickness map position 1. The displaced interneurons form around the rim of the fovea resulting in this area forming the thickest region in the retina (positions 2-5) after which the retinal thickness decreases with further distance from the pit (positions 6-9). The retinal thickness measurements obtained in our study clearly reflect the above retinal structure. Position 1 measured 195.84±18.32microns, the inner ring (2-5) exhibits retinal thickness measurements of between 259.04±12.75microns and 275.52±15.20microns (mean thickness 269.47microns) while the outer ring (positions 6-9) ranged from 216.74±13.11microns to 254.22±14.14microns (mean thickness 233.39microns).

This finding does not concur with Lim *et al.* (2005) who using horizontal and vertical OCT line scans 6mm in length through the fovea, concluded that while overall mean macular thickness is not affected by the degree of myopia, the thickest points at the parafoveal region decreases with myopia, whereas the fovea thickness increases with myopia.

In their investigation of the temporal peripapillary retina, Garcia-Valenzuela *et al.* (2000) suggest that retinal thickness may be unaffected by varying axial lengths as a result of the differential effects that the axial length has on the sensory layers

comprising the retinal tissue, particularly in this area, where retinal nerve fibre layer thickness is less than that of the inferior and superior disc margins.

5.12.5 Retinal nerve fibre layer thickness at the ONH

In our study, RNFL thickness at the optic disc margin was greatest in the inferior quadrant, followed by the superior, nasal quadrant and was thinnest in the temporal quadrant. For the 2nd and 3rd radii scans RNFL thickness was greatest in the superior and inferior quadrants and thinner in the nasal and temporal quadrants. This double hump pattern is widely reported in histological studies (Varma *et al.*, 1996; Dichtl *et al.*, 1999) and in studies using optical coherence tomography (Kanamori *et al.* 2003; Varma *et al.*, 2003; Budenz *et al.*, 2005). While direct comparisons of RNFL thickness from our work with others is not possible due to the fact that we used scans at different eccentricities from the optic disc margin, variations in thickness around the optic nerve head are very similar.

5.12.6 Relationship between axial length and RNFL at the optic nerve head

Surprisingly, little work has been published on the way in which nerve fibre layer is affected by axial length and refractive error despite the fact that optical coherence tomography scans of retinal nerve fibre layer thickness taken around the optic nerve head have been widely used in the diagnosis and monitoring of glaucomatous eye disease (Schuman *et al.*, 1995; Bowd *et al.*, 2000; Kanamori *et al.*, 2003; Nouri-Mahdavi *et al.*, 2004; Leung *et al.*, 2005).

To date, all RNFL studies using the OCT have employed the standard diameter (3.4mm) circle scan around the optic nerve to assess repeatability, reproducibility and pathological changes in glaucomatous optic neuropathy. Since disc size varies considerably between individuals, for each subject, the position at which the measurement is taken will also vary and may lead to inaccuracies in findings. Disc area has been considered a factor in the susceptibility of an individual to develop glaucoma (Klein and Klein, 1981; Seddon, Schwartz and Flowerdew, 1983) and therefore should be considered in all studies regarding the retinal nerve fibre layer and scan position. In

our study, the normal variation in disc size between subjects has been accounted for by scan design. The use of the different scan radii for each subject i.e. for the initial disc margin scan to be designed to fit closely around the optic disc margin whilst ensuring that the entire optic disc fell within the scanning circle, and the use of subsequent ratio scans meant that equivalent areas of the retina were measured for each patient. There was no evidence of a correlation between disc size and retinal nerve fibre layer thickness for each of the quadrants and mean for any of the three scan sizes. In this way we could confirm that our results reflected a true axial length effect and were not affected by the differential in disc size between subjects.

In summary, at the disc margin there were no significant correlations between axial length and RNFL thckness in any quadrant, although there appeared to be a trend between RNFL and the nasal quadrant. For the 2nd and 3rd radius scans RNFL thickness was correlated with axial length for the mean 360° thickness (p=0.000, p=0.000 respectively) and for the inferior (p=0.000, p=0.000 respectively), superior (p=0.000, p=0.000 respectively), and nasal quadrants (p=0.000, p=0.002 respectively) but not for the temporal quadrant (p=0.277, p=0.993 respectively).

Our findings may in part be explained by the anatomy of the retinal nerve fibre layer. Nerve fibres from the macular area follow a straight course to the optic nerve head, represented by the temporal quadrant fibres. Those from the nasal retina also follow a fairly straight course to the optic nerve head and form the nasal quadrant part of the scan. Fibres arising from the retina on the temporal side of the macula follow an arcuate pattern to reach the optic nerve head. As such, retinal fibre tissue at the optic disc margin is greatest at the inferior pole, followed by the superior pole, nasal pole and is thinnest at the temporal pole. Axial length effects may not be apparent in the temporal quadrant due to there being fewer fibres here.

The effect of increasing axial length on RNFL thickness is a important consideration since the link between increasing levels of myopia and ocular disease is not in dispute. There is considerable evidence of a relationship between myopia, particularly high myopia and glaucoma according to both clinical and population based studies. The Barbados Eye Study reported a myopic refraction to be a risk factor in adult black people with prevalent open-angle glaucoma Chihara *et al.* (1997). According to the Blue

Mountains Eye Study, myopic subjects aged between 49-97 years had a twofold to threefold increased risk of glaucoma compared with non myopic subjects after adjusting for known glaucoma risk factors (family history, diabetes, hypertension, steroid use etc). Glaucomatous damage to the optic disc and visual field was more than twice as frequent in eyes with low myopia (-1DS to -3DS spherical equivalent) than in eyes without myopia after adjusting for age and gender. A stronger association was found between moderate to high myopia (greater than -3DS) and glaucoma with glaucoma three times more frequent compared to nonmyopic eyes. Similarly, persons with myopia (defined -1DS or less) were 60% more likely to have prevalent glaucoma than emmetropes in a later study by Wong, Klein, Klein *et al.* (2003).

There have been several suggestions proposed to explain the link between myopia and glaucoma. Some reports postulate that the optic nerve head in the myopic eye is more susceptible to glaucomatous damage from elevated or normal IOP compared with the normal eye (Perkins and Phelps, 1982; Chihara *et al.*, 1997). The cup: disc ratio is higher in myopes which may make nerve fibres more prone to damage at any IOP level (Tomlinson and Phillips, 1969; Chihara and Sawada, 1990; Jonas and Dichtl, 1997, Jonas *et al.*, 1988a). Shearing forces exerted by scleral tension across the lamina cribrosa may play a role in the development of pathological glaucomatous changes according to Quigley (1987). Connective tissue changes and scleral tension are higher in eyes with greater axial length compared with shorter eyes with the same IOP (Cahane and Bartov, 1992). Glaucoma and myopia have a strong familial basis and may share a genetic link (Hammond, Snieder, Gilbert *et al.*, 2001; Stone *et al.*, 1997).

It is clear from the above review that comparisons between studies have many confounding variables. Several studies, including that of Lim *et al.* (2005) and ours employ subjects that are closely matched in age. Observable differences between subjects can therefore be solely attributed to axial length effects rather than possible differences due to age, the effects of which are explored in Chapter 6. This is not true for the study by Kremser *et al.* (1999), Garcia-Valenzuela *et al.* (2000) and Wakatani *et al.* (2003). Classification of myopia is not standardised across all studies with some authors using axial length measurements as the basis for their correlations, while others use degrees of refraction. Our study highlights the importance of classifying by axial length and not refraction in studies of this nature.

5.12.7 Future work

The majority of all the studies to date have imaged the posterior pole. Early reports have documented increasing choroidal degeneration in the peripheral fundus of the myopic eye (Karlin and Curtin, 1976) and reduced retinal thickness in the midperipheral regions of the myopic eye compared to the emmetrope (Chujo, Koboyashi, Emi *et al.* 1983). It would, therefore, be interesting to include investigations of the effects of axial length on retinal thickness of the peripheral retina although this would not be without its technical difficulties due to the required eccentric fixation of the patient, the lack of orientation clues i.e. non visibility of the optic disc margin etc during scanning and the difficulty in maintaining consistent scan positions for each subject.

There is clearly a need for more work to be undertaken in order that we fully understand the effects of axial length on retinal nerve fibre layer thickness. The use of a large normative database to compare normal eyes with eyes diagnosed with glaucoma or suspect glaucoma would be invaluable. An OCT software upgrade with such a database is available for the default retinal nerve fibre layer thickness scan (3.4mm in diameter centred around the optic disc margin). Future work may also include the investigation of the relationship between myopia and glaucoma and to fully research the basis of visual field loss in large eyes or those with large optic nerve heads.

5.13 Conclusion

Macular retinal thickness and retinal nerve fibre layer thickness around the optic nerve head correlate negatively with axial length which suggests that the longer eye may be more susceptible to ocular disease. As such, axial length and its associated risks should be considered during the clinical assessment of the myopic patient.

CHAPTER 6: The effect of age on retinal thickness and retinal nerve fibre layer thickness

6.1 The effect of age on retinal thickness at the macula and optic nerve head

6.1.1 Abstract

Purpose: To assess the effect of age on retinal thickness at the macula (MRt) and retinal nerve fibre layer thickness (RNFLt) around the optic nerve head measured by the Stratus Optical Coherence Tomographer (Model 3000, Carl-Zeiss Meditec, Dublin, CA).

Methods: The study comprised 2 parts: **Part 1.** MRt measurements were obtained using OCT multiple radial line scans, 6mm in length, centred through the fixation point of one eye each of 120 normal healthy volunteers subdivided according to age: group 1 under 40 years of age and group 2 over 40 years of age. Group 1 consisted of 66 subjects (mean age 22.45±4.3; range 19-39 years) with mean axial length of 24.27±1.3 mm. Group 2 consisted of 54 subjects (mean age 64.06.45±11.68; range 40-88 years) with mean axial length of 23.30±0.96 mm. Retinal thickness analysis produced a circular map comprising 9 sectors depicting average retinal thickness. **Part 2.** RNFLt measurements per quadrant and overall were obtained for a series of OCT circular scans centered on the optic disc, scanning around the optic disc margin at three different locations for one eye each of 115 normal healthy volunteers subdivided according to age. Group 1 consisted of 64 subjects (mean age 22.42±4.36; range 19-39 years) with mean axial length of 24.24±1.32 mm. Group 2 consisted of 51 normal subjects (mean age 64.76±11.82 years; range 40-88 years) with mean axial length 23.34±0.96 mm. Partial correlation was used to explore the relationship between age and MRt in all locations and RNFLt in all quadrants and overall for all subjects while controlling for axial length. A one-way between groups analysis of covariance was also conducted to compare MRt and RNFLt of group 1 and group 2 using axial length as the covariate and applying Bonferroni correction to correct for multiple comparisons.

Results: A significant positive correlation was found between age and MRt at the foveola only (p=0.000). Correlations between age and MRt at all remaining macular locations failed to reach significance. For the disc margin, 2nd and 3rd radius scans RNFLt was negatively correlated with age for the mean overall (p=0.006, p=0.000, p=0.000 respectively) and superior quadrant (p=0.002, p=0.000, p=0.000 respectively). RNFLt was negatively correlated with age for the inferior (p=0.000) and the temporal quadrant (p=0.007) for the 2nd radius scan only.

Conclusions: This study shows thickening at the foveola with age but no influence of age on the MRt at other positions. RNFLt around the optic nerve head decreases with age.

6.2 Introduction

Optical coherence tomography (OCT) is a non-contact and non-invasive method to assess and quantitatively measure the retinal nerve layer thickness and retinal thickness (Huang *et al.*, 1991; Chauhan and Marshall, 1999; Hee *et al.*, 1995a). Studies have shown that this technique is both an accurate and repeatable method of identifying early changes in normal and diseased eyes (Schuman *et al.*, 1995; Shuman *et al.*, 1996; Massin *et al.*, 2001; Sanchez-Tocino *et al.*, 2002; Muscat *et al.*, 2002; Budenz *et al.*, 2005; Olmedo *et al.*, 2005). It therefore has an important potential role in monitoring pathological changes in disease over time.

However, variations in retinal thickness and retinal nerve fibre layer (RNFL) thickness for normal healthy subjects may lead to difficulties in the interpretation of clinical OCT scans and subsequent mis-diagnosis of ocular pathology. There is some evidence to suggest that retinal and RNFL tissue may be affected by age. Conclusive findings are confounded by the variety of imaging techniques and particular type of scan employed in each study. Moreover, studies have reported that age effects on retinal thickness and retinal nerve fibre layer thickness are regional, whereby only certain sectors or locations of scanned tissue are affected.

A reduction in retinal thickness with increasing age has been reported (Baquero Aranda, *et al.*, 2005; Kanai *et al.*, 2002; Alamouti and Funk, 2003; Tewari *et al.*, 2004). Conversely, Oshima *et al.* (1999) and Wakatani *et al.* (2003) found no relationship between age and central macular thickness. Several studies describe an inverse correlation between RNFL and age (Poinoosawmy *et al.*, 1997; Funaki *et al*, 1999; Mok *et al.*, 2002; Kanamori *et al.*, 2003; Sony *et al.*, 2004), a result confirmed by histological studies (Varma *et al.*, 1996; Dichtl *et al.*, 1999).

Implications of age effects must be considered when monitoring disease effects, especially in long-term follow-up of conditions such as glaucoma. In order to determine whether any observed change in tissue thickness is attributable to disease alone and not due to age changes it is necessary to firstly establish whether age is a factor.

The purpose of this study was to determine the effect of age on retinal thickness at the macular and retinal nerve fibre layer thickness around the optic nerve head. This study will help to clarify the current theories regarding the effects of age on retinal tissue. It is likely that factors such as location (by quadrant or sector) around the optic nerve head and eccentricity from the optic nerve head will impact the volume of tissue available to firstly, to be measurable and secondly to show an age effect. Effects such as sampling, fibre distribution and signal: noise will all affect tissue thickness measures. Our objective is to determine age effects on retinal tissue while accounting for these factors.

6.3 Aims and objectives

This study comprises two parts:

1) To determine the effects of age on retinal thickness at the macula
2) To determine the effects of age on retinal nerve fibre layer thickness around the optic nerve head.

6.3.1 Hypothesis

Retinal thickness and retinal nerve fibre layer thickness decreases with age.

6.4 Materials and methods

6.4.1 Inclusion Criteria

Normal healthy subjects were recruited from staff at Birmingham Heartlands Hopsital Ophthalmology Department, staff in the Vision Sciences Department, Aston University, attendees at the Optometry Clinic at Aston University and from the University's student population. A full eye examination was carried at by an optometrist (HLW) to establish whether the study inclusion criteria were met. Subjects were included if they exhibited:

- No abnormalities on ophthalmoscopic examination
- Minimal or no lens opacities allowing a clear fundus view
- No history or evidence of intraocular surgery or laser therapy

- No history or evidence of retinal pathology or glaucoma
- Snellen visual acuity (VA) 6/9 or better
- Less than 6 dioptres of spherical ametropia and 2 dioptres of astigmatism
- Absence of visual field defects (Humphrey Visual Field Analyser program 24-2)
- Intraocular pressure (IOP) less than 21mmHg (Non-contact tonometry Pulsair 3000)

6.4.2 Subject sample:macular thickness measurements

The subject sample consisted of one eye each of 120 normal healthy volunteers (58 male, 62 female) aged between 19 and 88 (mean age 41.18 ± 22.42years). Volunteers were subdivided according to age- group 1 under 40 years of age and group 2 over 40 years of age. Subject sample characteristics are summarised in table 6.1.

Group 1 consisted of 66 normal healthy volunteers; 29 male, 37 female subjects. Their mean age was 22.45±4.30 years (range 19-39 years). The group mean axial length was 24.27±1.3 mm.

Group 2 consisted of 54 normal healthy volunteers; 29 male, 25 female subjects. Their mean age was 64.05±11.68 years (range 40-88 years). The group mean axial length was 23.30±0.96 mm.

	Gender		Test eye		Age mean ± SD (range)
	Male	Female	Right	Left	
Group 1 (young)	29	37	31	35	22.45±4.3 years (19-39)
Group 2 (mature)	29	25	29	25	64.05±11.68 years (40-88)

Table 6.1 Details of the subject sample (macular thickness measurements)

6.4.3 Ethical approval and informed consent

Ethical approval was obtained from the ethical committee boards of Aston University. Approval conformed to the tenets of the Declaration of Helsinki. Written informed consent was obtained from all subjects.

6.5 Methods

Following recruitment as per the requirements set and listed above, subjects attended for one visit only.

Following informed consent, axial length measurements were obtained using the IOL master in accordance with the method described in Chapter 4.

Retinal thickness scans of the macular were taken using the optical coherence tomographer in accordance with Chapter 3.

6.6 Statistical analysis

Our previous study (see chapter 5) established the existence of a relationship between axial length and both retinal thickness at the macula and retinal nerve fibre layer thickness around the optic nerve head. An independent samples *t*-test was therefore conducted for the subject sample to identify differences in axial length measurements between group 1 and 2. There was a significant difference in measures for group 1 and group 2 ($p=0.000$). In order to accurately assess the effects of age it was important therefore to account for the effects of axial length using appropriate statistical analyses.

Partial correlation was used to explore the relationship between age and retinal thickness in all scan positions and mean retinal thickness across the scan for all subjects while controlling for axial length. Preliminary analyses were performed to ensure no violation of the assumptions of normality, linearity and homoscedasticity. Bonferroni correction for multiple comparisons was used. p values less than 0.005 (i.e. 0.05/10 locations) were therefore considered significant.

A one-way between-groups analysis of covariance (ANCOVA) was conducted to compare the retinal thickness at each scan location 1-9 and mean retinal thickness of group 1 (under 40 years of age) and group 2 (over 40 years of age). Results are summarised in Appendix 1. The independent variable was the group type and the dependent variable was tissue thickness. Axial length was used as the covariate. After Bonferroni correction, p values less than 0.005 were considered significant. Preliminary checks were conducted to ensure that there was no violation of the assumptions of normality, linearity, homogeneity of variances, homogeneity of regression slopes and reliable measurement of the covariate.

6.7 Results

6.7.1 Macular retinal thickness values

Retinal thickness values for each group are displayed in table 6.2 below

	Retinal thickness (microns)	
Retinal location	Group 1 (young)	Group 2 (mature)
Position 1	195.84 ± 18.32	218.04 ± 22.91
Positon 2	272.52 ± 15.20	276.66 ± 17.86
Position 3	269.74 ± 13.15	275.08 ± 14.60
Position 4	259.04 ± 12.75	264.93 ± 14.54
Position 5	273.56 ± 14.03	276.0 ± 17.08
Position 6	254.22 ± 14.14	256.70 ± 19.62
Position 7	226.51 ± 12.69	232.96 ± 17.22
Position 8	216.74 ± 13.11	224.26 ± 15.18
Position 9	236.08 ± 13.52	239.40 ± 17.25
Mean	244.92 ± 11.74	251.56 ± 15.01

Table 6.2 Macular retinal thickness values mean ± SD for both groups at all locations

6.7.2 Correlation analysis: effects of age

A summary of the partial correlation is displayed in table 6.3 where * indicates statistical significance (p=0.005 after Bonferroni correction).

Retinal thickness scan position	Zero order partials	Sig (2-tailed)	Controlling for ax. Length	Sig (2-tailed)
Position 1	0.448	0.000*	0.486	0.000*
Position 2	0.024	0.792	0.003	0.973
Position 3	0.117	0.202	0.058	0.534
Position 4	0.128	0.162	0.089	0.338
Position 5	-0.011	0.903	-0.056	0.546
Position 6	-0.021	0.821	-0.119	0.196
Position 7	-0.163	0.075	0.015	0.870
Position 8	0.194	0.034	0.042	0.647
Position 9	0.014	0.880	-0.124	0.179
Mean RT	0.156	0.089	0.079	0.392

Table 6.3 Summary of partial correlation analysis for MRt of all subjects * denotes significance

Partial correlation analysis provides both the zero order partial and the normal Pearson product-moment correlation matrix between age and retinal thickness, and the correlation matrix controlling for axial length.

Table 6.3 shows a positive correlation between age and retinal thickness at the foveola (position 1) with increased age being associated with an increase in retinal thickness. An inspection of the zero order correlation suggested that controlling for axial length had very little effect on the strength of the relationship between these variables. This would suggest that the observed relationship between age and retinal thickness is not just due to the influence of axial length.

The output displayed no evidence of a relationship between age and retinal thickness in positions 2,3,4,5,6,7,8,9 and the mean retinal thickness of the scan.

Position 6 (outer nasal) and Position 9 (outer superior) displayed a very weak negative relationship with age. An inspection of the zero-order correlation suggests that controlling for axial length had a small effect on the strength of the relationship between these variables.

6.7.3 Differences between groups:effects of age - Analysis of covariance (ANCOVA)

Table 6.4 displays a summary of the ANCOVA output analysis where p values less than 0.005 after Bonferroni correction are considered significant.

	Levene's test	Signif	Eta squared (%)	Axial length Signif	Axial length Eta squared (%)
Position 1	0.138	0.000*	26.5	0.016	4.8
Position 2	0.541	0.219	1.3	0.946	0
Position 3	0.199	0.129	2	0.282	1
Position 4	0.293	0.048	3.3	0.648	0.2
Position 5	0.274	0.633	0.2	0.417	0.6
Position 6	0.007	0.914	0	0.027	4.1
Position 7	0.006	0.393	0.6	0.000*	10.7
Position 8	0.077	0.173	1.6	0.000*	11.1
Position 9	0.112	0.906	0	0.001*	8.3
Mean	0.047	0.052	3.2	0.146	1.8

Table 6.4 Summary of the ANCOVA output analysis comparing MRt of group 1 (young) and group 2 (mature) * denotes statistical significance

ANCOVA confirms the findings of partial correlation, with a significant positive relationship found between age and the foveola only. In no other locations was there evidence of a relationship between age and retinal thickness. 26.5% of the variance in retinal thickness in this location is explained by age effects.

There appears to be a significant relationship between axial length and retinal thickness at positions 7, 8 and 9, the outer ring of the retinal thickness map output (while

controlling for age). Axial length explains 10.7%, 11.1% and 8.3% of the variance in retinal thickness at position 7, 8 and 9. These findings confirm our study results in chapter 5 that macular retinal thickness correlates negatively with axial length.

Estimated marginal means i.e. mean of retinal thickness after removal of the effect of axial length, calculated from ANCOVA output are represented graphically below (see figure 6.1)

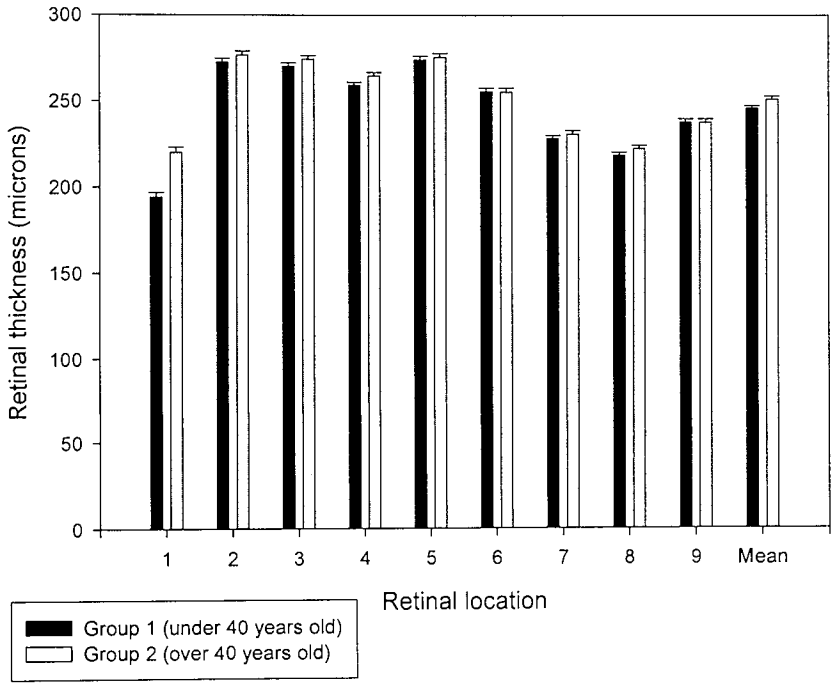

Figure 6.1 Vertical bar chart representing the estimated marginal means for macular retinal thickness (MRt) in all retinal locations

6.8 Subject sample- retinal nerve fibre layer thickness

The subject sample consisted of 115 normal healthy volunteers (56 male, 59 female) aged between 19 and 88 (mean age 41.18±22.42). Volunteers were subdivided according to age- group 1 under 40 years of age and group 2 over 40 years of age. Sample group characteristics are summarised in table 6.5.

Group1

The subject sample consisted of 64 normal healthy volunteers; 29 male, 35 female subjects. Their mean age was 22.42±4.36 years (range 19-39 years). The group had mean axial length 24.24±1.32 mm.

Group 2

The subject sample consisted of 51 normal healthy volunteers; 27 male, 24 female subjects. Their mean age was 64.76±11.82 years (range 40-88 years). The group had mean axial length 23.34±0.96 mm.

	Gender		Test eye		Age mean ± SD (range)
	Male	Female	Right	Left	
Group 1 (young)	29	35	32	32	22.42±4.36 years (19-39)
Group 2 (mature)	27	24	27	24	64.76±11.82 years (40-88)

Table 6.5 Details of the subjects sample (RNFLt measurements).

6.9 Methods

Following recruitment as per the requirements set and listed above (see section 6.4), subjects attended for one visit only.

Following informed consent, axial length measurements were obtained using the IOL master. See chapter 5 for details of IOL master.

Retinal nerve fibre layer thickness (RNFLt) was assessed using a series of OCT circular scans centred on the optic disc, scanning around the optic disc margin. Measurements of RNFLt were taken at or closest to the optic disc margin and at two further locations at increasing distance from the optic disc margin using circle scan radii specific to each subject. The initial scan was placed at the subject's disc margin and designed to fit closely around the optic disc margin whilst ensuring that the entire optic disc fell within the scanning circle. The radius of the circle scan was then increased to 2x and then 3x the initial radius to allow investigation of the RNFL at several eccentricities (i.e. using ratio of 1:2:3). Placement of the initial scan was achieved using the cursor and no further adjustment was required during the scanning process. Six scans of each circle

radii were taken, with a view to using the best five scans for analysis with the majority of patients requiring a initial scan radius of 1.0mm or 1.1mm which further increased to 2.0mm and 3.0mm (or 2.2mm and 3.3mm respectively) RNFL analysis software produced a circular map depicting RNFL thickness measurements for each of the four 90 degree quadrants (superior, nasal, inferior and temporal) and for the entire scan through 360 degrees.

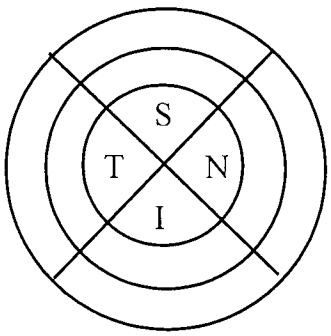

Figure 6.2 Schematic diagram showing OCT software generated concentric circle scan output.

6.10 Statistical analysis

An independent samples t-test was conducted to compare the axial length measurements of group 1 and 2. There was a significant difference in measures for group 1 and group 2 (p=0.000). In order to accurately assess the effects of age it was important therefore to account for the effects of axial length in our statistical analysis.

Partial correlation was used to explore the relationship between age and RNFLt in all quadrants and mean retinal nerve fibre thickness across the scan while controlling for axial length. Preliminary analyses were performed to ensure no violation of the assumptions of normality, linearity and homoscedasticity. Bonferroni correction was employed for multiple comparisons. For all tests a p value less than 0.01 (i.e. 0.05/5 analyses= 0.01) was considered significant.

A one-way between groups analysis of covariance was conducted to compare the RNFLt of each quadrant and mean RNFLt of group 1 (under 40 years of age) and group 2 (over 40 years of age). Results are summarised in Appendix 2. The independent

variable was the group type and the dependent variable was tissue thickness. Axial length was used as the covariate. Mean disc area for group 1 was 2.44 ± 0.37mm² (range 1.72-3.32mm²). Mean disc area for group 2 was 2.33 ± 0.36mm² (range 1.63-3.13mm²). An independent samples *t*-test revealed there were no statistically significant differences between groups in terms of their disc size (p=0.162) thus ensuring that any differences found between groups could not be explained by retinal nerve fibre layer thickness being measured at different location due to disc size variations.

Preliminary checks were conducted to ensure that there was no violation of the assumptions of normality, linearity, homogeneity of variances, homogeneity of regression slopes and reliable measurement of the covariate. A p value of less than 0.01 was considered significant (after Bonferroni correction for multiple comparisons). Estimated marginal means (i.e RNFLt values after controlling for axial length) were calculated using ANCOVA for each quadrant and group for every radius scan. This data can be seen in figures 6.3-6.5.

6.11 Results

6.11.1 Retinal nerve fibre layer thickness measures for both groups

Actual RNFLt measurements (raw data) for each group in each quadrant and overall for each scan are shown in table 6.6. Estimated marginal means for each quadrant (generated by ANCOVA analysis) are summarised in table 6.7.

Loc	Optic disc margin Actual RNFLt (microns)		2nd diameter scan Actual RNFLt (microns)		3rd diameter scan Actual RNFLt (microns)	
	1	2	1	2	1	2
Sup	165.77±19.73	154.24±25.96	101.89±14.53	90.15 ±15.75	66.44± 0.33	57.20±10.95
Nas	128.31±29.03	126.33±30.34	60.80±17.37	57.53±14.15	40.89± 7.10	40.42 ±6.79
Inf	178.13±27.98	174.18±30.13	101.04±12.93	94.70±16.59	64.17± 9.62	61.91±14.53
Tem	93.98±22.64	86.60±21.57	60.13± 9.53	53.24±10.26	45.23± 7.23	41.71±8.29
Mean	141.54±17.36	135.69±19.74	80.96± 9.20	73.91±11.20	54.18± 6.37	50.31±7.32

Table 6.6 Table showing actual retinal nerve fibre layer thickness values for each group in each quadrant for all scans

Loc	Optic disc margin RNFLt (microns)		2nd diameter scan RNFLt (microns)		3rd diameter scan RNFLt (microns)	
	1	2	1	2	1	2
Sup	166.37±2.90	153.49±3.31	103.30±1.87	88.25 ±2.11	67.35± 1.33	56.06±1.50
Nas	131.34±3.66	122.53±4.14	63.10±1.88	54.64±2.13	41.66± 0.85	39.44 ±0.96
Inf	179.93±3.69	171.91±4.17	105.25±1.71	91.93±1.93	65.87± 1.42	59.77±1.60
Tem	94.25±2.87	86.25±3.24	59.70± 1.30	53.78±1.47	45.23± 1.00	41.70±1.13
Mean	142.95±2.33	133.93±2.63	82.36± 1.20	72.15±1.36	55.03± 0.82	49.24±0.93

Table 6.7 Table showing estimated marginal means for retinal nerve fibre layer thickness for each group in each quadrant for all scans

6.11.2 Correlation analysis: effect of age

A summary of the partial correlation is displayed in tables 6.8-6.10 where * indicates statistical significance (p=0.01 after Bonferroni correction).

6.11.2.1 Disc margin

RNFL thickness quadrant	Zero order partials	Sig (2-tailed)	Controlling for ax length	Sig (2-tailed)
Superior	-0.276	0.003*	-0.290	0.002*
Nasal	-0.005	0.958	-0.119	0.209
Inferior	-0.104	0.268	-0.174	0.065
Temporal	-0.186	0.046	-0.191	0.042
Mean	-0.176	0.059	-0.254	0.006*

Table 6.8 Summary of partial correlation analysis for RNFL thickness at the disc margin of all subjects * indicates statistical significance (p=0.01)

6.11.2.2 2nd radius scan

RNFL thickness quadrant	Zero order partials	Sig (2-tailed)	Controlling for ax length	Sig (2-tailed)
Superior	-0.396	0.000*	-0.482	0.000*
Nasal	-0.060	0.523	-0.224	0.017
Inferior	-0.193	0.039	-0.361	0.000*
Temporal	-0.311	0.001*	-0.250	0.007*
Mean	-0.317	0.001*	-0.452	0.000*

Table 6.9 Summary of partial correlation analysis for RNFL thickness for the 2nd radius scan of all subjects * indicates statistical significance (p=0.01)

6.11.2.3 3rd radius scan

RNFL thickness quadrant	Zero order partials	Sig (2-tailed)	Controlling for ax length	Sig (2-tailed)
Superior	0.434	0.000*	-0.498	0.000*
Nasal	-0.001	0.992	-0.125	0.184
Inferior	-0.073	0.438	-0.237	0.011
Temporal	-0.196	0.036	-0.180	0.055
Mean	-0.263	0.004*	-0.388	0.000*

Table 6.10 Summary of partial correlation analysis for RNFL thickness for the 3rd radius scan of all subjects * indicates statistical significance (p=0.01)

As shown in table 6.8 at the disc margin scan for all quadrants and mean scan there is evidence of a moderate negative relationship between age and RNFL thickness with increasing age being associated with a decrease in nerve fibre layer thickness. This relationship appears strongest for the superior quadrant and for the mean scan. An inspection of the zero order correlation suggested that controlling of axial length had a variable effect on the strength of the relationship between these variables. Removing the effect of the axial length had little effect for the superior and temporal quadrant and mean fibre layer correlation, with a greater effect in the nasal and inferior quadrant (it should be noted that these relationships were weaker). RNFL in the superior quadrant is reduced with increasing age.

The effect of age on the retinal nerve fibre layer thickness for the 2nd radius scan is more marked in all locations compared to the disc margin scan with higher r-values in all quadrants (see table 6.9). The strongest negative correlation is observed for the superior quadrant followed by the mean, inferior quadrant, temporal quadrant and the nasal quadrant. With increasing age the RNFL decreases. This effect is more pronounced for the mean RNFL and in the superior, inferior, temporal quadrants.

For the 3rd radius scan, a summary of correlation matrices (shown in table 6.10) indicate a strong negative relationship between age and RNFLt in the superior quadrant and for the mean scan. This relationship is weaker for the inferior quadrant followed by that of the temporal quadrant and finally the nasal quadrant. This order follows that of the relationship strengths for the 2nd margin scan. At this distance from the optic disc margin, RNFL is affected to the greatest degree in the superior quadrant and for the mean RNFL.

6.11.3 Differences between groups: effects of age (ANCOVA)

Tables 6.11-6.13 display a summary of the ANCOVA output analysis where p values less than 0.01 after Bonferroni correction are considered statistically significant (shown by *) .

6.11.3.1 Disc margin scan

Parameter	Levene's test	Signif	Eta squared (%)	Axial length Signif	Axial length Eta squared (%)
Superior	0.035	0.006*	6.6	0.413	0.6
Nasal	0.717	0.126	2.1	0.001*	9
Inferior	0.976	0.166	1.7	0.051	3.3
Temporal	0.878	0.076	2.8	0.697	0.1
Mean	0.273	0.015	5.2	0.017	5

Table 6.11 Summary of the ANCOVA output analysis comparing RNFL at the disc margin of group 1 (young) and group 2 (mature) * indicates statistical significance (p=0.01)

6.11.3.2 2nd radius scan

Parameter	Levene's test	Signif	Eta squared (%)	Axial length Signif	Axial length Eta squared (%)
Superior	0.316	0.000*	19.5	0.001*	8.7
Nasal	0.337	0.005*	6.9	0.000*	17.8
Inferior	0.024	0.000*	13.9	0.000*	19.5
Temporal	0.501	0.004*	7.1	0.186	1.6
Mean	0.087	0.000*	21.0	0.000*	16.4

Table 6.12 Summary of the ANCOVA output analysis comparing RNFL at the 2nd radius scan of group 1 (young) and group 2 (mature) * indicates statistical significance (p=0.01)

6.11.3.3 3rd radius scan

Parameter	Levene's test	Signif	Eta squared (%)	Axial length signif	Axial length Eta squared (%)
Superior	0.611	0.000*	20.9	0.007*	6.3
Nasal	0.792	0.098	2.4	0.000*	10.6
Inferior	0.050	0.007*	6.4	0.000*	17.3
Temporal	0.284	0.025	4.4	0.972	0.0
Mean	0.157	0.000*	15.4	0.000*	13.4

Table 6.13 Summary of the ANCOVA output analysis comparing RNFL at the 3rd radius scan of group 1 (young) and group 2 (mature) * indicates statistical significance (p=0.01)

For the disc margin scan, a statistical difference between groups occurs in the superior quadrant only. The amount of variance however, as indicated by the eta squared value is low at 6.6%. In the nasal quadrant, there appears to be a significant relationship between axial length and RNFLt while controlling for age, which explained 9% of the variance. This would appear to confirm the trend observed in chapter 5 (section 5.11.3.1).

For the 2nd radius scan, significant differences between groups were observed for the mean RNFL and superior, nasal, inferior, and temporal quadrant. The amount of variance in RNFLt explained by age varies according to quadrant with superior, nasal,

inferior, temporal and mean exhibiting 19.5%, 6.9%, 13.9%, 7.1% and 21% respectively. The relationship between axial length and RNFLt (while controlling for the independent variable i.e. the group) reached statistical significance in all quadrants except the temporal quadrant. The variance of RNFLt explained by axial length for the superior, nasal, inferior amd mean was 8.7%, 17.8%, 19.5% and 16.4%.

For the 3rd radius scan, significant differences between groups were observed for the superior, inferior quadrant and mean RNFLt, with variance according to the eta squared values of 20.9, 6.4% and 15.4% respectively. The relationship between axial length and RNFLt, while controlling for age was significant in the superior, nasal, inferior quadrants and for the mean overall with variance values of 6.3%, 10.6%, 17.3% and 13.4% respectively.

6.11.4 Retinal nerve fibre layer thickness: Estimated marginal means

The following figures show the estimated marginal means (thickness values after controlling for axial length) of mean RNFLt and RNFLt per quadrant for all scan radii for all subjects.

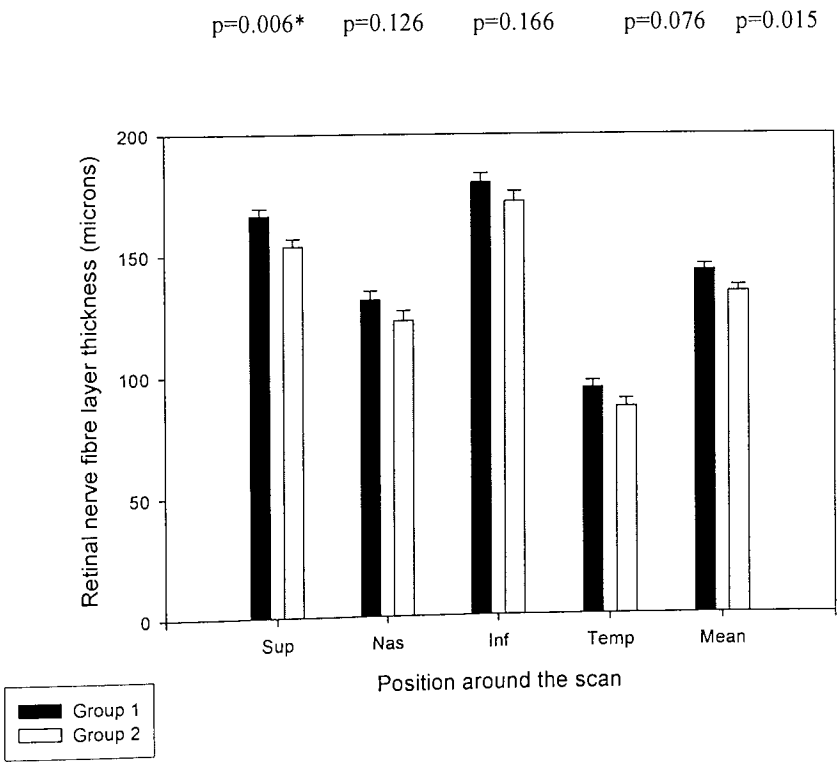

Figure 6.3 Vertical bar chart representing the estimated marginal means for retinal nerve fibre layer thickness in all quadrants of the disc margin scan * denotes statistical significance (p=0.01)

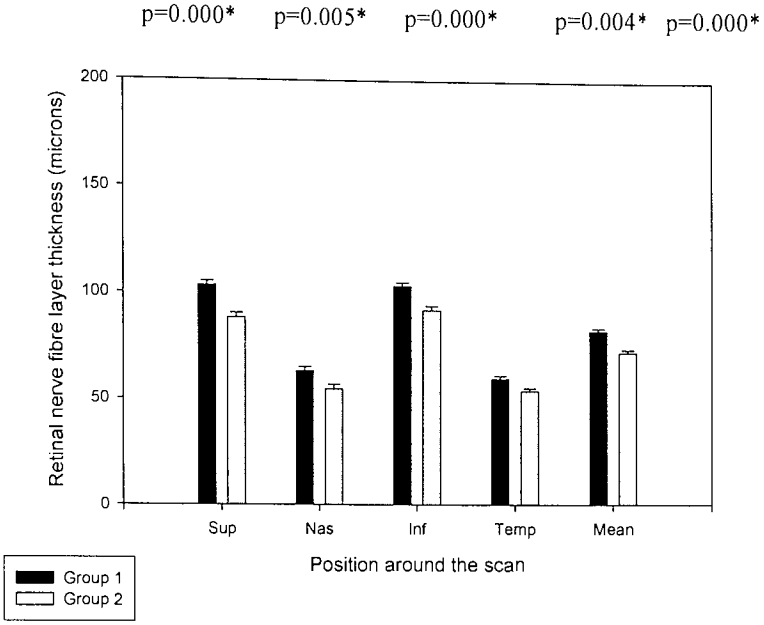

Figure 6.4 Vertical bar chart representing the estimated marginal means for retinal nerve fibre layer thickness in all quadrants of the 2nd radius scan * denotes statistical significance (p=0.01)

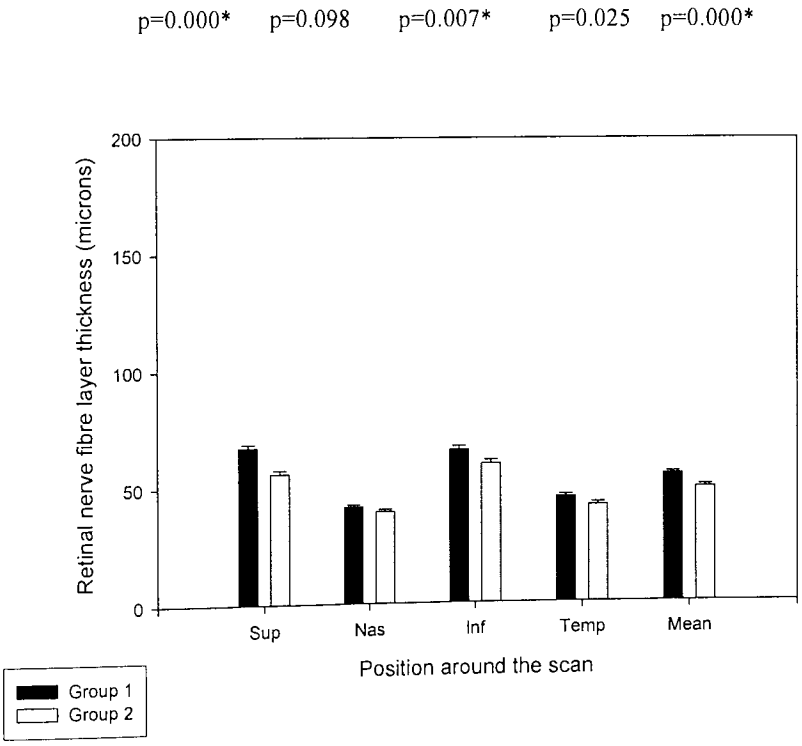

Figure 6.5 Vertical bar chart representing the estimated marginal means for retinal nerve fibre layer thickness in all quadrants of the 3rd radius scan * denotes statistical significance (p=0.01)

For the disc margin scan group 2 (over 40 years) had thinner RNFL layer in all quadrants compared to the younger group (see figure 6.3). This difference reached significance in the superior quadrant only where p=0.006 (see table 6.11). Significant differences in RNFL between groups occurred overall and in all the four quadrants (see table 6.12) for the 2nd radius scan. The estimated marginal means are summarised graphically in figure 6.4. RNFL thickness was greater for group 1 than group 2 in all quadrants and for the mean 360 degree scan for the 3rd margin scan (figure 6.5). However, significant differences in RNFL thickness between groups occurred for the overall mean scan and the superior quadrant only (see table 6.13).

6.12 Discussion

Our study found a significant positive correlation between age and macular retinal thickness in position 1 (fovea) only. For all other locations on the retinal thickness map analysis (2-9) correlations between age and retinal thickness failed to reach significance. Secondly, in terms of retinal nerve fibre layer thickness, for the disc margin, 2nd and 3rd radius scans RNFLt was negatively correlated with age for the mean overall and superior quadrant. RNFLt was negatively correlated with age for the inferior and the temporal quadrant for the 2nd radius scan only.

6.12.1 Effect of age on retinal thickness

Studies investigating the effect of age on retinal thickness report a range of findings. In a group of 40 normal subjects (mean age 53.2±15.8 (range 25-69) linear regression showed a non statistically significant correlation between macular thickness and age (r=0.12; p>0.99) (Landau *et al.*, 1997). Using a prototype Retinal Thickness Analyzer (RTA) instrument, the authors reported a tendency for foveola thickness to increase with age although they failed to prove statistical significance. They observed average retinal thickness of 166±38 microns for subjects younger than 31 years of age, 175±45 microns for subjects aged between 31 and 50 years. For their oldest group of subjects (aged over 50 years), foveola retinal thickness was 222±52 microns. However, Oshima *et al.* (1999) using a similar instrument found that central macular thickness was independent of age. Asrani *et al.* (1999) reported that age has little effect on the retinal thickness at the posterior pole. Kremser *et al.* (1999) using a prototype RTA reported

no association between age and retinal thickness in 129 eyes of 79 volunteers aged 16-80 years (mean age 41 years).

Similarly, Kanai *et al.* (2002) observed no change in retinal thickness at the foveola with increasing age in a group of 47 eyes from 47 normal volunteers aged from 21 to 79 years as measured by optical coherence tomograpy. These findings compare with a study by Massin *et al.* (2002) who, using the OCT six radial line macular scan found no significant difference in retinal thickness of the central 1mm sector (position 1) according to age. Wakatani *et al.* (2003), using a series of four OCT 2000 line scans, each 3mm in length centred through the fovea found no significant correlation between age and retinal thickness in three circular areas surrounding the central fovea (350, 1850 and 2850 μm in diameter).

The results of our study would appear to concur with the findings of Landau *et al.* (1997), with greater retinal thickness exhibited at foveal position 1 for group 2 (over 40 years old) than group 1 (under 40 years of age). Statistical analysis suggests a strong positive relationship between age and retinal thickness in this position. For all other locations, there was little evidence of a relationship between age and tissue thickness although inspection of the raw data (see table 6.2) suggest that in all locations retinal thickness is slightly greater in older individuals.

Kanai *et al.* (2002) using the OCT to measure points 1mm from the foveola in the superior, inferior nasal and temporal directions, observed reduced retinal thickness in this parafoveal region of the macula with age (note that no such effect was observed for the foveola). A Stratus OCT study by Baquero Aranda *et al.* (2005) of 40 normal subjects aged between 20 and 60 years (80 eyes) subdivided into 4 groups with the following age cut offs- group 1 aged 20-29 years, group 2 aged 30-39 years, group 3 aged 40-49 and group 4 aged 50-59 also revealed statistically significant differences in macular thickness between the study groups using the fast macular thickness scanning protocol. This was observed in particular locations and was not a uniform effect across the entire macular scan. Significant reductions with age according to ANOVA were observed in the superior outer sector (location 9; p=0.00), temporal outer sector (location 8; p=0.01), temporal inner sector (location 4; 0.04), nasal inner sector (location 2; p=0.03) and inferior inner sector (location 3; p=0.00). For all quadrants in

the 3mm ring, with the exception of position 5 (superior), differences in retinal thickness between groups existed. In the 6mm ring, only the superior (position 9) and temporal (position 8) showed differences in retinal thickness. Differences only reached significance between group 1 aged (20-29 years) and group 4 (50-59 years). Our study however, despite the use of the same OCT model (3000) and scan protocol failed to elicit the same results. This is explained by the fact that Bonferroni correction for multiple comparisons was not employed by Baquero Aranda and colleagues (2005) as we did in our study. It appears that all of the sectors they describe as reaching significance would have failed to do so using a p value of 0.005 as set in our criteria. In addition, there is no evidence that axial length was taken into account during their analysis.

Alalmouti and Funk (2003) investigated the effect of age on retinal thickness for a group of 100 subjects aged 6-79 years (mean age 39.5 years) using a vertical line measuring 2.3mm placed at the temporal disc margin. They observed a significant ($p=0.0002$) decrease of retinal thickness with increasing age and reported an average decrease of 0.53μm per year although they determined that 80% of changes in retinal thickness over time are caused by shrinkage of the retinal nerve fibre layer.

6.12.2 Effect of age on retinal nerve fibre layer thickness

In our study, it is clear that retinal nerve fibre layer thickness is inversely correlated with age. The extent to which this age effect occurs appears to vary according to both the distance from the optic disc and the location by quadrant, namely superior, inferior, nasal and temporal positions. At the disc margin, age primarily affects the superior retinal nerve fibres. At a scanning circle radius of approximately 2mm the effect of age is more pronounced with every quadrant affected. With greater eccentricity, using the scanning circle of radius approximately 3mm age effects are confined to the superior quadrant only.

Our findings may not entirely reflect the way in which age affects the retinal nerve fibre layer thickness per quadrant and distance from the optic nerve head. We suggest that the age effect is always present but the ability with which we can detect change varies

according to location by quadrant and distance from the optic nerve head. These factors govern the quantity of tissue available to show a reduction in tissue thickness with age and the quantity of tissue available to be measurable. Effects based on the sampling theory, distribution of fibres in the retina and the ratio of signal to noise will all impact the acquired RNFL measures and subsequent analysis. The sampling theory is as true for image analysis as it is for signal: noise. At the optic disc margin, RNFL thickness for all quadrants is greater than in the larger scan radii especially across the vertical poles. For our sample group, RNFL thickness at the optic disc margin according to tables 6.6 and 6.7 varies the most between groups in the superior quadrant (with only small differences for the other quadrants). Such a difference is likely to be regarded as due to the large amount of fibres available in this area. At the 2nd margin scan (where tissue is thinner in comparison to the disc margin scan) all quadrants differ significantly between groups and the effect due to sampling is more pronounced i.e. the relative percentage loss of tissue is greater, therefore the impact of loss as a percentage of fibres sampled is greater. This difference is, therefore, likely to be regarded as comparably more significant for all quadrants. For the 3rd margin scan, the retinal tissue is much reduced in thickness and the effect of signal: noise if greatest in this location. For every quadrant, except where the tissue is thickest i.e. in the superior quadrant the effect of age is not detectable and therefore significance is lost for every quadrant.

The majority of experimental studies, using a variety of techniques, report a reduction in RNFL thickness as age increases.

Prior to the introduction of sophisticated imaging techniques, the retinal nerve fibre layer had been shown to decrease with age. Jonas *et al.* (1989) used red-free photography to image the nerve fibre layer in normal eyes and found that the visibility of retinal nerve fibre bundles reduced with age. The authors suggested that this was the ophthalmoscopic correlate of the widely reported reduction in nerve fibres number with increased age (Dolman *et al.*, 1980; Johnson *et al.*, 1987). Balazsi *et al.* (1984) reported a significant age effect on nerve fibre counts of normal human optic nerves (n=16) with a mean annual loss of 5637 optic nerve fibres. Such findings were confirmed in a histomorphometric study by Jonas *et al.* (1990) who examined 22 eyes of 19 subjects between 20 and 75 years and derived an approximate annual loss of 5426 fibres per

year. As optic nerve axons diminish, reductions in the retinal nerve fibre layer thickness are likely.

6.12.2.1 Scanning laser polarimetry

Studies employing scanning laser polarimetry imaging techniques to assess retinal nerve fibre layer thickness are inconsistent. Some report a reduction in fibre layer with age (Weinreb, Shakiba and Zangwill, 1995; Chi *et al.*, 1995; Poinoosawmy *et al.*, 1997) while others have failed to demonstrate such a relationship (Funaki *et al.*, 1999). Funaki *et al.* (1999) found no significant relationship between RNFL thickness overall and at quadrant level along the 1.75 disc diameter scanning circle nor along the 0.8m ring for 60 normal volunteers (mean age 48.4 years). The authors suggest this may be explained by the wide variation in retinal nerve fibre layer thickness of their subject sample or their smaller sample size in comparison to previous studies.

The variability between the studies may be explained by the technology itself used to collect retinal nerve fibre layer thickness data. Laser scanning polarimetry technique is based on changes in polarisation of light and retardation which is related to retinal nerve fibre layer thickness. Change in polarisation is converted into a topographical map of RNFL thickness measurements from which software analysis can be performed. However, a limitation of the scanning laser polarimeter is that the RNFL is not the only birefringent structure of the eye- both the cornea and lens have birefringence properties. The possibility that they may influence findings should therefore be considered. These conflicting findings may also be explained by the wide variation in RNFLt among normal individuals. Another source of variability with this equipment is the inability to control for the size of the disc which differs between individuals. The distance from the outer margin of the optic disc to the measuring ring depends on the size of the optic disc.

6.12.2.2 Loss per decade

Contrary to the findings of Funaki *et al.* (1999), Poinoosawmy *et al.* (1997) obtained nerve fibre layer thickness measurements for 150 normal subjects along the measurement ring concentric with the optic disc margin located 1.5 disc diameters from the optic nerve and reported a progressive reduction in RNFL thickness as age

increases, with a decay of 0.38μm per year. Similar findings were reported by Chi *et al.* (1995) who calculated a decrease in RNFL thickness of 0.2μm per year as measured along the peripapillary ring (concentric with the optic disc margin) with a 1.5 disc diameter. Lee and Mok (2000) found a significant negative correlation between average RNFL values with increasing age (approximately 1.9μm per decade) and at regional locations, i.e. superior, inferior, nasal and temporal (1.8μm per decade) using a scanning ring located 1.75 disc diameters away from the optic disc for 159 normal volunteers.

While direct comparisons between studies are not appropriate due to the differences in imaging devices and scan types, similar calculations were performed for our study sample. The following figure (figure 6.6) summarises the way in which retinal nerve fibres are lost per decade in each quadrant and for each scan type. RNFL tissue loss ranges from 0.3μm to 1.7μm per decade which appears to be less than that observed in other OCT studies. Mok *et al.* (2002) using the OCT 2000 RNFL default circular scans of 3.4m around the optic disc suggested a decrease of approximately 3.3μm per decade while Alamouti and Funk also using the OCT 2000, quantified the loss of RNFL thickness at 0.44 μm per year (4.4 μm per decade). In an OCT study by Kanamori *et al.* (2003), based on their coefficient of correlation, they estimated RNFL thickness to decrease by 0.17% per year (1.7% per decade).

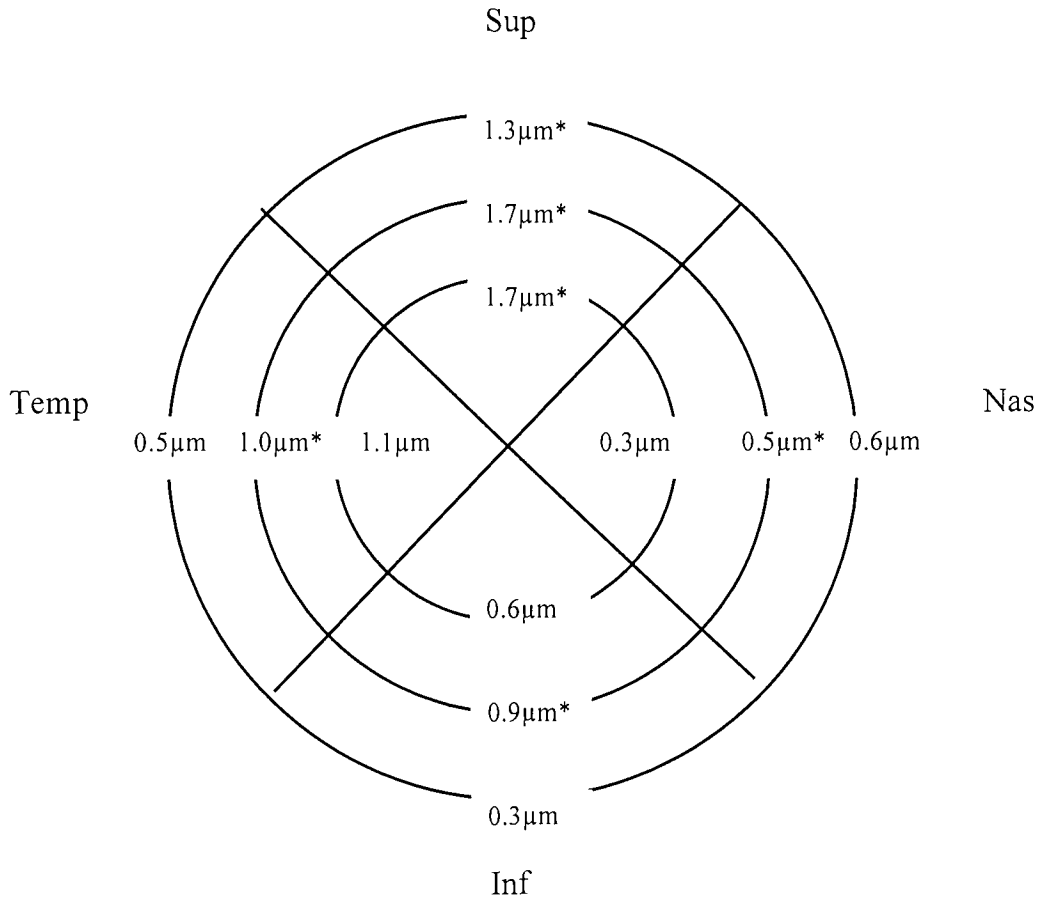

Figure 6.6 Schematic diagram showing RNFLt loss per decade in each quadrant for each scan * denotes statistical significance between groups

6.12.2.3 Optical coherence tomography

OCT is not subject to the limitations of scanning laser polarimetry, is unaffected by axial length and media opacities and throughout its development has been used in several investigations of the effect of age on retinal nerve fibre layer thickness. One of the first studies was carried out by Schuman *et al.* (1995) using a prototype OCT who reported a significant decrease in overall RNFL thickness with age. The RNFL of each subject was scanned using circular scans around the optic nerve, with circle sizes of either 2.25 or 3.37 mm, to best fit the optic nerve head of the patient without overlap. These scans therefore corresponded to an offset of approximately 500 and 750µm from the edge of the optic disc.

Soliman *et al.*, (2002) found that RNFL thickness decreased with increasing age when assessed by both the OCT and red-free photography.

Varma *et al.* (2003) found a statistical difference in the peripapillary RNFL thickness in each of the four quadrants between older and younger Latinos (n=312) using OCT circular scans of default radius of 1.74mm from the optic disc centre. Kanamori *et al.* (2003) reported that RNFL thickness around the optic disc significantly decreases with age in a study of 144 normal subjects (144 eyes) aged between 16 and 84 years of age. Using three OCT 1 circular scans, each 3.4mm in diameter Kanamori (2003) found that average RNFL exhibited the highest correlation with (r= -0.348, p,0.001). There was also evidence of a relationship between quadrantial RNFL. Correlation between age and temporal RNFL was highest and measured r-0.29,p=<0.001, for the superior quadrant correlation values were r=-0.24, p=0.035; inferior quadrant were -0.22 p=<0.001 and nasal RNFL r=0.14, p=0.355.

Furthermore, Mok *et al.* (2002) found a significant decrease in RNFLt with increasing age using the OCT model 2000 default circular scans of 3.4m around the optic disc to measure the RNFL of a cohort of 129 normal Hong Kong Chinese subjects aged between 24 and 78 years. Regression analysis revealed a significant negative linear correlation ($p<0.001$) between the average RNFL measurement and age ($r=-0.29$) and data suggested a decrease of approximately 3.3μm per decade of life. They also reported negative and gradual correlations between the superior ($r=-0.26$, $p<0.01$) inferior ($r=-0.24$, $p<0.01$) nasal ($r=-0.29$, $p<0.01$) and temporal ($r=-0.17$, $p=0.04$) values to age at a similar rate of about 3.2 μm per decade. Such findings are in keeping with those results found in a study by Alamouti and Funk (2003) using the same OCT model 2000 to examine 100 eyes of 100 healthy volunteers (age range 6-79 years) also show that RNFL thickness significantly decreases with age. They used vertical scans 2.3mm long, placed at the temporal edge of the optic disc and observed a significant ($p=0.00019$) decrease of the retinal nerve fibre layer thickness with increasing age quantified at 0.44 μm per year.

In a later study, Sony *et al.* (2004) report a significant age effect for the overall RNFL ($r=-0321$, $p=0.000$), superior ($r=-0.233$, $p=0.005$) and inferior quadrants ($r=-0.234$, $p=0.004$) using the OCT fast RNFL (3.4mm diameter circle scan) for a group of 146

normal subjects (mean age 44.55±16.14; range 20-70 years). There was no significant correlation between age and nasal or temporal retinal nerve fibre layer thickness. This agrees with our findings to a certain extent in that the vertical poles appear to be predominantly affected by age.

The effect of age on RNFL thickness was investigated by Baquero Aranda *et al.*, (2005) using the fast RNFL circular scan 3.4mm in diameter in a group of 40 normal subjects divided into age groups of 20-29 (group 1), 30-39 (group 2), 40-49 (group 3) and 50-59 (group 4). They found a progressive reduction in RNFL thickness across groups 1-4. Differences between groups only reached significance ($p=0.04$) in the inferior quadrant between groups 1 and 4. Again, no adjustment for multiple comparisons was employed unlike that in our study.

The above investigations can be confirmed by histological data. Varma (1996) found that the superonasal and inferotemporal RNFLt at the disc margin was inversely related to age. They were unable to detect a consistent negative association between all RNFLt measurements and age but their small sample size ($n=10$) may explain this.

6.13 Conclusion

This study shows thickening at the foveola with age but no influence of age on the macular retinal thickness at other positions. Retinal nerve fibre layer thickness around the optic nerve head decreases with age.

CHAPTER 7: Nerve fibre loss in glaucomatous optic neuropathy

7.1 Abstract

Purpose: To determine the pattern of retinal nerve fibre loss in patients with glaucomatous optic neuropathy using the Stratus Optical Coherence Tomographer (OCT 3 Model 3000, Carl-Zeiss Meditec, Dublin, CA).
Methods: RNFL thickness (RNFLt) measurements were obtained and compared for one eye each of 40 aged-matched normal control subjects (65.8±11.69years; range 40-84 years) and 40 glaucoma patients (mean age 68.0±10.53years; range 48-85 years). RNFLt was assessed using a series of OCT circular scans centered on the optic disc, scanning around the optic disc margin. Measurements of RNFLt were taken close to the optic disc margin and at two further locations at increasing distance from the optic disc margin using circle scan radii specific to each subject. The initial scan was placed at the subjects' disc margin and designed to fit closely around the optic disc margin whilst ensuring that the entire optic disc fell within the scanning circle. The radius of the circle scan was then increased to 2x and then 3x the initial radius to allow investigation of the RNFL at several eccentricities (i.e. using ratio of 1:2:3). Average RNFLt measurements were obtained for the overall 360 degree scan and for each of the superior, nasal, inferior and temporal quadrants for each of the three scan sizes. An independent samples t-test identified statistically significant differences in disc area between groups. Analysis of covariance (ANCOVA) was therefore used to identify differences between thickness measurements for the two groups using disc size as the covariate. Bonferroni correction was used to correct for multiple comparisons taking $p<0.003$ for significance.
Results: RNFL thickness decreases with increasing distance from the optic disc for both normal and glaucomatous eyes. Statistically significant differences in RNFL thickness occurred between normal and glaucomatous eyes for the mean scan and in all four quadrants for the optic disc margin scan and the 2nd radius scan ($p=0.0001$). Mean RNFL and RNFL thickness in the superior, inferior and temporal quadrant was greater for normal eyes than in glaucomatous eyes for the third radius scan but reached statistical significance only in the superior ($p=0.0001$) and inferior quadrants ($p=0.003$).
Conclusion: As the distance from the optic disc increases nerve fibre layer thickness generally decreases. RNFL thickness is reduced in glaucoma. With increasing distance from the disc the effects of glaucomatous damage are diminished. The retinal nerve fibres making up the superior and inferior quadrants are more susceptible to damage while those in the nasal and temporal quadrants appear to be spared to a certain extent. OCT provides a technique to measure the thickness of the RNFL which enables detection of nerve fibre loss and optic nerve head changes in the glaucamtous eye. OCT provides a means of monitoring disease over time.

7.2 Introduction

Optical coherence tomography (OCT) has been shown to be an objective and reliable method of providing quantitative measurements of retinal nerve fibre layer (RNFL) thickness (Huang *et al.*, 1991; Schuman *et al.*, 1995; Schuman *et al.*, 1996; Blumenthal *et al.*, 2000; Carpineto *et al.*, 2003). It utilises the differential properties of each of the retinal layers together with low coherence inteferometry to produce high resolution cross sectional images of ocular tissue and findings are confirmed by histological reports (Varma *et al.*, 1996). Glaucoma is a disease that is characterised by a loss of retinal ganglion cells and their axons and subsequent decrease in the retinal nerve fibre layer (RNFL). Studies have shown a reduction in RNFL thickness can precede both visual field defects (Quigley *et al.*, 1982; Sommer *et al.*, 1991) and pathological changes to the structure of the optic nerve head (Sommer *et al.*, 1977). OCT therefore has the potential to provide a means by which to identify early and longitudinal disease changes in the eye and monitoring the effect of any treatment or intervention.

The purpose of this study is to determine the impact of measuring RNFL thickness in different retinal locations around the optic nerve head to identify glaucomatous loss. This study uses the most recent version of OCT technology, the Stratus OCT to measure the RNFL in both glaucomatous and normal eyes.

7.3 Aims and objectives

To determine the rate of reduction in retinal nerve fibre layer thickness with eccentricity from the optic nerve head in normal subjects and glaucoma patients, in order to identify the most appropriate imaging protocol for the detection of glaucomatous nerve fibre loss.

7.3.1 Hypothesis

Retinal nerve fibre layer thickness decreases with distance from the optic nerve head, and as such glaucomatous loss will be less marked further away from the optic nerve head.

7.4 Materials and Methods

7.4.1 Inclusion criteria:Normal subjects

Normal healthy subjects were recruited from staff at Birmingham Heartlands Hospital Ophthalmology Department, staff in the Vision Sciences Department, Aston University and attendees at the Optometry Clinic at Aston University. A full eye examination was carried at by an optometrist (HLW) to establish whether the study inclusion criteria were met. Subjects were included if they exhibited:

- No abnormalities on ophthalmoscopic examination
- Minimal or no lens opacities allowing a clear fundus view
- No history or evidence of intraocular surgery or laser therapy
- No history or evidence of retinal pathology or glaucoma
- Snellen visual acuity (VA) 6/9 or better
- Less than 6 dioptres of spherical ametropia and 2 dioptres of astigmatism
- Intraocular pressure (IOP) less than 21mmHg (Non-contact tonometry-Pulsair 3000)

7.4.2 Glaucoma patients

Glaucoma patients were recruited from the Ophthalmology Department of Birmingham Heartlands Hospital Glaucoma Clinic and had previously been diagnosed with primary open angle glaucoma (POAG) by a collaborating ophthalmologist in the glaucoma clinic. Subjects were included in the study if they exhibited:

- Optic nerve head cupping consistent with glaucomatous changes:
  Notching (focal extension of the cup)
  Focal or geneneralised narrowing or disappearance of the neuroretinal rim
  Pallor of the neuro-retinal rim
  Cup-disc (C: D) asymmetry of >0.2

- Repeatable mild to moderate visual field defects consistent with a diagnosis of glaucoma on at least two consecutive assessments using the Humphrey Visual Field Analyser (program 24-2)
- Minimal or no lens opacities allowing a clear fundus view
- No history or evidence of intraocular surgery or laser therapy
- No history or evidence of retinal pathology other than glaucoma
- Snellen visual acuity (VA) 6/9 or better
- Less than 6 dioptres of spherical ametropia and 2 dioptres of astigmatism

7.4.3 Subject sample

The subject sample consisted of 40 normal subjects (20 male, 20 female) aged 65.8±11.69 years and 40 patients (20 male, 20 female) aged 68.0±10.53years diagnosed with primary open angle glaucoma (POAG). Data was collected from one eye each of each subject, equal numbers of R and L eyes were examined (20 R and 20 L eyes for both the normal and glaucoma group).

7.4.4 Ethical approval and informed consent

Ethical approval was obtained from the ethical committee boards of Birmingham Heartlands and Solihull NHS Trust and Aston University. Approval conformed to the tenets of the Declaration of Helsinki. Written informed consent was obtained from all subjects and patients.

7.5 Methods

Following recruitment as per the requirements set and listed above, subjects attended for one visit only.

7.5.1 OCT data acquisition

Retinal nerve fibre layer thickness scans around the optic nerve head were taken using the optical coherence tomographer. (For a detailed description of the OCT see section 1.13).

Prior to image acquisition, subject details were entered into the database of the OCT. The subjects were instructed to place their chin on the chin rest and forehead against the top bar and instructed to fixate on a green target. To optimise the scan image and yield the strongest scan signal both the Z-offset (axial range) and polarisation was adjusted.

Measurements of optic disc parameters were assessed for all participants using the OCT fast optical disc scan. Retinal nerve fibre layer thickness (RNFLt) was assessed using a series of OCT circular scans centered on the optic disc, scanning around the optic disc margin. Measurements of RNFLt were taken at or closest to the optic disc margin and at two further locations at increasing distance from the optic disc margin using circle scan radii specific to each subject. The initial scan was placed at the subject's disc margin and designed to fit closely around the optic disc margin whilst ensuring that the entire optic disc fell within the scanning circle. The radius of the circle scan was then increased to 2x and then 3x the initial radius to allow investigation of the RNFL at several eccentricities (i.e. using ratio of 1:2:3). Placement of the initial scan was achieved using the cursor and no further adjustment was required during the scanning process. Six scans of each circle radii were taken, with a view to using the best five scans for analysis with the majority of patients requiring a initial scan radius of 1.0mm or 1.1mm which further increased to 2.0mm and 3.0mm (or 2.2mm and 3.3mm respectively) RNFL analysis software produced a circular map depicting RNFL thickness measurements for each of the four 90 degree quadrants (superior, nasal, inferior and temporal) and for the entire scan through 360 degrees, comprising 12 segments or clock hours.

7.5.2 Retinal nerve fibre layer thickness

Prior to statistical analysis, actual recorded retinal nerve fibre layer thickness values around each scan (for each position 1-12 o'clock) were plotted for both normal subjects

and glaucoma patients (see figures 7.1-7.3). Table 7.1 summarises actual retinal nerve fibre layer thickness values per quadrant for both normal and glaucoma groups. Significant differences between groups according to analysis by ANCOVA are shown by *. (See section 7.6 for full description of ANCOVA)

Location	Optic disc margin Actual RNFLt (microns) [SD]		2nd diameter scan Actual RNFLt (microns) [SD]		3rd diameter scan Actual RNFLt (microns) [SD]	
Category	N	GL	N	GL	N	GL
Overall 360 degree scan	136.43 [19.89]	94.06* [22.86]	74.84 [10.86]	54.83* [11.42]	51.32 [7.85]	44.06 * [12.64]
Inferior 90 degree	174.70 [30.03]	116.91* [37.09]	95.87 [15.46]	70.29* [22.76]	64.13 [15.26]	49.27 * [23.21]
Superior 90 degree	149.27 [23.21]	104.76* [28.65]	91.86 [17.40]	61.70* [16.90]	58.96 [12.38]	43.51* [12.90]
Nasal 90 degree	128.23 [30.83]	89.13* [25.07]	57.95 [12.10]	46.78* [13.88]	39.93 [7.01]	42.00 [20.19]
Temporal 90 degree	86.75 [19.89]	65.46* [17.39]	53.68 [11.52]	40.56* [9.00]	42.28 [9.48]	41.45 [16.31]

Table 7.1 Actual RNFL thickness measures for each group at each diameter scan

* denotes statistical significance between groups (p=0.01 after Bonferroni correction).

For each size scan, RNFL thickness shows a characteristic double hump formation with peaks at the inferior and superior quadrants and troughs in the nasal and temporal quadrants for both groups. Nerve fibre layer thickness is greatest in the inferior quadrant followed by the superior and nasal quadrant and thinnest at the inferior part of the optic disc margin (7.1). The RNFL is thinner in all quadrants and for the mean scan in the glaucomatous eyes compared with their aged matched normals for all 3 scan radii (see figure 7.1-7.3). As shown in figure 7.2 and 7.3, with increasing distance from the optic nerve head, RNFL decreases. This is true for both the normal and glaucoma subjects.

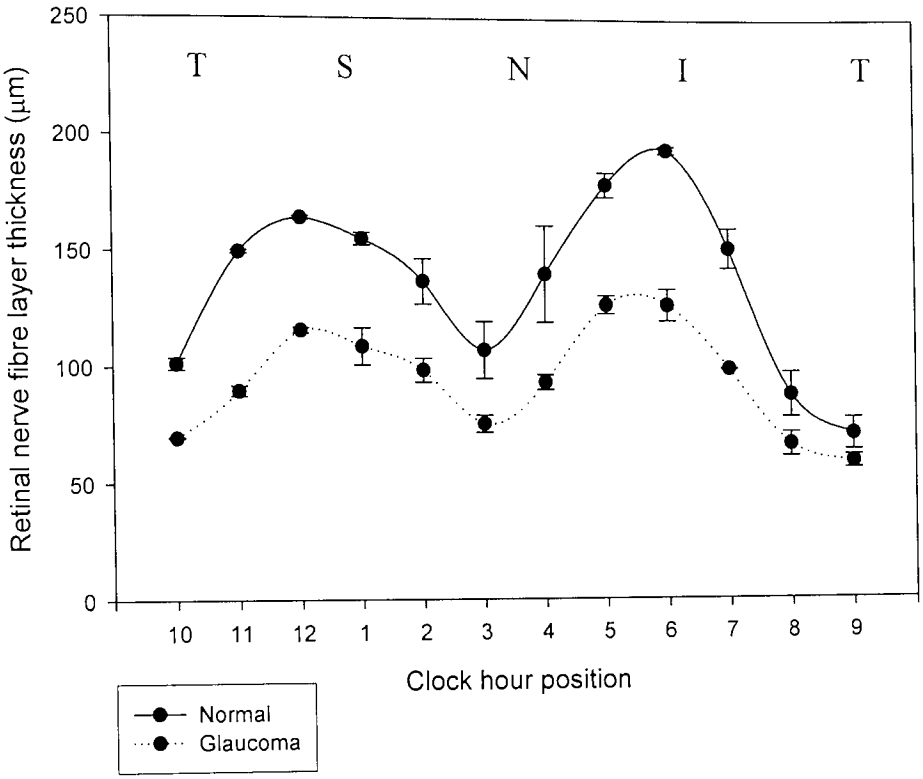

Figure 7.1 Graph to show the variation in RNFLt around the disc margin scan for normal subjects and glaucoma patients

As the distance from the optic nerve head increases the RNFL displays a progressive reduction for both the normal and glaucoma group. The double hump formation is shown for both the 2nd and 3rd radius although the pattern is less marked with increasing distance from the optic disc (see figures 7.2 and 7.3). The RNFL is thinner in all positions around the 2nd radius and 3rd radius scan in the glaucoma group compared with the normal group.

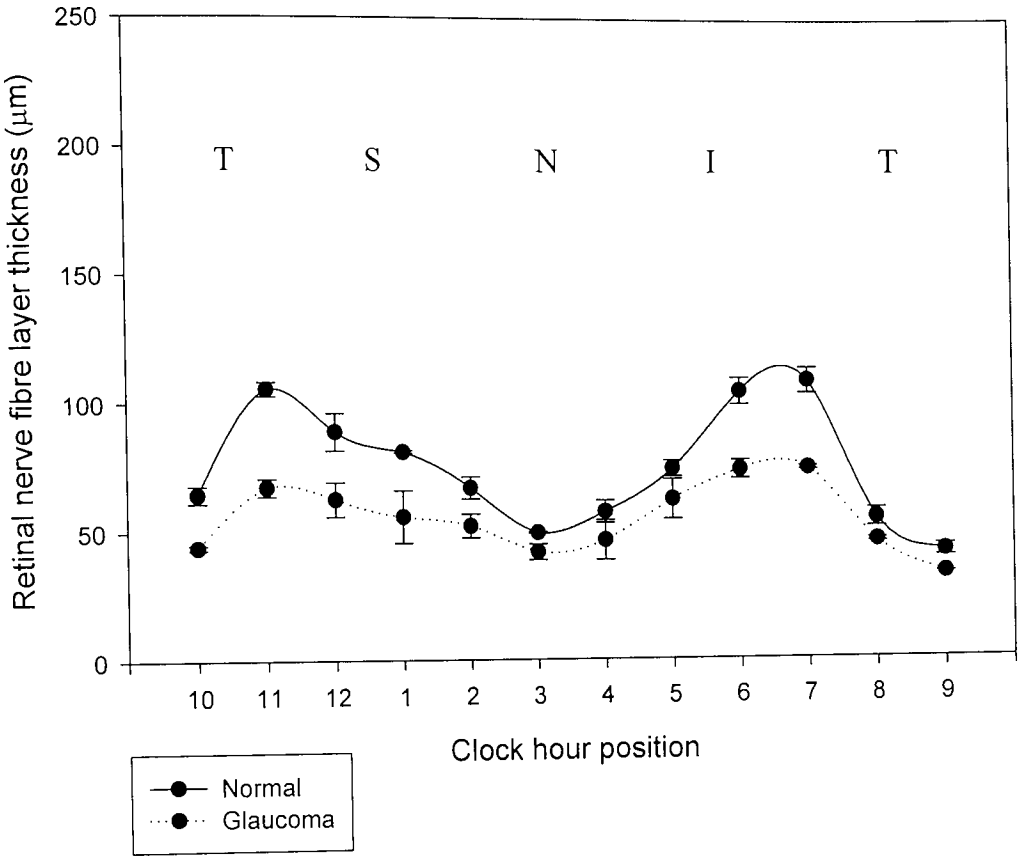

Figure 7.2 Graph to show the variation in RNFLt around the 2nd radius circle scan for normal subjects and glaucoma patients.

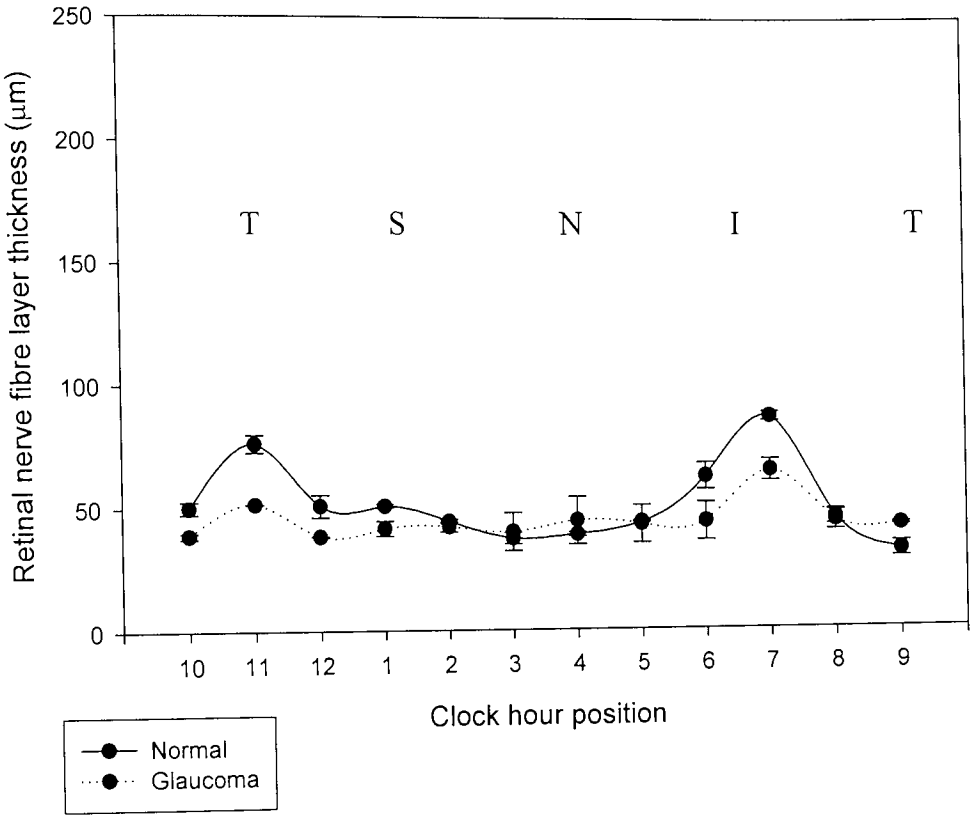

Figure 7.3 Graph to show the variation in RNFLt around the 3rd radius circle scan for normal subjects and glaucoma patients.

7.6 Statistical analysis

Mean disc area for normal subjects was 2.24 ± 0.31mm² (range 1.67-3.19mm²) and 2.48 ± 0.43mm² for the glaucoma group (range 1.67-3.61mm²). An independent samples *t*-test was conducted to assess whether differences in disc size between groups reached significance. There was a significant difference in disc size between normal subjects and glaucoma patients (p=0.006). In order to accurately assess the effects of disease it was important to account for the differences in disc area in our statistical analysis.

Analysis of covariance (ANCOVA) using Bonferroni correction for multiple analyses was used to assess whether statistical differences occurred between the groups with disc area assigned the covariate. A separate ANCOVA was carried out for RNFlt ineach quadrant (ISNT) and for the overall RNFLt. Results are summarised in Appendix 3. In this way we were able to assess whether differences occurred between the normal and

glaucoma group while controlling for the size of the disc. Bonferroni significance levels were set at 0.01 i.e. 0.05/5 where 5 is the number of analyses performed for each scan size. For each of the 3 scans analyses were carried out for the superior, nasal inferior, temporal quadrant and mean retinal nerve fibre layer thickness. ANCOVA analysis generated estimated marginal means for each parameter, details of which can be seen in the following figures (fig 7.4-7.6).

The relationship between RNFLt and visual field indices (MD and PSD) was assessed for the glaucoma patients using Pearson product-moment correlation.

7.7 Results

7.7.1 Differences between groups: analysis of covariance (ANCOVA)

Significance values of differences between groups for each quadrant and scan are summarised in table 7.2. Significant differences calculated by ANCOVA are shown by*

Estimated marginal means (RNFLt measures controlling for the effect of disc area) for each scan radius are shown in figures 7.4-7.6.

	p value (significance p=0.01)		
Location	Disc margin	2nd diameter	3rd diameter
Overall 360 degree scan	p<0.0001*	p<0.0001*	p=0.005*
Inferior 90 degree	p<0.0001*	p<0.0001*	p=0.003*
Superior 90 degree	p<0.0001*	p<0.0001*	p<0.0001*
Nasal 90 degree	p<0.0001*	p<0.0001*	p=0.518
Temporal 90 degree	p<0.0001*	p<0.0001*	p=0.718

Table 7.2 Statistical data for comparison of RNFLt between normal subjects and glaucoma group using ANCOVA * denotes statistical significance (p=0.01)

7.7.1.1 Optic disc margin

For the optic disc margin scan there was a statistical difference between RNFL measured in glaucoma and normals for each of the four quadrants and for the overall scan with $p<0.0001$.

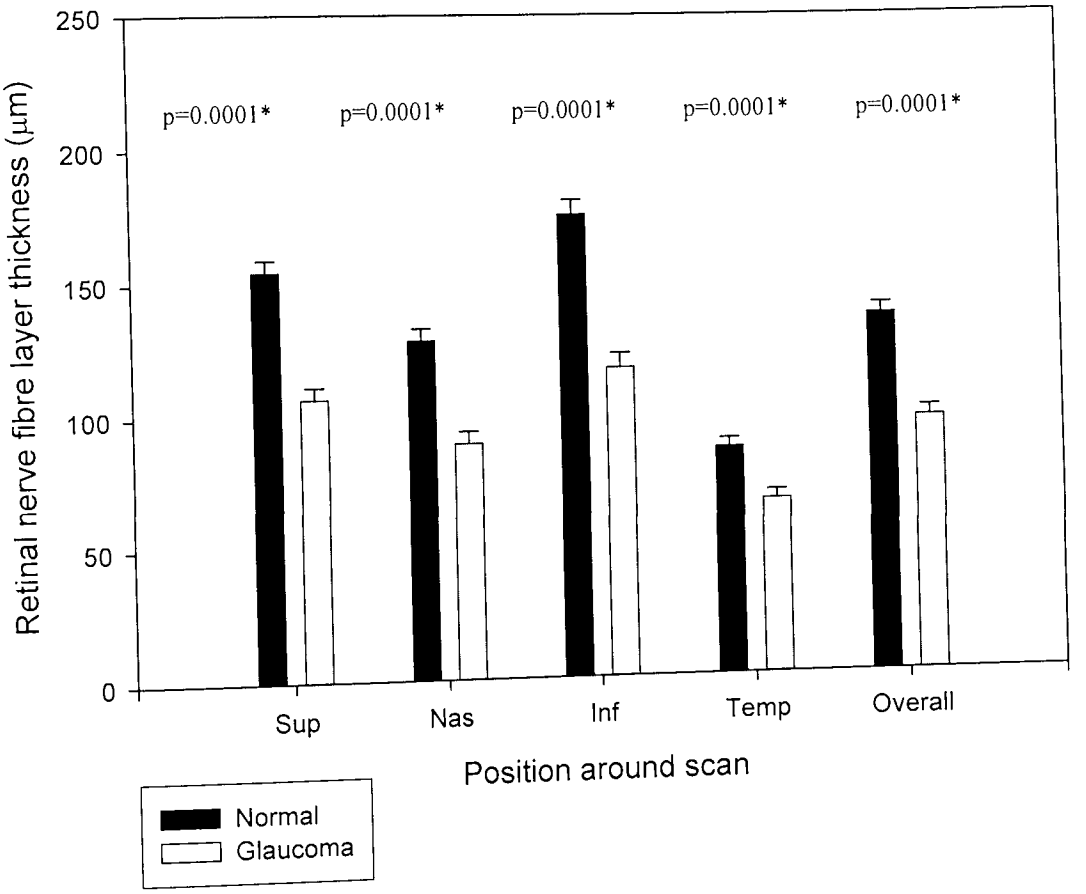

Figure 7.4 Graph to show the estimated marginal mean RNFLt from ANCOVA analysis for each group for the disc margin scan * denotes statistical significance (p=0.01 Bonferroni corrected)

7.7.1.2 2nd radius scan

RNFL thickness was significantly greater between diagnostic groups in each of the four quadrants and overall for the 2nd radius scan ($p<0.0001$) as shown in fig 7.5 and table7.2.

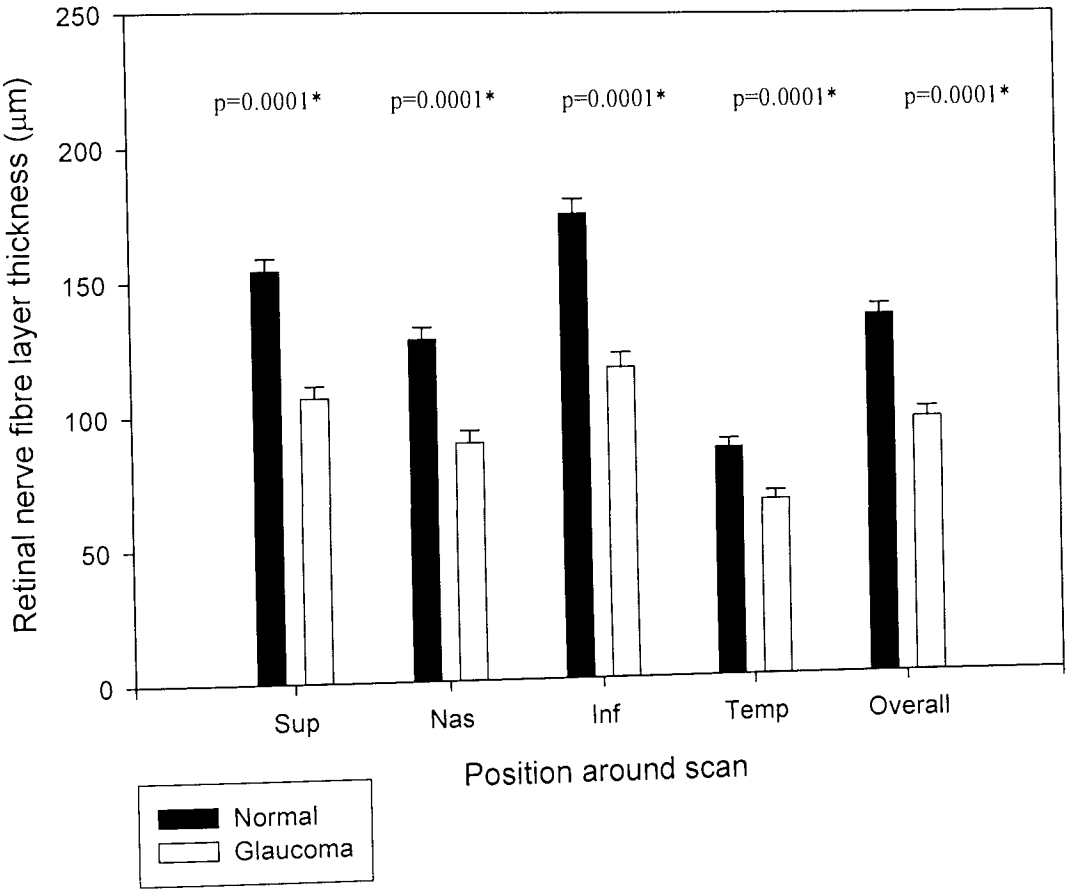

Figure 7.5 Graph to show the estimated marginal mean RNFLt from ANCOVA analysis for each group for the 2nd radius scan * denotes statistical significance (p=0.01 Bonferroni corrected)

7.7.1.3 3rd radius scan

For the 3rd radius scan, RNFL was thinner for the glaucomatous eyes compared to the normal eyes in the superior, inferior, temporal quadrants and overall (figure 7.6). However, this reached significance in only the superior and inferior quadrant according to our criteria.

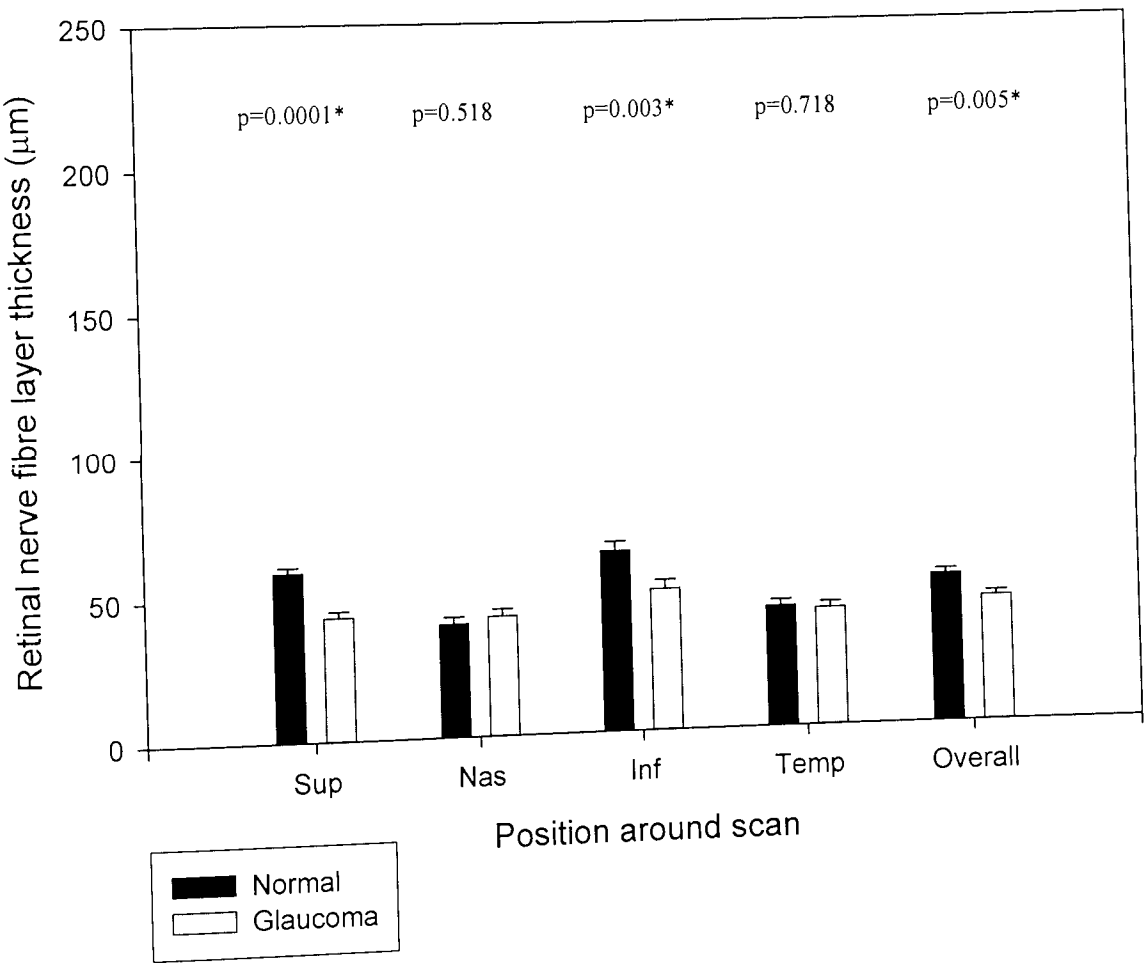

Figure 7.6 Graph to show the estimated marginal mean RNFLt from ANCOVA analysis for each group for the 3rd radius scan * denotes statistical significance (p=0.01 Bonferroni corrected)

7.7.2 Rate of change of retinal nerve fibre layer thickness with increasing distance from the optic nerve head.

Figures 7.7-7.11 show the decrease in RNFL in all quadrants and the mean RNFL with increasing distance from the optic nerve head for each scan size for the normal and glaucoma group.

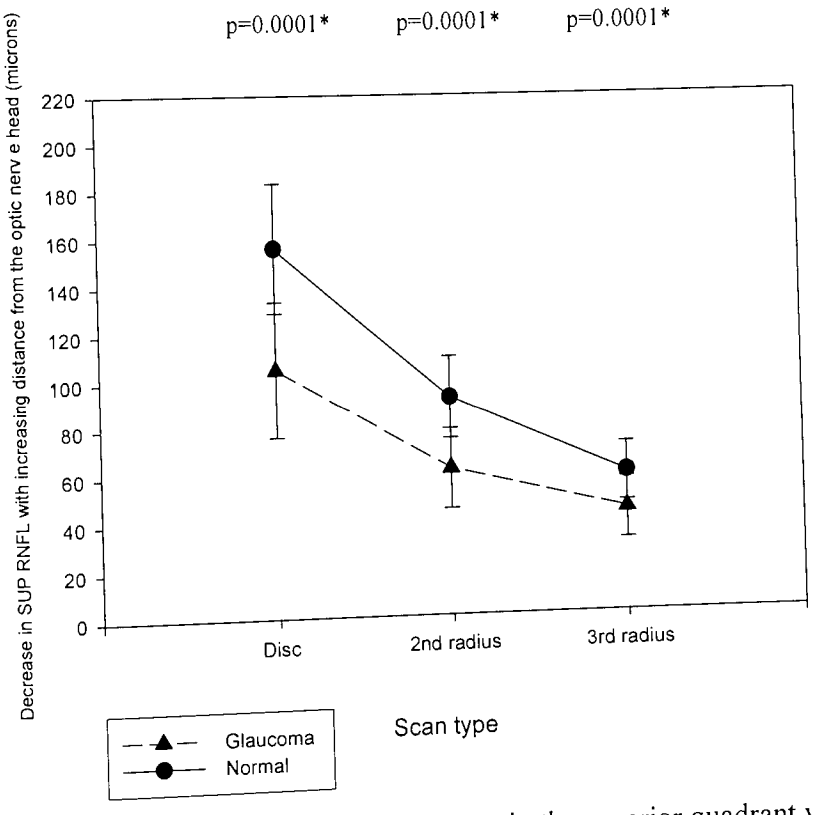

Figure 7.7 Graph to show the decrease in RNFLt in the superior quadrant with increasing eccentricity from the ONH * denotes statistical significance (p=0.01)

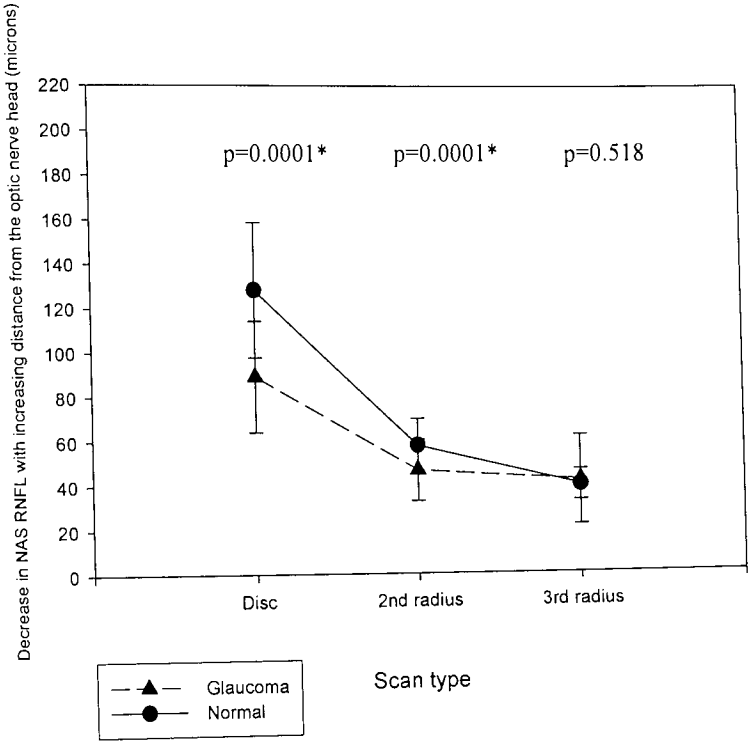

Figure 7.8 Graph to show the decrease in RNFLt in the nasal quadrant with increasing eccentricity from the ONH * denotes statistical significance (p=0.01)

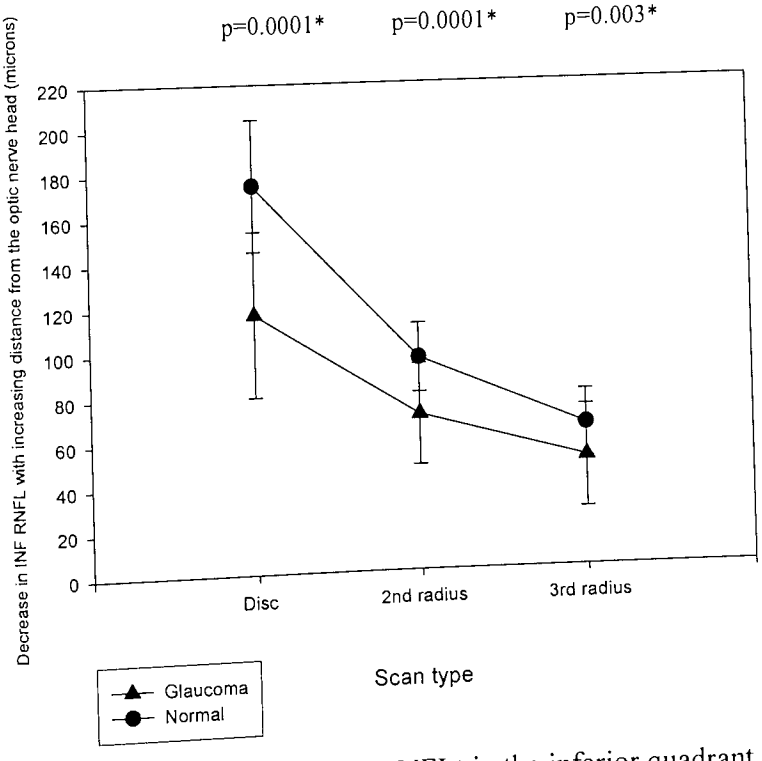

Figure 7.9 Graph to show the decrease in RNFLt in the inferior quadrant with increasing eccentricity from the ONH * denotes statistical significance (p=0.01)

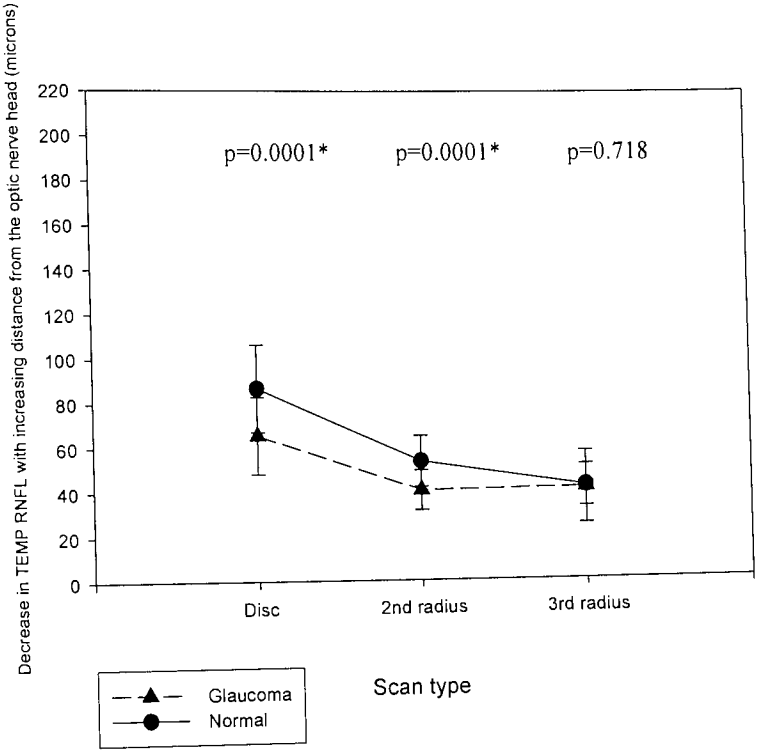

Figure 7.10 Graph to show the decrease in RNFLt in the temporal quadrant with increasing eccentricity from the ONH * denotes statistical significance (p=0.01)

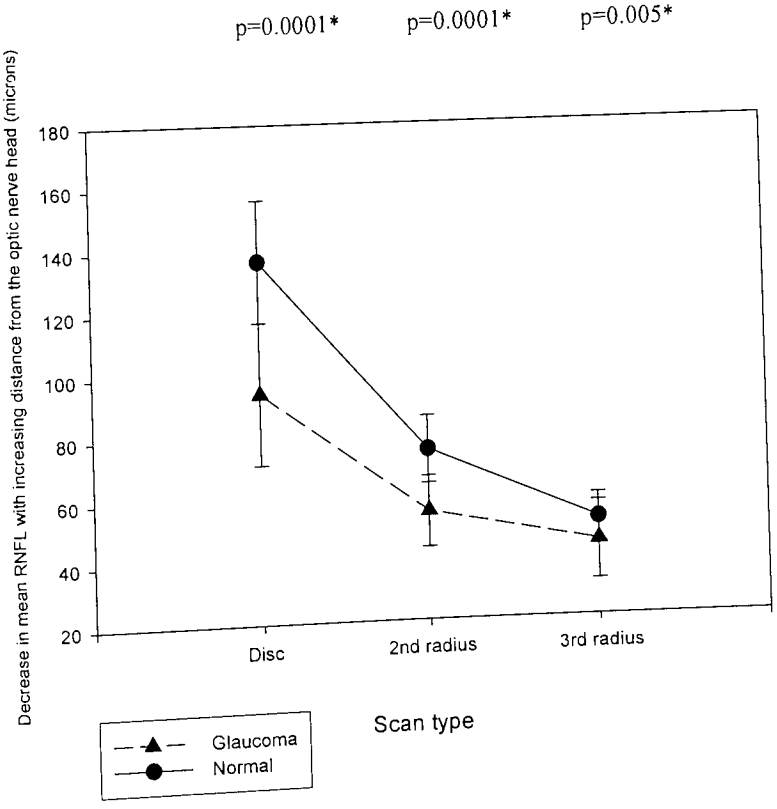

Figure 7.11 Graph to show the decrease in mean RNFLt with increasing eccentricity from the ONH* denotes statistical significance (p=0.01)

7.7.3 Relationship between RNFL and visual fields

For the glaucoma group mean MD was -3.04 ± 2.90dB while mean PSD was 4.39 ± 3.18 dB. After correction for multiple comparisons there was no correlation between mean deviation (MD), pattern standard deviation (PSD) and mean RNFLt mean and quadrant for any scan size.

7.8 Discussion

7.8.1 Anatomy of the RNFL

Our results confirm the findings of previous histological reports with regard to the pattern of nerve fibre distribution around the optic disc (Varma *et al.*, 1996). RNFLt is greater in the inferior quadrant followed by the superior, nasal and temporal quadrants for both the normal and glaucoma group. This double hump appearance is the most obvious at the optic disc margin itself and can also be observed at the 2nd and 3rd diameter scans though less marked here. At the majority of locations around the scan the RNFL thickness was greater in the normal group compared to the glaucoma group. This was true for each of the three scan diameters. As the scan size increases in diameter i.e with increasing distance from the optic disc margin the RNFL thickness reduces for both the normal and glaucoma group.

In terms of the pattern of nerve fibre loss, statistically significant differences occurred between groups in each of the four quadrants and overall for the optic disc margin scan. This was also true of the 2nd diameter scan. However, for the 3rd diameter scan difference between groups reached significance only at the inferior and superior quadrants. Our findings may be explained in terms of the anatomy of the retinal nerve fibre layer. Nerve fibres from the macular area follow a straight course to the optic nerve head, represented by the temporal quadrant fibres. Those from the nasal retina also follow a fairly straight course to the optic nerve head and form the nasal quadrant part of the scan. Fibres arising from the retina on the temporal side of the macula follow an arcuate pattern to reach the optic nerve head. According to Quigley *et al.* (1982) these arcuate fibres reaching the superior temporal and inferior temporal portions of the

optic nerve head have been shown to be most susceptible to damage. Our findings support the ISNT rule which describes the order in which retinal nerve fibres are lost. Inferior fibres are lost first, followed by the superior fibres and lastly nasal and temporal fibres are damaged.

Our study shows that patients with glaucoma exhibit reduced retinal nerve fibre thickness compared to normals. As the distance from the optic disc increases nerve fibre layer thickness generally decreases for all subjects. In addition, with increasing distance from the disc however, the effects of glaucomatous damage are diminished. The retinal nerve fibres making up the superior and inferior quadrants are more susceptible to damage while those in the nasal and temporal quadrants appear to be spared to a certain extent.

This study is the first of its kind to select scan size specific to the patient. A major complication in the process of diagnosing glaucoma in terms of pathological changes to the optic disc is that even in a normal population of eyes there is a considerable variation of disc size. In a population of normal eyes, there is a variation of both disc and cup size. A larger disc has a larger cup and a smaller disc may have little or no cup. In the glaucomatous eye, optic disc damage leads to a loss of neuroretinal rim and an increase in the optic disc cup. As a consequence the cup to disc ratio increases. Therefore, for a given cup to disc ratio, a small disc may have more damage. It is likely that larger optic discs have more nerve fibres and as a result measures from subjects with larger discs would be greater than those with smaller discs for the same size scan (Quigley *et al.*, 1991; Jonas *et al.*, 1992). In this study it was felt necessary to design each scan specifically to the subject rather than rely on an arbitary fixed dimension that would result in RNFL being measured at various differing locations from the optic disc centre. The majority of previous studies have used the standard RNFL scan protocol which comprises three fixed diameter circular scans (3.4mm in diameter) around the optic disc (Schuman *et al.*, 1996; Blumenthal *et al.*, 2000; Bowd *et al.*, 2000). In this study we used scans of appromimately 2.2mm diameter (disc margin scan), 4.4mm in diameter (2^{nd} scan) and 6.6mm diameter (3^{rd} scan) with each scan set designed to closely match the optic disc margin of each patient.

In this study, a circular scan was selected from the OCT scan protocol and a circle radius of 'best fit' applied to the optic nerve head shown on the fundus image, taking care to envelope the entire optic disc. Scans were taken at this radius before increasing the scan size to a radius twice the size of the original scan and then further to a scan radius three times the original, with five repetitions taken at each radius. While this is more time consuming in terms of set up and scan acquisition it was important that every subject had RNFL thickness measured in an identical place in order for reliable comparisons to be made. The position of the scan was recorded using x, y co-ordinates so detailed and reliable follow up of patients could be undertaken.

7.8.2 Reduction of RNFLt with increasing distance from the optic nerve head

This study also investigated the rate of reduction in nerve fibre layer thickness with increasing distance from the optic disc rate per quadrant in the normal and glaucoma group.

As expected, mean RNFL thickness and RNFL in each quadrant is greater in the normal group than in the glaucoma group for all scan radii. Between the disc margin and the 2nd radii scan, the decrease in RNFL thickness is greater than that between the 2nd and 3rd radii scans for all subjects. Statistical differences between normal subjects and glaucoma patients for the 3rd radii scan reached significance only for the superior, inferior quadrants and for the mean RNFL. The graphs for the superior and inferior quadrant (vertical pole) follow a similar pattern to each other while the nasal and temporal quadrants are similar in appearance to one another.

To our knowledge this has not been widely investigated. The majority of investigations of the RNFL report a reduction in the nerve tissue of glaucomatous eyes compared to the normal eye using the standard circle scan of diameter 3.4mm and at no other distances from the optic disc margin. Schuman *et al.* (1995) observed thinner RNFL in glaucomatous eyes compared to normal eyes, especially in the inferior quadrant ($p=0.04$) and reported a correlation between RNFL thickness and visual function. This finding is confirmed by Kanamori *et al.* (2003) who conclude that the OCT has the ability to detect early glaucomatous damage by measuring RNFL thickness particularly

in the inferior quadrant. Bowd *et al.* (2000) found significant differences in the RNFL thickness between the aged matched normal (n=28) and glaucoma group (n=30) in all quadrants and throughout 360 degrees.

One exception to this is a study by Rohrschneider, Gluck, Burk *et al.* (1995) who measured the retinal nerve fibre layer thickness of 4 quadrants in 10 healthy eyes and 10 glaucomatous eyes at four defined distances from the optic disc margin using the Nerve Fibre layer Analyser (NFA). The authors found a significant reduction in RNFL with increasing distance from the optic disc in the superior and inferior quadrant in normal subjects. However, no significant differences of RNFL thickness for different distances from the optic disc margin were observed in the glaucomatous eyes.

7.9 Conclusion

As the distance from the optic disc increases nerve fibre layer thickness generally decreases. RNFL thickness is reduced in glaucoma. With increasing distance from the disc the effects of glaucomatous damage are diminished. The retinal nerve fibres making up the superior and inferior quadrants are more susceptible to damage while those in the nasal and temporal quadrants appear to be spared to a certain extent. OCT examination of the RNFL thickness in the vertical pole around the disc margin provides the most useful information regarding the extent of glaucomatous damage. Our study suggests that OCT examination of RNFL thickness at a greater distance from the optic nerve head than traditionally employed may provide invaluable early indicators of the extent of glaucomatous damage and the efficacy of treatment protocols for the patient with primary open angle glaucoma.

CHAPTER 8: Short-term relationship between blood glucose levels and retinal thickness, retinal nerve fibre layer thickness and visual function.

8.1 Abstract

Purpose: Clinicians are aware of physiological diurnal variations in factors such as IOP and some, but not all, address these in clinical and experimental protocols of a longitudinal nature. There are no previous reports of diurnal variations in retinal thickness or visual function, either in normal subjects or in those known to be susceptible to greater variation such as that associated with glucose metabolism in diabetes. The purpose of this study was to determine the relationship between blood glucose levels, retinal thickness, retinal nerve fibre layer thickness and visual function over a 12 hour period.

Methods: Visual acuity (100% and 10% logMAR), contrast sensitivity (Pelli Robson), visual fields (Humphrey Field Analyser Program using 10-2 white on white automated static perimetry and 10-2 short wavelength automated perimetry (SWAP)), retinal thickness and retinal nerve fibre layer thickness (Optical Coherence Tomographer, Stratus OCT), tonometry (Pulsair 3000), blood pressure (Dinamap ProCare Monitor 300: GE Medical Systems) and measurements of blood glucose levels (Hemocue 201+) were acquired at two hourly intervals over a 12 hour period (6 visits) for a group of diabetic patients. Group 1 comprised 20 Type 1 diabetic patients (mean age 37.9±15.39 years: range 17-66 years) and Group 2 comprised 21 Type 2 diabetic patients (mean age 56.33±11.09 years: range 37-72 years). For each patient, a blood sample was collected at the start of the study day and analysed for haemoglobin (HbA1c) levels. A mixed between–within subject ANOVA was conducted to assess variation in test parameters over the course of the day for both groups. Post-hoc analysis identified the visits between which differences in parameters reached significant levels. A simultaneous regression model was used to explore the relationship between each of the test parameters: retinal thickness, retinal nerve fibre layer thickness, IOP, blood pressure, pulse rate and visual field data and a number of potential predictor variables: type of diabetes, haemoglobin levels, duration of diabetes and glucose level for each visit.

Results: Foveal retinal thickness, reduced contrast logMAR acuity, Pelli Robson contrast sensitivity, SWAP visual fields, diastolic pressure and IOP exhibited changes with fluctuation in blood glucose. 100% logMAR vision, retinal nerve fibre layer thickness, retinal thickness (except foveal thickness) and white-on-white perimetry was unaffected. Contrast sensitivity scores can be predicted by long-term metabolic control as indicated by HbA1c levels, inferior RNFL by type and duration of diabetes, and mean RNFL and superior macular retinal thickness by diabetes type.

Conclusion: Acute changes to blood glucose levels impact the visual function of the diabetic patient and should be considered during clinical examination.

8.2 Introduction

That several aspects of vision and visual function are affected by diabetes mellitus is widely reported by diabetic patients themselves and in experimental studies. Changes to contrast sensitivity, colour vision and SWAP visual fields are well documented in diabetic subjects compared to normals. Diabetic eyes exhibit reduced contrast sensitivity according to several reports (Arend *et al.*, 1997; Dosso *et al.*, 1996; Ismail and Whitaker, 1998; Sokol *et al.*, 1985; Verrotti *et al.*, 1998). Many studies have reported colour vision defects in diabetes (Green *et al.*, 1985; Bresnick *et al.*, 1985; Trick *et al.*, 1988; Roy *et al.*, 1984). Short wavelength sensitive cone mediated mechanisms are specifically affected in retinal diseases that involve the inner retina (Greenstein *et al.*, 1989; Nork *et al.*, 1994). It is therefore expected that the diabetic eye would exhibit functional loss. This has been confirmed by several authors who report reduced sensitivity to short wavelength stimuli and reduced hue discrimination (Greenstein *et al.*, 1990; Trick *et al.*, 1988; Utku and Atmaca, 1992; Kurtenbach *et al*, 1994; Greenstein *et al.*, 1989; Greenstein *et al.*, 1990; Nomura *et al.*, 2000).

There is evidence that the glycaemic state of a subject impacts their visual function, although the results are not consistent. Reports suggest that reductions in contrast sensitivity are associated with hypoglycaemia (Hyvarinen *et al.*, 1983; Ewing, Dreary, McCrimmon *et al.*, 1998; Tabandeh, Ranganath and Marks, 1996) while other studies have reported poor contrast sensitivity at high glucose levels and normal contrast sensitivity levels at reduced blood glucose levels (Verrotti *et al.*, 1998). A later study involving Type 1 diabetics and SWAP fields has shown that short wavelength sensitive cones are vulnerable to damage from hyperglycaemia (Afrashi *et al.*, 2003).

The majority of experimental studies to date have investigated visual performance by chemically inducing changes to blood glucose levels of the subject using insulin infusions (Harrad, Cockram and Plumb *et al.*, 1985; Ewing *et al.*, 1998; Tabandeh *et al.*, 1996; Volbrecht, Schneck, Adams *et al.*, 1994), by administration of glucose over a relatively short period of time (North, Cooney, Chambers *et al.*, 1997) and either fixing glucose levels at different levels (Hardy *et al.*, 1995) or comparing visual function at the highest and lowest glucose levels (Volbrecht *et al.*, 1994). No study has investigated

the impact of acute changes in glucose control on ocular anatomy or visual function over a period of time.

There is clear evidence of physiological diurnal variations in many biological systems in the body, for example, intraocular pressure, blood pressure and aqueous humour production. However, to date, there has been no investigation of diurnal variations in retinal thickness and visual function in the normal or diseased eye. This study assesses ocular and visual changes as glucose levels constantly change over the course of the day. The aim of this study is to investigate visual function in a more realistic situation to reflect the patient's daily life and visual experience.

8.3 Aims and objectives

To determine the short-term impact of fluctuations in blood glucose levels on retinal structure and function over a 12 hour period in patients with diabetes. Further, the relationship between long-term diabetic control (indicated by haemoglobin HbA1c) and duration of diabetes compared to visual function and structure were also explored.

8.3.1 Hypothesis

Acute changes in blood glucose levels in diabetic patients during routine activities have an acute impact on ocular structure and visual function over a 12 hour period.

8.4 Materials and methods

8.4.1 Inclusion Criteria

Subjects were recruited from staff and students from Aston University and volunteers from the general public in response to local advertising in medical centres and press articles. All patients were advised that a study report would be sent to their own GP/ hospital consultant if requested. Group 1 had been previously diagnosed with Type 1 diabetes by their own GP. Group 2 had been previously diagnosed with Type 2 diabetes by their own GP and patients were included in the study if they exhibited the following:

Ocular inclusion criteria

- Snellen visual acuity (VA) 6/9 or better
- Minimal or no lens opacities
- No history or evidence of intraocular surgery (with the exception of laser treatment for diabetic retinopathy)
- No history of amblyopia or squint
- No history of corneal abnormalities
- No history or evidence of retinal pathology other than diabetic retinopathy
- No history or evidence of glaucoma

Exclusion criteria

Due to the nature of the tests and their location in the Academy all patients were required to be mobile.

8.4.2 Subject sample

The subject sample consisted of one eye each of 41 diabetic patients. Group 1 comprised Type 1 diabetic patients (n=20) while Group 2 comprised Type 2 diabetics (n=21). Note that as patient groups act as their own controls over time, it was not necessary to recruit a normal sample.

Broad details of the subject sample are given in table 8.1. The mean age of the patients and the known duration of diabetes in group 1 was 37.90±15.39 years; duration 23.85±14.67 years and for group 2 was 56.33±11.09 years; duration 13.48±10.30 years.

	Gender		Test eye		Mean duration of diabetes ± SD (years)	Mean HbA1c ± SD (%)	Mean age± SD (years)
Subject Group	Male	Female	R	L			
1 Type 1 (n=20)	9	11	10	10	23.85± 14.67	8.42± 1.86	37.90 ± 15.39
2 Type 2 (n=21)	12	9	9	12	13.48± 10.30	7.62± 1.74	56.33 ±11.09

Table 8.1 Summary characteristics of Type 1 and Type 2 diabetics

In group 1, nine patients exhibited no diabetic retinopathy, eight subjects exhibited background retinopathic changes, and three patients had pre- proliferative changes.

In group 2, nine patients exhibited no diabetic retinopathy, ten patients exhibited background retinopathic changes, and two patients had pre- proliferative changes.

8.4.3 Ethical approval and informed consent

Ethical approval was obtained from the ethical committee board of Aston University. Approval conformed to the tenets of the Declaration of Helsinki. Written informed consent was obtained from all volunteers.

8.4.4 Methods

All patients arrived at 8am after fasting overnight. In the case of insulin dependent diabetics, instructions had been given to patients to refrain from taking their insulin the morning of their study day because breakfast would be provided shortly after arrival, having completed the first run of tests to be used as baseline measurements. During this period the patients were instructed to inform us if at any point they felt unwell.

At 2 hourly intervals over a 12 hour period several visual function tests and blood glucose monitoring were performed. Patients were required to complete a data sheet giving details of their medications, dosages and times taken and details of any drinks and food consumed over the course of the day. Patients were instructed wherever

possible to eat their normal diet and carry out their regular exercise routines in order that our results reflected their normal diabetic control. Fundus examination was performed on all volunteers and fundus photos taken using the Canon CR-DGi (non-mydriatic retinal camera) to assess the presence and grade of retinopathy and maculopathy. Patients were instructed to bring their most recent spectacle prescription and/or their distance spectacles on the day of the study from which a focimetry reading was taken. Refraction was performed at the beginning of the first test run only, to ensure that the best spectacle correction was worn. For the remainder of the day this correction was used by the patient when viewing the test charts.

8.4.5 Experimental investigations

A battery of tests was carried out in an identical order as detailed below at 2 hourly intervals in order that the time between blood glucose testing and each test parameter remained the same for comparison and analysis purposes. At visit 1 only, a blood sample was taken by a qualified phlebotomist.

8.4.5.1 Test run sequence

1. Visual acuity (VA) testing using LogMAR VA 100% and 10% contrast (Test Chart 2000 ^{PRO})
2. Contrast sensitivity (CS) testing using Pelli-Robson (Test Chart 2000 ^{PRO})
3. Visual field test 10-2 white-on-white static automated perimetry and 10-2 blue-on-yellow Short Wavelength Automated Perimetry (Humphrey Field Analyser)
4. Retinal thickness and retinal nerve fibre layer thickness (Optical coherence tomographer Stratus OCT)
5. Non-contact tonometry (Pulsair 3000)
6. Blood pressure (Dinamap ProCare Monitor 300: GE Medical Systems)
7. Blood glucose levels (Hemocue 201+)

8.4.5.2 Visual acuity testing

Visual acuity and contrast sensitivity testing was performed using the Test Chart 2000 ^{PRO} - (Thomson Software Solutions version 2.3.04), a Windows based program designed

to display a wide range of optometric test stimuli on a standard PC monitor. Prior to testing, screen and letter size was calibrated for use in the test room. Throughout the day of testing the position of the screen was not altered. LogMAR 100% and 10% were conducted with direct viewing at 6 metres. Letters on the logMAR chart increase in steps of 0.1 logMAR from the bottom to the top of the chart with each letter being assigned a value of 0.02. Limits of vision were recorded for each patient. Contrast sensitivity was performed at a 1 metre viewing distance. Subjects were asked to read letters (displayed in triplets of decreasing contrast) until they were unable to read two out of the three letters displayed. The contrast of the last row read was recorded.

8.4.5.3 Visual field testing

White-on-white perimetry was measured using program 10-2 with a stimulus size III and SITA standard program (Humphrey Visual Field Analyser). Mean Deviation (MD) and Pattern Standard Deviation (PSD) were entered into the study database for all visits.

SWAP (blue-on-yellow) was measured using program 10-2 Fastpac, Goldmann stimulus size V (Humprey Visual Field Analyser). MD and PSD were entered into the study database for all visits using values derived from a normal empirical database for the 10-2 SWAP program using 65 clinically normal subjects (Conway, 2003) due to the Humphrey Field Analyser (HFA) lacking a normative database for the SWAP 10-2 program.

8.4.5.4 Optical coherence tomography

Macular thickness

The fast macular thickness protocol was carried out to obtain macular thickness measurements for all subjects. The macular scans consist of six radial line scans (6mm in length) arranged in a spoke-like pattern centred on the fovea with each radial scan spaced 30 degrees from each other. The patient was instructed to fixate the central green light throughout each set of scans. 5 macular scans were taken for each subject and the best 3 averaged and used for analysis.

Retinal nerve fibre layer thickness

The fast retinal nerve fibre layer thickness protocol was carried out to obtain RNFL measurements around the optic nerve head. The patient was instructed to fixate the green light placed at the periphery of the camera view (right or left depending on which eye was being scanned). The scan position was altered manually using the cursor to best fit around the optic disc. This position was recreated for each subsequent scan set using the repeat mode from the scan selection menu. The fast RNFL scan protocol consists of 3 consecutive 360-degreee circular scans with a diameter of 3.4mm each containing 256 A-scans taken automatically in a single session of 1.92 seconds. A mean image was automatically created by the OCT software. Seven fast thickness scans were taken in total and the results of the five best scans were averaged.

a) b)

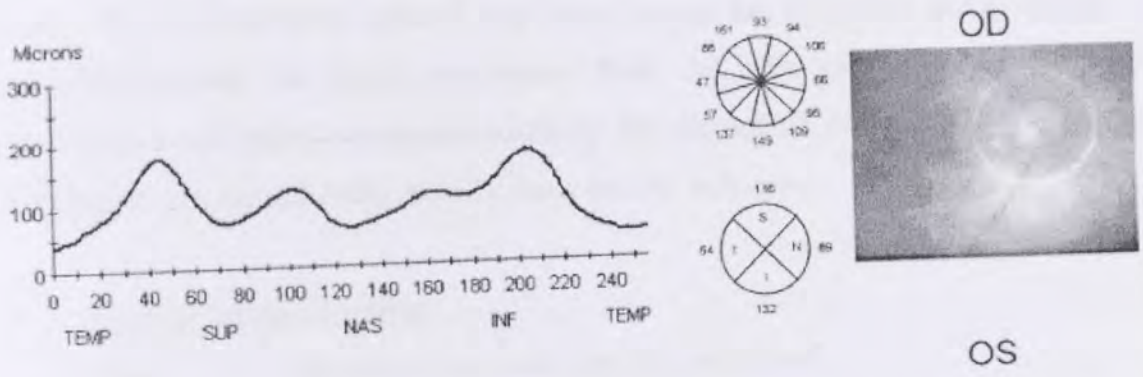

Figure 8.1 Example of a) OCT generated RNFL thickness output b) fundus image during fast RNFL scan acquistion

Non contact tonometry

Measurements of IOP were acquired using the Keeler Pulsair 3000. Four readings for each eye were taken and automatically averaged by the device (McCaghrey and Matthews, 2001).

Blood pressure

Systolic and diastolic blood pressure measurements were acquired using the Dinamap ProCare Monitor 300 (GE Medical Systems). These measurements were used as the basis for the calculation of mean arterial pressure and mean ocular perfusion pressure as detailed below:

Equation 8.1

$$MAP = \text{Diastolic BP} + \frac{1}{3}(\text{Systolic BP} - \text{Diastolic BP})$$

Equation 8.2

$$MOPP = \frac{2}{3}[\text{Diastolic BP} + \frac{1}{3}(\text{Systolic BP} - \text{Diastolic BP})] - IOP$$

Blood glucose

A baseline blood sample was taken at the start of the study day by a qualified phlebotomist and analysed by the laboratory for fasting blood glucose and HbA1c levels. At all visits blood glucose was tested using the HemoCue 201+ system. A controlled amount of blood was drawn from the side of the finger using the microcuvette and analysed automatically by the HemoCue system. The system was calibrated at the start of every test day using control solution.

Typical Study Timetable

8am	Px arrival and initial test run performed
9am	Blood sample taken by nurse/phlebotomist for haemoglobin testing and delivered to Aston Medical Centre for analysis
9.20 am	**Breakfast**
10am	2nd test run
12pm	3rd test run
1pm	**Lunch**
2pm	4th test run
4pm	5th test run
5pm	**Evening meal**
6pm	6th test run
7.15 pm	Px discharged

Patients were advised to maintain their normal diet and drinks throughout the course of the study, exercise according to their normal routine and take their regular medication in keeping with their normal frequency and dosage. Breakfast comprised choice of cereals, fruit, toast, tea and coffee. Patients had a choice of hot or cold buffet lunch and evening meal. Every effort was made to provide snacks if necessary and hot and cold drinks were made available for the patients throughout the study period.

Due to the length of test-runs and to give adequate time for the patient to rest between each test-run, only a single patient was seen on each test day.

8.5 Statistical analysis

All statistical analysis was performed using SPSS version 12.0.1 for Windows. Kolmogorov-Smirnov tests revealed no significant deviation from a normal distribution pattern for any of the test parameters ($p>0.05$). Parametric tests were subsequently used for analysis. Firstly, a mixed between–within subject ANOVA was conducted to assess variation in each test parameter over the course of the day (i.e. across test-runs) for all diabetic subjects using two independent variables – a between-subjects variable and a within-subjects variable. The between-subjects variable was diabetes type while the within-subjects variable was the test parameter. If between-subject effects reached statistical significance ($p=0.05$) during ANOVA, a separate ANOVA for group 1 and group 2 (i.e diabetes type) was performed where necessary. Results are summarised in Appendix 4. Post-hoc analysis identified the visits between which differences in parameters reached significant levels, where p values of 0.0033 (i.e. 0.05 divided by 15 comparsions) were regarded as significant. Results are summarised in Appendix 5. Secondly, a simultaneous regression model was used to explore the relationship between each of the test parameters: retinal thickness, retinal nerve fibre layer thickness, IOP, blood pressure and visual field parameters and a number of potential predictor variables: type of diabetes, haemoglobin levels, duration of diabetes and glucose level for each visit. Following study completion, a bivariate correlation analysis between the fasting blood glucose results obtained from the lab and by the Hemocue 201+ system (at visit 1) was conducted to ensure the reliability of the Hemocue system. The two measurements were highly correlated for diabetic subjects ($r=0.903$, $p=0.000$) and

normal subjects (r=0.980, p=0.000 Data courtesy of B. Huntjens, C. O'Donnell, with permission). Finally, Pearson product-moment correlation was conducted to investigate the relationships between visual function and retinal anatomy.

8.6 Results

8.6.1 Blood glucose variations

Blood glucose variations for group 1 and group 2 over the 12 hour period are shown in figure 8.2. A normal sample examined using the same model is shown for reference (data courtesy of B.Huntjens, C. O'Donnell, with permission). A one way repeated measures analysis of variance (ANOVA) was conducted to compare blood glucose variations for normal subjects, type 1 diabetic patients and type 2 diabetic patients where group type was identified as the independent variable and the blood glucose levels were the dependent variable. ANOVA revealed a significant difference between groups in terms of their blood glucose variations. Post-hoc analysis using Tukey's Honestly Significant Different (HSD) test revealed a significant difference between normal subjects and type 1 diabetic patients (p=0.001) and between normal subjects and type 2 diabetic patients (p=0.000). However, there were no statistically significant differences between type 1 and type 2 diabetics (p=0.947). It was not the purpose of this study to compare the outcomes between groups for the other test parameters.

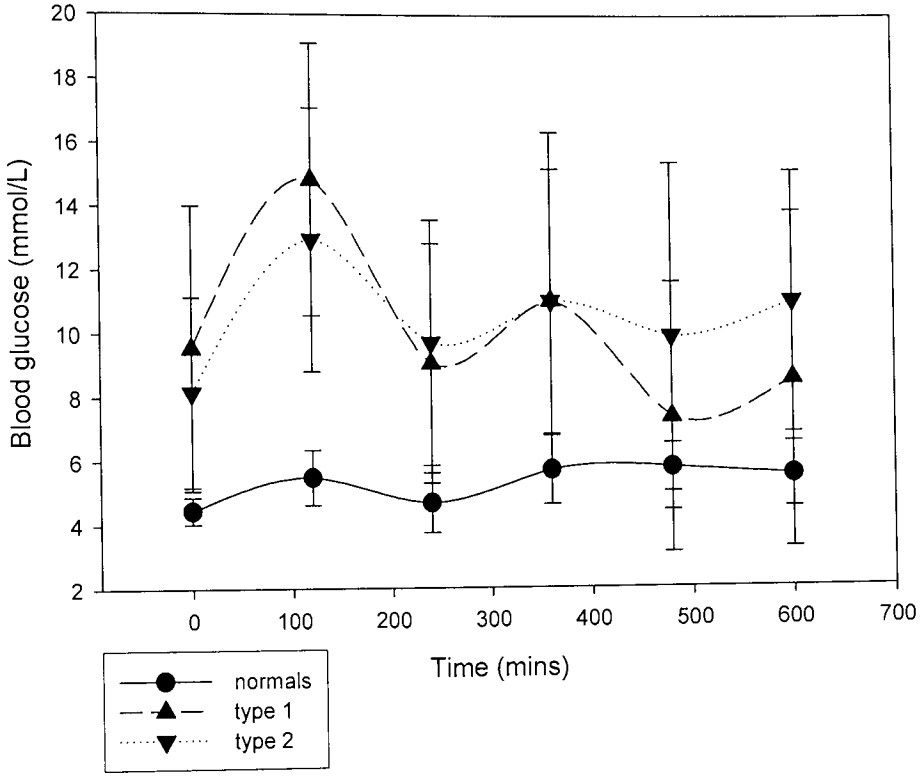

Figure 8.2 Graph to show blood glucose variation over a 12 hour time period in groups 1 and 2 and normal subjects.

A mixed between-within subject ANOVA revealed statistical differences in blood glucose levels occurred between visits for all diabetic subjects. Post-hoc analysis showed that statistical differences occurred only between visits 1 and 2 ($p=0.000$), visits 2 and 3 ($p=0.000$), visits 2 and 5 ($p=0.000$), visits 2 and 6 ($p=0.000$) and visits 4 and 5 ($p=0.001$).

8.6.2 Test parameter variations over time

The change of blood glucose and each test parameter over time are shown in the following figures (8.3-8.29). Data for type 1 and type 2 diabetics are presented separately in a graphical format for purposes of comparison and clarity.

Visual acuity (100% contrast)

ANOVA showed no statistical differences between visits for all patients.

(a)

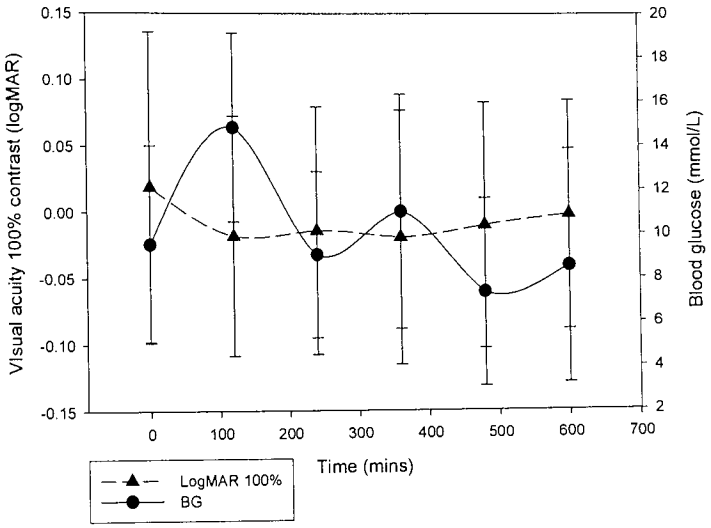

(b)

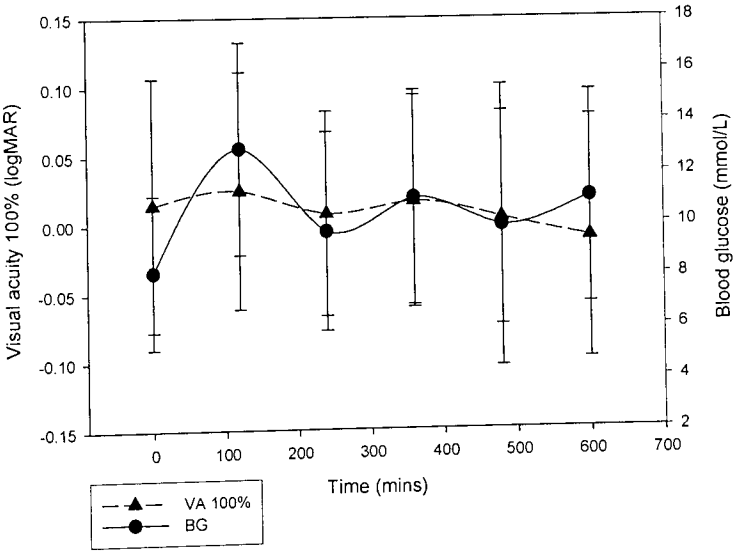

Figure 8.3 Graphs to show the change in blood glucose and visual acuity 100% over time in (a) type 1 diabetics and (b) type 2 diabetics

Visual acuity (10% contrast)

Visual acuity (10% contrast) varied over the course of the day as shown in figure 8.4. By observation, all diabetic patients exhibit highest VA at visit 1, followed by a VA reduction at visits 2 and 3, a small increase in VA at visit 4 before before reaching a plateau. ANOVA showed that statistical differences occurred between visits (p=0.030). However, during post-hoc analysis, differences between visits failed to reach significance after applying Bonferroni correction.

(a)

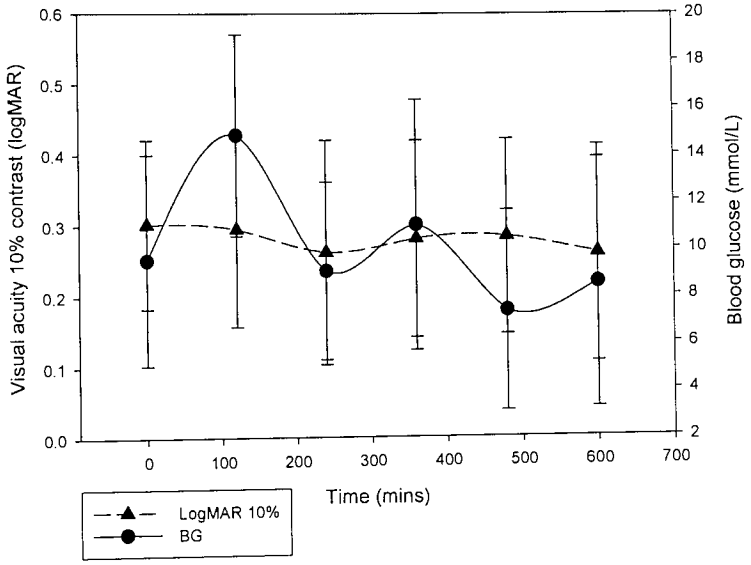

(b)

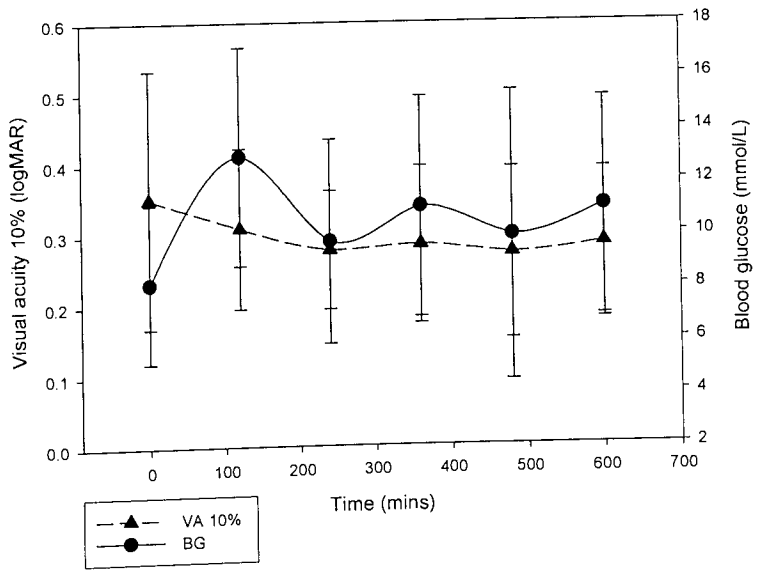

Figure 8.4 Graphs to show the change in blood glucose and visual acuity 10% over time in (a) type 1 diabetics and (b) type 2 diabetics

Contrast sensitivity

By observation, contrast sensitivity scores in diabetic subjects appear to rise steadily at each visit 1-5 before reaching a plateau or slight decline after visit 5 (figure 8.5). ANOVA for all patients revealed the presence of statistically significant differences between visits (p=0.000). Post-hoc analysis identified significantly different measures of CS occurring between visits 1 and 3 (p=0.002), 1and 4 (p=0.000), 1 and 5 (p=0.000), 1 and 6 (p=0.000) and 2 and 5 (p=0.003).

(a)

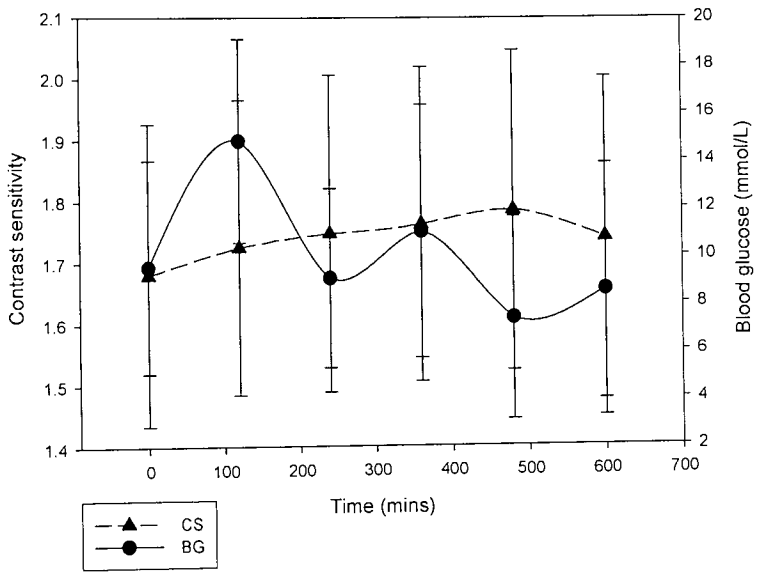

(b)

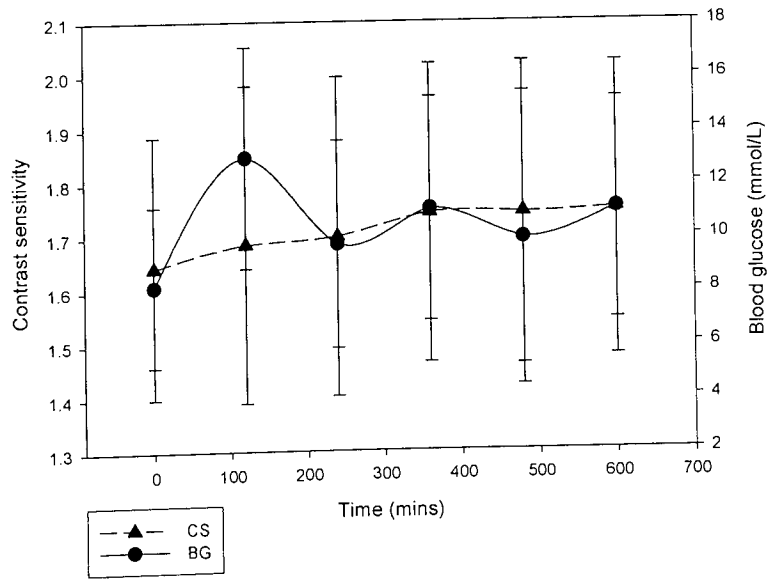

Figure 8.5 Graphs to show the change in blood glucose and contrast sensitivity over time in (a) type 1 diabetics and (b) type 2 diabetics

White-on-white visual fields

Mean deviation and pattern standard deviation for white-on-white fields for both type 1 and type 2 diabetics appeared to vary little over time despite the large variation in blood glucose levels as seen in figure 8.6 and 8.7. ANOVA for all patients revealed no statistical differences occurred between visits.

(a)

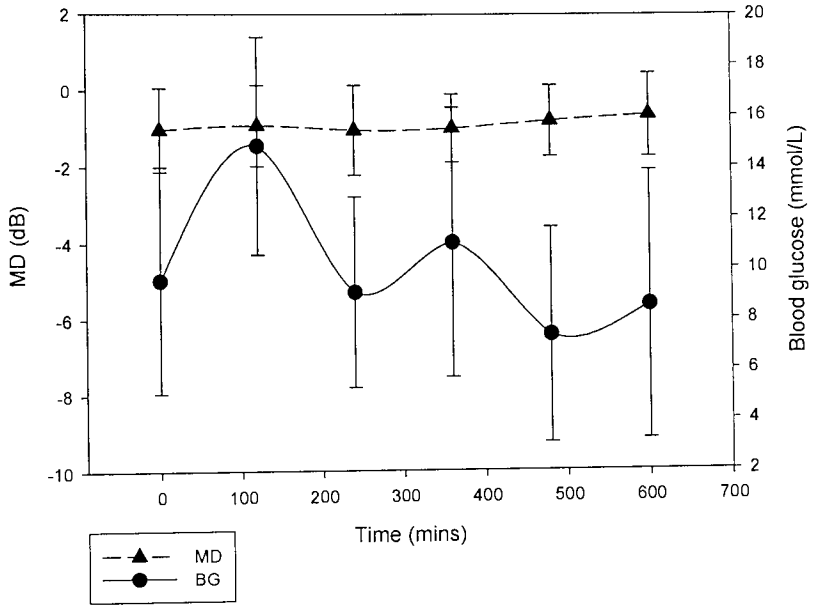

(b)

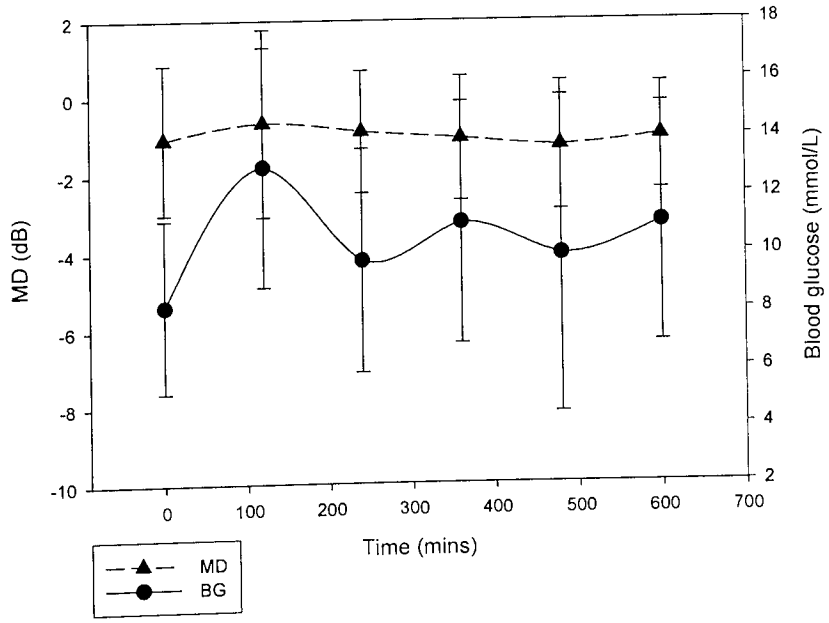

Figure 8.6 Graphs to show the change in blood glucose and MD (white-on white) over time in (a) type 1 diabetics and (b) type 2 diabetics

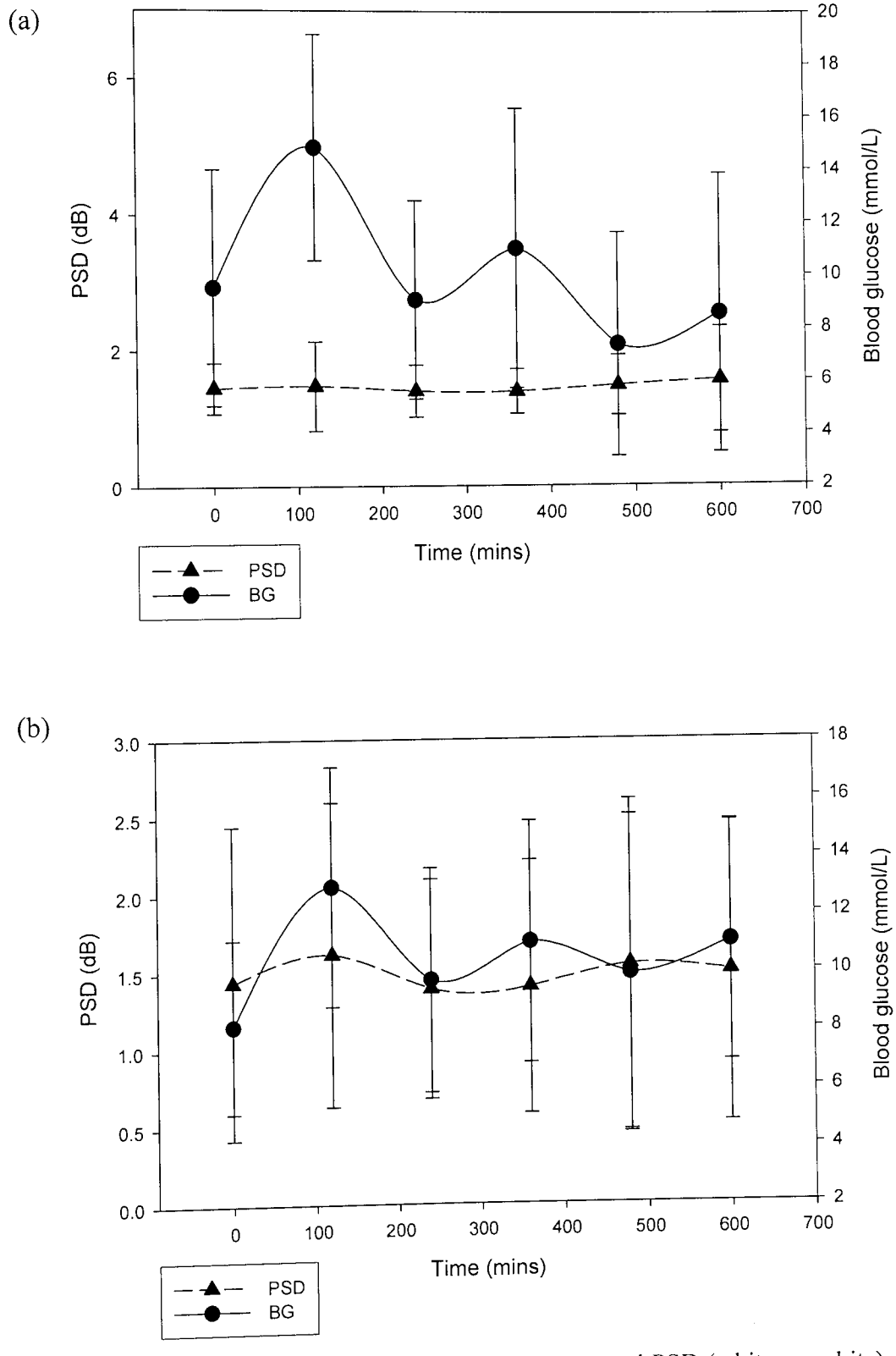

Figure 8.7 Graphs to show the change in blood glucose and PSD (white-on-white) over time in (a) type 1 diabetics and (b) type 2 diabetics

SWAP visual fields

Mean deviation and pattern standard deviation for SWAP fields for both type 1 and type 2 diabetics appeared to vary little over time despite the large variation in blood glucose levels as seen in figures 8.8 and 8.9. ANOVA revealed statistically significant differences occurred for SWAP MD only over the course of the day (p=0.023). Post-hoc analysis revelaed statistical differences occurred between visit 4 and 6 (0.001).

(a)

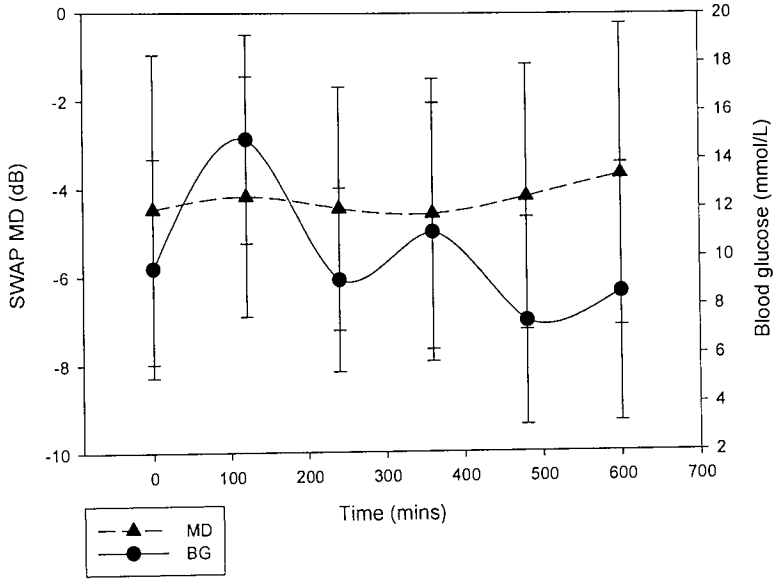

(b)

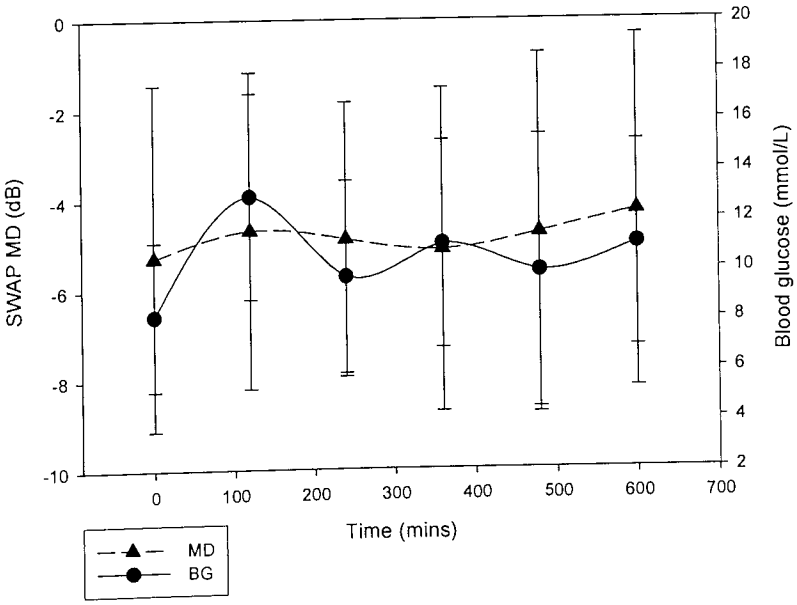

Figure 8.8 Graphs to show the change in blood glucose and SWAP MD over time in (a) type 1 diabetics and (b) type 2 diabetics

(a)

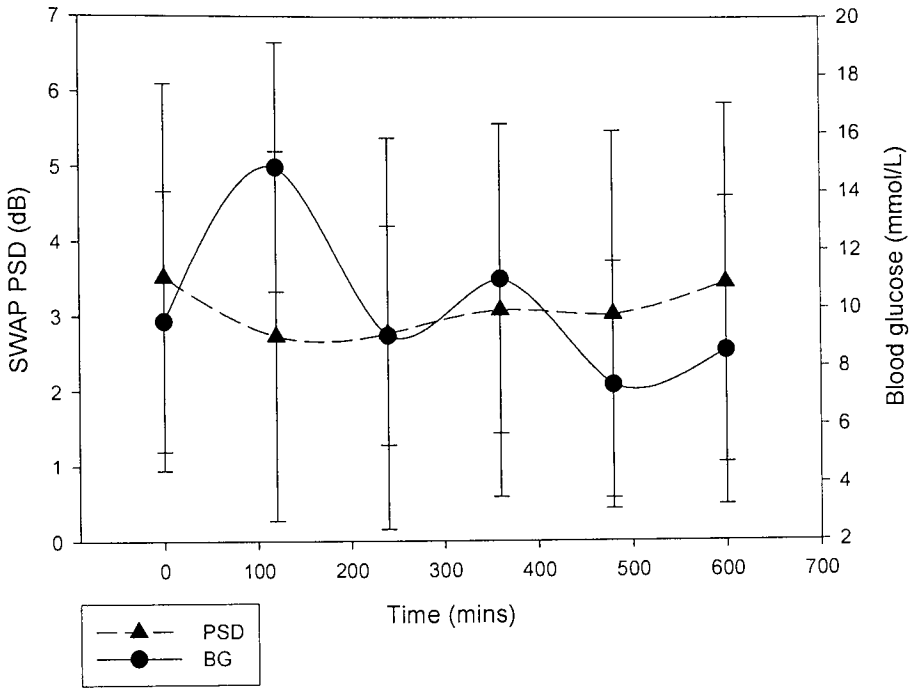

(b)

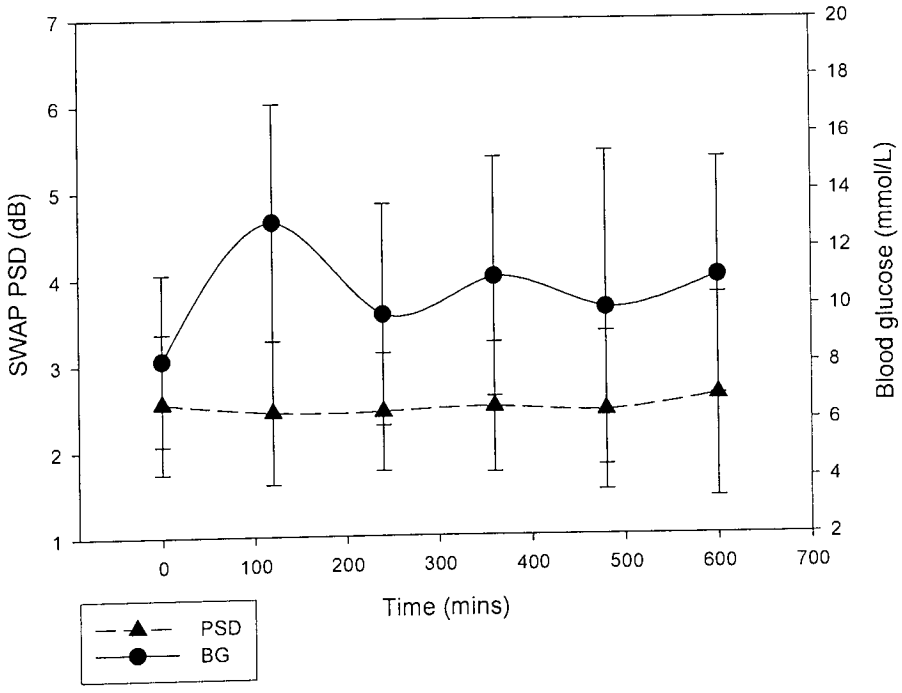

Figure 8.9 Graphs to show the change in blood glucose and SWAP PSD over time in (a) type 1 diabetics and (b) type 2 diabetics

Intraocular pressure (IOP)

By observation, IOP varies over the course of the day for both type 1 and type 2 diabetic subjects as shown in figure 8.10. IOP variation is more marked in type 2 subjects as shown graphically (Fig 8.10b) and there appears to be an inverse relationship between blood glucose and IOP. As blood glucose reached a peak the IOP was at its lowest and vice versa. ANOVA reveals statistically significant differences between visits (p=0.008) for all subjects. Post-hoc analysis identified differences between 2 and 3 only as reaching statistical significance (p=0.003).

(a)

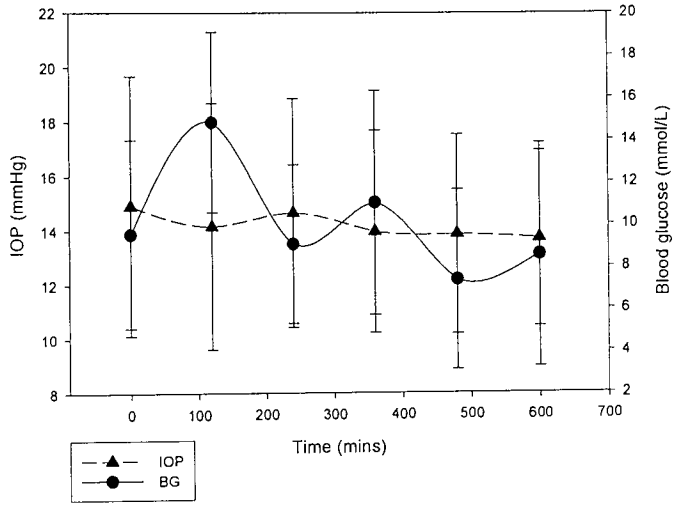

(b)

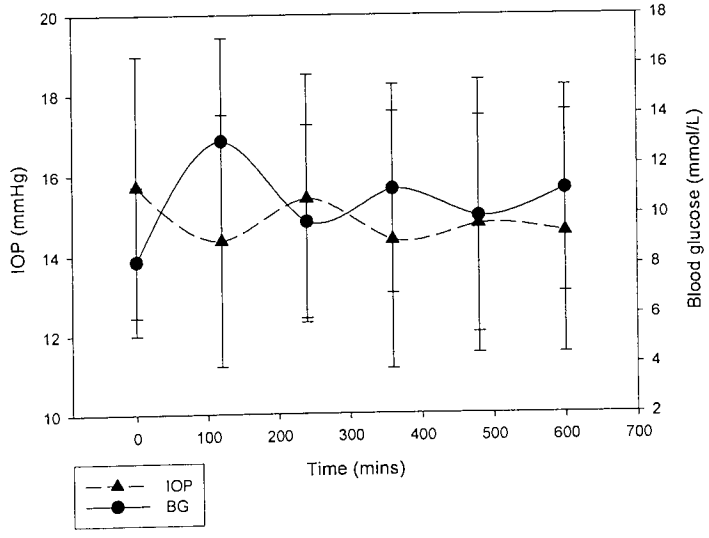

Figure 8.10 Graphs to show the change in blood glucose and IOP over time in (a) type 1 diabetics and (b) type 2 diabetics

Retinal nerve fibre layer thickness

Despite a large variation in blood glucose levels for all diabetic subjects, RNFL thickness in each quadrant and mean RNFL varies little over the course of the day as shown in figures 8.11-8.15. No statistically significant differences between-visits were observed.

Significant between-subject effects for mean RNFLt and RNFLt in the inferior quadrant were observed ($p=0.025$, $p=0.011$ respectively). Therefore a second ANOVA was conducted for each group separately. ANOVA showed no statistically siginificant differences between visits for group 1 or group 2.

Statistically significant interaction of type and visit was evident for the superior retinal nerve fibre layer ($p=0.005$). Separate analysis of variance revealed a statistically significant difference between visits for type 1 only with post-hoc analysis identifying the significant difference between visits 1 and 6 ($p=0.003$).

(a)

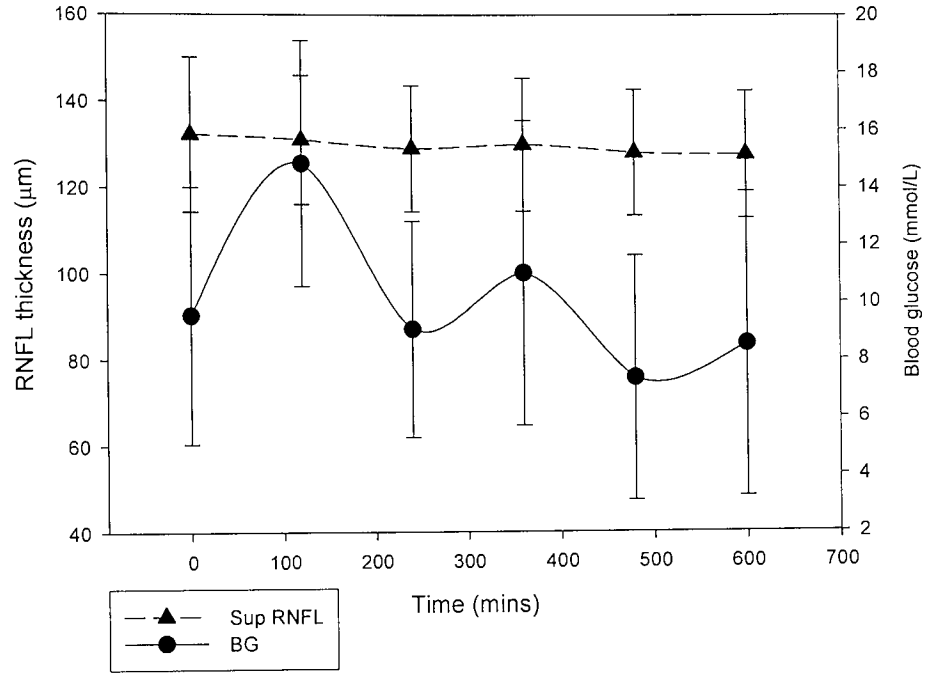

(b)

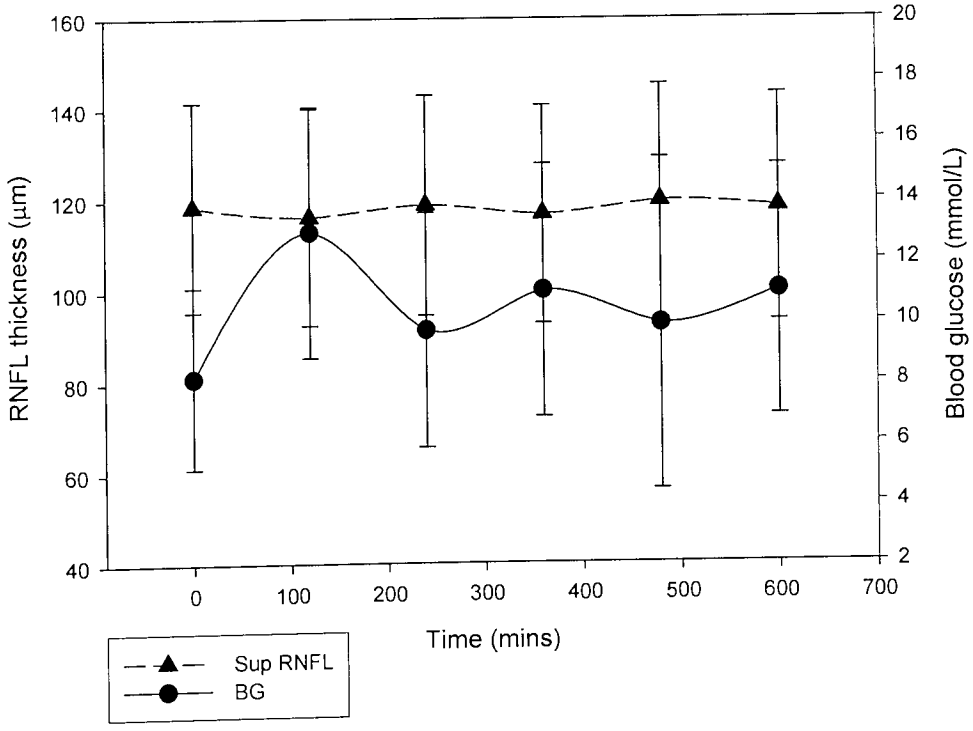

Figure 8.11 Graphs to show the change in blood glucose and superior RNFL over time in (a) type 1 diabetics and (b) type 2 diabetics

(a)

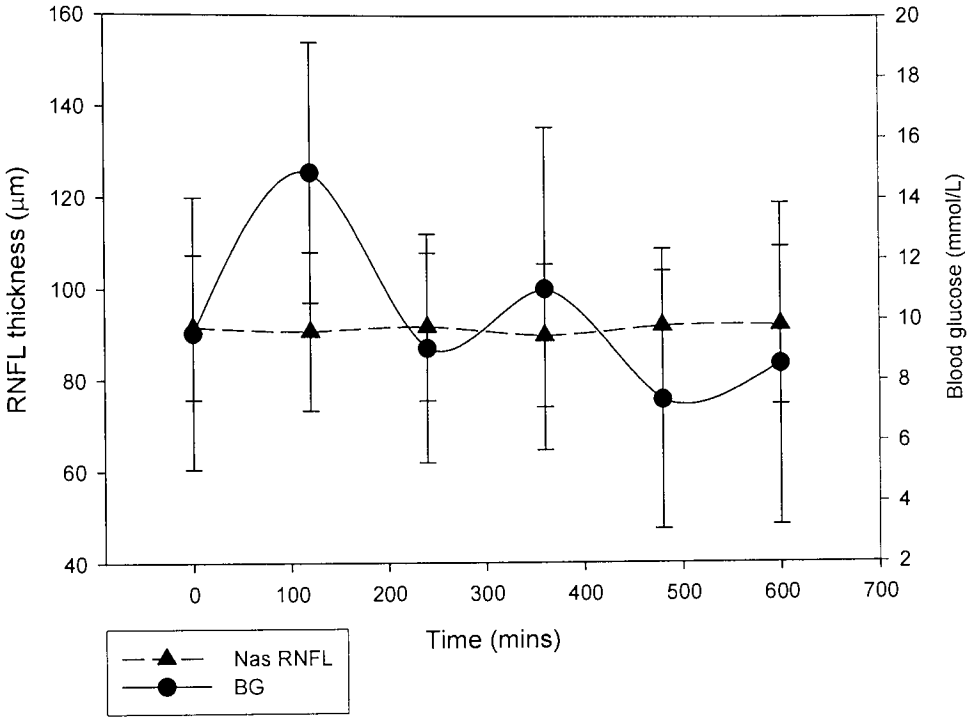

(b)

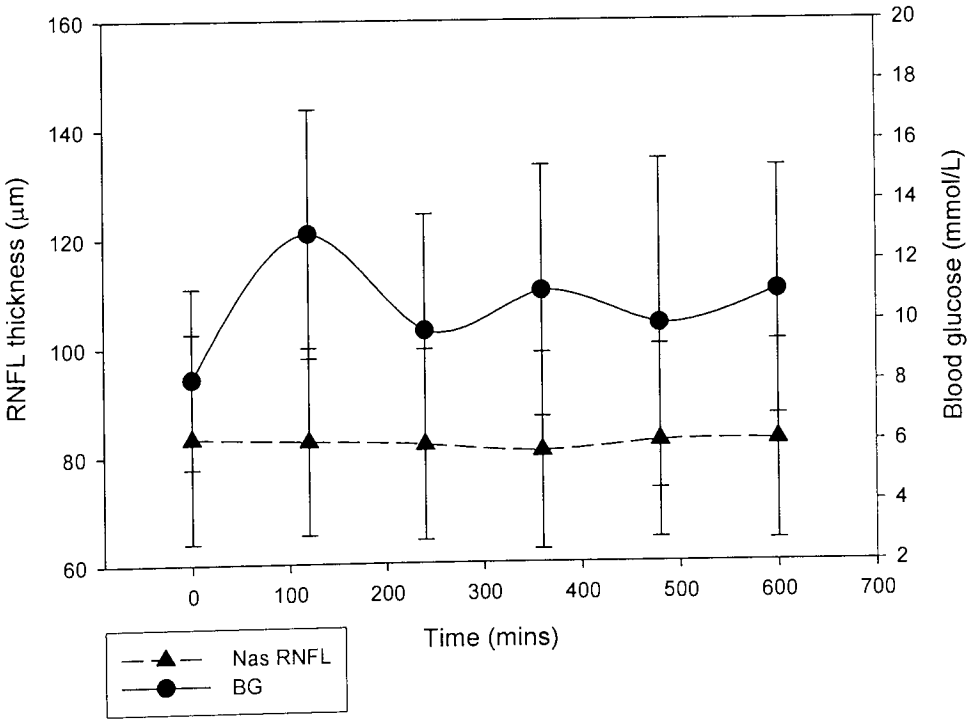

Figure 8.12 Graphs to show the change in blood glucose and nasal RNFL over time in (a) type 1 diabetics and (b) type 2 diabetics

(a)

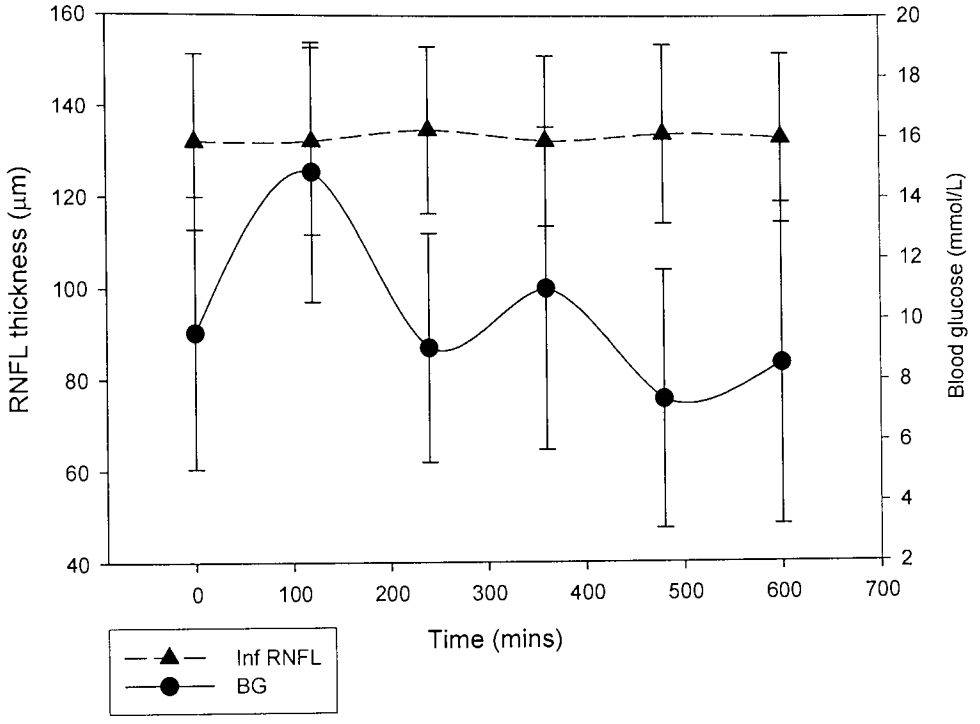

(b)

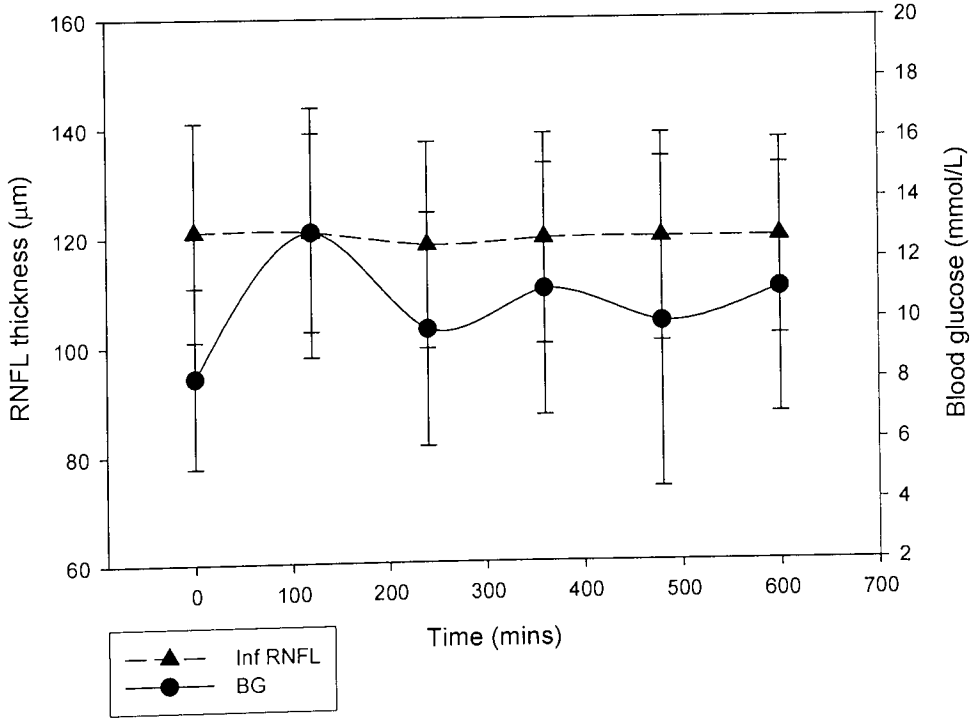

Figure 8.13 Graphs to show the change in blood glucose and inferior RNFL over time in (a) type 1 diabetics and (b) type 2 diabetics

(a)

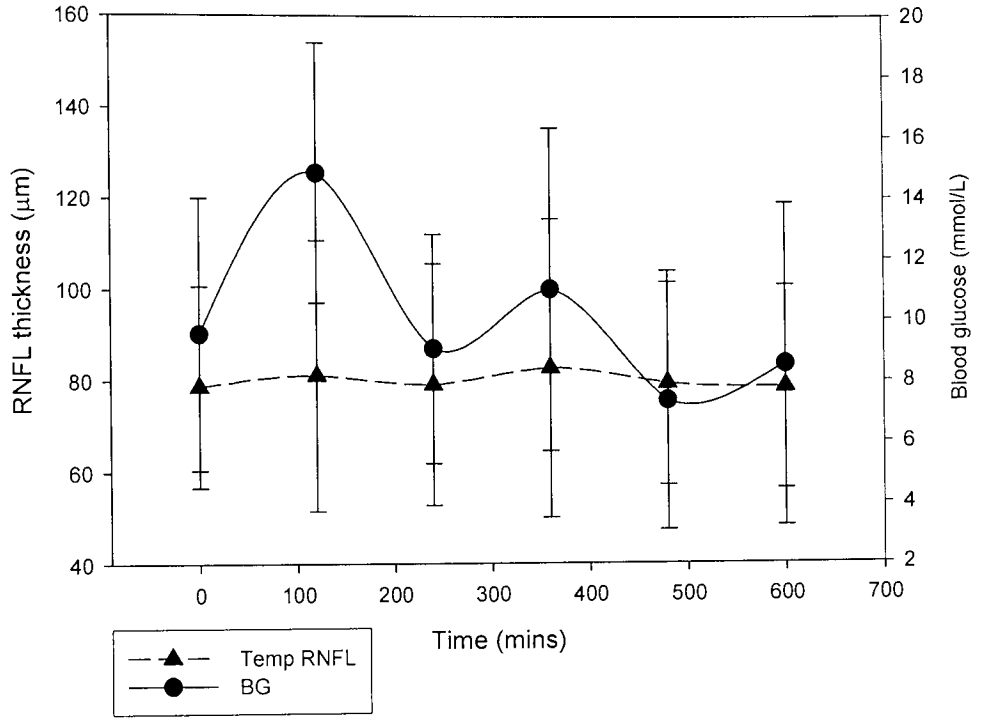

(b)

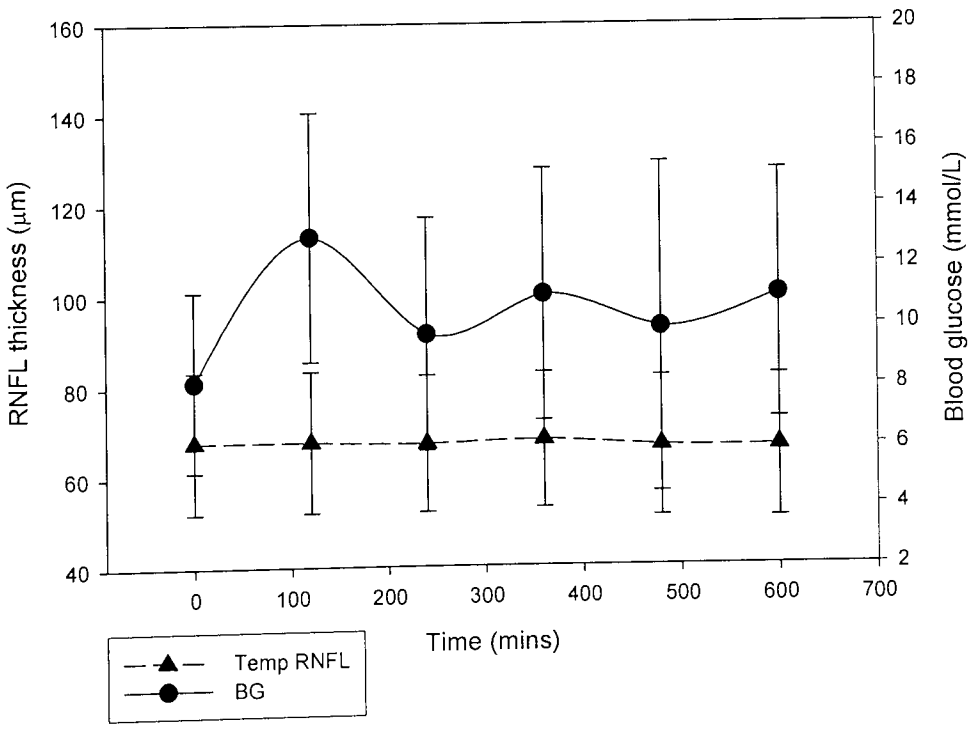

Figure 8.14 Graphs to show the change in blood glucose and temporal RNFL over time in (a) type 1 diabetics and (b) type 2 diabetics

(a)

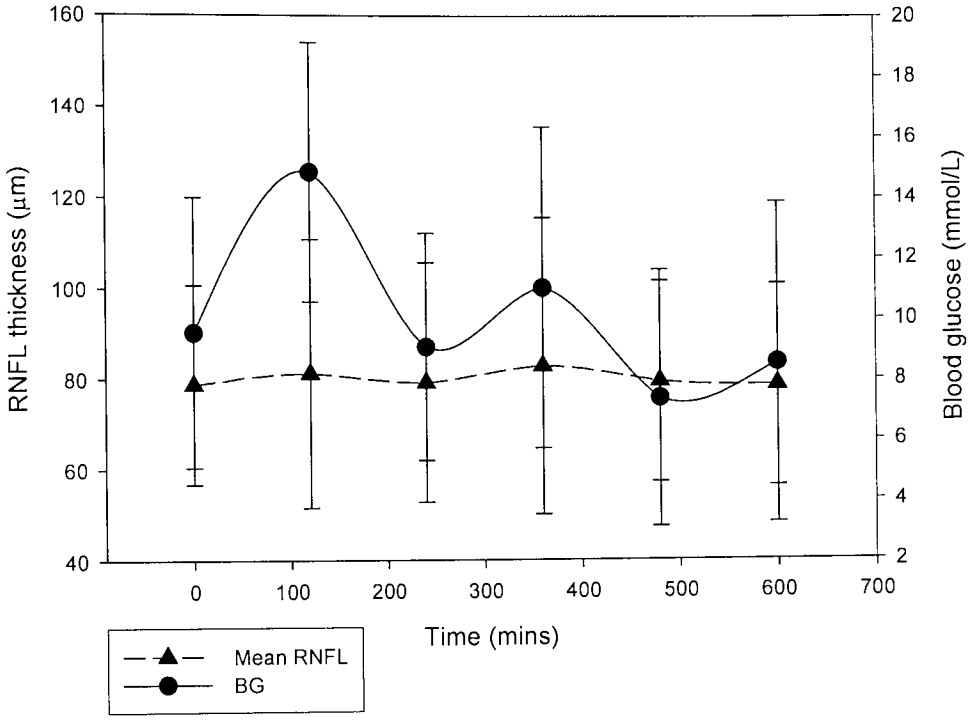

(b)

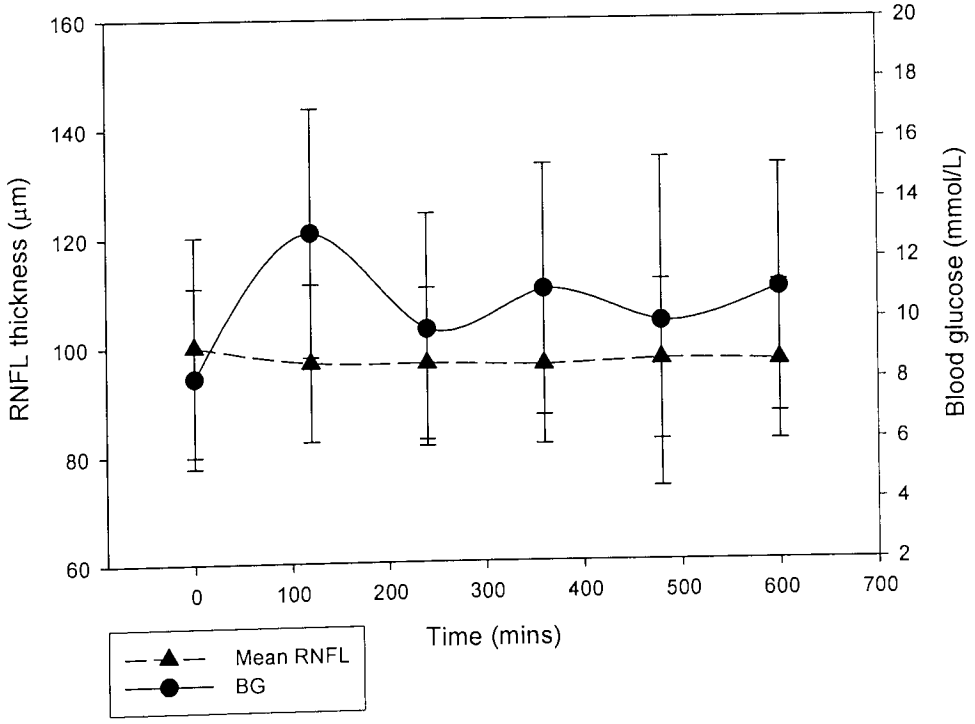

Figure 8.15 Graphs to show the change in blood glucose and mean RNFL over time in (a) type 1 diabetics and (b) type 2 diabetics

Macular retinal thickness (MRt)

Figures 8.16 to 8.25 illustrate how retinal thickness in each position 1-9 and mean retinal thickness varies little during the course of the day for groups 1 and 2 despite the variation in blood glucose levels. ANOVA revealed that for position 1 only (foveola) statistically significant differences occurred between visits ($p=0.004$). Post-hoc analysis identified significant differences occurring between visit 1 and 2 ($p=0.000$), 1 and 4 ($p=0.003$) and between visit 1 and 5 ($p=0.002$).

Significant between-subject effects for retinal thickness position 9 ($p=0.016$) were observed. Therefore a second ANOVA was conducted for each group separately. ANOVA showed no statistically siginificant differences between visits for group 1 or group 2.

(a)

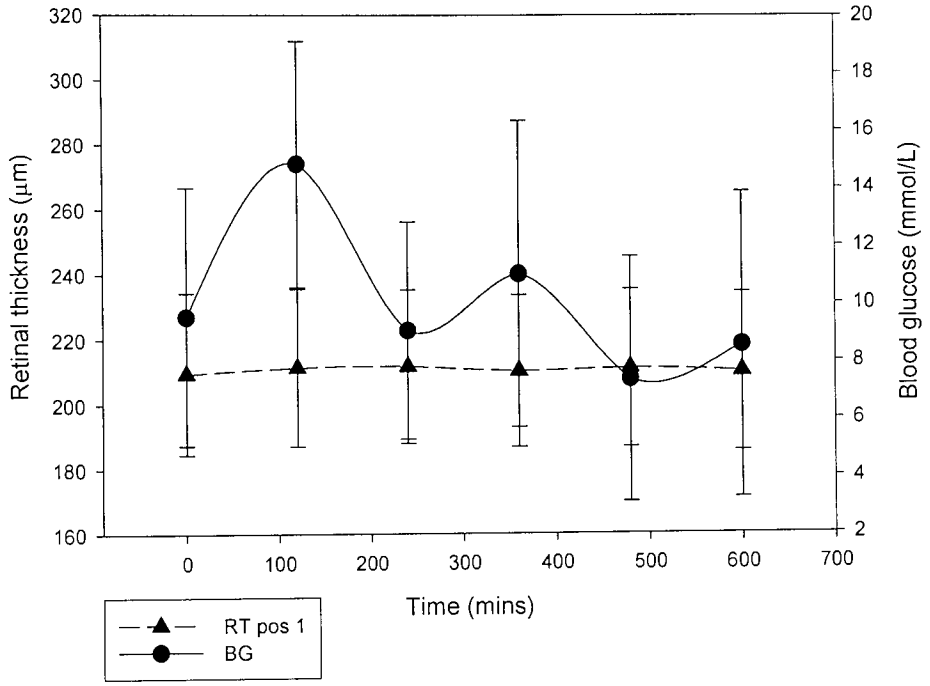

(b)

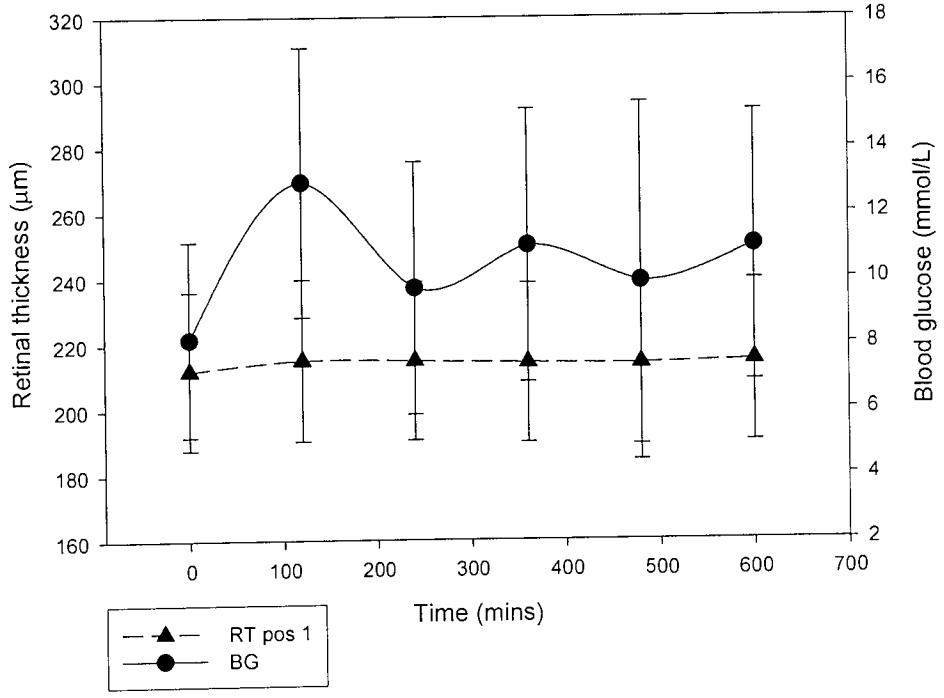

Figure 8.16 Graphs to show the change in blood glucose and macular retinal thickness in position 1 (fovea) over time in (a) type 1 diabetics and (b) type 2 diabetics

(a)

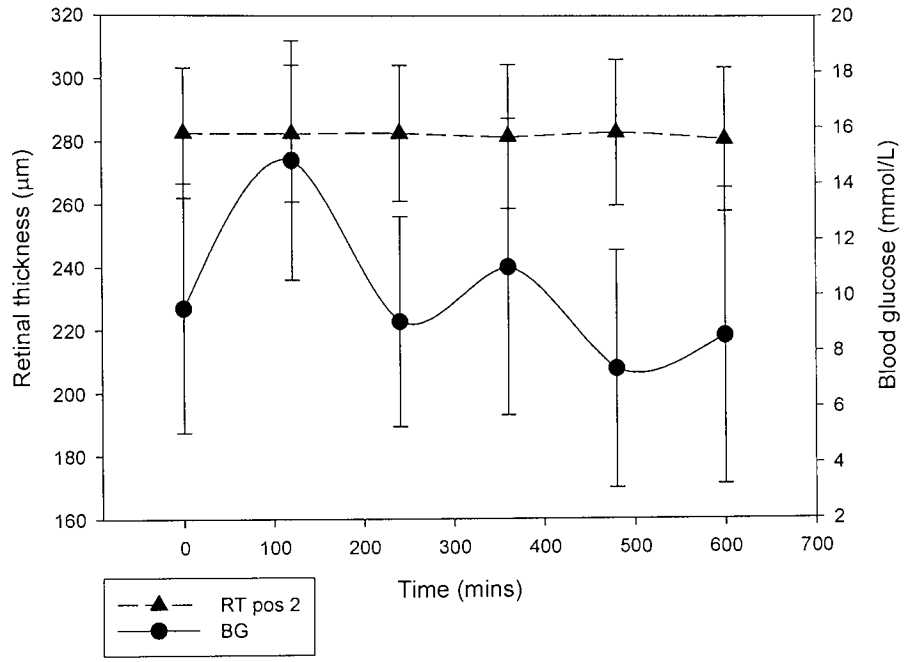

(b)

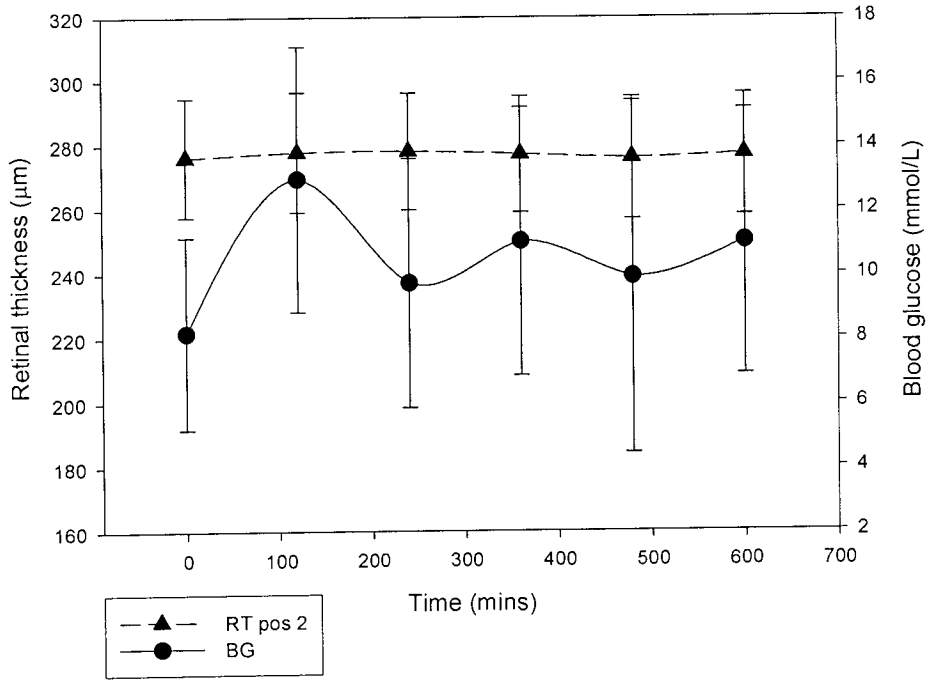

Figure 8.17 Graphs to show the change in blood glucose and macular retinal thickness in position 2 over time in (a) type 1 diabetics and (b) type 2 diabetics

(a)

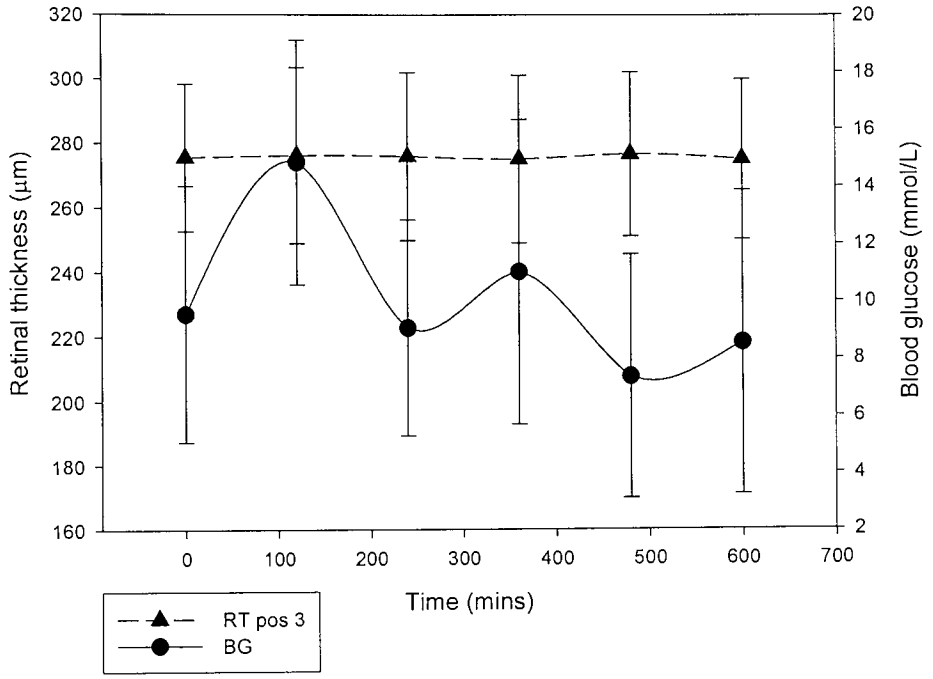

(b)

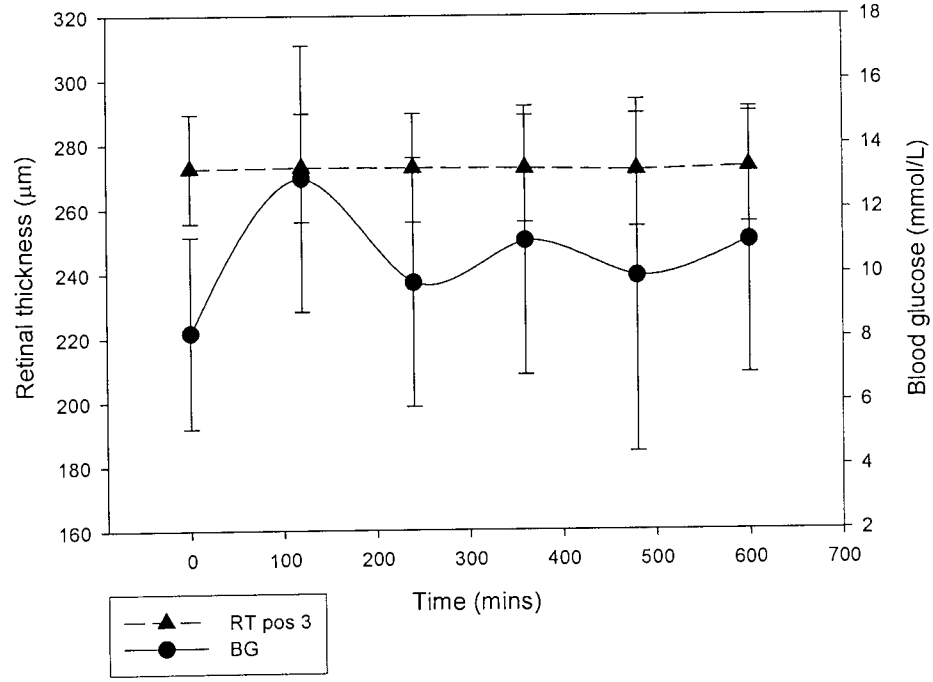

Figure 8.18 Graphs to show the change in blood glucose and macular retinal thickness in position 3 over time in (a) type 1 diabetics and (b) type 2 diabetics

(a)

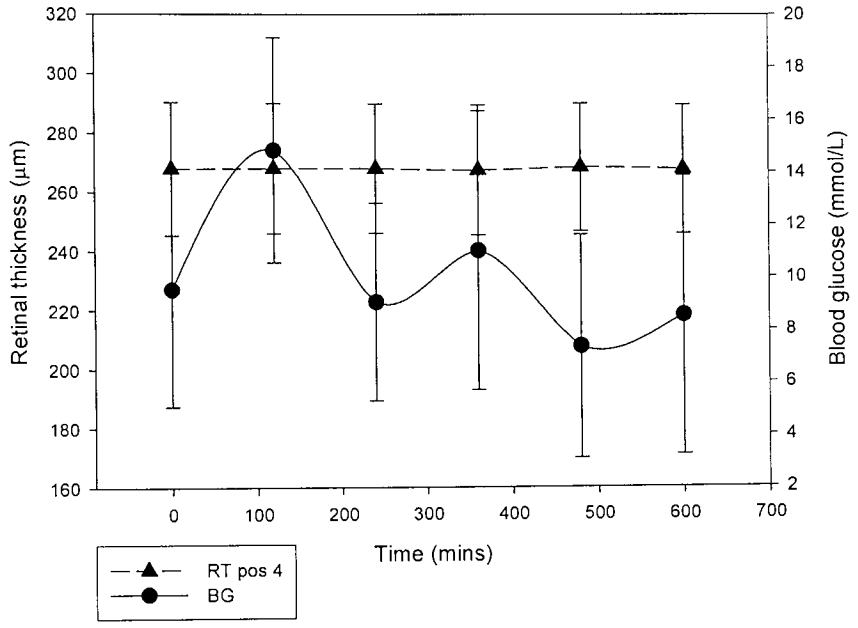

(b)

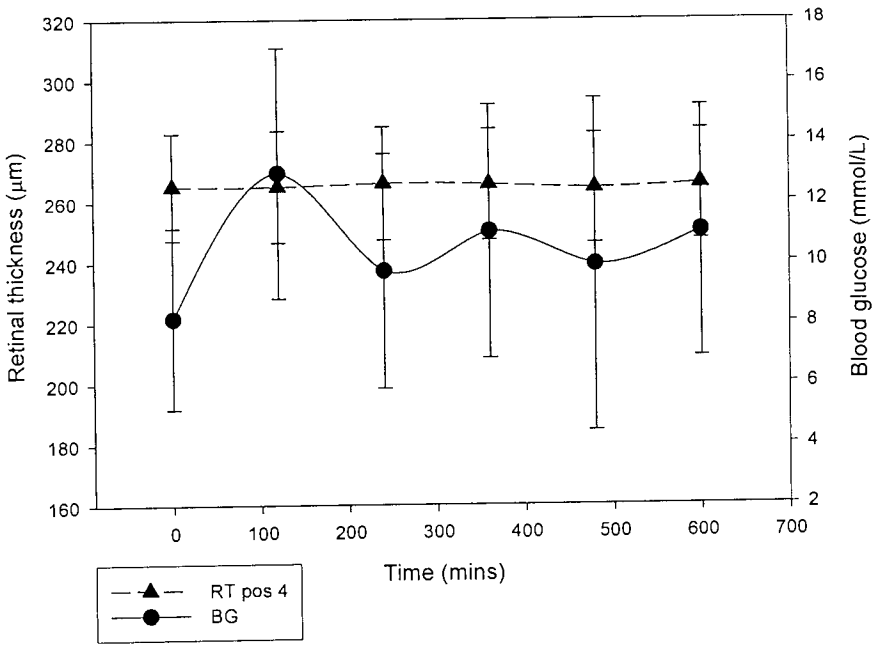

Figure 8.19 Graphs to show the change in blood glucose and macular retinal thickness in position 4 over time in (a) type 1 diabetics and (b) type 2 diabetics

(a)

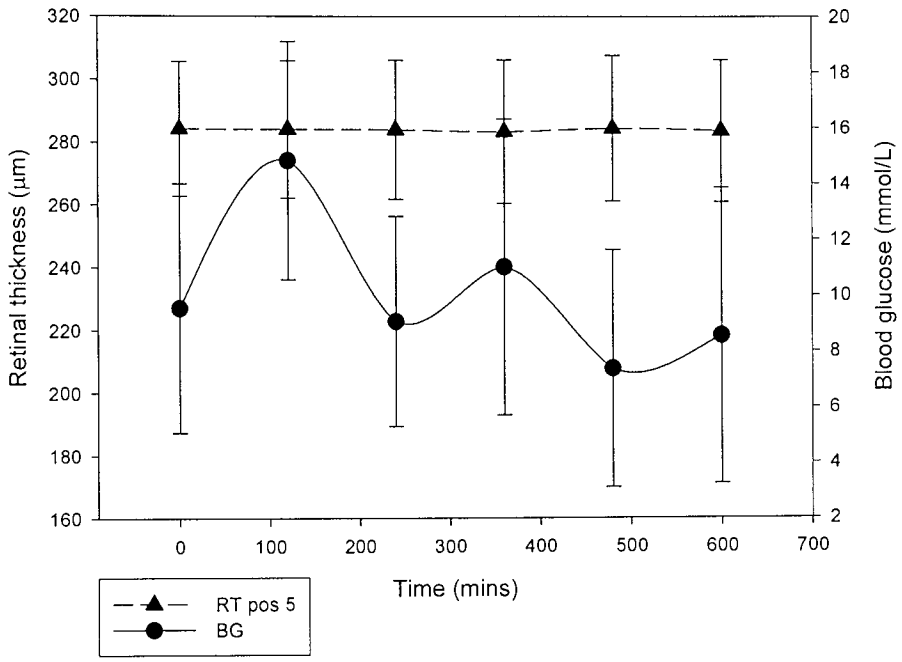

(b)

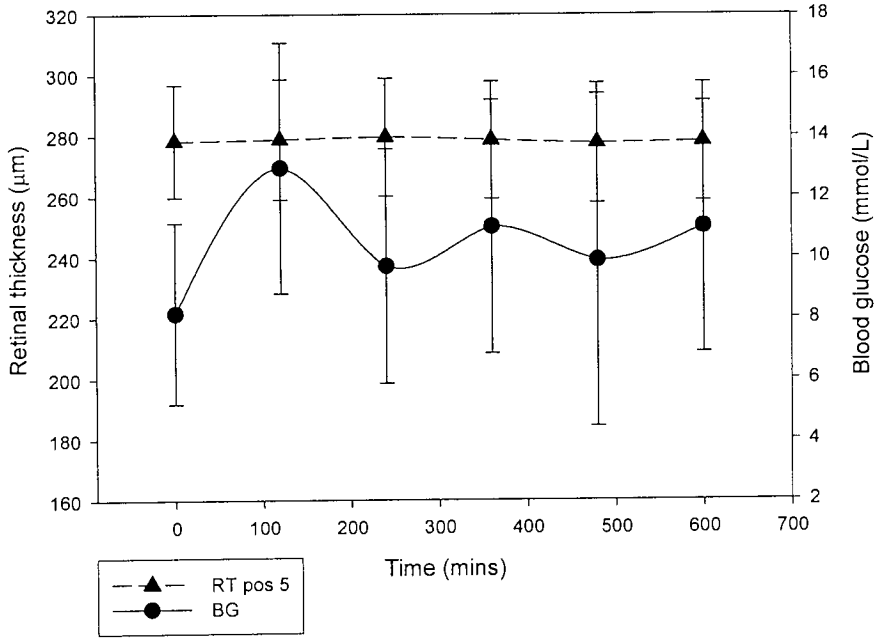

Figure 8.20 Graphs to show the change in blood glucose and macular retinal thickness in position 5 over time in (a) type 1 diabetics and (b) type 2 diabetics

(a)

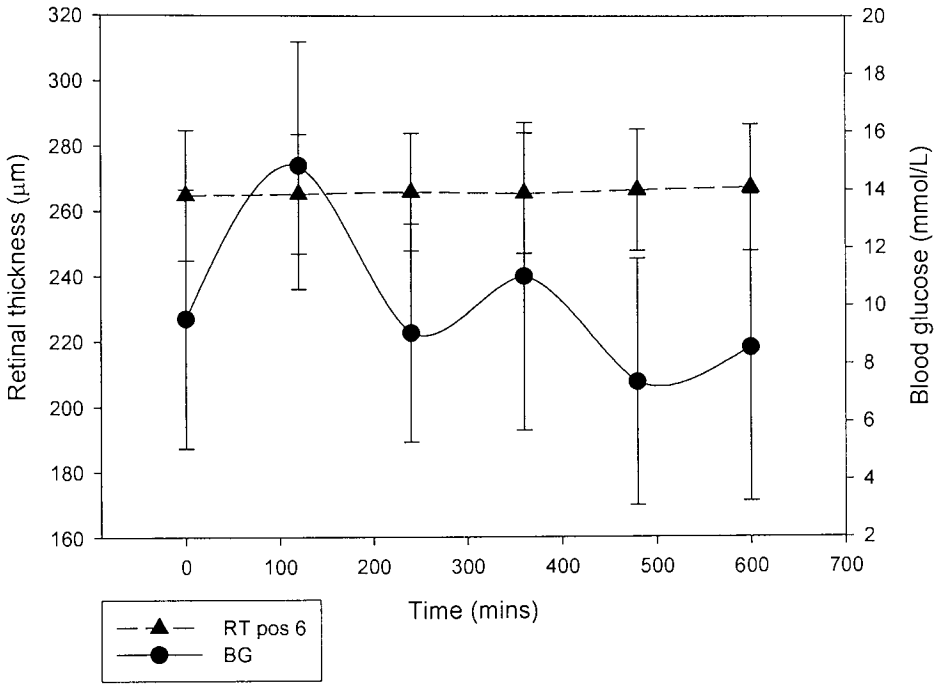

(b)

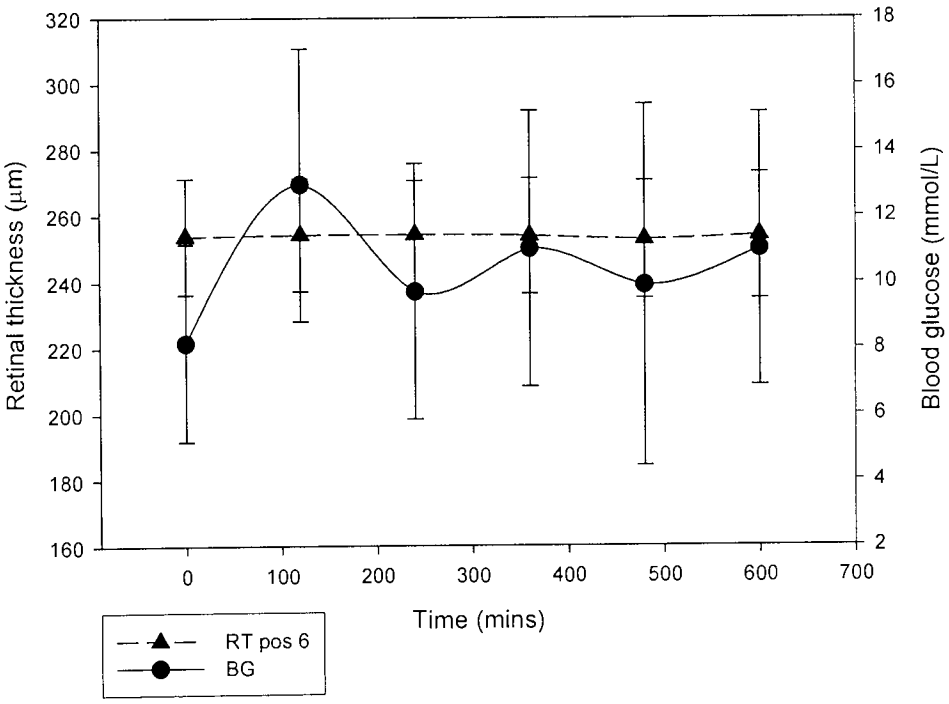

Figure 8.21 Graphs to show the change in blood glucose and macular retinal thickness in position 6 over time in (a) type 1 diabetics and (b) type 2 diabetics

(a)

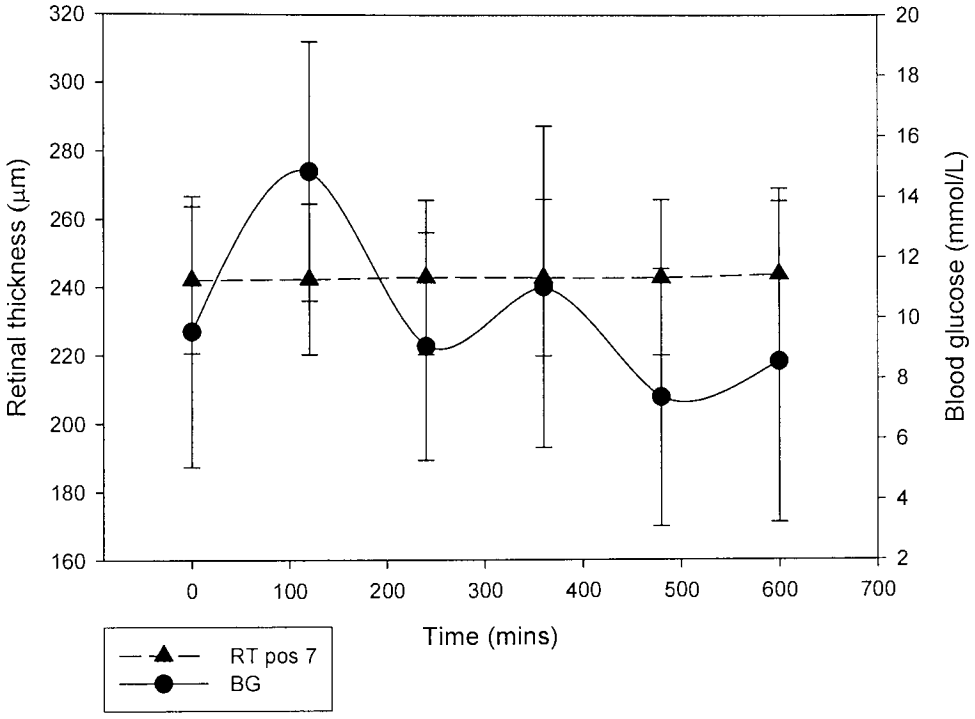

(b)

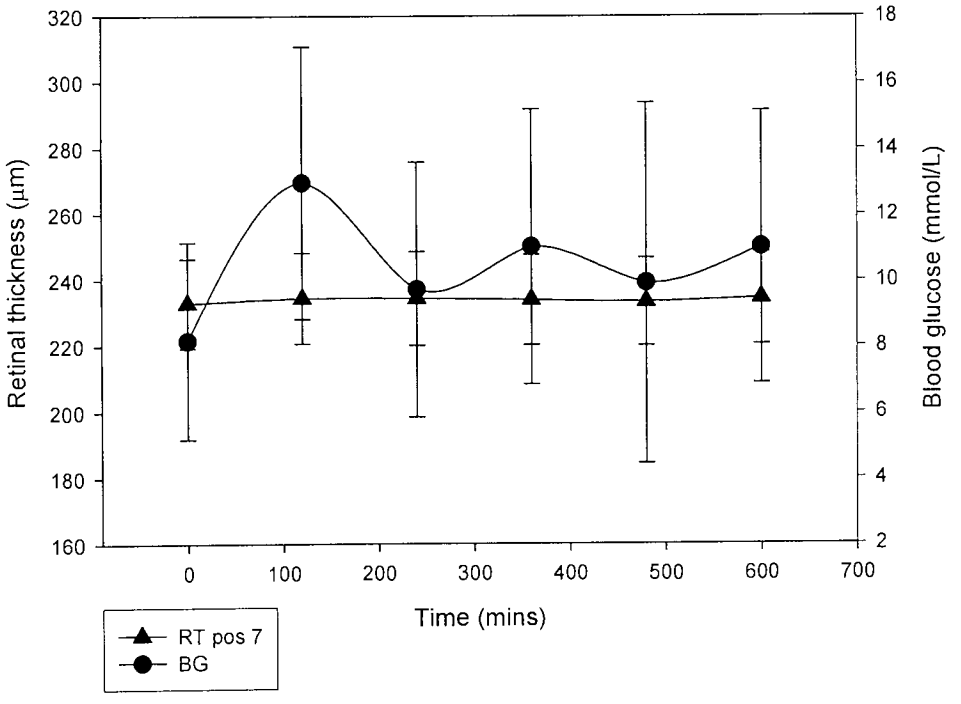

Figure 8.22 Graphs to show the change in blood glucose and macular retinal thickness in position 7 over time in (a) type 1 diabetics and (b) type 2 diabetics

(a)

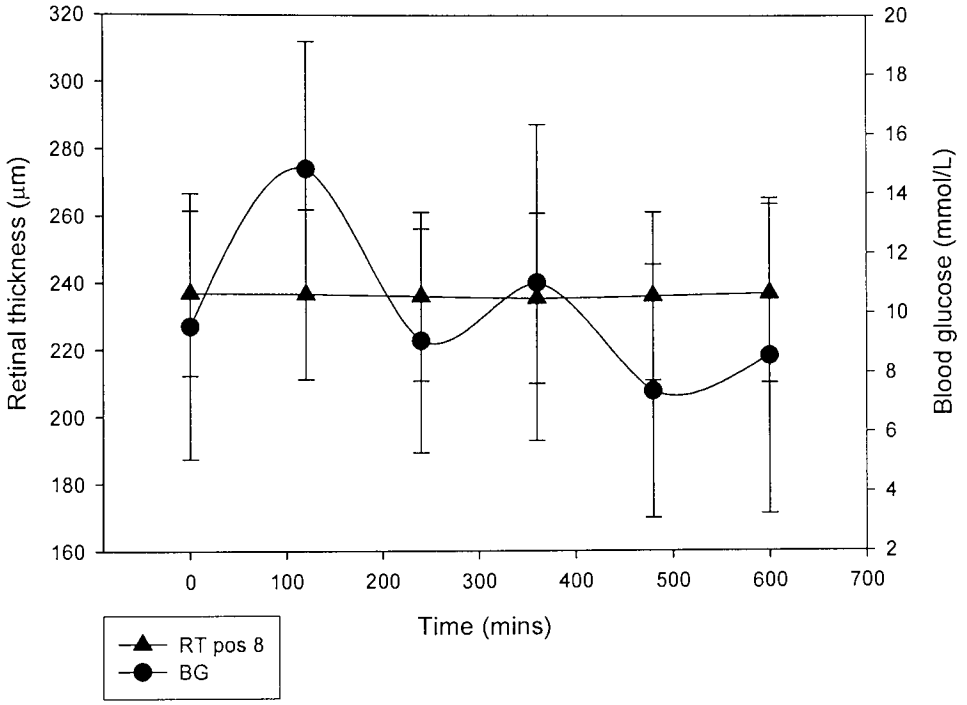

(b)

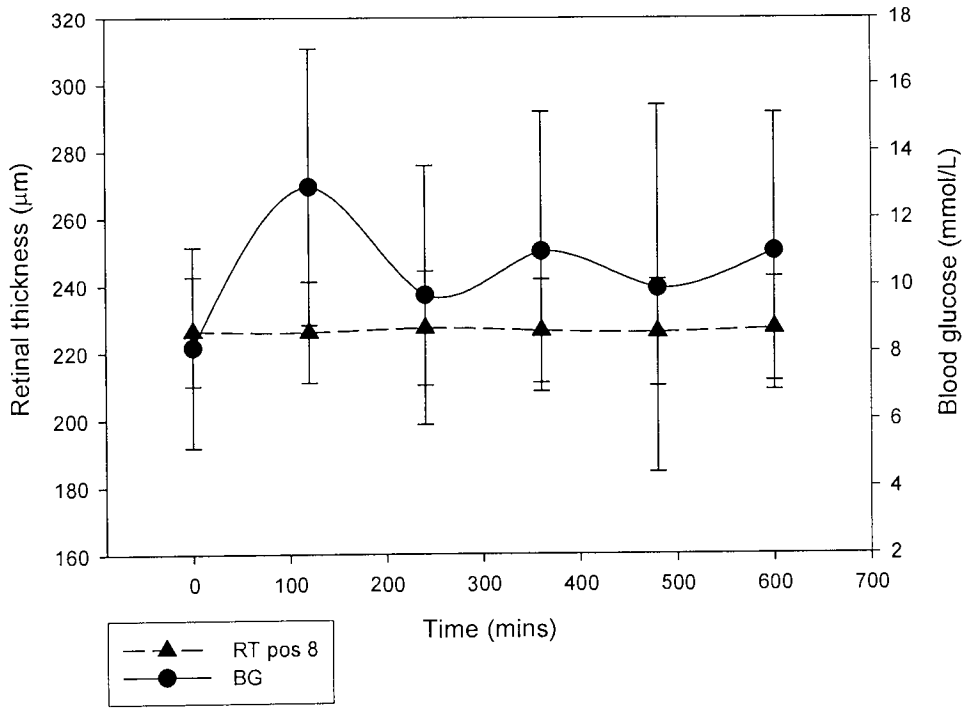

Figure 8.23 Graphs to show the change in blood glucose and macular retinal thickness in position 8 over time in (a) type 1 diabetics and (b) type 2 diabetics

(a)

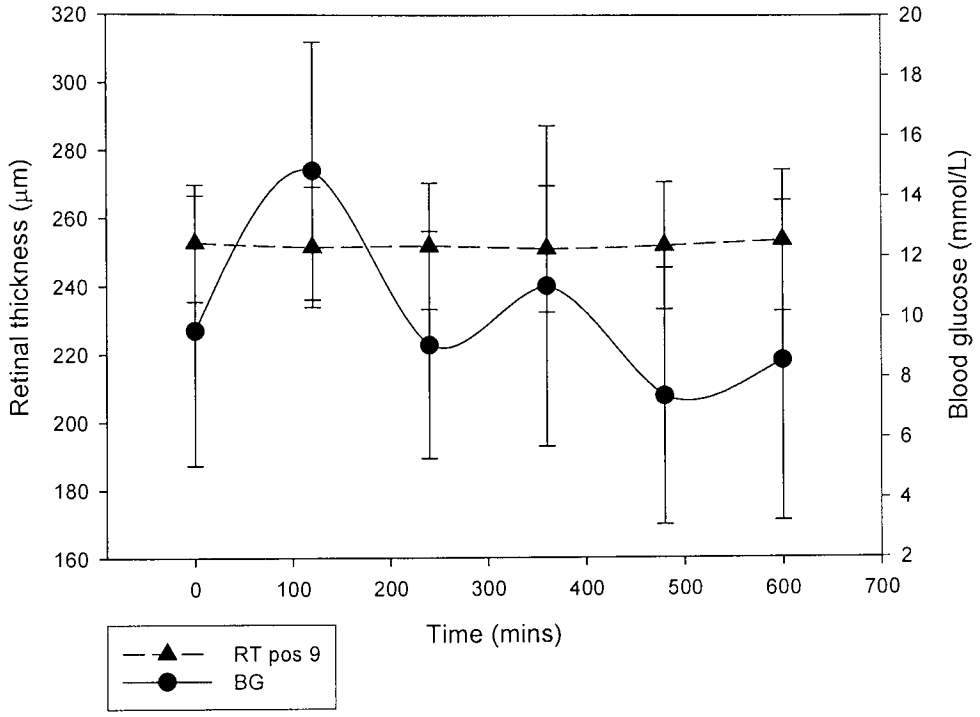

(b)

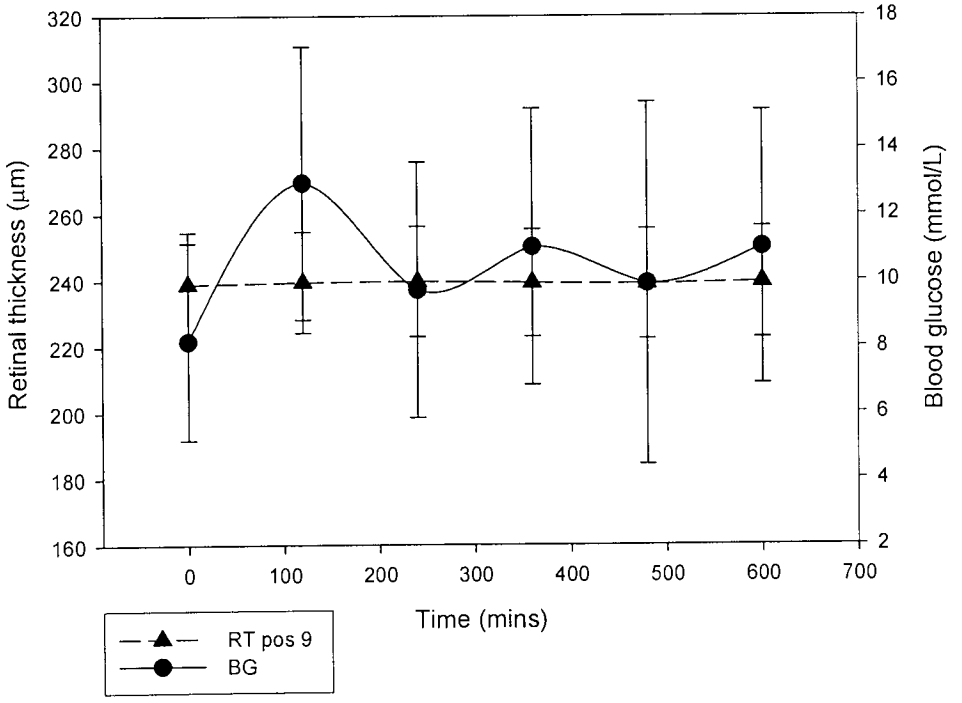

Figure 8.24 Graphs to show the change in blood glucose and macular retinal thickness in position 9 over time in (a) type 1 diabetics and (b) type 2 diabetics

(a)

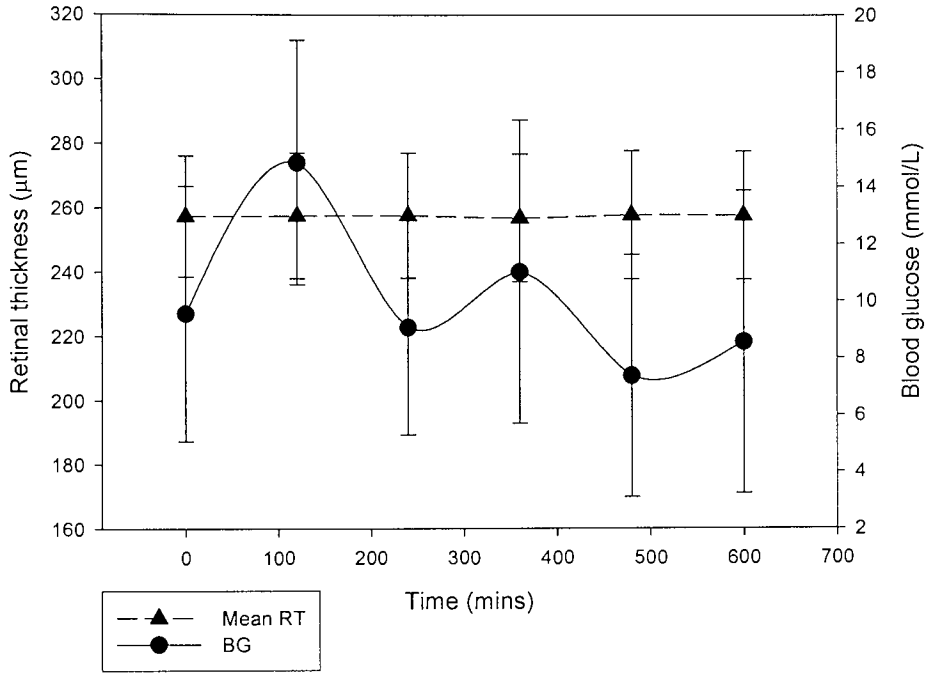

(b)

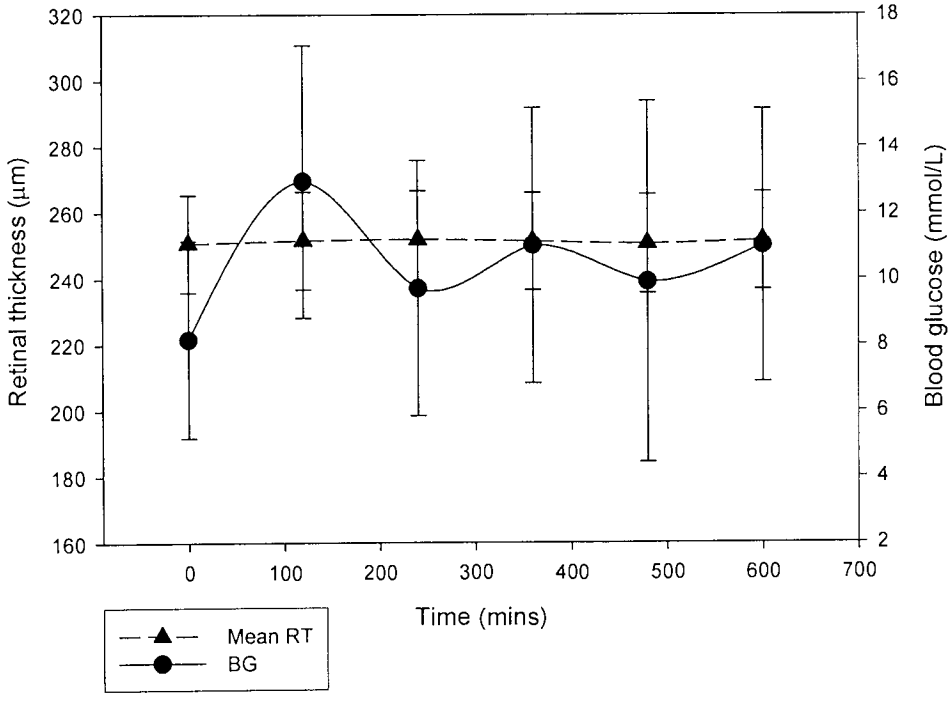

Figure 8.25 Graphs to show the change in blood glucose and mean macular retinal thickness over time in (a) type 1 diabetics and (b) type 2 diabetics

Systolic blood pressure

Systolic blood pressure varies minimally during the course of the day for both groups as shown in figure 8.26. ANOVA shows no statistically significant differences occurred between visits.

(a)

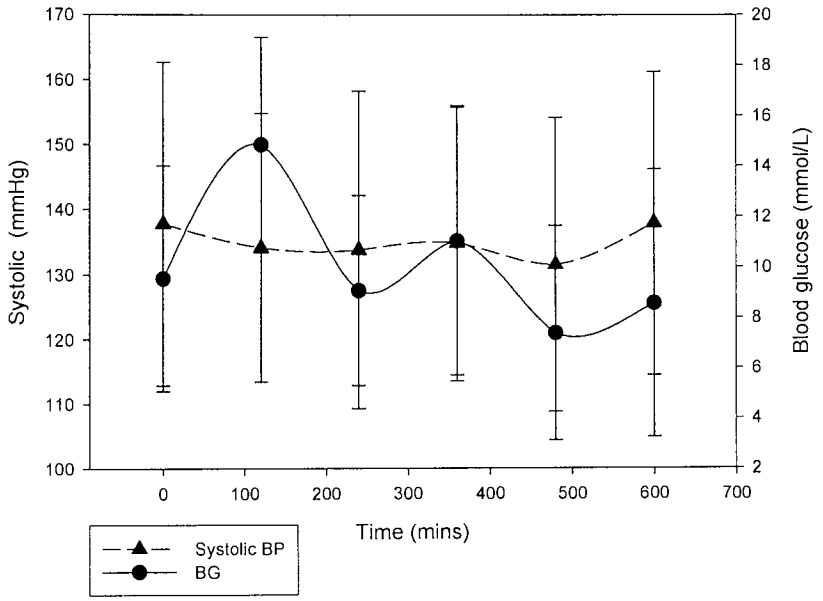

(b)

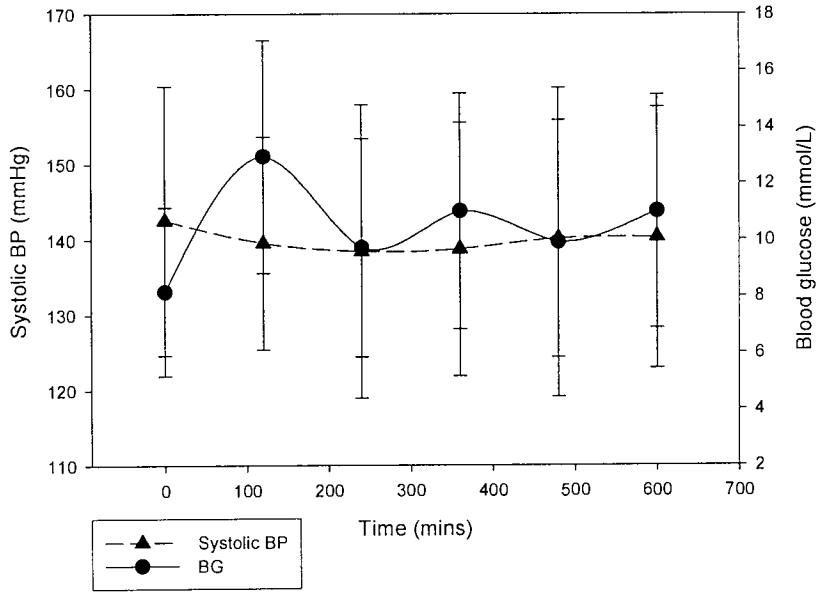

Figure 8.26 Graphs to show the change in blood glucose and systolic blood pressure over time in (a) type 1 diabetics and (b) type 2 diabetics

Diastolic blood pressure

Diastolic blood pressure varies significantly over the course of the day for all diabetic subjects as shown in figure 8.27. When blood glucose levels are high, diastolic blood pressure is low and vice versa. ANOVA reveals statistically significant differences between-visits for all subjects (p=0.000). Post-hoc analysis outline differences between visit 1 and 2 (p=0.001), 1 and 4 (p=0.000), 1 and 5 (p=0.000), 3 and 4 (p=0.000), and 4 and 6 (p=0.002) as being statistically significant.

(a)

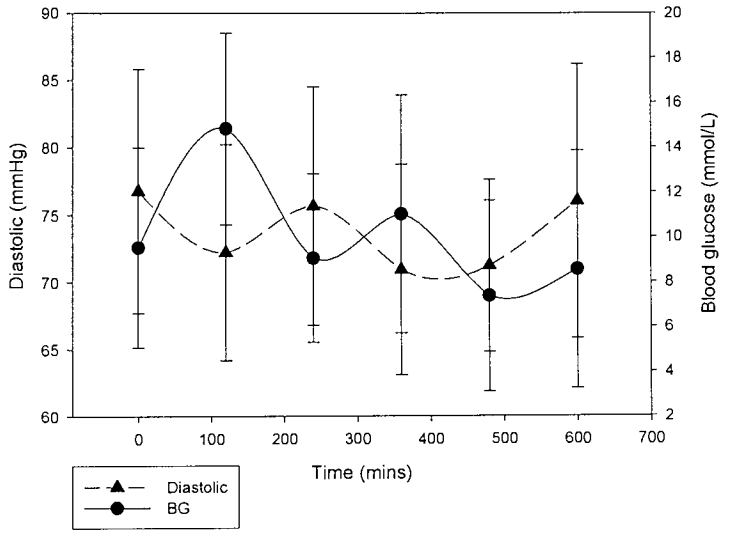

(b)

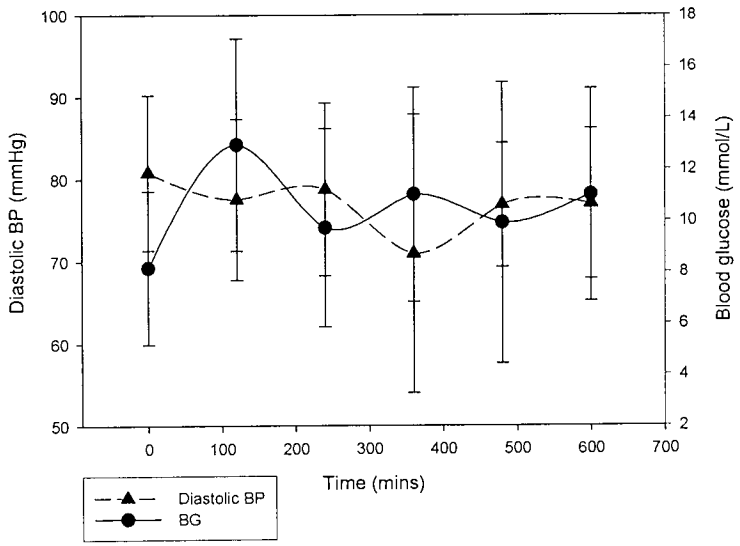

Figure 8.27 Graphs to show the change in blood glucose and diastolic blood pressure over time in (a) type 1 diabetics and (b) type 2 diabetics

Mean arterial pressure (MAP)

Mean arterial pressure varies significantly over the course of the day for diabetic subjects as shown in figure 8.28. When blood glucose levels are high, MAP is low and vice versa. ANOVA reveals statistically significant differences between-visits for all subjects (p=0.004). Post-hoc analysis outline differences only between visit 4 and 6 (p=0.003) as reaching statistical significance.

(a)

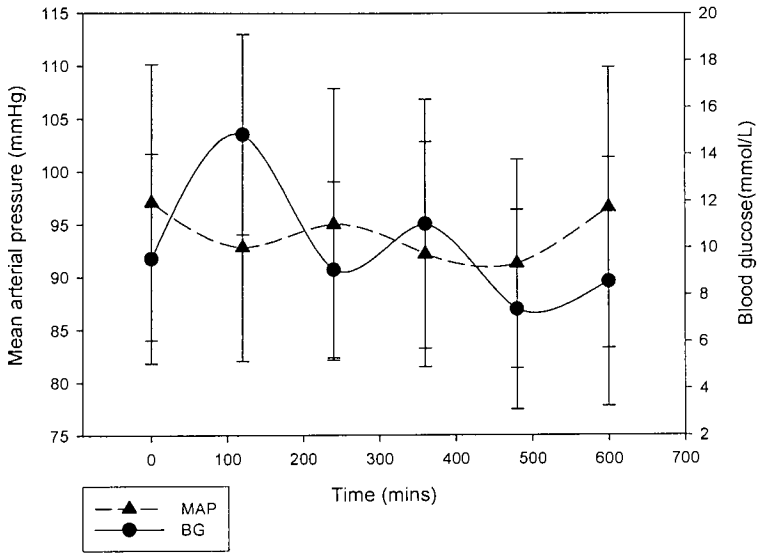

(b)

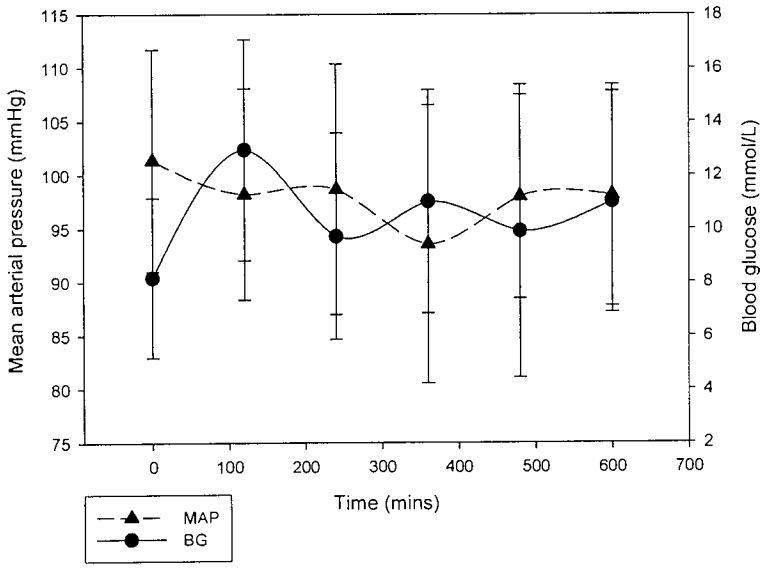

Figure 8.28 Graphs to show the change in blood glucose and mean arterial pressure (MAP) over time in (a) type 1 diabetics and (b) type 2 diabetics

Ocular perfusion pressure (OPP)

By observation, ocular perfusion pressure varies significantly over the course of the day for all diabetic subjects as shown in figure 8.29. When blood glucose levels are high, OPP is low and vice versa. ANOVA reveals statistically significant differences between-visits ($p=0.013$). However, post-hoc analysis using Bonferroni correction revealed that differences between visits failed to reach significance ($p=0.0033$).

(a)

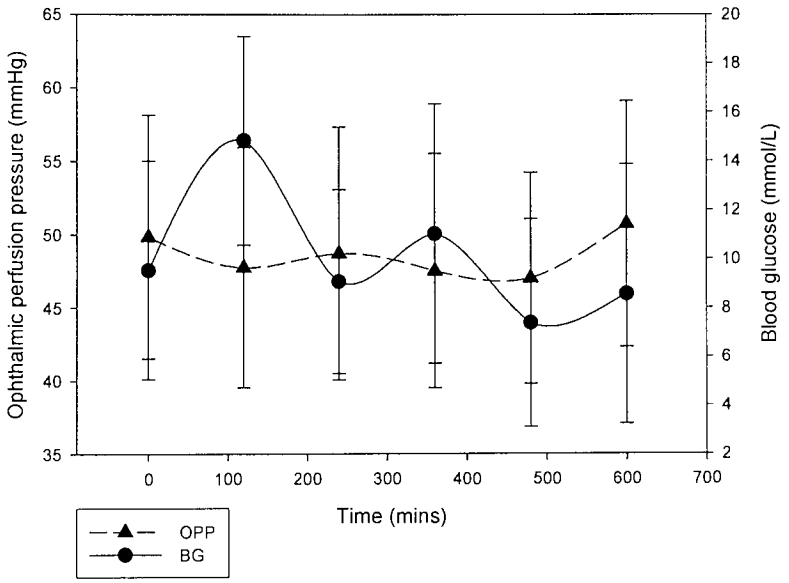

(b)

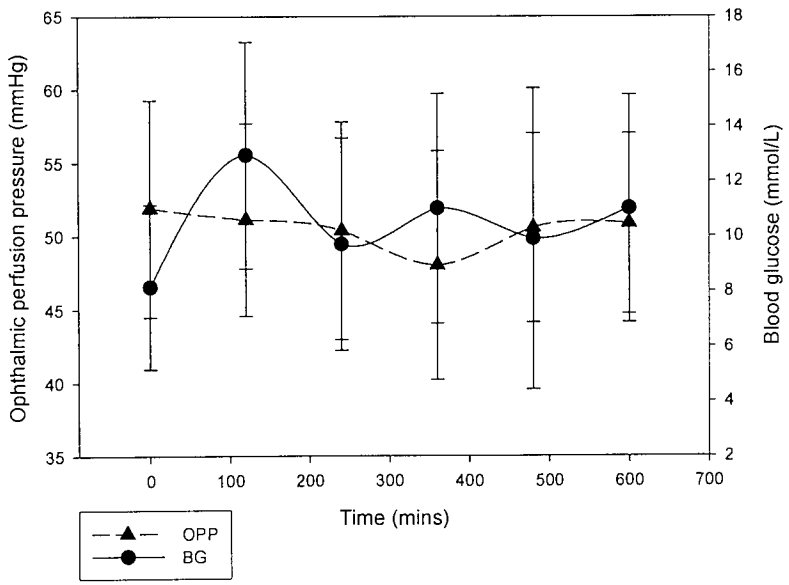

Figure 8.29 Graphs to show the change in blood glucose and ocular perfusion pressure pressure (OPP) over time in (a) type 1 diabetics and (b) type 2 diabetics

8.6.3 Correlation between test parameters and diabetic status

A simultaneous regression model was used to explore the relationship between each of the test parameters: VA (100 and 10%), contrast sensitivity, white-on-white fields (MD and PSD), SWAP fields (MD and PSD), IOP, retinal thickness (positions 1-9), retinal nerve fibre layer thickness (mean RNFL, superior, nasal, inferior, temporal quadrant) blood pressure, and a number of potential predictor variables: type of diabetes, haemoglobin levels, duration of diabetes and glucose level at each visit (1-6). Preliminary analyses were performed to ensure no violation of the assumptions of normality, linearity and homoscedasticity.

The multiple regression model was only significant for contrast sensitivity measures at visit 1, 2, 3 and visit 4. The regression model was significant for retinal thickness position 9 (outer superior sector) at visits 1, 2, 5 and 6 and for nasal retinal nerve fibre layer at visit 4. A significant model emerged for the inferior retinal nerve fibre layer for all visits (1-6). The simultaneous multiple regression model was significant for diastolic blood pressure at visit 4 only. Each of these models will be discussed further.

Contrast sensitivity : Visit 1

Predictor variable	Standardised coefficient (beta values)	Significance (p values)	Correlation (zero-order)	Correlation (part)
Type (1 or 2)	-0.248	0.124	-0.077	-0.225
HbA1c	**-0.455**	**0.005***	**-0.457**	**-0.425**
Glucose	-0.081	0.591	-0.169	-0.077
Duration	-0.137	0.393	-0.174	-0.124

Table 8.2 Table showing the results of simultaneous multiple regression analysis for contrast sensitivity visit 1

A significant model emerged for contrast sensitivity visit 1 (p=0.023) after using the following predictor values: type of diabetes, haemoglobin level (HbA1c), blood glucose level and duration (table 8.2). The R squared value was 0.265 which suggests that the model we used explained 26.5% of the variance in contrast sensitivity at visit 1. Inspection of the correlation revealed that HbA1c makes the strongest unique contribution to explaining contrast sensitivity scores when the variance explained by all

other variables in the model was controlled for. A significance value of 0.005 showed that HbA1c is making a statistically significant contribution to the equation. No other predictor reached significance. The beta value for HbA1c implied that some of the predictive power initially found (-0.455) was due to the variance it shared with the other predictors (part correlation -0.425). The zero-order correlation (-0.457) suggested that HbA1c had more predictive power when it was considered independently from the other predictive factors.

Contrast sensitivity:Visit 2

Predictor variable	Standardised coefficient (beta values)	Significance (p values)	Correlation (zero-order)	Correlation (part)
Type (1 or 2)	-0.173	0.279	-0.074	-0.157
HbA1c	**-0.534**	**0.002***	**-0.430**	**-0.486**
Glucose	0.246	0.131	0.059	0.221
Duration	-0.095	0.559	-0.094	-0.084

Table 8.3 Table showing the results of simultaneous multiple regression analysis for contrast sensitivity visit 2

A significant model emerged for contrast sensitivity visit 2 (p=0.022) after using the following predictor values: type of diabetes, haemoglobin level (HbA1c), blood glucose level and duration (table 8.3). The R squared value of 0.266 indicated that our model explained 26.6% of the variance in contrast sensitivity at visit 2. HbA1c makes the strongest unique contribution to explaining contrast sensitivity with a beta value 0.534. Inspection of the correlation revealed that HbA1c was the only significant predictor within the model (p=0.002). No other predictor reached significance. The beta value for HbA1c implied that some of the predictive power initially found (-0.534) was due to the variance it shared with the other predictors (part correlation -0.486).

Contrast sensitivity: Visit 3

Predictor variable	Standardised coefficient (beta values)	Significance (p values)	Correlation (zero-order)	Correlation (part)
Type (1 or 2)	-0.268	0.103	-0.087	-0.238
HbA1c	**-0.565**	**0.001***	**-0.391**	**-0.492**
Glucose	**0.334**	**0.048***	**0.059**	**-0.292**
Duration	-0.096	0.554	0.065	-0.085

Table 8.4 Table showing the results of simultaneous multiple regression analysis for contrast sensitivity visit 3

A significant model emerged for contrast sensitivity visit 3 (p=0.020) after using the following predictor values: type of diabetes, haemoglobin level (HbA1c), blood glucose level and duration (table 8.4). R squared value was 0.270. Inspection of the correlation revealed that HbA1c (0.001) and blood glucose level (0.048) were significant predictors within the model with HbA1c making the largest contribution (beta value 0.565) although glucose also made a statistically significant contribution (beta value 0.334). The beta value for HbA1c implied that some of the predictive power initially found (-0.565) was due to the variance it shared with the other predictors (part correlation -0.492). The beta value for glucose implied that some of the predictive power initially found (-0.334) was due to the variance it shared with the other predictors (part correlation -0.292).

Contrast sensitivity: Visit 4

Predictor variable	Standardised coefficient (beta values)	Significance (p values)	Correlation (zero-order)	Correlation (part)
Type (1 or 2)	-0.176	0.288	-0.038	-0.157
HbA1c	**-0.591**	**0.003***	**-0.429**	**-0.464**
Glucose	0.224	0.234	-0.124	0.176
Duration	-0.028	0.867	-0.057	-0.025

Table 8.5 Table showing the results of simultaneous multiple regression analysis for contrast sensitivity visit 4

A significant model emerged for contrast sensitivity visit 4 (p=0.043) after using the following predictor values: type of diabetes, haemoglobin level (HbA1c), blood glucose level and duration (table 8.5). The R squared value was 0.234. HbA1c makes the strongest statistically significant unique contribution to explaining contrast sensitivity at visit 4 with a beta value 0.591. Inspection of the correlation revealed that HbA1c was the only significant predictor within the model (p=0.003). No other predictor reached significance. The beta value for HbA1c implied that some of the predictive power initially found (-0.591) was due to the variance it shared with the other predictors (part correlation -0.464).

Contrast sensitivity: Visit 5

Predictor variable	Standardised coefficient (beta values)	Significance (p values)	Correlation (zero-order)	Correlation (part)
Type (1 or 2)	-0.230	0.203	-0.079	-0.191
HbA1c	**-0.520**	**0.006***	**-0.417**	**-0.433**
Glucose	0.126	0.485	-0.154	0.104
Duration	-0.007	0.968	-0.046	-0.006

Table 8.6 Table showing the results of simultaneous multiple regression analysis for contrast sensitivity visit 5

Despite the model just failing to reach significance for contrast sensitivity at visit 5 (p=0.061), a similar trend as that for visits 1-4 emerges. HbA1c makes the strongest statistically significant unique contribution to explaining contrast sensitivity at visit 5 with a beta value 0.520. Inspection of the correlation revealed that HbA1c was the only significant predictor within the model (p=0.006). No other predictor reached significance. The beta value for HbA1c implied that some of the predictive power initially found (-0.520) was due to the variance it shared with the other predictors (part correlation -0.433).

Contrast sensitivity: Visit 6

Predictor variable	Standardised coefficient (beta values)	Significance (p values)	Correlation (zero-order)	Correlation (part)
Type (1 or 2)	-0.111	0.526	-0.019	-0.095
HbA1c	**-0.445**	**0.009***	**-0.448**	**-0.405**
Glucose	0.016	0.923	-0.153	-0.014
Duration	-0.091	0.584	-0.166	-0.082

Table 8.7 Table showing the results of simultaneous multiple regression analysis for contrast sensitivity visit 6

Despite the model just failing to reach significance for contrast sensitivity at visit 6 (p=0.063), a similar trend as that for visits 1-4 emerges. HbA1c makes the strongest statistically significant unique contribution to explaining contrast sensitivity at visit 6 with a beta value 0.445. Inspection of the correlation revealed that HbA1c was the only significant predictor within the model (p=0.009). No other predictor reached significance. The beta value for HbA1c implied that some of the predictive power initially found (-0.445) was due to the variance it shared with the other predictors (part correlation -0.405).

Macular retinal thickness position 9- outer superior macular : Visit 1

Predictor variable	Standardised coefficient (beta values)	Significance (p values)	Correlation (zero-order)	Correlation (part)
Type (1 or 2)	**-0.450**	**0.007***	**-0.409**	**-0.407**
HbA1c	0.285	0.070	0.296	0.267
Glucose	-0.150	0.323	-0.015	-0.143
Duration	-0.190	0.239	0.037	-0.171

Table 8.8 Table showing the results of simultaneous multiple regression analysis for retinal thickness position 9 (outer superior) visit 1

A significant model emerged for retinal thickness at position 9 (outer superior) at visit 1 (p=0.023) after using the following predictor values: type of diabetes, haemoglobin level (HbA1c), blood glucose level and duration (table 8.6). R squared was 0.264.

Type makes the strongest unique contribution to explaining contrast sensitivity with a beta value 0.450. Inspection of the correlation revealed that the type of diabetes was the only significant predictor within the model (p=0.007). No other predictor reached significance. The beta value for diabetes type implied that some of the predictive power initially found (-0.450) was due to the variance it shared with the other predictors (part correlation -0.407). The zero-order correlation (-0.409) suggested that type had more predictive power when it was considered independently from the other predictive factors.

Macular retinal thickness position 9- outer superior : Visit 2

Predictor variable	Standardised coefficient (beta values)	Significance (p values)	Correlation (zero-order)	Correlation (part)
Type (1 or 2)	**-0.419**	**0.013***	**-0.371**	**-0.381**
HbA1c	0.278	0.091	0.262	0.253
Glucose	-0.162	0.324	-0.019	-0.146
Duration	-0.186	0.266	0.000	-0.165

Table 8.9 Table showing the results of simultaneous multiple regression analysis for retinal thickness position 9 (outer superior) visit 2

A significant model emerged for retinal thickness at position 9 (outer superior) at visit 2 (p=0.045) after using the following predictor values: type of diabetes, haemoglobin level (HbA1c), blood glucose level and duration (table 8.7). The R squared value was 0.231. Type makes the strongest unique contribution to explaining contrast sensitivity with a beta value 0.419. Inspection of the correlation revealed that the type of diabetes was the only significant predictor within the model (p=0.013). No other predictor reached significance. The beta value for diabetes type implied that some of the predictive power initially found (-0.419) was due to the variance it shared with the other predictors (part correlation -0.381).

Macular retinal thickness position 9- outer superior: Visit 5

Predictor variable	Standardised coefficient (beta values)	Significance (p values)	Correlation (zero-order)	Correlation (part)
Type (1 or 2)	**-0.433**	**0.019***	**-0.368**	**-0.359**
HbA1c	0.233	0.191	0.284	0.194
Glucose	0.057	0.748	0.021	0.047
Duration	-0.261	0.117	-0.027	-0.234

Table 8.10 Table showing the results of simultaneous multiple regression analysis for retinal thickness position 9 (outer superior) visit 5

A significant model emerged for retinal thickness at position 9 (outer superior) at visit 5 (p=0.023) after using the following predictor values: type of diabetes, haemoglobin level (HbA1c), blood glucose level and duration (table 8.8). The R squared value was 0.234. Type makes the strongest unique contribution to explaining contrast sensitivity with a beta value 0.433. Inspection of the correlation revealed that the type of diabetes was the only significant predictor within the model (p=0.019). No other predictor reached significance. The beta value for diabetes type implied that some of the predictive power initially found (-0.433) was due to the variance it shared with the other predictors (part correlation -0.359). The zero-order correlation (-0.368) suggested that type had slightly more predictive power when it was considered independently from the other predictive factors.

Macular retinal thickness position 9- outer superior: Visit 6

Predictor variable	Standardised coefficient (beta values)	Significance (p values)	Correlation (zero-order)	Correlation (part)
Type (1 or 2)	**-0.433**	**0.014***	**-0.371**	**-0.370**
HbA1c	0.267	0.100	0.295	0.243
Glucose	0.035	0.827	-0.022	0.032
Duration	-0.287	0.081	-0.048	-0.259

Table 8.11 Table showing the results of simultaneous multiple regression analysis for retinal thickness position 9 (outer superior) visit 6

A significant model emerged for retinal thickness at position 9 (outer superior) at visit 6 (p=0.030) after using the following predictor values: type of diabetes, haemoglobin level (HbA1c), blood glucose level and duration (table 8.9). The R squared value was 0.252. Type makes the strongest unique contribution to explaining contrast sensitivity with a beta value 0.433. Inspection of the correlation revealed that the type of diabetes was the only significant predictor within the model (p=0.014). No other predictor reached significance. The beta value for diabetes type implied that some of the predictive power initially found (-0.433) was due to the variance it shared with the other predictors (part correlation -0.370). The zero-order correlation (-0.371) suggested that type had only slightly more predictive power when it was considered independently from the other predictive factors.

Nasal RNFL around the optic nerve head: Visit 4

Predictor variable	Standardised coefficient (beta values)	Significance (p values)	Correlation (zero-order)	Correlation (part)
Type (1 or 2)	-0.190	0.233	-0.271	-0.170
HbA1c	**0.556**	**0.004***	**0.306**	**0.437**
Glucose	**-0.462**	**0.014***	**-0.159**	**-0.364**
Duration	-0.090	0.575	0.008	-0.079

Table 8.12 Table showing the results of simultaneous multiple regression analysis for retinal nerve fibre layer thickness nasal quadrant visit 4

A significant model emerged for retinal nerve fibre layer thickness in the nasal quadrant at visit 4 (p=0.012) after using the following predictor values: type of diabetes, haemoglobin level (HbA1c), blood glucose level and duration (table 8.10). R squared value was 0.295. Inspection of the correlation revealed that HbA1c (0.004) and blood glucose level (0.014) were significant predictors within the model with HbA1c making the largest contribution (beta value 0.556) although glucose also made a statistically significant contribution (beta value 0.462). Inspection of the correlation revealed that haemoglobin (p=0.004) and blood glucose (p=0.014) were the only significant predictors within the model. The beta value for HbA1c implied that some of the predictive power initially found (-0.556) was due to the variance it shared with the other predictors (part correlation -0.437). Likewise, the beta value for blood glucose implied

that some of the predictive power initially found (-0.462) was due to the variance it shared with the other predictors (part correlation -0.364).

Nasal RNFL around the optic nerve head: visit 6

Predictor variable	Standardised coefficient (beta values)	Significance (p values)	Correlation (zero-order)	Correlation (part)
Type (1 or 2)	-0.148	0.373	-0.283	-0.126
HbA1c	**0.427**	**0.009***	**0.330**	**-0.389**
Glucose	**-0.367**	**0.023***	**-0.307**	**-0.333**
Duration	-0.160	0.311	0.011	-0.144

Table 8.13 Table showing the results of simultaneous multiple regression analysis for retinal nerve fibre layer thickness nasal quadrant visit 6

A significant model emerged for retinal nerve fibre layer thickness in the nasal quadrant at visit 6 (p=0.012) after using the following predictor values: type of diabetes, haemoglobin level (HbA1c), blood glucose level and duration (table 8.11). R squared value was 0.294. Inspection of the correlation revealed that HbA1c (0.009) and blood glucose level (0.023) were significant predictors within the model with HbA1c making the largest contribution (beta value 0.427) although glucose also made a statistically significant contribution (beta value 0.367). Inspection of the correlation revealed that haemoglobin (p=0.009) and blood glucose level (p=0.023) were the only significant predictors within the model. The beta value for HbA1c implied that some of the predictive power initially found (-0.427) was due to the variance it shared with the other predictors (part correlation -0.389). Likewise, the beta value for blood glucose implied that some of the predictive power initially found (-0.367) was due to the variance it shared with the other predictors (part correlation -0.333).

Inferior RNFL around the optic nerve head :visit 1

Predictor variable	Standardised coefficient (beta values)	Significance (p values)	Correlation (zero-order)	Correlation (part)
Type (1 or 2)	**-0.409**	**0.016***	**-0.280**	**-0.370**
HbA1c	0.135	0.396	0.142	0.126
Glucose	0.025	0.870	0.027	0.024
Duration	**-0.422**	**0.014***	**-0.397**	**-0.380**

Table 8.14 Table showing the results of simultaneous multiple regression analysis for retinal nerve fibre layer thickness inferior quadrant visit 1

A significant model emerged for retinal nerve fibre layer thickness in the inferior quadrant at visit 1 (p=0.050) after using the following predictor values: type of diabetes, haemoglobin level (HbA1c), blood glucose level and duration (table 8.12). R squared value was 0.227. Inspection of the correlation revealed that type (0.016) and duration (0.014) were significant predictors within the model with duration making the largest contribution (beta value 0.422) although type also made a statistically significant contribution (beta value 0.409). Inspection of the correlation revealed that type of diabetes (p=0.016) and duration of the disease (p=0.014) were the only significant predictors within the model. The beta value for diabetes type implied that some of the predictive power initially found (-0.409) was due to the variance it shared with the other predictors (part correlation -0.370). Likewise, the beta value for disease duration implied that some of the predictive power initially found (-0.422) was due to the variance it shared with the other predictors (part correlation -0.380).

Inferior RNFL around the optic nerve head: visit 2

Predictor variable	Standardised coefficient (beta values)	Significance (p values)	Correlation (zero-order)	Correlation (part)
Type (1 or 2)	**-0.436**	**0.008***	**-0.298**	**-0.396**
HbA1c	0.073	0.640	0.098	0.066
Glucose	0.162	0.308	0.138	0.146
Duration	**-0.494**	**0.004***	**-0.256**	**-0.438**

Table 8.15 Table showing the results of simultaneous multiple regression analysis for retinal nerve fibre layer thickness inferior quadrant visit 2

A significant model emerged for retinal nerve fibre layer thickness in the inferior quadrant at visit 2 (p=0.014) after using the following predictor values: type of diabetes, haemoglobin level (HbA1c), blood glucose level and duration (table 8.13). R squared value was 0.286. Inspection of the correlation revealed that type (0.008) and duration (0.004) were significant predictors within the model with duration making the largest contribution (beta value 0.494) although type also made a statistically significant contribution (beta value 0.436). Inspection of the correlation revealed that type of diabetes (p=0.008) and duration of the disease (p=0.004) were the only significant predictors within the model. The beta value for diabetes type implied that some of the predictive power initially found (-0.436) was due to the variance it shared with the other predictors (part correlation -0.396). Likewise, the beta value for disease duration implied that some of the predictive power initially found (-0.494) was due to the variance it shared with the other predictors (part correlation -0.438).

Inferior RNFL around the optic nerve head: visit 3

Predictor variable	Standardised coefficient (beta values)	Significance (p values)	Correlation (zero-order)	Correlation (part)
Type (1 or 2)	**-0.622**	**0.000***	**-0.422**	**-0.552**
HbA1c	0.087	0.558	0.183	0.075
Glucose	0.236	0.114	0.115	0.206
Duration	**-0.531**	**0.001***	**-0.212**	**-0.469**

Table 8.16 Table showing the results of simultaneous multiple regression analysis for retinal nerve fibre layer thickness inferior quadrant visit 3

A significant model emerged for retinal nerve fibre layer thickness in the inferior quadrant at visit 3 (p=0.001) after using the following predictor values: type of diabetes, haemoglobin level (HbA1c), blood glucose level and duration (table 8.14). R squared value was 0.418. Inspection of the correlation revealed that type (0.000) and duration (0.001) were significant predictors within the model with type making the largest contribution (beta value 0.531) although duration also made a statistically significant contribution (beta value 0.531). Inspection of the correlation revealed that type of diabetes (p=0.000) and duration of the disease (p=0.001) were the only significant predictors within the model. The beta value for diabetes type implied that some of the predictive power initially found (-0.622) was due to the variance it shared with the other predictors (part correlation -0.552). Likewise, the beta value for disease duration implied that some of the predictive power initially found (-0.531) was due to the variance it shared with the other predictors (part correlation -0.469).

Inferior RNFL around the optic nerve head: visit 4

Predictor variable	Standardised coefficient (beta values)	Significance (p values)	Correlation (zero-order)	Correlation (part)
Type (1 or 2)	**-0.419**	**0.010***	**-0.335**	**-0.374**
HbA1c	0.312	0.083	0.139	0.245
Glucose	-0.282	0.115	-0.197	-0.222
Duration	**-0.383**	**0.019***	**-0.214**	**-0.338**

Table 8.17 Table showing the results of simultaneous multiple regression analysis for retinal nerve fibre layer thickness inferior quadrant visit 4

A significant model emerged for retinal nerve fibre layer thickness in the inferior quadrant at visit 4 (p=0.006) after using the following predictor values: type of diabetes, haemoglobin level (HbA1c), blood glucose level and duration (table 8.15). R squared value was 0.321. Inspection of the correlation revealed that type (0.010) and duration (0.019) were significant predictors within the model with type making the largest contribution (beta value 0.419) although duration also made a statistically significant contribution (beta value 0.383). Inspection of the correlation revealed that type of diabetes (p=0.010) and duration of the disease (p=0.019) were the only significant predictors within the model. The beta value for diabetes type implied that some of the predictive power initially found (-0.419) was due to the variance it shared with the other predictors (part correlation -0.374). Likewise, the beta value for disease duration implied that some of the predictive power initially found (-0.383) was due to the variance it shared with the other predictors (part correlation -0.338).

Inferior RNFL around the optic nerve head: visit 5

Predictor variable	Standardised coefficient (beta values)	Significance (p values)	Correlation (zero-order)	Correlation (part)
Type (1 or 2)	**-0.447**	**0.013***	**-0.356**	**-0.371**
HbA1c	0.184	0.286	0.134	-0.153
Glucose	-0.99	0.569	-0.170	-0.081
Duration	**-0.407**	**0.014***	**-0.192**	**-0.365**

Table 8.18 Table showing the results of simultaneous multiple regression analysis for retinal nerve fibre layer thickness inferior quadrant visit 5

A significant model emerged for retinal nerve fibre layer thickness in the inferior quadrant at visit 5 (p=0.017) after using the following predictor values: type of diabetes, haemoglobin level (HbA1c), blood glucose level and duration (table 8.16). R squared value was 0.278. Inspection of the correlation revealed that type (0.013) and duration (0.014) were significant predictors within the model with type making the largest contribution (beta value 0.447) although duration also made a statistically significant contribution (beta value 0.407). Inspection of the correlation revealed that type of diabetes (p=0.013) and duration of the disease (p=0.014) were the only significant predictors within the model. The beta value for diabetes type implied that some of the predictive power initially found (-0.447) was due to the variance it shared with the other predictors (part correlation -0.371). Likewise, the beta value for disease duration implied that some of the predictive power initially found (-0.407) was due to the variance it shared with the other predictors (part correlation -0.365).

Inferior RNFL around the optic nerve head: visit 6

Predictor variable	Standardised coefficient (beta values)	Significance (p values)	Correlation (zero-order)	Correlation (part)
Type (1 or 2)	**-0.405**	**0.017***	**-0.365**	**-0.346**
HbA1c	0.268	0.086	0.206	0.243
Glucose	-0.195	0.206	-0.245	-0.177
Duration	**-0.394**	**0.014***	**-0.167**	**-0.355**

Table 8.19 Table showing the results of simultaneous multiple regression analysis for retinal nerve fibre layer thickness inferior quadrant visit 6

A significant model emerged for retinal nerve fibre layer thickness in the inferior quadrant at visit 6 (p=0.007) after using the following predictor values: type of diabetes, haemoglobin level (HbA1c), blood glucose level and duration (table 8.17). R squared value was 0.316. Inspection of the correlation revealed that type (0.017) and duration (0.014) were significant predictors within the model with type making the largest contribution (beta value 0.405) although duration also made a statistically significant contribution (beta value 0.394). Inspection of the correlation revealed that type of diabetes (p=0.017) and duration of the disease (p=0.014) were the only significant predictors within the model. The beta value for diabetes type implied that some of the predictive power initially found (-0.405) was due to the variance it shared with the other predictors (part correlation -0.346). Likewise, the beta value for disease duration implied that some of the predictive power initially found (-0.394) was due to the variance it shared with the other predictors (part correlation -0.355). The zero-order correlation (-0.365) suggested that type had more predictive power when it was considered independently from the other predictive factors.

Mean RNFL around the optic nerve head: visit 2

Predictor variable	Standardised coefficient (beta values)	Significance (p values)	Correlation (zero-order)	Correlation (part)
Type (1 or 2)	**-0.478**	**0.004***	**-0.416**	**-0.435**
HbA1c	0.083	0.600	0.168	0.076
Glucose	0.165	0.307	0.212	0.148
Duration	-0.308	0.064	-0.050	-0.273

Table 8.20 Table showing the results of simultaneous multiple regression analysis for mean retinal nerve fibre layer thickness visit 2

A significant model emerged for mean retinal nerve fibre layer thickness at visit 2 (p=0.024) after using the following predictor values: type of diabetes, haemoglobin level (HbA1c), blood glucose level and duration (table 8.18). The R squared value was 0.263. Diabetes type makes the strongest statistically significant unique contribution to explaining contrast sensitivity at visit 2 with a beta value 0.478. Inspection of the correlation revealed that type was the only significant predictor within the model (p=0.004). No other predictor variables reached statistical significance. The beta value for type implied that some of the predictive power initially found (-0.478) was due to the variance it shared with the other predictors (part correlation -0.435).

Mean RNFL around the optic nerve head: visit 3

Predictor variable	Standardised coefficient (beta values)	Significance (p values)	Correlation (zero-order)	Correlation (part)
Type (1 or 2)	**-0.591**	**0.000***	**-0.440**	**-0.524**
HbA1c	0.04	0.797	0.196	0.035
Glucose	0.291	0.068	0.190	0.254
Duration	**-0.368**	**0.021***	**-0.061**	**-0.325**

Table 8.21 Table showing the results of simultaneous multiple regression analysis for mean retinal nerve fibre layer thickness visit 3

A significant model emerged for mean retinal nerve fibre layer thickness at visit 3 (p=0.004) after using the following predictor values: type of diabetes, haemoglobin

level (HbA1c), blood glucose level and duration (table 8.19). R squared value was 0.345. Inspection of the correlation revealed that type (0.000) and duration (0.021) were significant predictors within the model with type making the largest contribution (beta value 0.591) although duration also made a statistically significant contribution (beta value 0.368). Inspection of the correlation revealed that the type of diabetes (p=0.000) and duration of the disease (p=0.021) were the only significant predictors within the model. The beta value for type implied that some of the predictive power initially found (-0.591) was due to the variance it shared with the other predictors (part correlation -0.524). Likewise, the beta value for disease duration implied that some of the predictive power initially found (-0.368) was due to the variance it shared with the other predictors (part correlation -0.325).

Mean RNFL around the optic nerve head: visit 4

Predictor variable	Standardised coefficient (beta values)	Significance (p values)	Correlation (zero-order)	Correlation (part)
Type (1 or 2)	**-0.487**	**0.004***	**-0.430**	**-0.435**
HbA1c	0.210	0.255	0.191	0.165
Glucose	-0.100	0.584	-0.040	-0.079
Duration	-0.263	0.113	-0.045	-0.232

Table 8.22 Table showing the results of simultaneous multiple regression analysis for mean retinal nerve fibre layer thickness visit 4

A significant model emerged for mean retinal nerve fibre layer thickness at visit 4 (p=0.022) after using the following predictor values: type of diabetes, haemoglobin level (HbA1c), blood glucose level and duration (table 8.20). The R squared value was 0.266. Diabetes type makes the strongest statistically significant unique contribution to explaining contrast sensitivity at visit 4 with a beta value 0.487. Inspection of the correlation revealed that type was the only significant predictor within the model (p=0.004). No other predictor variables reached statistical significance. The beta value for type implied that some of the predictive power initially found (-0.487) was due to the variance it shared with the other predictors (part correlation -0.435).

Mean RNFL around the optic nerve head: visit 5

Predictor variable	Standardised coefficient (beta values)	Significance (p values)	Correlation (zero-order)	Correlation (part)
Type (1 or 2)	**-0.459**	**0.013***	**-0.398**	**-0.381**
HbA1c	0.175	0.323	0.182	-0.146
Glucose	-0.045	0.800	-0.114	-0.037
Duration	-0.287	0.085	-0.066	-0.257

Table 8.23 Table showing the results of simultaneous multiple regression analysis for mean retinal nerve fibre layer thickness visit 5

A significant model emerged for mean retinal nerve fibre layer thickness at visit 5 (p=0.039) after using the following predictor values: type of diabetes, haemoglobin level (HbA1c), blood glucose level and duration (table 8.21). The R squared value was 0.239. Diabetes type makes the strongest statistically significant unique contribution to explaining contrast sensitivity at visit 5 with a beta value 0.459. Inspection of the correlation revealed that type was the only significant predictor within the model (p=0.013). No other predictor variables reached statistical significance. The beta value for type implied that some of the predictive power initially found (-0.459) was due to the variance it shared with the other predictors (part correlation -0.381). The zero-order correlation (-0.398) suggested that type had more predictive power when it was considered independently from the other predictive factors.

Mean RNFL around the optic nerve head: visit 6

Predictor variable	Standardised coefficient (beta values)	Significance (p values)	Correlation (zero-order)	Correlation (part)
Type (1 or 2)	**-0.415**	**0.018***	**-0.383**	**-0.355**
HbA1c	0.269	0.095	0.260	0.245
Glucose	-0.089	0.574	-0.141	-0.081
Duration	-0.302	0.066	-0.069	-0.272

Table 8.24 Table showing the results of simultaneous multiple regression analysis for mean retinal nerve fibre layer thickness visit 6

A significant model emerged for mean retinal nerve fibre layer thickness at visit 6 (p=0.024) after using the following predictor values: type of diabetes, haemoglobin level (HbA1c), blood glucose level and duration (table 8.22). The R squared value was 0.262. Diabetes type makes the strongest statistically significant unique contribution to explaining contrast sensitivity at visit 6 with a beta value 0.415. Inspection of the correlation revealed that type was the only significant predictor within the model (p=0.018). No other predictor variables reached statistical significance. The beta value for type implied that some of the predictive power initially found (-0.415) was due to the variance it shared with the other predictors (part correlation -0.355). The zero-order correlation (-0.383) suggested that type had more predictive power when it was considered independently from the other predictive factors.

Diastolic blood pressure: visit 5

Predictor variable	Standardised coefficient (beta values)	Significance (p values)	Correlation (zero-order)	Correlation (part)
Type (1 or 2)	0.272	0.126	0.370	0.226
HbA1c	0.176	0.316	0.148	0.147
Glucose	0.211	0.235	0.341	0.174
Duration	-0.210	0.199	-0.254	-0.189

Table 8.25 Table showing the results of simultaneous multiple regression analysis for diastolic blood pressure visit 5

A significant model emerged for diastolic blood pressure at visit 5 (p=0.030) after using the following predictor values: type of diabetes, haemoglobin level (HbA1c), blood glucose level and duration (table 8.23). Inspection of the correlation revealed that none of the predictor variables alone reached significance.

8.6.4 Multiple regression model summary

The following table (table 8.26) summarises the multiple regression analysis.

Parameter	Predictor variables significance			
	Type	HbA1c	Glucose	Duration
CS Visit 1	0.124	0.005*	0.591	0.393
CS Visit 2	0.279	0.002*	0.131	0.559
CS Visit 3	0.103	0.001*	0.048*	0.554
CS Visit 4	0.288	0.003*	0.234	0.867
CS Visit 5	0.203	0.006*	0.485	0.968
CS Visit 6	0.526	0.009*	0.923	0.584
MRt Pos 9 V1	0.007*	0.070	0.323	0.239
MRt Pos 9 V2	0.013*	0.091	0.324	0.266
MRt Pos 9 V5	0.019*	0.191	0.748	0.117
MRt Pos 9 V6	0.014*	0.100	0.827	0.081
Nas RNFL V4	0.233	0.004*	0.014*	0.575
Nas RNFL V6	0.373	0.009*	0.023*	0.311
Inf RNFL V1	0.016*	0.396	0.870	0.014*
Inf RNFL V2	0.008*	0.640	0.308	0.004*
Inf RNFL V3	0.000*	0.558	0.114	0.001*
Inf RNFL V4	0.010*	0.083	0.115	0.019*
Inf RNFL V5	0.013*	0.286	0.569	0.014*
Inf RNFL V6	0.017*	0.086	0.206	0.014*
Mean RNFL V2	0.004*	0.600	0.307	0.064
Mean RNFL V3	0.000*	0.797	0.068	0.021*
Mean RNFL V4	0.004*	0.255	0.584	0.113
Mean RNFL V5	0.013*	0.323	0.800	0.085
Mean RNFL V6	0.018*	0.095	0.574	0.066

Table 8.26 Summary of multiple regression analysis for all diabetic subjects * denotes statistical significance

8.6.5 Relationship between visual function and retinal anatomy

8.6.5.1 Retinal tissue and vision

Macular retinal thickness

Pearson product moment correlation revealed no relationship between macular retinal thickness at the fovea (position 1) and visual acuity (10% and 100%) and Pelli Robson contrast sensitivity.

Retinal nerve fibre layer thickness

Pearson product moment correlation revealed significant relationships between mean retinal nerve fibre layer thickness around the optic nerve head and visual acuity measures as summarised in table 8.27. Significant correlations were observed for visits 1,2,3,5,6 while a similar trend was noted for visit 4. Significant correlations were found between RNFL and 10% logMAR at visit 1 only.

Mean	100% logMAR		10% LogMAR		Contrast sensitivity (PR)	
RNFL	Pearson	Sig	Pearson	Sig	Pearson	Sig
Visit 1	-0.456	0.003*	-0.464	0.002*	-0.167	0.295
Visit 2	-0.478	0.002*	-0.398	0.010	0.132	0.412
Visit 3	-0.423	0.006*	-0.254	0.110	0.140	0.382
Visit 4	-0.321	0.041	-0.198	0.214	0.140	0.383
Visit 5	-0.440	0.004*	-0.296	0.060	0.125	0.437
Visit 6	-0.422	0.006*	-0.356	0.023	0.086	0.592

Table 8.27 Correlation between mean RNFL and vision * denotes statistical significance (p=0.00833 after Bonferroni correction)

8.6.5.2 Retinal nerve fibre layer thickness (ONH) and visual fields

Pearson product moment correlation revealed significant relationships between mean retinal nerve fibre layer thickness around the optic nerve head and visual field indices obtained with white-on-white perimetry. No significant correlations were found between mean RNFL and SWAP visual field indices. Results are summarised in tables 8.28.

	MD (dB)		PSD (dB)	
Mean RNFL	Pearson Corr	Significance	Pearson Corr	Significance
Visit 1	0.428	0.005*	-0.358	0.022
Visit 2	0.345	0.027	-0.432	0.005*
Visit 3	0.314	0.047	-0.314	0.046
Visit 4	0.436	0.004*	-0.352	0.024
Visit 5	0.459	0.003*	-0.324	0.039
Visit 6	0.475	0.002*	-0.238	0.134

Table 8.28 Correlation between mean RNFL and visual field indices (white-on-white perimetry) * denotes statistical significance (p=0.00833 after Bonferroni correction)

SWAP fields

Pearson product moment correlation revealed no significant correlations between mean RNFL and SWAP visual field indices. Results are summarised in tables 8.29.

	MD (dB)		PSD (dB)	
Mean RNFL	Pearson Corr	Significance	Pearson Corr	Significance
Visit 1	0.262	0.098	-0.244	0.125
Visit 2	0.201	0.207	-0.139	0.385
Visit 3	0.028	0.863	-0.051	0.751
Visit 4	0.142	0.376	-0.173	0.280
Visit 5	0.157	0.327	-0.173	0.280
Visit 6	0.152	0.342	-0.145	0.364

Table 8.29 Correlation between mean RNFL and visual field indices (SWAP perimetry)
* denotes statistical significance (p=0.00833 after Bonferroni correction)

8.6.6 Relationship between blood pressure and intraocular pressure

Systolic

Pearson product moment correlation revealed a statistically significant relationship between IOP and systolic blood pressure at visit 6 only (r=0.372, p=0.016). At no other visit was there evidence of a correlation.

Diastolic

Pearson product moment correlation revealed a statistically significant relationship between IOP and diastolic blood pressure at visit 6 only (r=0.322, p=0.040). At no other visit was there evidence of a correlation.

8.7 Discussion

This study showed for the first time acute changes in retinal structure and function associated with blood glucose fluctuation in diabetic patients. Previous studies have investigated changes in visual function with changes in blood glucose by chemical induction using insulin infusions (Harrad *et al.*, 1985; Ewing *et al*, 1998; Tabandeh *et al.*, 1996; Volbrecht *et al.*, 1994) or administration of glucose over a relatively short period of time (North *et al.*, 1997). In contrast, our study was over a far longer period of time and our patients did not alter their routine in terms of food consumption, medication type and dosage or exercise.

The fluctuation pattern of the majority of test parameters throughout the course of the day was the same for type 1 and type 2 diabetic patients. The only exceptions to this finding were for macular retinal thickness position 9, inferior RNFL thickness and mean RNFL where ANOVA identified statistically significant between-subject effects. However, separate ANOVA analysis for each group in terms of these test parameters identified no statistically significant differences between-visits.

The way in which each test parameter is affected by blood glucose over the course of the 12 hour period differs. Visual acuity 100% remains unchanged throughout the course of the day, while both reduced contrast visual acuity (10%) and Pelli-Robson contrast sensitivity are affected by variations in blood glucose levels. White-on-white perimetry indices show no variation over the six visits, while MD in SWAP fields shows a statistical difference between visits. This is likely to be explained by the process of selective sampling. Contrast sensitivity tests (10% and Pelli-Robson) and SWAP are all selective sampling devices and as such will detect more subtle effects. While this shows that these tests are effective at identifying subtle variations, it also

suggests that test results must be interpreted with caution in relation to the observations of disease progression.

The most marked fluctuations over the course of the study are exhibited by the intraocular pressure readings which fluctuate inversely with blood glucose levels. High levels of blood glucose are associated with low IOP and vice versa. This is also the case for diastolic blood pressure, mean arterial pressure and mean ocular perfusion pressure. Retinal nerve fibre layer thickness remains unaltered throughout the day despite changes in blood glucose levels. Retinal thickness measurements in position 1 only (fovea) exhibit statistically significant differences between particular visits.

Multiple simultaneous regression was performed to determine which diabetic status variable would predict each test parameter at every visit. The most dominant predictor variables varied for each test parameter and was not always consistent throughout the day.

8.7.1 Blood glucose variation

Observation of figure 8.2 indicates very little change in the blood glucose levels of the normal subject over the course of the day, while changes in the blood glucose levels of the diabetic patients are marked. ANOVA revealed statistically significant differences between the blood glucose variation of normals and both type 1 and 2 subjects. Glucose levels of both diabetic groups are higher overall than in normal subjects with greater fluctuations apparent over the course of the 12 hour study. In all diabetic subjects, as expected, baseline data (fasting) shows a low glucose level with an increase after breakfast (approximately 120 mins). Blood glucose levels fall approximately 240 mins (before lunch) and rise to a lesser extent after lunch. Another decrease at approximately 480 minutes just prior to tea is followed by a final increase in blood glucose following the patients final meal of the day. The graph would suggest that type 1 diabetics display even greater changes than type 2 diabetics when considering the peaks and troughs of their glucose levels. However, ANOVA revealed no statistical differences between type 1 and type 2 diabetics.

8.7.2 Relationship between blood glucose levels and haemoglobin

The range (i.e. minimum to maximum) of blood glucose levels differed between individual subjects. Those patients with poorer long term control indicated by a higher HbA1c may be expected to have a larger variation in blood glucose levels throughout the day. Figure 8.30 shows the relationship between long term and short term control. By observation, there appears to be a positive relationship between long and short term metabolic control. As HbA1c increases, the range of blood glucose measurements also increases.

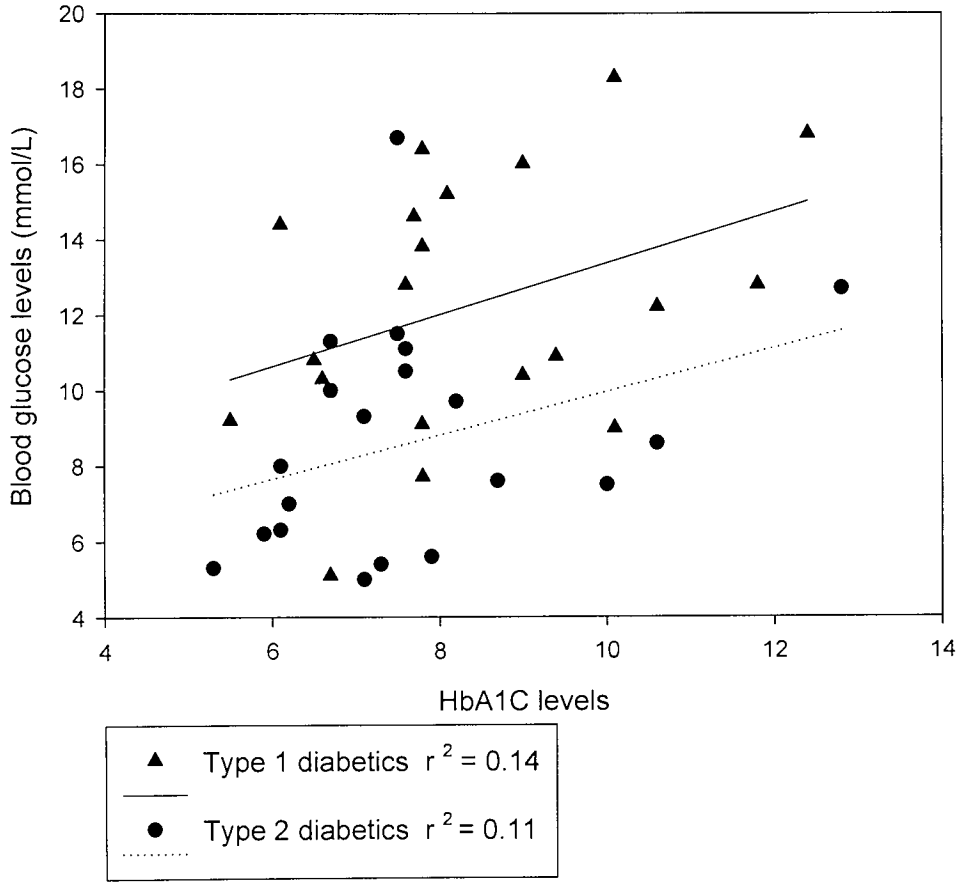

Figure 8.30 Graph to show the relationship between HbA1c levels and blood glucose range (Max-min) duirng a 12 hour period.

Pearson product-moment correlation was performed between HbA1c and the blood glucose range for all subjects. Analysis confirmed the graphical findings of a significant positive relationship between long and short term control ($r=0.409$; $p=0.008$).

8.7.3 Visual function variation

Visual symptoms in hypoglycaemia may be a consequence of metabolic disturbances in the visual pathways within the central nervous system or due to the impairment of the refractive status of the eye and binocular vision. Early reports suggested that visual symptoms experienced by the diabetic patient during a period of hypoglycaemia were related to changes in the eye (Duke-Elder, 1925).

Visual acuity

In our study 100% contrast visual acuity remained unchanged throughout the day despite there being fluctuations of blood glucose. This concurs with several studies who found no evidence of a relationship between glycaemic state and visual acuity. A number of investigators have reported no changes in visual acuity during acute episodes of low blood glucose levels in diabetic patients (Harrad *et al.*, 1985; McCrimmon, Deary, Huntly *et al.*, 1996). In a study of 5 insulin dependent diabetic subjects and 6 normal subjects, Harrad *et al.* (1985) measured corrected visual acuity during a stepwise induction of hypoglycaemia using insulin infusion. Visual acuity remained unchanged despite fluctuations in blood glucose. Similarly, Ewing *et al.* (1998) observed the effect of acute hypoglycaemia on the visual information processing in 16 type 1 diabetic subjects with no diabetic retinopathy and normal visual acuity (mean age 24 years; range 18-47 years). They reported no significant differences between distance or near snellen visual acuity in the hypoglycaemic (low blood glucose level) or euglycaemic (normal blood glucose level) state. Visual acuity, fusion and stereopsis remained unaffected by a decrease in blood glucose levels according to a study by Tabandeh *et al.* (1996) who investigated visual function in 10 normal subjects prior to, during and following an acute chemically induced state of hypoglycaemia.

Contrast sensitivity

There is considerable evidence to suggest that contrast sensitivity is affected by acute changes in blood glucose. An early study by Hyvarinen *et al.* (1983) suggested that contrast sensitivity fluctuates with blood glucose levels, with reductions in scores associated with hypoglycaemia. This is confirmed in a later study by Tabandeh *et al.* (1996) who investigated levels of visual acuity, contrast sensitivity and binocular status in 10 normal subjects prior to, during and following an acute chemically induced state

of hypoglycaemia. Visual acuity, fusion and stereopsis remained unaffected by the decrease in blood glucose levels. However, 80% of the subjects experienced a significant reduction in contrast sensitivity which was closely related to the decrease in blood sugar concentration. Tabandeh *et al.* (1996) concluded that visual symptoms were due to a shortage of glucose (neuroglycopenia) of the central visual pathways in the brain and not due to localized changes in the refractive elements of the eye itself. Verrotti and colleagues (1998) investigated the use of contrast sensitivity on diabetic patients to assess metabolic control and grade severity of diabetic retinopathy. They reported poor contrast sensitivity at high glucose levels, with normal contrast sensitivity levels at reduced blood glucose levels.

Ewing *et al.* (1998) observed the effect of acute hypoglycaemia on the visual information processing in 16 type 1 diabetic subjects with no diabetic retinopathy and normal visual acuity (mean age 24 years; range 18-47 years). Using insulin infusions, blood glucose levels were lowered and maintained at 2.6mmol/L during hypoglycaemia and at 5mmol/L during euglycaemia. Significant reductions were found in both general cognitive performance and visual information processing tasks when patients were in a hypoglycaemic state. Contrast sensitivity tended to deteriorate during hypoglycaemia although this failed to reach statistical significance ($p=0.06$). Such findings were consistent with an early study for normal subjects (McCrimmon *et al.*, 1996).

In our study, contrast sensitivity varies over the course of the day and significant differences were observed between visit 1 and visits 3, 4, 5, and 6 as well as between visit 2 and 5. There does not appear to be a particular relationship between blood glucose and contrast sensitivity, rather that it increases at each visit compared with the previous visit. Our results may be explained by the effect of learning, especially since most of the significant differences occur between visit 1 and subsequent visits. Nevertheless, according to our work and that of others, contrast sensitivity appears to be a more sensitive indicator of visual function than that of 100% contrast visual acuity.

Conversely, Banford *et al.* (1994) observed no correlation between blood glucose levels and contrast sensitivity at any spatial frequency measured. Trick *et al.* (1988) found no correlation between contrast sensitivity at any of the tested spatial frequencies and fasting blood glucose levels.

Colour vision

A number of investigators have attempted to explore the relationship between blood glucose levels and visual function, namely colour vision with conflicting results. Several reports suggest that variations in colour vision upon repeated testing may be explained by changes in the plasma glucose level of the diabetic patient (Lakowski *et al.*, 1972; Harrad *et al.*, 1985; Volbrecht *et al.*, 1994). In a study involving 5 diabetic patients and 6 healthy control subjects, Harrad *et al.* (1985) carried out colour vision testing using the FM 100-hue test at three different blood glucose levels. A general reduction in colour vision performance across all wavelengths was observed as glucose levels decreased suggesting that fluctuations in short-wavelength sensitivity may be attributable to fluctuations in blood glucose levels across test sessions.

A later study by Volbrecht *et al.* (1994) investigated the relationship between blood glucose level and colour sensitivity in 18 diabetic patients of which there were 5 type 1 patients and 13 type 2 (mean age 46 years; mean duration of the disease 8.6 years). Patients were subjected to acute rapid changes in blood glucose over a period of up to 2 hours. After insulin administration, blood glucose and threshold measurements were taken at 10, 20, 30, 45, 69, 90 and 120 mins. Medium and long wavelength sensitivity showed no change with a rapid drop in blood glucose when comparing the highest and lowest glucose levels. However, with an acute decrease in blood glucose levels there is an increase in short wavelength sensitivity. It is not clear in this study how sensitivity changed with repeated measures during the 2 hour study period. The authors conclude that such acute and reversible changes may be directly related to the transient metabolic state of diabetes and immediately linked to diabetic blood glucose levels rather than to structural loss of vascular or neural tissues. Their findings do not concur with earlier reports suggesting that lens changes or photoreceptor loss is responsible for SWS sensitivity loss since these procedures are not reversible.

Hardy *et al.* (1995) tested the hypothesis that changes in blood glucose are responsible for visual pathway abnormalities of the insulin diabetic patient, by measuring colour vision with the 100-hue test in a group of 10 subjects with no diabetic retinopathy (mean age 28 years; mean duration 9 years). On three individual occasions, separated by at least seven days, either hyperglycaemia (14mmol/L), hypoglycaemia (2.5mmol/L) or euglycaemia (5mmol/L) in random order was induced following a stable period of

euglycaemia. Mean error score in the hypoglycaemic, euglycaemic and hyperglycaemic states were 34±22, 35±33, and 39±28 respectively. The authors concluded that short term changes of 1-2 hours in plasma glucose levels had no effect on colour vision. Similarly, Trick *et al.* (1988) observed no significant correlation between hue discrimination scores and the fasting blood glucose level of their diabetic patients.

Hyperglycaemia has no influence on colour vision (as measured by the Desaturated D15 test) according to a study by North *et al.* (1997) who tested 16 subjects with non-insulin diabetes (mean age 59.8±7.5 years; mean duration 4.7±7.5 6.9 years). Colour vision and blood glucose levels were monitored every 30 minutes over a 4 hour period during three different test conditions: a meal tolerance test (MTT) in which glucose is administered orally, an intravenous glucose intolerance test whereby an intravenous infusion of glucose was administered or prolonged fasting during which time the blood glucose levels were relatively stable. The total error score did not vary significantly between the three test conditions. Over the course of the test periods, colour vision did fluctuate but exhibited no consistent trend. However, there was no significant difference observed between test scores for the same subjects when subjected to the MTT and fasting conditions. There was no evidence of a relationship between the change in blood glucose level and the change in total error scores.

Visual fields

In our study there were no significant changes between visits in the MD or PSD of the white-on-white fields for all subjects. Observation of change over the day also appeared to show little fluctuation for visual field indices of SWAP fields. However, while PSD showed no statistical difference bewteen visits, MD exhibited a statistically significant difference between visits 4 and 6. This appears to suggest that SWAP testing is a more senstive functional test in diabetic patients than conventional periemtry which supports the findings of several investigators. Short-wavelength sensitive (SWS) cone mediated mechanisms are reported to be susceptible to damage in diabetic retinopathy (Greenstein *et al.*, 1989; Greenstein *et al.*, 1990; Nomura *et al.*, 2000).

Afrashi *et al.* (2003) compared white-on-white perimetric parameters with SWAP perimetric parameters in a group of 43 type 1 diabetic patients without diabetic

retinopathy and visual acuity of 6/6 (mean age 31.03±5.2 years) and 30 normal subjects. They found that achromatic visual indices (MD, SF, PSD and CPSD) were similar between the diabetic subjects and their control subjects. SWAP SF, PSD and CPSD values were also similar between groups. However, the blue-on-yellow perimetry MD score was significantly different between groups (p=0.001). Mean MD for the diabetic group was -5.23±3.67dB and -1.18±2.40dB for the normal subjects. The authors suggest that SWAP perimetry reveals the loss of S cone sensitivity and as such has the potential to detect early reductions in visual function in pre-clinical diabetes in the absence of retinopathy and be used in the follow up of such patients.

8.7.4 Retinal thickness and retinal nerve fibre layer thickness variation

Retinal nerve fibre layer thickness around the optic nerve head in all quadrants and mean RNFL does not vary despite fluctuations in blood glucose. In all macular retinal locations except the fovea (position 1) there is no evidence of a relationship between blood glucose and retinal thickness. Statistically significant differences between visits occurred only between visit 1 and 2, 4, and 5. Our findings may be explained by patient fixation losses at the beginning of the day, when the patient has no experience of retinal imaging. As the day progresses the patient is likely to exhibit learning effects. To our knowledge there are no published reports regarding the effects of acute changes in blood glucose on retinal structure.

8.7.5 IOP variation

There appears to be an inverse relationship between blood glucose and IOP according to our findings. As blood glucose reached a peak the IOP was at its lowest and vice versa. This would appear to disagree with the results of a number of studies where acute hypoglycaemia has been shown to provoke a reduction in intraocular pressure both in patients with insulin diabetes (Frier, Hepburn, Fisher *et al.*, 1987) and in normal subjects (Hepburn, Fisher, Thomson *et al.*, 1991). The relationship between diabetes and IOP is unclear. Studies regarding the effect of blood glucose on IOP are also inconsistent. Mitchell *et al.* (1997) suggest that increases in blood glucose levels lead to an induction of an osmotic gradient with a subsequent movement of fluid into the

intraocular space, resulting in an increase in IOP. Conversely, Dielemans *et al.* (1994) suggest that the reverse is true, with an increase in blood glucose giving rise to a reduction in IOP due to a fluid shift out of the intraocular compartment.

Difficulities in interpreting study results stem from the fact that IOP in all subjects, regardless of metabolic factors or disease, exhibits changes throughout the day. In the normal eye IOP exhibits a period of elevation above the mean mid-morning-approximately 11am and a depression mid-afternoon-approximately 3pm (Pointer, 1997). Aqueous humour production also varies according to a circadian rhythm with lower rates of secretion occurring during the night and higher rates during the day (Cole, 1977; Reiss, Lee, Topper *et al.*, 1984).

Studies have shown that aqueous humour is subject to alterations in the diabetic eye. Decreased aqueous humour flow rates have been observed in type 1 diabetic patients (Hayashi, Yablonski, Boxrud *et al.*, 1989; Larsson, Pach, and Brubaker, 1995) although this is not the case for type 2 diabetics (Larsson *et al.*, 1995). There is also evidence that blood flow increases are related to increases in insulin and glucose concentrations (Schmetterer, Muller, Fasching *et al.*, 1997; Bursell, Clermont, Kinsley *et al.*, 1996; Luksch, Polak, Matulla *et al.*, 2001). Since blood flow clearly plays a role in the production of aqueous humour, any increase in blood flow may provoke a similar increase in aqueous flow. In the first study of its kind, Lane, Toris, Nakhle *et al.* (2001) investigated whether this reduced flow is the result of the diabetic state or alterations in glucose or insulin concentrations in a sample of 11 type 1 diabetic patients and 17 control subjects. Subjects in their study were well matched for age, body mass index, gender and degree of insulin sensitivity and unlike previous work, glucose and insulin concentrations were controlled for. Aqueous flow was measured for all subjects at different insulin concentrations. Controls were studied during fasting concentrations with no intravenous insulin infusion and during a hyperinsulinemic-euglycaemic glucose clamp. Diabetic patients were studied under low and high insulin states. A reduction in aqueous flow was observed for type 1 diabetic patients compared with normal controls under both low and high insulin concentrations, despite the lack of significant changes in intraocular pressure or ocular blood flow.

8.7.6 Blood pressure variation

Systolic blood pressure is unaffected by blood glucose variations, while diastolic pressure, mean arterial pressure (MAP) and ocular perfusion pressure (OPP) undergo changes throughout the day. Graphical observations appear to suggest that diastolic blood pressure exhibits an inverse relationship with blood glucose. This is also true for MAP and OPP. Drawing conclusions about the relationship between blood glucose and measures of blood pressure are confounded by the existence of the normal variation in the blood pressure of normal subjects, in the same way as differentiating between normal and causative IOP variations are. Positive associations between systolic and diastolic blood pressure and IOP have been reported (Tielsch *et al.*, 1995; Bonomi, Marchini, Marraffa *et al.*, 2000). The mechanism between blood pressure and IOP is unclear but is thought to be the result of increased aqueous production by means of an elevation in ciliary artery pressure associated with an increase in systemic blood pressure (Bulpitt, Hodes and Everitt, 1975; Shiose and Kawase, 1986).

Blood pressure exhibits a circadian pattern of variation throughout the day. Systolic blood pressure rises rapidly by 20-25mmHg upon waking while diastolic pressure is subject to an increase of 10-15mmHg. Both systolic and diastolic pressures are highest in the late afternoon, decreasing in the evening and are at their minimum levels during sleep. Blood pressure fluctuations are governed by variations in physical and mental activity, stress and postural changes (Gherghel, Hosking and Orgul, 2004). The pattern of change that we observed cannot be explained by the diurnal variation alone. The reasons for an inverse relationhip between blood glucose and blood pressure are unclear at this stage.

8.7.7 Predictive factors

Multiple simultaneous regression was performed to determine which diabetic status variable would predict each test parameter at every visit. Predictor variables included type of diabetes, haemoglobin levels, glucose level and duration of diabetes. Analysis revealed the extent to which the variance of each test parameter was explained by each of the independent variables. The model was only significant for some of the test

parameters and with the exception of the inferior retinal nerve fibre layer predictions proved to be inconsistent throughout the day.

Haemoglobin was the best predictor of contrast sensitivity scores at visits 1, 2, 3 and 4 where the regression model was significant. Contrast sensitivity scores at visits 5 and 6 followed this same trend although the model just failed to reach statistical significance. Our findings agree with Banford *et al.* (1994) who reported a negative correlation between HbA1c and contrast sensitivity at 6 and 12 cyc/deg. However, the subject of a relationship between contrast sensitivity and long term control is controversial. Trick *et al.* (1998) found no relationship between contrast sensitivity and haemoglobin levels. They did however observe an inverse correlation between hue discrimination deficits and patients' glycosylated haemoglobin (HbA1) levels. Others found no correlation between colour vision and haemoglobin levels (Roy *et al.*, 1986; Hardy *et al.*, 1995). This appears to be confirmed by Banford *et al.* (1994) who found no significant correlation between haemoglobin and colour vision scores on the D15 or desaturated D15 in a group of young type 1 diabetics. Differences in findings may be explained by the differences in subject samples, presence of diabetic retinopathy and duration of the disease. Nasal quadrant retinal nerve fibre layer thickness around the optic nerve head at visits 4 and 6 was best predicted by the haemoglobin level and to a lesser degree by the glucose level at that particular visit.

Inferior retinal nerve fibre layer around the optic nerve head exhibited the most consistent results over the course of the day for each visit. For every visit, measures were best predicted by the type of diabetes followed by the duration of the disease. Finally, the type of diabetes was the best predictor of mean RNFL for visits 2,3,4,5 and 6 with duration also contributing to mean RNFL measurement at visit 3. The type of diabetes (1 or 2) was also the best predictor of macular retinal thickness at position 9 for visits 1, 2, 5 and 6.

The impact of duration on deficits of visual function has been investigated with regard to contrast sensitivity and colour vision only. Sokol *et al.* (1985) found that diabetic patients with background retinopathy and abnormal contrast sensitivity has the longest mean duration (17 years) while patients with no retinopathy and normal contrast sensitivity has the shortest mean duration of diabetes (9 years). Those with either

retinopathy or abnormal contrast sensitivity had duration of 14 years. Ismail and Whitaker (1998) calculated from their study of 74 non-insulin diabetics, that a 10 year increase in the duration of diabetes is likely to result in a change of contrast sensitivity of only about one letter on the Pelli-Robson chart. They report that the error scores of the 100-Hue colour test do not correlate well with duration of diabetes. Trick *et al.* (1988) in a group of 57 diabetic patients with little or minimal retinopathy, found a negative correlation between contrast sensitivity at 6.0cyc/deg and the duration of diabetes. However, they observed no relationship between hue discrimination scores and duration.

8.7.8 Correlation analysis

8.7.8.1 Macular retinal thickness and vision

No significant relationships between macular retinal thickness at the fovea (position 1) and visual acuity (10% and 100% contrast) and Pelli-Robson contrast sensitivity were observed for any visit.

8.7.8.2 Retinal nerve fibre layer thickness and vision

Statistically significant relationships between mean retinal nerve fibre layer thickness around the optic nerve head and 100% contrast logMAR visual acuity were observed for visits 1,2,3,5,6. This trend was also observed at visit 4 although the correlation failed to reach significance. A significant correlation between 10% logMAR visual acuity was observed for visit 1 only. There was no evidence of a relationship at all other visits.

There was no evidence of a correlation between contrast sensitivity scores using Pelli-Robson and retinal nerve fibre layer thicknes around the optic nerve head at any visit.

8.7.8.3 Retinal nerve fibre layer thickness (ONH) and visual fields

Statistically significant correlations between mean retinal nerve fibre layer thickness around the optic nerve head and MD (white-on-white perimetry) were observed for visits 1,4,5 and 6. This trend was also apparent for visits 2 and 3 although the correlation failed to reach significance after Bonferroni correction ($p=0.00833$).

No significant correlations were found between mean RNFL and SWAP visual field indices.

8.7.8.4 Blood pressure and intraocular pressure

Statistically significant relationships between IOP and systolic and diastolic blood pressure were observed only at visit 6. At no other visit was there evidence of a correlation.

8.7.9 Correlations of functional loss with degree of diabetic retinopathy

8.7.9.1 Colour vision

Reports concerning the relationship between colour defects and the level of diabetic retinopathy provide conflicting evidence. Several authors conclude that no such correlation exists (Moloney and Drury 1982; Roy *et al.*, 1986; Greenstein *et al.*, 1990). This is disputed by Green *et al.* (1985) who observed that the prevalence of significant colour deficiencies increased from 32% in diabetics with no retinopathy to 35% in diabetics with background diabetic changes. Similarly, Bresnick *et al.* (1985) noted that 41% of patients with pre-proliferative changes exhibited scores that fell outside tha 95th percentile of normal values on the 100-hue test. Trick *et al.* (1988) reported significant reductions in hue discrimination in 18.9% of diabetic patients with no retinopathy and 25.0% of those with mild-moderate background retinopathy. Ismail and Whitaker (1998) also found an increase in the Farnsworth-Munsell 100-hue error score with an increase in the retinopathy progression.

8.7.9.2 Visual acuity

Ismail and Whitaker (1998) found no significant difference in visual acuity levels between their aged matched control group, NIDDM patients with no retinopathy, and NIDDM patients with early background diabetic changes. Visual acuity in the group of NIDDM patients with proliferative retinopathy however, was significantly different to that of the other subjects.

8.7.9.3 Contrast sensitivity

The use of routine contrast sensitivity testing lead to suggestions by some authors that a relationship may exist between deficits in contrast sensitivity and the severity of diabetic retinopathy, although results were not always consistent. An early report by Arden and Jacobson (1978) suggested that normal subjects and diabetic patients without retinopathy exhibited no differences in terms of their contrast sensitivity scores, while diabetic patients with background retinopathy had abnormal contrast sensitivity at all spatial frequencies. In the same way, Ghafour *et al.* (1982) found that diabetic patients with background retinopathy had reduced contrast sensitivity. However, they also reported abnormal contrast sensitivity scores in patients without retinopathy at specific spatial frequencies. Hyvarinen *et al.* (1983) reported abnormal contrast sensitivity in patients with normal visual acuity (6/6 Snellen) and background retinopathy. In a later study, Sokol *et al.* (1985) observed that insulin dependent diabetic subjects aged between 8 and 22 years (n=31) with good visual acuity and no retinopathy exhibited normal contrast sensitivity, while patients with non-insulin diabetes aged between 18 to 67 years (n=33), good visual acuity and no retinopathy exhibited abnormal contrast sensitivity only at high spatial frequencies. Non-insulin diabetic patients with good visual acuity and background retinopathy had abnormal contrast sensitivity at all tested spatial frequencies. Trick *et al.* (1988) reported significant reductions in contrast sensitivity at mid-to-high spatial frequencies in 24.3% of diabetic patients with no retinopathy and 45.0 % of patients with mild to moderate background retinopathy. Della Sala *et al.* (1985) observed contrast sensitivity reductions in 41% of diabetics with no retinopathy (n=22) and 30% diabetics with background retinopathy (n=20). Changes to low-to-medium spatial frequencies have also been documented (Brinchmann-Hansen, Bangstad, Hultgren *et al.*, 1993). In a later study by Ismail and Whitaker (1998) using the Pelli-Robson chart, contrast sensitivity was found be inversely related to the extent of diabetic retinopathy. They found that while the test was able to distinguish non-diabetic patients from early diabetic groups, it was relatively insensitive to the degree of diabetic retinopathy i.e. the test was unable to reliably distinguish between diabetics without retinopathy from those with. Apparent discrepancies in reported findings may be explained by differences in methods and, more likely, in sample groups.

8.8 Conclusion

Foveal retinal thickness, reduced contrast logMAR acuity, Pelli-Robson contrast sensitivity and SWAP visual fields exhibited changes throughout the day while 100% logMAR vision, retinal nerve fibre layer thickness, retinal thickness (except foveal thickness) and white-on-white perimetry was unaffected by fluctuations in blood glucose. Contrast sensitivity scores can be predicted by long-term metabolic control as indicated by HbA1c levels. Inferior RNFL can be predicted by type and duration of diabetes, while mean RNFL can be predicted according to diabetes type.

8.9 Future work

A recommendation for future work would be to explore the relationship between the degree of retinopathy and the visual function of the diabetic patient. Fundus images will be independently assessed in a masked experiment by a collaborating ophthalmologist and graded according to the EDTRS guidelines.

CHAPTER 9: Anatomical and functional changes in the visual cortex of patients with glaucoma: A pilot study and case discussions

9.1 Abstract

Purpose: To study the relationship between visual function as derived by subjective visual field examination and objective cortical responses, and anatomy of the visual pathway from retinal ganglion cells and their fibres to cortical cell distribution.
Methods: Study participants comprised a control group of 6 normal subjects (mean age 41.5±9.1years; range 28-49years) and a group of 4 patients diagnosed with primary open angle glaucoma (POAG) (mean age 59.0±5.6 years; range 52-64 years). Optical Coherence Tomography (OCT) fast optical disc scans consisting of six radial lines (4mm in length) arranged in a spoke-like pattern centred on the optic disc, were performed to obtain optic nerve head measurements for all study participants. Retinal nerve fibre layer thickness (RNFLt) was assessed using a series of OCT circular scans centered on the optic disc, scanning around the optic disc margin. Measurements of RNFLt were taken close to the optic disc margin and at two further locations at increasing distance from the optic disc margin using circle scan radii specific to each subject. Visual fields were assessed using the Humphrey Visual Field Analyser (program 24-2) and retrobulbar optic nerve diameter was measured by ultrasound was obtained for each subject. Anatomical and functional magnetic resonance imaging (MRI) scans were performed using the Siemens Trio 3T Scanner to assess the density of grey matter in the visual cortex and the cortical activation response to a series of visual stimuli for each group. For each group, correlation between anatomical structures was assessed using Pearsons correlation coefficient. In the same way functional data was assessed for each group. Differences between groups in terms of anatomical structure and cortical response were assessed using analysis of variance (ANOVA). Grey matter density for all subjects was compared to a normal database (n=80).
Results: This study showed a significant positive correlation between rim area and RNFLt ($p=0.000$), and negative correlation between rim area and PSD ($p=0.021$). There was also a strong negative correlation between PSD and retrobulbar optic nerve diameter in all positions measured ($p<0.05$). Grey matter density reduced with age at a rate of 3.85% per decade, but did not appear to be exacerbated in the glaucoma patients. Binocular cortical activation measured by MRI was highly correlated with both rim area ($p=0.009$) and PSD ($p=0.057$).
Conclusion Rim area and retrobulbar optic nerve diameter but not RNFLt were strong indicators of glaucomatous visual field loss. Glaucoma damage did not appear to result in cortical grey matter loss in excess of that expected due to ageing, however, cortical activation as measured by fMRI was a strong indicator of functional damage due to glaucoma.

9.2 Introduction

Primary open angle glaucoma (POAG) is a chronic, slowly progressive, multifactorial and usually bilateral, though not necessarily symmetrical, optic neuropathy. The glaucomatous eye undergoes a number of well documented pathological changes including retinal nerve fibre loss and optic nerve head damage which is correlated with loss of functional vision (Pieroth *et al.*, 1999; Schuman *et al.*, 1995; Zangwill *et al.*, 2000; Kanamori *et al.*, 2003; Tuulonen and Airaksen, 1991; Jonas *et al.*, 1989, 1993). Retrobulbar optic nerve diameter has also been found to be reduced in glaucoma (Dichtl and Jonas, 1996; Beatty *et al.*, 1998c) while a significant and positive correlation between retrobulbar and optic nerve dimensions has been reported (Beatty *et al.*, 1998a). To our knowledge there have been no studies investigating the relationship between retrobulbar optic nerve diameter and visual function.

There is well documented evidence that glaucomatous damage extends from retinal ganglion cells in the eye, along the visual pathway, to vision centres in the brain. Several experimental glaucoma studies have reported a significant loss of lateral geniculate nucleus relay neurons terminating in the primary visual cortex in both the magnocellular and parvocellular layers (Dandona *et al.*, 1991; Chaturvedi *et al.*, 1993; Crawford, Harwerth, Smith *et al.*, 2000; Weber *et al.*, 2000; Yucel *et al.*, 2000; Yucel, Zhang, Weinreb *et al.*, 2001, 2003). A later study by Yucel *et al.* (2001) suggest that relay neurons in the LGN undergo significant shrinkage in glaucoma, the effect of which is more pronounced for neurons in parvocellular layers compared with neurons in LGN magnocellular layers. MRI studies have shown that glaucoma affects the anterior visual pathway of human subjects at least up to the optic chiasm and these changes in the anterior visual pathway are correlated with glaucomatous optic nerve damage (Kashiwagi *et al.*, 2004).

Andrews *et al.* (1997) using a series of morphometic and cytoarchitectonic techniques, suggest that amongst normal human brains there is a wide variation in sizes of the optic tract, lateral geniculate nucleus (LGN) and the primary visual cortex. The authors also report the existence of a relationship between the dimensions of the human visual system amongst the normal population whereby a large visual cortex is associated with a large LGN and optic tract and vice versa.

Such a variation in the normal structure of eyes must be considered before conclusions can be accurately drawn from studies involving diseased eyes, namely glaucoma. While several studies have investigated the differences between the structure of the eye in glaucomatous and normal eyes and others the effect of disease on visual function, this study aims to investigate both the relationship between the anatomical structure of the visual pathway from retinal nerve fibre layer, along the optic nerve at retinal and retrobulbar level to the grey matter in the visual cortex and its relationship with visual function in normal and diseased eyes. It aims to determine and quantify the changes that occur along the entire visual pathway from eye to the brain in patients diagnosed with glaucoma. This will lead to a greater understanding of the nature of visual loss in glaucoma which in turn has important implications for the detection and treatment of glaucoma.

Although it is beyond the scope of a single thesis to conduct this investigation in its entirety, preliminary results using our methodology are presented and the findings of pilot data and case discussions.

9.3 Aims and Objectives

The aim of this study is to explore the relationship between visual function, cortical responses, and anatomy of the visual pathway in normal and diseased eyes. Key objectives are:

1. To determine a methodology by which to investigate structural and functional changes in the cortex of patients with glaucoma.
2. To present pilot data demonstrating structural and functional losses resulting from glaucomatous optic neuropathy which exceed those typically associated with normal ageing.

9.3.1 Hypotheses

1. fMRI can be used to measure objectively and *in vivo*, structural and functional cortical changes.
2. Structural and functional losses are evident in the cortex of patients with established glaucoma.

3. Structural cortical changes lag behind measurable fibre loss in the anterior optic nerve.

9.4 Study sample and investigations

9.4.1 Inclusion criteria

Prior to recruitment, a magnetic resonance imaging (MRI) information sheet and a detailed initial screening form was sent to each patient. The first screening form served to identify and eliminate at-risk individuals as part of the recruitment procedure. The second screening form was presented on the day of the scan to ensure that scanning was safe at the time of the scan. Both forms were completed on the study day before scanning in the presence of the MRI operator. In this way, patients had the opportunity to ask any questions and the MRI operator could confirm that the patients were suitable for scanning. All subjects and patients were subjected to a clinical eye examination to assess their fitness to participate in the study based on the following criteria.

9.4.2 Normal subjects

Normal healthy subjects were recruited from staff in the Vision Sciences Department, Aston University, staff at Aston Academy of Life Sciences, Aston University and attendees at the Optometry Clinic at Aston University. A full eye examination was carried at by an optometrist (HLW) to establish whether the study inclusion criteria were met. Subjects were included if they exhibited:

- No abnormalities on ophthalmoscopic examination
- Minimal or no lens opacities allowing a clear fundus view
- No history or evidence of intraocular surgery or laser therapy
- No history or evidence of retinal pathology or glaucoma
- Snellen visual acuity (VA) 6/9 or better
- Less than 6 dioptres of spherical ametropia and 2 dioptres of astigmatism
- Absence of visual field defects (Humphrey Visual Field Analyser program 24-2)

- Intraocular pressure (IOP) less than 21mmHg (Non-contact tonometry-Pulsair 3000)

9.4.3 Glaucoma patients

Glaucoma patients were recruited by a consultant ophthalmic surgeon (SV) and had therefore been previously diagnosed with primary open angle glaucoma (POAG) at the time of the study. They were included if they exhibited:

- Confirmed optic nerve head cupping consistent with glaucomatous changes:
  Notching (focal extension of the cup)
  Focal or generalised narrowing or disappearance of the neuro-retinal rim
  Pallor of the neuro-retinal rim
  Cup:Disc (C:D) asymmetry >0.2
  AND/OR:
- Repeatable moderate visual field defect consistent with glaucoma and as defined by Hodapp and Parrish (1993), assessed using the Humphrey Visual Field Analyser with the central 24-2 full threshold standard test program
  AS WELL AS:
- Snellen visual acuity (VA) 6/12 or better
- Less than 6 dioptres of spherical ametropia and 2 dioptres of astigmatism
- IOP>21 mmHg on at least two occasions (as part of their diagnosis prior to treatment)
- No other ocular disease evident by indirect binocular ophthalmoscopy

9.5 MRI exclusion criteria

Strict exclusion criteria for MRI scanning exists and careful screening of study participants was required. Patients were excluded if there was a possibility that they may be pregnant, wore a hearing aid or if they had:

- been fitted with a pacemaker, artificial heart valve, cochlear implant or any other implanted device

- any surgical clips, aneurysm clips, shunts or stents in their body
- any metal fragments in their eyes
- any metal fragments, e.g. shrapnel in any other part of their body
- any surgically implanted metal in any part of their body (e.g. joint replacement or bone reconstruction).
- any surgery that might have involved metal implants of which they were not aware
- been sterilised using clips
- ever suffered from any of: epilepsy, diabetes or thermoregulatory problems
- ever suffered from any heart disease
- any permanent eye makeup
- any tattoos
- any dental work (including dentures, crowns, bridgework, braces) in their mouth, other than simple fillings

9.5.1 Other exclusion criteria

Due to the close confines of the MRI scanner, patients suffering with claustrophobia did not take part in the study.

9.5.2 Subject sample

Group 1 comprised 6 normal subjects (mean age 41.5±9.1years; range 28-49 years). Group 2 consisted of 4 patients diagnosed with primary open angle glaucoma (POAG) (mean age 59.0±5.6 years; range 52-64 years). For each study participant data was collected for both the R and L eyes.

9.5.3 Ethical approval and informed consent

Ethical approval was obtained from the ethical committee boards of Aston University. Approval conformed to the tenets of the Declaration of Helsinki. Written informed consent was obtained from all volunteers.

9.6 Methods

Subjects were required to visit Aston Academy of Life Sciences on one occasion to undergo all testing procedures.

9.6.1 Visual acuity testing

All vision testing was performed using the Test Chart 2000 ^{PRO} - (Thomson Software Solutions version 2.3.04). LogMAR 100% and 10% were recorded at the beginning of the test run.

9.6.2 Visual field testing

Visual fields were assessed for the right and left eyes of each participant using the Humphrey Visual Field Analyser program 24-2.

9.6.3 Optical coherence tomography

The Stratus OCT was used to scan the macular, optic nerve head and retinal nerve fibre layer around the optic nerve head for each subject. The patient was instructed to fixate the green light placed at the centre of the camera view (macular imaging) or the periphery of the camera view (optic disc imaging and retinal nerve fibre layer imaging).

9.6.4 Optic disc scan acquisition

The fast optical disc scanning protocol carried out to obtain optic nerve head measurements for all subjects. This scan consists of six radial lines (4mm in length) arranged in a spoke-like pattern centred on the optic nerve head. The OCT interpolates between the scans to provide measurements of the optic nerve head. Optic nerve head analysis results combines the analysis and measurement of each individual scan to give vertical integrated rim area (volume), horizontal integrated rim width (area), disc area, cup area, rim area, cup:disc area ratio, cup:disc horizontal ratio and cup:disc vertical ratio.

9.6.5 Retinal nerve fibre layer thickness scan acquisition

The fast retinal nerve fibre layer thickness protocol was carried out to obtain RNFL measurements around the optic nerve head. The scan position was altered manually using the cursor to best fit around the optic disc. The fast RNFL scan protocol consists of 3 consecutive 360-degreee circular scans with a diameter of 3.4mm each containing 256 A-scans taken automatically in a single session of 1.92 seconds. A mean image was automatically created by the OCT software. Seven fast thickness scans were taken in total and the results of the five best scans were averaged.

OCT software generates an output displaying average RNFL thickness measurements for the overall 360 degree scan, 12 clock hour sectors and for each of the superior, nasal, inferior and temporal quadrants.

9.6.6 Non contact tonometry

Measurements of IOP were acquired using the Keeler Pulsair 3000. Four readings for each eye were taken and automatically averaged by the device.

9.6.7 Ultrasound imaging

The retrobulbar optic nerve was imaged using the 8v5 transducer probe of the Siemens Seqoiua. With each patient in the supine position, the transducer was applied gently to the closed eyelid. An example of the scan and the use of calipers to measure optic nerve width and different distances from the globe (5,10 and 15mm) can be seen in figure 9.1.

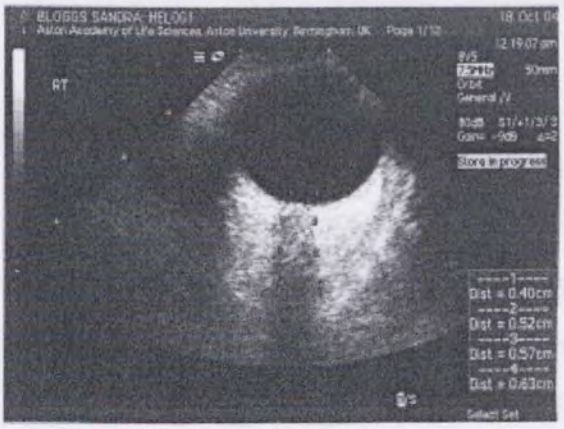

Figure 9.1 Example of an orbit and retrobulbar optic nerve scan using ultrasound technology

9.7 MRI scanning

Before entering the MRI suite, subjects and operators were required to remove all metal from their pockets (coins, keys), remove articles of clothing which have metal fasteners (belts, bras, etc) jewellery and place watches and credit cards in the lockers provided. Prior to the day of study patients had been instructed to wear clothing without metal fastenings, e.g belts, zips or to provide alternative clothing to wear during MRI scanning.

9.7.1 MRI data acquisition

The Siemens Trio 3T Scanner was used to collect all anatomical and functional MRI data. A standard birdcage quadrature RF coil was used to both transmit and receive the radiofrequency signal.

All participants were required to lie on their backs on a narrow bed on runners, which was moved fully into the magnet during data acquisition. The MRI coil was placed over the patient's head and they were instructed to keep their head as still as possible during scanning, helped by padded headrest. All subjects were required to wear ear-plugs and sound-attenuating headphones to reduce the level of noise generated during the scanning process. Subjects and operators were able to talk via an intercom system and

if the patient felt unable to continue with the scanning procedure for any reason they could alert MRI staff by activating a hand held alarm.

Visual stimuli were presented to the participant in the scanner using an LCD projector (Sanyo XP41) located in the rear equipment room, which projects through a custom waveguide onto a projection screen located in the rear of the magnet bore, effectively behind the patient's head. Subjects viewed all visual stimuli via a small mirror placed just above their eyes. The full stimulus subtended a circular patch of approximately 30 degrees diameter. Throughout the scanning process participants were instructed to look at the central fixation target.

Anatomical MRI data acquisition

For each participant, a high-quality MRI scan was acquired of the whole brain using a Magnetization Prepared rApid Gradient Echo (MP-RAGE) sequence with 1mm isotropic voxels and excellent grey-white matter contrast.

Functional MRI data acquisition

Retinotopic mapping stimuli was generated using software written by a colleague, MRI scientist (KDS) using a Macintosh computer. The stimulus consisted of a wedge containing a checkerboard pattern flickering at 8Hz, subtending 80 degrees of visual polar angle and extending to 15 degrees eccentricity. The wedge rotated slowly around a central fixation point. A test run comprised 4 complete rotations lasting 216 seconds in total. As the wedge rotated, areas of visual cortex that were being retinotopically mapped showed a rise and fall of activation at a fundamental frequency of 1/54 Hz. The magnitude of the signal at 1/54Hz represents the amount of retinotopic signal in each voxel, whilst the phase of the 1/54Hz signal indicates the polar angle in visual space that the voxel is sensitive to.

Functional images consisted of gradient-echo echo-planar (EPI) sequences made up of 50 slices placed axially throughout the entire brain. The slices each measuring 3mm in width, had a 64x64 matrix, 192 mm field-of-view and were acquired in an interleaved fashion with no inter-slice gap. The acquired isotropic voxels measured 3x3x3mm. A

repetition time (TR) of 3 seconds was employed, creating a functional volume output every 3 seconds during retinotopic mapping stimulus presentation. The echo time (TE) was 30 milliseconds and the flip-angle was 90 degrees. Seventy two functional volumes were collected during each test run (of 216 seconds).

MRI data was acquired monocularly and binocularly. Six runs were performed on each participant. In order to cancel out the unknown haemodynamic delay from subsequent analyses, clockwise and anticlockwise stimulus runs are conducted as follows:

1. Left eye monocular viewing, checkerboard wedge pattern stimulus rotating anticlockwise.
2. Right eye monocular viewing, stimulus rotating anticlockwise.
3. Binocular viewing, stimulus rotating anticlockwise.
4. Left eye monocular viewing, stimulus rotating clockwise.
5. Right eye monocular viewing, stimulus rotating clockwise.
6. Binocular viewing, stimulus rotating clockwise.

9.8 Data analysis

9.8.1 Optical coherence tomography

The average of five scans was calculated for the retinal nerve fibre layer thickness scans and the fast optic disc scan of each participant.

9.8.2 Ultrasound imaging

Seven images were acquired and saved. The five best images i.e. those with the most clearly demarcated optic nerve dimensions were used for analysis. Using a series of cursors the optic nerve width was measured at the globe and at three further distances from the globe at 5mm intervals.

9.8.3 Anatomical MRI analysis

Anatomical MRI data for each study participant was segmented into different tissue types: grey matter, white matter, cerebrospinal fluid using the FAST software tool and the density of grey matter within the right occipital lobe, left occipital lobe and total visual cortex calculated.

9.8.4 Functional MRI data analysis

In order to increase the signal-to-noise ratio and cancel phase-delays due to the slow haemodynamic response the clockwise and anti-clockwise runs were averaged during data analysis.

Retinotopic mapping data was analysed using a combination of tools from the FSL software suite and custom written retinotopic mapping analysis software (developed by KDS). In order to eliminate the effects of head movement by the patient during scan acquisition the data was corrected for movement by re-aligning each of the functional volumes to best-fit the first volume acquired. The signal-to-noise in the data was maximized using a spatial filter (Gaussian, SD=2.0 mm).

The retinotopic signal in each voxel of the cortex was analysed using Fourier techniques to yield power (signal magnitiude) and phase values of the 1/54 Hz component, from which a 3 dimensional map could be generated. The phase-angle was directly converted into a wedge position, to identify the portion of retinotopic space the voxel is responding to. Amplitude and phase maps were visualised in 3D for each subject by combining the functional map with the anatomical scan as shown in figure 9.2. The upper row of images illustrates the magnitude of the retinotopic signal (darker colours indicating greater power) while the lower row illustrates the phase of the retinotopic signal (where colour scale indicates wedge position with blue/purple representing the upper vertical meridian, orange/yellow representing horizontal meridians, and green representing the lower vertical meridian).

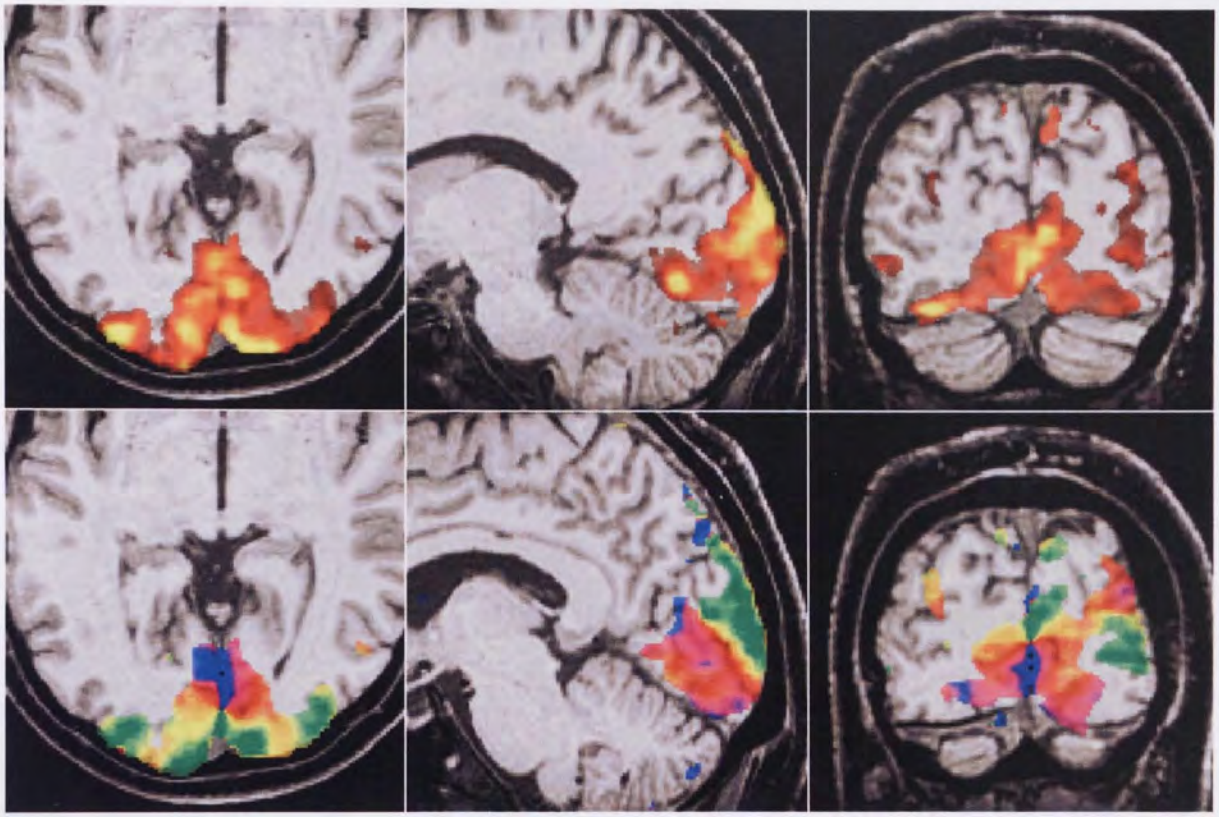

Figure 9.2 Example of MRI scan indicating the magnitude of the retinotopic signal (upper row) and the phase of the retinotopic signal (lower row) superimposed on the anatomical scan of a normal subject during fMRI retinotopic mapping

In this study a threshold of 0.3 for the correlation coefficient of the signal amplitude was employed in order to give an appropriate level of control between noise and signal.

The magnitude and phase data from each patient was analysed to calculate the amount of activation generated in the entire visual cortex, at each phase angle. Polar-plots of activation versus wedge-angle were generated for each subject for monocular and binocular viewing.

9.9 Statistical analysis

Pearson's product moment correlation was used to assess the relationships between each anatomical structure along the visual pathway for all subjects and to assess whether there was a relationship between anatomical structure and visual function. Throughout

all analyses significance levels were treated with caution due to the very small sample sizes in the study.

9.9.1 Relationship between anterior eye structure and visual fields

Pearson product moment correlation was conducted to explore the relationship between retrobulbar optic nerve, rim area, mean RNFL and visual fields. Data from all eyes of all subjects was used in the analysis (n=20).

9.9.2 Relationship between anterior eye structure, visual cortex structure and visual function

Pearson product moment correlation was conducted to explore the relationship between the anatomy of the anterior eye structure and visual cortex and visual function. Due to the fact that as a result of nasal fibre decussation at the chiasm there is representation of nerve fibres from both the R and L eyes in the R and L occipital lobes, it was felt appropriate that mean anterior eye measurements were explored. Therefore, during analysis the mean values of R and L anterior anatomy and mean visual field analyses were correlated against grey matter percentage in the R and L cortices (n=10).

9.9.3 Relationship between cortical activation and visual pathway anatomy

Pearson product moment correlation was conducted to explore the relationship between firstly, the level of activation in the visual cortex and the amount of grey matter and secondly the level of activation in the visual cortex and the anatomy of the anterior eye. Binocular activation data was available for only 9 subjects because one glaucoma subject felt unable to continue with the MRI scanning process. Mean measurements of anatomical structure were used during this analysis (n=9).

9.9.4 The effects of disease and age on grey matter in the visual cortex

The relationship between age and grey matter was initially explored using Pearson product moment correlation. Graphical representation of age versus grey matter was plotted with regression line and 95% confidence intervals. The effect of the disease

process on grey matter was investigated on a case-wise basis using graphical observations.

9.10 Results: Anatomical data

The mean and standard deviation measurement of each anatomical structure of the normal group 1 and glaucoma group 2 and individual study participants are displayed in tables 9.1 to 9.4.

9.10.1 Optic nerve head characteristics

The group mean characteristics of optic nerve head tomography as derived from OCT data are shown for group 1 and group 2 in table 9.1. Rim area measurements for individual subjects in the normal (N) and glaucoma (G) group are summarised in table 9.2.

	Group 1 (Normal) n=6		Group 2 (Glaucoma) n=4	
	Right eye	Left eye	Right eye	Left eye
Vert. int. rim area (Vol) (mm^3)	0.55 ± 0.39	0.69 ± 0.39	0.12 ± 0.08	0.11 ± 0.03
Horiz. int. rim width (Area) (mm^2)	1.83 ± 0.40	1.92 ± 0.46	1.26 ± 0.28	1.28 ± 0.18
Disc area (mm^2)	2.25 ± 0.34	2.36 ± 0.42	2.70 ± 0.47	2.74 ± 0.29
Cup area (mm^2)	0.43 ± 0.28	0.48 ± 0.28	1.72 ± 0.47	1.75 ± 0.26
Rim area (mm^2)	1.82 ± 0.50	1.91 ± 0.55	0.99 ± 0.36	0.99 ± 0.25
Cup/Disc Area ratio	0.24 ± 0.11	0.24 ± 0.12	0.64 ± 0.12	0.64 ± 0.08
Cup/Disc Horiz ratio	0.50 ± 0 .10	0.48 ± 0.13	0.86 ± 0.06	0.84 ± 0.05
Cup/Disc Vert ratio	0.46 ± 0.14	0.45 ± 0.15	0.74 ± 0.08	0.75 ± 0.04

Table 9.1 Mean (±SD) optic nerve head characteristics of the normal and glaucoma groups

Patient	Right eye (mm^2)	Left eye (mm^2)
N1	1.75	1.61
N2	2.10	2.48
N3	1.99	2.43
N4	2.55	2.29
N5	1.23	1.33
N6	1.30	1.33
Mean ±SD	**1.82 ±0.50**	**1.91±0.55**
G1	1.02	1.21
G2	0.63	0.65
G3	0.82	1.15
G4	1.46	0.96
Mean±SD	**0.99 ±0.36**	**0.99±0.25**

Table 9.2 Rim area for the right and left eyes of each subject in the normal (N) group and glaucoma (G) group and mean (±SD) for each group using optical coherence tomography

9.10.2 Retinal nerve fibre layer thickness

The group mean retinal nerve fibre layer thickness measurements as derived from OCT data are shown for group 1 (normal) and group 2 (glaucoma) in table 9.3. Retinal nerve fibre layer thickness measurements for individual subjects in the normal (N) and glaucoma (G) group are summarised in table 9.4.

Quad	Normal		Glaucoma	
	Right eye (μm)	Left eye (μm)	Right eye (μm)	Left eye (μm)
S	119.87 ± 10.71	130.47 ± 19.41	108.40±28.14	99.70± 15.57
N	77.13 ± 11.73	77.03 ± 9.72	71.45±17.50	68.80 ± 14.25
I	119.10 ± 15.79	123.03 ± 14.93	102.40±23.48	99.55± 19.59
T	62.60.46 ± 7.94	68.13 ± 19.08	59.10±21.83	57.45 ± 7.46
Ave	94.68 ± 6.33	99.67 ±12.06	85.34±20.34	81.38 ±12.40

Table 9.3 Mean (±SD) RNFL measurements of the normal and glaucoma group using OCT

Patient	Right eye (μm)	Left eye (μm)
N1	96.25	99.3
N2	97.50	116.4
N3	97.35	96.95
N4	101.90	110.9
N5	91.30	88.65
N6	83.75	85.80
Mean±SD	**94.68±6.33**	**99.67±12.06**
G1	87.75	94.50
G2	69.95	73.15
G3	70.45	68.70
G4	113.2	89.15
Mean±SD	**85.34±20.34**	**81.38±12.40**

Table 9.4 Mean retinal nerve fibre layer (RNFL) thickness for the right and left eyes of each subject in the normal (N) group and glaucoma (G) group and mean (±SD) for each group using optical coherence tomography

9.10.3 Retrobulbar optic nerve diameter

The group mean retrobulbar optic nerve diameter measured with ultrasound are shown for group 1 and group 2 in table 9.5. Retinal nerve fibre layer thickness measurements for individual subjects in the normal (N) and glaucoma (G) group are summarised in table 9.6.

	Retrobulbar optic nerve diameter (cm)			
Patient	Normal		Glaucoma	
Distance behind globe (cm)	Right eye	Left eye	Right eye	Left eye
0	0.43 ± 0.07	0.45 ± 0.04	0.35 ± 0.03	0.35 ± 0.03
0.50	0.54 ± 0.07	0.55 ± 0.03	0.44 ± 0.07	0.46 ± 0.09
1.00	0.61 ± 0.08	0.62 ± 0.04	0.51 ± 0.09	0.52 ± 0.07
1.50	0.68 ± 0.08	0.68 ± 0.04	0.59 ± 0.10	0.60 ± 0.10

Table 9.5 Mean (±SD) retrobulbar optic nerve diameters of the right and left normal and glaucoma groups using ultrasound

	RETROBULBAR OPTIC NERVE DIAMETER							
	Right eye (cm):Distance behind globe				Left eye (cm) Distance behind globe			
	0cm	0.50cm	1.00cm	1.50cm	0cm	0.50cm	1.00cm	1.50cm
N1	0.44	0.57	0.61	0.65	0.43	0.53	0.58	0.66
N2	0.51	0.59	0.67	0.75	0.47	0.56	0.62	0.69
N3	0.41	0.47	0.53	0.59	0.42	0.52	0.55	0.59
N4	0.31	0.47	0.54	0.62	0.40	0.56	0.64	0.70
N5	0.41	0.51	0.60	0.66	0.49	0.60	0.65	0.69
N6	0.49	0.63	0.73	0.81	0.47	0.56	0.65	0.73
Mean ±SD	**0.43 ±0.07**	**0.54 ±0.07**	**0.61 ±0.08**	**0.68 ±0.08**	**0.45 ±0.04**	**0.55 ±0.03**	**0.62 ±0.04**	**0.68 ±0.05**
G1	0.39	0.48	0.55	0.62	0.33	0.43	0.51	0.56
G2	0.38	0.49	0.61	0.68	0.40	0.58	0.62	0.75
G3	0.35	0.45	0.54	0.61	0.35	0.46	0.53	0.58
G4	0.30	0.34	0.39	0.40	0.33	0.38	0.44	0.5
Mean ±SD	**0.35 ±0.04**	**0.44 ±0.07**	**0.52 ±0.09**	**0.59 ±0.10**	**0.35 ±0.03**	**0.46 ±0.09**	**0.52 ±0.07**	**0.59 ±0.10**

Table 9.6 Retrobulbar optic nerve diameter at increasing distance from the globe for the right (R) and left (L) eyes of normal (N) subjects and glaucoma (G) patients and mean (±SD) for each group

9.10.4 Grey matter percentages for individual subjects

Grey matter percentages for the right, left occipital lobe and total cortex for individual subjects in the normal (N) and glaucoma (G) group are summarised in table 9.7.

Patient	R occipital grey matter percentage	L occipital grey matter percentage	Total occipital grey matter percentage
N1	41.3	50.2	44.3
N2	53.0	54.2	49.4
N3	52.8	51.9	46.0
N4	50.1	51.9	45.8
N5	49.8	51.3	45.9
N6	45.9	47.1	40.9
Mean ±SD	**48.82 ±4.49**	**51.1±2.36**	**45.38±2.77**
G1	48.3	51.2	44.0
G2	50.5	52.8	48.4
G3	40.9	45.6	42.6
G4	48.0	50.7	42.9
Mean ±SD	**46.93 ±4.17**	**50.08±3.11**	**44.48±2.68**

Table 9.7 Grey matter percentages in the right (R) and left (L) occipital lobe and in the visual cortex of each subject in the normal (N) and glaucoma (G) group using anatomical MRI scanning

9.11 Results: Functional data

Functional data results are summarised in tables 9.8 and 9.9

Visual field indices of mean deviation (MD) and pattern standard deviation (PSD) for each participant are displayed in table 9.8 (see section 1.10.2 for definition).

Patient	R MD (dB)	L MD (dB)	R PSD (dB)	L PSD (dB)
N1	0.12	1.22	1.33	1.25
N2	0.44	-0.96	1.52	1.59
N3	0.89	0.58	1.12	1.39
N4	0.51	-0.03	1.34	1.29
N5	0.82	1.24	1.61	1.50
N6	-0.31	-0.40	1.58	1.18
Mean ±SD	**0.41 ±0.45**	**0.28±0.89**	**1.42±0.19**	**1.37±0.16**
G1	-3.80	-5.19	3.56	5.03
G2	-3.44	-3.49	4.86	3.23
G3	0.65	-1.10	1.71	1.41
G4	-7.23	-10.44	3.17	8.68
Mean ±SD	**-3.46 ±3.23**	**-5.06±3.96**	**3.33±1.30**	**4.59±3.10**

Table 9.8 Table showing the visual field indices: mean deviation (MD) and pattern standard deviation (PSD) for each subject in the normal (N) and glaucoma (G) group

Measures of total activation power for each subject are displayed in table 9.9 for all 6 normal subjects and 3 glaucoma patients only, due to 1 glaucoma patient being unable to complete the MRI scanning process. Activation power data for separate eyes was available for 2 normal subjects and 3 glaucoma patients only due to time constraints in the scanner.

These data are represented in the polar plots shown in figure 9.3 for normal subjects and figure 9.4 for glaucoma subjects.

Patient	R activation power	L activation power	Total activation power
N1	n/a	n/a	48759.11
N2	83159.15	61552.65	64610.79
N3	n/a	n/a	38976.15
N4	30291.34	39619.42	46480.55
N5	n/a	n/a	37902.31
N6	n/a	n/a	33842.04
Mean±SD			**45095.16**
G1	n/a	n/a	n/a
G2	25798.06	65842.77	18124.74
G3	35263.25	27517.84	33291.70
G4	20889.85	30874.26	23651.04
Mean±SD			**25122.49**

Table 9.9 Table to show the activation power of each subject in the normal (N) and glaucoma (G) group using functional MRI scanning

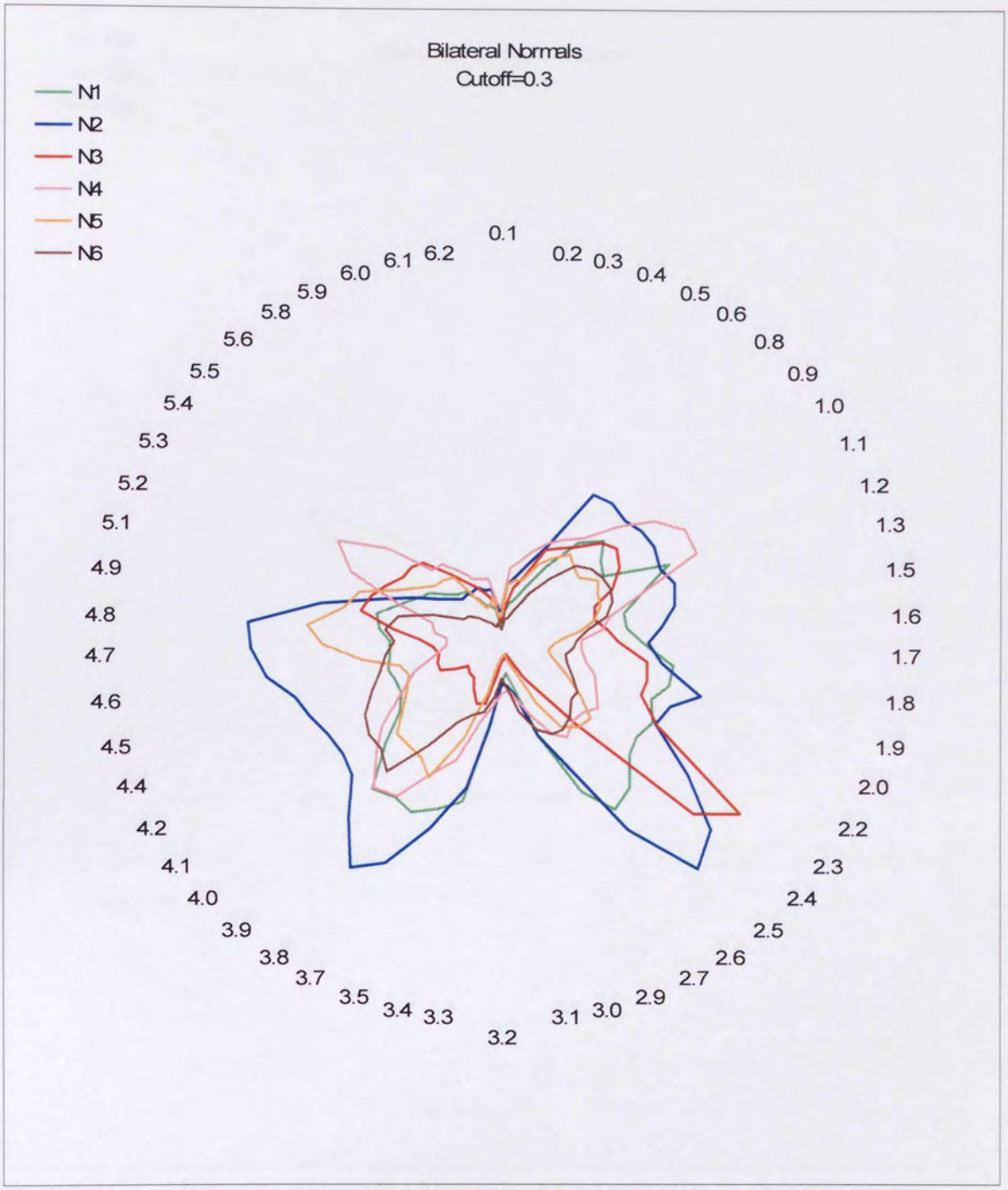

Figure 9.3 Polar plot representing binocular cortical activation in normal subjects

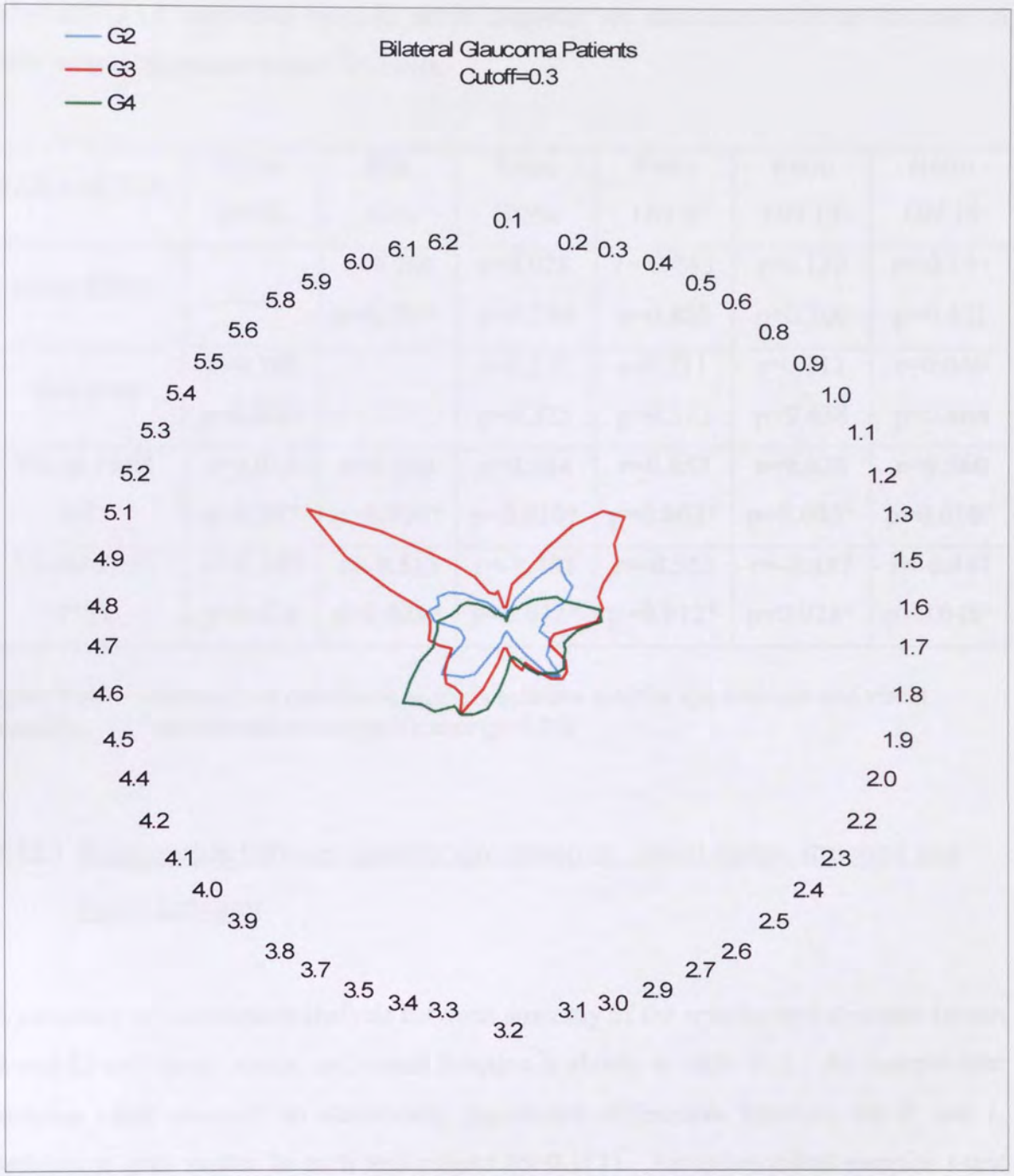

Figure 9.4 Polar plot representing binocular cortical activation in glaucoma patients

9.12 Relationship between anterior eye structure and visual fields

A summary of the results of Pearson product-moment correlation are shown in table 9.10 (n=20). There was a strong positive correlation between mean rim area and mean retinal nerve fibre layer thickness. Rim area and MD were significantly correlated while rim area and PSD exhibited a statistically significant inverse relationship i.e. as rim area decreases, PSD increases, indicating more marked visual field loss. Retrobulbar optic nerve diameter at all distances from the globe showed a statistically significant inverse

relationship i.e. decreases in optic nerve diameter are associated with an increase in PSD indicating greater visual field loss.

PARAMETER	Mean RNFL	Rim Area	Retro Globe	Retro ON 5	Retro ON 10	Retro ON 15
Mean RNFL	———	**r=0.780 p=0.000***	r=0.078 p=0.744	r=-0.045 p=0.850	r=0.139 p=0.560	r=-0.191 p=0.421
Rim Area	**r=0.780 p=0.000***	———	r=0.232 p=0.325	r=0.211 p=0.372	r=0.112 p=0.638	r=0.040 p=0.868
Visual Field MD	r=0.028 p=0.907	**r=0.444 p=0.050***	**r=0.564 p=0.010***	**r=0.653 p=0.002***	**r=0.628 p=0.003***	**r=0.560 p=0.010***
Visual Field PSD	r=-0.189 p=0.426	**r=-0.513 p=0.021***	**r=-0.481 p=0.032***	**r=-0.553 p=0.012***	**r=-0.497 p=0.026***	**r=-0.447 p=0.048***

Table 9.10 Summary of correlation analysis between anterior eye structure and visual function * denotes statistical significance (p=0.05)

9.12.1 Relationship between anterior eye structure, visual cortex structure and visual function

A summary of correlation analysis between anatomy of the anterior eye structure (mean R and L) and visual cortex and visual function is shown in table 9.11. An independent samples *t*-test revealed no statistically significant differences between the R and L percentage grey matter in each test subject (p=0.111). An independent samples *t*-test revealed no statistically significant differences between the right and left eyes of all subjects in terms of the anterior eye anatomical structures i.e. rim area (p=0.846), RNFL (p=0.827), retrobulbar optic nerve diameter at the globe (p=0.719), and at 5, 10, 15mm from the globe (p=0.631, p=0.953, p=0.976 respectively) and disc area (0.692). It was therefore felt appropriate at this stage in the pilot study to consider the average of each of the anterior eye structures in the analysis. RNFL as a whole, without the need to consider the nasal and temporal fibre input into the occipital lobes. As shown in table 9.11, there was no statistically significant correlation between the R or L grey matter and any anterior eye anatomical or visual field parameter (p>0.05).

	R % grey matter	L % grey matter
Mean rim area	r=0.408 p=0.242	r=0.412 p=0.236
Mean RNFL	r=0.420 p=0.226	r=0.556 p=0.095
Retro ON (10mm)	r=0.101 p=0.781	r=0.052 p=0.886
MD	r=-0.055 p=0.880	r=-0.092 p=0.801
PSD	r=0.104 p=0.774	r=0.174 p=0.630

Table 9.11 Summary of correlation analysis between anterior eye structure, visual cortex and visual function – for 10 eyes of 6 normal and 4 glaucoma patients

9.12.2 Relationship between cortical activation and visual pathway anatomy

Correlation analysis of the relationship between level of activation in the visual cortex and the amount of grey matter and the anatomy of the anterior eye are summarised in table 9.12. The table shows a strong positive correlation between binocular activation and mean rim area and a strong negative correlation between binocular activation and mean PSD.

	Binocular Activation	
	Pearson correlation (r)	Significance (p)
R percentage grey matter	r=0.152	p=0.697
L percentage grey matter	r=0.320	p=0.400
Total percentage grey matter	r=0.353	p=0.352
Mean rim area	r=0.801	p=0.009*
Mean RNFL	r=0.647	p=0.060
Retrobulbar ON	r=0.379	p=0.314
Mean MD	r=0.585	p=0.098
Mean PSD	r=-0.652	p=0.057*

Table 9.12 Summary of correlation analysis between anterior eye, visual cortex and cortical activation * denotes statistical significance (p=0.05)

9.12.3 Effect of age and disease on grey matter

The effect of age on grey matter, right occipital, left occipital and total cortex is shown in figure 9.5, 9.6, 9.7. The regression line and 95% confidence intervals were generated using a database of 80 normal subjects recruited from among friends, colleagues and staff of Aston University; mean age 28.1±9.80 years, range 19-55 years (raw data courtesy of Prof K.D.Singh). According to Pearson correlation coefficient of the normative database, age and grey matter in normals exhibit a significant inverse relationship for the right occipital lobe (r=-0.252, p=0.024), left occipital lobe (r=-0.402, p=0.000) and total grey matter (r=-0.658, p=0.000).

The data for the study sample are shown superimposed, with normal subjects indicated by a solid circle and glaucoma patients by dotted circles.

Graph 9.7 indicates a loss of 3.85% grey matter density in the visual cortex per decade.

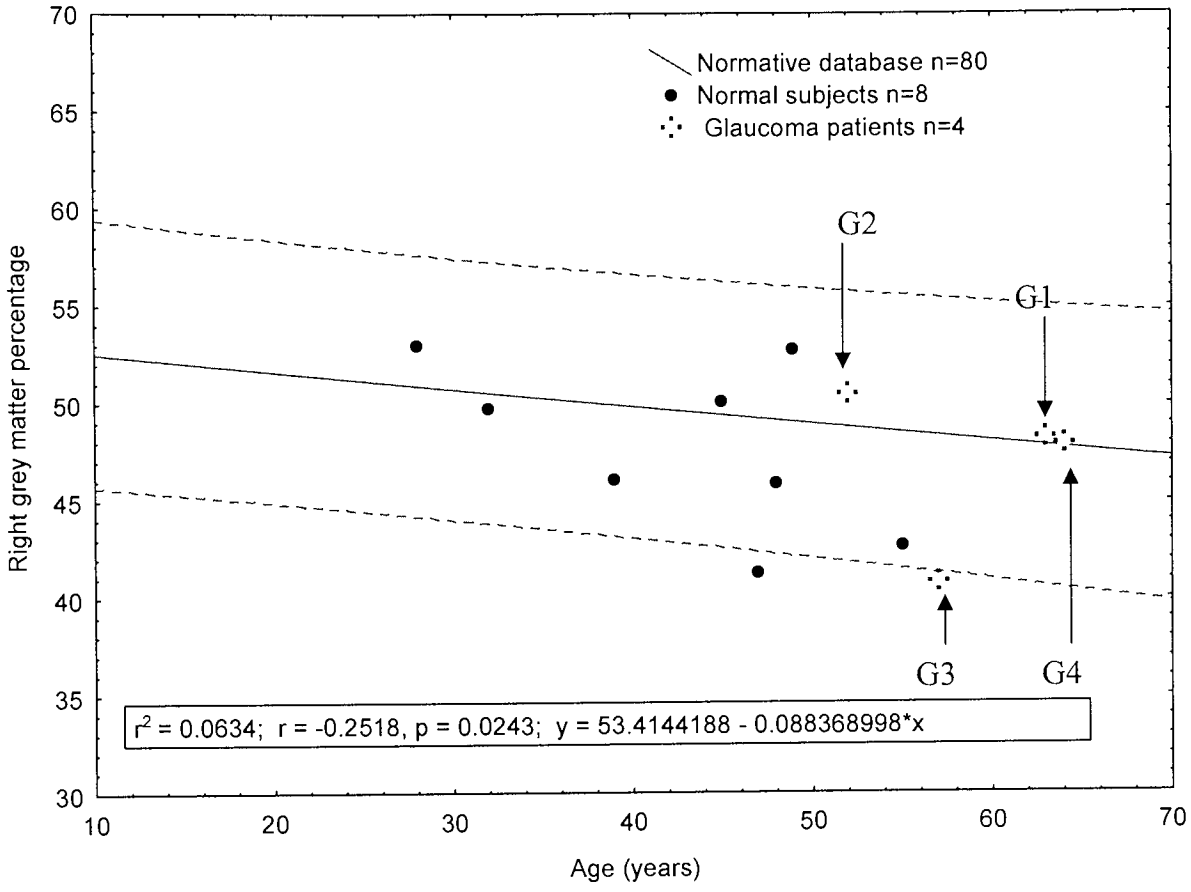

Figure 9.5 Graph showing a significant negative relationship between age and percentage grey matter R occipital lobe for a cohort of 80 normal subjects. Data for the study sample are superimposed.

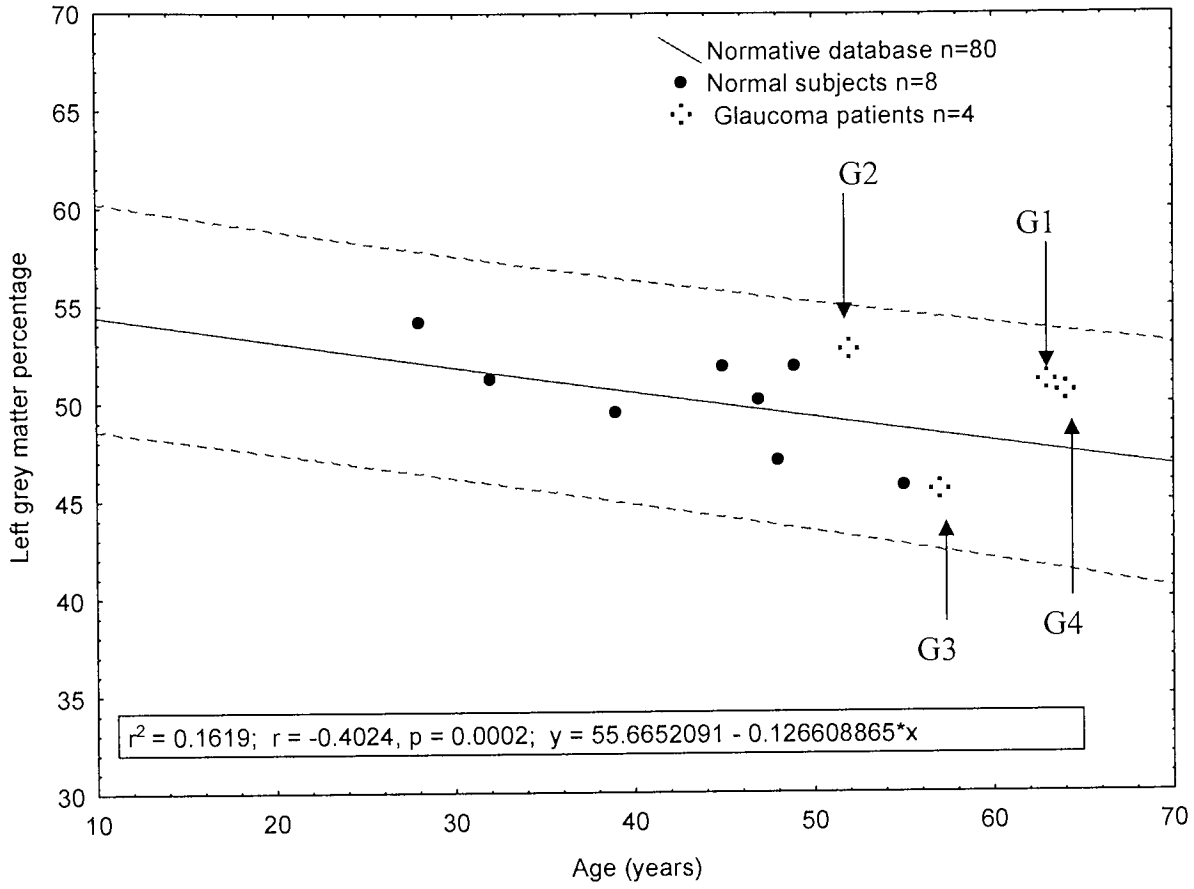

Figure 9.6 Graph showing a significant negative relationship between age and percentage grey matter L occipital lobe for a cohort of 80 normal subjects. Data for the study sample are superimposed.

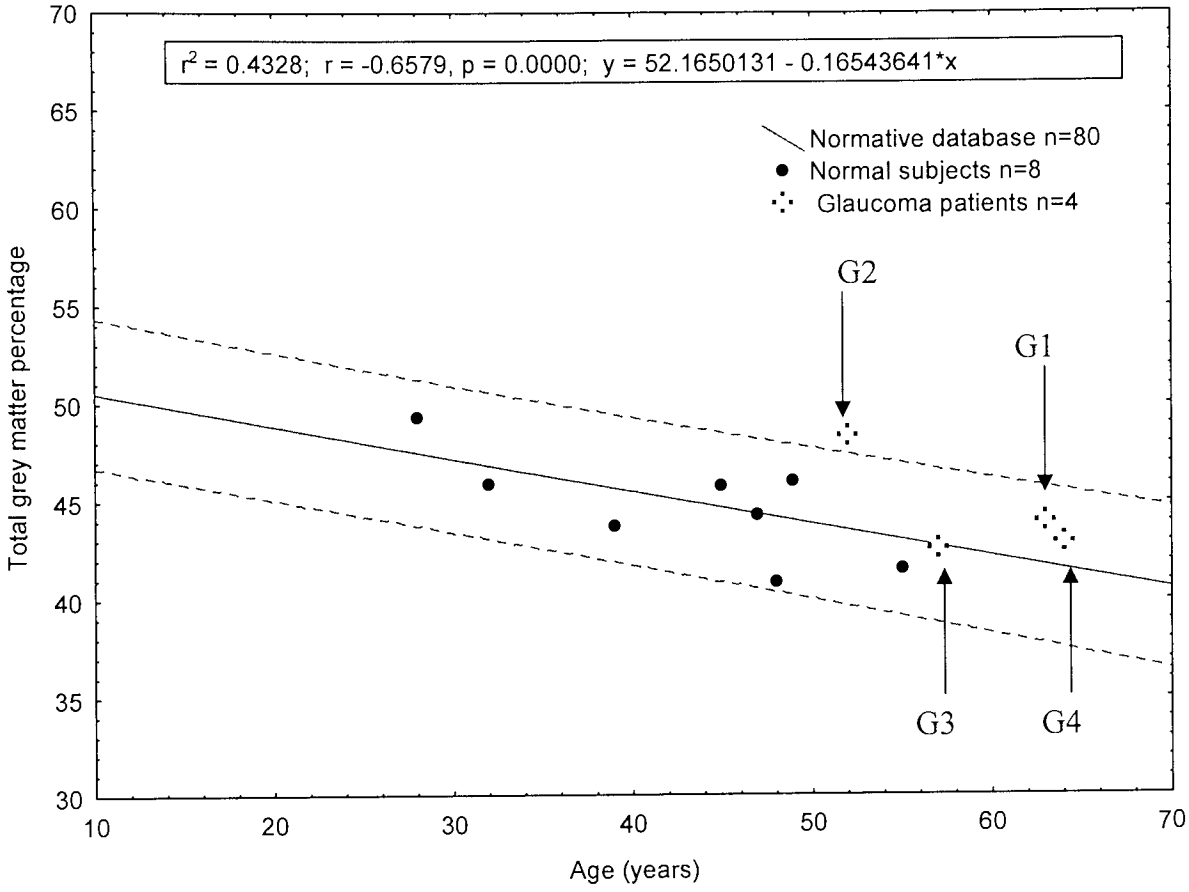

Figure 9.7 Graph showing a significant negative relationship between age and percentage grey matter in the total visual cortex for a cohort of 80 normal subjects. Data for the study sample are superimposed.

9.13 Case discussions

9.13.1 Glaucoma patient G2

A summary of the anatomical and functional characteristics of glaucoma patient G2 is shown in table 9.13. Of all three glaucoma patients G2 exhibited the least mean rim area and RNFL thickness but the highest retrobular optic nerve diameter (tables 9.5-9.7). As indicated in figures 9.5-9.7, R and L grey matter percentages fall within normal limits while the grey matter percentage in the entire visual cortex is better than expected for the age of the patient. Visual field PSD for the right and left eyes were 4.86 and 3.23 respectively (table 9.8). The visual field plot for the R eye shows an inferior arcuate loss (figure 9.8) while L eye exhibits scattered peripheral loss (figure 9.9).

Binocular activation as indicated by the polar plot (figure 9.4) and table 9.9 was the least of all the glaucoma patients.

	R	L	Total
Rim area	0.634 mm^2	0.647mm^2	_____
RNFL	69.95µm	73.15 µm	_____
Retro ON (10mm)	0.605cm	0.62cm	_____
Grey matter	50.5	52.8	48.4
Visual field MD	-3.44dB	-3.49dB	_____
Visual field PSD	4.86dB	3.23dB	_____
Activation	25798.06	65842.77	18124.74

Table 9.13 Anatomical structure and visual and cortical function summary for glaucoma patient G2

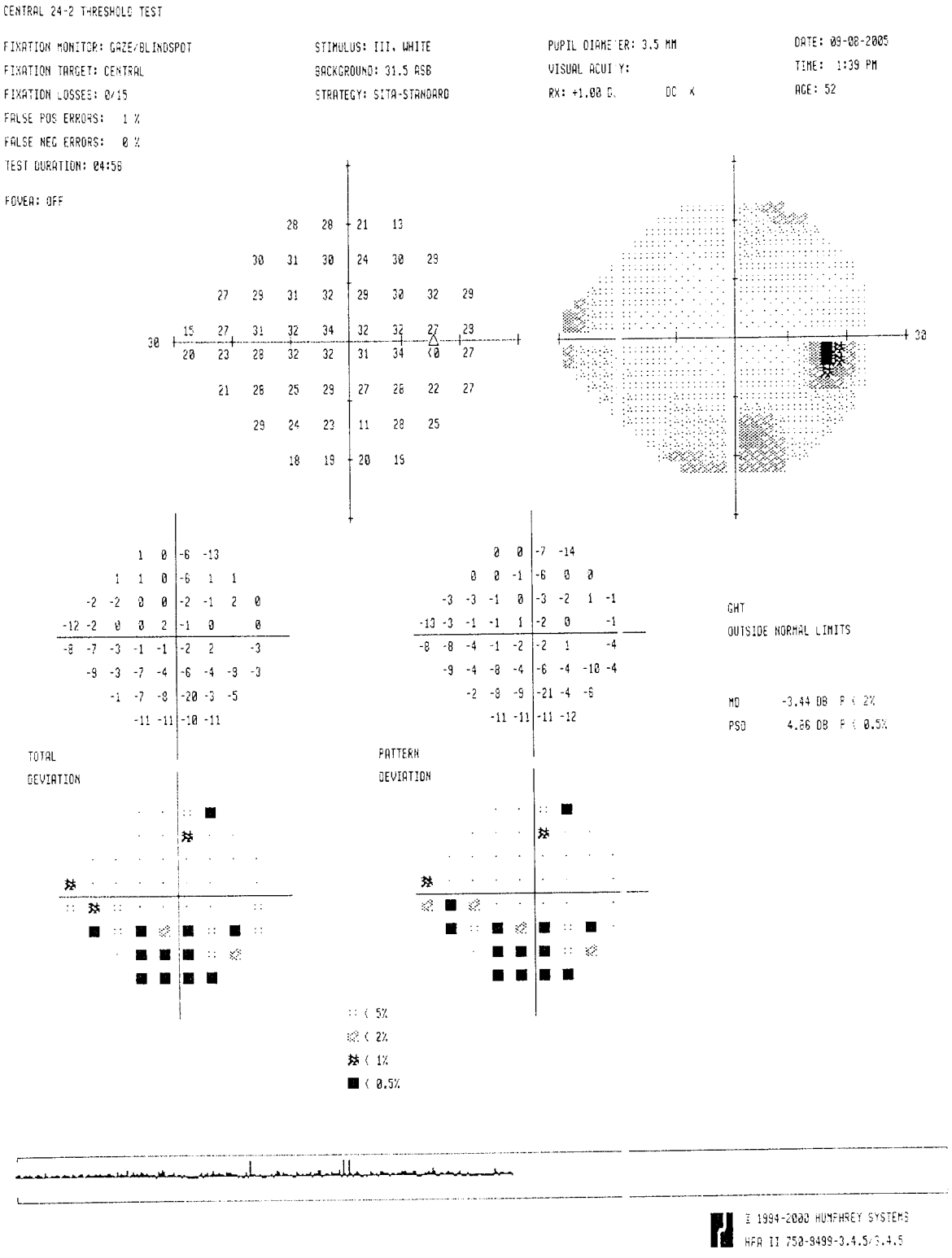

Figure 9.8 Humphrey Visual field (24-2) plot for R eye of patient G2

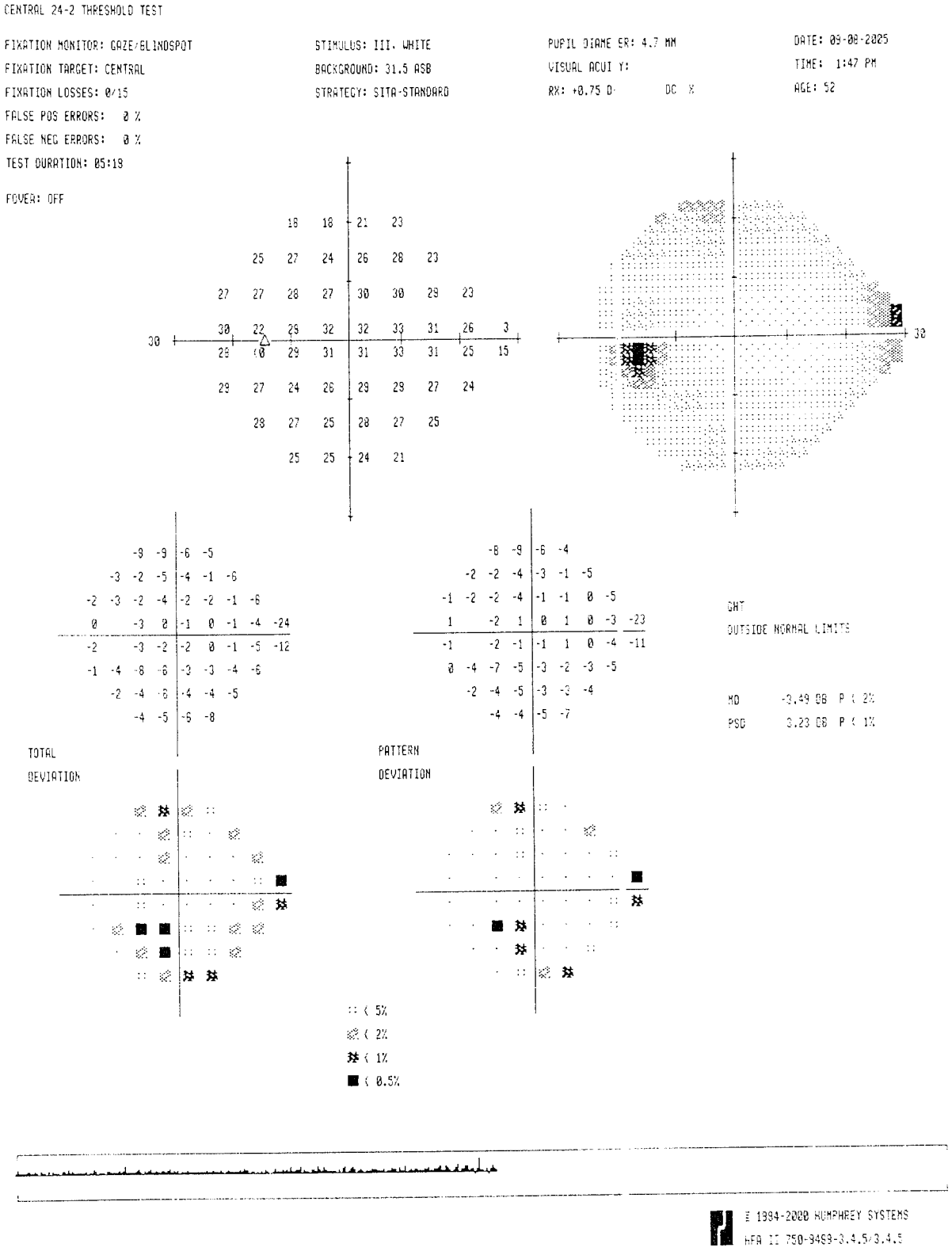

Figure 9.9 Humphrey Visual field plot (24-2) for L eye of glaucoma patient G2

This would suggest that loss of retinal nerve fibres leading to a reduction of rim area and RNFL thickness, has little direct impact on the diameter of the retrobulbar optic nerve. Despite a reduction in fibre number, the retrobulbar nerve structure appears to be maintained. The larger retrobulbar optic nerve diameter compared to the other glaucoma subjects suggests that prior to the onset of disease this patient had a large number of fibres. Accordingly, the fact that RNFL is thinnest in this patient indicates extensive fibre loss.

Although there is extensive fibre loss as evidenced by significant reduction in RNFL thickness, grey matter of this patient remains within normal limits suggesting that the cortex is resistant to anatomical loss in a similar way to the retrobulbar optic nerve. This indicates that grey matter is affected more slowly by the disease process or less likely, that it is unaffected in glaucoma. Our study would suggest that changes to cortical grey matter may lag reductions in rim area and retinal nerve fibre layer.

The relative lack of visual loss indicated by PSD (compared to glaucoma patient G4) may be explained by the fact this patient had a higher number of fibres before the onset of glaucoma. However, binocular activation as indicated by fMRI was the lowest of all the glaucoma patients and apparently not consistent with field defect, which may suggest that fMRI was a good indicator of functional loss. Consequently, fMRI may be a superior method of detecting generalized fibre loss than visual field testing. The comparatively greater effect of the disease on cortical activation may be explained by multiplicity of connection that occurs in the cortex.

9.13.2 Glaucoma patient G4

A summary of the anatomical and functional characteristics of glaucoma patient G4 is shown in table 9.14. Rim area in the right eye was greater compared to the other glaucoma patients, as was RNFL in both eyes (table 9.2 and 9.4). Retrobulbar optic nerve diameter however was lowest of all the glaucoma patients (table 9.6). Right, left and total grey matter percentage appears normal for age. However, visual field defects were greater for patient G4 compared to G2 and G3. Visual field plots (figure 9.10 and 9.11) show marked inferior arcuate loss in both right and left eyes. Of all three

glaucoma patients, binocular activation as indicated by the polar plot is the second highest (or second lowest).

	R	L	Total
Rim area	1.465 mm^2	0.956 mm^2	_____
RNFL	113.2μm	89.15μm	_____
Retro ON (10mm)	0.39cm	0.44cm	_____
Grey matter	48.0	50.7	42.9
Visual field MD	-7.23dB	-10.44dB	_____
Visual field PSD	3.17dB	8.68dB	_____
Activation	20889.85	30874.26	23651.04

Table 9.14 Anatomical structure and visual and cortical function summary for glaucoma patient G4

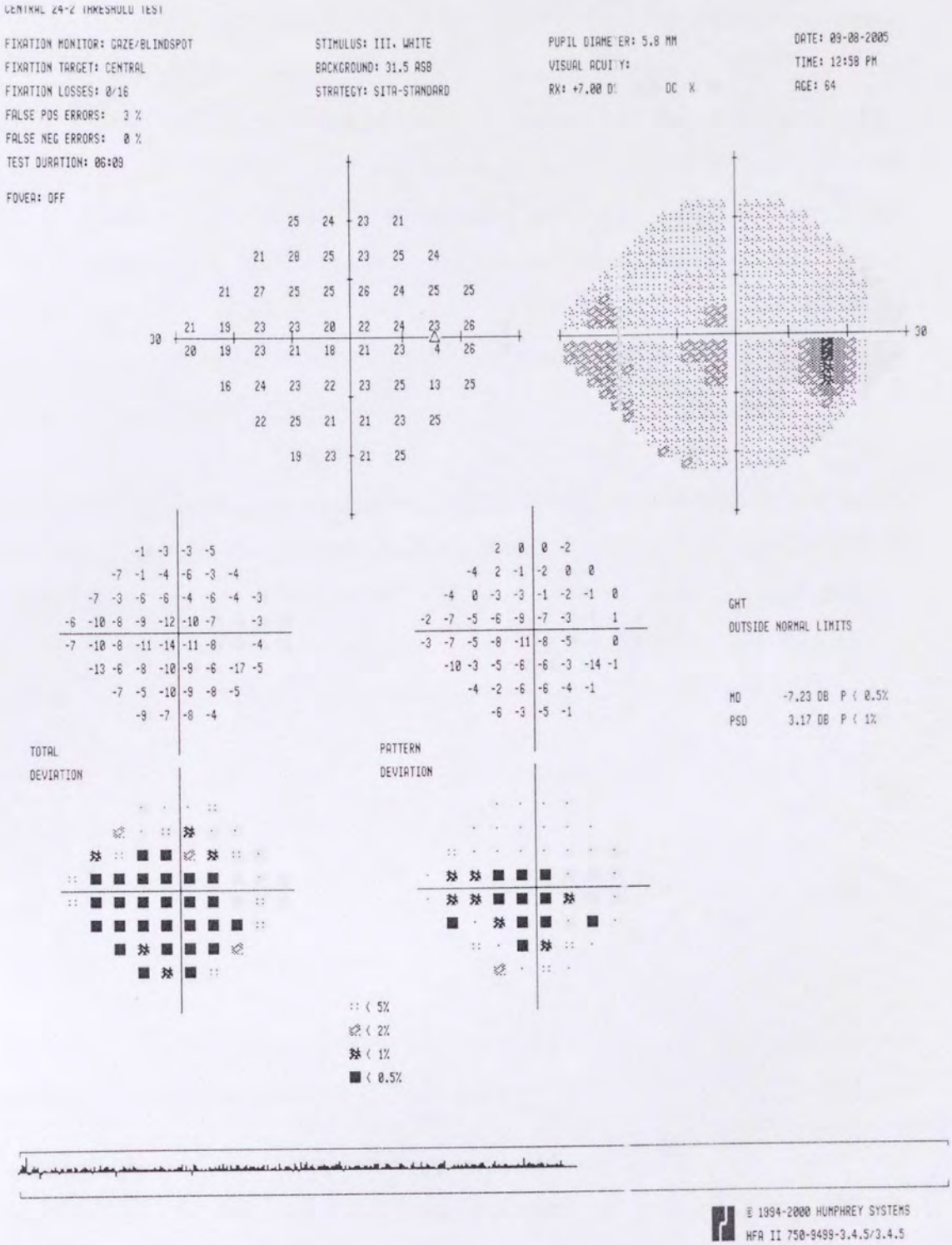

Figure 9.10 Humphrey Visual field (24-2) plot for the R eye of glaucoma patient G4

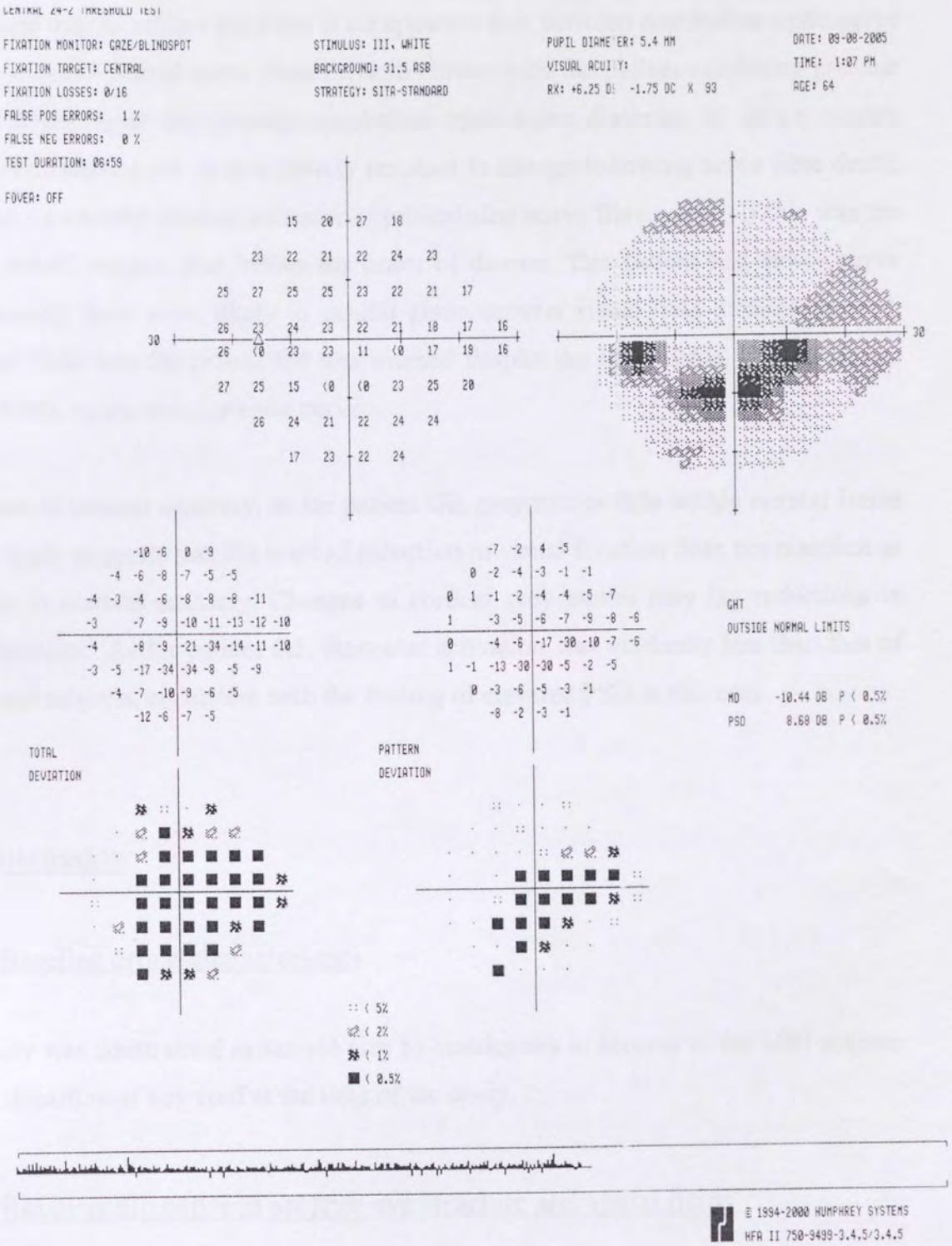

Figure 9.11 Humphrey Visual field (24-2) plot for the L eye of glaucoma patient G4

In a similar way to patient G2 there is no apparent link between retrobulbar optic nerve and rim area and retinal nerve fibre layer thickness with the patient exhibiting greatest rim and RNFL layer but thinnest retrobulbar optic nerve diameter. If, as we expect, optic nerve diameter *per se* is relatively resistant to change following nerve fibre death, it may act as a useful clinical indicator of pre-existing nerve fibre count. If this was the case, it would suggest that before the onset of disease, this patient had fewer nerve fibres making them more likely to exhibit glaucomatous visual field damage. Indeed, the visual field loss for patient G4 was marked despite the lack of real change in rim area or RNFL in the anterior optic nerve.

In relation to cortical anatomy, as for patient G2, grey matter falls within normal limits and our study suggests that the marked reduction in visual function does not manifest as a change in cortical anatomy. Changes to cortical grey matter may lag reductions in visual function. As for patient G2, binocular activation was markedly less than that of our normal subjects, consistent with the finding of elevated PSD in this case.

9.14 Discussion

9.14.1 Baseline group characteristics

This study was constrained in sample size by restrictions in acccess to the MRI scanner and the departure of key staff at the time of the study.

9.14.2 Relationship between anterior eye structure and visual fields

As expected, anterior optic nerve head parameters and visual field indices differed between groups which support the characteristic presentation of patients with a diagnosis of glaucoma. Retinal nerve fibre layer and rim area was greater in normal subjects compared to the glaucoma patients while visual field indices MD and PSD were lower in the normal group compared to the diseased eyes.

The small group sample sizes preclude sensible between-group comparisons in this study. However, by observation, retrobulbar optic nerve diameter was less in glaucoma

subjects compared with normals in accordance with previously reported findings of Dichtl and Jonas (1996) and Beatty *et al.* (1998c) who observed reduced retrobulbar optic nerve diameter in patients with glaucoma. Retrobulbar optic nerve diameter for all subjects increased with increasing distance from the globe which differs from other findings by Ossoinig, Cennamo and Frazier-Byrne (1981) who found the orbital optic nerve to be of uniform thickness throughout its course.

There is a clear correlation between rim area and retinal nerve fibre layer which is expected. However, despite this correlation there is no apparent correlation with retrobulbar optic nerve diameter. This contradicts the findings of Dichtl and Jonas (1996) who, in a group of 31 glaucoma subjects and 16 normal controls, observed a significant correlation between echographic measurements of the pial optic nerve width and glaucomatous changes of the optic disc and retinal nerve fibre layer. Similarly, Beatty *et al.* (1998a) report that retrobulbar optic nerve dimensions correlated positively and significantly with the neuroretinal rim area. This may be explained by our small sample and warrants further work with a larger study cohort.

Our study shows that while rim area correlates with visual field parameters, retinal nerve fibre layer *per se*, is a poor indicator of visual field loss. The statistically significant inverse relationship between retrobulbar optic nerve diameter and PSD indicates that a decrease in optic nerve diameter is associated with increasing visual field loss. Interestingly, the data suggest that retrobulbar optic nerve diameter is at least as good an indicator of glaucomatous visual field loss as rim area such that eyes with small optic nerve diameters are more inclined to exhibit a higher PSD in visual field analysis. Confirmation of our findings with a larger sample size would be appropriate. To our knowledge there are no studies investigating the relationship between visual function and retrobulbar optic nerve characteristics and this warrants further work.

While there is considerable evidence of a link between visual field loss and reductions in retinal nerve fibre layer thickness (Quigley *et al.*, 1980; Airaksinen *et al.*, 1984; Sommer *et al.*, 1991; Kanamori *et al.*, 2003; El Beltagi *et al.*, 2003) this is not the case according to our data. We suggest that the correlation with visual field loss is less strong than for other indicators and requires analysis of a larger sample size. Nevertheless, in our study there were stronger indicators than RNFL for predicting loss.

There was no evidence of a relationship between disc area with rim area (p=0.804), retinal nerve fibre layer (0.939), or visual field indices MD (p=0.129) and PSD (p=0.341). However, disc area correlated significantly and negatively with retrobulbar optic nerve diameter at the globe, and at 5mm, 10mm and 15mm behind the globe (p=0.048, p=0.043, p=0.027, p=0.041 respectively). This is in keeping with the findings of Jonas *et al.* (1992) who observed that optic nerve cross section area was related to optic disc size.

At first glance this result may be somewhat unexpected as one might imagine that ganglion cell fibres pass through the widest diameter of the optic disc and so dimensions might be similar or even less than disc area. Experimental artifacts due to anatomical measures of disc area being derived from the OCT and retrobulbar optic nerve diameter by ultrasonography, either of which could induce errors relating to absolute size, may explain the finding. However, consideration of the clinical anatomy of the optic nerve offers a better explanation, based on the additional thickness resulting from the presence of fibre myelination, the three cerebral membranes and subarachnoid space around the optic nerve. Figure 9.12 shows a histological cross-section of a normal optic nerve. The disc area, identified by the OCT using reference points located at the disc edge where the RPE ends, is narrower than the diameter of the retrobulbar portion of the optic nerve.

Figure 9.12. Histological section through a normal optic nerve showing relative thickening of the retrobulbar nerve section compared to optic disc diameter. (Image provided for Dr S L Hosking courtesy of Prof G L Ruskell).

While it is not clear whether retrobulbar optic nerve diameter reduces as a consequence of reduced nerve fibre loss, we suggest, according to the findings of glaucoma patient G2, that nerve fibre loss does not impact the structure of the retrobulbar optic nerve. A much larger sample size will be needed in subsequent studies to confirm this finding. That disc area may explain our findings regarding the correlation between retrobulbar optic nerve diameter and visual function should be considered. The subject of whether disc size is correlated with glaucoma susceptibility has long been discussed. Support for a relationship between large disc size and increased glaucoma susceptibility comes from observations of larger disc size and higher glaucoma susceptibility in African-American subjects compared to white subjects (Seddon *et al.*, 1983). Conversely, there is evidence that eyes with small optic discs are predisposed to glaucomatous optic nerve damage due to the fact that optic nerve fibres in the small optic nerve head are more crowded (Jonas, Mardin, Schlotzer-Schrehardt *et al.*, 1991) and may be more susceptible to the effects of mechanical lamina deformation than the larger optic nerve head. It has also been reported that the small disc possesses a smaller number of fibres than those with larger optic nerve heads (Quigley *et al.*, 1991) suggesting a smaller anatomic reserve capacity. Factoring in the size of the optic disc into our analyses helps to negate the effect of structural size to some extent. The relationship between retrobulbar optic nerve and visual field indices were therefore explored using a partial correlation with disc area as the covariate. In this way we were able to control for the effect of disc size on our findings. The results are summarised below (table 9.15). A strong negative relationship was exhibited between retrobulbar optic nerve and PSD which implies that controlling for disc size had very little effect on the strength of the relationship between these two parameters.

PARAMETER	Retro Globe	Retro ON 5	Retro ON 10	Retro ON 15
Visual Field MD	**r=0.486 P=0.035***	**r=0.592 p=0.008***	**r=0.558 p=0.013***	**r=0.480 p=0.038***
Visual Field PSD	**r=-0.437 p=0.061**	**r=-0.519 p=0.023***	**r=-0.456 p=0.050***	**r=-0.397 p=0.092**

Table 9.15 Summary of partial correlation analysis between retrobulbar optic nerve diameter and visual field indices, where disc area is the covariate * denotes statistical significance

9.14.3 Relationship between anterior eye structure, visual cortex structure and visual function

For all subjects, there were no significant relationships between percentage grey matter in either occipital lobe and anterior eye structure mean rim area, mean RNFL, retrobulbar optic nerve nor visual function as indicated by visual field indices. To our knowledge, the relationship between visual function and grey matter has not been considered before and there has been no published work regarding this matter.

9.14.4 Relationship between cortical activation and visual pathway anatomy

Reduced binocular activation was associated with reduced neuroretinal rim area and worsening visual field as indicated by increased PSD, but was not linked with retrobulbar optic nerve diameter. Our study therefore suggests that there is a clear link between reduction in cortical activation and loss of functional vision and neuroretinal rim tissue at the optic nerve head. Glaucoma case studies suggest that fMRI provides a potential alternative method of detecting glaucomatous optic nerve damage. In particular, our initial findings suggest that fMRI may offer a technique by which to explore functional damage in patients with relatively well preserved visual field data, such as those for whom large ganglion cell fibre numbers protect vision due to sampling issues. Cortical activation was not correlated with grey matter indicating no real change in grey matter anatomy.

9.14.5 Effect of age and disease on grey matter

The data show that percentage grey matter in the right and left occipital lobe and total cortex diminishes with age in normal volunteers. In normal subjects (normative database) grey matter loss per decade of life for the visual cortex was calculated as 3.85%. Age effects have also been reported in anterior eye structures. Kanamori *et al.* (2003), suggest that retinal nerve fibre layer thickness around the optic nerve head decreases to a lesser degree at 1.7% per decade while Balazsi *et al.* (1984) reported a significant age effect on nerve fibre counts of normal human optic nerves (n=16) with a mean annual loss of 5637 optic nerve fibres. Similarly, Jonas *et al.* (1990) who examined 22 eyes of 19 subjects between 20 and 75 years and derived an approximate annual loss of 5426 fibres per year. As optic nerve axons diminish, reductions in the retinal nerve fibre layer thickness are likely. Loss of RNFL varies according to the location in which it is measured, according to our study (Chapter 6). We estimated mean RNFL loss per decade at the disc margin, 2nd margin scan and 3rd margin scan to be 1.5μm, 1.5 μm and 0.83μm respectively. In percentage terms this is calculated as a percentage loss per decade of 1.09%, 1.94% and 1.62% respectively which appears to approximate to the findings of Kanamori *et al.* (2003).

By graphical observation, in each case (right, left and binocular cortex) the study participants fell within or close to the expected normal confidence intervals for age suggesting that data were within the normal range. The few exceptions were that, as shown in figure 9.5, one normal subject (N6) and one glaucoma patient (G3) fell just below the normal range. This could be explained by, for example, the normal subject being normal but within the lower 5% of values of normality i.e. a false +ve defect), while the glaucoma patient could be explained the same way, or this could in fact be a genuine reduction in grey matter as a result of the disease process. Further data would be required to make a compelling argument either way. Similarly, in Figure 9.7, one glaucoma patient (G2) appears to have scored better than the 95% confidence interval. In this case one might consider a possible explanation that despite presenting among those individuals with a particular high density of fibres and cells, the disease has progressed sufficiently for a visual defect to manifest itself.

9.15 Conclusion

This study shows that despite there being a clear relationship between RNFL and rim area, any loss of nerve fibre tissue is not apparent along the next stage of the visual pathway, the retrobulbar optic nerve for all study participants. In all subjects, visual field defects are significantly related to both the rim area and retrobulbar optic nerve diameter, although the RNFL thickness around the optic nerve head is unrelated to field loss. That the retrobulbar optic nerve diameter is a strong indicator of visual field loss, apparently even more so than rim area, is an unexpected finding.

Binocular activation appears to be related to mean rim area and mean PSD. Interestingly, this suggests that fMRI is more powerful than visual fields in predicting loss of functional vision. This may be explained by differences between tests in terms of the very nature of their testing strategy. fMRI is objectively sampling the entire visual field during stimulus presentation to the patient while subjective visual field examination uses a sampling protocol to calculate visual loss. Visual field testing is inherently noisy, relying on good patient co-operation for reliable results. We suggest that compared to fMRI testing, visual field testing requires more functional loss before a defect is detected. Cortical grey matter in normal subjects reduces with increasing age which corresponds to findings that anterior eye structure are also affected by age. Disease does not appear to heighten the effects of age on grey matter with the majority of our study patients lying within or near to normal limits. This appears to suggest that any potential pathological change in the visual cortex lags the changes in the anterior eye structures.

9.16 Future work

Our study suggests that fMRI scanning of the visual cortex may provide important clues regarding the effects of glaucoma on visual function. It is clear the assessment of a larger subject sample is necessary before accurate conclusions can be drawn. We suggest that computational modelling of nerve fibres based on rim area, retrobulbar optic nerve diameter, cortical anatomy, compared to fMRI will increase the diagnostic ability of the ophthalmologist in a clinical setting. Following the assessment of substantial numbers of normal subjects and calculation of a normal database for anterior

eye structures, it may be possible to identify whether subjects fall within the normal centile ranges and offer a prediction as to their likelihood of developing glaucomatous optic neuropathy or at the very least enable the clinician additional methods of assessment.

Acknowledgements:
The author wishes to thank Mr Stephen Vernon for providing glaucoma patients for the study and Prof Krish Singh for allowing use of a cohort of normal data for comparison.

CHAPTER 10: Discussion

This thesis was divided into several sections. Initial studies were performed to assess the ability of the new Stratus OCT to provide repeatable and reproducible measures of retinal thickness and retinal nerve fibre layer thickness of normal eyes and diseased eyes. Secondly the normal physiological variations of anatomical structure with regards to age and axial length were explored. Finally, we explored the relationship between morphological changes along the visual pathway and visual function in disease.

10.1 Repeatability and reproducibility of the Stratus OCT

In order for any technology to be useful in monitoring changes over time it must be both repeatable and reproducible. Any observed detectable changes in ocular structure can therefore be attributed to the disease process and not to the variability of the equipment itself. Chapter 3 investigated the within-visit repeatability and between-visit reproducibility of macular thickness measurements in the normal and diabetic eye made by the newest OCT model, the Stratus Optical Coherence Tomographer. There is considerable evidence that its predecessors provide repeatable and reproducible measures in the normal and diseased eye, though very little had been reported for this third generation instrument. Compared to the OCT 1 and OCT 2000, the Stratus OCT offers higher resolution, increased sampling density and a variety of fast scanning protocols to more quickly acquire retinal scans. Repeatability and reproducibility was assessed using a variety of statistical methods in order to provide a basis for drawing accurate comparisons between similar studies. Our study showed that measurements of retinal macular thickness made with the Stratus OCT are highly repeatable and reproducible for both normal subjects and diabetic patients. The lack of significant differences between normal and diabetic patients in terms of their repeatability and reproducibility suggest that measurements are robust even in eyes with some degree of pathology. A further extension of this work would be to assess the repeatability and reproducibility characteristics of the Stratus OCT in diabetic patients with more advanced retinal changes and possible accompanying reductions in vision leading to greater fixation losses.

Our findings therefore suggest, that Stratus OCT has a role in monitoring the effects of disease and treatment over a period of time. Our findings were confirmed by a later study by Polito *et al.* (2005) who investigated the repeatability and reproducibility of macular thickness measures of normal subjects and the repeatability only of diabetic patients exhibiting clinically significant oedema. In general our study indicated higher repeatability and reproducibility of measures than observed by Polito *et al.* (2005) for normal subjects, although it is not clear why this is the case. It is possible that the lower repeatability scores reported for diabetic patients in the study by Polito *et al.* (2005) is due to the lower acuity of their subject sample compared to ours.

Chapter 2 investigated the within-visit repeatability and between-visit reproducibility of optic nerve head measurements in the normal and glaucomatous eye made by the Stratus Optical Coherence Tomographer. Despite the provision, by optical coherence tomography, of a cross-sectional scan to image the optic nerve head there had been little work reported on the use of such a scan and, as a consequence, nor on the repeatability and reproducibility of acquired measures. The majority of OCT studies into the glaucoma eye had focused primarily on retinal nerve fibre layer thickness changes around the optic nerve head, rather than using the OCT to quantify pathological changes to the optic nerve head itself such as loss of the neuroretinal rim and subsequent increase in the cup: disc ratio. Measurements of the retinal nerve fibre layer thickness using the OCT 1 and OCT 2000 had proved repeatable and reproducible while little had been reported on the ability of these instruments to image the optic nerve head. At the time of embarking on the study no work had been published regarding the ability of the Stratus OCT to acquire meaningful and reliable measurements of optic nerve head characteristics in the normal subject and the glaucoma patient.

This study showed that measurements of optic disc parameters made with the Stratus OCT are repeatable and reproducible for both normal and glaucoma patients. For the majority of the repeatability and reproducibility measures, with the exception of the intraclass coefficient (ICC) there were no significant differences between the two groups. This statistical difference is of no clinical concern since overall the ICCs were high in the glaucoma group, ranging from 90.6% to 95.3%, indicating excellent reproducibility. Since completion of our work, two recent studies confirm our findings. Paunescu *et al.* (2004) reported similarly reproducible optic nerve head measures in

normal subjects while Olmedo *et al.* (2004) found reproducible measures in normal and glaucoma patients. Reproducibility values are generally higher in our study than the observed values by Olmedo *et al.* (2004) while reproducibility values on normal subjects exceeded that of the glaucoma group in our study, unlike that of Olmedo *et al.* (2004).

Generally the repeatability and reproducibility values of optic nerve head measurements are less than for the retinal macular thickness measurements. This may be explained by the increased difficulty for the patients in looking at an eccentrically placed target within the OCT during optic nerve head scanning rather than fixating centrally during macular scanning and the increased difficulty for the examiner to check that fixation is being accurately maintained. Furthermore, since the topography of the optic nerve head compared to the macular area is much more varied, small decentration issues or fixation losses will increase the variability of measurements.

For routine clinical imaging, one scan does provide adequate data. However, for more detailed investigation such as that undertaken in research, we recommend three scans to provide robust measurements from which to detect change.

10.2 Effect of axial length on macular retinal thickness and retinal nerve fibre layer thickness

Ocular disease may impact retinal tissue thickness and structure in a number of ways. Decreases in retinal thickness may accompany degenerative diseases through atrophy, in age related macular degeneration or through ganglion cell axon loss exhibited in glaucoma. Macular oedema, arising from complications of uveitis, diabetic retinopathy or retinal vein occlusion will be exhibited as an increase in retinal thickness. In a clinical situation where retinal tissue changes are observed, it is important to consider normal physiological variations in retinal tissue, prior to conclusions being drawn and diagnoses being made. Scleral thinning and potentially retinal thickness reductions are associated with myopia. To date, studies investigating the effects of axial length on retinal thickness and retinal nerve fibre layer thickness have provided conflicting evidence. Our study attempted to determine the relationship between axial length and

retinal thickness at the macular and retinal nerve fibre layer thickness around the optic nerve head in normal human eyes.

Our study suggests that the impact of increased axial length in higher degrees of myopia affects retinal thickness non-uniformly across a circular scanning area, 6mm in diameter centred on the fovea. The foveal retinal thickness, represented by the inner ring scan, 1mm in diameter and retinal thickness in an annulus measuring 3mm across does not correlate with axial length. However, with increasing distance from the fovea, the effects of increasing axial length are marked. For retinal tissue located in the outer ring of the macular scan measuring 6mm in diameter, our study revealed an inverse relationship between axial length and thickness.

Similarly, in terms of retinal nerve fibre layer thickness the effects of axial length are not consistent in terms of position around the optic nerve head, or distance from the optic disc margin. At the optic disc margin, axial length exerts no measurable influence on retinal nerve fibre layer thickness. At increasing distance from the optic disc margin, our study revealed regional variations in axial length effects. Mean retinal nerve fibre layer thickness around the optic nerve head and nerve fibre layer thickness in the superior, nasal and inferior quadrants were significantly inversely correlated with axial length. No such effect was found for the temporal quadrant at any distance from the optic disc margin. This effect may be attributed to the fact that fibres in the temporal quadrant of the normal human eye are fewer in number compared to that in the inferior, superior and nasal quadrants (ISNT rule) and as a consequence, axial length effects are not apparent in this region.

The increased prevalence of disease in eyes with high myopia is not in question. Myopic subjects have been reported as having a twofold to threefold increased risk of developing glaucoma (Mitchell *et al.*, 1999). Pathology in the retinal periphery such posterior vitreous detachment, lattice degeneration, and pigmentary degeneration are more prevalent in myopic eyes (Akiba, 1993; Celorio and Pruett, 1991; Hoffman and Heath, 1997). A person with 5 dioptres of myopia is at a fifteen times greater risk of developing retinal detachment than an emmetrope, increasing to 110 times with 20 dioptres of myopia (Blacharski, 1988). Effects of myopia also are exhibited in the posterior pole with increased likelihood of optic disc crescents (Hendicott and Lam,

1991), posterior staphylomas (Steidl and Pruet, 1997), lacquer cracks (Klein and Curtin, 1975; Ohno-Matsui and Tokoro, 1996) and chorioretinal atrophy (Ito-Ohara, Seko, Morita *et al.*, 1998).

Our study shows that macular retinal thickness and retinal nerve fibre layer thickness around the optic nerve head correlates negatively with axial length which suggests that the individual with higher degrees of axial myopia may be more susceptible to ocular disease. Our study design was able to highlight regional variations of the impact of axial length on retinal thickness measurements which explain inconsistencies in previous studies.

Future work could include investigating the effects of axial length on peripheral retinal thickness, where the majority of degenerative conditions are observed and investigation of the relationship between myopia and glaucoma.

10.3 Effect of age on macular retinal thickness and retinal nerve fibre layer thickness

Normal physiological variations in retinal tissue, whether due to axial length or age are considerable and lead to difficulties in the interpretation of clinical data with respect to disease monitoring. Although studies to date have proved inconsistent it is thought that the retina and nerve fibre tissue are affected by age. Such suggestions have important implications for the long-term monitoring of disease, especially for conditions such as glaucoma for which there is an expected reduction in retinal nerve fibre layer thickness. In a clinical situation, in order for tissue changes to be ascribed to disease alone, it is imperative that the effects of age on retinal structure are established.

Our study explored the relationship between age and macular retinal thickness and retinal nerve fibre layer thickness around the optic nerve head. We found a significant positive correlation between age and retina thickness at the fovea only. In no other locations across the 6mm circular macular scan was there an effect of age on tissue thickness. Physiological ageing processes of the human eye including accumulation of lipofuscin in the retinal pigment epithelium (RPE) and extracellular deposits (drusen)

between the RPE basal lamina and the inner collagenous layer of the Bruch's membrane (a basement membrane situated between the RPE and the choriocapillaris) are well documented (Bonnel, Mohand-Said and Sahel, 2003). It is possible that these structural changes may account for the foveal thickening we observed in our study and the loss of the foveal reflex in elderly patients compared to young patients.

In terms of retinal nerve fibre layer thickness, at all distances from the optic disc margin there was evidence of a negative correlation between mean RNFL and superior retinal nerve fibre layer thickness. Retinal nerve fibre layer thickness was inversely correlated with age in the inferior and temporal quadrant only for the scanning circle imaging the retinal nerve fibre layer at a distance approximately 1mm from the disc edge. On initial consideration our results suggest that the effect of age is both sectoral in terms of which retinal area is primarily affected and dependent on the distance from the margin that retinal tissue is measured. Rather we suggest that an age effect is always present in our subject sample but the ability to detect this change varies according to location. Superiorly, where there is a comparatively larger number of fibres, an age effect is clearly pronounced at all distances from the optic disc margin. At approximately 1mm from the disc margin an age effect was found for every quadrant and for the mean RNFL. It is likely that this can be explained by the relative fewer number of fibres in this area and as a result, age effects will be more apparent here. For the largest scanning circle the effect of age is only detected for the superior quadrant. We suggest that age effects are not identified for the other quadrants at this distance due to the lack of retinal tissue here and the subsequent effect of signal:noise particularly in this region and the inability of the imaging device to detect changes of this magnitude.

This study suggests that decreases in retinal thickness and retinal nerve fibre layer thickness due to age effects must be considered during the examination of the eye with suspect pathology and in the long-term monitoring of ocular disease such as glaucoma.

10.4 Nerve fibre loss in glaucomatous neuropathy

It has long been established that nerve fibre layer defects precede loss of visual function (Quigley *et al.*, 1982) and glaucomatous changes to the optic nerve head (Sommer *et*

al., 1977) and as such, examination of the RNFL plays a key role in the initial diagnosis of the suspect glaucoma and monitoring of the glaucoma patient. The effect of glaucoma on the retinal nerve fibre layer thickness around the optic nerve head has been extensively investigated using a variety of techniques including red-free photography and more recently using imaging technologies such as optical coherence tomography and scanning laser polarimetry. OCT studies of the retinal nerve fibre layer have employed the default scanning radius for all subjects and to our knowledge no study has been conducted to quantify the way in which the RNFL changes with increasing distance from the optic nerve head. Our study hypothesised that retinal nerve fibre layer thickness decreases with increasing distance from the optic nerve head and as a result, glaucomatous loss will be less marked further away from the optic nerve head. Early detection of retinal nerve fibre layer thickness reductions at this increased distance from the optic nerve head would be a useful predictor of future glaucomatous loss.

The double hump formation of the RNFL as documented in several histological studies was found in our study for both the normal and glaucoma group. Retinal nerve fibre thickness was greater in normal subjects than for glaucoma patients in every location for every scan. Statistically significant differences occurred between groups in all quadrants for the disc margin scan and the second radius scan. However, as predicted for the third radius scan, difference in RNFL thickness reached statistical significance across the vertical pole. This supports early findings that the superior and inferior quadrants are more susceptible to glaucomatous damage while the nasal and temporal fibres are spared to a certain degree (Quigley *et al.*, 1982).

Our study suggests that OCT examination of RNFL thickness at a greater distance from the optic nerve head than traditionally employed may provide invaluable early indicators of the extent of glaucomatous damage and the efficacy of treatment protocols for the patient with primary open angle glaucoma.

10.5 Short term relationship between blood glucose levels, retinal thickness, retinal nerve fibre layer thickness and visual function

It is universally accepted that visual function of the diabetic patient is reduced compared to normal subjects and this has been reported for a variety of investigations including contrast sensitivity, colour vision, and SWAP visual fields whether in the presence or absence of diabetic retinopathy. It is also shown that visual function is affected by the glycaemic state of the diabetic patient. While disease monitoring in diabetes is a significant financial burden to healthcare systems, it is essential if early progression is to be detected and understood. By their very nature, subjective visual investigations can be highly valuable and quantitative objective measures would be desirable. At the same time, the impact of physiological diurnal variations such as those pertaining to intraocular pressure are well reported and often factored into research study designs or careful clinical monitoring in diseases such as glaucoma. For diabetics, the picture is more complex, because while acknowledgement is made of the fact that visual status is affected by long term control, the impact of acute changes in blood sugar during the course of the day have been much ignored. In this study we examined the relationship between retinal structure and visual function over a 12 hour cycle to determine the impact of long term control and variability of blood sugar levels in type 1 and type 2 diabetics.

No previous study to our knowledge has investigated the diurnal variation in retinal structure and visual function in diabetic subjects who by nature of their disease may be more susceptible to a greater variation in these parameters. We investigated the short-term impact of fluctuations in blood glucose levels in retinal structure and function over a 12 hour period in patients with diabetes. Unlike other studies that induced changes to blood glucose level using insulin infusions or glucose administration, our patients were instructed to maintain their daily routine of diet and medication in order that we could account for the fluctuations in visual performance often reported over the course of the day by the diabetic individual.

By observation, blood glucose levels appeared to differ according to diabetic type with greater variation between peaks and troughs in type 1 diabetic patients compared to type 2 diabetics, although analysis revealed no statistical difference between the two groups.

For the majority of test parameters the experience of type 1 and type 2 diabetic patients was identical. 100% logMAR vision, retinal nerve fibre layer thickness, retinal thickness (except foveal thickness) and white-on-white perimetry was unaffected by fluctuations in blood glucose.

Our findings of consistent 100% contrast visual acuity levels throughout the day despite there being fluctuations of blood glucose, concurs with several studies that found no evidence of a relationship between glycaemic state and visual acuity. A number of investigators have reported no changes in visual acuity during acute episodes of low blood glucose levels in diabetic patients (Harrad *et al.*, 1985; McCrimmon *et al.*, 1996). Ewing *et al.* (1998) reported no significant differences between distance or near Snellen visual acuity in the hypoglycaemic (low blood glucose level) or euglycaemic (normal blood glucose level) state of type 1 diabetic patients while Tabandeh *et al.* (1996) observed that visual acuity of normal subjects remained unaffected by an acute decrease in blood glucose levels.

Diurnal variations of retinal thickness and retinal nerve fibre layer thickness have not been reported to our knowledge with the exception of Frank *et al.* (2004) who reported fluctuations in diabetic macular oedema over the course of the day. Retinal thickness, as measured by the OCT was greatest at the start of the day, just after waking and decreased over subsequent visits. The authors suggest that a decrease in macular retinal thickness is most likely to be explained by the shift from recumbent to upright body position of their patients. They recommend that clinical assessment of diabetic patients using OCT should consider the time of day when measurements were acquired. Despite the lack of changes in retinal structure throughout the day, the OCT has a potentially useful role in detecting early diabetic retinopathic changes in the eye compared to traditional assessments using funduscopy and photography (Sugimoto, Sasoh, Ido *et al.*, 2005).

Foveal retinal thickness, reduced contrast logMAR acuity, Pelli Robson contrast sensitivity and SWAP visual fields exhibited changes throughout the day. We suggest this may be explained by the nature of such tests, with the latter three visual function tests based on selective sampling and, as such, will detect more subtle effects.

Our findings of a differential between visual acuity and contrast sensitivity show agreement with early studies which report that reduced visual acuity is often preceded by central vision abnormalities in diabetic eyes which may by exhibited as contrast sensitivity defects (Moloney and Drury, 1982; Della Salla *et al.*, 1985; Sokol *et al.*, 1985; Gharfour *et al.*, 1982). Clinical studies have shown that there is often dissociation between contrast sensitivity scores and levels of visual acuity in patients with diseased eyes (Wolkstein *et al.*, 1980; Hyvarinen *et al.*, 1983).

That contrast sensitivity is affected by acute changes in blood glucose is well documented. Reduced contrast sensitivity scores are associated with hypoglycaemia (Hyvarinen *et al.*, 1983; Tabandeh, Ranganath and Marks, 1996). Verrotti *et al.* (1998) however, reported poor contrast sensitivity at high glucose levels, with normal contrast sensitivity levels at reduced blood glucose levels.

Our observations that SWAP varied over the course of the day but not white-on-white perimetry receives support from several studies. Short-wavelength sensitive (SWS) cone mediated mechanisms are reported to be susceptible to damage in diabetic retinopathy (Greenstein *et al.*, 1989; Greenstein *et al.*, 1990; Nomura *et al.*, 2000). We suggest that SWAP perimetry may be a useful indicator of functional loss in the diabetic eye.

Intraocular pressure, diastolic blood pressure, mean arterial pressure and mean ocular perfusion pressure exhibited an apparent inverse relationship with blood glucose levels. The reasons for these relationships are unclear at this stage and warrant further investigation. Difficulities in interpreting study results are confounded by the fact that IOP and blood pressure in all subjects, regardless of metabolic factors or disease, exhibits changes throughout the day.

The observed inverse relationship between blood glucose and IOP according to our findings appears to disagree with the results of a number of studies where acute hypoglycaemia has been shown to provoke a reduction in intraocular pressure both in patients with insulin diabetes (Frier, Hepburn, Fisher *et al.*, 1987). Mitchell *et al.* (1997) suggest that increases in blood glucose levels lead to an induction of an osmotic gradient with a subsequent movement of fluid into the intraocular space, resulting in an

increase in IOP. Conversely, Dielemans *et al.* (1994) suggest that the reverse is true, with an increase in blood glucose giving rise to a reduction in IOP due to a fluid shift out of the intraocular compartment.

We suggest large fluctuations in blood glucose levels and/or visual function and structure over a 12 hour period may be indicative of an increased risk of developing or progression of existing diabetic retinopathy.

Long-term control, as indicated by HbA1c levels was the best indicator for Pelli Robson contrast sensitivity scores which confirms the earlier findings of Banford *et al.* (1994) who report a negative correlation between contrast sensitivity and HbA1c. Conclusions regarding this relationship, however, are far from consistent. Variation in the inferior retinal nerve fibre layer thickness over the course of the day, for all visits was best predicted by the type of diabetes and the duration of the disease. Diabetic type was also the best predictor for mean retinal nerve fibre layer and for superior macular retinal thickness for some, but not all visits.

Our study suggests that there is little difference in the visual experience of all diabetic subjects, despite the differences in their physiological status. Blood glucose notably affects visual function and diastolic blood pressure, yet the reasons for this are not established.

A recommendation for future work would be to explore the relationship between the degree of retinopathy and visual function of the diabetic patient. To date, conflicting reports have been published regarding this issue. A study of these variables in normal subjects is currently in progress.

10.6 Anatomical and functional changes in the visual cortex of patients with glaucoma: A pilot study and case discussions

This study explored the anatomical changes along the visual pathway and functional changes of the glaucomatous patient. With regards anatomy, the findings of this study

suggest that RNFLt in the study sample was a less reliable indicator of glaucoma damage that neuroretinal rim area or retrobulbar optic nerve diameter. In relation to the latter there remains a contradiction. On the one hand these preliminary data do not seem to suggest that the retrobulbar optic nerve diameter reduce with disease, however smaller diameters were associated with glaucomatous visual field loss. Further study with larger sample numbers will unravel the question. However, a possible explanation would be that the supporting structures of the optic nerve such as neuroglia preserve optic nerve diameter even after fibres have died, while smaller diameter optic nerves may be those of eyes with reduced redundancy and thus a tendency for earlier or more marked disease in glaucoma.

A measurable reduction in grey matter density was observed with age. This may be the result of cortical cell loss, perhaps through absorption, or through cell shrinkage with age. Case studies of glaucoma patients revealed no obvious exacerbation of age-related losses in patients with significant glaucomatous visual field loss. There are three explanations for this finding: i) There is no impact on cortical cell numbers or size in patients with glaucoma, ii) Reductions in cortical cell density substantially lag anatomical changes in the anterior visual pathway, iii) There is a reduction in grey matter density but the sample size in this study was too low to detect it reliably. Only further study will address this question.

Visual field data are known to lag anterior optic nerve damage in glaucoma. Numerous theories have been suggested as to why these psychophysical responses appear relatively robust to the impact of even moderate to advanced ganglion cell death. However, the most well supported, relates to sampling theory in which it is suggested that redundancy due to over supply of fibres masks functional loss to varying extents. Coupled with inherent variability due to their subjective nature, they remain an important but flawed clinical tool by which to diagnose and monitor diseases such as glaucoma.

This pilot study demonstrates that fMRI offers a potentially important method by which to assess visual status in patients with glaucoma. Inspection of data on a case-wise basis leads to the suggestion that in some patients, particularly those for whom it is believed they had a large number of fibres at the outset, or a high degree of redundancy in the

visual pathway, fMRI may even be a more reliable indicator of functional damage. If verified through future studies, the possible reasons for this, are multifold. For example, if there is significant redundancy, the relatively non-specific sampling volume of normal visual field investigations masks the effects of damage, while cortical responses, sampled objectively over the entire visual field and interpreted via vascular activity changes in the cortex, appear to be more marked. Extensive additional data would be required to verify these preliminary findings.

Future investigations are required to establish the normal variation of cortical activation with respect to anterior optic nerve and visual field parameters and to confirm or rebuke suggestions of reduced grey matter density in glaucomatous patients. These investigations will aid the understanding of mechanisms of glaucoma and offer new diagnostic tools for the disease.

10.7 Final conclusion

These investigations have shown that the effects of senescence are evident in both the anterior and posterior visual pathway. A variety of anatomical and functional diagnostic protocols for the investigation of damage to the visual pathway in ocular disease are required to maximise understanding of the disease processes and thereby optimising patient care.

REFERENCES

Abate, N and Chandalia, M (2003). The impact of ethnicity on type 2 diabetes. Journal of Diabetes and Its complications **17**(1): 39-58.

Abate, N, Garg, A, Peschock, R M, Stray-Gundersen, J, Adams-Huet, B and Grundy, S M (1996). Relationship of generalised and regional adiposity to insulin sensitivity in men with IDDM. Diabetes **45**(12): 1684-1693.

Aclimandos, W A and Galloway, N R (1988). Blindness in the city of Nottingham (1980-1985). Eye **2**: 431-434.

Afrashi, F, Erakgun, T, Kose, S, Ardic, K and Mentes, J (2003). Blue-on-yellow perimetry versus achromatic perimetry in type 1 diabetes patients without retinopathy. Diabetes research and clinical practice **61**: 7-11.

Airaksinen, P J (1989). Retinal nerve fiber layer and neuroretinal rim changes in ocular hypertension and early glaucoma (summary). Surv Ophthalmol **33**(Supplement 1): 413-414.

Airaksinen, P J, Drance, S M and Douglas, G R (1984). Diffuse and localised nerve fibre loss in glaucoma. Am J Ophthalmol **98**: 566-572.

Airaksinen, P J, Mustonen, E and Alanko, H I (1981). Optic disc haemorrhages precede retinal nerve fibre layer defects in ocular hypertension. Acta Ophthalmol **59**: 637-641.

Aizenman, Y and de Vellis, J (1987). Synergistic action of thyroid hormone, insulin and hydrocortisone on astrocyte differentiation. Brain Res **414**:301-308

Akiba, J (1993). Prevalence of posterior vitreous detachment in high myopia. Ophthalmology **100**: 1384-1388.

Alamouti, B and Funk, J (2003). Retinal thickness decreases with age: an OCT study. Br J Ophthalmol **87**: 899-901.

Alberti, K G M M and Zimmer, P Z (1998). Definition, diagnosis and classification of diabetes mellitus and its complications. Part 1: Diagnosis and classification of diabetes mellitus. Diabetic medicine **15**: 539-553.

Aldebasi, Y, Drasdo, N, Morgan, J and North, R (2003). Cortical OFF-potentials from the S-cone pathway reveal neural damage in early glaucoma. Vis Res **43**(2): 221-226.

Anderson, D R (1977). Axonal transport in the retina and optic nerve. In Neuroophthalmology. Ed. Glasser,J.S. CV Mosby Co, St Louis **9**: 140-153.

Anderson, D R (1989). Glaucoma: the damage caused by pressure. Am J Ophthalmol **108**: 485-495.

Anderson, R S and O'Brien, C (1997). Psychophysical Evidence for a Selective Loss of M Ganglion Cells in Glaucoma. Vis Res **37**(8): 1079-1083.

Andrews, T J, Halpern, S D and Purves, D (1997). Correlated size variations in human visual cotrex, lateral geniculate nucleus and optic tract. J Neuroscience **17**(8): 2859-2868.

Ang, A, Tong, L and Vernon, S A (2000). Improvement of reproducibilty of macular volume measurements using the Heidelberg retinal tomograph. Br J Ophthalmol **84**: 1194-1197.

Antcliff, R J, Ffytche, T J, Shilling, J S and Marshall, J (2000). Optical coherence tomography of melanocytoma. Am J Ophthalmol **130**(6): 845-847.

Antonetti, D A, Barber, A J, Hollinger, L A, Wolpert, E B and Gardner, T W (1999). Vascular endothelial growth factor induces parid phosphorylation of tight junction proteins occludin and zonula occludin-1. A potential mechanism for vascular permeability in diabetic retinopathy and tumours. J Biol Chem **274**: 23463-23467.

Antonetti, D A, Barber, A J, Khin, A J, Lieth, E, Tarbell, J M and Gardner, T W (1998). Vascular permeability in experimental diabetes is associated with reduced endothelial occludin content:vascular endothelial growth factor decreases occludin in retinal endothelial cells. Diabetes **47**: 1953-1959.

Applegate, R A, Adams, A J, Cavender, J C and Zisman, F (1987). Early colour vision changes in age -related maculopathy. Applied Optics **26**(8): 1458-1463.

Arden, G B and Jacobson, J (1978). A simple grating test for contrast sensitivity-glaucoma screening. Invest Ophthalmol Vis Sci **17**: 23-32.

Arend, O, Remky, A, Evans, R et al., (1997). Contrast sensitivity loss is coupled with capillary dropout in patients with diabetes. Invest Ophthalmol Vis Sci **38**: 1819-1824.

Armaly, M F (1965). On the distribution of applanation pressure. Arch Ophthalmol **73**: 11-18.

Armaly, M F, Kreuger, D E and Maunder, L (1980). Biostatistical analysis of the collaborative glaucoma study. I. Summary report of the risk factors for glaucomatous visual field defects. Arch Ophthalmol **98**: 2163-2171.

Armstrong, J R, Daily, R K, Dobson, H L and Girard, L J (1960). The incidence of glaucoma on diabetes mellitus. Am J Ophthalmol **50**: 55-63.

Arndt C. F., Desmettre T., Montreuil E. and Herbinet B. (1995). 3136 Magnocellular pathways in glaucoma and ocular hypertension. Vis Res **35**(Supplement 1): S124.

Ashton, N (1974). Vascular basement membrane changes in diabetic retinopathy. Montgomery Lecture 1973. Br J Ophthalmol **58**(4): 344-366.

Asrani, S, Zou, S, d'Anna, S, Vitale, S and Zeiner, R (1999). Noninvasive mapping of the normal retinal thickness at the posterior pole. Ophthalmology **106**: 269-273.

Awata, T, Kurihara, S, Takata, N, Neda, T, Iizuka, H, Ohkubo, T, Osaki, M, Watanabe, M, Nakashima, Y and Inukai, K (2005). Functional VEGF C-634G polymorphism is associated with development of diabetic macular edema and correlated with macular retinal thickness in type 2 diabetes. Biochemical and Biophysical Research Communications **333**(3): 679-685.

Aydin, A, Wollstein, G, Price, L L, Fujimoto, J G and Schuman, J S (2003). Optical coherence tomography assessment of retinal nerve fiber layer thickness changes after glaucoma surgery. Ophthalmology **110**(8): 1506-1511.

Aydin, A, Wollstein, G, Price, L L and Schuman, J S (2003). Evaluating pulsatile ocular blood flow analysis in normal and treated glaucomatous eyes. Am J Ophthalmol **136**(3): 448-453.

Azuara-Blanco, A, Harris, A and Cantor, L B (1998). Reproducibility of optic disc topographic measurements with the Topcon Imagenet and the Heidelberg retina tomograph. Ophthalmologica **212**: 95-98.

Bagga, H and Greenfield, D S (2004). Quantitative assessment of structural damage in eyes with localized visual field abnormalities. Am J Ophthalmol **137**(5): 797-805.

Bagga, H, Greenfield, D S, Feuer, W and Knighton, R W (2003). Scanning laser polarimetry with variable corneal compensation and optical coherence tomography in normal and glaucomatous eyes. Am J Ophthalmol **135**(4): 521-529.

Bagga, H, Greenfield, D S and Feuer, W J (2005). Quantitative assessment of atypical birefringence images using scanning laser polarimetry with variable corneal compensation. Am J Ophthalmol **139**(3): 437-446.

Balazsi, A G, Rootman, J, Drance, S M, Sculze, M and Douglas, G R (1984). The effect of age on the nerve fibre population of the human optic nerve. Am J Ophthalmol **97**: 760-767.

Banford, D, North, R V, Dolben, J, Butler, G and Owens, D R (1994). Longitudinal study of visual functions in young insulin dependent diabetics. Ophthal Physiol Opt **14**: 339-346.

Baquero-Aranda, I M, Morillo Sanchez, M J and Garcia Campos, J M (2005). Use of optical coherence tomography to study variations of normal parameters with age. Archivos De La Sociedad Espanola De Oftalmologia **80**(4): 225-231.

Barber, A J (2003). A new view of diabetic retinopathy: a neurodegenerative disease of the eye. Progress in Neuro-Psychopharmacology and Biological Psychiatry **27**: 283-290.

Barber, A J, Antonetti, D A, Gardner, T W (2000). Altered expression of retinal occludin and glial fibrillary acidic protein in experimental diabetes. Invest Ophthalmol Vis Sci **41**:3561-3568

Barber, A J, Lieth, E, Khin, S A, Antonetti, D A, Buchanan, A G, Gardner, T W (1998). Neural Apoptosis in the retina during experimental and human diabetes. J Clin Invest **102**(4): 783-791.

Barboni, P, Savini, G, Valentino, M L, Montagna, P, Cortelli, P, De Negri, A M, Sadun, F, Bianchi, S, Longanesi, L and Zanini, M (2005). Retinal nerve fiber layer evaluation by optical coherence tomography in Leber's hereditary optic neuropathy. Ophthalmology **112**(1): 120-126.

Bartz-Schmidt, K U and Schmitz-Valckenberg P (1994). Retinal nerve fibre layer photography and papillometry in juvenile diabetes mellitus. Ophthalmologe **91**:3643-3731

Baumann, M, Gentile, R C, Liebman, J M and Ritch, R (1998). Reproducibility of retinal thickness measurements in normal eyes using optical coherence tomography. Ophthalmic Surg Lasers **29**(4): 280-285.

Bayer, A, Harasymowycz, P, Henderer, J D, Steinmann, W G and Spaeth, G L (2002). Validity of a new disk grading scale for estimation glaucomatous damage: correlation with visual field damage. Am J Opthalmol **133**: 758-763.

Beatty, S, Good, P A, McLaughlin, J and O'Neill, E C (1998a). Correlation between the orbital and intraocular portions of the optic nerve in glaucomatous and ocular hypertensive eyes. Eye **12**: 707-713.

Beatty, S, Good, P A, McLaughlin, J, Tsaloumas, M and O'Neill, E C (1998b). Evaluation of optic disc cupping using high -resolution ocular ultrasound. Eye **12**: 54-60.

Beatty, S, McLaughlin, J and O'Neill, E C (1998c). Echographic measurements of the retrobulbar optic nerve in normal and glaucomatous eyes. Br J Ophthalmol **82**: 43-47.

Becker, B (1971). Diabetes and primary open-angle glaucoma. Am J Ophthalmol **71**: 1-16.

Bengttson, B (1981). The prevalence of glaucoma. Br J Ophthalmol **65**: 46-49.

Benhamou, N, Massin, P, Haouchine, B, Erginay, A and Gaudric, A (2002). Macular retinoschisis in highly myopic eyes. Am J Ophthalmol **133**(6): 794-800.

Bennett, A G, Rudnicka, A R and Edgar, D F (1994). Improvements on Littmann's method of determining the size of retinal features by fundus photography. Graefe's Arch Clin Exp Ophthalmol **232**: 361-367.

Birch, M, Brotchie, D, Roberts, N and Grierson, I (1997). The three-dimensional structure of the connective tissue in the lamina cribrosa of the human optic nerve head. Ophthalmologica **211**: 183-191.

Blacharski, P A (1988). Pathologic progressive myopia, in DA Newsome Ed. Retinal dystrophies and degenerations **Raven Press, New York**.

Bland, J M and Altman, D G (1986). Statistical methods for assessing agreement between two methods of clinical measurement. Lancet **2**:307-310

Bland, J M and Altman, D G (1996). Measurement error and correlation coefficients. BMJ **313**:41-42.

Blumenthal, E Z and Weinreb, R N (2001). Assessment of the Retinal Nerve Fiber Layer in Clinical Trials of Glaucoma Neuroprotection. Surv Ophthalmol **45**(Supplement 3): S305-S312.

Blumenthal, E Z, Williams, J M, Weinreb, R N, Girkin, C A, Berry, C C and Zangwill, L M (2000). Reproducibility of nerve fiber layer thickness measurements by use of optical coherence tomography. Ophthalmology **107**(12): 2278-2282.

Bonnel, S, Mohand-Said, S and Sahel, J A (2003). The aging of the retina. Exp Gerontology **38**: 825-831.

Bonomi, L, Marchini, G, Marraffa, M et al (1998). Prevalence of glaucoma and intraocular pressure in a defined population. The Egna-Neumarkt Study. Ophthalmology **105**: 209-215.

Bonomi, L, Marchini, G, Marraffa, M, Bernardi, P, Morbio, R and Varotto, A (2000). Vascular risk factors for primary open angle glaucoma: The Egna-Neumarkt Study. Ophthalmology **107**(7): 1287-1293.

Bowd, C, Weinreb, R N, Williams, J M and Zangwill, L M (2000). The retinal nerve fiber layer thickness in ocular hypertensive, normal, and glaucomatous eyes with optical coherence tomography. Arch Ophthalmol **118**: 22-26.

Bowd, C, Zangwill, L M, Berry, C C, Blumenthal, E Z, Vasile, C, Sanchez-Galeana, C, Bosworth, C F, Sample, P A and Weinreb, R N (2001). Detecting early glaucoma by assessment of retinal nerve fibre layer thickness and visual function. Invest Ophthalmol Vis Sci **42**: 1993-2003.

Bresnick, G H, Condit, R S, Palta, M, Korth, K, Groo, A and Syrjala, S (1985). Association of hue discrimination loss and diabetic retinopathy. Arch Ophthalmol **103**: 1317-1324.

Bressler, N M (1998). Evaluating new retinal imaging techniques. Arch Ophthalmol **116**: 521-522.

Bressler, S B, Bressler, N M, Fine, S L, Hillis, A, Murphy, R P, Olk, R J and Patz, A (1982). Natural course of CNV membranes within the foveal avascular zone in senile macular degeneration. Am J Ophthalmol **93**: 157-163.

Brinchmann-Hansen, O, Bangsatd, H J, Hultgren S, Fletcher, R, et al., (1993). Psychophysical visual function, retinopathy, and glycaemic control in insulin-dependent diabetics with normal visual acuity. Acta Ophthalmol **71** 230-257.

Brigatti, L, Weitzman, M and Caprioli, J (1995). Regional test-retest variability of confocal scanning laser tomography. Am J Ophthalmol **120**: 433-440.

British Standards Institution. Accuracy (trueness and precision) of measurement methods and results. General Principles and definitions. BS ISO 5725 part 1. London: British Standards Institution: 1994.

British Standards Institution. Accuracy (trueness and precision) of measurement methods and results: basic methods for the determination of repeatability and reproducibility of a standard measurement method. BS ISO 5725 part 2. London: British Standards Institution: 1994.

Broadway, D C, Nicolela, M T and Drance, S M (1999). Optic disc appearances in Primary open angle glaucoma. Surv Ophthalmol **43(Suppl)**(1): S223-S243.

Brown, G C, Brown, M M, Sharma, S, Brown, H and Tasman, W (2000). Incremental cost effectiveness of laser photocoagulation for subfoveal choroidal neovascularisation. Ophthalmology **107**: 1374-1380.

Browning, D J and Fraser, C M (2005). Regional Patterns of Sight-Threatening Diabetic Macular Edema. Am J Ophthalmol **140** (1): 117-124

Browning, D J, McOwen, M D, Bowen, R M and O'Marah, T L (2004). Comparison of the clinical diagnosis of diabetic macular oedema with diagnosis by optical coherence tomography. Ophthalmology **111**: 712-715.

Brunk, U T and Terman, A (2002). Lipofuscin:mechanisms of age related accumulation and influence on cell function. Free radical biology and medicine **33**(5): 611-619.

Budenz, D, L, Chang, R T, Huang, X-R, Knighton, R W, and Tielsch, J M (2005). Reproducibility of Retinal Nerve Fiber Thickness Measurements Using the Stratus OCT in Normal and Glaucomatous Eyes. Invest Ophthalmol Vis Sci **46**: 2440-2443.

Budenz, D L, Michael, A, Chang, R T, McSoley, J and Katz, J (2005). Sensitivity and specificity of the StratusOCT for perimetric glaucoma. Ophthalmology **112**(1): 3-9.

Bulpitt, C J, Hodes, C and Everitt, M G (1975). Intraocular pressure and systemic blood pressure in the elderly. Br J Ophthalmol **59**: 717-720.

Burk, R O W and Rendon, R (2001). Clinical detection of optic nerve damage: Measuring changes in cup steepness with use of a new image alignment algorithm. Surv Ophthalmol **45(Suppl)** (3): S297-S303.

Burk, R O W, Rohrschneider, K, Takamoto, T, Volcker, H E and Schwartz, B (1993). Laser scanning tomography and stereophotogrammetry in three-dimensional optic disc analysis. Graefe's Arch Clin Exp Ophthalmol **231**: 193-198.

Bursell, S E, Clermont, A, Kinsley, B, Simonsen, D, Aiello, L and Wolpert, H (1996). Retinal blood flow changes in patients with insulin-dependent diabetes mellitus and no diabetic retinopathy. Invest Ophthalmol Vis Sci **37**: 886-897.

Cahane, M and Bartov, E (1992). Axial length and scleral thickness effect on susceptibility to glaucomatous damage: a theoretical model implementing Laplace's law. Ophthalmic Res **24**: 280-284.

Carpineto, P, Ciancaglini, M, Zuppardi, E, Falconio, G, Doronzo, E and Mastropasqua, L (2003). Reliability of nerve fibre layer thickness measurements using optical coherence tomography. Ophthalmology **110**: 190-195.

Cartwright, M J and Anderson, D R (1988). Correlation of assymetric damage with assymetric intraocular pressure in normal-tension glaucoma (low tension glaucoma). Arch Ophthalmol **106**: 898-900.

Catier, A, Tadayoni, R, Paques, M, Erginay, A, Haouchine, B, Gaudric, A and Massin, P (2005). Characterization of Macular Edema from Various Etiologies by Optical Coherence Tomography. Am J Ophthalmol **140**(2): 200-206.

Celorio, J M and Pruett, R C (1991). Prevalence of lattice degeneration and its relation to axial length in severe myopia. Am J Ophthalmol **111**: 20-23.

Cerutti, F, Sacchetti, C, Vigo, A, Dianzani, I, Barateno, S, Bessone, A, Vaona, P and Furlotti, F (1989). Course of retinopathy in children and adolescents with insulin-dependent diabetes mellitus: A ten-year study. Ophthalmol Scand **198**: 116-123.

Chan, A, Duker, J S, Schuman, J S and Fujimoto, J G (2004). Stage 0 macular holes: Observations by optical coherence tomography. Ophthalmology **111**(11): 2027-2032.

Charman, W N (1998). Imaging in the 21st Century. Ophthal Physiol Opt **18**(2): 210-233.

Chaturvedi, N, Hedley-White, E T and Dreyer, D B (1993). Lateral geniculate nucleus. Am J Ophthalmol **116**: 182-188.

Chauhan, B C, LeBlanc, R P, McCormick, T A and Rogers, J B (1994). Test-retest variability of topographic measurements with confocal scanning laser tomography in patients with glaucoma and control subjects. Am J Ophthalmol **15**: 118-119.

Chauhan, B C and MacDonald, C A (1995). Influence of time separation on variability estimates of topgraphic measurements with confocal scanning laser tomography. J Glaucoma **4**: 189-193.

Chauhan, D S and Marshall, J (1999). The interpretation of optical coherence tomography images of the retina. Invest Ophthalmol Vis Sci **40**(10): 2332-2342.

Chen, H C, Newsom, R S, Patel, V et al., (1994). Retinal blood flow changes during pregnancy in women with diabetes. Invest Ophthalmol Vis Sci **35**: 3199-3208.

Cheung, C, Liu, C J, Chiou, H, Chou, J C, Hsu, W and Liu, J (2001). Colour doppler imaging of retrobulbar haemodynamics in chronic angle closure glaucoma. Ophthalmology **108**: 1445-1451.

Chi, Q M, Tomita, G, Inazumi, K, Hayakawa, T, Ido, T and Kitazawa, Y (1995). Evaluation of the effect of aging on the retinal nerve fibre layer thickness using scanning laser polarimetry. J Glaucoma **94**: 406-413.

Chihara, E, Matsuoka, T, Ogura, Y et al., (1993). Retinal nerve fibre layer defect as an early manifestation of diabetic retinopathy. Ophthalmology **100**:1147-1151.

Chihara, E, Liu, X, Dong, J et al., (1997). Severe myopia as a risk factor for progressive visual field loss in primary open angle glaucoma. Ophthalmologica **211**: 66-71.

Chihara, E and Sawada, A (1990). Atytpical nerve fibre layer defects in high myopes with high-tension glaucoma. Arch Ophthalmol **108**: 228-232.

Choplin, N T (2001). Effect of corneal polarization axis on assessment of retinal nerve fiber layer thickness by scanning laser polarimetry. Am J Ophthalmol **131**(4): 528.

Choplin, N T, Zhou, Q and Knighton, R W (2003). Effect of individualized compensation for anterior segment birefringence on retinal nerve fiber layer assessments as determined by scanning laser polarimetry. Ophthalmology **110**(4): 719-725.

Christiannson, J (1961). Intraocular pressure in diabetes mellitus. Acta Ophthalmol **39**: 155-167.

Chujo, S, Kobayashi, Y, Emi, K et al., (1983). The biometry of each thickness of the human retina, choroid, sclera by using ultrasound and Fourier Analysis. Acta Soc Ophthalmol Jpn **87**: 70-73.

Cioffi, G A (2001). Three common assumptions about ocular blood flow and glaucoma. Surv Ophthalmol **45(Suppl)**: S325-S331.

Cioffi, G A, Robin, A L, Eastman, R D, Perell, H F, Sarfarazi, F A and Kelman, F E (1993). Confocal Laser Scanning Ophthalmoscope. Reproducibility of optic nerve head topographic measurements with the confocal scanning laser ophthalmoscope. Ophthalmology **100**: 57-62.

Coffey, M, Reidy, A and Wormaid, R (1993). Prevalence of glaucoma in the west of Ireland. Br J Ophthalmol **77**: 17-21.

Cohen, K L, Patel, S B and Ray, N (2004). Retinal thickness measurement after phacoemulsification. J Cat Refract Surg **30**(7): 1501-1506.

Cohen, M S and Bookheimer, S Y (1994). Localization of brain function using magnetic resonance imaging. Trends Neurosci **17**: 268-277.

Cole, D F (1977). Secretion of the aqueous humour. Exp Eye Res **38 (Suppl)**: 161-176.
Colen, T P and Lemij, H G (2002). Motion artifacts in scanning laser polarimetry. Ophthalmology **109**(8): 1568-1572.

Conway, M (2004). Investigation of visual defects attributed to vigabatrin **(PhD Thesis)**

Courtney, S M and Ungerleider, L G (1997). What fMRI has taught us about human vision. Curr Opin Neurobiol **7**: 554-561.

Crawford, M L J, Harwerth, R S, Smith, E L, Shen, F and Carter-Dawson, L (2000). Glaucoma in primates: cytochrome oxidase reactivity in parvo and magnocellular pathways. Invest Ophthalmol Vis Sci **41**: 1791-1802.

Cunha-Vaz, J, Faria de Abreu, J R and Campos, A J (1975). Early breakdown of the blood-retinal barrier in diabetes. Br J Ophthalmol **59**: 649-656.

Cunha-Vaz, J, Gray, J R, Zeimer, R, Mota, M C, Ishimoto, B M and Leite, E B (1985). Characterisation of the early stages of diabetic retinopathy by vitreous fluorophotometry. Diabetes **34**: 53-59.

Cunha-Vaz, J, Lobo, C L, Sousa, J C, Oliveiros, B, Leite, L and de Abreu, F (1985). Progression of retinopathy and alteration of the blood-retinal barrier in patients with type 2 diabetes: a 7-year prospective follow-up study. Graefe's Arch Clin Exp Ophthalmol **236**: 264-268.

Curcio, C A, Allen, K A, Sloan, K R et al., (1991). Distribution and morphology of human cone photoreceptors stained with anti-blue opsin. J Com Neurol **312**: 610-624.

Curtin, B J and Karlin, D B (1971). Axial length measurements and fundus changes of the myopic eye. Am J Ophthalmol **71**(1): 42-53.

Dandona, L, Hendrickson, A and Quigley, H A (1991). Selective effects of experimental glaucoma on axonal transport by retinal ganglion cells to the dorsal lateral geniculate nucleus. Invest Ophthalmol Vis Sci **32**: 1593-1599.

Dandona, L, Quigley, H A and Jampel, H D (1989). Variabilty of depth measurements of the optic nerve head and peripapillary retina with computerised image analysis. Arch Ophthalmol **107**: 1786-1792.

Dandona, L, Quigley, H A, Brown, A E, Enger, C (1990). Quantitative regional structure of the normal human lamina cribrosa. A racial comparison. Arch Ophthalmol **108** (3): 393-398

Danesh-Meyer, H, Savino, P J, Spaeth, G L and Gamble, G D (2005). Comparison of Arteritis and Nonarteritic Anterior Ischemic Optic Neuropathies with the Heidelberg Retina Tomograph. Ophthalmology **112**(6): 1104-1112.

David, R, Livingston D.G and Luntz, M H (1977). Ocular hypertension: a long term follow-up of treated and untreated patients. Br J Ophthalmol **61**: 668-674.

Di Leo, M A, Caputo, S, Falsini, B, Porciatti V, Minella A, Greco AV, Ghirlanda G (1992). Nonselective loss of contrast sensitivity in visual system testing in early type 1 diabetes. Diabetes Care **15**: 620-625.

Degenring, R F, Aschmoneit, I, Kamppeter, B, Budde, W M and Jonas, J B (2004). Optical coherence tomography and confocal scanning laser tomography for assessment of macular edema. Am J Ophthalmol **138**(3): 354-361.

Della-Sala, S, Bertoni, G, Somazzi, L, Stubbe, F and Wilkins, A J (1985). Impaired contrast sensitivity in diabetic patients with and without retinopathy: a new technique for rapid assessment. Br J Ophthalmol **69**: 136-142.

Dichtl, A, Jonas, J B (1996). Echographic measurement of optic nerve thickness correlated with neuroretinal rim area and visual field defect in glaucoma. Am J Ophthalmol **122**: 514–519.

Dichtl, A, Jonas, J B and Naumann, G O H (1999). Retinal nerve fibre layer thickness in human eyes. Graefe's Arch Clin Exp Ophthalmol **237**: 474-479.

Dielemans, I, Vingerling, J R and Wolfs, R C (1994). The prevalence of primary open angle glaucoma in a population based study in The Netherlands. The Rotterdam Study. Ophthalmology **101**: 1851-1855.

Dielemans, I, Vingerling, J R, Algra, D et al. (1995). Primary open-angle glaucoma, intraocular pressure and systemic blood pressure in the general elderly population. The Rotterdam Study. Ophthalmology **102**: 54-60.

Dolman, C L, McCormick, A Q and Drance, S M (1980). Aging of the optic nerve. Arch Ophthalmol **98**: 2053-2058.

Dosso, A A, Bonvin, E R, Morel, Y et al., (1996). Risk factors associated with contrast sensitivity loss in diabetic patients. Graefe's Arch Clin Exp Ophthalmol **234**: 300-305.

Drance, S M, Sweeney, V P, Morgan, R W and Feldman, F (1973). Studies of factors involved in the production of low tension glaucoma. Arch Ophthalmol **89**: 457-465.

Dreher, A W, Tso, P C and Weinreb, R N (1991). Reproducibility of topographic measurements of the normal and glaucomatous optic nerve head with the laser tomographic scanner. Am J Ophthalmol **111**: 221-229.

Dreyer, E B, Zurakowski, D, Schumer, R A et al., (1996). Elevated glutamate levels in the vitreous body of humans and monkeys with glaucoma. Arch Ophthalmol **114**: 299-305.

Duke-Elder S (1995). Changes in refraction in diabetes mellitus. Br J Ophthalmol **9**:167-187.

Ekstrom, C (1996). Prevalence of open-angle glaucoma in central Sweden. Acta Ophthalmol Scand **74**: 107-112.

El Beltagi, T A, Bowd, C, Boden, C, Amini, P, Sample, P A, Zangwill, L M and Weinreb, R N (2003). Retinal nerve fiber layer thickness measured with optical coherence tomography is related to visual function in glaucomatous eyes. Ophthalmology **110**(11): 2185-2191.

Engler, C, Krogsaa, B and Lund-Andersen, H (1991). Blood-retinal barrier permeability and its relation to the progression of diabetic retinopathy in type 1 diabetics: an 8-year follow-up study. Graefe's Arch Clin Exp Ophthalmol **229**: 442-446.

Early Treatment of Diabetic Retinopthy Study (ETDRS), (1985). Photocoagulation for diabetic macular oedema. Arch Ophthalmol **103**: 1796-1806.

Early Treatment of Diabetic Retinopthy Study (ETDRS), (1987). Treatment techniques and clinical guidelines for photocoagulation of diabetic macular oedema. Ophthalmology **94**: 761-774.

Early Treatment of Diabetic Retinopthy Study (ETDRS), (1995). Focal photocoagulation treatment of diabetic macular oedema. Arch Ophthalmol **113**: 1144-1155.

Ewing, F M E, Dreary, I J, McCrimmon, R J, Strachan, M W J and Frier, B M (1998). Effect of acute hypoglyacaemia on visual information processing in adults with type 1 diabetes mellitus. Physiology and Behaviour **64**(5): 653-600.

Farnsworth, D (1943). The Farnsworth-Munsell 100 hue and dichomatous tests for colour vision. J Opt Soc Am **33**: 568-578.

Fechtner, R D and Weinreb, R N (1994). Mechanisms of optic nerve damage in primary open angle glaucoma. Surv Ophthalmol **39**: 23-42.

Ferris, F L (1993). Diabetic Retinopathy. Diabetes Care **16**: 322-325.

Ferris, F L and Patz, A (1984). Macular oedema: A complication of diabetic retinopathy. Surv Ophthalmol **28**: 452-461.

Fingeret, M, Medeiros, F A, Susanna, J, Remo and Weinreb, R N (2005). Five rules to evaluate the optic disc and retinal nerve fiber layer for glaucoma. Optometry - Journal of the American Optometric Association **76**(11): 661-668.

Fisher, J B, Jacobs, D A, Markowitz, C E, Galetta, S L, Volpe, N J, Nano-Schiavi, M L, Baier, M L, Frohman, E M, Winslow, H and Frohman, T C Relation of Visual Function to Retinal Nerve Fiber Layer Thickness in Multiple Sclerosis. Ophthalmology **In Press, Corrected Proof**.

Flammer, J and Orgul, S (1998). Optic nerve blood-flow abnormalities in glaucoma. Prog Ret Eye Res **17**(2): 267-289.

Flammer, J, Orgul, S, Costa, V P, Orzalesi, N, Krieglstein, G K, Serra, L M, Renard, J-P and Stefansson, E (2002). The impact of ocular blood flow in glaucoma. Prog Ret Eye Res **21**(4): 359-393.

Fodera, F A (1999). Diabetes:diagnosis, management and patient education. Clin Eye Vis Care **11**: 183-186.

Frank, R N, Schulz, L, Abe, K and Iezzi, R L (2004). Temporal variation in diabetic macular oedema measured by optical coherence tomography. Ophthalmology **111**: 211-217.

Freeman, W R, Bartsch, D U, Mueller, A J, Banker, A S and Weinreb, R N (1998). Simultaneous indocyanine green and fluorescein angiography using a confocal scanning laser ophthalmoscope. Arch Ophthalmol **116**: 455-463.

Frenkel, S, Slonim, E, Horani, A, Molcho, M, Barzel, I and Blumenthal, E Z (2005). Operator learning effect and interoperator reproducibility of the scanning laser polarimeter with variable corneal compensation. Ophthalmology **112**(2): 257-261.

Friedman, D S, Nordstrom, B, Mozaffari, E and Quigley, H A (2005). Variations in Treatment among Adult-Onset Open-Angle Glaucoma Patients. Ophthalmology **112**(9): 1494-1499.

Frier, B M, Hepburn, D A, Fisher, B M and Barrie, T (1987). Fall in intraocular pressure during acute hypoglycaemia in patients with insulin dependent diabetes. Br Med J **294**: 610-611.

Fritsche, P, van der Heijde, R, Suttorp-Schulten, M S A and Polak, B C (2002). An objective method to assess and quantify the retinal thickness in healthy controls without diabetic retinopathy. Retina **22**: 768-771.

Frost-Larsen, K, Larsen, H W and Simonsen, S E (1980). Oscillatory potential and nyctometry in insulin-dependent diabetics. Acta Ophthalmol **58**: 879-888.

Fujita, Y, Imagawa, T and Uehara, M (2001). Fine structure of the retino-optic nerve junction in the chicken. Tissue and Cell **33**(2): 129-134.

Fukuchi, T, Takahashi, K, Ida, H, Sho, K and Matsumura, M (2001). Staging of idiopathic choroidal neovascularization by optical coherence tomography. Graefe's Arch Clin Exp Ophthalmol **239**: 424-429.

Funaki, S, Shirakashi, M, Funaki, H, Yaoeda, K and Abe, H (1999). Relationship Between Age and the Thickness of the Retinal Nerve Fiber Layer in Normal Subjects. Jpn J Ophthalmol **43**(3): 180-185.

Funatsu, H, Yamashita, H, Shimizu, E, Mimura, T, Nakamura, S and Hori, S (2004). Quantitative measurement of retinal thickness in patients with diabetic macular edema is useful for evaluation of therapeutic agents. Diabetes Research and Clinical Practice **66**(3): 219-227.

Gadsby, R (2002). Epidemiology of diabetes. Advanced Drug Delivery Reviews **54**: 1165-1172.

Garcia-Valenzuela, E, Mori, M, Edward, D P and Shahidi, M (2000). Thickness of the peripapillary retina in healthy subjects with different degrees of ametropia. Ophthalmology **107**: 1321-1327.

Gardner, T W, Antonetti, D A, Barber, A J, LaNoue K.F and Levison, S W (2002). Diabetic retinopathy:more than meets the eye. Surv Ophthalmol **47**(Suppl 2): S253-262.

Garway-Heath, D F, Caprioli, J, Fitzke, F W and Hitchings, R A (2000). Scaling the hill of vision: the physiological relationship between light sensitivity and ganglion cell numbers. Invest Ophthalmol Vis Sci **41**: 1174-1182.

Garway-Heath, D F, Poinoosawmy, D, Fitzke, F W and Hitchings, R A (2000). Mapping the visual field to the optic disc in normal tension glaucoma eyes. Ophthalmology **107**(10): 1809-1815.

Garway-Heath, D F, Rudnicka, A R, Lowe, T, Foster, P J, Fitzke, F W and Hitchings, R A (1998). Measurements of optic disc size: equivalence of methods to correct for ocular magnification. Br J Ophthalmol **82**: 643-649.

Gaucher, D, Tadayoni, R, Erginay, A, Haouchine, B, Gaudric, A and Massin, P (2005). Optical Coherence Tomography Assessment of the Vitreoretinal Relationship in Diabetic Macular Edema. Am J Ophthalmol **139**(5): 807-813.

Gharfour, I M, Foulds, W S, Allan, D and McClure, E (1982). Contrast sensitivity in diabetic subjects with and without retinopathy. Br J Ophthalmol **66**: 492-495.

Gherghel, D, Hosking, S L and Orgul, S (2004). Autonomic nervous system, circadian rhythms and primary open angle glaucoma. Surv Ophthalmol **49**(5): 491-508.

Giovannini, A, Amato, G and Mariotti, C (2002). The macular thickness and volume in glaucoma: an analysis in normal and glaucomatous using OCT. Acta Ophthalmol Scand Suppl **236**: 34-36.

Giovannini, A, Amato, G P, Mariotti, C and Scassellati-Sforzolini, B (1999). OCT imaging of choroidal neovascularisation and its role in the determination of patients' eligibility for surgery. Br J Ophthalmol **83**: 438-442.

Giuffre, G, Giammanco, R, Dardanoni, G and Ponte, F (1995). Prevalence of glaucoma and distribution of intraocular pressure. Acta Ophthalmol Scand **73**: 222-225.

Glovinsky, Y, Quigley, H A and Dunkelberger, G R (1991). Retinal ganglion cell loss is size dependent in experimental glaucoma. Invest Ophthalmol Vis Sci **32**: 484-491.

Glovinsky, Y, Quigley, H A and Pease, M, E. (1993). Foveal ganglion cell loss is size dependent in experimental glaucoma. Am J Ophthalmol **34**: 395-404.

Goebel, W, Hartmann, F and Haigis, W (2001). Determination of retinal thickness in relation to the age and axial length using optical coherence tomography. Der Ophthalmologe:Zeitschrift Der Deutschen Ophthalmologischen Gesellschaft **98**(2).

Goebel, W and Kretzchmar-Gross, T (2002). Retinal thickness in diabetic retinopathy: a study using Optical coherence tomography. Retina **22**: 759-767.

Greaney, M J, Hoffman, D C, Garway-Heath, D F, Nakla, M, Coleman, A L and Caprioli, J (2002). Comparison of optic nerve imaging methods to distinguish normal eyes from those with glaucoma. Invest Ophthalmol Vis Sci **43**: 140-145.

Green, F D, Ghafour, I M, Allan, D, Barrie, T, McCluire, E and Foulds, W S (1985). Colour vision of diabetics. Br J Ophthalmol **69**: 533-536.

Green, W R, McDonnell, P J and Yeo, J H (1985). Pathologic features of senile macular degeneration. Ophthalmology **92**: 615-627.

Greenfield, D S, Bagga, H and Knighton, R, W. (2003). Macular thickness changes in glaucomatous optic neuropathy detected using optical coherence tomography. Arch Ophthalmol **121**: 41-46.

Greenfield, D S and Knighton, R W (2001). Stability of corneal polarization axis measurements for scanning laser polarimetry. Ophthalmology **108**(6): 1065-1069.

Greenfield, D S, Knighton, R W, Feuer, W J, Schiffman, J C, Zangwill, L and Weinreb, R N (2002). Correction for corneal polarization axis improves the discriminating power of scanning laser polarimetry. Am J Ophthalmol **134**(1): 27-33.

Greenfield, D S, Knighton, R W and Huang, X R (2000). Effect of corneal polarization axis on assessment of retinal nerve fiber layer thickness by scanning laser polarimetry. Am J Ophthalmol **129**(6): 715-722.

Greenfield, S, Knighton, R W and Huang, X R (2001). Effect of corneal polarization axis on assessment of retinal nerve fiber layer thickness by scanning laser polarimetry. Am J Ophthalmol **131**(3): 403-404.

Greenstein, V C, Hood, D C, Ritch, R, Steinberger, D and Carr, R E (1989). S (blue) cone pathway vulnerability in retinitis pigmentosa, diabetes and glaucoma. Invest Ophthalmol Vis Sci **30**: 1732-1737.

Greenstein, V C, Sarter, B, Hood, D, Noble, K and Carr, R E (1990). Hue discrimination and S cone sensitivity in early diabetic retinopathy. Invest Ophthalmol Vis Sci **31**: 1008-1014.

Greenstein, V C, Shapiro, A, Zaidi, Q and Hood, D, C. (1992). Psychophysical evidence for post-receptoral sensitivity loss in diabetics. Invest Ophthalmol Vis Sci **33**: 2781-2790.

Grehn, F (1981). The sensitivity of the retinal nerve fibre layer to elevated intraocular pressure and graded hypoxia in the cat. Vis Res **21**(11): 1697-1701.

Guedes, V, Schuman, J S, Hertzmark, E, Wollstein, G, Correnti, A, Mancini, R, Lederer, D, Voskanian, S, Velazquez, L and Pakter, H M (2003). Optical coherence tomography measurement of macular and nerve fiber layer thickness in normal and glaucomatous human eyes. Ophthalmology **110**(1): 177-189.

Gurses-Ozden, R, Liebmann, J M, Schuffner, D, Buxton, D F, Soloway, B D and Ritch, R (2001). Retinal nerve fiber layer thickness remains unchanged following laser-assisted in situ keratomileusis. Am J Ophthalmol **132**(4): 512-516.

Gurses-Ozden, R, Pons, M E, Barbieri, C, Ishikawa, H, Buxton, D F, Liebmann, J M and Ritch, R (2000). Scanning laser polarimetry measurements after laser-assisted in situ keratomileusis. Am J Ophthalmol **129**(4): 461-464.

Gurses-Ozden, R, Teng, C, Vessani, R, Zafar, S, Liebmann, J M and Ritch, R (2004). Macular and retinal nerve fibre layer thickness measurement reproducibility using Optical Coherence Tomography (OCT 3). J Glaucoma **13**: 238-244.

Haefliger, I O and Hitchings, R A (1990). Relationship between asymmetry of visual field defects and intraocular pressure difference in an untreated normal (low) tension glaucoma population. Acta Ophthalmol **68**: 654-657.

Haley, M J E (1987). The field analyser primer. Humphrey Allergan, San Leandro.

Halkiadakis, I, Anglionto, L, Ferensowicz, M, Triebwasser, R W, van Westenbrugge, J A and Gimbel, H V (2005). Assessment of nerve fiber layer thickness before and after laser in situ keratomileusis using scanning laser polarimetry with variable corneal compensation. J Cat Refract Surg **31**(5): 1035-1041.

Hammond, C J, Snieder, H, Gilbert, C E and Spector, T D (2001). Genes and environment in refractive error: the twin eye study. Invest Ophthalmol Vis Sci **42**: 1232-1236.

Haouchine, B, Massin, P, Tadayoni, R, Erginay, A and Gaudric, A (2004). Diagnosis of macular pseudoholes and lamellar macular holes by optical coherence tomography. Am J Ophthalmol **138**(5): 732-739.

Hardy, K J, Scase, M O, Foster, D H and Scarpello, J H (1995). Effect of short-term changes of blood glucose on visual pathway function in insulin-dependent diabetics. Br J Ophthalmol **79**: 38-41.

Hardy, K J, Lipton, J, Scase, M O, Foster, D H and Scarpello, J H (1992). Detection of colour vision abnormalities in uncomplicated type 1 diabetic patients with angiographically normal retinas. Br J Ophthalmol **76**: 461-464.

Harper, C A, O'Day, J and Taylor, H R (1995). Early detection of diabetic retinopathy. The Medical Journal of Australia **162**: 536-538.

Harrad, R A, Cockram, C S, Plumb, A P, Stone, S, Fenwick, P and Sonksen, P H (1985). The effect of hypoglycaemia on visual function: A clinical and electrophysiological study. Clin Sci **69**: 673-679.

Harris, M, Flegal, K M, Cowie, C C, Eberhardt, D E, Goldstein, R R, Little, H, M, and Bryd-Holt, D D (1998). Prevalence of diabetes, impaired fasting glucose and impaired fasting glucose in US adults, the third National health and Nutrition examination survey 1988-1994. Diabetes Care **21**: 518-524.

Harris, M, Klein, R, Cowie, C C, Rowland, M and Byrd-Holt, D D (1998). Is the risk of diabetic retinopathy greater in non-hispanic blacks and mexican americans than in non-hispanic whites with Type 2 diabetes? Diabetes Care **21**(8): 1230-1235.

Harris, M, Sherman, S H and Georgopoulos, A (1999). Black-white differences in risk of developing retinopathy among individuals with type 2 diabetes. Diabetes Care **22**(5): 779-783.

Hart, W M and Becker, B (1982). The onset and evolution of glaucomatous visual field defects. Ophthalmology **89**: 268-279.

Hayashi, M, Yablonski, M, Boxrud, C, Fong, N, Berger, C and Jovanovic, L (1989). Decreased formation of aqueous humour in insulin-dependent diabetics. Br J Ophthalmol **73**: 621-623.

Hayreh, S S and Jonas, J B (2000). Appearance of the optic disk and retinal nerve fiber layer in atherosclerosis and arterial hypertension: an experimental study in rhesus monkeys. Am J Ophthalmol **130**(1): 91-96.

Hayreh, S S and Jonas, J B (2000). Ophthalmoscopic detectability of the parafoveal annular reflex in the evaluation of the optic nerve: An experimental study in rhesus monkeys. Ophthalmology **107**(5): 1009-1014.

Hayreh, S S and Jonas, J B (2000). Optic disk and retinal nerve fiber layer damage after transient central retinal artery occlusion: an experimental study in rhesus monkeys. Am J Ophthalmol **129**(6): 786-795.

Hee, M R, Izatt, J A, Swanson, E A, Huang, D, Schuman, J S, Lin, C P, Puliafito, C A and Fujimoto, J G (1995a). Optical coherence tomography of the human retina. Arch Ophthalmol **113**: 325-332.

Hee, M R, Puliafito, C A, Duker, J S, Reichel, E, Coker, J G, Wilkins, J R, Schuman, M D, Swanson, E A and Fujimoto, J G (1998). Topography of diabetic macular oedema with optical coherence tomography. Ophthalmology **105**: 360-370.

Hee, M R, Puliafito, C A, Wong, C, Duker, J S, Reichel, E, Rutledge, B, Schuman, J S, Swanson, E A and Fujimoto, J G (1995b). Quantitative assessment of macular oedema with optical coherence tomography. Arch Ophthalmol **113**: 1019-1029.

Hendicott, P and Lam, C (1991). Myopic crescent, refractive error and axial length in Chinese eyes. Clin Exp Optom **74**: 42-53.

Henson, D B (1993). Visual fields. Oxford University Press, Oxford.

Hepburn, D A, Fisher, B M, Thomson, I, Barrie, T and Frier, B M (1991). Autonomic mechanisms underlying intraocular pressure changes during insulin-induced hypoglycaemia in normal human subjects:effecst of pharmacological blockade. Clin Sci **80**(4): 333-338.

Hernandez, M R (1992). Ultrastructural immunocytochemical analysis of elastin in the human lamina cribrosa. Changes in elastic fibres in primary open-angle glaucoma. Invest Ophthalmol Vis Sci **33**: 2891-2903.

Hernandez, M R, Luo, X X, Igoe, F and Neufield, A H (1987). Extracellular matrix of the human lamina cribrosa. Am J Ophthalmol **104**: 567-576.

Heron, G, Adams, A J and Husted, R (1988). Central visual field for short wavelength sensitive pathways in glaucoma and hypertension. Invest Ophthalmol Vis Sci **29**: 64-72.

Hess, D B, Asrani, S G, Bhide, M G, Enyedi, L B, Stinnett, S S and Freedman, S F (2005). Macular and retinal nerve fiber layer analysis of normal and glaucomatous eyes in children using optical coherence tomography. Am J Ophthalmol **139**(3): 509-517.

Hildebrand, C and Waxman, S G (1983). Regional node-like membrane specializations in non-myelinated axons of rat retinal nerve fiber layer. Brain Res **258**(1): 23-32.

Hodapp, E and Parrish, R K, Anderson, D (1993). Follow-up of primary open angle glaucoma. In Clinical decision in glaucoma **Mosby, St. Louis, Missouri**: 84-126.

Hoffman, D J and Heath, D A (1987). Staphyloma and other risk factors in axial myopia. J Am Optom Assoc **58**: 907-913.

Hoh, S T, Greenfield, D S, Mistlberger, A, Liebmann, J M, Ishikawa, H and Ritch, R (2000). Optical coherence tomography and scanning laser polarimetry in normal, ocular hypertensive, and glaucomatous eyes. Am J Ophthalmol **129**(2): 129-135.

Hollows, F C and Graham, P A (1966). Intraocular pressure, glaucoma, and glaucoma suspects in a defined population. Br J Ophthalmol **50**: 570-586.

Horn, F K, Nguyen, N X, Mardin, C Y and Jnemann, A G (2003). Combined use of frequency doubling perimetry and polarimetric measurements of retinal nerve fiber layer in glaucoma detection. Am J Ophthalmol **135**(2): 160-168.

Hoskins, H D, Hetherington, J, Glendlay, M, Samuels, S J and Verdooner, S R (1994). Repeatability of the Glaucoma-scope mesurements of optic nerve head topography. J Glaucoma **3**(1): 17-37.

Hoye, V J, Berrocal, A M, Hedges, T R and Amaro-Quireza, M L (2001). Optical coherence tomography demonstrates subretinal macular oedema from papilloedema. Arch Ophthalmol **119**: 1287-1290.

Hoyt, W F, Frisen, L L and Newman, N M (1973). Fundoscopy of nerve fibre layer defects in glaucoma. Invest Ophthalmol Vis Sci **12**: 814-829.

Hrynchak, P and Simpson, T (2000). Optical coherence tomography: An introduction to the technique and its use. Optom Vis Sci **77**(7): 347-356.

Huang, D, Swanson, E A, Lin, C P, Schuman, J S, Stinson, W G, Chang, W, Hee, M R, Flotte, T, Gregory, K, Puliafito, C A and Fujimoto, J G (1991). Optical coherence tomography. Science **254**: 1178-1181.

Huang, L N, Schuman, J, S, Pedut-Kloizman, T et al., (1997). The comparison of nerve fibre layer thickness in glaucomatous monkey eyes measured by optical coherence tomography and histomorphometry. Invest Ophthalmol Vis Sci **38**: S838.

Hubel, D (1988). Eye, Brain and Vision. Scientific American Library

Hudson, C (1997). Nerve fibre layer thickness measurements derived by scanning laser polarimetry: the jury is out. Br J Ophthalmol **81**: 338-339.

Hudson, C, Charles, S J, Flanagan, J G, Brahma, A K, Turner, G S and D, M (1997). Objective morphological assessment of macular hole surgery by scanning laser tomography. Br J Ophthalmol **81**: 107-116.

Hudson, C, Flanagan, J G, Turner, G S and McLeod, D (1998). Scanning laser tomography Z profile signal width as an objective index of macular retinal thickening. Br J Ophthalmol **82**: 121-130.

Hudson, C, Flanagan, J G, Turner, G S, Chen H C, Young L B, McLeod D (1998). Short-wavelength sensitive visual field loss in patients with clinically significant diabetic macular oedema. Diabetologia **41**:918-928

Hussain, A, Hussain, N and Nutheti, R (2005). Comparison of mean macular thickness using optical coherence tomography and visual acuity in diabetic retinopathy. Clin Exp Ophthalmol **33**: 240.

Hyvarinen, L, Laurinen, P and Rovamo, J (1983). Contrast sensitivity in evaluation of visual impairment due to diabetes. Acta Ophthalmol **61**: 94-101.

Hyrnchak, P, Simpson, T (2000). Optical coherence tomography: an introduction to the technique and its use. Optom and Vis Sci **77** (7):347-356

Iacono, P, Da Pozzo, S, Vattovani, O, Tognetto, D and Ravalico, G (2005). Scanning laser polarimetry of nerve fiber layer thickness in normal eyes after cataract phacoemulsification and foldable intraocular lens implantation. J Cat Refract Surg **31**(5): 1042-1049.

Iester, M, Broadway, D C, Mikelberg, F S and Drance, S M (1997). A comparison of healthy, ocular hypertensive and glaucomatous optic disc topographic parameters. J Glaucoma **6**: 363-370.

Iester, M, Capris, P, Pandolfo, A, Zingirian, M and Traverso, C E (2000). Learning effect, short-term fluctuation, and long-term fluctuation in frequency doubling technique. Am J Ophthalmol **130**(2): 160-164.

Iester, M, Mikelberg, F S and Drance, S M (1997). The effect of optic disc size on diagnostic precision with the Heidelberg Retina Tomograph. Ophthalmology **104** 545-548.

Iester, M, Mermoud, A and Schynder, C (2000). Frequency doubling technique in patients with ocular hypertension and glaucoma: a correlation with Octopus perimeter indices. Ophthalmology **107** (2): 288-294.

Iester, M, Tizte, P and Mermoud, A (2002). Retinal nerve fiber layer thickness changes after an acute increase in intraocular pressure. J Cat Refract Surg **28**(12): 2117-2122.

Iijima, H (2001). Macular Diseases-Application of Automated Static Perimetry and Optical Coherence Tomography. Jpn J Ophthalmol **45**(3): 324-325.

Imai, M, Lijima, H and Hanada, N (2001). Optical coherence tomography of tractional macular elevations in eyes with proliferative diabetic retinopathy. Am J Ophthalmol **132**(3): 458-461.

Inzelberg, R, Ramirez, J A, Nisipeanu, P and Ophir, A (2004). Retinal nerve fiber layer thinning in Parkinson disease. Vis Res **44**(24): 2793-2797.

Ip, M, Garza-Karren, C, Duker, J S, Reichel, E, Swartz, J C, Amirikia, A and Puliafito, C A (1999). Differentiation of degenerative retinoschisis from retinal detachment using optical coherence tomography. Ophthalmology **106**: 600-605.

Ishida, K, Yamamoto, T, Sugiyama, K and Kitazawa, Y (2000). Disk haemorrhage is a significantly negative prognostic factor in normal-tension glaucoma. Am J Ophthalmol **129**(6): 707-714.

Ismail, G M and Whitaker, D (1998). Early detection of changes in visual function in diabetes mellitus. Ophthal Physiol Opt **18**(1): 3-12.

Itai, N, Tanito, M and Chihara, E (2003). Comparison of Optic Disc Topography Measured by Retinal Thickness Analyzer with Measurement by Heidelberg Retina Tomograph II. Jpn J Ophthalmol **47**(2): 214-220.

Ito-Ohara, M, Seko, Y and Morita, H (1998). Clinical course of newly developed or progressive patchy chorioretinal atrophy in pathological myopia. Ophthalmologica **212**: 23-29.

Iwata, K (1989). Ophthalmoscopy in the detection of optic disc and retinal nerve fiber layer changes in early glaucoma (summary). Surv Ophthalmol **33**(Supplement 1): 447-448.

Izatt, J A, Hee, M R, Swanson, E A, Lin, C P, Huang, D, Schuman, J S, Puliafito, C A and Fujimoto, J G (1994). Micrometer-scale resolution imaging of the anterior eye in vivo with optical coherence tomography. Arch Ophthalmol **112**: 1584-1589.

Jaffe, G J and Caprioli, J (2004). Optical coherence tomography to detect and manage retinal disease and glaucoma. Am J Ophthalmol **137**(1): 156-169.

Jain, A, Sarraf, D and Fong, D (2003). Preventing diabetic retinopathy through control of systemic factors. Curr Opin Ophthalmol **14**: 389-394.

Janknecht, P and Funk, J (1994). Optic nerve head analyser and Heidelberg retina tomograph: accuracy and reproducibility of topographic measurements in a model eye and in volunteers. Br J Ophthalmol **78**: 760-768.

Janknecht, P and Funk, J (1995). Optic nerve head analyzer and Heidelberg retina tomograph: relative error and reproducibility of topographic measurements in a model eye with simulated cataract. Graefe's Arch Clin Exp Ophthalmol **233**: 523-529.

Jeoung, J W, Park, K H, Kim, T W, Khwarg, S I and Kim, D M (2005). Diagnostic Ability of Optical Coherence Tomography with a Normative Database to Detect Localized Retinal Nerve Fiber Layer Defects. Ophthalmology **112**(12): 2157-2163.

Johnson, B M, Miao, M and Sadun, A A (1987). Age-related decline of the human optic nerve axon populations. Age **10**: 5.

Johnson, C A, Adams, A J, Casson, E J et al., (1993). Progression of early glaucomatous visual field loss as detected by blue-on-yellow and standard white-on - white automated perimetry. Arch Ophthalmol **111**: 651-656.

Johnson, C A and Samuels, S J (1997). Screening for glaucomatous visual field loss with frequency-doubling perimetry. Invest Ophthalmol Vis Sci **38**(2): 413-425.

Jonas, J B and Budde, W M (2000). Diagnosis and pathogenesis of glaucomatous optic neuropathy: morphological aspects. Prog Ret Eye Res **19**(1): 1-40.

Jonas, J B and Budde, W M (2000). Optic nerve head appearance in juvenile-onset chronic high-pressure glaucoma and normal-pressure glaucoma. Ophthalmology **107**(4): 704-711.

Jonas, J B, Budde, W M and Panda-Jonas, S (1999). Ophthalmoscopic Evaluation of the Optic Nerve Head. Surv Ophthalmol **43**(4): 293-320.

Jonas, J B and Dichtl, A (1996). Evaluation of the retinal nerve fibre layer. Surv Ophthalmol **40**: 369-378.

Jonas, J B and Dichtl, A (1997). Optic disc morphology in myopic primary open-angle glaucoma. Graefe's Arch Clin Exp Ophthalmol **235**: 627-633.

Jonas, J B, Fernandez, I and Naumann, G O H (1990). Glaucomatous optic nerve atrophy in small discs with low cup-to-disc ratios. Ophthalmology **97**: 1211-1215.

Jonas, J B, Fernandez, I and Naumann, G O H (1991). Correlation of the optic disc size to glaucoma susceptibility. Ophthalmology **98**: 675-680.

Jonas, J B, Fernandez, I and Sturmer, J (1993). Pattern of glaucomatous neuroretinal rim loss. Ophthalmology **100**: 63-68.

Jonas, J B, Gusek, G C and Naumann, G O H (1988a). Optic disc, cup and neuroretinal rim size, configuration and correlations in normal eyes. Invest Ophthalmol Vis Sci **29**: 1151-1158.

Jonas, J B, Gusek, G C and Naumann, G O H (1988b). Optic disc morphometry in chronic primary open angle glaucoma I Morphometric intrapapillary characteristics. Graefe's Arch Clin Exp Ophthalmol **226**: 522-526.

Jonas, J B, Mardin, C Y, Schlotzer-Schrehardt, U, Naumann, G O H (1991). Morphometry of the human lamina cribrosa surface. Invest Ophthalmol Vis Sci **32**:401-405.

Jonas, J B, Muller-Bergh, J A, Schlotzer- Schrehardt, U M and Naumann, G O H (1990). Histomorphometry of the human optic nerve. Invest Ophthalmol Vis Sci **31**: 736-744.

Jonas J B, Nguyen X N, Naumann G O H (1989). The retinal nerve fiber layer in normal eyes. Ophthalmology **96**: 627-632

Jonas, J B and Schiro, D (1994). Localised wedge shaped defects of the retinal nerve fibre layer in glaucoma. Br J Ophthalmol **78**: 285-290.

Jonas, J B, Schmidt, A M, Muller-Bergh, J A and Naumann, G O H (1995). Optic nerve fibre count and diameter of the retrobulbar optic nerve in normal and glaucomatous eyes. Graefe's Arch Clin Exp Opthalmol **233**: 421-424.

Jonas, J B, Schmidt, J C, Muller-Bergh, J A, Schlotzer- Schrehardt, U M and Naumann, G O H (1992). Human optic nerve fibre count and optic disc size. Invest Ophthalmol Vis Sci **33**(6): 2012-2018.

Jonas, J B and Xu, L (1994). Optic disc haemorrhages in glaucoma. Am J Ophthalmol **118**: 1-8.

Jones, A L, Sheen, N J L, North, R V and Morgan, J E (2001). The Humphrey optical coherence tomography scanner: quantitative analysis and reproducibility study of the normal human retinal nerve fiber layer. Br J Ophthalmol **85**: 673-677.

Juen, S and Kieselbach, G F (1990). Electrophysiological changes in juvenile diabetics without retinopathy. Arch Ophthalmol **108**: 372-375.

Justino, L, Kergoat, M-J, Bergman, H, Chertkow, H, Robillard, A and Kergoat, H (2001). Neuroretinal function is normal in early dementia of the Alzheimer type. Neurobiology of Aging **22**(4): 691-695.

Kagemann, L, Harris, A, Chung, H S, Evans, D, Buck, S and Martin, B (1998). Heidelberg retinal flowmetry: factors affecting blood flow measurement. Br J Ophthalmol **82**: 131-136.

Kahn, H A, Leibowitz, H M, Ganley, J P et al., (1977). The Framingham Eye Study II Association of ophthalmic pathology with single variables previously mentioned in the Framingham Heart Study. Am J Epidemiol **106**: 33-41.

Kahn, H A and Milton, R C (1980). Revised Framingham Eye study prevalence of glaucoma and diabetic retinopathy. Am J Epidemiol **111**: 769-776.

Kaiser, P K, Riemann, C D, Sears, J E and Lewis, H (2001). Macular traction detachment and diabetic macular edema associated with posterior hyaloidal traction. Am J Ophthalmol **131**(1): 44-49.

Kanai, K, Abe, T, Murayama, K and Yoneya, S (2002). Retinal thickness and changes with age. Nippon Ganka Gakkai Zasshi **106**(3): 162-165.

Kanamori, A, Escano, M F T, Eno, A, Nakamura, M, Maeda, H, Seya, R, Ishibashi, K and Negi, A (2003). Evaluation of the effect of aging on retinal nerve fibre layer thickness measured by Optical Coherence Tomography. Ophthalmologica **217**: 273-278.

Kanamori, A, Nakamura, M, Escano, M F T, Seya, R, Maeda, H and Negi, A (2003). Evaluation of the glaucomatous damage on retinal nerve fiber layer thickness measured by optical coherence tomography. Am J Ophthalmol **135**(4): 513-520.

Kanamori, A, Nakamura, M, Matsui, N, Nagai, A, Nakanishi, Y, Kusuhara, S, Yamada, Y and Negi, A (2004). Optical coherence tomography detects characteristic retinal nerve fiber layer thickness corresponding to band atrophy of the optic discs. Ophthalmology **111**(12): 2278-2283.

Kang, S W, Park, C Y and Ham, D I (2004). The correlation between fluorescein angiographic and optical coherence tomographic features in clinically significant diabetic macular oedema. Am J Ophthalmol **137**: 313-322.

Karlin, D B and Curtin, B J (1976). Peripheral chorioretinal lesions and axial length of the myopic eye. Am J Ophthalmol **81**: 625-635.

Kashwagi, K, Okubo, T and Tsukahara, S (2004). Association of magnetic resonance imaging of anterior optic pathway with glaucomatous visual field damage and optic disc cupping. J Glaucoma **13**: 189-195.

Kato, S, Takemori, M, Kitano, S, Hori, S, Fukushima, H, Numaga, J and Yamashita (2002). Retinopathy in older patients with diabetes mellitus. Diabetes research and clinical practice **58**: 187-192.

Kerrigan-Baumrind, L A, Quigley, H A, Pease, M E, Kerrigan, D F and Mitchell, R S (2000). Number of ganglion cells in glaucoma eyes compared with threshold visual field tests in the same persons. Invest Ophthalmol Vis Sci **41**: 741-748.

Kerrigan, L A, Zack, D J, Quigley, H A et al., (1997). TUNEL-positive ganglion cells in human primary open-angle glaucoma. Arch Ophthalmol **115**: 1031-1035.

Kern T S, Engerman R L (1995). Vascular lesion in diabetes is distributed non-uniformly within the retina. Exp Eye Res **60**: 545-549.

Kielhorn, I, Rajan, M S, Tesha, P M, Subryan, V R and Bell, J A (2003). Clinical assessment of the Zeiss IOLMaster. J Cat Refract Surg **29**(3): 518-522.

Kim, D M, Hwang, U S, Park, K H and Kim, S H (2005). Retinal Nerve Fiber Layer Thickness in the Fellow Eyes of Normal-tension Glaucoma Patients With Unilateral Visual Field Defect. Am J Ophthalmol **140**(1): 165-166.

King, A J W, Bolton, N, Aspinall, P and O'Brien, C J (2000). Measurement of peripapillary retinal nerve fiber layer volume in glaucoma. Am J Ophthalmol **129**(5): 599-607.

King, G L and Brownlee, M (1996). The cellular and molecular mechanisms of diabetic complications. Endocrinol Metab Clin N Am **25**: 255-270.

King, H, Aubert, R E and Herman, W H (1998). Global burden of diabetes, 1995-2025 prevalence, numerical estimates and projections, Diabetes Care 21. Diabetes Care **21**: 1414-1431.

King, H and Rewers, M (1993). Global estimates for prevalence of diabetes and impaired glucose tolerance in adults. Diabetes Care **16**: 157-177.

Kirkpatrick, J N P, Manivannan, A, Gupta, A K, Hipwell, J, Forrester, J V and Sharp, P F (1995). Fundus imaging in patients with cataract: role of a variable wavelength scanning laser ophthalmoscope. Br J Ophthalmol **79**: 892-899.

Klein, B E and Klein, R (1981). Intraocular pressure and cardiovascular risk variables. Arch Ophthalmol **99**: 837-839.

Klein, B E, Klein, R and Jensen, S C (1994). Open-angle glaucoma and older-onset diabetes: the Beaver Dam Study. Ophthalmology **101**: 1173-1177.

Klein, R, Klein, B E, Moss S E et al., (1984). The Wisconsin Epidemiologic Study of Diabetic Retinopathy. IV. Diabetic macular edema. Ophthalmology **91**:1464–74.

Klein, B E, Klein, R and Ritter, L L (1993). Relationship of drinking alcohol and smoking to prevalence of open angle glaucoma. Ophthalmology **100**: 1609-1613.

Klein, B E, Klein, R, Sponsel, W E et al (1992). Prevalence of glaucoma. The Beaver Dam Study. Ophthalmology **99**: 1499-1504.

Klein, R M and Curtin, B J (1975). Lacquer crack lesions in pathological myopia. Am J Ophthalmol **79**: 386-392.

Kogure, S and Iijima, H (2001). Effect of corneal polarization axis on assessment of retinal nerve fiber layer thickness by scanning laser polarimetry. Am J Ophthalmol **131**(3): 403.

Kohner, E M (1976). Problems of retinal blood flow in diabetes. Diabetes **25**: 839-844.

Konno, S, Akiba, J and Yoshida, A (2001). Retinal thickness measurements with optical coherence tomography and the scanning retinal thickness analyser. Retina **21**: 57-61.

Kook, M S, Cho, H-s, Seong, M and Choi, J (2005). Scanning Laser Polarimetry Using Variable Corneal Compensation in the Detection of Glaucoma with Localized Visual Field Defects. Ophthalmology **112**(11): 1970-1978.

Kook, M S, Lee, S-U, Tchah, H-W, Sung, K-R, Park, R-H and Kim, K-R (2002). Effect of laser in situ keratomileusis on retinal nerve fiber layer thickness measurements by scanning laser polarimetry. J Cat Refract Surg **28**(4): 670-675.

Koozekanani, D, Roberts, C, Katz, S E and Herderick, E E (2000). Intersession repeatability of macular thickness measurements with the Humphrey 2000 OCT. Invest Ophthalmol Vis Sci **41**: 1486-1491.

Kremser, B, Troger, J, Baltaci, M, Kralinger, M and Kieselbach, G (1999). Retinal thickness analysis in subjects with different refractive conditions. Ophthalmologica **213**: 376-379.

Kruse, F, Burk, R O W, Volcker, H, Zinser, G and Harbarth, U (1989). Reproducibility of topographic measurements of the optic nerve head with laser tomographic scanning. Ophthalmology **96**: 1320-1324.

Kurimoto, Y, Kaneko, Y, Matsuno, K, Akimoto, M and Yoshimura, N (2001). Evaluation of the retinal nerve fiber layer thickness in eyes with idiopathic macular holes. Am J Ophthalmol **131**(6): 756-760.

Kurimoto, Y, Matsuno, K, Kaneko, Y, Umihira, J and Nagahisa, Y (2000). Asymmetries of the retinal nerve fibre layer thickness in normal eyes. Br J Ophthalmol **84**: 469-472.

Kurtenbach, A, Wagner, U, Neu, A, Schiefer, M, Ranke, E and Zrenner, E (1994). Brightness matching and colour discrimination in young diabetics without retinopathy. Vis Res **34**: 115-122.

Kusuhara, S, Teraoka Escano, M F, Fujii, S, Nakanishi, Y, Tamura, Y, Nagai, A, Yamamoto, H, Tsukahara, Y and Negi, A (2004). Prediction of postoperative visual outcome based on hole configuration by optical coherence tomography in eyes with idiopathic macular holes. Am J Ophthalmol **138**(5): 709-716.

Lai, J C, Stinnett, S S and Jaffe, G J (2003). B-scan ultrasonography for the detection of macular thickening. Am J Ophthalmol **136**(1): 55-61.

Lai, J S M, Tham, C C Y, Chan, J C H, Yip, N K F, Tang, W W T, Li, P S H, Yeung, J C C and Lam, D S C (2003). Scanning laser polarimetry in patients with acute attack of primary angle closure. Jpn J Ophthalmol **47**(6): 543-547.

Lakowski, R, Aspinall, P A and Kinneer, P R (1972). Association between colour vision and diabetes mellitus. Ophthalmic Res **4**: 145-159.

Lam, A K C, Chang, P and Pang, P C K (2001). The repeatability and accuracy of axial length and anterior chamber depth measurements from the IOLMaster. Ophthal Physiol Opt **21**(6): 477-483.

Landau, D, Schneidman, E M, Jacobovitz, T and Rozenman, Y (1997). Quantitative in vivo retinal thickness measurements in healthy subjects. Ophthalmology **104**: 639-642.

Lane, J T, Toris, C B, Nakhle, S N, Chacko, D M, Wang, Y L and Yablonski, M (2001). Acute effects of insulin on aqueous humour flow in patients with type 1 diabetes. Am J Ophthalmol **132**: 321-327.

Larrson, L, Pach, J and Brubaker, R (1995). Aqueous humour dynamics in patients with diabetes mellitus. Am J Ophthalmol **120**: 362-367.

Lawrenson, J G (1998). Anatomy and physiology of aqueous production and drainage. Optometry Today Glaucoma Module Parts 1-12: 1-5.

Lederer, D E, Schuman, J S, Hertzmark, E, Heltzer, J, Velazques, L J, Fujimoto, J G and Mattox, C (2003). Analysis of macular volume in normal and glaucomatous eyes using optical coherence tomography. Am J Ophthalmol **135**(6): 838-843.

Lee, V W H and Mok, K H (2000). Nerve fibre layer measurement of the Hong Kong Chinese Population by scanning laser polarimetry. Eye **14**: 371-374.

Lee, V W H and Mok, K H (1999). Retinal nerve fiber layer measurement by nerve fiber analyzer in normal subjects and patients with glaucoma. Ophthalmology **106**(5): 1006-1008.

Leske, M C, Connell, A M, Schachat, A P and Hyman, L (1994). The Barbados Eye Study. Prevalence of open angle glaucoma. Arch Ophthalmol **112**: 821-829.

Leske, M C, Connell, A M and Wu, S Y (1995). Risk factors for open-angle glaucoma. The Barbados Eye Study. Arch Ophthalmol **113**: 918-924.

Leske, M C and Podgor, M J (1983). Intraocular pressure, cardiovascular risk variables and visual field defects. Am J Epidemiol **118**: 280-287.

Leung, C K S, Chan, W M, Yung, W H, Ng, A C K, Woo, J, Tsang, M K and Tse, K K (2005). Comparison of macular and peripapillary measurements for the detection of glaucoma: An Optical Coherence Tomography study. Ophthalmology **112**(3): 391-400.

Levkovitch-Verbin, H, Quigley, H A, Martin, K R G, Harizman, N, Valenta, D F, Pease, M E and Melamed, S (2005). The transcription factor c-jun is activated in retinal ganglion cells in experimental rat glaucoma. Exp Eye Res **80**(5): 663-670.

Lim, M C C, Hoh, S T, Foster, P J, Lim, T, H, Chew, S J, Seah, S K L and Aung, T (2005). Use of the optical coherence tomography to assess variations in macular retinal thickness in myopia. Invest Ophthalmol Vis Sci **46**: 974-978.

Liou, S-Y, Sugiyama, K, Uchida, H, Gu, Z-B, Yamamoto, T, Tomita, G and Kitazawa, Y (2001). Morphometric characteristics of optic disk with disk hemorrhage in normal-tension glaucoma. Am J Ophthalmol **132**(5): 618-625.

Lloyd, C E, Klein, R, Maser, R E, Kuller, L H, Becker, D J and Orchard, T J (1995). The progression of retinopathy over 2 years: The Pittsburgh Epidemiology of Diabetes Complications (EDC) study. Journal of Diabetes and Its Complications **9**(3): 140-148.

Lobo, C L, Bernandes, R C and Cunha-Vaz, J (2000). Alterations of the blood-retinal barrier and retinal thickness in preclinical retinopathy in subjects with type 2 diabetes. Arch Ophthalmol **118**: 1364-1369.

Lobo, C L, Bernandes, R C, de Abreu, F and Cunha-Vaz, J (2001). One-year follow-up of blood retinal barrier and retinal thickness alterations in patients with type 2 diabetes mellitus and mild nonproliferative retinopathy. Arch Ophthalmol **119**: 1469-1474.

Lobo, C L, Bernandes, R C, Figueira, J P, de Abreu, F and Cunha-Vaz, J (2004). Three-year follow-up study of blood retinal barrier and retinal thickness alterations in patients with type 2 diabetes mellitus and mild nonproliferative diabetic retinopathy. Arch Ophthalmol **122**: 211-217.

Lopes de Faria, J M, Russ, H and Costa, V P (2002). Retinal nerve fibre loss in patients with type 1 diabetes mellitus without retinopathy. Br J Ophthalmol **86**: 725-728.

Luksch, A, Polak, K, Matulla, B et al., (2001). Glucose and insulin exert additive ocular and renal vasodilator effects on healthy humans. Diabetologia **44**: 95-103.

Lundh (1983). Central contrast sensitivity tests in the detection of early glaucoma. Acta Ophthalmol Scand **63**: 481-486.

Lusky, M, Bosem, M E and Weinreb, R N (1993). Reproducibility of optic nerve head topography measurements in eyes with undilated pupils. J Glauc **2**: 104-109.

Mackie, S W and Walsh, G (1998). Contrast and glare sensitivity in diabetic patients with and without pan-retinal photocoagulation. Ophthal Physiol Opt **18**(2): 173-181.

Majid, M A, Smith, V A, Easty, D L, Baker, A H and Newby, A C (2002). Adenoviris medicated gene delivery of tissue inhibitor of metalloproteinases-3 induces death of retinal pigment epithelial cells. Br J Ophthalmol **86**: 97-101.

Manassakorn, A, Nouri-Mahdavi, K and Caprioli, J (2006). Comparison of Retinal Nerve Fiber Layer Thickness and Optic Disk Algorithms with Optical Coherence Tomography to Detect Glaucoma. Am J Ophthalmol **141**(1): 105.

Mansberger, S L, Zangwill, L M, Sample, P A, Choi, D and Weinreb, R N (2003). Relationship of optic disk topography and visual function in patients with large cup-to-disk ratios. Am J Ophthalmol **136**(5): 888-894.

Mapstone, R and Clark, C V (1985). Prevalence of diabetes in glaucoma. Br Med J **291**: 93-95.

Markomichelakis, N N, Halkiadakis, I, Pantelia, E, Peponis, V, Patelis, A, Theodossiadis, P and Theodossiadis, G (2004). Patterns of macular edema in patients with uveitis: Qualitative and quantitative assessment using optical coherence tomography. Ophthalmology **111**(5): 946-953.

Martin, M J, Sommer, A, Gold, E B and Diamond, E L (1985). Race and primary open angle glaucoma. Am J Ophthalmol **99**: 383-387.

Martin, P, White, A, Goodchild, A, Wilder, H and Sefton, A (1997). Evidence that blue-on yellow cells are part of the third geniculocortical pathway in primates. Proc Natl Acad Sci **27**: 5900-5905.

Mason, R P, Kosoko, O, Wilson, R et al., (1989). National Survey of the Prevalence and Risk Factors of Glaucoma in St. Lucia, West Indies. Ophthalmology **96**: 1363-1368.

Massin, P, Allouch, C, Haouchine, B, Metge, F, Paques, M, Tangui, L, Erginay, A and Gaudric, A (2000). Optical coherence tomography of idiopathic macular epiretinal membranes before and after surgery. Am J Ophthalmol **130**(6): 732-739.

Massin, P, Audren, F, Haouchine, B, Erginay, A, Bergmann, J-F, Benosman, R, Caulin, C and Gaudric, A (2004). Intravitreal triamcinolone acetonide for diabetic diffuse macular edema: Preliminary results of a prospective controlled trial. Ophthalmology **111**(2): 218-224.

Massin, P, Duguid, G, Erginay, A, Haouchine, B and Gaudric, A (2003). Optical coherence tomography for evaluating diabetic macular edema before and after vitrectomy. Am J Ophthalmol **135**(2): 169-177.

Massin, P, Erginay, A, Haouchine, B, Mehidi, A B, Paques, M and Gaudric, A (2002). Retinal thickness in healthy and diabetic subjects measured using optical coherence tomography mapping software. Eur J Ophthalmol **12**(2): 102-108.

Massin, P, Vicaut, E, Haouchine, B, Erginay, A, Pacques, M and Gaudric, A (2001). Reproducibility of retinal mapping using optical coherence tomography. Arch Ophthalmol **119**: 1135-1142.

Matsumoto, C, Shirato, S, Haneda, M, Yamashiro, H and Saito, M (2003). Study of Retinal Nerve Fiber Layer Thickness Within Normal Hemivisual Field in Primary Open-Angle Glaucoma and Normal-Tension Glaucoma. Jpn J Ophthalmol **47**(1): 22-27.

McCrimmon, R, J, Dreary, I J, Huntly, B J H, Macleod, K J M and Frier, B M (1996). Visual information processing during controlled hypoglycaemia in humans. Brain **119**: 1277-1287.

McCarty, D and Zimmet, P Z (1994). Diabetes 1994 to 2010. Global estimates and projections. Melbourne, International Diabetes Institute.

McCarty, T M, Hardten, D R, Anderson, N J, Rosheim, K and Samuelson, T W (2003). Evaluation of neuroprotective qualities of brimonidine during LASIK. Ophthalmology **110**(8): 1615-1625.

McClure, M E, Hart, P M, Jackson, A J, Stevenson, M R and Chakravarthy, U (2000). Macular degeneration: do conventional measurements of impaired visual function equate with visual disabilty? Br J Ophthalmol **84**: 244-250.

McNaught, A I, Allen, J, G,, Healey, D L, McCartney, P J, Coote, M A, Wong, T L, Craig, J E, Green, C M, Rait, J L and Mackey, D A (2000). Accuracy and implications of a reported family history of glaucoma. Arch Ophthalmol **118**: 900-904.

Medeiros, F A, Moura, F C, Vessani, R M and Susanna, J, Remo (2003). Axonal loss after traumatic optic neuropathy documented by optical coherence tomography. Am J Ophthalmol **135**(3): 406-408.

Medeiros, F A, Zangwill, L M, Bowd, C, Vessani, R M, Susanna, J, Remo and Weinreb, R N (2005). Evaluation of retinal nerve fiber layer, optic nerve head, and macular thickness measurements for glaucoma detection using optical coherence tomography. Am J Ophthalmol **139**(1): 44-55.

Meier, F M, Bernasconi, P, Sturmer, J, Caubergh, M J and Landau, K (2002). Axonal loss from acute optic neuropathy documented by scanning laser polarimetry. Br J Ophthalmol **86**: 285-287.

Menezes, A V, Giunta, M, Chisholm, L, Harvey, P T, Tuli, R and Devenyi, R G (1995). Reproducibility of topographic measurements of the macula with a scanning laser ophthalmoscope. Ophthalmology **102**: 230-235.

Miglior, S, Albe, E, Guareschi, M, Rossetti, L and Orzalesi, N (2002). Intraobserver and interobserver reproducibility in the evaluation of optic disc stereometric parameters by Heidelberg retina tomograph. Ophthalmology **109**(6): 1072-1077.

Miglior, S, Casula, M, Guareschi, M, Marchetti, I, Iester, M and Orzalesi, N (2001). Clinical ability of Heidelberg Retinal Tompgraph examination to detect glaucomatous visual field changes. Ophthalmology **108**: 1621-1627.

Miglior, S, Rossetti, L, Brigatti, L, Bujtar, E and Orzalesi, N (1994). Reproducibility of retinal nerve fibre layer evaluation by dynamic scanning laser ophthalmoscopy. Am J Ophthalmol **118**: 16-23.

Mikelberg, F S (1993). Intraocular pressure and glaucoma. Can J Ophthalmol **28**: 251-252.

Mikelberg, F S, Drance, S M, Schulzer, M, Yidegiligne, H M and Weis, M, M. (1989). The normal human optic nerve: axon count and diameter and distribution. Ophthalmology **96**: 1325-1328.

Mikelberg, F S, Wijsman, K and Schulzer, M (1993). Reproducibility of topographic parameters obtained with the Heidelberg Retina Tomograph. J Glaucoma **2**: 101-103.

Miller, K N and Quigley, H A (1988). The clinical appearance of the lamina cribrosa as a function of the extent of glaucomatous optic nerve damage. Ophthalmology **95**: 135-138.

Minckler, D S, Bunt, A H and Johanson, G W (1977). Orthograde and retrograde axoplasmic transport during acute ocular hypertension in the monkey. Invest Ophthalmol Vis Sci **16**: 426-441.

Minckler, D S, Bunt, A H and Klock, I B (1978). Radiographic and cytochemical ultrastructural studies of axoplasmic transport in the monkey optic nerve head. Invest Ophthalmol Vis Sci **17**: 33-50.

Mistlberger, A, Liebmann, J M, Greenfield, D S, Pons, M E, Hoh, S-T, Ishikawa, H and Ritch, R (1999). Heidelberg retina tomography and optical coherence tomography in normal, ocular-hypertensive, and glaucomatous eyes. Ophthalmology **106**(10): 2027-2032.

Mitamura, Y, Suzuki, T, Kinoshita, T, Miyano, N, Tashimo, A and Ohtsuka, K (2004). Optical coherence tomographic findings of dissociated optic nerve fiber layer appearance. Am J Ophthalmol **137**(6): 1155-1156.

Mitchell, P, Hourihan, F, Sandbach, J and Jin Wang, J (1999). The relationship between glaucoma and myopia: The Blue Mountains eye study. Ophthalmology **106**(10): 2010-2015.

Mitchell, P, Smith, W, Attebo, K and Healey, P R (1996). Prevalence of open-angle glaucoma in Australia. Ophthalmology **103**: 1661-1669.

Mitchell, P, Smith, W, Chey, T, Stat, M and Healey, P R (1997). Open-angle glaucoma and diabetes. Ophthalmology **104**: 712-718.

Miyake, K, Uchida, H, Sugiyama, K, Yamamoto, T, Kitazawa, Y and Shinohara, H (2003). Quantification of retinal nerve fiber defects in Glaucoma: three-dimensional analysis by Heidelberg retina tomograph. Jpn J Ophthalmol **47**(4): 347-350.

Mohammadi, K, Bowd, C, Weinreb, R N, Medeiros, F A, Sample, P A and Zangwill, L M (2004). Retinal nerve fiber layer thickness measurements with scanning laser polarimetry predict glaucomatous visual field loss. Am J Ophthalmol **138**(4): 592-601.

Mok, K H, Lee, V, W H and So, K F (2002). Retinal nerve fibre layer measurement of the Hong Kong Chinese Population by Optical Coherence Tomography. J Glaucoma **11**: 481-483.

Mok, K H and Lee, V W H (2000). Nerve fiber analyzer and short-wavelength automated perimetry in glaucoma suspects: A pilot study. Ophthalmology **107**(11): 2101-2104.

Mok, K H, Lee, V W H and So, K F (2003). Retinal nerve fibre loss pattern in high-tension glaucoma by Optical Coherence Tomography. J Glaucoma **12**: 255-259.

Moloney, J B and Drury, M I (1982). Retinopathy and retinal function in insulin dependent diabetes mellitus. Br J Ophthalmol **66**: 759-761.

Morgan, J E, Uchida, H and Caprioli, J (2000). Retinal ganglion cell death in experimental glaucoma. Br J Ophthalmol **84**: 303-310.

Morgan, J E (1994). Selective cell death in glaucoma, does it really occur? Br J Ophthalmol **78**: 875-880.

Morgan, J E and Waldock, A (2000). Scanning laser polarimetry of the normal human retinal nerve fiber layer: a quantitative analysis. Am J Ophthalmol **129**(1): 76-82.

Moss, S E, Klein, B E and Klein, R (1996). Cigarette smoking and ten-year progression of diabetic retinopathy. Ophthalmology **103**: 1438-1442.

Mrugacz, M and Bakunowicz-Lazarczyk, A (2005). Measurement of retinal thickness using optical coherence tomography in patients with myopia. Klinika Oczna **107**(1-3): 68-69.

Mueller, A J, Freeman, W R, Folberg, R, Bartsch, D U, Schneider, A, Schaller, U and Kampik, A (1999). Evaluation of microvascularisation pattern visibilty in human choroidal melanomas: comparison of confocal fluorescein with indocyanine angiography. Graefe's Arch Clin Exp Ophthalmol **237**: 448-456.

Mulhauser, I, Bender, R, Bott, U et al., (1996). Cigarette smoking and progression of retinopathy and nephropathy in type 1 diabetics. Diabetic Medicine **13**: 536-543.

Murata, T, Cui, J, Taba, K E, Oh, J, Spee, C, Hinton, D R and Ryan, S J (2000). The possibilty of gene therapy for the treatment of choroidal neovascularisation. Ophthalmology **107**: 1364-1373.

Muscat, S, Parks, S, Kemp, E and Keating, D (2002). Repeatability and reproducibility of macular thickness measurements with the Humphrey OCT system. Invest Ophthalmol Vis Sci **43**: 490-495.

Nakamura, H, Maeda, T, Suzuki, Y and Inoue, Y (1999). Scanning Laser Tomography to Evaluate Optic Discs of Normal Eyes. Jpn J Ophthalmol **43**(5): 410-414.

Nakamura, M, Barber, A J, Antonetti, D A, La Noue, K F, Robinson, K A, Buse, M G and Gardner, T W (2001). Excessive hexosamines block the neuroprotective effect of insulin and induce aptosis in retinal neurons. J Biol Chem **276**: 43748-43755.

Neubauer, A S, Priglinger, S, Ullrich, S et al., (2001). Comparison of foveal thickness measured with the retinal thickness analyser and optical coherence tomography. Retina **21**(6): 596-601.

Ningerling, J R, Dielemans, I, Hofman, A, Grobbee, D E, Hijmering, M, Kramer, C F L and de Jong, P T V M (1995). The prevalence of age related maculopathy in the Rotterdam study. Ophthalmology **102**: 201-210.

Nomura, R, Terasaki, H, Hirose, H and Miyake, Y (2000). Blue-on-yellow perimetry to evaluate S cone sensitivity in diabetics. Ophthalmic Res **32**: 69-72.

Nork, T M, Wang, L P and Poulson, G L (1994). Selective loss of photoreceptors in human diabetic retinopathy. Invest Ophthalmol Vis Sci **35**: 1588.

North, R V, Cooney, O, Chambers, D, Dolben, J and Owens, D R (1997). Does hyperglycaemia have an influence upon colour vision of patients with diabetes mellitus. Ophthal Physiol Opt **17**(2): 95-101.

Nouri-Mahdavi, K, Hoffman, D, Tannenbaum, D P, Law, S and Caprioli, J (2004). Identifying early glaucoma with optical coherence tomography. Am J Ophthalmol **137**: 228-235.

Nowomiejska, K, Vonthein, R, Paetzold, J, Zagorski, Z, Kardon, R and Schiefer, U (2005). Comparison between Semiautomated Kinetic Perimetry and Conventional Goldmann Manual Kinetic Perimetry in Advanced Visual Field Loss. Ophthalmology **112**(8): 1343-1354.

Nussenblatt, R B, Kaufman, S C, Palestine, A G, Davis, M D and Ferris, F L (1987). Macular thickening and visual acuity; Measurement in patients with cystoid macular oedema. Ophthalmology **94**: 1134-1139.

O'Brien, C (1998). The optic disc in glaucoma. Ophthal Physiol Opt **18**(2): 238.

Ogawa, S, Tank, D W, Menon, R, Ellerman, J M, Kim, S G, Merkle, H and Uburbil, K (1992). Intrinsic signal changes accompanying sensory stimulation: functional brain mapping with magnetic resonance imaging. Proc Natl Acad Sci **89**: 5951-5955.

Ogden, T E and Miller, R F (1966). Studies of the optic nerve of the rhesus monkey: Nerve fiber spectrum and physiological properties. Vis Res **6**(5): 485-488.

Ohashi, H, Oh, H, Nishiwaki, H, Nonaka, A and Takagi, H (2004). Delayed absorption of macular edema accompanying serous retinal detachment after grid laser treatment in patients with branch retinal vein occlusion. Ophthalmology **111**(11): 2050-2056.

Ohno-Matsui, K and Tokoro, T (1996). The progression of lacquer crack lesions in pathological myopia. Retina **16**: 29-37.

Ossoinig K C, Cennamo G and Frazier-Byrne S (1981). Echographic differential diagnosis of optic nerve lesions. Docum Ophthalmol Proc Ser **29**:327-32.

Olmedo, M, Cardarso-Suarez, C, Gomez-Ulla, F, Val, C and Fernandez, I (2005). Reproducibility of optic nerve head measurements obtained by optical coherence tomography. Eur J Ophthalmol **15**(4): 486-492.

Olsen, T (1989). The accuracy of ultrasonic determination of axial length in pseuodphakic eyes. Acta Ophthalmol **67**: 141-144.

Onda, E, Cioffi, G A, Bacon, D R and Van Buskirk, E M (1995). Microvasculature of the human optic nerve. Am J Ophthalmol **120**: 92-102.

Orgul, S, Flammer, J, Gasser, P (1995). Female preponderance in normal tension glaucoma. Ann Ophthalmol Glaucoma **27**: 355-359

Orgul, S, Cioffi, G A, Bacon, D R and Van Buskirk, M (1995). Sources of variability of topometric data with a scanning laser ophthalmoscope. Arch Ophthalmol **113**: 161-164.

Orgul, S, Cioffi, G A and Van Buskirk, E M (1997). Variability of contour alignment on sequential images with the Heidelberg Retina Tomograph. Graefe's Arch Clin Exp Ophthalmol **235**: 82-86.

Orzalesi, N, Miglior, S, Lonati, C and Rosetti, L (1998). Microperimetry of localized retinal nerve fiber layer defects. Vis Res **38**(5): 763-771.

Oshima, Y, Emi, K, Yamanishi, S and Motokura, M (1999). Quantitative assessment of macular thickness in normal subjects and patients with diabetic retinopathy by scanning retinal thickness analyser. Br J Ophthalmol **83**: 54-61.

Otani, T and Kishi, S (2000). Tomographic assessment of vitreous surgery for diabetic macular oedema. Am J Ophthalmol **129**: 487-494.

Otani, T, Kishi, S and Maruyama, Y (1999). Patterns of diabetic macular edema with optical coherence tomography. Am J Ophthalmol **127**(6): 688-693.

Paczka, J A, Friedman, D S, Quigley, H A, Barron, Y and Vitale, S (2001). Diagnostic capabilities of frequency-doubling technology, scanning laser polarimetry, and nerve fiber layer photographs to distinguish glaucomatous damage. Am J Ophthalmol **131**(2): 188-197.

Palmowski, A M, Allgayer, R, Heinemann-Vernaleken, B and Ruprecht, K W (2002). Influence of PDT in choroidal neovascularisation on focal retinal function assessed with the multifocal electroretinalgram and perimetry. Ophthalmology **109**: 1788-1792.

Panda S and Jonas J B (1992). Decreased photoreceptor count in human eyes with secondary angle-closure glaucoma. Invest Ophthalmol Vis Sci **33** (8):2532-2536.

Panda-Jonas, S, Jonas, J B, Jakobczyk, M and Schneider, U (1994). Retinal photoreceptor count, retinal surface area, and optic disc size in normal human eyes. Ophthalmology **101**: 519-523.

Panozzo, G, Parolini, B, Gussan, I, Mercanti, A, Pinackatt, S, Bertoldo, G and Pignatto, S (2004). Diabetic macular oedema: an OCT based classification. Semin Ophthalmol **19**(1-2): 13-20.

Patel (2002). Current theories of primary open-angle glaucoma. Optician **223**(5856): 22-25.

Paunescu, L A, Schuman, J S, Price, L L, Stark, P C, Beaton, S A, Ishikawa, H, Wollstein, G and Fujimoto, J G (2004). Reproducibility of nerve fibre thickness, macular thickness and optic nerve head measurements using Stratus OCT. Invest Ophthalmol Vis Sci **45**: 1716-1724.

Pavlin, C J, Harsiewicz, K, Sherar, M D and Foster, F S (1991). Clinical use of ultrasound biomicroscopy. Ophthalmology **98**: 287-295.

Pavlin, C J, Sherar, M D and Foster, F S (1990). Subsurface ultrasound microscopic imaging of the intact eye. Ophthalmology **97**: 244-250.

Pendergast, S D and Shields, M B (1995). Reproducibility of optic nerve head topographic measurements with the Glaucoma-scope. J Glaucoma **4**: 170-176.

Perkins, E S and Phelps, C D (1982). Open angle glaucoma, ocular hypertension, low-tension glaucoma, and refraction. Arch Ophthalmol **100**: 1464-1467.

Perry, V H, Oehler, R and Cowey, A (1984). Retinal ganglion cells that project to the dorsal lateral geniculate nucleus in the macaque monkey. Neuroscience **12**: 1101-1123.

Pieroth, L, Schuman, J S, Hertzmark, E, Hee, M R, Wilkins, J R, Coker, J, Mattox, C, Pedut-Kloizman, T, Puliafito, C A, Fujimoto, J G and Swanson, E (1999). Evaluation of focal defects of the nerve fibre layer using optical coherence tomography. Ophthalmology **106**: 570-579.

Pierre-Kahn, V, Tadayoni, R, Haouchine, B, Massin, P and Gaudric, A (2005). Comparison of optical coherence tomography models OCT1 and Stratus OCT for macular retinal thickness measurement. Br J Ophthalmol **89**: 1581-1585.

Pires, I, Bernandes, R C, Lobo, C L, Soares, M A and Cunha-Vaz, J (2002). Retinal thickness in eyes with mild nonproliferative retinopathy in patients with type 2 diabetes mellitus. Arch Ophthalmol **120**: 1301-1306.

Poinoosawmy, D, Fontana, L, Wu, J X, Fitzke, F W and Hitchings, R A (1997). Variation of nerve fibre layer thickness measurements with age and ethnicity by scanning laser polarimetry. Br J Ophthalmol **81**: 350-354.

Pointer, J S (1997). The diurnal variation of intraocular pressure in non-glaucomatous subjects: relevance in a clinical context. Ophthal Physiol Opt **17**(6): 456-465.

Polito, A, Del Borello, M, Isola, M, Zemella, N and Bandello, F (2005). Repeatability and Reproducibility of Fast Macular Thickness Mapping With Stratus Optical Coherence Tomography. Arch Ophthalmol **123**: 1330-1337.

Polito, A, Shah, S M, Haller, J A, Zimmer-Galler, I, Zeimer, R, Campochiaro, P A and Vitale, S (2002). Comparison between retinal thickness analyzer and optical coherence tomography for assessment of foveal thickness in eyes with macular disease. Am J Ophthalmol **134**(2): 240-251.

Polo, V, Larrosa, J M, Pinilla, I, Pablo, L and Honrubia, F M (2001). Optimum criteria for short-wavelength automated perimetry. Ophthalmology **108**(2): 285-289

Polo, V, Larrosa, J M, Pinilla, I, Perez, S, Gonzalvo, F and Honrubia, F M (2002). Predictive value of short-wavelength automated perimetry: A 3-year follow-up study. Ophthalmology **109**(4): 761-765.

Pons, M E and Garcia-Valenzuela, E (2005). Redefining the Limit of the Outer Retina in Optical Coherence Tomography Scans. Ophthalmology **112**(6): 1079-1085.

Pons, M E, Rothman, R F, Ozden, R G, Liebmann, J M and Ritch, R (2001). Vitreous opacities affect scanning laser polarimetry measurements. Am J Ophthalmol **131**(4): 511-513.

Porciatti, V (1997). Retinal and cortical EPs to chromatic contrast stimuli. Electroencephalography and Clinical Neurophysiology **103**(1): 43.

Puliafito, C.A, Hee, M R, Lin, C P, Reichel, E, Schuman, J S, Duker, J S, Izatt, J A, Swanson, E A and Fujimoto J G (1995). Imaging of macular diseases with optical coherence tomography. Ophthalmology **102**: 217-229.

Quigley, H A (1985). Early detection of glaucomatous damage: II. Changes in the appearance of the optic disk. Surv Ophthalmol **30**(2): 117-126.

Quigley, H A (1986). Regenerating fish optic nerves and a regeneration-like response in injured optic nerves of adult rabbits : by M. Schwartz, M. Belkin, A. Harel, et al. Science 228:600-602, 1985. Surv Ophthalmol **30**(5): 348.

Quigley, H A (1987). Reappraisal of the mechanisms of glaucomatous optic nerve damage. Eye **1**: 318-322.

Quigley, H A (1989). Primary trabeculectomy in congenital glaucoma : by J.P. Burke and R. Rowell. Br J Ophthalmol 73: 186-190, 1989. Surv Ophthalmol **34**(3): 233.

Quigley, H A (1991). Retinal nerve fiber layer photography : by Lewis W. Roloff, M.D., Thorofare, N.J., Slack Inc., 1990, Surv Ophthalmol **36**(1): 77.

Quigley, H A (1996). Number of people with glaucoma worldwide. Br J Ophthalmol **80**: 389-393.

Quigley, H A (1998). Identification of glaucoma-related visual field abnormality with the screening protocol of frequency doubling technology. Am J Ophthalmol **125**(6): 819-829.

Quigley, H A (1998). Recognizing structural damage to the optic nerve head and nerve fiber layer in glaucoma. Am J Ophthalmol **125**(4): 563.

Quigley, H A (1999). Neuronal death in glaucoma. Prog Ret Eye Res **18**(1): 39-57.

Quigley, H A (1999). Proportion of those with open-angle glaucoma who become blind. Ophthalmology **106**(11): 2039.

Quigley, H A (2005). European Glaucoma Prevention Study. Ophthalmology **112**(9): 1642-1643.

Quigley, H A and Addicks, E M (1981). Regional differences in the structure of the lamina-cribrosa and their relation to glaucomatous optic nerve damage. Arch Ophthalmol **99**: 137-143.

Quigley, H A, Addicks, E M and Green, W R (1982). Optic nerve damage in human glaucoma: III. Quantitative correlation of nerve fibre loss and visual field deficit in glaucoma, Ischaemic neuropathy, papilloedema and toxic neuropathy. Arch Ophthalmol **100**: 135-146.

Quigley, H A, Addicks, E M, Green, W R and Maumenee (1981). Optic nerve damage in human glaucoma: II. the site of injury and susceptibility to damage. Arch Ophthalmol **99**: 635-649.

Quigley, H A, Coleman, A L and Dorman-Pease, M E (1991). Larger optic nerve heads have more nerve fibres in normal monkey eyes. Arch Ophthalmol **109**: 1441-1443.

Quigley, H A, Dunkelberger, G R and Green, W R (1988). Chronic human glaucoma causing selectively greater loss of large optic nerve fibres. Ophthalmology **95**: 357-363.

Quigley, H A, Hohman, R M and Addicks, E M (1980). Chronic experimental glaucoma in primates: II. effect of extended intraocular pressure elevation on optic nerve head and axonal transport. Invest Ophthalmol Vis Sci **19**: 137-152.

Quigley, H A, Katz, J, Derick, R J, Gilbert, D and Sommer, A (1992). An evaluation of optic disc and nerve fibre layer examination in monitoring progression of early glaucoma damage. Ophthalmology **99**: 19-28.

Quigley, H A, Kee Park, C, Tracey, P A and Pollack, I P (2002). Community screening for eye disease by laypersons: the Hoffberger program. Am J Ophthalmol **133**(3): 386-392.

Quigley, H A, Miller, N R and George, T (1980). Clinical evaluation of nerve fibre atrophy as indicator of glaucomatous optic nerve damage. Arch Ophthalmol **98**: 1564-1571.

Quigley, H A and Pease, M E (1996). Change in the optic disc and nerve fibre layer thickness estimated with the Glaucoma-scope in monkey eyes. J Glaucoma **5**: 106-116.

Quigley, H A, Pease, M E and Thibault, D (1994). Change in the appearance of elastin in the lamina cribrosa of glaucomatous optic nerve heads. Graefe's Arch Clin Exp Ophthalmol **232**: 257-261.

Quigley, H A, Sanchez R.M and Dunkelberger, G R (1987). Chronic glaucoma selectively damages large optic nerve fibres. Invest Ophthalmol Vis Sci **28**: 913-920.

Radius, R L (1981). Regional specificity in anatomy at the lamina cribrosa. Arch Ophthalmol **99**: 478-480.

Radius, R L and Gonzales, M (1981). Anatomy of the lamina cribrosa in human eyes. Arch Ophthalmol **99**: 2159-2162.

Rath, E Z, Shin, D H, Kim, C, Tsai, C S, Zeiter, J H and Hong, Y J (1996). Relationship between optic disc cupping change and intraocular pressure control in adult glaucoma patients. Graefe's Arch Clin Exp Ophthalmol **234**: 434-439.

Ray, R, Stinnett, S S and Jaffe, G J (2005). Evaluation of image artifact produced by optical coherence tomography of retinal pathology. Am J Ophthalmol **139**(1): 18-29.

Realini, T, Lai, M Q, and Barber, L (2004). Impact of diabetes on glaucoma screening using frequency-doubling perimetry. Ophthalmology **111**: 2133-2136.

Regan, D and Neima, D (1984). Low contrast letter charts in early diabetic retinopathy, ocular hypertension, glaucoma and Parkinson's disease. Br J Ophthalmol **68**: 885-889.

Reiss, G R, Lee D A, Topper, J E and Brubaker, R F (1984). Aqueous humour flow during sleep. Invest Ophthalmol Vis Sci **25**: 776-778.

Remky, A, Arend, O and Hendricks, S (2000). Short-wavelength automated perimetry and capillary density in early diabetic maculopathy. Invest Ophthalmol Vis Sci **41**: 274-281.

Remsch, H, Spraul, C W, Lang, G K and Land, G E (2000). Changes of retinal capillary blood flow in age related maculopathy. Graefe's Arch Clin Exp Ophthalmol **238**: 960-964.

Repka, M X and Quigley, H A (1989). The effect of age on normal human optic nerve fibre number and diameter. Ophthalmology **96**: 26-32.

Resnikoff, Pascolini, Etya'ale et al., (2002). WHO statistics. Bull World Health Organisation **82**(11): 844-851.

Reus, N J, Colen, T P and Lemij, H G (2003). Visualization of localized retinal nerve fiber layer defects with the GDx with individualized and with fixed compensation of anterior segment birefringence. Ophthalmology **110**(8): 1512-1516.

Reus, N J and Lemij, H G (2004). Scanning laser polarimetry of the retinal nerve fiber layer in perimetrically unaffected eyes of glaucoma patients. Ophthalmology **111**(12): 2199-2203.

Rivero, M E, Bartsch, D, Otto, T and Freeman, W R (1999). Automated scanning laser ophthalmoscope image montages of retinal diseases. Ophthalmology **106**: 2296-2300.

Rohrschneider, K, Burk, R O W, Kruse, F E and Volcker, H E (1994). Reproducibility of the optic nerve head topography with a new laser tomographic scanning laser device. Ophthalmology **101**: 1044-1049.

Rohrschneider, K, Burk, R O W and Volcker, H E (1993). Reproducibility of topometric data acquisition in normal and glaucomatous optic nerve heads with the laser tomographic scanner. Graefe's Arch Clin Exp Ophthalmol **231**: 457-464.

Rohrschneider, K, Gluck, R, Burk, R O W, Kruse, F E and Volcker, H E (1995). Retinal nerve fiber layer thickness measurements in different distances from the optic disc. Vis Res **35**(Supplement 1): S123.

Ross, J E, Bron, A J and Clarke, D D (1984). Contrast sensitivity and visual disability in chronic simple glaucoma. Br J Ophthalmol **68**: 821-827.

Roth, J A (1969). Central visual field in diabetes. Br J Ophthalmol **53**:16-25.

Roy, M S, Gunkel, R D and Podgor, M J (1986). Colour vision defects in early diabetic retinopathy. Arch Ophthalmol **104**: 225-228.

Roy, M S, McCulloch, C, Hanna, A K and Mortimer, C (1984). Colour vision in longstanding diabetes mellitus. Br J Ophthalmol **68**: 215-217.

Rubin, G S, Bandeen Roche, K, Prasada-Rao, P and Fried, L P (1994). Visual impairment and disability in older adults. Optom Vis Sci **71**(12): 750-760.

Rudnicka, A R, Burk, R O W, Edgar, D F, Fitzke, F W (1998). Magnification characteristics of fundus imaging systems. Ophthalmology **105**: 2186-2192.

Rylander III, H G, Kemp, N J, Park, J, Zaatari, H N and Milner, T E (2005). Birefringence of the primate retinal nerve fiber layer. Exp Eye Res **81**(1): 81-89.

Sadda, S R, Wu, Z, Walsh, A C, Richine, L, Dougall, J, Cortez, R and LaBree, L D (2006). Errors in Retinal Thickness Measurements Obtained by Optical Coherence Tomography. Ophthalmology **113**(2):285-293.

Saiki, S, Tanaka, T, Miyamoto, T and Ohnishi, Y (2001). Surgical posterior vitreous detachment combined with gas/air tamponde for treating macular oedema associated with branch retinal vein occlusion: retinal tomography and visual outcome. Graefe's Arch Clin Exp Ophthalmol **239**: 729-732.

Salmon, J F, Mermoud, A and Ivey, A (1993). The prevalence of primary angle closure glaucoma and open angle glaucoma in Mamre, Western Cape, South Africa. Arch Ophthalmol **111**: 1263-1269.

Sample P A, (2000). Short-wavelength automated perimetry: it's role in the clinic and for understanding ganglion cell function. Prog Ret Eye Res **19** (4):369-383.

Sample, P A, Bosworth, C F and Weinreb, R N (1997). Short-wavelength automated perimetry and motion automated perimetry in patients with glaucoma. Arch Ophthalmol **115**: 1129-1133.

Sample, P A, Taylor, J D N, Martinez, G A et al., (1993). Short-wavelength colour visual fields in glaucoma suspects at risk. Am J Ophthalmol **115**: 225-233.

Sample, P A, and Weinreb, R N. (1990). Colour perimetry for assessment of primary open angle glaucoma. Invest Ophthalmol Vis Sci **31**: 1869-1875.

Sample, P A (2001). What does functional testing tell us about optic nerve damage? Surv Ophthalmol **45(Suppl)**(3): S319-S324.

Sanchez-Galeana, C A, Bowd, C, Zangwill, L M, Sample, P A and Weinreb, R N (2004). Short-wavelength automated perimetry results are correlated with optical coherence tomography retinal nerve fiber layer thickness measurements in glaucomatous eyes. Ophthalmology **111**(10): 1866-1872.

Sanchez-Tocino, H, Alvarez-Vidal, A, Maldonado, M J, Moreno-Montanes, J and Garcia-Layana, A (2002). Retinal thickness study with optical coherence tomography in patients with diabetes. Invest Ophthalmol Vis Sci **43**: 1588-1594.

Schaudig U H, Glaefke C, Scholz F, Richard G (2000). Optical coherence tomography for retinal thickness measurement in diabetic patients without clinically significant macular oedema. Ophthalmic Surg Lasers **31**:182-186.

Schmetterer, L, Muller, M, Fasching, P et al., (1997). Renal and ocular haemodynamic effects of insulin. Diabetes **46**: 1868-1874.

Schocket, L S, Grunwald, J E, Tsang, A F et al., (1999). The effect of pregnancy on retinal haemodynamics in diabetic versus nondiabetic mothers. Am J Ophthalmol **128**: 477-484.

Schuman J S, Puliafito C A and Fujimoto J G (2004). Optical Coherence Tomography of Ocular Diseases. 2nd Edition. Slack Incorporated.

Schuman, J S, Pedut-Kloizman, T, Hertzmark, E, Hee, M R, Wilkins, J R, Coker , J G, Puliafito, C A, Fujimoto, J G and Swanson, E A (1996). Reproducibility of nerve fibre layer thickness measurements using optical coherence tomography. Ophthalmology **103**: 1889-1898.

Schuman, J S, Hee, M R, Puliafito, C A, Wong, C, Pedut-Kloizman, T, Lin, C P, Hertzmark, E, Izatt, J A, Swanson, E A and Fujimoto, J G (1995). Quantification of nerve fibre layer thickness in normal and glaucomatous eyes using optical coherence tomography. Arch Ophthalmol **113**: 586-596.

Schwartz, B (1994). Circulatory defects of the optic disk and retina in ocular hypertension and high pressure open-angle glaucoma. Surv Ophthalmol **38**(Supplement 1): S23-S34.

Scott, T M, Foote, J, Peat, B, Galway, G (1986). Vascular and neural changes in the rat optic nerve following induction of diabetes with streptozotocin. J Anat **144**: 145-152.

Seddon, J M, Schwartz, B and Flowerdew, G (1983). Case-control study of ocular hypertension. Arch Ophthalmol **101**: 891-894.

Shabana, N, Peres, V C, Carkeet, A and Chew, P T K (2003). Motion Perception in Glaucoma Patients: A Review. Surv Ophthalmol **48**(1): 92-106.

Shahidi, M, Ogura, Y, Blair, N and Zeimer, R (1994). Retinal thickness changes after focal laser treatment of diabetic macular oedema. Br J Ophthalmol **78**: 827-830.

Shahidi, M, Ogura, Y, Blair, N P, Rusin, M M and Zeimer, R (1991). Retinal thickness analysis for quantitative assessment of diabetic macular oedema. Arch Ophthalmol **109**: 1115-1119.

Shahidi, M, Wang, Z and Zelkha, R (2005). Quantitative Thickness Measurement of Retinal Layers Imaged by Optical Coherence Tomography. Am J Ophthalmol **139**(6): 1056-1061.

Shahidi, M, Zeimer, R C and Mori, M (1990). Topography of the retinal thickness in normal subjects. Ophthalmology **97**: 1120-1124.

Sharma, S, Brown, G C, Brown, M M, Hollands, H and Shah, G K (2001). The cost-effectiveness of photo dynamic therapy for fellow eyes with subfoveal choroidal neovascularisation secondary to age-related macular degeneration. Ophthalmology **108**: 2051-2059.

Shiose, Y (1990). Intraocular pressure. New perspectives. Surv Ophthalmol **34**: 413-435.

Shiose, Y, Kitazawa, Y, Tsukuhara, S, Akamatsu, T, Mizokami, K, Futa, R et al (1991). Epidemiology of glaucoma in Japan- a nationwide glaucoma survery. Jpn J Ophthalmol **35**: 133-155.

Shiose, Y and Kawase, Y (1986). A new approach to stratified normal intraocular pressure in general population. Am J Ophthalmol **101**: 714-721.

Simonsen, S E (1980). The value of the oscillatory potential in selecting diabetics at risk of developing proliferative retinopathy. Acta Ophthalmol **58**: 865-878.

Sinclair, S H, Graunwald, J E, Riva, C, Braunstein, S, N, Nichols, C W and Scwartz, S (1982). Retinal vascular autoregulation in diabetes mellitus. Ophthalmology **89**: 748-750.

Smith, E L, Chino, Y M, Harwerth, R S, Ridder, W H, Crawford, M L J and DeSantis, L (1993). Retinal inputs to the monkey geniculate nucleus in experimental glaucoma. Clin Vis Sci **8**: 113-139.

Sokol, S, Moskowitz, A, Skarf, B, Evans, R, Molitch, M and Senior, B (1985). Contrast sensitivity in diabetics with and without background retinopathy. Arch Ophthalmol **103**: 51-54.

Soliman, M A E, van den Berg, T J T P, Ismaeil, A A, de Jong, L A and de Smet, M D (2002). Retinal nerve fibre layer analysis: relationship between optical coherence tomography and red- free photography. Am J Ophthalmol **133**: 187-195.

Sommer, A (1989). Intraocular pressure and glaucoma. Am J Ophthalmol **107**: 186-188.

Sommer, A, Katz, J, Quigley, H A, Miller, R N, Richter, R C and Witt, K A (1991). Clinically detectable nerve fibre atrophy precedes the onset of visual field loss. Arch Ophthalmol **109**: 77-83.

Sommer, A, Miller, N R, Pollack, I P, Maumenee, A E and George, T (1977). The nerve fibre layer in the diagnosis of glaucoma. Arch Ophthalmol **95**: 2149-2156.

Sommer, A, Pollack, I P and Maumenee, A E (1979). Optic disc parameters and onset of glaucomatous visual field loss. Arch Ophthalmol **97**: 1449-1454.

Sommer, A, Tielsch, J, M, Katz, J, Quigley, H A, Gottsch, J D, Javitt, J and Singh, K (1991). Relationship between introcular pressure and primary open angle glaucoma among white and black Americans: The Baltimore Eye Survey. Arch Ophthalmol 109: 1090-1095.

Sonnsjo, B, Dokmo, Y and Krakau, T (2002). Disc haemorrhages, precursors of open angle glaucoma. Prog Ret Eye Res **21**(1): 35-56.

Sony, P, Sihota, R, Tewari, H K, Venkatesh, P and Singh, R (2004). Quantification of the retinal nerve fibre layer thickness in normal Indian eyes with optical coherence tomography. Ind J Ophthalmol **52**(4): 303-309.

Spaeth, G L. (1994). Reversible changes in the optic disc and visual field in glaucoma. Curr Opin Ophthalmol **5**: 36-45.

Spaide, R F, Wong, D, Fisher, Y and Goldbaum, M (2002). Correlation of vitreous attachment and foveal deformation in early macular hole states. Am J Ophthalmol **133**: 226-229.

Spencer, A F, Sadiq, S A, Pawson, P and Vernon, S A (1995). Vertical optic disc diameter: discrepancy between planimetric and SLO measurements. Invest Ophthalmol Vis Sci **36**: 796-803.

Steidl, S M and Pruet, R C (1997). Macular complications associated with posterior staphyloma. Am J Ophthalmol **123**: 181-187.

Stone, E M, Fingert, J H, Alward, W L M, Nguyen, T, D, Polansky, J R, Sunden, S L F et al., (1997). Identification of a gene that causes primary open angle glaucoma. Science **275**: 668-670.

Sugimoto, M, Sasoh, M, Ido, M, Wakatani, Y, Takahashi C, Uji, Y (2005). Detection of Early Diabetic Change with Optical Coherence Tomography in Type 2 Diabetes Mellitus Patients without Retinopathy. Ophthalmologica **219**: 379-385.

Sugiyama, K, Uchida, H, Tomita, G, Sato, Y, Iwase, A and Kitazawa, Y (1999). Localized wedge-shaped defects of retinal nerve fiber layer and disc hemorrhage in glaucoma. Ophthalmology **106**(9): 1762-1767.

Sung Chung, H, Harris, A, Kagemann, L and B, M (1999). Peripapillary retinal blood flow in normal tension glaucoma. Br J Ophthalmol **83**(466-469).

Suzuma, K, Kita, M, Yamana, T, Ozaki, S, Takagi, H, Kiryu, J and Ogura, Y (1998). Quantitative assessment of macular edema with retinal vein occlusion. Am J Ophthalmol **126**(3): 409-416.

Tabandeh, H, Ranganath, L and Marks, V (1996). Visual function during acute hypoglycaemia. Eur J Ophthalmol **6**(1): 81-86.

Tannenbaum, D P, Zangwill, L M, Bowd, C, Sample, P A and Weinreb, R N (2001). Relationship between visual field testing and scanning laser polarimetry in patients with a large cup-to-disk ratio. Am J Ophthalmol **132**(4): 501-506.

Tate, G W and Lynn, J R (1977). Principles and quantitative perimetry, testing and interpreting visual fields. New York, Grune and Stratton: 8-10.

Teesalu, P, Airaksinen, P J and Tuulonen, A (1998). Blue-on-yellow visual field and retinal nerve fiber layer in ocular hypertension and glaucoma. Ophthalmology **105**(11): 2077-2081.

Terasaki, H, Kojima, T, Niwa, H, Piao, C H, Ueno, S, Kondo, M, Ito, Y and Miyake, Y (2003). Changes in focal macular electroretinograms and foveal thickness after vitrectomy for diabetic macular oedema. Invest Ophthalmol Vis Sci **44**: 4465-4472.

Tewari, H K, Wagh, V B, Sony, P, Venkatesh, P and Singh, R (2004). Macular thickness evaluation using the optical coherence tomography in normal Indian eyes. Ind J Ophthalmol **52**(3): 199-204.

Theodossiadis, P G, Kollia, A K, Gogas, P, Panagiotidis, D, Moschos, M and Theodossiadis, G P (2002). Retinal disorders in preeclampsia studied with optical coherence tomography. Am J Ophthalmol **133**(5): 707-709.

Tielsch, J M, Katz, J, Quigley, H A, Javitt, J and Sommer, A (1995). Diabetes, Intraocular pressure, and Primary Open-angle Glaucoma in the Baltimore Eye Survey. Ophthalmology **102**: 48-53.

Tielsch, J M, Katz, J, Quigley, H A, Miller, N R, and Sommer, A (1988). Intraobserver and interobserver agreement in measurement of optic disc characteristics. Ophthalmology **95**: 350-356.

Tielsch, J M, Katz, J, Sommer, A, Quigley, H A and Javitt, J (1995). Hypertension, perfusion pressure and primary open angle glaucoma. Arch Ophthalmol **113**: 216-221.

Tielsch, J M, Sommer, A, Katz, J, Quigley, H A and Javitt, J (1991). Racial variations in the prevalence of Primary Open-angle Glaucoma. JAMA **266**: 369-374.

Tjon-Fo-Sang, M J, de Vries, J and Lemij, H G (1996). Measurement by nerve fibre analyser of retinal nerve fibre layer thickness in normal subjects and patients with ocular hypertension. Am J Ophthalmol **122**: 220-227.

Tjon-Fo-Sang, M J and Lemij, H G (1998). Retinal nerve fiber layer measurements in normal black subjects as determined with scanning laser polarimetry. Ophthalmology **105**(1): 78-81.

Tomlinson, A and Phillips, C I (1970). Applanation tension and axial length of the eyeball. Br J Ophthalmol **54**: 548-553.

Toth, C A, Narayan, D G, Boppart, S A et al., (1997). A comparison of retinal morphology viewed by optical coherence tomography and by light microscopy. Arch Ophthalmol **115**: 1425-1428.

Trick, G L, Burde, R M, Gordon, M O, Santiago, J V and Kilo, C (1988). The relationship between hue discrimination and contrast sensitivity deficits in patients with diabetes mellitus. Ophthalmology **95**: 693-698.

Tuulonen, A and Airaksinen, P J (1991). Initial glaucomatous optic disc and retinal nerve fibre layer abnormalities and their progression. Am J Ophthalmol **111**:485-490.

Tuulonen, A, Lehtola, J and Airaksinen, P J (1992). Nerve fibre layer defects with normal visual fields. Ophthalmology **100**: 587-598.

UK Prospective Diabetes Study (UKPDS) (1998). Tight blood pressure control and risk of macrovascular and microvascular complications in type 2 diabetes. UKPDS report number 38. BMJ **317**: 703-713.

Utku, D and Atmaca, L S (1992). Farnsworth-Munsell 100 hue test for patient with diabetes mellitus. Ann Ophthalmol **24**: 205-208.

Van Buskirk, E M and Cioffi, G A (1992). Glaucomatous optic neuropathy. Am J Ophthalmol **113**: 447-452.

VanNewkirk, M R, Nanjan, M B, Wang, J J, Mitchell, P, Taylor, H R and McCarty, C A (2000). The prevalence of age related maculopathy. Ophthalmology **107**: 1593-1600.

Varma, R, Bazzaz, S and Lai, M (2003). Optical tomography-measured retinal nerve fibre layer thickness in normal latinos. Invest Ophthalmol Vis Sci **44**: 3369-3373.

Varma, R, Skaf, M and Barron, E (1996). Retinal nerve fibre layer thickness in norman human eyes. Ophthalmology **103**: 2114-2119.

Varma, R, Steinmann, W C and Scott, I U (1992). Expert agreement in evaluating the optic disc for glaucoma. Ophthalmology **99**: 215-221.

Vermeer, K A, Vos, F M, Lemij, H G and Vossepoel, A M (2003). Detecting glaucomatous wedge shaped defects in polarimetric images. Medical Image Analysis **7**(4): 503-511.

Vermeer, K A, Vos, F M, Lemij, H G and Vossepoel, A M (2004). A model based method for retinal blood vessel detection. Computers in Biology and Medicine **34**(3): 209-219.

Verrotti, A, Lobefalo, L, Petitti, M, T, et al., (1998). Relationship between contrast sensitivity and metabolic control in diabetics with and without retinopathy. Ann Med **30**: 369-374.

Vickers, J C, Schumer, R A, Podos, S M, Wang, R F, Riederer, B M and Morrison, J H (1995). Differential vulnerability of neurochemically identified subpopulations of retinal neurons in a monkey model of glaucoma. Brain Research **680**(1-2): 23-35.

Vingerling, J R, Dielemans, I, Hofman, A, Grobbee, D E, Hijmering, M, Kramer, C F L and de Jong, P T V M (1995). The prevalence of age related maculopathy in the Rotterdam study. Ophthalmology **102**: 205-210.

Vogel, R, Crick, R P, Newson, R B, Shipley, M, Blackmore, H and Bulpitt, C J (1990). Association between intraocular pressure and loss of visual field in chronic simple glaucoma. Br J Ophthalmol **74**: 3-6.

Volbrecht, V J, Schneck, M E, Adams, A J, Linfoot, J A and Ai, E (1994). Diabetic short-wavelength sensitivity: variations with induced changes in blood glucose level. Invest Ophthalmol Vis Sci **35**: 1243-1246.

Wakatani, Y, Sasoh, M, Sugimoto, M, Ito, Y, Ido, M and Uji, Y (2003). Macular thickness measurements in healthy subjects with different axial lengths using optical coherence tomography. Retina **23**: 177-182.

Weber, J, Koll, W, Krieglstein, G K (1993). Intraocular pressure and visual field decay in chronic glaucoma. Ger J Ophthalmol **2** (3): 165-169

Weber, A J, Chen, H C, Hubbard, W C and Kaufman, P, L. (2000). Experimental glaucoma and cell size, density, and number in the primate lateral geniculate. Invest Ophthalmol Vis Sci **41**: 1370-1379.

Weber, A J, Kaufmann, P L and Hubbard, W C (1998). Morphology of single ganglion cells in the glaucomatous primate retina. Invest Ophthalmol Vis Sci **39**: 2304-2320.

Weih, L M, Nanjam, M, McCarty, C A and Taylor, H R (2001). Prevalence and predictors of open-angle glaucoma. Ophthalmology **108**: 1966-1972.

Weinberger , A W A, Kirchhof, B, Mazinani, B E and Schrage, N F (2001). Persistent indocyanine green (ICG) fluorescence 6 weeks after intraocular ICG administration for macular hole surgery. Graefe's Arch Clin Exp Ophthalmol **239**: 388-390.

Weinberger, D, Axer-Siegel, R and Landau, D (1998). Retinal thickness variation in the diabetic patient measured by the retinal thickness analyser. Br J Ophthalmol **82**: 1003-1006.

Weinberger, D, Stiebel, H, Gaton, D G, Priel, E and Yassur, Y (1995). Three - dimensional measurements of idiopathic macular holes using a scanning laser tomograph. Ophthalmology **102**: 1445-1449.

Weinreb, R N and Khaw, P T (2004). Primary open-angle glaucoma. Lancet **363**(9422): 1711-1720.

Weinreb, R N, Lusky, M, Bartsch, D and Morsman, D (1993). Effect of repetitive imaging on topographic measurements of the optic nerve head. Arch Ophthalmol **111**: 636-638.

Weinreb, R N, Shakiba, S, Zangwill L (1995). Scanning laser polarimetry to measure the nerve fibre layer of normal and glaucomatous eyes. Am J Ophthalmol **119**:627-636

Wensor, M D, McCarty, C A, Stanislavsky, Y L, Livingston, P M and Taylor, H R (1998). The Prevalence of Glaucoma in the Melbourne Visual Impairment project. Ophthalmology **105**: 733-739.

Williams, Z Y, Schman, J S, Gamell, L, Nemi, A, Hertzmark, E, Fujimoto, J G, Mattox, C, Simpson, J and Wollstein, G (2002). Optical coherence tomography measurement of nerve fibre layer thickness and the likelihood of a visual field defect. Am J Ophthalmol **134**: 538-546.

Wilson, M R, Hertzmark, E, Walker, A M, Childs, K, Epstein, D L (1987). A case-control study of risk factors in open angle glaucoma. Arch Ophthalmol **105**: 1066-1071.

Winder, S and Atta, H R (1996). Ultrasonography of the optic disc cup in discs of various sizes. Eye **10**: 732-736.

Wolfs, R C, Klaver, C C W, Ramrattan, R S, van Duijn, C M, Hofman, A and de Jong, P T V M (1998). Genetic risk of primary open-angle glaucoma. Arch Ophthalmol **116**: 1640-1645.

Wolkstein, M, Atkin, A and Bodis-Wollner, I (1980). Contrast sensitivity in retinal disease. Ophthalmology **87**: 1140-1149.

Wollstein, G, Schuman, J S, Price, L L, Aydin, A, Beaton, S A, Stark, P C, Fujimoto, J G and Ishikawa, H (2004). Optical coherence tomography (OCT) macular and peripapillary retinal nerve fiber layer measurements and automated visual fields. Am J Ophthalmol **138**(2): 218-225.

Wong, T Y, Klein, B E, Klein, R, Knudtson, M and Lee, K E (2003). Refractive errors, intraocular pressure, and glaucoma in a white population. Ophthalmology **110**: 211-217.

World Health Organisation, WHO (1994). Prevention of diabetes mellitus. Geneva, Technical Report Series no. 844.

Wu, A W, Coleson, L C, Holbrook, J and Jabs, D A (1996). Measuring visual function and quality of life in patients with cytomegalovirus retinitis. Arch Ophthalmol **114**: 841-847.

Wu, D, Wu, L, Chang, F, Jin, C and Padula, W (1995). Visual rehabilitation in low vision patients with aging macular degeneration. J Am Optom Assoc **66**: 39-41.

Yamamoto, T, Hitani, K, Tsukahara, I, Yamamoto, S, Kawasaki, R, Yamashita, H and Takeuchi, S (2003). Early postoperative retinal thickness changes and complications after vitrectomy for diabetic macular edema. Am J Ophthalmol **135**(1): 14-19.

Yan, D B, Coloma, F M, Metheetraiurut, A, Trope, G E, Heathcote, J G and Ethier, C R (1994). Deformation of the lamina cribrosa by elevated intraocular pressure. Br J Ophthalmol **78**: 643-648.

Yan, D B, Flanagan, J G, Farra, T, Trope, G E and Ethier, C R (1998). Study of regional deformation of the optic nerve head using scanning laser tomography. Curr Eye Res **17**: 903-16.

Yang, C S, Cheng, C Y, Lee, F L, Hsu, W M and Liu, J H (2001). Quantitative assessment of retinal thickness in diabetic patients with and without clinically significant macular oedema using optical coherence tomography. Acta Ophthalmol Scand **79**: 266-270.

Yanoff, M and Fine, B S (1989). Ocular pathology: A text and atlas. Hagerstown, MD:Harper & Row.

Yarmish, G and Lipton, M L (2003). Functional magnetic resonance imaging:from acquisition to application. Einstein J Biol Med **20**: 2-9.

Yoshida, A (2001). New Examination Methods for Macular Disorders: Application of Diagnosis and Treatment. Jpn J Ophthalmol **45**(3): 323-324.

Yucel, I, Akar, Y, Yucel, G, Ciftcioglu, M A, Keles, N, Aslan, M (2005). Effect of hypercholesterolemia on inducible nitric oxide synthase expression in a rat model of elevated intraocular pressure. Vis Res **45**(9): 1107-1114.

Yucel, Y H, Gupta, N, Kalichman, M W, Mizisin, A P, Hare, W, de Souza Lima, M, Zangwill, L and Weinreb, R N (1998). Relationship of optic disc topography to optic nerve fibre number in glaucoma. Arch Ophthalmol **116**: 493-497.

Yucel, Y H, Zhang, Q, Gupta, M S, Kaufman, P L, and Weinreb, R N. (2000). Loss of neurons in magnocellular and parvocellular layers of the lateral geniculate nucleus. Arch Ophthalmol **118**: 378-384.

Yucel, Y H, Zhang, Q, Weinreb, R N, Kaufman, P L, and Gupta, M S, (2001). Atrophy of relay neurons in magno- and parvocellular layers in the lateral geniculate nucleus in experimental glaucoma. Invest Ophthalmol Vis Sci **42**: 3216-3222.

Yucel, Y H, Zhang, Q, Weinreb, R N, Kaufman, P L and Gupta, N (2003). Effects of retinal ganglion cell loss on magno-, parvo-, koniocellular pathways in the lateral geniculate nucleus and visual cortex in glaucoma. Prog Ret Eye Res **22**(4): 465-481.

Zafar, S, Gurses-Ozden, R, Vessani, R, Makornwattana, M, Liebmann, J M, Tello, C and Ritch, R (2004). Effect of pupillary dilation on retinal nerve fibre layer thickness measurements using optical coherence tomography. J Glaucoma **13**: 34-37.

Zambarakji, H J, Amoaku, W M and Vernon, S A (1998). Volumetric analysis of early macular oedema with the Heidelberg retina tomograph in diabetic retinopathy. Ophthalmology **105**: 1051-1059.

Zambarakji, H J, Butler, T K H and Vernon, S A (1999). Assessment of the Heidelberg retinal tomograph in the detection of sight threatening diabetic maculopathy. Eye **13**: 136-144.

Zambarakji, H J, Evans, J E, Amoaku, W M K and Vernon, S A (1998). Reproducibility of volumetric measurements of normal maculae with the Heidelberg Retinal Tomograph. Br J Ophthalmol **82**: 884-891.

Zangwill, L, Bowd, C, Berry, C C, et al., (2001). Discriminating between normal and glaucomatous eyes using the Heidelberg Retina Tomograph, GDx Nerve Fibre Analyser, and Optical Coherence Tomograph. Arch Ophthalmol **119**: 985-993.

Zangwill, L, Shakiba, S, Caproili, J and Weiner, R N (1994). Agreement between clinicians and a confocal scanning laser ophthalmoscope in estimating cup/disc ratios. Am J Ophthalmol **119**: 415-421.

Zangwill, L, Van Horn, S, de Souza Lima, M, Sample, P A, and Weinreb, R N. (1996). Optic nerve head topography in ocular hypertensive eyes using confocal scanning laser ophthalmoscopy. Am J Ophthalmol **122**: 520-525.

Zangwill, L M, Abunto, T, Bowd, C, Angeles, R, Schanzlin, D J and Weinreb, R N (2005). Scanning laser polarimetry retinal nerve fiber layer thickness measurements after LASIK. Ophthalmology **112**(2): 200-207.

Zangwill, L M, Williams, J, Berry, C C, Knauer, S and Weinreb, R N (2000). A comparison of optical coherence tomography and retinal nerve fiber layer photography for detection of nerve fiber layer damage in glaucoma. Ophthalmology **107**(7): 1309-1315.

Zeimer, R, Asrani, S, Zou, S et al., (1998). Quantitative detection of glaucomatous damage at the posterior pole by retinal thickness mapping. A pilot study. Ophthalmology **105**: 224-231.

Zeimer, R, Blair, N and Cunha-Vaz, J (1983). Pharmokinetic interpretation of vitreous fluorophotometry. Invest Ophthalmol Vis Sci **24**: 1374-1381.

Zeimer, R, Shahidi, M, Mori, M, Zou, S and Asrani, S (1996). A new method for rapid mapping of the retinal thickness at the posterior pole. Invest Ophthalmol Vis Sci **37**: 1994-2001.

Zeimer, R C, Mori, M T and Khoobehi, B (1989). Feasibility test of a new method to measure retinal thickness non-invasively. Invest Ophthalmol Vis Sci **30**(10): 2099-2105.

Zhang, L, Inoue, M, Dong, J and Yamamoto, M (2000). Retrograde axonal transport impairment of large and medium-sized retinal ganglion cells in diabetic rat. Curr Eye Res **20**: 131-136.

Zhang, L, Inoue, M, Dong, K and Yamamoto, M (1998). Alterations in retrograde axonal transport in optic nerve of type 1 and type 2 diabetic rats. Kobe J Med Sco **44**: 205-215.

Zhao, D Y and Cioffi, G A (2000). Anterior optic nerve microvascular changes in human glaucomatous optic neuropathy. Eye **14**: 445-449.

Zhu, S Q, Kum, W, Ho, S K, Young, J D and Cockram, C S (1990). Structure-function relationships of insulin receptor interactions in cultured mouse astrocytes. Brain Research **529**: 329-332.

Zimmet, P Z, McCarty, D J and De Courten, M P (1997). The Global Epidemiology of non-insulin dependent diabetes mellitus and the metabolic syndrome. Journal of Diabetes and Its complications **11**(2): 60-68.

APPENDICES

Appendix 1

ANCOVA summary tables for retinal thickness in all retinal locations 1-9 and mean retinal thickness

Appendix 2

2.1 ANCOVA summary tables for retinal nerve fibre layer thickness in all quadrants (SNIT) and mean retinal nerve fibre layer thickness for the disc margin scan
2.2 ANCOVA summary tables for retinal nerve fibre layer thickness in all quadrants (SNIT) and mean retinal nerve fibre layer thickness for the 2nd radius scan
2.3 ANCOVA summary tables for retinal nerve fibre layer thickness in all quadrants (SNIT) and mean retinal nerve fibre layer thickness for the 3rd radius scan

Appendix 3

3.1 ANCOVA summary tables for retinal nerve fibre layer thickness in all quadrants (SNIT) and overall retinal nerve fibre layer thickness for the disc margin scan
3.2 ANCOVA summary tables for retinal nerve fibre layer thickness in all quadrants (SNIT) and overall retinal nerve fibre layer thickness for the 2nd radius scan
3.3 ANCOVA summary tables for retinal nerve fibre layer thickness in all quadrants (SNIT) and overall retinal nerve fibre layer thickness for the 3rd radius scan

Appendix 4

Mixed between-within subject ANOVA summary tables for each test parameter across test-runs

Appendix 5

Post-hoc analysis on repeated measures ANOVA

Appendix 1

ANCOVA summary tables for retinal thickness in all retinal locations 1-9 and mean retinal thickness

Tests of Between-Subjects Effects

Dependent Variable: Pos1

Source	Type III Sum of Squares	df	Mean Square	F	Sig.	Partial Eta Squared	Noncent. Parameter	Observed Power(a)
Corrected Model	17045.400(b)	2	8522.700	21.113	.000	.265	42.227	1.000
Intercept	3803.376	1	3803.376	9.422	.003	.075	9.422	.861
axlen	2406.276	1	2406.276	5.961	.016	.048	5.961	.678
group	17043.936	1	17043.936	42.223	.000	.265	42.223	1.000
Error	47228.632	117	403.664					
Total	5148192.700	120						
Corrected Total	64274.032	119						

a Computed using alpha = .05
b R Squared = .265 (Adjusted R Squared = .253)

Tests of Between-Subjects Effects

Dependent Variable: Pos2

Source	Type III Sum of Squares	df	Mean Square	F	Sig.	Partial Eta Squared	Noncent. Parameter	Observed Power(a)
Corrected Model	510.552(b)	2	255.276	.936	.395	.016	1.871	.209
Intercept	21890.819	1	21890.819	80.234	.000	.407	80.234	1.000
axlen	1.241	1	1.241	.005	.946	.000	.005	.051
group	416.441	1	416.441	1.526	.219	.013	1.526	.232
Error	31922.028	117	272.838					
Total	9066668.460	120						
Corrected Total	32432.580	119						

a Computed using alpha = .05
b R Squared = .016 (Adjusted R Squared = -.001)

Tests of Between-Subjects Effects

Dependent Variable: Pos3

Source	Type III Sum of Squares	Df	Mean Square	F	Sig.	Partial Eta Squared	Noncent. Parameter	Observed Power(a)
Corrected Model	1070.188(b)	2	535.094	2.805	.065	.046	5.609	.542
Intercept	25790.880	1	25790.880	135.180	.000	.536	135.180	1.000
axlen	223.080	1	223.080	1.169	.282	.010	1.169	.189
group	446.491	1	446.491	2.340	.129	.020	2.340	.329
Error	22322.273	117	190.789					
Total	8910763.691	120						
Corrected Total	23392.461	119						

a Computed using alpha = .05
b R Squared = .046 (Adjusted R Squared = .029)

Tests of Between-Subjects Effects

Dependent Variable: Pos4

Source	Type III Sum of Squares	Df	Mean Square	F	Sig.	Partial Eta Squared	Noncent. Parameter	Observed Power(a)
Corrected Model	1068.581(b)	2	534.291	2.878	.060	.047	5.756	.554
Intercept	21412.876	1	21412.876	115.351	.000	.496	115.351	1.000
axlen	38.909	1	38.909	.210	.648	.002	.210	.074
group	741.325	1	741.325	3.994	.048	.033	3.994	.509
Error	21718.930	117	185.632					
Total	8240429.230	120						
Corrected Total	22787.511	119						

a Computed using alpha = .05
b R Squared = .047 (Adjusted R Squared = .031)

Tests of Between-Subjects Effects

Dependent Variable: Pos5

Source	Type III Sum of Squares	Df	Mean Square	F	Sig.	Partial Eta Squared	Noncent. Parameter	Observed Power(a)
Corrected Model	335.960(b)	2	167.980	.699	.499	.012	1.398	.166
Intercept	25457.246	1	25457.246	105.971	.000	.475	105.971	1.000
axlen	159.335	1	159.335	.663	.417	.006	.663	.127
group	55.035	1	55.035	.229	.633	.002	.229	.076
Error	28106.819	117	240.229					
Total	9080934.253	120						
Corrected Total	28442.778	119						

a Computed using alpha = .05
b R Squared = .012 (Adjusted R Squared = -.005)

Tests of Between-Subjects Effects

Dependent Variable: Pos6

Source	Type III Sum of Squares	Df	Mean Square	F	Sig.	Partial Eta Squared	Noncent. Parameter	Observed Power(a)
Corrected Model	1557.496(b)	2	778.748	2.845	.062	.046	5.690	.549
Intercept	30157.062	1	30157.062	110.174	.000	.485	110.174	1.000
axlen	1375.509	1	1375.509	5.025	.027	.041	5.025	.604
group	3.234	1	3.234	.012	.914	.000	.012	.051
Error	32025.386	117	273.721					
Total	7857315.386	120						
Corrected Total	33582.882	119						

a Computed using alpha = .05
b R Squared = .046 (Adjusted R Squared = .030)

Appendix 1

Tests of Between-Subjects Effects

Dependent Variable: Pos7

Source	Type III Sum of Squares	Df	Mean Square	F	Sig.	Partial Eta Squared	Noncent. Parameter	Observed Power(a)
Corrected Model	4032.317(b)	2	2016.158	10.089	.000	.147	20.177	.984
Intercept	30865.052	1	30865.052	154.445	.000	.569	154.445	1.000
axlen	2797.529	1	2797.529	13.998	.000	.107	13.998	.960
group	146.775	1	146.775	.734	.393	.006	.734	.136
Error	23381.876	117	199.845					
Total	6343048.552	120						
Corrected Total	27414.192	119						

a Computed using alpha = .05
b R Squared = .147 (Adjusted R Squared = .133)

Tests of Between-Subjects Effects

Dependent Variable: Pos8

Source	Type III Sum of Squares	Df	Mean Square	F	Sig.	Partial Eta Squared	Noncent. Parameter	Observed Power(a)
Corrected Model	4263.898(b)	2	2131.949	11.994	.000	.170	23.989	.994
Intercept	28463.559	1	28463.559	160.135	.000	.578	160.135	1.000
axlen	2586.253	1	2586.253	14.550	.000	.111	14.550	.966
group	333.805	1	333.805	1.878	.173	.016	1.878	.274
Error	20796.447	117	177.747					
Total	5839596.182	120						
Corrected Total	25060.345	119						

a Computed using alpha = .05
b R Squared = .170 (Adjusted R Squared = .156)

Tests of Between-Subjects Effects

Dependent Variable: Pos9

Source	Type III Sum of Squares	Df	Mean Square	F	Sig.	Partial Eta Squared	Noncent. Parameter	Observed Power(a)
Corrected Model	2624.372(b)	2	1312.186	6.056	.003	.094	12.111	.878
Intercept	30630.984	1	30630.984	141.361	.000	.547	141.361	1.000
axlen	2298.017	1	2298.017	10.605	.001	.083	10.605	.898
group	3.042	1	3.042	.014	.906	.000	.014	.052
Error	25352.346	117	216.687					
Total	6800953.559	120						
Corrected Total	27976.718	119						

a Computed using alpha = .05
b R Squared = .094 (Adjusted R Squared = .078)

Tests of Between-Subjects Effects

Dependent Variable: Mean RT

Source	Type III Sum of Squares	Df	Mean Square	F	Sig.	Partial Eta Squared	Noncent. Parameter	Observed Power(a)
Corrected Model	1686.194(b)	2	843.097	4.805	.010	.076	9.610	.788
Intercept	23144.365	1	23144.365	131.900	.000	.530	131.900	1.000
axlen	376.555	1	376.555	2.146	.146	.018	2.146	.306
group	673.543	1	673.543	3.839	.052	.032	3.839	.493
Error	20529.917	117	175.469					
Total	7397074.270	120						
Corrected Total	22216.111	119						

a Computed using alpha = .05
b R Squared = .076 (Adjusted R Squared = .060)

Appendix 2

2.1 ANCOVA summary tables for retinal nerve fibre layer thickness in all quadrants (SNIT) and mean retinal nerve fibre layer thickness for the disc margin scan

Tests of Between-Subjects Effects

Dependent Variable: Superior quadrant disc

Source	Type III Sum of Squares	df	Mean Square	F	Sig.	Partial Eta Squared	Noncent. Parameter	Observed Power(a)
Corrected Model	4121.190(b)	2	2060.595	3.987	.021	.066	7.975	.704
Intercept	10513.486	1	10513.486	20.344	.000	.154	20.344	.994
AXLEN	348.806	1	348.806	.675	.413	.006	.675	.129
GROUP	4099.476	1	4099.476	7.933	.006	.066	7.933	.797
Error	57879.448	112	516.781					
Total	3030306.600	115						
Corrected Total	62000.638	114						

a Computed using alpha = .05
b R Squared = .066 (Adjusted R Squared = .050)

Tests of Between-Subjects Effects

Dependent Variable: Nasal quadrant disc

Source	Type III Sum of Squares	Df	Mean Square	F	Sig.	Partial Eta Squared	Noncent. Parameter	Observed Power(a)
Corrected Model	9024.330(b)	2	4512.165	5.602	.005	.091	11.205	.849
Intercept	25934.957	1	25934.957	32.202	.000	.223	32.202	1.000
AXLEN	8913.504	1	8913.504	11.067	.001	.090	11.067	.910
GROUP	1916.158	1	1916.158	2.379	.126	.021	2.379	.334
Error	90204.304	112	805.396					
Total	1966734.400	115						
Corrected Total	99228.634	114						

a Computed using alpha = .05
b R Squared = .091 (Adjusted R Squared = .075)

Tests of Between-Subjects Effects

Dependent Variable: Inferior quadrant disc

Source	Type III Sum of Squares	Df	Mean Square	F	Sig.	Partial Eta Squared	Noncent. Parameter	Observed Power(a)
Corrected Model	3614.840(b)	2	1807.420	2.211	.114	.038	4.422	.443
Intercept	22084.470	1	22084.470	27.014	.000	.194	27.014	.999
AXLEN	3173.208	1	3173.208	3.881	.051	.033	3.881	.497
GROUP	1589.313	1	1589.313	1.944	.166	.017	1.944	.282
Error	91562.452	112	817.522					
Total	3672639.920	115						
Corrected Total	95177.292	114						

a Computed using alpha = .05
b R Squared = .038 (Adjusted R Squared = .021)

Tests of Between-Subjects Effects

Dependent Variable: Temporal quadrant disc

Source	Type III Sum of Squares	Df	Mean Square	F	Sig.	Partial Eta Squared	Noncent. Parameter	Observed Power(a)
Corrected Model	1620.841(b)	2	810.420	1.636	.199	.028	3.272	.339
Intercept	3136.737	1	3136.737	6.332	.013	.054	6.332	.704
AXLEN	75.451	1	75.451	.152	.697	.001	.152	.067
GROUP	1584.463	1	1584.463	3.198	.076	.028	3.198	.426
Error	55486.468	112	495.415					
Total	1003208.080	115						
Corrected Total	57107.309	114						

a Computed using alpha = .05
b R Squared = .028 (Adjusted R Squared = .011)

Tests of Between-Subjects Effects

Dependent Variable: MEAN RNFLt disc

Source	Type III Sum of Squares	Df	Mean Square	F	Sig.	Partial Eta Squared	Noncent. Parameter	Observed Power(a)
Corrected Model	2887.885(b)	2	1443.943	4.422	.014	.073	8.844	.751
Intercept	13539.306	1	13539.306	41.465	.000	.270	41.465	1.000
AXLEN	1913.558	1	1913.558	5.860	.017	.050	5.860	.670
GROUP	2012.129	1	2012.129	6.162	.015	.052	6.162	.692
Error	36570.661	112	326.524					
Total	2259678.070	115						
Corrected Total	39458.546	114						

a Computed using alpha = .05
b R Squared = .073 (Adjusted R Squared = .057)

2.2 ANCOVA summary tables for retinal nerve fibre layer thickness in all quadrants (SNIT) and mean retinal nerve fibre layer thicknessfor the 2nd radius scan

Tests of Between-Subjects Effects

Dependent Variable: Superior quadrant 2nd radius

Source	Type III Sum of Squares	Df	Mean Square	F	Sig.	Partial Eta Squared	Noncent. Parameter	Observed Power(a)
Corrected Model	6135.837(b)	2	3067.918	14.632	.000	.207	29.264	.999
Intercept	9496.175	1	9496.175	45.290	.000	.288	45.290	1.000
AXIALLE	2224.943	1	2224.943	10.611	.001	.087	10.611	.898
GROUP	5672.500	1	5672.500	27.054	.000	.195	27.054	.999
Error	23483.435	112	209.674					
Total	1104565.520	115						
Corrected Total	29619.272	114						

a Computed using alpha = .05
b R Squared = .207 (Adjusted R Squared = .193)

Tests of Between-Subjects Effects

Dependent Variable: Nasal quadrant 2nd radius

Source	Type III Sum of Squares	Df	Mean Square	F	Sig.	Partial Eta Squared	Noncent. Parameter	Observed Power(a)
Corrected Model	5456.172(b)	2	2728.086	12.809	.000	.186	25.619	.996
Intercept	10551.397	1	10551.397	49.542	.000	.307	49.542	1.000
AXIALLE	5153.878	1	5153.878	24.199	.000	.178	24.199	.998
GROUP	1767.340	1	1767.340	8.298	.005	.069	8.298	.815
Error	23853.495	112	212.978					
Total	434382.320	115						
Corrected Total	29309.667	114						

a Computed using alpha = .05
b R Squared = .186 (Adjusted R Squared = .172)

Tests of Between-Subjects Effects

Dependent Variable: Inferior quadrant 2nd radius

Source	Type III Sum of Squares	Df	Mean Square	F	Sig.	Partial Eta Squared	Noncent. Parameter	Observed Power(a)
Corrected Model	5881.800(b)	2	2940.900	16.850	.000	.231	33.701	1.000
Intercept	14421.492	1	14421.492	82.630	.000	.425	82.630	1.000
AXIALLE	4742.549	1	4742.549	27.173	.000	.195	27.173	.999
GROUP	3165.129	1	3165.129	18.135	.000	.139	18.135	.988
Error	19547.470	112	174.531					
Total	1135030.440	115						
Corrected Total	25429.271	114						

a Computed using alpha = .05
b R Squared = .231 (Adjusted R Squared = .218)

Tests of Between-Subjects Effects

Dependent Variable: Temporal quadrant 3rd radius

Source	Type III Sum of Squares	df	Mean Square	F	Sig.	Partial Eta Squared	Noncent. Parameter	Observed Power(a)
Corrected Model	1525.078(b)	2	762.539	7.535	.001	.119	15.070	.939
Intercept	266.963	1	266.963	2.638	.107	.023	2.638	.363
AXIALLE	179.345	1	179.345	1.772	.186	.016	1.772	.262
GROUP	865.209	1	865.209	8.549	.004	.071	8.549	.826
Error	11334.457	112	101.201					
Total	387429.920	115						
Corrected Total	12859.535	114						

a Computed using alpha = .05
b R Squared = .119 (Adjusted R Squared = .103)

Tests of Between-Subjects Effects

Dependent Variable: MEAN RNFLt 2nd radius

Source	Type III Sum of Squares	Df	Mean Square	F	Sig.	Partial Eta Squared	Noncent. Parameter	Observed Power(a)
Corrected Model	3314.725(b)	2	1657.362	19.107	.000	.254	38.213	1.000
Intercept	7081.089	1	7081.089	81.633	.000	.422	81.633	1.000
AXIALLE	1901.702	1	1901.702	21.923	.000	.164	21.923	.996
GROUP	2576.315	1	2576.315	29.701	.000	.210	29.701	1.000
Error	9715.225	112	86.743					
Total	709690.173	115						
Corrected Total	13029.950	114						

a Computed using alpha = .05
b R Squared = .254 (Adjusted R Squared = .241)

2.3 ANCOVA summary tables for retinal nerve fibre layer thickness in all quadrants (SNIT) and mean retinal nerve fibre layer thickness for the 3rd radius scan

Tests of Between-Subjects Effects

Dependent Variable: Superior quadrant 3rd radius

Source	Type III Sum of Squares	Df	Mean Square	F	Sig.	Partial Eta Squared	Noncent. Parameter	Observed Power(a)
Corrected Model	3223.648(b)	2	1611.824	15.142	.000	.213	30.284	.999
Intercept	3679.614	1	3679.614	34.568	.000	.236	34.568	1.000
AXLEN	800.081	1	800.081	7.516	.007	.063	7.516	.776
GROUP	3148.127	1	3148.127	29.575	.000	.209	29.575	1.000
Error	11922.013	112	106.447					
Total	462104.760	115						
Corrected Total	15145.661	114						

a Computed using alpha = .05
b R Squared = .213 (Adjusted R Squared = .199)

Tests of Between-Subjects Effects

Dependent Variable: Nasal quadrant 3rd radius

Source	Type III Sum of Squares	Df	Mean Square	F	Sig.	Partial Eta Squared	Noncent. Parameter	Observed Power(a)
Corrected Model	589.593(b)	2	294.797	6.743	.002	.107	13.486	.911
Intercept	2064.142	1	2064.142	47.213	.000	.297	47.213	1.000
AXLEN	583.275	1	583.275	13.341	.000	.106	13.341	.952
GROUP	121.667	1	121.667	2.783	.098	.024	2.783	.380
Error	4896.623	112	43.720					
Total	195779.120	115						
Corrected Total	5486.216	114						

a Computed using alpha = .05
b R Squared = .107 (Adjusted R Squared = .092)

Tests of Between-Subjects Effects

Dependent Variable: Inferior quadrant 3rd radius

Source	Type III Sum of Squares	Df	Mean Square	F	Sig.	Partial Eta Squared	Noncent. Parameter	Observed Power(a)
Corrected Model	2969.941(b)	2	1484.970	12.271	.000	.180	24.541	.995
Intercept	7420.192	1	7420.192	61.314	.000	.354	61.314	1.000
AXLEN	2825.611	1	2825.611	23.349	.000	.173	23.349	.998
GROUP	919.628	1	919.628	7.599	.007	.064	7.599	.780
Error	13554.106	112	121.019					
Total	475406.720	115						
Corrected Total	16524.047	114						

a Computed using alpha = .05
b R Squared = .180 (Adjusted R Squared = .165)

Tests of Between-Subjects Effects

Dependent Variable: Temporal quadrant 3rd radius

Source	Type III Sum of Squares	Df	Mean Square	F	Sig.	Partial Eta Squared	Noncent. Parameter	Observed Power(a)
Corrected Model	350.786(b)	2	175.393	2.917	.058	.050	5.833	.559
Intercept	531.640	1	531.640	8.841	.004	.073	8.841	.838
AXLEN	.073	1	.073	.001	.972	.000	.001	.050
GROUP	308.769	1	308.769	5.135	.025	.044	5.135	.613
Error	6735.032	112	60.134					
Total	226359.440	115						
Corrected Total	7085.818	114						

a Computed using alpha = .05
b R Squared = .050 (Adjusted R Squared = .033)

Tests of Between-Subjects Effects

Dependent Variable: MEAN RNFLt 3rd radius

Source	Type III Sum of Squares	Df	Mean Square	F	Sig.	Partial Eta Squared	Noncent. Parameter	Observed Power(a)
Corrected Model	1125.676(b)	2	562.838	13.898	.000	.199	27.797	.998
Intercept	2896.875	1	2896.875	71.534	.000	.390	71.534	1.000
AXLEN	700.446	1	700.446	17.296	.000	.134	17.296	.985
GROUP	827.075	1	827.075	20.423	.000	.154	20.423	.994
Error	4535.607	112	40.496					
Total	322194.433	115						
Corrected Total	5661.283	114						

a Computed using alpha = .05
b R Squared = .199 (Adjusted R Squared = .185)

Appendix 3

3.1 ANCOVA summary tables for retinal nerve fibre layer thickness in all quadrants (SNIT) and overall retinal nerve fibre layer thickness for the disc margin scan

Tests of Between-Subjects Effects

Dependent Variable: Superior quadrant disc

Source	Type III Sum of Squares	df	Mean Square	F	Sig.	Partial Eta Squared	Noncent. Parameter	Observed Power(a)
Corrected Model	55166.668(b)	2	27583.334	35.776	.000	.482	71.552	1.000
Intercept	52911.821	1	52911.821	68.628	.000	.471	68.628	1.000
discarea	2573.900	1	2573.900	3.338	.072	.042	3.338	.438
group	41246.066	1	41246.066	53.497	.000	.410	53.497	1.000
Error	59366.772	77	770.997					
Total	1474866.240	80						
Corrected Total	114533.440	79						

a Computed using alpha = .05
b R Squared = .482 (Adjusted R Squared = .468)

Tests of Between-Subjects Effects

Dependent Variable: Nasal quadrant disc

Source	Type III Sum of Squares	df	Mean Square	F	Sig.	Partial Eta Squared	Noncent. Parameter	Observed Power(a)
Corrected Model	30588.138(b)	2	15294.069	19.127	.000	.332	38.253	1.000
Intercept	23513.539	1	23513.539	29.406	.000	.276	29.406	1.000
discarea	11.938	1	11.938	.015	.903	.000	.015	.052
group	27407.477	1	27407.477	34.275	.000	.308	34.275	1.000
Error	61571.252	77	799.627					
Total	1036979.840	80						
Corrected Total	92159.390	79						

a Computed using alpha = .05
b R Squared = .332 (Adjusted R Squared = .315)

Appendix 3.1

Tests of Between-Subjects Effects

Dependent Variable: Inferior quadrant disc

Source	Type III Sum of Squares	df	Mean Square	F	Sig.	Partial Eta Squared	Noncent. Parameter	Observed Power(a)
Corrected Model	66818.199(b)	2	33409.099	28.976	.000	.429	57.953	1.000
Intercept	38515.164	1	38515.164	33.405	.000	.303	33.405	1.000
discarea	24.517	1	24.517	.021	.884	.000	.021	.052
group	61375.807	1	61375.807	53.232	.000	.409	53.232	1.000
Error	88779.401	77	1152.979					
Total	1856208.800	80						
Corrected Total	155597.600	79						

a Computed using alpha = .05
b R Squared = .429 (Adjusted R Squared = .415)

Tests of Between-Subjects Effects

Dependent Variable: Temporal quadrant disc

Source	Type III Sum of Squares	Df	Mean Square	F	Sig.	Partial Eta Squared	Noncent. Parameter	Observed Power(a)
Corrected Model	9450.545(b)	2	4725.273	13.551	.000	.260	27.101	.997
Intercept	15444.622	1	15444.622	44.291	.000	.365	44.291	1.000
discarea	381.005	1	381.005	1.093	.299	.014	1.093	.178
group	7192.379	1	7192.379	20.626	.000	.211	20.626	.994
Error	26850.734	77	348.711					
Total	499628.520	80						
Corrected Total	36301.279	79						

a Computed using alpha = .05
b R Squared = .260 (Adjusted R Squared = .241)

Appendix 3.1

Tests of Between-Subjects Effects

Dependent Variable: Overall RNFLt disc

Source	Type III Sum of Squares	Df	Mean Square	F	Sig.	Partial Eta Squared	Noncent. Parameter	Observed Power(a)
Corrected Model	33365.806(b)	2	16682.903	28.330	.000	.424	56.660	1.000
Intercept	31745.250	1	31745.250	53.908	.000	.412	53.908	1.000
discarea	331.582	1	331.582	.563	.455	.007	.563	.115
group	28102.582	1	28102.582	47.722	.000	.383	47.722	1.000
Error	45343.873	77	588.881					
Total	1157174.193	80						
Corrected Total	78709.679	79						

a Computed using alpha = .05
b R Squared = .424 (Adjusted R Squared = .409)

3.2 ANCOVA summary tables for retinal nerve fibre layer thickness in all quadrants (SNIT) and overall retinal nerve fibre layer thickness for the 2nd radius scan

Tests of Between-Subjects Effects

Dependent Variable: Superior quadrant 2nd radius

Source	Type III Sum of Squares	Df	Mean Square	F	Sig.	Partial Eta Squared	Noncent. Parameter	Observed Power(a)
Corrected Model	18864.106(b)	2	9432.053	32.601	.000	.459	65.202	1.000
Intercept	17269.015	1	17269.015	59.689	.000	.437	59.689	1.000
disc	665.562	1	665.562	2.300	.133	.029	2.300	.322
group	14567.314	1	14567.314	50.351	.000	.395	50.351	1.000
Error	22277.413	77	289.317					
Total	512724.280	80						
Corrected Total	41141.520	79						

a Computed using alpha = .05
b R Squared = .459 (Adjusted R Squared = .444)

Tests of Between-Subjects Effects

Dependent Variable: Nasal quadrant 2nd radius

Source	Type III Sum of Squares	Df	Mean Square	F	Sig.	Partial Eta Squared	Noncent. Parameter	Observed Power(a)
Corrected Model	2822.960(b)	2	1411.480	8.425	.000	.180	16.851	.959
Intercept	8110.911	1	8110.911	48.416	.000	.386	48.416	1.000
disc	325.348	1	325.348	1.942	.167	.025	1.942	.280
group	1775.579	1	1775.579	10.599	.002	.121	10.599	.895
Error	12899.447	77	167.525					
Total	235068.920	80						
Corrected Total	15722.407	79						

a Computed using alpha = .05
b R Squared = .180 (Adjusted R Squared = .158)

Tests of Between-Subjects Effects

Dependent Variable: Inferior quadrant 2nd radius

Source	Type III Sum of Squares	Df	Mean Square	F	Sig.	Partial Eta Squared	Noncent. Parameter	Observed Power(a)
Corrected Model	13088.148(b)	2	6544.074	17.073	.000	.307	34.145	1.000
Intercept	13406.732	1	13406.732	34.977	.000	.312	34.977	1.000
disc	1.420	1	1.420	.004	.952	.000	.004	.050
group	11800.904	1	11800.904	30.787	.000	.286	30.787	1.000
Error	29514.602	77	383.307					
Total	594719.200	80						
Corrected Total	42602.750	79						

a Computed using alpha = .05
b R Squared = .307 (Adjusted R Squared = .289)

Tests of Between-Subjects Effects

Dependent Variable: Temporal quadrant 2nd radius

Source	Type III Sum of Squares	Df	Mean Square	F	Sig.	Partial Eta Squared	Noncent. Parameter	Observed Power(a)
Corrected Model	3505.720(b)	2	1752.860	16.327	.000	.298	32.654	.999
Intercept	5319.324	1	5319.324	49.546	.000	.392	49.546	1.000
disc	64.343	1	64.343	.599	.441	.008	.599	.119
group	2857.575	1	2857.575	26.617	.000	.257	26.617	.999
Error	8266.794	77	107.361					
Total	189405.490	80						
Corrected Total	11772.514	79						

a Computed using alpha = .05
b R Squared = .298 (Adjusted R Squared = .280)

Tests of Between-Subjects Effects

Dependent Variable: Overall RNFLt 2nd radius

Source	Type III Sum of Squares	Df	Mean Square	F	Sig.	Partial Eta Squared	Noncent. Parameter	Observed Power(a)
Corrected Model	8183.390(b)	2	4091.695	33.108	.000	.462	66.217	1.000
Intercept	10516.162	1	10516.162	85.092	.000	.525	85.092	1.000
disc	175.888	1	175.888	1.423	.237	.018	1.423	.218
group	6598.353	1	6598.353	53.391	.000	.409	53.391	1.000
Error	9516.070	77	123.585					
Total	353975.913	80						
Corrected Total	17699.460	79						

a Computed using alpha = .05
b R Squared = .462 (Adjusted R Squared = .448)

3.3 ANCOVA summary tables for retinal nerve fibre layer thickness in all quadrants (SNIT) and overall retinal nerve fibre layer thickness for the 3rd radius scan

Tests of Between-Subjects Effects

Dependent Variable: Superior quadrant 3rd radius

Source	Type III Sum of Squares	Df	Mean Square	F	Sig.	Partial Eta Squared	Noncent. Parameter	Observed Power(a)
Corrected Model	4797.971(b)	2	2398.986	14.845	.000	.278	29.690	.999
Intercept	4277.430	1	4277.430	26.469	.000	.256	26.469	.999
disc	28.555	1	28.555	.177	.675	.002	.177	.070
group	4545.714	1	4545.714	28.129	.000	.268	28.129	.999
Error	12443.307	77	161.601					
Total	227233.050	80						
Corrected Total	17241.279	79						

a Computed using alpha = .05
b R Squared = .278 (Adjusted R Squared = .260)

Tests of Between-Subjects Effects

Dependent Variable: Nasal quadrant 3rd radius

Source	Type III Sum of Squares	Df	Mean Square	F	Sig.	Partial Eta Squared	Noncent. Parameter	Observed Power(a)
Corrected Model	97.506(b)	2	48.753	.211	.810	.005	.422	.082
Intercept	3581.624	1	3581.624	15.495	.000	.168	15.495	.973
disc	11.393	1	11.393	.049	.825	.001	.049	.056
group	97.348	1	97.348	.421	.518	.005	.421	.098
Error	17798.102	77	231.144					
Total	152129.720	80						
Corrected Total	17895.608	79						

a Computed using alpha = .05
b R Squared = .005 (Adjusted R Squared = -.020)

Tests of Between-Subjects Effects

Dependent Variable: Inferior quadrant 3rd radius

Source	Type III Sum of Squares	Df	Mean Square	F	Sig.	Partial Eta Squared	Noncent. Parameter	Observed Power(a)
Corrected Model	4566.463(b)	2	2283.232	5.871	.004	.132	11.742	.862
Intercept	8190.884	1	8190.884	21.062	.000	.215	21.062	.995
disc	154.528	1	154.528	.397	.530	.005	.397	.095
group	3541.414	1	3541.414	9.106	.003	.106	9.106	.846
Error	29944.846	77	388.894					
Total	291691.170	80						
Corrected Total	34511.310	79						

a Computed using alpha = .05
b R Squared = .132 (Adjusted R Squared = .110)

Tests of Between-Subjects Effects

Dependent Variable: Temporal quadrant 3rd radius

Source	Type III Sum of Squares	Df	Mean Square	F	Sig.	Partial Eta Squared	Noncent. Parameter	Observed Power(a)
Corrected Model	32.595(b)	2	16.297	.091	.914	.002	.181	.063
Intercept	2859.957	1	2859.957	15.887	.000	.171	15.887	.976
disc	18.734	1	18.734	.104	.748	.001	.104	.062
group	23.636	1	23.636	.131	.718	.002	.131	.065
Error	13861.370	77	180.018					
Total	154099.850	80						
Corrected Total	13893.965	79						

a Computed using alpha = .05
b R Squared = .002 (Adjusted R Squared = -.024)

Tests of Between-Subjects Effects

Dependent Variable: Overall RNFLt 3rd radius

Source	Type III Sum of Squares	Df	Mean Square	F	Sig.	Partial Eta Squared	Noncent. Parameter	Observed Power(a)
Corrected Model	1057.412(b)	2	528.706	4.719	.012	.109	9.438	.774
Intercept	4530.327	1	4530.327	40.437	.000	.344	40.437	1.000
disc	2.352	1	2.352	.021	.885	.000	.021	.052
group	929.136	1	929.136	8.293	.005	.097	8.293	.812
Error	8626.571	77	112.033					
Total	191628.486	80						
Corrected Total	9683.982	79						

a Computed using alpha = .05
b R Squared = .109 (Adjusted R Squared = .086)

Appendix 4

Mixed between-within subject ANOVA summary tables for each test parameter across test-runs

Tests of Within-Subjects Effects

Measure: Blood glucose

Source		Type III Sum of Squares	df	Mean Square	F	Sig.
factor1	Sphericity Assumed	748.872	5	149.774	10.707	.000
	Greenhouse-Geisser	748.872	3.348	223.691	10.707	.000
	Huynh-Feldt	748.872	3.794	197.390	10.707	.000
	Lower-bound	748.872	1.000	748.872	10.707	.002
factor1 * type	Sphericity Assumed	209.432	5	41.886	2.994	.013
	Greenhouse-Geisser	209.432	3.348	62.558	2.994	.028
	Huynh-Feldt	209.432	3.794	55.203	2.994	.023
	Lower-bound	209.432	1.000	209.432	2.994	.091
Error(factor1)	Sphericity Assumed	2727.662	195	13.988		
	Greenhouse-Geisser	2727.662	130.564	20.891		
	Huynh-Feldt	2727.662	147.961	18.435		
	Lower-bound	2727.662	39.000	69.940		

Tests of Between-Subjects Effects

Measure: Blood glucose
Transformed Variable: Average

Source	Type III Sum of Squares	df	Mean Square	F	Sig.
Intercept	26031.491	1	26031.491	532.514	.000
type	6.618	1	6.618	.135	.715
Error	1906.481	39	48.884		

Tests of Within-Subjects Effects

Measure: logMAR 100% contrast

Source		Type III Sum of Squares	Df	Mean Square	F	Sig.
VISIT	Sphericity Assumed	.014	5	.003	1.045	.393
	Greenhouse-Geisser	.014	3.572	.004	1.045	.382
	Huynh-Feldt	.014	4.077	.003	1.045	.387
	Lower-bound	.014	1.000	.014	1.045	.313
VISIT * TYPE	Sphericity Assumed	.022	5	.004	1.635	.153
	Greenhouse-Geisser	.022	3.572	.006	1.635	.175
	Huynh-Feldt	.022	4.077	.005	1.635	.167
	Lower-bound	.022	1.000	.022	1.635	.209
Error(VISIT)	Sphericity Assumed	.525	195	.003		
	Greenhouse-Geisser	.525	139.299	.004		
	Huynh-Feldt	.525	159.004	.003		
	Lower-bound	.525	39.000	.013		

Tests of Between-Subjects Effects

Measure: logMAR 100% contrast
Transformed Variable: Average

Source	Type III Sum of Squares	df	Mean Square	F	Sig.
Intercept	.000	1	.000	.007	.933
TYPE	.017	1	.017	.489	.489
Error	1.368	39	.035		

Tests of Within-Subjects Effects

Measure: logMAR10% contrast

Source		Type III Sum of Squares	Df	Mean Square	F	Sig.
VISIT	Sphericity Assumed	.097	5	.019	3.010	.012
	Greenhouse-Geisser	.097	3.177	.031	3.010	.030
	Huynh-Feldt	.097	3.581	.027	3.010	.025
	Lower-bound	.097	1.000	.097	3.010	.091
VISIT * TYPE	Sphericity Assumed	.022	5	.004	.674	.643
	Greenhouse-Geisser	.022	3.177	.007	.674	.578
	Huynh-Feldt	.022	3.581	.006	.674	.595
	Lower-bound	.022	1.000	.022	.674	.417
Error(VISIT)	Sphericity Assumed	1.260	195	.006		
	Greenhouse-Geisser	1.260	123.919	.010		
	Huynh-Feldt	1.260	139.652	.009		
	Lower-bound	1.260	39.000	.032		

Tests of Between-Subjects Effects

Measure: logMAR 10% contrast
Transformed Variable: Average

Source	Type III Sum of Squares	df	Mean Square	F	Sig.
Intercept	20.442	1	20.442	277.981	.000
TYPE	.015	1	.015	.197	.659
Error	2.868	39	.074		

Appendix 4

Tests of Within-Subjects Effects

Measure: Contrast sensitivity (Pelli Robson)

Source		Type III Sum of Squares	df	Mean Square	F	Sig.
VISIT	Sphericity Assumed	.291	5	.058	8.999	.000
	Greenhouse-Geisser	.291	4.350	.067	8.999	.000
	Huynh-Feldt	.291	5.000	.058	8.999	.000
	Lower-bound	.291	1.000	.291	8.999	.005
VISIT * TYPE	Sphericity Assumed	.024	5	.005	.726	.604
	Greenhouse-Geisser	.024	4.350	.005	.726	.586
	Huynh-Feldt	.024	5.000	.005	.726	.604
	Lower-bound	.024	1.000	.024	.726	.399
Error(VISIT)	Sphericity Assumed	1.262	195	.006		
	Greenhouse-Geisser	1.262	169.663	.007		
	Huynh-Feldt	1.262	195.000	.006		
	Lower-bound	1.262	39.000	.032		

Tests of Between-Subjects Effects

Measure: Contrast sensitivity (Pelli Robson)
Transformed Variable: Average

Source	Type III Sum of Squares	df	Mean Square	F	Sig.
Intercept	731.871	1	731.871	1841.211	.000
TYPE	.053	1	.053	.133	.718
Error	15.502	39	.397		

Tests of Within-Subjects Effects

Measure: MD White on white fields

Source		Type III Sum of Squares	Df	Mean Square	F	Sig.
VISIT	Sphericity Assumed	1.282	5	.256	.818	.538
	Greenhouse-Geisser	1.282	3.589	.357	.818	.505
	Huynh-Feldt	1.282	4.098	.313	.818	.518
	Lower-bound	1.282	1.000	1.282	.818	.371
VISIT * TYPE	Sphericity Assumed	2.771	5	.554	1.769	.121
	Greenhouse-Geisser	2.771	3.589	.772	1.769	.145
	Huynh-Feldt	2.771	4.098	.676	1.769	.136
	Lower-bound	2.771	1.000	2.771	1.769	.191
Error(VISIT)	Sphericity Assumed	61.102	195	.313		
	Greenhouse-Geisser	61.102	139.954	.437		
	Huynh-Feldt	61.102	159.839	.382		
	Lower-bound	61.102	39.000	1.567		

Tests of Between-Subjects Effects

Measure: MD white on white fields
Transformed Variable: Average

Source	Type III Sum of Squares	df	Mean Square	F	Sig.
Intercept	250.103	1	250.103	24.903	.000
TYPE	3.003	1	3.003	.299	.588
Error	391.677	39	10.043		

Tests of Within-Subjects Effects

Measure: PSD white on white fields

Source		Type III Sum of Squares	Df	Mean Square	F	Sig.
VISIT	Sphericity Assumed	.949	5	.190	2.169	.059
	Greenhouse-Geisser	.949	3.522	.269	2.169	.084
	Huynh-Feldt	.949	4.013	.236	2.169	.075
	Lower-bound	.949	1.000	.949	2.169	.149
VISIT * TYPE	Sphericity Assumed	.274	5	.055	.625	.681
	Greenhouse-Geisser	.274	3.522	.078	.625	.625
	Huynh-Feldt	.274	4.013	.068	.625	.646
	Lower-bound	.274	1.000	.274	.625	.434
Error(VISIT)	Sphericity Assumed	17.063	195	.088		
	Greenhouse-Geisser	17.063	137.348	.124		
	Huynh-Feldt	17.063	156.526	.109		
	Lower-bound	17.063	39.000	.438		

Tests of Between-Subjects Effects

Measure: PSD white on white fields
Transformed Variable: Average

Source	Type III Sum of Squares	df	Mean Square	F	Sig.
Intercept	535.679	1	535.679	168.383	.000
TYPE	.057	1	.057	.018	.895
Error	124.071	39	3.181		

Tests of Within-Subjects Effects

Measure: MD SWAP fields

Source		Type III Sum of Squares	df	Mean Square	F	Sig.
VISIT	Sphericity Assumed	22.790	5	4.558	3.081	.011
	Greenhouse-Geisser	22.790	3.539	6.440	3.081	.023
	Huynh-Feldt	22.790	4.035	5.647	3.081	.017
	Lower-bound	22.790	1.000	22.790	3.081	.087
VISIT * TYPE	Sphericity Assumed	.877	5	.175	.119	.988
	Greenhouse-Geisser	.877	3.539	.248	.119	.966
	Huynh-Feldt	.877	4.035	.217	.119	.976
	Lower-bound	.877	1.000	.877	.119	.733
Error(VISIT)	Sphericity Assumed	288.452	195	1.479		
	Greenhouse-Geisser	288.452	138.021	2.090		
	Huynh-Feldt	288.452	157.381	1.833		
	Lower-bound	288.452	39.000	7.396		

Tests of Between-Subjects Effects

Measure: MD SWAP fields
Transformed Variable: Average

Source	Type III Sum of Squares	df	Mean Square	F	Sig.
Intercept	5239.282	1	5239.282	83.083	.000
TYPE	31.893	1	31.893	.506	.481
Error	2459.361	39	63.061		

Tests of Within-Subjects Effects

Measure: PSD SWAP fields

Source		Type III Sum of Squares	df	Mean Square	F	Sig.
VISIT	Sphericity Assumed	.455	5	.091	.445	.817
	Greenhouse-Geisser	.455	3.611	.126	.445	.757
	Huynh-Feldt	.455	4.127	.110	.445	.782
	Lower-bound	.455	1.000	.455	.445	.509
VISIT * TYPE	Sphericity Assumed	.874	5	.175	.855	.513
	Greenhouse-Geisser	.874	3.611	.242	.855	.484
	Huynh-Feldt	.874	4.127	.212	.855	.496
	Lower-bound	.874	1.000	.874	.855	.361
Error(VISIT)	Sphericity Assumed	39.877	195	.204		
	Greenhouse-Geisser	39.877	140.817	.283		
	Huynh-Feldt	39.877	160.939	.248		
	Lower-bound	39.877	39.000	1.022		

Tests of Between-Subjects Effects

Measure: PSD SWAP fields
Transformed Variable: Average

Source	Type III Sum of Squares	df	Mean Square	F	Sig.
Intercept	1561.200	1	1561.200	640.894	.000
TYPE	.073	1	.073	.030	.863
Error	95.003	39	2.436		

Tests of Within-Subjects Effects

Measure: IOP

Source		Type III Sum of Squares	df	Mean Square	F	Sig.
VISIT	Sphericity Assumed	57.165	5	11.433	3.996	.002
	Greenhouse-Geisser	57.165	3.267	17.499	3.996	.008
	Huynh-Feldt	57.165	3.692	15.482	3.996	.005
	Lower-bound	57.165	1.000	57.165	3.996	.053
VISIT * TYPE	Sphericity Assumed	3.214	5	.643	.225	.952
	Greenhouse-Geisser	3.214	3.267	.984	.225	.894
	Huynh-Feldt	3.214	3.692	.870	.225	.913
	Lower-bound	3.214	1.000	3.214	.225	.638
Error(VISIT)	Sphericity Assumed	557.908	195	2.861		
	Greenhouse-Geisser	557.908	127.404	4.379		
	Huynh-Feldt	557.908	144.000	3.874		
	Lower-bound	557.908	39.000	14.305		

Tests of Between-Subjects Effects

Measure: IOP
Transformed Variable: Average

Source	Type III Sum of Squares	df	Mean Square	F	Sig.
Intercept	51781.308	1	51781.308	829.456	.000
TYPE	24.040	1	24.040	.385	.539
Error	2434.692	39	62.428		

Appendix 4

Tests of Within-Subjects Effects

Measure: Superior quadrant RNFLt

Source		Type III Sum of Squares	df	Mean Square	F	Sig.
VISIT	Sphericity Assumed	160.426	5	32.085	1.382	.233
	Greenhouse-Geisser	160.426	4.483	35.785	1.382	.238
	Huynh-Feldt	160.426	5.000	32.085	1.382	.233
	Lower-bound	160.426	1.000	160.426	1.382	.247
VISIT * TYPE	Sphericity Assumed	399.597	5	79.919	3.443	.005
	Greenhouse-Geisser	399.597	4.483	89.134	3.443	.007
	Huynh-Feldt	399.597	5.000	79.919	3.443	.005
	Lower-bound	399.597	1.000	399.597	3.443	.071
Error(VISIT)	Sphericity Assumed	4526.971	195	23.215		
	Greenhouse-Geisser	4526.971	174.841	25.892		
	Huynh-Feldt	4526.971	195.000	23.215		
	Lower-bound	4526.971	39.000	116.076		

Tests of Between-Subjects Effects

Measure: Superior quadrant RNFLt
Transformed Variable: Average

Source	Type III Sum of Squares	df	Mean Square	F	Sig.
Intercept	3762374.330	1	3762374.330	1564.220	.000
TYPE	7743.242	1	7743.242	3.219	.081
Error	93805.619	39	2405.272		

Tests of Within-Subjects Effects

Measure: Superior quadrant RNFLt TYPE 1 diabetic

Source		Type III Sum of Squares	df	Mean Square	F	Sig.
VISIT	Sphericity Assumed	387.415	5	77.483	3.427	.007
	Greenhouse-Geisser	387.415	3.744	103.464	3.427	.015
	Huynh-Feldt	387.415	4.778	81.085	3.427	.008
	Lower-bound	387.415	1.000	387.415	3.427	.080
Error(VISIT)	Sphericity Assumed	2147.934	95	22.610		
	Greenhouse-Geisser	2147.934	71.145	30.191		
	Huynh-Feldt	2147.934	90.780	23.661		
	Lower-bound	2147.934	19.000	113.049		

Tests of Between-Subjects Effects

Measure: Superior quadrant RNFLt TYPE 1 diabetic
Transformed Variable: Average

Source	Type III Sum of Squares	df	Mean Square	F	Sig.
Intercept	2006796.382	1	2006796.382	1500.193	.000
Error	25416.152	19	1337.692		

Appendix 4

Tests of Within-Subjects Effects

Measure: Superior quadrant RNFLt TYPE 2 diabetic

Source		Type III Sum of Squares	df	Mean Square	F	Sig.
VISIT	Sphericity Assumed	167.238	5	33.448	1.406	.229
	Greenhouse-Geisser	167.238	3.698	45.221	1.406	.243
	Huynh-Feldt	167.238	4.641	36.031	1.406	.233
	Lower-bound	167.238	1.000	167.238	1.406	.250
Error(VISIT)	Sphericity Assumed	2379.038	100	23.790		
	Greenhouse-Geisser	2379.038	73.965	32.164		
	Huynh-Feldt	2379.038	92.829	25.628		
	Lower-bound	2379.038	20.000	118.952		

Tests of Between-Subjects Effects

Measure: Superior quadrant RNFLt TYPE 2 diabetic
Transformed Variable: Average

Source	Type III Sum of Squares	df	Mean Square	F	Sig.
Intercept	1757234.311	1	1757234.311	513.890	.000
Error	68389.467	20	3419.473		

Appendix 4

Tests of Within-Subjects Effects

Measure: Inferior quadrant RNFLt

Source		Type III Sum of Squares	df	Mean Square	F	Sig.
VISIT	Sphericity Assumed	19.939	5	3.988	.188	.967
	Greenhouse-Geisser	19.939	3.724	5.355	.188	.936
	Huynh-Feldt	19.939	4.271	4.669	.188	.952
	Lower-bound	19.939	1.000	19.939	.188	.667
VISIT * TYPE	Sphericity Assumed	227.989	5	45.598	2.148	.061
	Greenhouse-Geisser	227.989	3.724	61.229	2.148	.083
	Huynh-Feldt	227.989	4.271	53.381	2.148	.073
	Lower-bound	227.989	1.000	227.989	2.148	.151
Error(VISIT)	Sphericity Assumed	4138.561	195	21.223		
	Greenhouse-Geisser	4138.561	145.217	28.499		
	Huynh-Feldt	4138.561	166.567	24.846		
	Lower-bound	4138.561	39.000	106.117		

Tests of Between-Subjects Effects

Measure: Inferior quadrant RNFLt
Transformed Variable: Average

Source	Type III Sum of Squares	df	Mean Square	F	Sig.
Intercept	3939905.031	1	3939905.031	1883.705	.000
TYPE	11434.412	1	11434.412	5.467	.025
Error	81571.298	39	2091.572		

Tests of Within-Subjects Effects

Measure: Inferior quadrant RNFLt TYPE 1 diabetic

Source		Type III Sum of Squares	df	Mean Square	F	Sig.
VISIT	Sphericity Assumed	149.181	5	29.836	1.276	.281
	Greenhouse-Geisser	149.181	3.320	44.932	1.276	.290
	Huynh-Feldt	149.181	4.107	36.320	1.276	.286
	Lower-bound	149.181	1.000	149.181	1.276	.273
Error(VISIT)	Sphericity Assumed	2221.969	95	23.389		
	Greenhouse-Geisser	2221.969	63.084	35.223		
	Huynh-Feldt	2221.969	78.041	28.472		
	Lower-bound	2221.969	19.000	116.946		

Tests of Between-Subjects Effects

Measure: Inferior quadrant RNFLt TYPE 1 diabetic
Transformed Variable: Average

Source	Type III Sum of Squares	Df	Mean Square	F	Sig.
Intercept	2135827.395	1	2135827.395	1009.088	.000
Error	40215.264	19	2116.593		

Tests of Within-Subjects Effects

Measure: Inferior quadrant RNFLt TYPE 2 diabetic

Source		Type III Sum of Squares	df	Mean Square	F	Sig.
VISIT	Sphericity Assumed	97.486	5	19.497	1.017	.412
	Greenhouse-Geisser	97.486	3.494	27.898	1.017	.398
	Huynh-Feldt	97.486	4.325	22.542	1.017	.407
	Lower-bound	97.486	1.000	97.486	1.017	.325
Error(VISIT)	Sphericity Assumed	1916.592	100	19.166		
	Greenhouse-Geisser	1916.592	69.887	27.424		
	Huynh-Feldt	1916.592	86.493	22.159		
	Lower-bound	1916.592	20.000	95.830		

Tests of Between-Subjects Effects

Measure: Inferior quadrant RNFLt TYPE 2 diabetic
Transformed Variable: Average

Source	Type III Sum of Squares	Df	Mean Square	F	Sig.
Intercept	1807504.165	1	1807504.165	874.119	.000
Error	41356.034	20	2067.802		

Tests of Within-Subjects Effects

Measure: Nasal quadrant RNFLt

Source		Type III Sum of Squares	df	Mean Square	F	Sig.
VISIT	Sphericity Assumed	140.521	5	28.104	1.517	.186
	Greenhouse-Geisser	140.521	4.578	30.696	1.517	.192
	Huynh-Feldt	140.521	5.000	28.104	1.517	.186
	Lower-bound	140.521	1.000	140.521	1.517	.225
VISIT * TYPE	Sphericity Assumed	42.434	5	8.487	.458	.807
	Greenhouse-Geisser	42.434	4.578	9.270	.458	.791
	Huynh-Feldt	42.434	5.000	8.487	.458	.807
	Lower-bound	42.434	1.000	42.434	.458	.502
Error(VISIT)	Sphericity Assumed	3611.968	195	18.523		
	Greenhouse-Geisser	3611.968	178.534	20.231		
	Huynh-Feldt	3611.968	195.000	18.523		
	Lower-bound	3611.968	39.000	92.615		

Tests of Between-Subjects Effects

Measure: Nasal quadrant RNFLt
Transformed Variable: Average

Source	Type III Sum of Squares	Df	Mean Square	F	Sig.
Intercept	1857529.302	1	1857529.302	1087.209	.000
TYPE	5610.152	1	5610.152	3.284	.078
Error	66632.687	39	1708.530		

Tests of Within-Subjects Effects

Measure: Temporal quadrant RNFLt

Source		Type III Sum of Squares	Df	Mean Square	F	Sig.
VISIT	Sphericity Assumed	246.385	5	49.277	.991	.424
	Greenhouse-Geisser	246.385	1.378	178.792	.991	.350
	Huynh-Feldt	246.385	1.449	170.082	.991	.354
	Lower-bound	246.385	1.000	246.385	.991	.326
VISIT * TYPE	Sphericity Assumed	138.066	5	27.613	.556	.734
	Greenhouse-Geisser	138.066	1.378	100.189	.556	.513
	Huynh-Feldt	138.066	1.449	95.308	.556	.522
	Lower-bound	138.066	1.000	138.066	.556	.461
Error(VISIT)	Sphericity Assumed	9692.438	195	49.705		
	Greenhouse-Geisser	9692.438	53.744	180.344		
	Huynh-Feldt	9692.438	56.496	171.558		
	Lower-bound	9692.438	39.000	248.524		

Tests of Between-Subjects Effects

Measure: Temporal quadrant RNFLt
Transformed Variable: Average

Source	Type III Sum of Squares	df	Mean Square	F	Sig.
Intercept	1331847.889	1	1331847.889	509.492	.000
TYPE	10055.477	1	10055.477	3.847	.057
Error	101948.779	39	2614.071		

Appendix 4

Tests of Within-Subjects Effects

Measure: Mean RNFLt

Source		Type III Sum of Squares	Df	Mean Square	F	Sig.
VISIT	Sphericity Assumed	110.501	5	22.100	1.350	.245
	Greenhouse-Geisser	110.501	1.769	62.479	1.350	.265
	Huynh-Feldt	110.501	1.894	58.345	1.350	.265
	Lower-bound	110.501	1.000	110.501	1.350	.252
VISIT * TYPE	Sphericity Assumed	105.023	5	21.005	1.283	.273
	Greenhouse-Geisser	105.023	1.769	59.381	1.283	.281
	Huynh-Feldt	105.023	1.894	55.453	1.283	.282
	Lower-bound	105.023	1.000	105.023	1.283	.264
Error(VISIT)	Sphericity Assumed	3193.132	195	16.375		
	Greenhouse-Geisser	3193.132	68.976	46.293		
	Huynh-Feldt	3193.132	73.863	43.230		
	Lower-bound	3193.132	39.000	81.875		

Tests of Between-Subjects Effects

Measure: Mean RNFLt
Transformed Variable: Average

Source	Type III Sum of Squares	Df	Mean Square	F	Sig.
Intercept	2603395.896	1	2603395.896	2339.324	.000
TYPE	7995.097	1	7995.097	7.184	.011
Error	43402.467	39	1112.884		

Appendix 4

Tests of Within-Subjects Effects

Measure: Mean RNFLt TYPE 1 diabetic

Source		Type III Sum of Squares	df	Mean Square	F	Sig.
VISIT	Sphericity Assumed	20.193	5	4.039	.518	.762
	Greenhouse-Geisser	20.193	2.104	9.599	.518	.609
	Huynh-Feldt	20.193	2.372	8.515	.518	.630
	Lower-bound	20.193	1.000	20.193	.518	.480
Error(VISIT)	Sphericity Assumed	740.327	95	7.793		
	Greenhouse-Geisser	740.327	39.967	18.523		
	Huynh-Feldt	740.327	45.059	16.430		
	Lower-bound	740.327	19.000	38.965		

Tests of Between-Subjects Effects

Measure: Mean RNFLt TYPE 1 diabetic
Transformed Variable: Average

Source	Type III Sum of Squares	Df	Mean Square	F	Sig.
Intercept	1415444.440	1	1415444.440	1614.463	.000
Error	16657.827	19	876.728		

Appendix 4

Tests of Within-Subjects Effects

Measure: Mean RNFLt TYPE 2 diabetic

Source		Type III Sum of Squares	df	Mean Square	F	Sig.
VISIT	Sphericity Assumed	199.710	5	39.942	1.628	.159
	Greenhouse-Geisser	199.710	1.237	161.397	1.628	.217
	Huynh-Feldt	199.710	1.278	156.226	1.628	.217
	Lower-bound	199.710	1.000	199.710	1.628	.217
Error(VISIT)	Sphericity Assumed	2452.805	100	24.528		
	Greenhouse-Geisser	2452.805	24.748	99.112		
	Huynh-Feldt	2452.805	25.567	95.937		
	Lower-bound	2452.805	20.000	122.640		

Tests of Between-Subjects Effects

Measure: Mean RNFLt TYPE 2 diabetic
Transformed Variable: Average

Source	Type III Sum of Squares	df	Mean Square	F	Sig.
Intercept	1190459.106	1	1190459.106	890.241	.000
Error	26744.640	20	1337.232		

Appendix 4

Tests of Within-Subjects Effects

Measure: RT Pos 1

Source		Type III Sum of Squares	Df	Mean Square	F	Sig.
VISIT	Sphericity Assumed	204.055	5	40.811	4.267	.001
	Greenhouse-Geisser	204.055	3.630	56.217	4.267	.004
	Huynh-Feldt	204.055	4.151	49.158	4.267	.002
	Lower-bound	204.055	1.000	204.055	4.267	.046
VISIT * TYPE	Sphericity Assumed	34.519	5	6.904	.722	.608
	Greenhouse-Geisser	34.519	3.630	9.510	.722	.566
	Huynh-Feldt	34.519	4.151	8.316	.722	.583
	Lower-bound	34.519	1.000	34.519	.722	.401
Error(VISIT)	Sphericity Assumed	1865.256	195	9.565		
	Greenhouse-Geisser	1865.256	141.562	13.176		
	Huynh-Feldt	1865.256	161.889	11.522		
	Lower-bound	1865.256	39.000	47.827		

Tests of Between-Subjects Effects

Measure: RT Pos 1
Transformed Variable: Average

Source	Type III Sum of Squares	df	Mean Square	F	Sig.
Intercept	11034753.939	1	11034753.939	3149.793	.000
TYPE	340.154	1	340.154	.097	.757
Error	136629.748	39	3503.327		

Appendix 4

Tests of Within-Subjects Effects

Measure: RT Pos 2

Source		Type III Sum of Squares	Df	Mean Square	F	Sig.
VISIT	Sphericity Assumed	58.676	5	11.735	1.523	.184
	Greenhouse-Geisser	58.676	3.570	16.438	1.523	.204
	Huynh-Feldt	58.676	4.074	14.402	1.523	.197
	Lower-bound	58.676	1.000	58.676	1.523	.225
VISIT * TYPE	Sphericity Assumed	78.409	5	15.682	2.035	.075
	Greenhouse-Geisser	78.409	3.570	21.966	2.035	.101
	Huynh-Feldt	78.409	4.074	19.245	2.035	.091
	Lower-bound	78.409	1.000	78.409	2.035	.162
Error(VISIT)	Sphericity Assumed	1502.768	195	7.707		
	Greenhouse-Geisser	1502.768	139.213	10.795		
	Huynh-Feldt	1502.768	158.895	9.458		
	Lower-bound	1502.768	39.000	38.533		

Tests of Between-Subjects Effects

Measure: RT Pos 2
Transformed Variable: Average

Source	Type III Sum of Squares	df	Mean Square	F	Sig.
Intercept	19131049.596	1	19131049.596	7558.553	.000
TYPE	2634.762	1	2634.762	1.041	.314
Error	98710.819	39	2531.047		

Appendix 4

Tests of Within-Subjects Effects

Measure: RT Pos 3

Source		Type III Sum of Squares	df	Mean Square	F	Sig.
VISIT	Sphericity Assumed	14.332	5	2.866	.303	.911
	Greenhouse-Geisser	14.332	3.015	4.754	.303	.824
	Huynh-Feldt	14.332	3.379	4.241	.303	.846
	Lower-bound	14.332	1.000	14.332	.303	.585
VISIT * TYPE	Sphericity Assumed	38.944	5	7.789	.823	.535
	Greenhouse-Geisser	38.944	3.015	12.918	.823	.484
	Huynh-Feldt	38.944	3.379	11.525	.823	.496
	Lower-bound	38.944	1.000	38.944	.823	.370
Error(VISIT)	Sphericity Assumed	1845.232	195	9.463		
	Greenhouse-Geisser	1845.232	117.569	15.695		
	Huynh-Feldt	1845.232	131.785	14.002		
	Lower-bound	1845.232	39.000	47.314		

Tests of Between-Subjects Effects

Measure: RT Pos 3
Transformed Variable: Average

Source	Type III Sum of Squares	df	Mean Square	F	Sig.
Intercept	18385817.652	1	18385817.652	6512.991	.000
TYPE	1339.447	1	1339.447	.474	.495
Error	110094.871	39	2822.945		

Appendix 4

Tests of Within-Subjects Effects

Measure: RT Pos 4

Source		Type III Sum of Squares	df	Mean Square	F	Sig.
VISIT	Sphericity Assumed	8.618	5	1.724	.426	.830
	Greenhouse-Geisser	8.618	4.112	2.096	.426	.795
	Huynh-Feldt	8.618	4.775	1.805	.426	.822
	Lower-bound	8.618	1.000	8.618	.426	.518
VISIT * TYPE	Sphericity Assumed	31.446	5	6.289	1.553	.175
	Greenhouse-Geisser	31.446	4.112	7.647	1.553	.188
	Huynh-Feldt	31.446	4.775	6.585	1.553	.178
	Lower-bound	31.446	1.000	31.446	1.553	.220
Error(VISIT)	Sphericity Assumed	789.667	195	4.050		
	Greenhouse-Geisser	789.667	160.378	4.924		
	Huynh-Feldt	789.667	186.240	4.240		
	Lower-bound	789.667	39.000	20.248		

Tests of Between-Subjects Effects

Measure: RT Pos 4
Transformed Variable: Average

Source	Type III Sum of Squares	df	Mean Square	F	Sig.
Intercept	17388577.718	1	17388577.718	7067.616	.000
TYPE	919.050	1	919.050	.374	.545
Error	95952.377	39	2460.317		

Appendix 4

Tests of Within-Subjects Effects

Measure: RT Pos 5

Source		Type III Sum of Squares	Df	Mean Square	F	Sig.
VISIT	Sphericity Assumed	21.887	5	4.377	1.187	.317
	Greenhouse-Geisser	21.887	3.988	5.488	1.187	.319
	Huynh-Feldt	21.887	4.614	4.744	1.187	.318
	Lower-bound	21.887	1.000	21.887	1.187	.283
VISIT * TYPE	Sphericity Assumed	33.673	5	6.735	1.826	.109
	Greenhouse-Geisser	33.673	3.988	8.443	1.826	.127
	Huynh-Feldt	33.673	4.614	7.299	1.826	.116
	Lower-bound	33.673	1.000	33.673	1.826	.184
Error(VISIT)	Sphericity Assumed	719.118	195	3.688		
	Greenhouse-Geisser	719.118	155.550	4.623		
	Huynh-Feldt	719.118	179.928	3.997		
	Lower-bound	719.118	39.000	18.439		

Tests of Between-Subjects Effects

Measure: RT Pos 5
Transformed Variable: Average

Source	Type III Sum of Squares	df	Mean Square	F	Sig.
Intercept	19388162.113	1	19388162.113	7495.600	.000
TYPE	2383.006	1	2383.006	.921	.343
Error	100877.622	39	2586.606		

Appendix 4

Tests of Within-Subjects Effects

Measure: RT Pos 6

Source		Type III Sum of Squares	Df	Mean Square	F	Sig.
VISIT	Sphericity Assumed	48.571	5	9.714	.989	.425
	Greenhouse-Geisser	48.571	3.058	15.883	.989	.401
	Huynh-Feldt	48.571	3.433	14.149	.989	.407
	Lower-bound	48.571	1.000	48.571	.989	.326
VISIT * TYPE	Sphericity Assumed	70.776	5	14.155	1.442	.211
	Greenhouse-Geisser	70.776	3.058	23.144	1.442	.234
	Huynh-Feldt	70.776	3.433	20.618	1.442	.229
	Lower-bound	70.776	1.000	70.776	1.442	.237
Error(VISIT)	Sphericity Assumed	1914.401	195	9.817		
	Greenhouse-Geisser	1914.401	119.263	16.052		
	Huynh-Feldt	1914.401	133.876	14.300		
	Lower-bound	1914.401	39.000	49.087		

Tests of Between-Subjects Effects

Measure: RT Pos 6
Transformed Variable: Average

Source	Type III Sum of Squares	df	Mean Square	F	Sig.
Intercept	16600675.695	1	16600675.695	8774.744	.000
TYPE	9485.427	1	9485.427	5.014	.031
Error	73782.935	39	1891.870		

Appendix 4

Tests of Within-Subjects Effects

Measure: RT Pos 7

Source		Type III Sum of Squares	Df	Mean Square	F	Sig.
VISIT	Sphericity Assumed	63.713	5	12.743	1.077	.374
	Greenhouse-Geisser	63.713	2.070	30.786	1.077	.347
	Huynh-Feldt	63.713	2.243	28.400	1.077	.351
	Lower-bound	63.713	1.000	63.713	1.077	.306
VISIT * TYPE	Sphericity Assumed	14.169	5	2.834	.240	.945
	Greenhouse-Geisser	14.169	2.070	6.846	.240	.795
	Huynh-Feldt	14.169	2.243	6.316	.240	.812
	Lower-bound	14.169	1.000	14.169	.240	.627
Error(VISIT)	Sphericity Assumed	2307.078	195	11.831		
	Greenhouse-Geisser	2307.078	80.712	28.584		
	Huynh-Feldt	2307.078	87.494	26.368		
	Lower-bound	2307.078	39.000	59.156		

Tests of Between-Subjects Effects

Measure: RT Pos 7
Transformed Variable: Average

Source	Type III Sum of Squares	df	Mean Square	F	Sig.
Intercept	13972914.732	1	13972914.732	6861.241	.000
TYPE	5072.488	1	5072.488	2.491	.123
Error	79423.483	39	2036.500		

Appendix 4

Tests of Within-Subjects Effects

Measure: RT Pos 8

Source		Type III Sum of Squares	Df	Mean Square	F	Sig.
VISIT	Sphericity Assumed	26.453	5	5.291	.340	.888
	Greenhouse-Geisser	26.453	2.918	9.065	.340	.791
	Huynh-Feldt	26.453	3.260	8.114	.340	.813
	Lower-bound	26.453	1.000	26.453	.340	.563
VISIT * TYPE	Sphericity Assumed	29.043	5	5.809	.373	.867
	Greenhouse-Geisser	29.043	2.918	9.953	.373	.767
	Huynh-Feldt	29.043	3.260	8.908	.373	.789
	Lower-bound	29.043	1.000	29.043	.373	.545
Error(VISIT)	Sphericity Assumed	3036.607	195	15.572		
	Greenhouse-Geisser	3036.607	113.802	26.683		
	Huynh-Feldt	3036.607	127.152	23.882		
	Lower-bound	3036.607	39.000	77.862		

Tests of Between-Subjects Effects

Measure: RT Pos 8
Transformed Variable: Average

Source	Type III Sum of Squares	df	Mean Square	F	Sig.
Intercept	13127044.995	1	13127044.995	5079.993	.000
TYPE	6896.234	1	6896.234	2.669	.110
Error	100778.641	39	2584.068		

Appendix 4

Tests of Within-Subjects Effects

Measure: RT Pos 9

Source		Type III Sum of Squares	Df	Mean Square	F	Sig.
VISIT	Sphericity Assumed	44.491	5	8.898	.804	.548
	Greenhouse-Geisser	44.491	2.560	17.377	.804	.477
	Huynh-Feldt	44.491	2.826	15.744	.804	.488
	Lower-bound	44.491	1.000	44.491	.804	.375
VISIT * TYPE	Sphericity Assumed	38.866	5	7.773	.702	.622
	Greenhouse-Geisser	38.866	2.560	15.180	.702	.531
	Huynh-Feldt	38.866	2.826	13.754	.702	.545
	Lower-bound	38.866	1.000	38.866	.702	.407
Error(VISIT)	Sphericity Assumed	2158.341	195	11.068		
	Greenhouse-Geisser	2158.341	99.852	21.615		
	Huynh-Feldt	2158.341	110.208	19.584		
	Lower-bound	2158.341	39.000	55.342		

Tests of Between-Subjects Effects

Measure: RT Pos 9
Transformed Variable: Average

Source	Type III Sum of Squares	df	Mean Square	F	Sig.
Intercept	14815974.148	1	14815974.148	8462.805	.000
TYPE	11097.605	1	11097.605	6.339	.016
Error	68277.948	39	1750.717		

Appendix 4

Tests of Within-Subjects Effects

Measure: RT Pos 9 TYPE 1 diabetic

Source		Type III Sum of Squares	df	Mean Square	F	Sig.
VISIT	Sphericity Assumed	73.654	5	14.731	.975	.437
	Greenhouse-Geisser	73.654	1.670	44.101	.975	.374
	Huynh-Feldt	73.654	1.812	40.647	.975	.380
	Lower-bound	73.654	1.000	73.654	.975	.336
Error(VISIT)	Sphericity Assumed	1434.863	95	15.104		
	Greenhouse-Geisser	1434.863	31.732	45.218		
	Huynh-Feldt	1434.863	34.429	41.676		
	Lower-bound	1434.863	19.000	75.519		

Tests of Between-Subjects Effects

Measure: RT Pos 9 TYPE 1 diabetic
Transformed Variable: Average

Source	Type III Sum of Squares	df	Mean Square	F	Sig.
Intercept	7632858.223	1	7632858.223	3799.713	.000
Error	38167.173	19	2008.799		

Appendix 4

Tests of Within-Subjects Effects

Measure: RT Pos 9 TYPE 2 diabetic

Source		Type III Sum of Squares	df	Mean Square	F	Sig.
VISIT	Sphericity Assumed	8.103	5	1.621	.224	.951
	Greenhouse-Geisser	8.103	3.321	2.440	.224	.896
	Huynh-Feldt	8.103	4.061	1.995	.224	.926
	Lower-bound	8.103	1.000	8.103	.224	.641
Error(VISIT)	Sphericity Assumed	723.478	100	7.235		
	Greenhouse-Geisser	723.478	66.412	10.894		
	Huynh-Feldt	723.478	81.217	8.908		
	Lower-bound	723.478	20.000	36.174		

Tests of Between-Subjects Effects

Measure: RT Pos 9 TYPE 2 diabetic
Transformed Variable: Average

Source	Type III Sum of Squares	df	Mean Square	F	Sig.
Intercept	7183247.413	1	7183247.413	4771.214	.000
Error	30110.775	20	1505.539		

Appendix 4

Tests of Within-Subjects Effects

Measure: Mean RT

Source		Type III Sum of Squares	df	Mean Square	F	Sig.
VISIT	Sphericity Assumed	18.345	5	3.669	1.293	.269
	Greenhouse-Geisser	18.345	3.635	5.046	1.293	.277
	Huynh-Feldt	18.345	4.158	4.412	1.293	.274
	Lower-bound	18.345	1.000	18.345	1.293	.262
VISIT * TYPE	Sphericity Assumed	17.566	5	3.513	1.238	.293
	Greenhouse-Geisser	17.566	3.635	4.832	1.238	.298
	Huynh-Feldt	17.566	4.158	4.225	1.238	.297
	Lower-bound	17.566	1.000	17.566	1.238	.273
Error(VISIT)	Sphericity Assumed	553.416	195	2.838		
	Greenhouse-Geisser	553.416	141.774	3.904		
	Huynh-Feldt	553.416	162.159	3.413		
	Lower-bound	553.416	39.000	14.190		

Tests of Between-Subjects Effects

Measure: Mean RT
Transformed Variable: Average

Source	Type III Sum of Squares	df	Mean Square	F	Sig.
Intercept	15859422.062	1	15859422.062	8838.549	.000
TYPE	3156.116	1	3156.116	1.759	.192
Error	69979.521	39	1794.347		

Appendix 4

Tests of Within-Subjects Effects

Measure: Systolic blood pressure

Source		Type III Sum of Squares	df	Mean Square	F	Sig.
VISIT	Sphericity Assumed	646.365	5	129.273	.976	.433
	Greenhouse-Geisser	646.365	2.375	272.162	.976	.392
	Huynh-Feldt	646.365	2.604	248.219	.976	.398
	Lower-bound	646.365	1.000	646.365	.976	.329
VISIT * TYPE	Sphericity Assumed	214.918	5	42.984	.325	.898
	Greenhouse-Geisser	214.918	2.375	90.494	.325	.760
	Huynh-Feldt	214.918	2.604	82.533	.325	.779
	Lower-bound	214.918	1.000	214.918	.325	.572
Error(VISIT)	Sphericity Assumed	25818.432	195	132.402		
	Greenhouse-Geisser	25818.432	92.622	278.750		
	Huynh-Feldt	25818.432	101.556	254.228		
	Lower-bound	25818.432	39.000	662.011		

Tests of Between-Subjects Effects

Measure: Systolic blood pressure
Transformed Variable: Average

Source	Type III Sum of Squares	df	Mean Square	F	Sig.
Intercept	4630105.392	1	4630105.392	2659.726	.000
TYPE	1299.668	1	1299.668	.747	.393
Error	67892.006	39	1740.821		

Appendix 4

Tests of Within-Subjects Effects

Measure: Diastolic blood pressure

Source		Type III Sum of Squares	Df	Mean Square	F	Sig.
VISIT	Sphericity Assumed	1049.034	5	209.807	7.357	.000
	Greenhouse-Geisser	1049.034	4.008	261.737	7.357	.000
	Huynh-Feldt	1049.034	4.639	226.135	7.357	.000
	Lower-bound	1049.034	1.000	1049.034	7.357	.010
VISIT * TYPE	Sphericity Assumed	140.123	5	28.025	.983	.430
	Greenhouse-Geisser	140.123	4.008	34.961	.983	.419
	Huynh-Feldt	140.123	4.639	30.206	.983	.426
	Lower-bound	140.123	1.000	140.123	.983	.328
Error(VISIT)	Sphericity Assumed	5561.308	195	28.520		
	Greenhouse-Geisser	5561.308	156.311	35.578		
	Huynh-Feldt	5561.308	180.920	30.739		
	Lower-bound	5561.308	39.000	142.598		

Tests of Between-Subjects Effects

Measure: Diastolic blood pressure
Transformed Variable: Average

Source	Type III Sum of Squares	df	Mean Square	F	Sig.
Intercept	1403741.149	1	1403741.149	4510.591	.000
TYPE	778.060	1	778.060	2.500	.122
Error	12137.192	39	311.210		

Appendix 4

Tests of Within-Subjects Effects

Measure: MAP

Source		Type III Sum of Squares	Df	Mean Square	F	Sig.
VISIT	Sphericity Assumed	806.942	5	161.388	4.056	.002
	Greenhouse-Geisser	806.942	2.943	274.216	4.056	.009
	Huynh-Feldt	806.942	3.291	245.223	4.056	.007
	Lower-bound	806.942	1.000	806.942	4.056	.051
VISIT * TYPE	Sphericity Assumed	152.377	5	30.475	.766	.575
	Greenhouse-Geisser	152.377	2.943	51.781	.766	.513
	Huynh-Feldt	152.377	3.291	46.306	.766	.526
	Lower-bound	152.377	1.000	152.377	.766	.387
Error(VISIT)	Sphericity Assumed	7758.817	195	39.789		
	Greenhouse-Geisser	7758.817	114.766	67.605		
	Huynh-Feldt	7758.817	128.335	60.457		
	Lower-bound	7758.817	39.000	198.944		

Tests of Between-Subjects Effects

Measure: MAP
Transformed Variable: Average

Source	Type III Sum of Squares	df	Mean Square	F	Sig.
Intercept	2271409.845	1	2271409.845	4382.326	.000
TYPE	937.000	1	937.000	1.808	.187
Error	20214.149	39	518.312		

Appendix 4

Tests of Within-Subjects Effects

Measure: OPP

Source		Type III Sum of Squares	Df	Mean Square	F	Sig.
VISIT	Sphericity Assumed	289.410	5	57.882	3.599	.004
	Greenhouse-Geisser	289.410	4.118	70.281	3.599	.007
	Huynh-Feldt	289.410	4.783	60.510	3.599	.005
	Lower-bound	289.410	1.000	289.410	3.599	.065
VISIT * TYPE	Sphericity Assumed	95.862	5	19.172	1.192	.314
	Greenhouse-Geisser	95.862	4.118	23.279	1.192	.316
	Huynh-Feldt	95.862	4.783	20.043	1.192	.315
	Lower-bound	95.862	1.000	95.862	1.192	.282
Error(VISIT)	Sphericity Assumed	3135.799	195	16.081		
	Greenhouse-Geisser	3135.799	160.599	19.526		
	Huynh-Feldt	3135.799	186.530	16.811		
	Lower-bound	3135.799	39.000	80.405		

Tests of Between-Subjects Effects

Measure: OPP
Transformed Variable: Average

Source	Type III Sum of Squares	df	Mean Square	F	Sig.
Intercept	601024.075	1	601024.075	2334.402	.000
TYPE	184.163	1	184.163	.715	.403
Error	10041.090	39	257.464		

Appendix 5

Post-hoc analysis on repeated measures ANOVA

Blood glucose

Paired Samples Test

		Paired Differences					t	df	Sig. (2-tailed)
		Mean	Std. Deviation	Std. Error Mean	95% Confidence Interval of the Difference Lower	Upper			
Pair 1	v1 - v2	-4.77073	4.09410	.63939	-6.06299	-3.47848	-7.461	40	.000
Pair 2	v1 - v3	-.22683	5.41964	.84641	-1.93748	1.48382	-.268	40	.790
Pair 3	v1 - v4	-1.89024	6.02556	.94103	-3.79215	.01166	-2.009	40	.051
Pair 4	v1 - v5	.31707	6.80452	1.06269	-1.83070	2.46484	.298	40	.767
Pair 5	v1 - v6	-.87073	6.54547	1.02223	-2.93674	1.19527	-.852	40	.399
Pair 6	v2 - v3	4.54390	4.49739	.70237	3.12435	5.96345	6.469	40	.000
Pair 7	v2 - v4	2.88049	6.11863	.95557	.94921	4.81177	3.014	40	.004
Pair 8	v2 - v5	5.08780	6.50151	1.01536	3.03568	7.13993	5.011	40	.000
Pair 9	v2 - v6	3.90000	6.39433	.99863	1.88170	5.91830	3.905	40	.000
Pair 10	v3 - v4	-1.66341	4.12733	.64458	-2.96616	-.36067	-2.581	40	.014
Pair 11	v3 - v5	.54390	4.49633	.70221	-.87532	1.96312	.775	40	.443
Pair 12	v3 - v6	-.64390	4.92621	.76934	-2.19881	.91100	-.837	40	.408
Pair 13	v4 - v5	2.20732	4.02116	.62800	.93808	3.47655	3.515	40	.001
Pair 14	v4 - v6	1.01951	5.00156	.78111	-.55918	2.59820	1.305	40	.199
Pair 15	v5 - v6	-1.18780	5.04501	.78790	-2.78021	.40460	-1.508	40	.140

Appendix 5

logMAR 10% contrast

Paired Samples Test

		Paired Differences					t	df	Sig. (2-tailed)
					95% Confidence Interval of the Difference				
		Mean	Std. Deviation	Std. Error Mean	Lower	Upper			
Pair 1	V1 - V2	.0249	.13113	.02048	-.0165	.0663	1.215	40	.232
Pair 2	V1 - V3	.0571	.14970	.02338	.0098	.1043	2.441	40	.019
Pair 3	V1 - V4	.0444	.15359	.02399	-.0041	.0929	1.851	40	.072
Pair 4	V1 - V5	.0493	.14900	.02327	.0022	.0963	2.117	40	.041
Pair 5	V1 - V6	.0541	.14685	.02293	.0078	.1005	2.361	40	.023
Pair 6	V2 - V3	.0322	.08245	.01288	.0062	.0582	2.500	40	.017
Pair 7	V2 - V4	.0195	.07301	.01140	-.0035	.0426	1.711	40	.095
Pair 8	V2 - V5	.0244	.07622	.01190	.0003	.0484	2.049	40	.047
Pair 9	V3 - V4	-.0127	.08897	.01389	-.0408	.0154	-.913	40	.367
Pair 10	V3 - V5	-.0078	.09673	.01511	-.0383	.0227	-.517	40	.608
Pair 11	V3 - V6	-.0029	.12021	.01877	-.0409	.0350	-.156	40	.877
Pair 12	V4 - V5	.0049	.06896	.01077	-.0169	.0266	.453	40	.653
Pair 13	V4 - V6	.0098	.10041	.01568	-.0219	.0414	.622	40	.537
Pair 14	V5 - V6	.0049	.10448	.01632	-.0281	.0379	.299	40	.767
Pair 15	V2 - V6	.0293	.09911	.01548	-.0020	.0605	1.891	40	.066

Appendix 5

Contrast sensitivity (Pelli Robson)

Paired Samples Test

		Paired Differences					t	df	Sig. (2-tailed)
		Mean	Std. Deviation	Std. Error Mean	95% Confidence Interval of the Difference Lower	Upper			
Pair 1	V1 – V2	-.0439	.11247	.01756	-.0794	-.0084	-2.499	40	.017
Pair 2	V1 – V3	-.0622	.12082	.01887	-.1003	-.0241	-3.296	40	.002
Pair 3	V1 – V4	-.0915	.12937	.02020	-.1323	-.0506	-4.527	40	.000
Pair 4	V1 – V5	-.1024	.11830	.01847	-.1398	-.0651	-5.545	40	.000
Pair 5	V1 – V6	-.0841	.12116	.01892	-.1224	-.0459	-4.447	40	.000
Pair 6	V2 – V3	-.0183	.08997	.01405	-.0467	.0101	-1.302	40	.200
Pair 7	V2 – V4	-.0476	.10305	.01609	-.0801	-.0150	-2.955	40	.005
Pair 8	V2 – V5	-.0585	.12037	.01880	-.0965	-.0205	-3.114	40	.003
Pair 9	V2 – V6	-.0402	.11137	.01739	-.0754	-.0051	-2.314	40	.026
Pair 10	V3 – V4	-.0293	.10184	.01591	-.0614	.0029	-1.840	40	.073
Pair 11	V3 – V5	-.0402	.12561	.01962	-.0799	-.0006	-2.052	40	.047
Pair 12	V3 – V6	-.0220	.11404	.01781	-.0579	.0140	-1.232	40	.225
Pair 13	V4 – V5	-.0110	.09715	.01517	-.0416	.0197	-.723	40	.474
Pair 14	V4 – V6	.0073	.11595	.01811	-.0293	.0439	.404	40	.688
Pair 15	V5 – V6	.0183	.11223	.01753	-.0171	.0537	1.044	40	.303

Appendix 5

MD SWAP fields

Paired Samples Test

		Paired Differences					t	df	Sig. (2-tailed)
		Mean	Std. Deviation	Std. Error Mean	95% Confidence Interval of the Difference Lower	Upper			
Pair 1	V1 - V2	-.4344	1.65312	.25817	-.9562	.0874	-1.683	40	.100
Pair 2	V1 - V3	-.2205	1.98393	.30984	-.8467	.4057	-.712	40	.481
Pair 3	V1 - V4	-.0505	2.16973	.33886	-.7353	.6344	-.149	40	.882
Pair 4	V1 - V5	-.3807	2.06463	.32244	-1.0324	.2709	-1.181	40	.245
Pair 5	V1 - V6	-.9173	2.32810	.36359	-1.6522	-.1825	-2.523	40	.016
Pair 6	V2 - V3	.2139	1.26072	.19689	-.1840	.6118	1.086	40	.284
Pair 7	V2 - V4	.3839	1.40606	.21959	-.0599	.8277	1.748	40	.088
Pair 8	V2 - V5	.0537	1.60831	.25118	-.4540	.5613	.214	40	.832
Pair 9	V2 - V6	-.4829	1.55910	.24349	-.9750	.0092	-1.983	40	.054
Pair 10	V3 - V4	.1700	1.11495	.17413	-.1819	.5219	.976	40	.335
Pair 11	V3 - V5	-.1602	1.47293	.23003	-.6252	.3047	-.697	40	.490
Pair 12	V3 - V6	-.6968	1.74991	.27329	-1.2492	-.1445	-2.550	40	.015
Pair 13	V4 - V5	-.3302	1.34858	.21061	-.7559	.0954	-1.568	40	.125
Pair 14	V4 - V6	-.8668	1.62766	.25420	-1.3806	-.3531	-3.410	40	.001
Pair 15	V5 - V6	-.5366	1.67733	.26195	-1.0660	-.0072	-2.048	40	.047

Appendix 5

IOP

Paired Samples Test

		Paired Differences					t	df	Sig. (2-tailed)
					95% Confidence Interval of the Difference				
		Mean	Std. Deviation	Std. Error Mean	Lower	Upper			
Pair 1	V1 - V2	1.0244	3.06992	.47944	.0554	1.9934	2.137	40	.039
Pair 2	V1 - V3	.3171	3.02852	.47298	-.6388	1.2730	.670	40	.506
Pair 3	V1 - V4	1.2439	3.33752	.52123	.1905	2.2974	2.386	40	.022
Pair 4	V1 - V5	1.0976	2.76410	.43168	.2251	1.9700	2.543	40	.015
Pair 5	V1 - V6	1.2439	2.97305	.46431	.3055	2.1823	2.679	40	.011
Pair 6	V2 - V3	-.7073	1.43603	.22427	-1.1606	-.2540	-3.154	40	.003
Pair 7	V2 - V4	.2195	2.16232	.33770	-.4630	.9020	.650	40	.519
Pair 8	V2 - V5	.0732	2.00487	.31311	-.5596	.7060	.234	40	.816
Pair 9	V2 - V6	.2195	2.13907	.33407	-.4557	.8947	.657	40	.515
Pair 10	V3 - V4	.9268	2.10226	.32832	.2633	1.5904	2.823	40	.007
Pair 11	V3 - V5	.7805	1.87766	.29324	.1878	1.3732	2.662	40	.011
Pair 12	V3 - V6	.9268	1.91560	.29917	.3222	1.5315	3.098	40	.004
Pair 13	V4 - V5	-.1463	1.90474	.29747	-.7476	.4549	-.492	40	.625
Pair 14	V4 - V6	.0000	1.94936	.30444	-.6153	.6153	.000	40	1.000
Pair 15	V5 - V6	.1463	1.89157	.29541	-.4507	.7434	.495	40	.623

Superior quadrant RNFLt TYPE 1

Paired Samples Test

		Paired Differences					t	df	Sig. (2-tailed)
		Mean	Std. Deviation	Std. Error Mean	95% Confidence Interval of the Difference Lower	Upper			
Pair 1	V1 - V2	1.7400	6.93272	1.55020	-1.5046	4.9846	1.122	19	.276
Pair 2	V1 - V3	4.2725	8.55151	1.91218	.2703	8.2747	2.234	19	.038
Pair 3	V1 - V4	2.1075	6.90031	1.54296	-1.1219	5.3369	1.366	19	.188
Pair 4	V1 - V5	4.5617	6.76295	1.51224	1.3965	7.7268	3.016	19	.007
Pair 5	V1 - V6	4.9867	6.68942	1.49580	1.8559	8.1174	3.334	19	.003
Pair 6	V2 - V3	2.5325	7.28105	1.62809	-.8751	5.9401	1.556	19	.136
Pair 7	V2 - V4	.3675	7.29459	1.63112	-3.0465	3.7815	.225	19	.824
Pair 8	V2 - V5	2.8217	4.23210	.94633	.8410	4.8024	2.982	19	.008
Pair 9	V2 - V6	3.2467	6.98105	1.56101	-.0206	6.5139	2.080	19	.051
Pair 10	V3 - V4	-2.1650	8.22576	1.83934	-6.0148	1.6848	-1.177	19	.254
Pair 11	V3 - V5	.2892	6.95978	1.55625	-2.9681	3.5464	.186	19	.855
Pair 12	V3 - V6	.7142	5.80890	1.29891	-2.0045	3.4328	.550	19	.589
Pair 13	V4 - V5	2.4542	6.28604	1.40560	-.4878	5.3961	1.746	19	.097
Pair 14	V4 - V6	2.8792	5.06640	1.13288	.5080	5.2503	2.541	19	.020
Pair 15	V5 - V6	.4250	5.57724	1.24711	-2.1852	3.0352	.341	19	.737

MRT pos 1 (fovea)

Paired Samples Test

		Paired Differences					t	df	Sig. (2-tailed)
		Mean	Std. Deviation	Std. Error Mean	95% Confidence Interval of the Difference Lower	Upper			
Pair 1	V1 - V2	-2.6671	4.03143	.62960	-3.9396	-1.3946	-4.236	40	.000
Pair 2	V1 - V3	-2.7878	5.80456	.90652	-4.6200	-.9557	-3.075	40	.004
Pair 3	V1 - V4	-1.8573	3.72394	.58158	-3.0327	-.6819	-3.194	40	.003
Pair 4	V1 - V5	-2.0988	4.02614	.62878	-3.3696	-.8280	-3.338	40	.002
Pair 5	V1 - V6	-1.8378	4.80360	.75020	-3.3540	-.3216	-2.450	40	.019
Pair 6	V2 - V3	-.1207	5.08460	.79408	-1.7256	1.4842	-.152	40	.880
Pair 7	V2 - V4	.8098	3.88869	.60731	-.4177	2.0372	1.333	40	.190
Pair 8	V2 - V5	.5683	3.39208	.52975	-.5024	1.6390	1.073	40	.290
Pair 9	V2 - V6	.8293	4.59381	.71743	-.6207	2.2793	1.156	40	.255
Pair 10	V3 - V4	.9305	4.83917	.75575	-.5969	2.4579	1.231	40	.225
Pair 11	V3 - V5	.6890	5.15196	.80460	-.9371	2.3152	.856	40	.397
Pair 12	V3 - V6	.9500	5.35532	.83636	-.7403	2.6403	1.136	40	.263
Pair 13	V4 - V5	-.2415	2.94287	.45960	-1.1703	.6874	-.525	40	.602
Pair 14	V4 - V6	.0195	3.33731	.52120	-1.0339	1.0729	.037	40	.970
Pair 15	V5 - V6	.2610	3.13790	.49006	-.7295	1.2514	.533	40	.597

Diastolic blood pressure

Paired Samples Test

		Paired Differences					t	df	Sig. (2-tailed)
		Mean	Std. Deviation	Std. Error Mean	95% Confidence Interval of the Difference Lower	Upper			
Pair 1	V1 - V2	3.9268	6.85708	1.07090	1.7625	6.0912	3.667	40	.001
Pair 2	V1 - V3	1.7073	8.80126	1.37453	-1.0707	4.4853	1.242	40	.221
Pair 3	V1 - V4	6.2195	9.11458	1.42346	3.3426	9.0964	4.369	40	.000
Pair 4	V1 - V5	4.7805	7.35701	1.14897	2.4583	7.1026	4.161	40	.000
Pair 5	V1 - V6	2.2683	8.57620	1.33938	-.4387	4.9753	1.694	40	.098
Pair 6	V2 - V3	-2.2195	7.75085	1.21048	-4.6660	.2270	-1.834	40	.074
Pair 7	V2 - V4	2.2927	7.04004	1.09947	.0706	4.5148	2.085	40	.043
Pair 8	V2 - V5	.8537	6.72518	1.05030	-1.2691	2.9764	.813	40	.421
Pair 9	V2 - V6	-1.6585	7.98627	1.24725	-4.1793	.8622	-1.330	40	.191
Pair 10	V3 - V4	4.5122	6.54264	1.02179	2.4471	6.5773	4.416	40	.000
Pair 11	V3 - V5	3.0732	7.48128	1.16838	.7118	5.4346	2.630	40	.012
Pair 12	V3 - V6	.5610	8.64595	1.35027	-2.1680	3.2900	.415	40	.680
Pair 13	V4 - V5	-1.4390	5.73170	.89514	-3.2482	.3701	-1.608	40	.116
Pair 14	V4 - V6	-3.9512	7.47981	1.16815	-6.3121	-1.5903	-3.382	40	.002
Pair 15	V5 - V6	-2.5122	6.24549	.97538	-4.4835	-.5409	-2.576	40	.014

MAP

Paired Samples Test

		Paired Differences					t	df	Sig. (2-tailed)
		Mean	Std. Deviation	Std. Error Mean	95% Confidence Interval of the Difference Lower	Upper			
Pair 1	V1 - V2	3.7573	10.77803	1.68324	.3554	7.1593	2.232	40	.031
Pair 2	V1 - V3	2.4480	11.91782	1.86125	-1.3138	6.2097	1.315	40	.196
Pair 3	V1 - V4	5.3830	12.08448	1.88728	1.5687	9.1973	2.852	40	.007
Pair 4	V1 - V5	4.7164	11.23449	1.75453	1.1704	8.2625	2.688	40	.010
Pair 5	V1 - V6	1.9685	12.58559	1.96554	-2.0040	5.9410	1.002	40	.323
Pair 6	V2 - V3	-1.3093	7.61317	1.18898	-3.7124	1.0937	-1.101	40	.277
Pair 7	V2 - V4	1.6257	6.00674	.93810	-.2703	3.5217	1.733	40	.091
Pair 8	V2 - V5	.9591	6.87283	1.07336	-1.2102	3.1284	.894	40	.377
Pair 9	V2 - V6	-1.7888	8.02253	1.25291	-4.3210	.7434	-1.428	40	.161
Pair 10	V3 - V4	2.9350	7.83023	1.22288	.4635	5.4066	2.400	40	.021
Pair 11	V3 - V5	2.2685	6.70014	1.04639	.1536	4.3833	2.168	40	.036
Pair 12	V3 - V6	-.4794	8.36032	1.30566	-3.1183	2.1594	-.367	40	.715
Pair 13	V4 - V5	-.6666	5.26086	.82161	-2.3271	.9939	-.811	40	.422
Pair 14	V4 - V6	-3.4145	6.90417	1.07825	-5.5937	-1.2352	-3.167	40	.003
Pair 15	V5 - V6	-2.7479	6.38370	.99697	-4.7628	-.7329	-2.756	40	.009

OPP

Paired Samples Test

		Paired Differences					t	df	Sig. (2-tailed)
					95% Confidence Interval of the Difference				
		Mean	Std. Deviation	Std. Error Mean	Lower	Upper			
Pair 1	V1 - V2	1.4798	5.24931	.81980	-.1771	3.1367	1.805	40	.079
Pair 2	V1 - V3	1.3144	5.23328	.81730	-.3374	2.9662	1.608	40	.116
Pair 3	V1 - V4	2.3439	5.46626	.85369	.6185	4.0692	2.746	40	.009
Pair 4	V1 - V5	2.0461	5.41275	.84533	.3376	3.7545	2.420	40	.020
Pair 5	V1 - V6	.0676	6.06868	.94777	-1.8480	1.9831	.071	40	.944
Pair 6	V2 - V3	-.1654	5.50173	.85923	-1.9020	1.5712	-.192	40	.848
Pair 7	V2 - V4	.8641	4.14771	.64776	-.4451	2.1732	1.334	40	.190
Pair 8	V2 - V5	.5663	4.93825	.77122	-.9924	2.1250	.734	40	.467
Pair 9	V2 - V6	-1.4122	5.59747	.87418	-3.1790	.3545	-1.616	40	.114
Pair 10	V3 - V4	1.0295	5.20199	.81241	-.6125	2.6714	1.267	40	.212
Pair 11	V3 - V5	.7317	4.27652	.66788	-.6182	2.0815	1.095	40	.280
Pair 12	V3 - V6	-1.2469	5.42392	.84707	-2.9589	.4651	-1.472	40	.149
Pair 13	V4 - V5	-.2978	4.01910	.62768	-1.5664	.9708	-.474	40	.638
Pair 14	V4 - V6	-2.2763	5.36994	.83864	-3.9713	-.5814	-2.714	40	.010
Pair 15	V5 - V6	-1.9785	4.23273	.66104	-3.3145	-.6425	-2.993	40	.005